Münchener Abhandlungen
zum Alten Orient 6

Kai Kaniuth (ed.)

Karacamirli — Tepe 5
A multi-period necropolis in Western Azerbaijan

with contributions by
Andrei Asăndulesei, Florian Becker, Jörg W.E. Fassbinder,
Andrea Göhring, Martin Gruber, Gisela Grupe, Stefan Hölzl,
Michael Joachimski, Christoph Mayr and Michaela Schauer

PeWe-Verlag

Münchener Abhandlungen zum Alten Orient
Band 6

Münchener Abhandlungen zum Alten Orient

herausgegeben von

Adelheid Otto

unter Mitarbeit von

Ursula Calmeyer-Seidl

Berthold Einwag

Michael Herles

Kai Kaniuth

Simone Mühl

Michael Roaf

Elisa Roßberger

Karacamirli — Tepe 5
A multi-period necropolis in Western Azerbaijan

edited by
Kai Kaniuth

with contributions by Andrei Asăndulesei, Florian Becker,
Jörg W.E. Fassbinder, Andrea Göhring, Martin Gruber, Gisela Grupe,
Stefan Hölzl, Michael Joachimski, Christoph Mayr and Michaela Schauer

PeWe-Verlag
2020

Gedruckt mit Unterstützung der Fritz Thyssen Stiftung.

Bibliografische Information der Deutschen Nationalbibliothek
Die Deutsche Nationalbibliothek verzeichnet diese Publikation in der Deutschen Nationalbibliografie; detaillierte bibliografische Daten sind im Internet über http://dnb.dnb.de abrufbar.

© PeWe-Verlag – Gladbeck 2020

Alle Rechte, insbesondere das Recht der Vervielfältigung und Verbreitung sowie der Übersetzung, vorbehalten. Kein Teil des Werkes darf in irgendeiner Form durch Fotokopie, Mikrofilm usw. ohne schriftliche Genehmigung des Verlages reproduziert oder unter Verwendung elektronischer Systeme verarbeitet, vervielfältigt oder verbreitet werden.

Layout und Prepress: Martin Gruber, München/Berlin
Umschlaggestaltung: PeWe-Verlag, Gladbeck
Umschlagabbildung: Bronze Disks 0179 and 0180 from Burial 9 of Karacamirli, Tepe 5 © Martin Gruber

Druck und Verarbeitung: Memminger MedienCentrum
Gedruckt auf alterungsbeständigem Papier

Printed in Germany

ISBN: 978-3-935012-44-7

In Memory of
İlyas Babayev (1935–2017)

Gurban Tepe, August 2017

Table of Contents

List of Figures XI

List of Tables XIX

Preface XXI

I. Introduction to the volume 1
Kai Kaniuth

I.1 The site of Tepe 5 3
I.2 The organization of the present volume 5

II. The Geophysical prospection around Tepe 5 7
Jörg W. E. Fassbinder, Florian Becker, Andrei Asăndulesei

II.1 Introduction 7
II.2 The Geophysical Prospection of Tepe 5 9
II.3 Conclusion 13

III. The Chalcolithic Pits 15
Martin Gruber

III.1 Pit KG-016/KG-019 15
III.2 Pit-KG-049 17
III.3 The Chalcolithic pottery in Pit-Complexes A and B 17
III.4 Dating 19
III.5 Conclusions 26

IV. The Tepe 5 Cemetery 29
Martin Gruber

IV.1 Introductory remarks 29
IV.2 Late Bronze/Early Iron Age 32
IV.2.1 A short history of research 32
IV.2.2 The Khojaly-Gadabay-Culture 33
IV.2.3 General description of burials and grave contents 35
IV.2.4 Radiocarbon dates 39
IV.2.5 The sequence of Late Bronze/Early Iron Age burials at Tepe 5 40
IV.3 Late Antique Period 41

IV.3.1 Historical background 41
IV.3.2 Regional Context 42
IV.3.3 General description of burials and grave contents 43
IV.3.4 Radiocarbon dates 46
IV.4 Medieval Period 46
IV.4.1 Historical Background 46
IV.4.2 Regional Context 47
IV.4.3 General description of the burials 49
IV.4.4 Radiocarbon dates 51
IV.5 Undated burials 52
IV.6 Pit-Complexes 53
IV.6.1 Pit-Complex A 54
IV.6.2 Pit-Complex B 54
IV.6.3 Pit-Complex C 55
IV.7 KG-100 and KG-101 56
IV.8 Stray finds 57
IV.9 Detailed description of the burials 60

V. Morphological and histological survey of human remains from Tepe 5 163
Andrea Göhring

V.1 Introduction 163
V.2 Methods 163
V.2.1 Morphological analysis 163
V.2.2 Histological analysis 168
V.2.3 X-ray analysis 170
V.2.4 Data analysis and software 170
V.3 Catalogue of human remains 170
V.3.1 Late Bronze Age/Early Iron Age burials 170
V.3.2 Late Antique burials 176
V.3.3 Medieval Burials 183
V.3.4 Undated burials 200
V.4 Morphological results and discussion 202
V.4.1 State of preservation 202
V.4.2 Age and sex distribution 202
V.4.3 Osteometry 204
V.4.3.1 Cranial measurements 204
V.4.3.2 Postcranial measurements 209
V.4.4 Joint status 211
V.4.5 Pathological alterations of bones and teeth 212
V.4.6 Acquired and epigenetic non-metric variants of bones 214
V.5 Summary 216

VI. Multi-isotope fingerprint of humans, animals, and environmental samples from Karacamirli 217
Andrea Göhring, Stefan Hölzl, Michael Joachimski, Christoph Mayr, Gisela Grupe

VI.1 Introduction 217
VI.2 Material and Methods 220
VI.2.1 Material 220
VI.2.2 Extraction of collagen and apatite and mass spectrometry 220
VI.2.2.1 Extraction and measurement of $\delta^{13}C_{collagen}$ and $\delta^{15}N_{collagen}$ of bone collagen 220
VI.2.2.2 Extraction and measurement of $\delta^{13}C_{carbonate}$ and $\delta^{18}O_{carbonate}$ of bone apatite 222
VI.2.2.3 Extraction and measurement of $\delta^{18}O_{phosphate}$ of bone apatite 222
VI.2.2.4 Extraction and measurement of $^{87}Sr/^{86}Sr$ of bones, teeth, and environmental samples 223
VI.2.3 Data analysis 223
VI.3 Results 225
VI.3.1 Diet reconstruction 225
VI.3.2 Assessment of the places of origin 230
VI.3.3 Cluster analysis 233
VI.4 Discussion 237
VI.5 Conclusion 242

VII. Portable X-ray Analysis 245
Michaela Schauer

VII.1 Geological background 246
VII.1.1 Geology of the Caucasus and Azerbaijan 246
VII.1.2 Geology of the Ganja-Qazakh region 248
VII.1.3 The Location of Tepe 5 251
VII.1.4 Soil samples 251
VII.1.4.1 Dataset 253
VII.1.4.2 Comments on the chemistry 255
VII.2 Pottery 256
VII.2.1 The Pottery of Tepe 5 257
VII.2.1.1 Results of p-XRF analyses 257
VII.2.1.2 Chemical groups and related fabric types (Martin Gruber, Kai Kaniuth) 276
VII.2.1.3 The pottery of Tepe 5 through time 278
VII.3 Obsidian 282
VII.3.1 Sources 282

VII.3.2 The obsidian from Tepe 5 286
VII.4 Metal analyses 289
VII.4.1 Copper 292
VII.4.2 Arsenical Copper 292
VII.4.3 Tin Bronze 292
VII.4.4 Iron 293
VII.4.5 Silver 293
VII.4.6 Summary 293
VII.5 Conclusion 293

VIII. Summary 295
Kai Kaniuth

IX. List of contexts 299

X. List of finds 303

XI. Bibliography 311

List of Figures

Unless otherwise indicated the copyright of figures and drawings lies with the individual authors. All drawings by Manfred Lercнl are labelled [ml].

Fig. 1. Archaeological sites (blue and red) and obsidian deposits (green) mentioned in this volume 1
Fig. 2. Archaeological sites north of Garajamirli 2
Fig. 3. Survey grid showing Tepe 5 in relation to Gurban Tepe and other archaeological sites of Karacamirli 3
Fig. 4. Location of Tepe 5 on a satellite image (© Quickbird, April 12, 2007) 4
Fig. 5. Karacamirli. Satellite overview of the total area overlaid by the grey scale images of the magnetometer survey areas (Quickbird imagery © 2013 DigitalGlobe from April 12th, 2007) ... 7
Fig. 6. Karacamirli. Tepe 5 area: Quickbird satellite image from April 12th 2007 (© 2013 DigitalGlobe); WGS 84 UTM 38N 8
Fig. 7. Karacamirli. Tepe 5 area: Quickbird Satellite image from 2007 (© 2013 DigitalGlobe), overlaid by the magnetogram of the area. The location of former and still existing mounds is marked in yellow; WGS 84 UTM 38N 9
Fig. 8. Karacamirli. Tepe 5 and its surroundings: Magnetogram of the burials and mounds, the »inner enclosure« and its periphery 10
Fig. 9. Karacamirli, Tepe 5. Detail of the magnetogram with the burial mound 11
Fig. 10. Karacamirli, Tepe 5. Detail of the magnetogram 12
Fig. 11. Karacamirli, Tepe 5. Detail of the magnetogram (30 % overlay by inverted high-pass filtered data) overlaid by photogrammetric image of the excavation (© Martin Gruber) ... 13
Fig. 12. Detail of the fill of pit KG-016. The transition from light to dark brown soil in the west marks the edge of the pit 15
Fig. 13. Location of the Chalcolithic pits on Tepe 5 16
Fig. 14. Finds from pit KG-016 [ml] 17
Fig. 15. Selected pottery from pit KG-016 [ml] 20
Fig. 16. Selected pottery from Chalcolithic contexts (KG-016-0045, KG-049-0196, KG-022-0073 and KG-023–0082) [ml] 21
Fig. 17. Selected pottery from pit KG-016 22
Fig. 18. Selected pottery from pit KG-016 23
Fig. 19. Selected pottery from contexts KG-016 and KG-018 23
Fig. 20. Cross-section of a sherd (0045-01) revealing the impressions of two jointed slabs 23
Fig. 21. Contour map of Tepe 5 with orthophotos of the excavated area 29
Fig. 22. Location of burials and Pit-Complexes on Tepe 5 30
Fig. 23. Temporary southern section of the south-western quadrant of square 6300/7990 showing the three natural layers on Tepe 5; the eastern part (right side) was disturbed by the grave-pit of the Medieval Burial 38 31
Fig. 24. Radiocarbon dates showing the three occupation phases of the cemetery 31
Fig. 25. Proposed subdivision of the Late Bronze/Early Iron Age (Khojaly-Gadabay-Culture) in north-western Azerbaijan after Минкевич-Мустафаева 1962, Гусейнова 1989; 2011 and Погребова 2011 33
Fig. 26. Punctate ornamentation on pot 0200-03 from Burial 2 34
Fig. 27. Location of Late Bronze/Early Iron Age burials 36
Fig. 28. Orientation of the grave-pits and skeletons in the Late Bronze/Early Iron Age 37
Fig. 29. Radiocarbon dates of Late Bronze/Early Iron Age burials 39
Fig. 30. Proposed chronological sequence of Late Bronze/Early Iron Age burials 40
Fig. 31. Location of Late Antique burials 42
Fig. 32. Orientation of the grave-pits and skeletons in the Late Antique period 44
Fig. 33. Typical black coloured stains on a Late Antique vessel from Burial 25 (0209-01) 44
Fig. 34. Radiocarbon dates of Late Antique burials 45
Fig. 35. Location of Medieval burials 47

Fig. 36. Burial 29 (KG-031) with an individual placed on its right side (first group)....49
Fig. 37. Burial 37 (KG-052) with an individual laying on its back with stretched legs (second group)....50
Fig. 38. Orientation of the grave-pits and skeletons in the Medieval period....50
Fig. 39. Radiocarbon dates of Medieval burials....51
Fig. 40. Undated Burial 42 (KG-035) with an infant individual....52
Fig. 41. Location of undated burials....53
Fig. 42. Plan of Pit-Complex A....54
Fig. 43. Plan of Pit-Complex B....55
Fig. 44. Plan of Pit-Complex C....56
Fig. 45. Pit-Complex C with Burial 21 (KG-074) and remains of Burial 1 (KG-094)....56
Fig. 46. Distribution of stray finds....57
Fig. 47. Stray finds (KG-024) [ml]....58
Fig. 48. Plan of Burial 1 (KG-094); Pit-Complex C-3....61
Fig. 49. Black-polished pot KG-094-0425-01 from Burial 1 with punctate ornamentation....62
Fig. 50. Black-polished bowl KG-094-0425-03 from Burial 1....62
Fig. 51. Pottery from Burial 1 (KG-094) [ml]....63
Fig. 52. Pottery from the fill of Burial 1 (KG-094) [ml] 63
Fig. 53. Finds from the fill of Burial 1 (KG-094) [ml]... 64
Fig. 54. Distribution of beads and obsidian flakes in the fill of Burials 1 (KG-094) and 21 (KG-074). 64
Fig. 55. Light blue frit bead (0453) with a cylindrical body and three applied knobs....65
Fig. 56. Black-polished pot with punctate ornamentation (0200-04) from Burial 2 (KG-044)....67
Fig. 57. Black-polished bowl (0200-07) from Burial 2 (KG-044)....67
Fig. 58. Plan of Burial 2 (KG-044)....68
Fig. 59. Pottery from Burial 2 (KG-044) [ml]....69
Fig. 60. Walnut-shaped bowl (0200-02) from Burial 2 (KG-044)....70
Fig. 61. Plan of Burial 3 (KG-051)....72
Fig. 62. Pottery from Burial 3 (KG-051) [ml]....72
Fig. 63. Pit-Complex A with Burials 4 (KG-039 & KG-040) and 5 (KG-038)....73
Fig. 64. Plan of Burials 4 (KG-039 & KG-040) and 5 (KG-038); Pit-Complex A....74
Fig. 65. Finds from Burial 4 (KG-039 & KG-040) [ml] ..75
Fig. 66. Finds from Burial 5 (KG-038) [ml]....76
Fig. 67. Pit-Complex C-1 and 2 with Burial 6 (KG-095-0497) in the south, Burial 45 (KG-096) in the west and Burial 22 (KG-095-0496) in the north....77
Fig. 68. Plan of Burials 6 (KG-095-0497), 22 (KG-095-0496) and 45 (KG-096); Pit Complex C-1–2....78
Fig. 69. Finds from Burial 6 (KG-095-0497) [ml]....79
Fig. 70. Bowl 0498-01 from Burial 6 (KG-095-0497) 79
Fig. 71. Pot 0498-02 with decorated lug from Burial 6.79
Fig. 72. Pottery from Burial 6 (KG-095-0497) [ml] 80
Fig. 73. Pot 0498-03 with polished decoration and disc-shaped lug from Burial 6 (KG-095-0497) . 81
Fig. 74. Pot 0498-06 from Burial 6 (KG-095-0497) with circular impressions on the shoulder.... 81
Fig. 75. Pit-Complex A with Burial 7 (KG-026) and the Medieval Burial 28 (KG-027)....84
Fig. 76. Pottery from Burial 7 (KG-026) [ml] 84
Fig. 77. Plan of Burial 7 (KG-026); Pit-Complex A 85
Fig. 78. Black-polished pot 0100-03 from Burial 7 (KG-026)....86
Fig. 79. Fragment of pot 0100-01 from Burial 7 (KG-026)....86
Fig. 80. Black-polished bowl 0100-02 from Burial 7 (KG-026)....86
Fig. 81. Pot 0100-09 from Burial 7 (KG-026)....86
Fig. 82. Pottery from the fill of Burial 7 (KG-026) [ml] 86
Fig. 84. Pit KG-057 with remains of Burial 8 in the south-eastern (pot 0417-01) and north-western corner (KG-057-0247 and KG-057-0404 with one half of bowl 0418-01), and the Late Antique Burials 23 (KG-057-0415) and 24 (KG-057-0414)....88
Fig. 83. Grey coloured pot 0417-01 from Burial 8 (KG-057-0247 and KG-057-0404)....88
Fig. 85. The rejoined halves of bowl 0418-01 (Burial 8) and 0241-02 (fill of Burial 15)....89
Fig. 86. Pottery from Burial 8 (KG-057-0247 & KG-057-0404) [ml]....89
Fig. 87. Plan of the remains of Burial 9 (KG-043)....90
Fig. 88. Bronze objects and adornment of the individual in Burial 9 (KG-043)....91
Fig. 89. Ornamented bronze discs (0179 and 0180) *in situ* with remains of a human skull in between....91
Fig. 90. Finds from Burial 9 (KG-043) [ml]....92
Fig. 91. Finds from Burial 9 (KG-043) [ml]....93
Fig. 92. Grey coloured pot (0164-02) from Burial 10 (KG-041)....94
Fig. 93. Grey coloured cup (0164-01) from Burial 10 (KG-041)....94
Fig. 94. Pottery from Burial 10 (KG-041) [ml]....94
Fig. 95. Plan of Burials 10 (KG-041) and 11 (KG-029); Pit-Complex A....96
Fig. 96. Grey coloured jug (0112-01) from Burial 11 (KG-029)....97
Fig. 97. Grey coloured churn (0112-02) from Burial 11 (KG-029)....97

Fig. 98. Pottery from Burial 11 (KG-029) [ml] 98
Fig. 99. Plan of Burial 12 (KG-064) 99
Fig. 100. Pottery from Burial 12 (KG-064) [ml] 100
Fig. 101. Plan of Burial 13 (KG-032) 100
Fig. 102. Burial 13 (KG-032) 101
Fig. 103. Finds from Burial 13 (KG-032) [ml] 101
Fig. 104. Pot 0144-01 from Burial 13 (KG-032) 101
Fig. 105. Pottery from Burial 13 (KG-032) [ml] 102
Fig. 106. Pot 0144-02 from Burial 13 (KG-032) 103
Fig. 107. Pot 0144-04 from Burial 13 (KG-032) 103
Fig. 108. Small beaker 0144-05 from Burial 13 (KG-032) 103
Fig. 109. Pottery from Burial 14 (KG-059) [ml] 105
Fig. 110. Plan of Burial 14 (KG-059) 106
Fig. 111. Pot 0252-01 from Burial 14 (KG-059) 107
Fig. 112. Finds from Burial 14 (KG-059) [ml] 107
Fig. 113. Carnelian beads from Burial 14 (KG-059) [ml] 108
Fig. 114. Frit beads and other finds from Burial 14 (KG-059) [ml] 109
Fig. 115. Plana A and B of Burial 15 (KG-058); Pit-Complex B 114
Fig. 116. Bowl 0241-03 from Burial 15 (KG-058) 115
Fig. 117. Bowl 0241-04 from Burial 15 (KG-058) 115
Fig. 118. Bowl 0241-01 from Burial 15 (KG-058) 115
Fig. 119. Pottery from Burial 15 (KG-059) [ml] 116
Fig. 120. Small pot 0241-05 from Burial 15 (KG-058) 117
Fig. 121. Pot 0241-07 from Burial 15 (KG-058) 117
Fig. 122. Finds from Burial 15 (KG-059) [ml] 118
Fig. 123. Plan of Burial 16 (KG-055) 120
Fig. 124. Pottery and finds from Burial 16 (KG-065) [ml] 120
Fig. 125. Jug 0221-01 from Burial 16 (KG-055) 120
Fig. 126. Pottery from Burial 17 (KG-065) [ml] 121
Fig. 127. Plan of Burial 18 (KG-015) 121
Fig. 128. Pottery from Burial 18 (KG-015) [ml] 122
Fig. 129. Plan of Burial 19 (KG-063) 122
Fig. 130. Finds from Burial 19 (KG-063) [ml] 123
Fig. 131. Plan of Burial 20 (KG-030 & KG-102); Pit-Complex A 123
Fig. 132. Plan of Burial 21 (KG-074); Pit-Complex C-3–4 124
Fig. 133. Finds from Burial 21 (KG-074) that probably originate from Burial 1 (KG-094) [ml] 125
Fig. 134. Trefoil jug 0506-01 from Burial 21 (KG-074) 125
Fig. 135. Pottery from Burial 21 (KG-074) [ml] 125
Fig. 136. Find from Burial 21 (KG-074) [ml] 126
Fig. 137. Two-handled pot (0419-01) from Burial 23 127
Fig. 138. Plan of Burials 8 (KG-057-0247 & KG-057-0404), 23 (KG-057-0415) and 24 (KG-057-0414); Pit-Complex B 128
Fig. 139. Pottery from Burial 23 (KG-057-0415) [ml] 129
Fig. 140. Distribution of finds in the fill of pit KG-057 (Pit-Complex B) 129
Fig. 141. Finds from the fill of pit KG-057 (Pit-Complex B) [ml] 130
Fig. 142. Burial 25 (KG-053) 132
Fig. 143. Plan of Burial 25 (KG-053) 133
Fig. 144. Finds from Burial 25 (KG-053) [ml] 134
Fig. 145. Pottery from Burial 25 (KG-053) [ml] 134
Fig. 146. Plan of Burial 26 (KG-066) 135
Fig. 147. Burial 26 (KG-066) 136
Fig. 148. Pottery from Burial 26 (KG-066) [ml] 136
Fig. 149. Pottery from Burial 27 (KG-097) [ml] 136
Fig. 150. Plan of Burial 27 (KG-097) 137
Fig. 151. Burial 27 (KG-097) 138
Fig. 152. Burial 27 Finds from Burial 27 (KG-097) [ml] 138
Fig. 153. Plan of Burial 28 (KG-027); Pit-Complex A 139
Fig. 154. Plan of Burial 29 (KG-031) with bronze object (0123) 140
Fig. 155. Burial 30 (KG-036) 141
Fig. 156. Plan of Burial 30 (KG-036) 142
Fig. 157. Burial 31 (KG-042) 143
Fig. 158. Plan of Burial 31 (KG-042) 144
Fig. 159. Plan of Burial 32 (KG-045) 145
Fig. 160. The southern part of Burial 33 (KG-046) in 2017 146
Fig. 161. Plan of Burial 33 (KG-046) 147
Fig. 162. Burial 34 (KG-048) and parts of the pottery inventory of Burial 2 (KG-044) 148
Fig. 163. Plan of Burial 34 (KG-048) 149
Fig. 164. Plan of Burial 35 (KG-047 & KG-098) 150
Fig. 165. Burial 36 (KG-050) 151
Fig. 166. Plan of Burial 36 (KG-050) 152
Fig. 167. Burial 38 (KG-073) 153
Fig. 168. Plan of Burial 37 (KG-052) 154
Fig. 169. Plan of Burial 38 (KG-073) 155
Fig. 170. Finds from Burial 38 (KG-073) [ml] 155
Fig. 171. Plan of Burials 39 (KG-077) and 43 (KG-076) 156
Fig. 172. Find from Burial 39 (KG-077) [ml] 157
Fig. 173. Burials 39 (KG-077) and 43 (KG-076) 157
Fig. 174. Plan of Burial 40 (KG-089) 158
Fig. 175. Plan of Burial 41 (KG-093) 159
Fig. 176. Burial 41 (KG-093) 160
Fig. 177. Plan of Burial 42 (KG-035) 160
Fig. 178. Plan of Burial 44 (KG-092) 161
Fig. 180. Example of the histological composition of bone in a young individual. Histological thin section of a femur diaphysis sample of individual KG-095-0496, Burial 22 (photograph by A. Alesi) 168
Fig. 181. Example of the histological composition of bone in a young individual. Histological thin section of a femur diaphysis sample

of individual KG-095-0496, Burial 35 (photograph by A. Alesi) 168
Fig. 182. Example of the histological composition of bone in a mature or senile individual. Histological thin section of a femur diaphysis sample (periosteal part) of individual KG-092-0398, Burial 44 (photograph by A. Alesi) 169
Fig. 183. Example of the TCA analysis of a tooth in an adult or mature individual. Histological thin section of an upper premolar sample of individual KG-097-0455, Burial 27 (photograph by A. Alesi)..... 169
Fig. 184. Example of the TCA analysis of a tooth in a mature or senile individual. Histological thin section of a lower premolar sample of individual KG-090-0398, Burial 44 (photograph by A. Alesi)..... 169
Fig. 185. Skeletal scheme of KG-094-0474 (Burial 1).....171
Fig. 186. Skeletal scheme of KG-039-0163 and KG-040-0165 (Burial 4) 171
Fig. 187. Skeletal scheme of KG-038-0146 (Burial 5)..... 172
Fig. 188. Norma frontalis of the skull of individual KG-026-0105 (Burial 7)..... 172
Fig. 189. Norma lateralis of the skull of individual KG-026-0105 (Burial 7)..... 172
Fig. 190. Skeletal scheme of individual KG-095-0497 (Burial 6) 173
Fig. 191. Skeletal scheme of individual KG-026-0105 (Burial 7) 173
Fig. 192. Skeletal scheme of KG-057-0247 and KG-057-0404 (Burial 8) 174
Fig. 193. Skeletal scheme of KG-032-0166 (Burial 13) ... 175
Fig. 194. Healed rib fracture (see arrows) on a right rib of individual KG-032-0166 (Burial 13) 175
Fig. 195. Skeletal scheme of KG-058-0243 (Burial 15)... 175
Fig. 196. Skeletal scheme of KG-030-0113 and KG-102-0491 (Burial 20) 176
Fig. 197. Skeletal scheme of KG-095-0496 (Burial 22) .. 176
Fig. 198. Skeletal scheme of KG-074-0507 (Burial 21)....177
Fig. 199. Skeletal scheme of KG-057-0415 (Burial 23) 177
Fig. 200. Lambdoid ossicles (see arrows) at the Sutura lambdoidea of individual KG-057-0415 (Burial 23)..... 178
Fig. 201. Ossicle at the lambda and lambdoid ossicles (see arrows) at the Sutura lambdoidea of individual KG-057-0415 178
Fig. 202. Canalis condylaris patent at the right side of the Foramen magnum (see arrow) of individual KG-057-0415 (Burial 23) 178
Fig. 203. Skeletal scheme of KG-057-0414 (Burial 24)... 179
Fig. 204. Osteomyelitis (see arrows) at the anterior-lateral side of the left tibia of individual KG-057-0414 (Burial 24)..... 179
Fig. 205. Periostitis on the anterior side of the left tibia of individual KG-053-0208 (Burial 25) ... 179
Fig. 206. Skeletal scheme of KG-053-0208 (Burial 25) ..180
Fig. 207. Lambdoid ossicles at the Sutura lambdoidea of individual KG-053-0208 (Burial 25).....180
Fig. 208. Norma frontalis of the skull of individual KG-053-0208 (Burial 25) 180
Fig. 209. Norma lateralis of the skull of individual KG-053-0208 (Burial 25) 181
Fig. 211. Skeletal scheme of KG-066-0392 (Burial 26) ...181
Fig. 210. Healed fracture (see arrows) of the posterior part of the left ulna of individual KG-066-0392 (Burial 26).....181
Fig. 212. Skeletal scheme of KG-097-0455 (Burial 27)... 182
Fig. 213. Foramen transversum bipartitum (see upper arrow) as well as Processus spinosus bipartitus (see lower arrow) on the sixth cervical vertebra of individual KG-097-0455 (Burial 27) 182
Fig. 214. Norma occipitalis of the skull of individual KG-097-0455 (Burial 27) with an ossicle at the lambda (see arrows)..... 182
Fig. 215. Skeletal scheme of KG-027-0106 (Burial 28) ... 183
Fig. 216. Anterior-lateral view on the right tibia of individual KG-027-0106 (Burial 28) with an osteomyelitis at the proximal part of the bone shaft including a central sisus (cloaca) for pus drainage. The central sisus (cloaca) and the coarsely woven bone at the cortex are clearly visible 183
Fig. 217. Lateral view on the right tibia of individual KG-027-0106 (Burial 28) with an osteomyelitis at the proximal part of the bone shaft. The coarsely woven bone at the cortex and consequent thickening of the bone are clearly visible 183
Fig. 218. X-ray Image (10 mAs, 52 kVp) of the proximal part of the right tibia of individual KG-027-0106 (Burial 28) from anterior (left) and lateral (right)..... 184
Fig. 219. Cribra orbitalia (see arrows) in the right and left orbit of individual KG-031-0120 (Burial 29)..... 184
Fig. 220. Exsutural Foramen mastoideum (see arrow) on the left side of the skull of individual KG-031-0120 (Burial 29)..... 184
Fig. 221. Skeletal scheme of KG-031-0120 (Burial 29) ... 185
Fig. 222. Processi spinosi bipartiti (see arrows) on cervical vertebrae C3–C6 of individual KG-031-0120 (Burial 29)..... 185

Fig. 223. Foramen transversum bipartitum (see arrrow) on the right side of cervical vertebra C7 of individual KG-031-0120 (Burial 29)..... 185
Fig. 224. Norma frontalis of the skull of individual KG-031-0120 (Burial 29)..... 186
Fig. 225. Norma lateralis of the skull of individual KG-031-0120 (Burial 29)..... 186
Fig. 226. Doubled Foramen zygomaticofaciale (see arrows) on the left Os zygomaticum of individual KG-036-0134 (Burial 30)..... 186
Fig. 227. Skeletal scheme of KG-036-0134 (Burial 30)... 187
Fig. 228. Norma frontalis of the skull of individual KG-036-0134 (Burial 30)..... 187
Fig. 229. Norma lateralis of the skull of individual KG-036-0134 (Burial 30)..... 187
Fig. 230. Skeletal scheme of KG-042-0173 (Burial 31).... 188
Fig. 231. Skeletal scheme of KG-045-0193 (Burial 32)... 188
Fig. 232. Skeletal scheme of KG-046-0192 (Burial 33)... 189
Fig. 233. Norma frontalis of the skull of individual KG-046-0192 (Burial 33)..... 189
Fig. 234. Norma lateralis of the skull of individual KG-046-0192 (Burial 33)..... 189
Fig. 235. Skeletal scheme of KG-048-0197 (Burial 34)... 190
Fig. 236. Bony spurs (see arrows) at the Os ischii projecting in the Foramen obturatum of the right pelvis of individual KG-038-0197 (Burial 34)..... 190
Fig. 237. Fusion of the second and third cervical vertebrae (see arrows) of individual KG-048-0197 (Burial 34)..... 190
Fig. 238. Supraorbital notches (see arrows above orbits) and accessory Foramina infraorbitalia (see arrows below orbits) on both sides of the facial skull of individual KG-048-0197 (Burial 34)..... 191
Fig. 239. Facies articularis superior atlantis bipartita on the superior side of the atlas of individual KG-048-0197 (Burial 34)..... 191
Fig. 240. Norma frontalis of the skull of individual KG-048-0197 (Burial 34)..... 191
Fig. 241. Norma lateralis of the skull of individual KG-048-0197 (Burial 34)..... 191
Fig. 242. Skeletal scheme of KG-047-0217 and KG-098-0467 (Burial 35)..... 192
Fig. 243. Skeletal scheme of KG-050-0203 (Burial 36).. 193
Fig. 244. Lambdoid ossicles (see arrows) on the Sutura lambdoidea of individual KG-050-0203 (Burial 36)..... 193
Fig. 245. Canalis condylaris on the right side of the Foramen magnum (left arrow) of individual KG-050-0203 (Burial 36), while the canal is not patent on the left side (right arrow)..... 193
Fig. 246. Foramen supratrochleare (see arrows) on the distal end of the left Humerus of individual KG-050-0203 (Burial 36)..... 194
Fig. 247. Norma frontalis of the skull of individual KG-050-0203 (Burial 36)..... 194
Fig. 248. Norma lateralis of the skull of individual KG-050-0203 (Burial 36)..... 194
Fig. 249. Skeletal scheme of KG-052-0205 (Burial 37)... 195
Fig. 250. Foramen transversum bipartitum (see arrows) on two cervical vertebrae (vertebra C4 and C5) of individual KG-052-0205 (Burial 37). The foramina on the fifth vertebra (right) are damaged and only partly visible..... 195
Fig. 251. Norma frontalis of the skull of individual KG-073-0508 (Burial 38)..... 195
Fig. 252. Norma lateralis of the skull of individual KG-073-0508 (Burial 38)..... 195
Fig. 253. Skeletal scheme of KG-073-0508 (Burial 38) .. 196
Fig. 254. Skeletal scheme of KG-077-0517 (Burial 39).... 196
Fig. 255. Skeletal scheme of KG-089-0387 (Burial 40) .. 197
Fig. 256. Osteophytes (see arrows) at the anterior side of four lumbar vertebrae of individual KG-093-0480 (Burial 41)..... 197
Fig. 257. Skeletal scheme of KG-093-0480 (Burial 41) .. 198
Fig. 258. Posterior view on the proximal part of the left tibia of individual KG-093-0480 (Burial 41) with osteophytes (see arrows) at the medial side, probably caused by an injury of the Ligamentum collaterale tibiae..... 198
Fig. 259. Osteophytes (see arrows) at the Facies auricularis of the left pelvis of individual KG-093-0480 (Burial 41)..... 198
Fig. 260. Damage of the right joint (left nd) of the sacrum of individual KG-093-0480 (Burial 41) with relatively large osteophytes (see arrows). The corresponding Facies auricularis of the right pelvis could not be examined..... 198
Fig. 261. Enthesiopathy (lateral) and rhomboid fossae (medial) on both clavicles of individual KG-093-0480 (Burial 41)..... 198
Fig. 262. Variant of Allen's fossa (see arrows) at the femoral neck of the left femur of individual KG-093-0480 (Burial 41)..... 199
Fig. 263. Processus supracondylaris (see arrow) on the posterior side of the left humerus diaphysis of individual KG-093-0480 (Burial 41)..... 199
Fig. 264. Canales condylares (see arrows) present on both sides of the Foramen Magnum of individual KG-093-0480 (Burial 41)..... 199

Fig. 265. Foramen supraorbitale with a vertical septum (see arrows) on the left side of the skull of individual KG-093-0480 (Burial 41)..... 199
Fig. 266. Skeletal scheme of KG-035-0136 (Burial 42).. 200
Fig. 267. Cribra orbitalia (see arrows) on both orbits of individual KG-035-0136 (Burial 42)..... 200
Fig. 268. Foramen transversum bipartitum (see left arrow) as well as Processus spinosus bipartitus (see right arrow) at the sixth cervical vertebra of individual KG-076-0515 (Burial 43)..... 200
Fig. 269. Skeletal scheme of KG-075-0515 (Burial 43)... 201
Fig. 270. Skeletal scheme of KG-092-0398 (Burial 44).. 201
Fig. 271. Osteomyelitis (see arrows) on the distal diaphyseal part of the left radius of individual KG-099-0460 (Burial 46)..... 201
Fig. 272. Skeletal scheme of KG-099-0460 (Burial 46). 202
Fig. 273. Sex distribution of the individuals from Karacamirli separated by ^{14}C dating..... 202
Fig. 274. Distribution of age classes of the individuals from Karacamirli separated by ^{14}C dating.... 204
Fig. 275. Distribution of sex per age class of the individuals from Karacamirli..... 204
Fig. 276. Cranial index and basio-bregmatic longitudinal index of nine individuals from Karacamirli.....205
Fig. 277. Cranial index and basio-bregmatic transversal index of nine individuals from Karacamirli.....205
Fig. 278. Basio-bregmatic longitudinal index and basio-bregmatic transversal index of nine individuals from Karacamirli.....206
Fig. 279. Jugo-frontal index and jugo-mandibular index of seven individuals from Karacamirli. Diagonal: jugo-frontal index = jugo-mandibular index.....206
Fig. 280. Total facial index and superior facial index of eight individuals from Karacamirli.....206
Fig. 281. Orbital index and nasal index of nine individuals from Karacamirli.....206
Fig. 282. Pairwise bivariate plot of the resulting three clusters on the twelve-dimensional craniometry dataset of nine humans from Karacamirli.....207
Fig. 283. Index platymericus of eight individuals from Karacamirli.....209
Fig. 284. Index cnemicus of six individuals from Karacamirli.....210
Fig. 285. Mean estimated body height (after Trotter/Gleser 1958) for seven at least juvenile individuals from Karacamirli. Error bars indicate standard deviations.....210
Fig. 286. $\delta^{13}C_{collagen}$ and $\delta^{15}N_{collagen}$ values of twelve individuals from Karacamirli differentiated by age, sex, and ^{14}C dating 225
Fig. 287. $\Delta\delta^{13}C_{carbonate\text{-}collagen}$ and $\delta^{15}N_{collagen}$ values of twelve individuals from Karacamirli differentiated by age and sex, and ^{14}C dating 225
Fig. 288. Diet-adjusted $\delta^{13}C$ and $\delta^{15}N$ of possible food sources and humans from Karacamirli.....226
Fig. 289. Concentration-weighted mixing model for the humans (green squares) from Karacamirli calculated with SISUS using eight different food sources (red circles) 228
Fig. 290. $\delta^{18}O_{carbonate}$ and $\delta^{18}O_{phosphate}$ values of twelve individuals from Karacamirli differentiated by age, sex, and ^{14}C dating 231
Fig. 291. $^{87}Sr/^{86}Sr$ values of human bones and teeth (enamel), animal bones and teeth (enamel), as well as modern environmental samples from Karacamirli.....232
Fig. 292. $\delta^{18}O_{phosphate}$ and $^{87}Sr/^{86}Sr$ values of ten individuals from Karacamirli differentiated by age, sex, and ^{14}C dating 233
Fig. 293. Pairwise bivariate plot of the resulting two clusters on the five-dimensional isotopic dataset of the humans from Karacamirli..... 234
Fig. 294. Pairwise bivariate plot of the resulting two clusters on the six-dimensional isotopic dataset ($\delta^{13}C_{collagen}$, $\delta^{15}N_{collagen}$, $\delta^{13}C_{carbonate}$, $\delta^{18}O_{carbonate}$, $\delta^{18}O_{phosphate}$, $^{87}Sr/^{86}Sr_{bone}$) of the humans from Karacamirli 236
Fig. 295. Pairwise bivariate plot of the resulting two clusters on the six-dimensional isotopic dataset ($\delta^{13}C_{collagen}$, $\delta^{15}N_{collagen}$, $\delta^{13}C_{carbonate}$, $\delta^{18}O_{carbonate}$, $\delta^{18}O_{phosphate}$, $^{87}Sr/^{86}Sr_{enamel}$) of the humans from Karacamirli 237
Fig. 296. Map approximatively indicating the (most probable) regions of origins for the primarily non-local individuals from Karacamirli.....239
Fig. 297. Tectonic map of the Caucasus (after Vincent et al. 2016: Fig. 1) 246
Fig. 298. Physical map of Azerbaijan 247
Fig. 299. Geological map of the Ganja-Qazakh region (IHPA NGO 2013: 28 Fig. 1.6).....249
Fig. 300. The location of Tepe 5.....250
Fig. 301. The location of clay samples used in this study..... 251
Fig. 302. The location of clay samples from the vicinity of Tepe 5.....252
Fig. 303. Tepe 5. Scatterplot of clay samples (n=30) showing SiO_2-Al_2O_3-ratio..... 254
Fig. 304. Tepe 5. Ternary plot of soil samples (n=30) showing Fe_2O_3-, CaO-, and MgO-ratio.....255

Fig. 305. Tepe 5. Ternary plot of pottery samples (n=30) showing Al_2O_3-, K_2O-, and CaO-ratio 256
Fig. 306. Tepe 5. Scatterplot of Early Chalcolithic pottery samples (n=21) and clay samples (n=20) showing Rb/Sr-ratio 257
Fig. 307. Tepe 5. Scatterplot of Early Chalcolithic pottery samples (n=21) and clay samples (n=20) showing Cr-/Zn-ratio 260
Fig. 308. Tepe 5. Scatterplot of Early Chalcolithic pottery samples (n=21) and clay samples (n=20) showing Fe_2O_3/Zn-ratio 260
Fig. 309. Tepe 5. Scatterplot of Early Chalcolithic pottery samples (n=21) and clay samples (n=20) showing K_2O/CaO-ratio 261
Fig. 310. Tepe 5. Scatterplot of Early Chalcolithic pottery samples (n=21) and clay samples (n=20) showing Zr/Rb-ratio 262
Fig. 311. Tepe 5. Scatterplot of Early Chalcolithic pottery samples (n=21) and clay samples (n=20) showing CaO/Zr-ratio 262
Fig. 312. Tepe 5. Scatterplot of Early Chalcolithic pottery samples (n=21) and clay samples (n=20) showing SiO_2/Al_2O_3-ratio 263
Fig. 313. Tepe 5. Scatterplot of Early Chalcolithic pottery samples (n=21) and clay samples (n=20) showing SiO_2/K_2O-ratio 263
Fig. 314. Tepe 5. Scatterplot of Late Bronze Age pottery samples (n=8) and clay samples (n=20) showing Sr/Rb-ratio 264
Fig. 315. Tepe 5. Scatterplot of Late Bronze Age pottery samples (n=8) and clay samples (n=20) showing CaO/Sr-ratio 265
Fig. 316. Tepe 5. Scatterplot of Late Bronze Age pottery samples (n=8) and clay samples (n=20) showing SiO_2/Al_2O_3-ratio 265
Fig. 317. Tepe 5. Scatterplot of Late Bronze Age pottery samples (n=8) and clay samples (n=20) showing Sr/Pb-ratio 266
Fig. 318. Tepe 5. Scatterplot of Early Iron Age pottery samples (n=18) and clay samples (n=20) showing Rb/Sr-ratio 267
Fig. 319. Tepe 5. Scatterplot of Early Iron Age pottery samples (n=18) and clay samples (n=20) showing CaO/S-ratio 268
Fig. 320. Tepe 5. Scatterplot of Early Iron Age pottery samples (n=18) and clay samples (n=20) showing SiO_2/Al_2O_3-ratio 268
Fig. 321. Tepe 5. Scatterplot of Early Iron Age pottery samples (n=18) and clay samples (n=20) showing SiO_2/Al_2O_3-ratio after removing CaO from the calculation 269
Fig. 322. Tepe 5. Scatterplot of Early Iron Age pottery samples (n=18) and clay samples (n=20) showing CaO/Sr-ratio 269
Fig. 323. Tepe 5. Scatterplot of Early Iron Age pottery samples (n=18) and clay samples (n=20) showing Sr/Pb-ratio 270
Fig. 324. Tepe 5. Scatterplot of Early Iron Age pottery samples (n=18) and clay samples (n=20) showing Cr/Zn-ratio 271
Fig. 325. Tepe 5. Scatterplot of Early Iron Age pottery samples (n=18) and clay samples (n=20) showing CaO/SiO_2-ratio 271
Fig. 326. Tepe 5. Scatterplot of Late Antique pottery samples (n=3) and clay samples (n=30) showing Sr/Rb-ratio 272
Fig. 327. Tepe 5. Scatterplot of Late Antique pottery samples (n=3) and clay samples (n=30) showing V/Cr-ratio 273
Fig. 328. Tepe 5. Scatterplot of Late Antique pottery samples (n=3) and clay samples (n=30) showing Cu/Zn-ratio 273
Fig. 329. Tepe 5. Scatterplot of Late Antique pottery samples (n=3) and clay samples (n=30) showing CaO/Zr-ratio 274
Fig. 330. Tepe 5. Scatterplot of Late Antique pottery samples (n=3) and clay samples (n=30) showing SiO_2/Al_2O_3-ratio 274
Fig. 331. Tepe 5. Scatterplot of Late Antique pottery samples (n=3) and clay samples (n=30) showing SiO_2/K_2O-ratio 275
Fig. 332. Tepe 5. Scatterplot of Late Antique pottery samples (n=3) and clay samples (n=30) showing Cl/S-ratio 275
Fig. 333. Ratio of hardness and grain size of the analysed samples according to their dating 277
Fig. 334. Tepe 5. Scatterplot of Early Chalcolithic (n=21), Late Bronze Age (n=8), Early Iron Age pottery samples (n=18) and clay samples (n=20) showing Rb/Sr-ratio 279
Fig. 335. Tepe 5. Scatterplot of Early Chalcolithic (n=21), Late Bronze Age (n=8) and Early Iron Age pottery samples (n=18) as well as clay samples (n=20) showing S/Cl-ratio 279
Fig. 336. Tepe 5. Scatterplot of Late Bronze Age (n=8) and Early Iron Age pottery samples (n=18) as well as clay samples (n=20) showing Rb/Sr-ratio 280
Fig. 337. Map of obsidian sources (after Chataigner/Gratuze 2014: Fig. 1) 282
Fig. 338. Tepe 5. PCA of obsidian artefacts (n=48) and source regions (n=37) 283
Fig. 339. Tepe 5. Scatterplot of obsidian artefacts (n=48) and sources (n=37) showing Zr/Sr-ratio 283

Fig. 340. Tepe 5. Scatterplot of obsidian artefacts (n=48) and sources (n=17) showing Zr/Sr-ratio 285
Fig. 341. Tepe 5. Scatterplot of obsidian artefacts (n=48) and sources (n=34) showing Zr/Rb-ratio 285
Fig. 342. Tepe 5. Scatterplot of obsidian artefacts (n=48) and reference material (n=37) showing Nb/Y-ratio.....286
Fig. 343. Tepe 5. Scatterplot of copper (n=5), arsenic copper (n=13), tin bronze (n=17) and leaded tin bronze artefacts (n=1) showing Zr/Sr-ratio ... 288
Fig. 344. Percentage of metals identified at Tepe 5 288
Fig. 345. Tepe 5. Scatterplot of copper (n=5), arsenical copper (n=13), tin bronze (n=17) and leaded tin bronze artefacts (n=1) showing Ni/Sb-ratio.....289
Fig. 346. Tepe 5. Scatterplot of copper (n=5), arsenical copper (n=13), tin bronze (n=17) and leaded tin bronze artefacts (n=1) showing Cu/Sn-ratio..... 290
Fig. 347. Tepe 5. Scatterplot of copper (n=5), arsenical copper (n=13), tin bronze (n=17) and leaded tin bronze artefacts (n=1) showing Sn/Pb-ratio 291
Fig. 348. Tepe 5. Scatterplot of copper (n=5), arsenical copper (n=13), tin bronze (n=17) and leaded tin bronze artefacts (n=1) showing Fe/Cu-ratio 291

List of Tables

Table 1. Types of vessels attested in each of the Chalcolithic contexts 19
Table 2. General features and orientation of grave-pits and skeletons of Late Bronze/Early Iron Age burials 37
Table 3. Type and number of objects found in Late Bronze/Early Iron Age burials and in their fill 38
Table 4. Radiocarbon dates of Late Bronze/Early Iron Age burials 39
Table 5. General features and orientation of grave-pits and skeletons of Late Antique burials 43
Table 6. Type and number of objects found in Late Antique burials and in their fill 44
Table 7. Radiocarbon dates of Late Antique burials 45
Table 8. General features and orientation of grave-pits and skeletons of Late Antique burials 48
Table 9. Burials of the Medieval period with burial gifts 50
Table 10. Radiocarbon dates of Medieval burials 52
Table 11. Criteria for sex determination of adult and non-adult skeletons 164
Table 12. Overview of the cranial measures including sections of measurement and measurement tools 165
Table 13. Cranial indices calculated from cranial measures 165
Table 14. Overview of the postcranial measures including measurement tools for humerus, radius, ulna, femur, and tibia 166
Table 15. Postcranial indices calculated from postcranial measures 167
Table 16. Summary of determined sex and age of the individuals from Karacamirli sorted by context 203
Table 17. Results of the cranial indices for nine individuals from Karacamirli, where cranial measurements were possible 205
Table 18. Mean (μ) and standard deviation (sd) of the twelve-dimensional craniometry dataset of nine humans from Karacamirli according to GMM clustering performed with three clusters 208
Table 19. Results of GMM cluster analyses on the twelve-dimensional craniometry dataset 208
Table 20. Results of the postcranial Indices for nine individuals from Karacamirli, where postcranial measurements were possible 210
Table 21. Overview of the distribution of the joint status for different joints and vertebrae of all 34 at least adult individuals from Karacamirli 211
Table 22. Overview of the distribution of the status of the bone surfaces (see ch. V.2.1) for different bones of all 34 at least adult individuals from Karacamirli 212
Table 23. Overview of the distribution of the status of the bone surfaces for different bones of all eight infant or juvenile individuals from Karacamirli 213
Table 24. Overview of the archaeological and modern samples from Karacamirli used for stable isotope analysis 221
Table 25. Results of isotope analyses of collagen and apatite for humans, animals and environmental samples from Karacamirli 224
Table 26. Overview of minimum, mean (μ), standard deviation (sd), and maximum isotope value of the analysed isotopic systems for the humans from Karacamirli 225
Table 28. Isotope values (mean μ, standard deviation sd) of the food sources (input data) from Karacamirli 227
Table 27. Diet-adjusted $\delta^{13}C$ and $\delta^{15}N$ values for the human consumers from Karacamirli 227
Table 29. Source contributions (minimum, mean, maximum) for the individuals from Karacamirli calculated with SISUS using eight food sources (see Table 27 and Table 28) 229
Table 30. Results of GMM cluster analyses with five and six isotopic dimensions 233
Table 31. Mean (μ) and standard deviation (sd) of

the five-dimensional isotopic dataset of the humans from Karacamirli according to GMM clustering performed with two clusters 235
Table 32. Mean (μ) and standard deviation (sd) of the six-dimensional isotopic dataset of the humans from Karacamirli according to GMM clustering performed with two clusters 235
Table 33. Mean (μ) and standard deviation (sd) of the six-dimensional isotopic dataset of the humans from Karacamirli according to GMM clustering performed with two clusters 235
Table 34. List of chemical values of the clay samples discussed in this study 253
Table 35. List of discussed chemical values of the sampled ceramics in this study 258
Table 36. System of ceramic ware codes 277
Table 37. List of sampled obsidian from Tepe 5 284
Table 38. Measurement results of significant elements for the metal artefacts of Tepe 5 and a stray find from the survey (0007) 287

Preface

The Tepe 5 north of the village of Qarajamirli is a small site of less than 0.2 ha, but the cemetery on its top neatly encompasses remains from almost all occupational periods documented up to now in the micro-region south of the Yenikand reservoir in western Azerbaijan. The relevance of the investigations reported on here therefore belies the small number of burials investigated: It provides us with a corpus of dated and analysed material which ideally complements the data collected in our larger project, the Karacamirli survey.

This volume contains the results of a concerted effort which extended over the past 5 years. It started with fieldwork in the years 2015–2017, continued with the subsequent analyses carried out in Baku and Munich between 2018 and 2019 and culminated in the writing and editing process which took another 18 months. As all group efforts tend to do, work on Tepe 5 has brought out the best and worst in the people involved. The exhilarating moment of discovery triggers the excavators as much as popular imagination, but there follows a phase when that beautifully preserved vessel or piece of jewellery discovered just before the close of work must be described, dated, discussed and contextualised, when different strands of information (some of them contradictory!) must be reconciled and synthesized. Now that the results are ready to be published, I am happy to admit that the major efforts were other peoples' – mostly the individual authors' –, and that bringing together the various chapters was the least effort of all, and probably the most pleasurable.

The privilege of working with a devoted and assiduous team of colleagues from Germany and Azerbaijan is only eclipsed by seeing their efforts come to fruition. My thanks go first and foremost to the people who have contributed to this publication, spending their time and energy, and undoubtedly foregoing other duties, in the process. My most sincere thanks are due to our Azeri colleagues who went out of their way to facilitate the collaborative work at Karacamirli. Dr. Maisa Rahimova, director of the Institute of Archaeology and Ethnography of the Academy of Sciences of Azerbaijan, granted permissions for fieldwork and material analyses and took a keen interest in our progress. Numerous other colleagues helped, not only in the preparation of this volume. Emil Iskenderov and Lachin Mustafaev were, in addition to pursuing their own research programmes, responsible for all facets of organization in the field, and in access to archives and collections in the post-excavation phase. All along, they managed to introduce us to current developments in Azeri archaeology and to impart a lasting impression of selfless collegiality and true hospitality.

Closer to home, Giulio Palumbi (Lyon) kindly checked parts of this manuscript. He and Bertille Lyonnet (Paris) supplied publications unavailable to us and kindly discussed aspects of their work. Most small find drawings are from the hands of Manfred Lerchl (Munich). We thank Simon Trixl for the archaeozoological determination of the animal bones and Alina Alesi (both Munich) for the preparation of the histological samples. M. Mach, B. Seelwald (Munich) and D. Steiniger (Berlin) gave us access to standards for our portable XRF instruments.

All research and analysis on Tepe 5 was funded by grants from the Fritz Thyssen Stiftung, which generously supported us for four years, from 2015 until 2018.

The man who made everything possible is, unfortunately, no longer with us. Academician Ilyas Babaev, head of the Institute of Ethnography and Archaeology's expedition and cooperation partner of a succession of German missions, passed away in December 2017. He is sorely missed and this book, which he anticipated as much as anybody, will be dedicated to his memory.

Kai Kaniuth Munich, July 2020

I. Introduction to the volume

Kai Kaniuth

Archaeological fieldwork along the middle stretch of the Kura river was, until recently, mostly linked to industrial or infrastructural projects. In the southern part of the region, in the foothills of the Lesser Caucasus, it was engineers who initiated excavations of Early Iron Age graveyards which they encountered in the vicinity of their mines or refining plants (Belck 1893). Later, in the 1930s, local schoolteachers were a driving force behind the fieldwork (Hummel 1929; Гуммель 1940). A first concerted effort in the documentation and investigation of archaeological remains started in 1946, flanking the Azerbaijan Soviet Socialist Republic's first major infrastructure project, the building of the Mingachevir dam (Асланов et al. 1959; Казиев 1960; Ваидов 1961).

The toponym Karacamirli commonly refers to a number of archaeological sites located on the southern side of

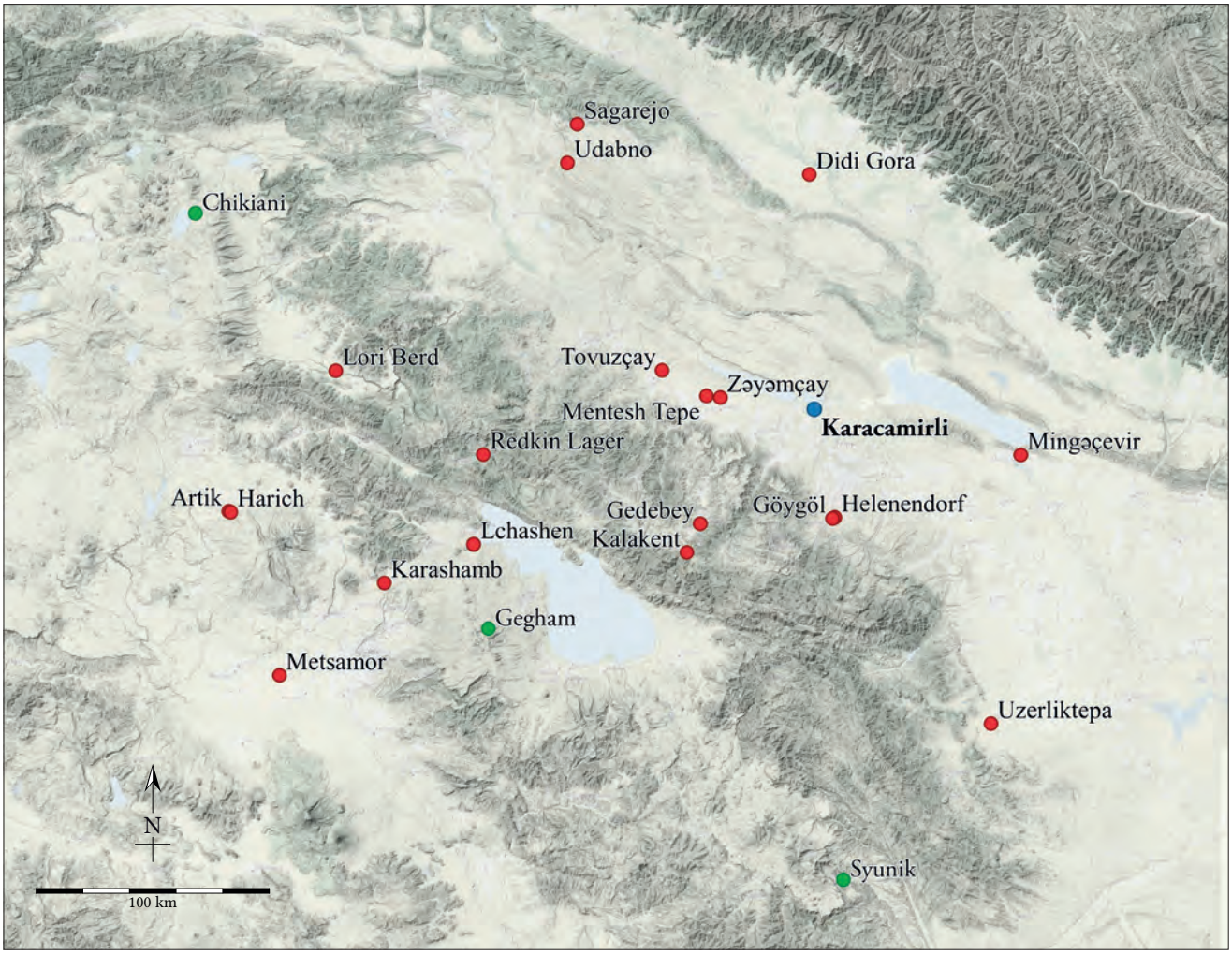

Fig. 1. Archaeological sites (blue and red) and obsidian deposits (green) mentioned in this volume

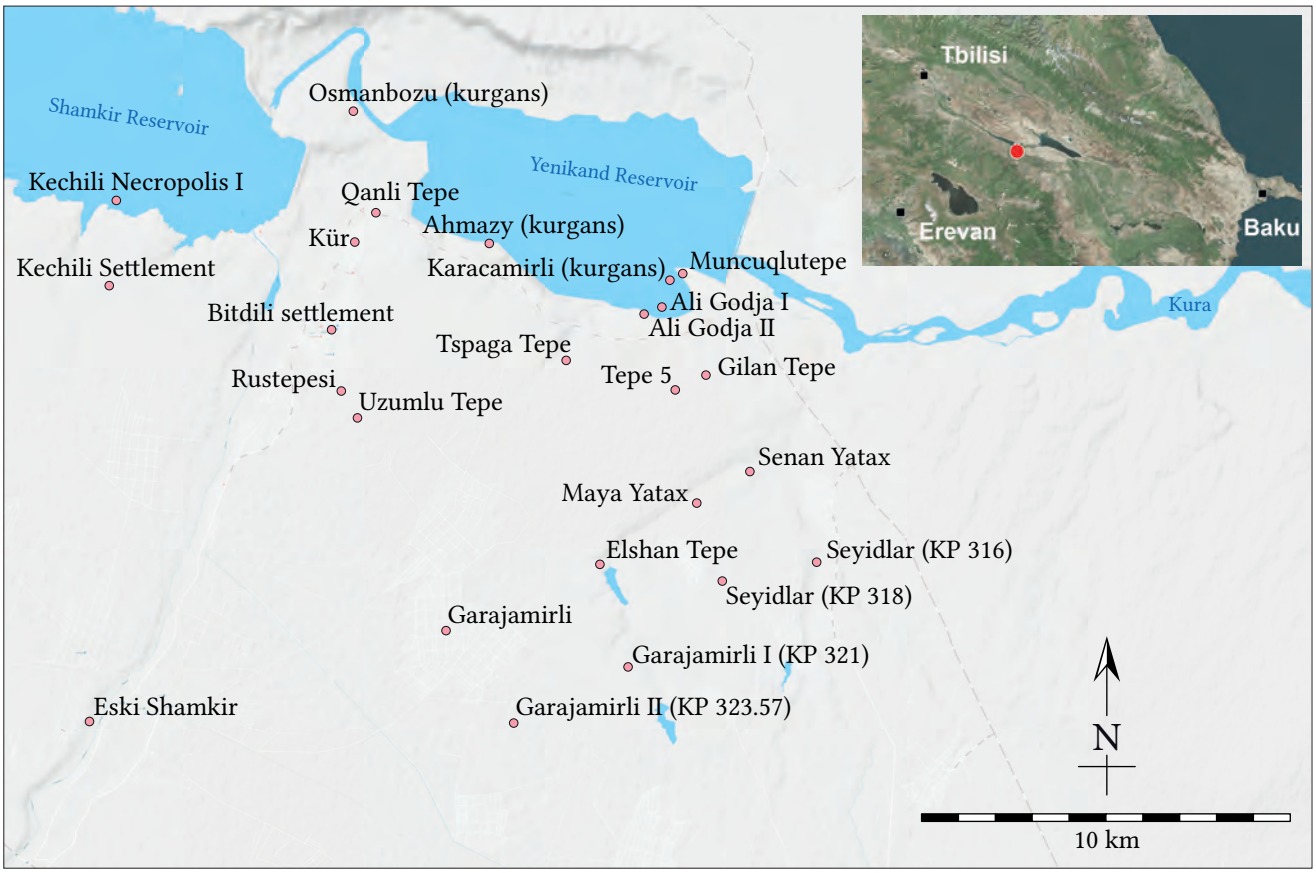

Fig. 2. Archaeological sites north of Garajamirli (basemap: Open Street Map)

the middle Kura valley north of the village of the same name (modern az. Garajamirli/Qaracamirli) in the Shamkir region of the Republic of Azerbaijan (Fig. 1 and Fig. 2).

Systematic archaeological fieldwork in this micro-region began in the early 1970s, when the Shamkir expedition was formed by the Azeri Academy of Sciences' Institute of Archaeology in advance of the construction of the Shamkir dam, designed to use the ponded waters of the Kura river (az. Kür) for use in a hydroelectric power plant above the modern town of Kür. Since 1973, annual work was carried out under the direction of G. P. Kesamanly at several sites, dating from the Chalcolithic until the late Medieval period (Кесаманлы et al. 1976; 1978a; 1978b; Кесаманлы 1981; 2003; Кесаманлы/Джафаров 1977; Джафаров et al. 1982). In the mid-1980s, responsibility for the work was transferred to G. Aslanov and A. Aliev, who shifted their attention further east, where a second, smaller dam was planned near the village of Yenikand (Алиев/Велиев 1986; Алиев 1987; n. d.; Алиев et al. 1988).

The years 2001–2005 saw yet another major infrastructure project, the building of the Baku-Tbilisi-Ceyhan pipeline (BTC). Four sites were discovered near Garajamirli, between kilometres 316 and 323 of the pipeline route, again confirming the general chronological bracket between the Chalcolithic and Middle Ages (Huseynov et al. 2007; Jalilov 2007; Agayev 2006; Dostiyev 2007a).[1]

In 2006, a fourth phase of research started with a joint project by the Institute of Archaeology, Azerbaijan Academy of Sciences (I. Babaev), the Georgian National Museum (I. Gagoshidze) and the Glyptothek and State Collections of Antiquities in Munich (F. Knauss). The aim of their excavations was a suite of Achaemenid period monumental buildings, focusing on the palace of Gurban Tepe (Babaev et al. 2006; 2009; Babaev/Knauss 2010; 2016; Knauss 2007; Knauss et al. 2010; 2013). From 2006–2019, annual campaigns were carried out by the team, documenting the virtual identity of the structure's dimensions with the Hadiš of Xerxes on the Persepolis terrace. The discovery of a spectacular residential and administrative complex, modelled in every respect on an imperial Achaemenid prototype, is at the heart of Karacamirli's international renown today.

1 For the results of the BTC project in general see Taylor/Maynard 2011, Taylor et al. 2011 and Taylor 2018 (for Azerbaijan) and Gamkrelidze 2010 (for Georgia).

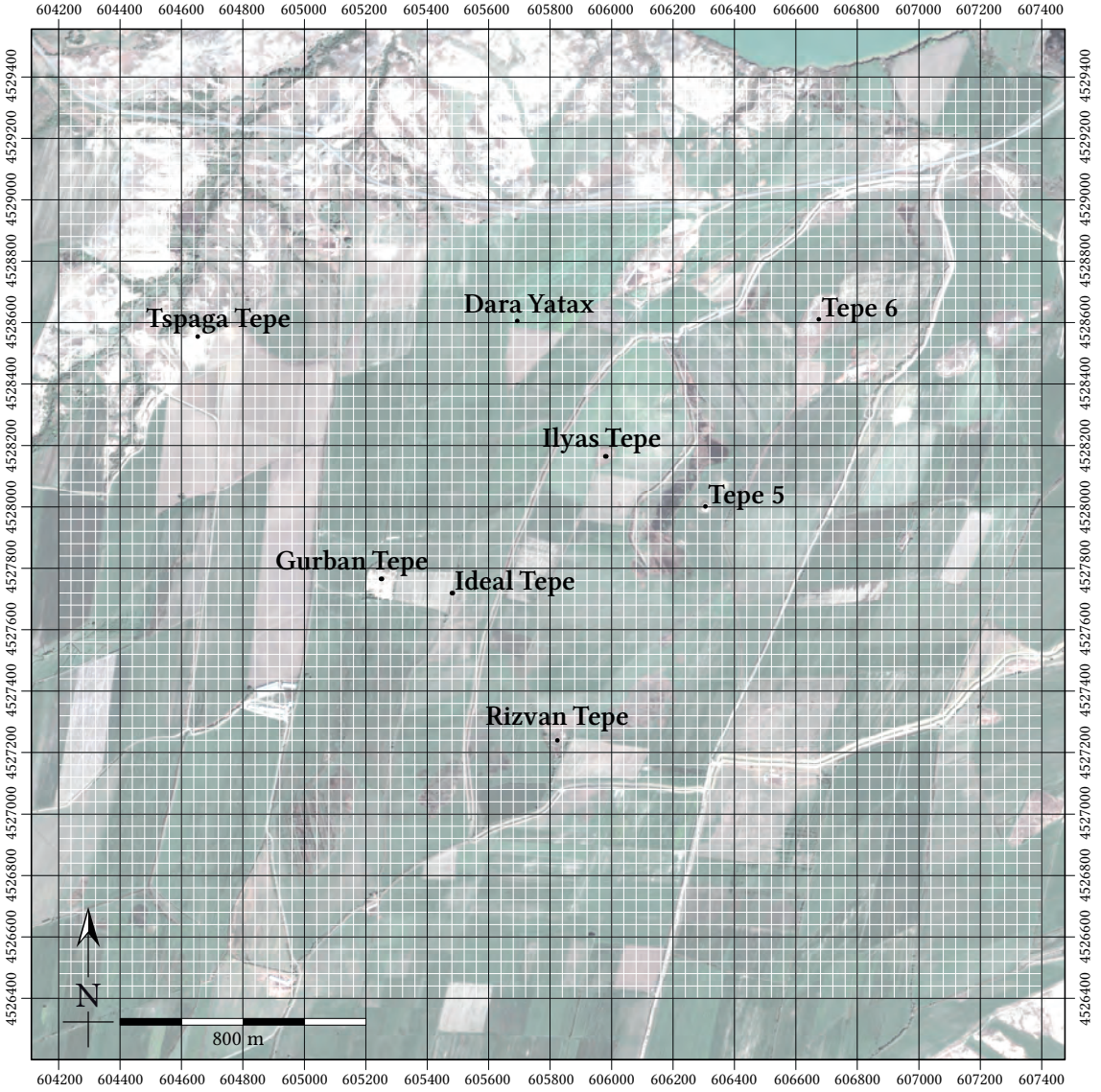

Fig. 3. The Karacamirli survey grid showing Tepe 5 in relation to Gurban Tepe and other archaeological sites of Karacamirli (map base: Quickbird, April 12, 2007)

The desire to study the Achaemenid complex in depth and to situate it within the local settlement history led to the conception of the Karacamirli survey. This project was carried out in cooperation of the Academy of Sciences (I. Babaev) and this author, as representative of Ludwig-Maximilians-University Munich. Funded by the *Deutsche Forschungsgemeinschaft* (DFG Az. KA2288/3, 2013–2014. KA2288/4, 2017–2018) and the *Fritz- Thyssen-Stiftung* (Thyssen-Stiftung Az. 10.14.2.053, 2015– 2018) an intensive surface survey led to the discovery of a number of new sites, the localisation of others, previously known only from short preliminary reports, and, above all, the clarification of the spatial structuration of an Achaemenid centre in the periphery of the empire (Babaev et al. 2016; 2017a; 2017b; Babaev et al. in print). While our research consisted mostly of surface survey work, several excavations were undertaken along. One of these is dealt with in this report.

I.1 The site of Tepe 5

Tepe 5 lies in the eastern part of the Karacamirli survey grid, at 606300.8 E/4527994.3 N (WGS 84, UTM 38N) (Fig. 3).[2] The terrain slopes down from south-east to north-

2 In the early phases of their project, the team of Babaev and Knauss numbered the hitherto unknown sites in the Karacamirli area. Thus, the propylon of the palace complex was labelled Tepe 1

Fig. 4. Location of Tepe 5 on a satellite image (© Quickbird, April 12, 2007)

west, where a small ditch visually and physically separates the site from the Achaemenid occupation further west. Surrounded by modern fields, the tepe forms the second of a row of originally at least four small elevations strung out in north-south direction (Fig. 4). The remaining three have been ploughed under, but were still visible on satellite imagery as late as 2007.

Today, Tepe 5 measures 35 × 40 m. It is a rectangular mound, whose edges have been somewhat cut and straightened by decades of ploughing. Even though some attempts are visible to level the site with the surrounding fields, the elevation still stands some 2.5 m high in its north-western corner (at a max. height of 174.18 m a.s.l.), while in the southeast it rises barely above the cultivated ground. The natural soil of Tepe 5 differs from that of the nearby fields. It is of lighter shade, and harder to work. While we have not undertaken a geomorphological identification, it appears that Tepe 5, like the other three hillocks visible on Fig. 4, and like another, smaller hill west of the ditch, are relicts of an underlying geomorphological stratum which was selected, for one reason or another, as a focus of human activity.

The area around Tepe 5 was included in our survey on 24 September 2015 as part of grid numbers Z41 (6280/7960) and Z53 (6280/8000). The topography of the site stood out, as did the finds collected on the surface nearby (among them a bronze dagger (Fd. no. 0007, picked up 45 m northeast of the tepe), i. e., between Tepe 5 and the next relict tepe. This, of course, opens the possibility that the ancient burial ground may have been considerably larger. The ceramic material was inconspicuous.

The geophysical survey, on the other hand, showed more tangible results and suggested the hill as a very

(later: Ideal Tepe), the palace itself Tepe 2 (later: Gurban Tepe), and the administrative sites in the periphery Tepes 3 (Rizvan Tepe) and 4 (Ilyas Tepe). Only Tepes 5 and 6 – a medieval site several hundred meters to the north (Babaev et al. in print) – retain their original names.

promising location for a detailed investigation. At that time, in late 2015, the nature of the pre-modern use of Tepe 5 was very much open to debate. The regular pattern of the anomalies visible on the magnetometer image (see ch. II) made the presence of a built structure as likely as any other. Our excavations began in the following summer with the only certainty, that conditions and archaeological remains promised to be much different from any other we were likely to encounter in the surroundings of Gurban Tepe.

Since our excavations in the years 2016 and 2017 have provided much more detailed information, a discussion of the survey results – including the comparison of survey and excavation data – will be deferred to the final publication of that work package.

The excavation of Tepe 5 began on the 3rd of August and lasted until the 27th of August 2016. A surface area of 140 sqm was opened in this year in three trenches (Babaev et al. in print). In the following year, the investigations were resumed from 24th of July until 18th of August 2017. Work was carried out by two to three archaeologists and up to 14 workmen from the town of Kür.[3] The excavation was carried out with the help of a Leica TC407 Total Station, within a grid staked out by a GS10 GNSS system. Archaeological deposits were recorded in a single context-system. Contexts numbers consist of three digits preceded by KG (for *Karacamirli Grabung*, i. e. KG-999), small finds, sherd lots, skeletons and samples are identified by a four-digit code (KG-[context]-8888). Individual sherd numbers are listed with reference to the sherd lot-numbers.[4] A Filemaker© database was used to enter the form-based in-field documentation. In the field, no drawings were made. Instead, all visual documentation was photographic, and of all features three-dimensional models were created employing Structure from Motion (SfM) with Agisoft Metashape©. Subsequent to the excavation, the interpretation of remains involved the creation of vector graph plans and drawings. Starting with the 2017 campaign, a portable XRF instrument, Niton XL3t, was used extensively in the Karacamirli project, and a substantial number of finds from Tepe 5 were analysed.[5] In the same year, the anthropological material from both campaigns was studied. A number of samples were exported to Germany for isotope analyses.[6]

I.2 The organization of the present volume

The present volume is the final report on our excavations at Tepe 5. It therefore discusses all parts of our work exhaustively, presenting the entirety of relevant data gathered. The first results obtained at the site will be reported by Jörg Fassbinder and his team, who opened our investigations in the year 2015 with their geophysical prospection (ch. II). Next, Martin Gruber publishes the excavations results, contexts and small finds, which were documented under his supervision (chs. III and IV). Andrea Göhring, who joined our team in 2017, then deals with all aspects of the anthropological remains (ch. V), followed by a report on isotope analyses carried out on the human bone material (ch. VI). Michaela Schauer covers the material science aspects of the Tepe 5 finds (ch. VII), carried out within the larger analytic program run at Karacamirli. Finally, an overview is provided summarising the most important results of our work (ch. VIII).

3 In 2016, the excavation staff consisted of M. Gruber (site supervisor, Munich University), M. Uehara, S. Forstreuter (archaeologists), R. Aliev, H. Aliev, E. Mamedov, Farid Aliev, Fariz Aliev, V. Cəfərov, C. Hüseynov, T. Jusifov, E. Cafarov, C. Qafarov, Z. Məhərrəmov, R. Ahmedov, N. Abdullaev, S. Amiraslanov, E. Bajramov, A. Musayev, S. Namazov, V. Pirverdiev, T. Gasimov, A. Akbarov, S. Askarov, S. Ələkbərov, N. İmamverdiyev and E. Ağayev (workmen). In 2017 M. Gruber was again in charge, aided by M. Uehara, E. Güneş, A. Rybalchenko (archaeologists), N. İmamverdiyev, Z. Məhərrəmov, F. Abdullayev, S. Ələkbərov, N. Abdullayev, C. Ələkbərov, E. Əliyev, E. Mamedov, A. Pənahov, Y. Alnağıyev, A. Həsənov, M. Abdullayev, Q. İmamverdiyev, N. Şahbazi, A. Paşayev, S. İmamverdiyev, A. Mehdiyev, V. Pirverdiyev, M. İbrahimov, E. Ağayev, G. Mamedov, M. Ağayev, A. Süleymanov, A. Musayev, V. Cəfərov, F. Chernasov, N. Seyidov, V. Gasimov, M. Mamedov, V. Aslanov and E. Bogrov (workmen).

4 Hence, KG-010-2222-03 would refer to the third sherd of lot 2222, belonging to context 010.

5 For details concerning the analytic protocol see M. Schauer, in this vol.

6 See Göhring and Göhring et al., in this vol.

II. The Geophysical prospection around Tepe 5

Jörg W. E. Fassbinder / Florian Becker / Andrei Asăndulesei

II.1 Introduction

Karacamirli, a major Achaemenid palatial structure, has been under excavation since 2006 by F. Knauss and I. Babaev (Babaev et al. 2016; Knauss et al. 2013). From 2013–2017 a systematic archaeological survey combined with a large-scale magnetometer prospection undertaken by Kai Kaniuth and Jörg Fassbinder (Ludwig Maximilians University, Munich) followed up these ground-breaking studies by considering patterns of land use and the spatial structuration of an Achaemenid imperial site.

According to the ceramic finds, the area of Karacamirli was occupied from the Chalcolithic period until the Middle Ages. The intensive archaeological survey target-

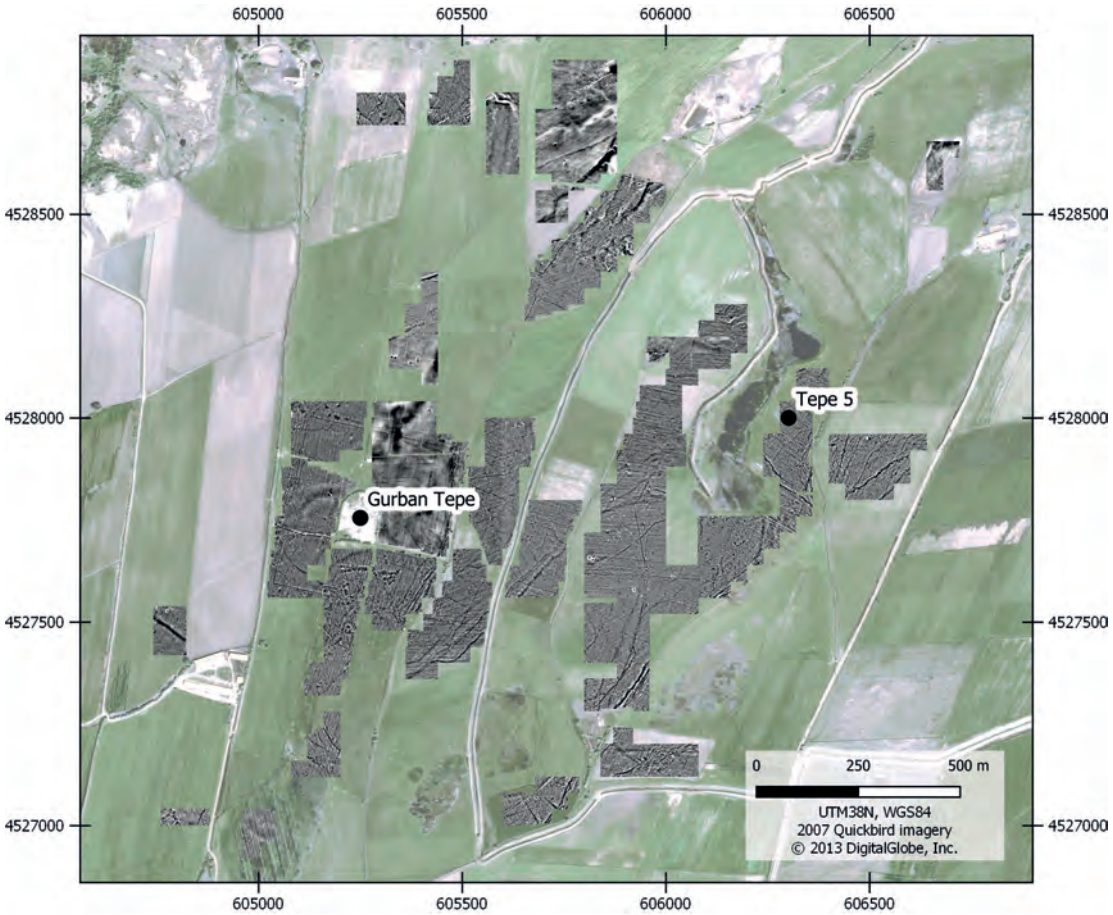

Fig. 5. Karacamirli. Satellite overview of the total area overlaid by the grey scale images of the magnetometer survey areas. The grey scale patchwork is due to the application of different instruments (caesium and fluxgate magnetometer) with different sensitivities/dynamics (Quickbird imagery © 2013 DigitalGlobe from April 12th, 2007)

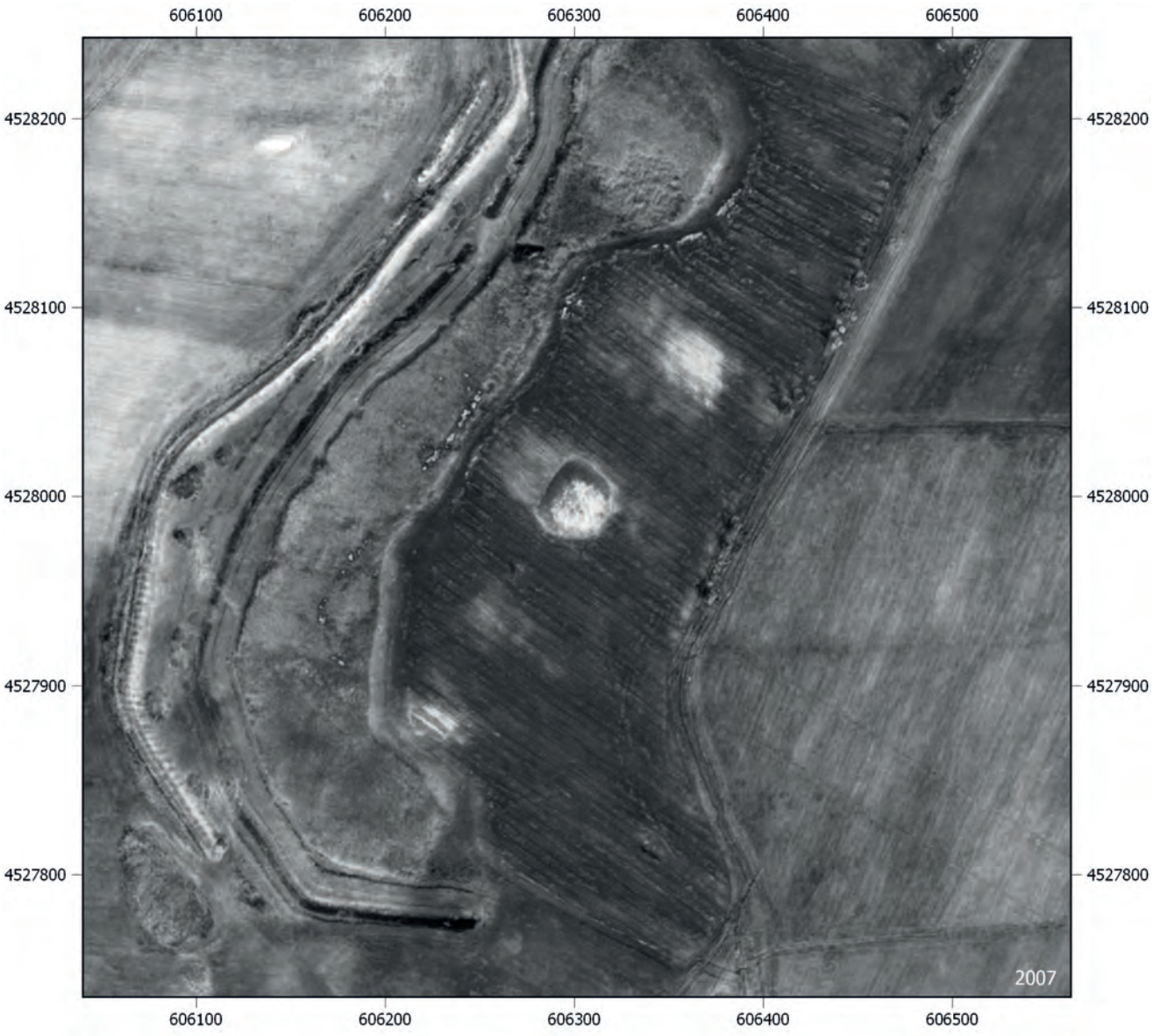

Fig. 6. Karacamirli. Tepe 5 area: Quickbird satellite image from April 12th 2007 (© 2013 DigitalGlobe); WGS 84 UTM 38N

ed an area of c. 4 km², of which more than 1.5 km² were prospected by a magnetometer survey (Fig. 5).

Our first tests for the suitability of magnetometer prospecting in 2013 were undertaken with the Scintrex SM-4G-Special caesium magnetometer to prove the feasibility of the site for geophysical prospection. In three field seasons from 2015–2017 we applied all our disposable magnetometers (fluxgate and caesium magnetometers) to cover all accessible areas adjacent to the palace and in its periphery.

For this purpose, we worked with several teams and applied two 4-sensor (Förster-Ferex) fluxgate magnetometer units and two Caesium-magnetometers. The prospecting areas were selected according to their accessibility and suitability for a high-resolution magnetometer prospection. All these areas were scanned with a sampling interval of 10 × 50 cm.

For a better understanding, the magnetometer measurements were complemented by Earth Resistance Tomography (ERT) measurements, susceptibility measurements, some trial excavations and additional mineral magnetic analyses of archaeological soils and typical soil layers. The results of this part of the project will be published in a separate report.

Apart from the known sites which had formed part of the Achaemenid administrative centre, geophysics were employed predominantly, whenever noteworthy topographic features, remote sensing data or concentrations of ceramic finds indicated sub-surface archaeological structures. All of this was the case at Tepe 5.

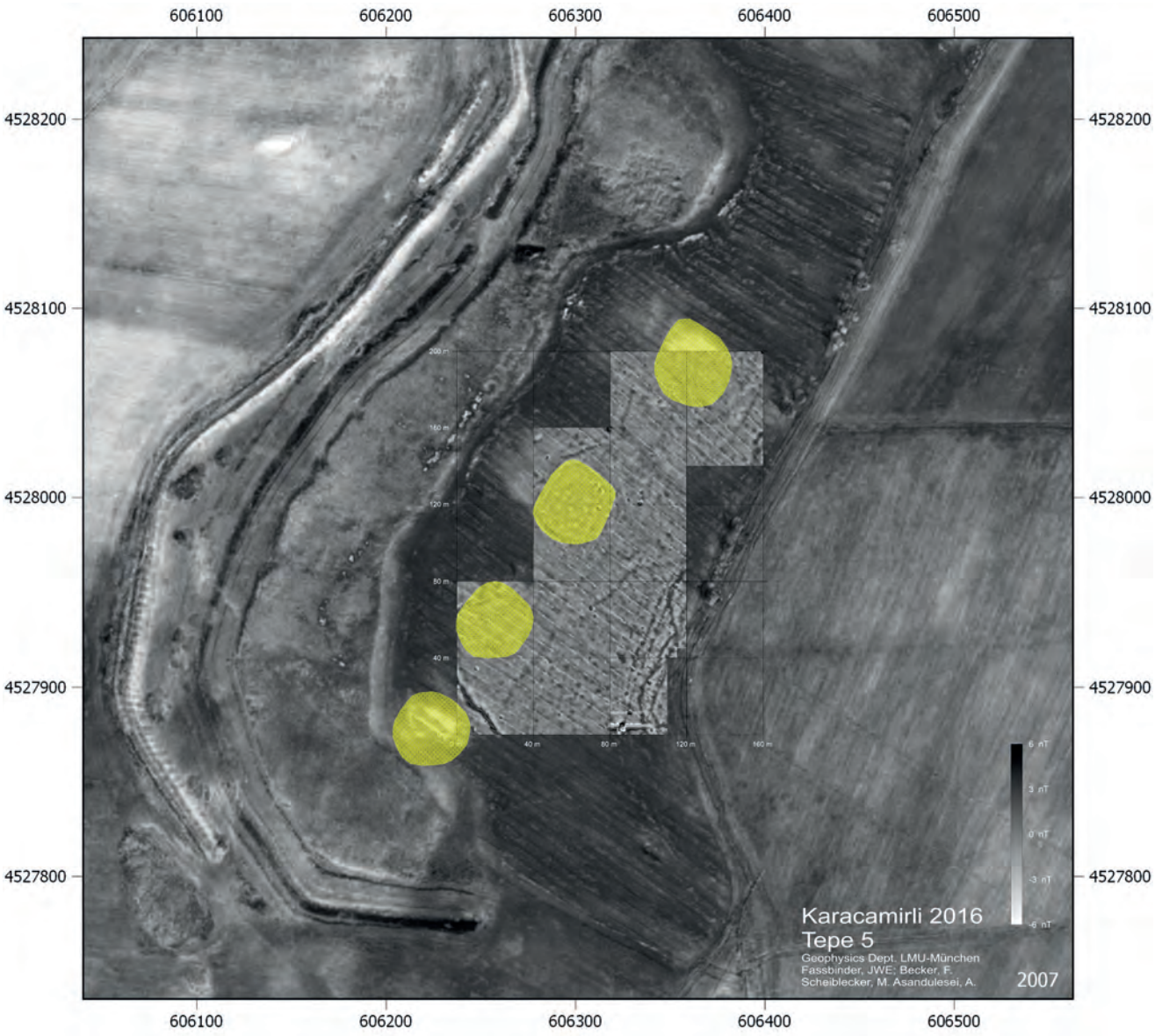

Fig. 7. Karacamirli. Tepe 5 area: Quickbird Satellite image from 2007 (© 2013 DigitalGlobe), overlaid by the magnetogram of the area. The location of former and still existing mounds is marked in yellow; WGS 84 UTM 38N

II.2 The Geophysical Prospection of Tepe 5

The mound named »Tepe 5«, is situated c. 1200 m northeast of Gurban Tepe. It is visible on vintage CORONA and more recent Quickbird satellite images (Fig. 6) which show a more or less regular row of four white spots in this area, indicating burial mounds or other undated archaeological sites. Three of these sites were already intensively ploughed and hence invisible from the ground. Only one mound appeared fairly untouched. It forms a square shaped elevation of c. 2.5 m height and c. 40 m diameter. Previous to our measurements nothing was known about the constitution, composition or the function of this site. The controlled sherd pickup did demonstrate, however, that we were dealing with an archaeological site.

The mound, so far excluded from modern farming, was overgrown by high grass and bushes. We prepared the area for the magnetometer prospection manually by cutting and clearing the vegetation. While the periphery and the area adjacent to the mound had already been measured with a fluxgate magnetometer, we decided to survey the mound itself with a more sensitive caesium magnetometer (Geometrics G-585) in duo-sensor configuration. Caesium magnetometers usually have five times higher intensity anomalies than gradiometers which allows an insight to deeper soil horizons (Linford et al. 2007; Mathé et al. 2009; Fassbinder 2015).

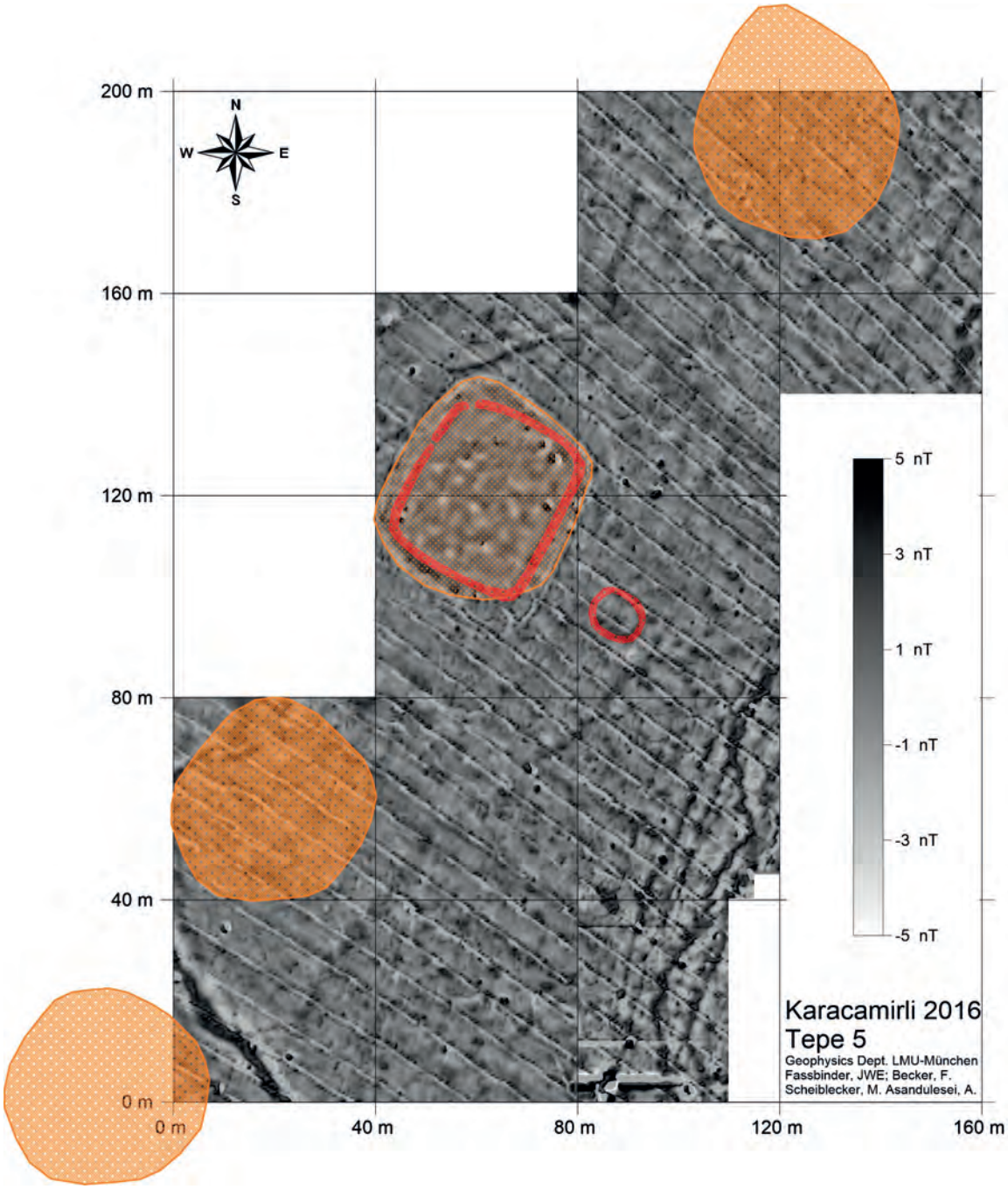

Fig. 8. Karacamirli. Tepe 5 and its surroundings: Magnetogram of the burials and mounds, the »inner enclosure« and its periphery. Caesium total field magnetometer (Geometrics, G-585 in duo-sensor variometer configuration) in the area on top of the mound and Ferex Foerster (four sensor fluxgate gradiometer) applied in the periphery of the mound. Sampling density 12.5 × 50 cm resp. 10 x 50 cm, interpolated to 12.5 × 12.5 cm, dynamics ±15 resp. 3 nT fused to ±4 nT in 256 grey-scales, 40 m grid

Analysing the magnetogram in detail, we believe that the inner structure of the mound forms a rectangle with rounded edges, c. 35 × 25 m in size. The longer side is tilted clockwise by c. 27°. The mound itself was never touched by modern farming. Irrigation canals and ploughmarks are only visible around the mound. Possibly, the agricultural activity is in part responsible for the rhomboid shape of the hill. The periphery of the mound, like the predominant part of the landscape in Karacamirli (see magnetograms in Fig. 5), is seriously disturbed by modern irrigation canals, which run parallel to each other at a distance of 5 m. They are c. 30 cm wide and incised c. 20–30 cm deep into the ground. Due to their short distance to the magnetometer probes during the

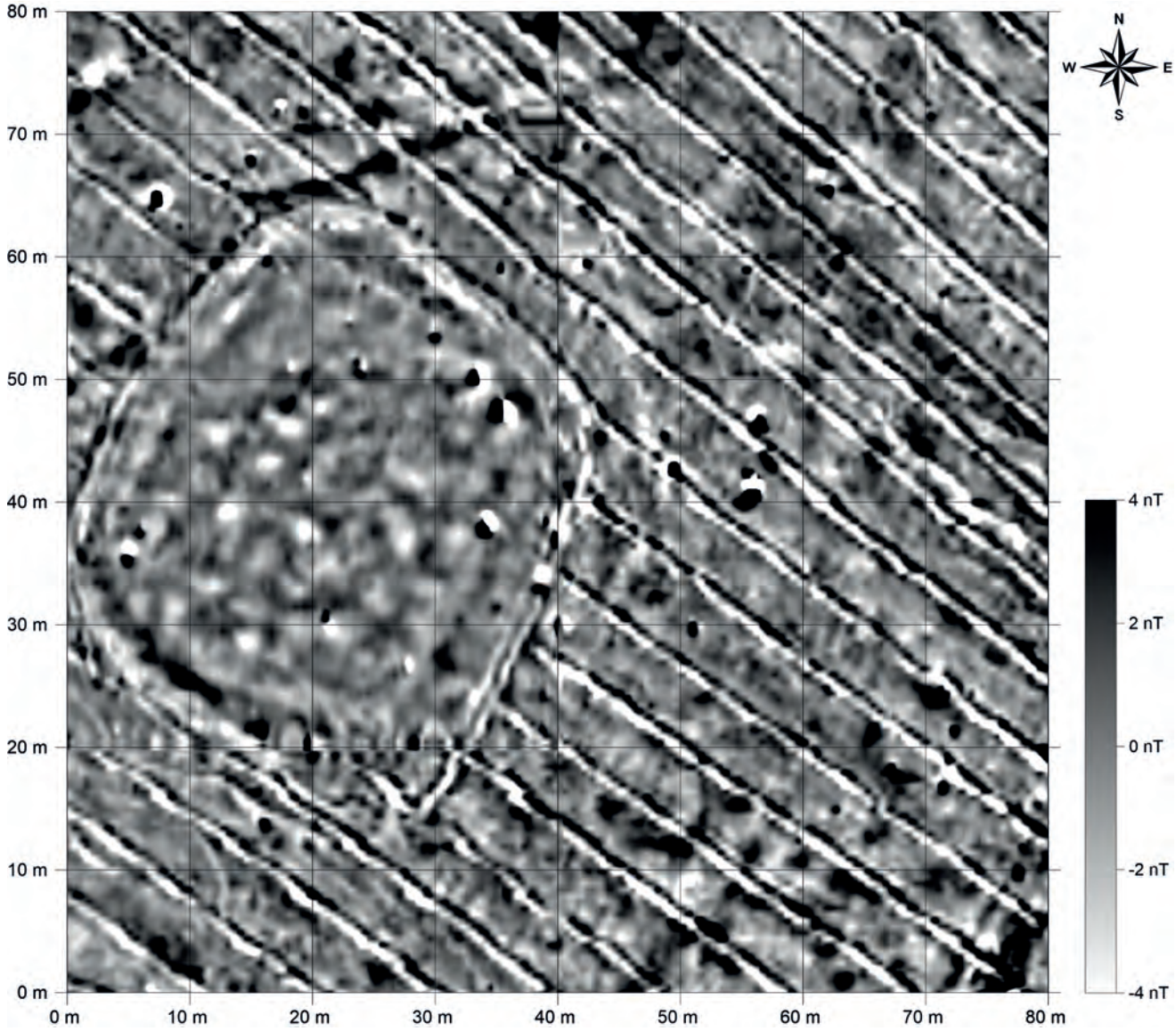

Fig. 9. Karacamirli, Tepe 5. Detail of the magnetogram with the burial mound. Notice that the magnetic anomalies of the pits on top of the mound are positive and negative; while in the periphery these are almost only positive ones (for technical details see Fig. 8)

survey these features show up very sharply and obscure the image as from a window blind.

The magnetogram clearly indicated the presence of non-natural subsurface structures on the mound. At first sight it appeared to conform to the ground plan of a massive building complex (Fig. 8 and Fig. 9). The more or less regular pattern of »negative« white anomalies led us to the assumption that we had discovered a monumental building complex possibly linked functionally to the administrative complex centred on Gurban Tepe.

Comparing our first geophysical assessment, the excavation and discovery of a cemetery therefore came as a surprise. On the other hand, previous measurements of burial grounds and cemeteries elsewhere show similar results with burial pits showing up as negative (white) anomalies (Fassbinder et al. 1999; Fassbinder/Becker 2003; Fassbinder 2017).

The burials on the mound seem to be arranged as within an »enclosure«, oriented by c. 27° towards the north-east. The burials here show up as negative and positive magnetic anomalies. Together they form a square shaped pattern of burial pits, which is enclosed by a linear feature. Within this rectangular structure with rounded edges, was the trace of a palisade, a ditch or a wall of rammed earth, the nature of which cannot be determined solely by the magnetic image. Extensive agriculture deformed the mound already and gives it its rhomboid shape (Fig. 10 and Fig. 11).

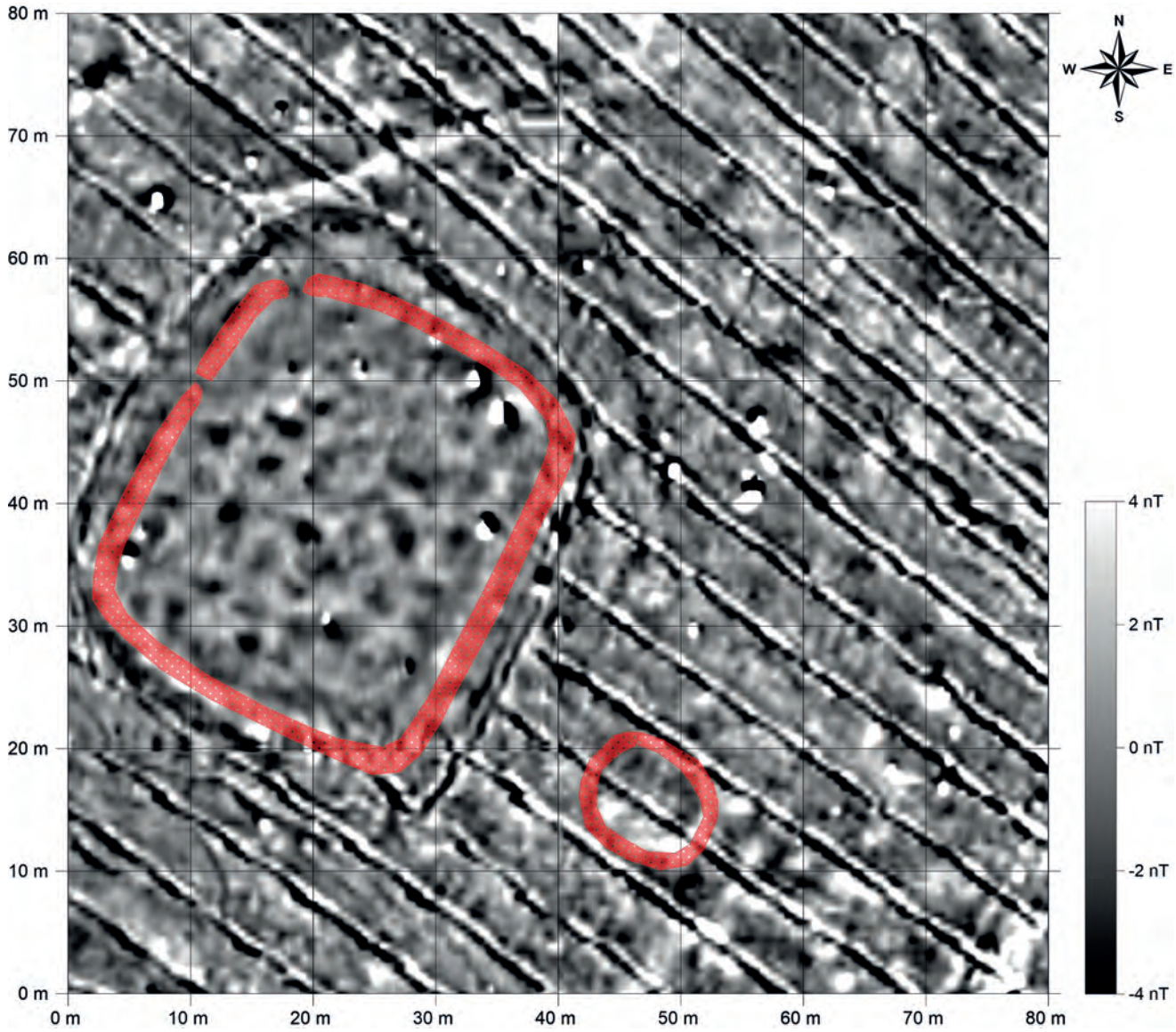

Fig. 10. Karacamirli, Tepe 5. Detail of the magnetogram (like Fig. 5, but with inverted greyscale). The layout of the presumed enclosure is marked in red

Whether burials show up as »positive« (= black) or as »negative« (= white) anomalies, depends on the magnetic susceptibility of the infill and the demagnetized natural remanent magnetization of the adjacent sediments in the burial pit. In the area of the mound, we detect both types; however, both are similarly arranged (see Fig. 9 and Fig. 10). South-east of the mound, we detect another enclosed feature with pits inside. Such features are reminiscent of Iron Age kurgan sites in the Northern Caucasus, the Volga steppe and Kazakhstan (Gass et al. 2019; Парцингер et al. 2018). In addition to this small enclosure, a multitude of other pits of more or less of similar size are discernible to the east of Tepe 5. Nearly all of them show positive anomalies. We therefore suggest that these pits could be further burials and that the whole area represents a large cemetery. Usually, pits of a settlement should come in different sizes, shapes and diameters. Linear features, indicating ground plans of houses or buildings, were not detected, but could be still there and overprinted and masked by the sharp and strong traces of the irrigation canals. Even though we consider the presence of a major cemetery very likely, we cannot entirely exclude the possibility that (at least some of) these traces are simply from a settlement.

The question may arise, why there are burial pits with positive and negative anomalies on the mound, but only positive ones in the periphery. The answer probably lies in the different geological background and composition

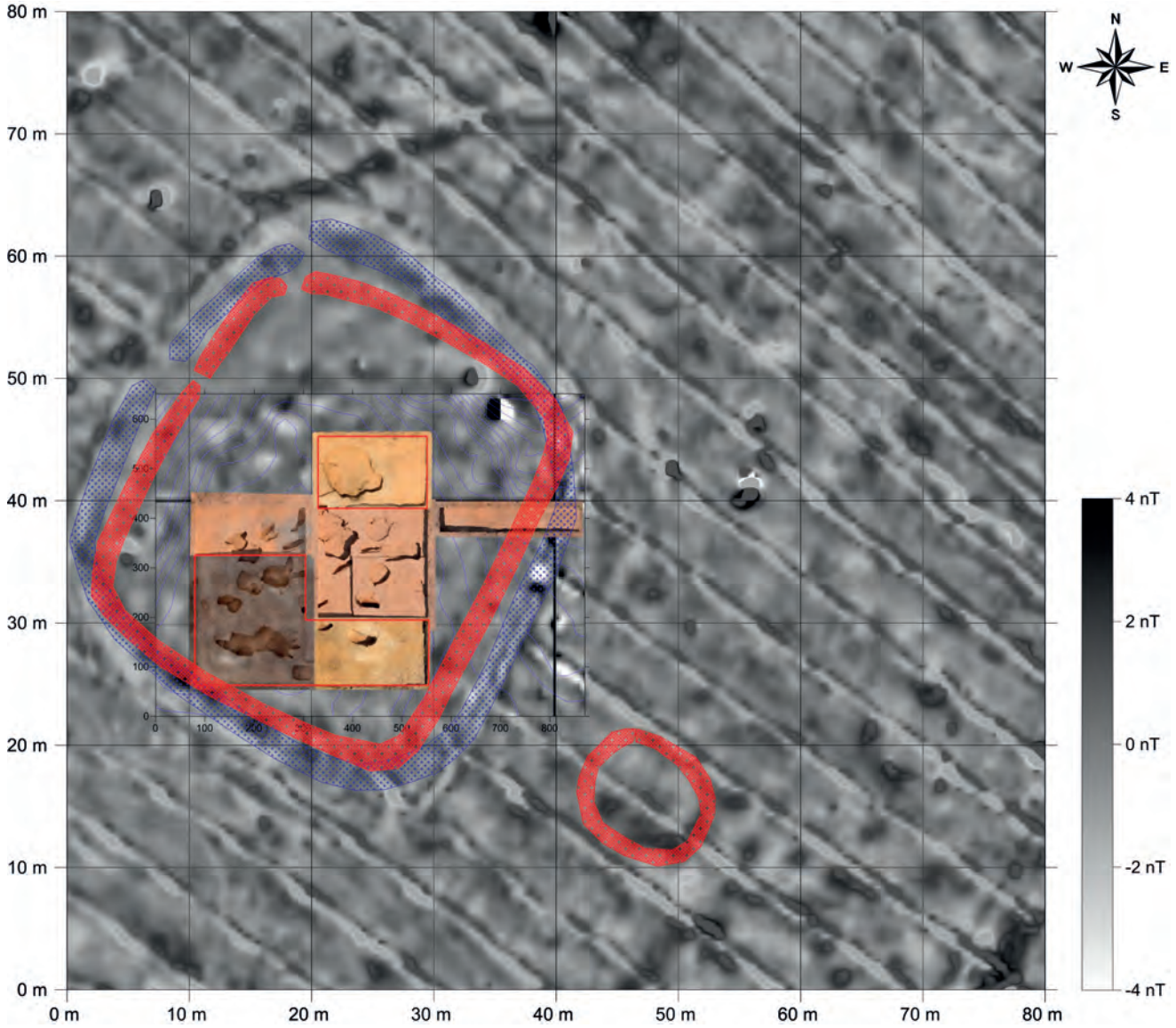

Fig. 11. Karacamirli, Tepe 5. Detail of the magnetogram (30% overlay by inverted high-pass filtered data) overlaid by photogrammetric image of the excavation (© Martin Gruber). The »enclosure« is marked in red; the outer shape of the butte is marked in blue

of the adjacent sediment. All four little hills in the area are geological relics, which survived as butte and were then used as prominent locations for burial. Three of these four buttes are now destroyed by recent farming and erosion and no archaeological record survived.

II.3 Conclusion

Satellite remote sensing, ground survey and magnetometer prospecting confirmed and revealed the existence of an archaeological site at Tepe 5. However, the »laboratory analyses« left room for misinterpretation. In combination with a detailed scientific excavation and mineral-magnetic analysis of sediments and soils, our research combines to produce to a valuable case study for the joint application of archaeological and geophysical fieldwork.

III. The Chalcolithic Pits

Martin Gruber

In the 2016 field campaign two pits of the Chalcolithic period were uncovered in square 6300/7990 (Fig. 22). A notable quantity of Chalcolithic pottery and obsidian flakes in Pit-Complex A indicated a possible third, completely destroyed pit (see ch. IV.6.1). The pits were dug from a now completely eroded occupation level of unknown nature. Apart from the pits, the Chalcolithic occupation on Tepe 5 was further attested by single sherds and obsidian flakes in the topsoil and subsoil layers as well as occasional intrusive sherds in grave-pits.

As none of the relevant contexts contained bones or any other organic material, which could provide samples for radiocarbon dating, the proposed date of the remains relies solely on the morphological characteristics of the recovered pottery. Of particular importance for regional comparisons are the results of the recent excavations at Mentesh Tepe, located in the Tovuz district, c. 36 km west of Tepe 5 (Lyonnet 2014; Lyonnet/Quliyev 2017; Lyonnet et al. 2012: 86–121; 2016). After a Neolithic occupation (Mentesh Period I) and a settlement hiatus, Mentesh Tepe was re-occupied in the Chalcolithic period during the first half of the 5th mill. BC (Mentesh Period II), probably by a mobile population. The subsequent occupation of the second half of the 5th mill. BC (Mentesh Period III) was more substantial and attests to links with Northern Mesopotamia. At the end of the 5th mill. BC the site was again abandoned for the entire duration of the Leilatepe Culture until the 2nd half of the 4th mill. BC – the onset of the Early Bronze Age.

III.1 Pit KG-016/KG-019

Pit KG-016 was discovered in the northern half of square 6300/7990, c. 40 cm below the modern surface (Fig. 13). Its flat bottom was reached at c. 40 cm depth (173.10 m). It had a round outline with a diameter of 1.9 m and its north-western edge was cut by the undated child Burial 42. The majority of sherds was concentrated in the uppermost 25 cm (KG-016-0045), whereas the lowest 15 cm (KG-019-0062) contained much less pottery. Apart from the changing density of finds, the brown clay material of the fill did not differ significantly in both contexts and therefore they can be considered as a single entity.

The pit was filled with a considerable number of sherds (n = 262, of which 71 were diagnostic sherds; see Table 1). Although some of them could be joined to larger vessel parts, none of these was complete, suggesting that the pit primarily contained settlement refuse (Fig. 12). Of particular interest was the large quantity of obsidian flakes (n = 54) scattered throughout the fill (0038–0040,

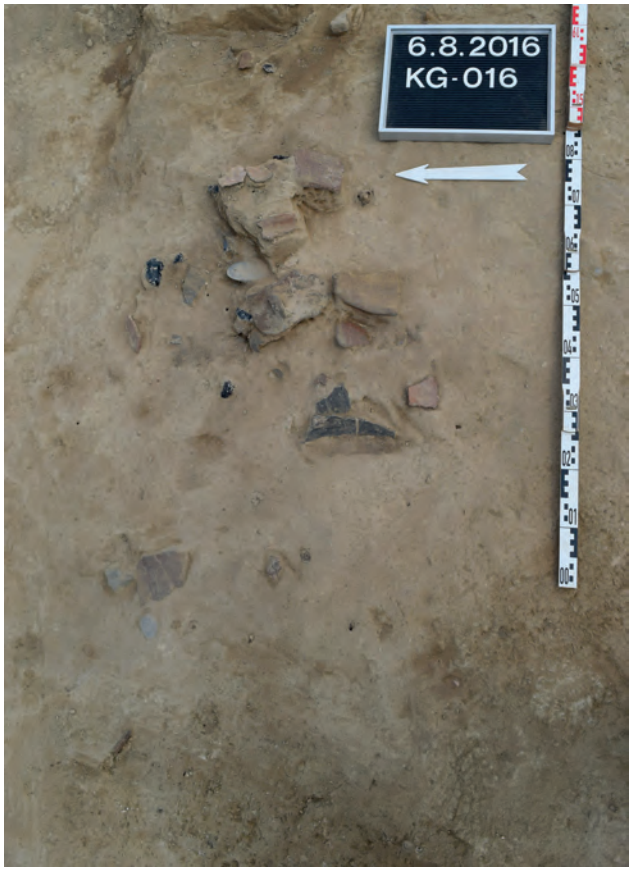

Fig. 12. Detail of the fill of pit KG-016. The transition from light to dark brown soil in the west marks the edge of the pit

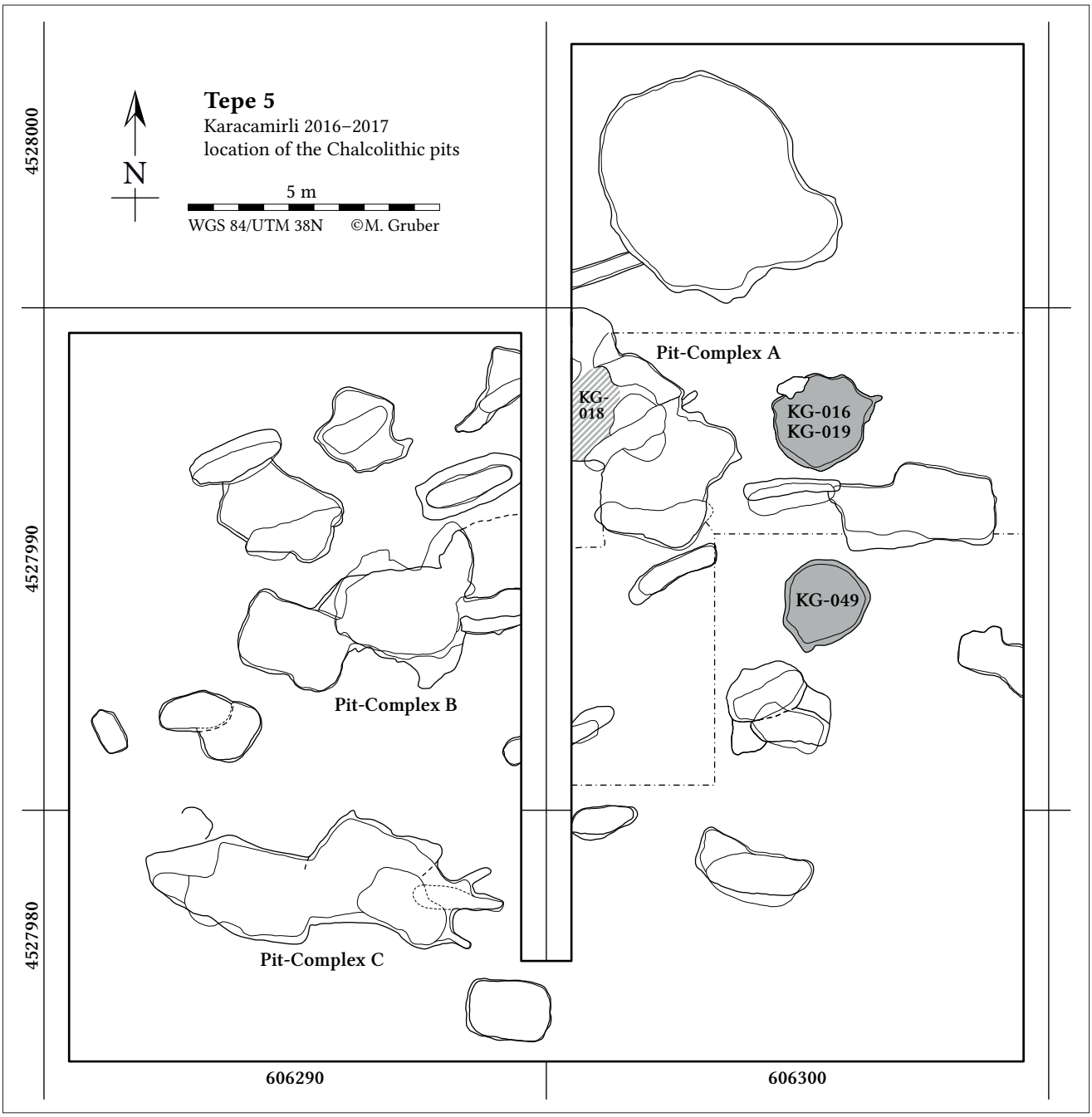

Fig. 13. Location of the Chalcolithic pits on Tepe 5

0042–0044, 0063). Because they were largely unworked and barely revealed any signs of retouching, they are most likely production waste. Nevertheless, the strikingly high proportion of obsidian flakes in this pit (28.1 %) and in the other potentially Chalcolithic contexts (12.5 %; see below) in relation to the total number of obsidian flakes discovered on Tepe 5 suggests that most of them, if not all, are remnants of the Chalcolithic occupation.

The fill was also interspersed with unworked small cobblestones, some of which were split. The only worked example was a flat oval stone that bore several parallel incisions or traces of abrasion at its lateral sides (0046, Fig. 14). Else, only one half of a limestone ring or whorl was found (0038, Fig. 14), 2)

List of finds

KG-016-0038 (half of limestone ring) Fig. 14,2
Diam: 28.0 mm; inner diam.: 10.5 mm; Th.: 10.0–15.0 mm; Wt: 9 g
606304.565 E; 4527997.699 N; 173.428 m

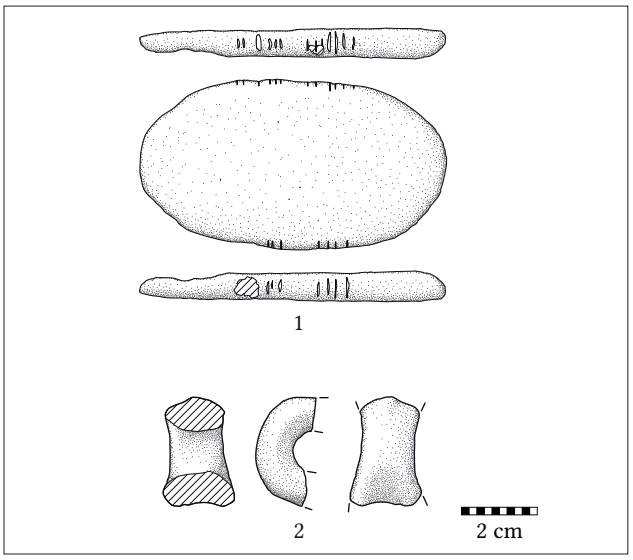

Fig. 14. Finds from pit KG-016: 1 – worked stone (0046); 2 – limestone ring (0038)

KG-016-0046 (flat stone with incised lines) Fig. 14, 1
L: 81.0 mm; W: 45.0 mm; Th: 8.0 mm; Wt: 51 g
606305.400 E; 4527997.656 N; 173.500 m

KG-016-0038 (obsidian flake)
L: 55.0 mm; W: 32.0 mm; Th: 15.0 mm; Wt: 14 g
606305.000 E; 4527997.659 N; 173.490 m

KG-016-0039 (obsidian flake)
L: 41.0 mm; W: 39.0 mm; Th: 13.0 mm; Wt: 6 g
606304.980 E; 4527997.439 N; 173.390 m

KG-016-0040 (obsidian flake)
L: 21.0 mm; W: 20.0 mm; Th: 6.0 mm; Wt: 2 g
606305.262 E; 4527997.351 N; 173.400 m

KG-016-0041 (stone flake)
L: 42.0 mm; W: 19.0 mm; Th: 6.0 mm; Wt: 7 g
606305.262 E; 4527997.351 N; 173.400 m

KG-016-0042 (obsidian flake)
L: 26.0 mm; W: 26.0 mm; Th: 4.0 mm; Wt: 3 g
606305.282 E; 4527997.661 N; 173.510 m

KG-016-0043 (cobblestone)
L: 59.0 mm; W: 56.0 mm; Th: 10.0 mm; Wt: 35 g
606305.262 E; 4527997.351 N; 173.400 m

KG-016-0044 (43 obsidian flakes)

KG-016-0047 (retouched flint)
L: 62.0 mm; W: 26.0 mm; Th: 9.0 mm; Wt: 13 g

KG-019-0063 (collection of 7 obsidian flakes)

III.2 Pit-KG-049

The second pit was located further south in the south-western quadrant of square 6300/7990 (Fig. 22). Its shape, size and depth were very similar to KG-016, but it contained far less sherds (n = 50) and no obsidian flakes or other finds. The attested vessel forms and fabrics (KG-049-0196), are, however, nearly identical with the Chalcolithic material from pit KG-016.

III.3 The Chalcolithic pottery in Pit-Complexes A and B

The existence of a possible third pit was suggested by a considerable amount of Chalcolithic pottery in the fill of Pit-Complex A (Fig. 13 and Fig. 42). Using the longitudinal axis of Burial 28 as dividing line, the northern part of the fill was defined as context KG-018 and the southern part as context KG-022. The highest concentration of scattered sherds was detected immediately south of the grave-pit of Burial 20, near the western baulk at an elevation of c. 173.20 m (KG-018-0049) and in the context below (KG-023-0082). Moreover, the soil east of the sherds was intermixed with fine ashy material. As the area between Burials 7 and 20 contained no interment, these sherds mark the most likely location of a Chalcolithic feature – probably another rubbish pit, that was destroyed by the adjacent grave-pits. Due to repeated interments of the Late Bronze/Early Iron Age and the Medieval Period in Pit-Complex A, the pottery sherds were scattered all over its fill and ended up also in the southern part (KG-022-0073) and even in Burials 5 (KG-038-0141-01) and 7 (KG-026, see Fig. 82, 4–5). It seems that along with the sherds a significant number of obsidian flakes was spread throughout the fill. This might explain the large amount of obsidian in the fill of Pit-Complex A: If all pieces from the contexts KG-018, KG-022 and KG-023 are added up, they account for 12.5 % of all obsidian flakes on Tepe 5 (Fig. 46). A further pit might have existed at the north-eastern end of Pit-Complex B (KG-056), as some sherds and a high density of obsidian flakes suggest, but the mixed nature of this area remains difficult to assess.

List of finds

KG-018-0051 (obsidian flake)
L: 41.0 mm; W: 28.0 mm; Th: 12.0 mm; Wt: 16 g
606301.426 E; 4527997.990 N; 173.460 m

KG-018-0053 (obsidian flake)
L: 34.0 mm; W: 19.0 mm; Th: 7.0 mm; Wt: 4 g
606301.185 E; 4527998.790 N; 173.263 m

KG-018-0057 (obsidian flake)
L: 19.0 mm; W: 16.0 mm; Th: 9.0 mm; Wt: 1 g
606302.113 E; 4527998.659 N; 173.214 m

KG-018-0060 (2 obsidian flakes)
L: 43.0 mm; W: 27.0 mm; Th: 8.0 mm; Wt: 8 g
606300.712 E; 4527998.226 N; 173.166 m

KG-018-0056 (obsidian flake)
L: 40.0 mm; W: 27.0 mm; Th: 9.0 mm; Wt: 5 g
606300.769 E; 4527997.774 N; 173.229 m

KG-022-0069 (obsidian flake)
L: 12.0 mm; W: 11.0 mm; Th: 4.0 mm; Wt: 1 g

KG-022-0071 (obsidian flake)
L: 26.0 mm; W: 19.0 mm; Th: 5.0 mm; Wt: 3 g
606302.092 E; 4527997.523 N; 173.368 m

KG-022-0075 (obsidian flake)
L: 38.0 mm; W: 34.0 mm; Th: 12.0 mm; Wt: 16 g
606302.846 E; 4527997.697 N; 173.268 m

KG-022-0076 (obsidian flake)
L: 14.0 mm; W: 10.0 mm; Th: 8.0 mm; Wt: 1 g
606302.092 E; 4527996.060 N; 173.197 m

KG-022-0077 (obsidian flake)
L: 20.0 mm; W: 17.0 mm; Th: 6.0 mm; Wt: 2 g
606301.362 E; 4527996.640 N; 173.143 m

KG-022-0079 (obsidian flake)
L: 32.0 mm; W: 35.0 mm; Th: 9.0 mm; Wt: 5 g
606302.968 E; 4527997.638 N; 173.101 m

KG-022-0080 (obsidian flake)
L: 23.0 mm; W: 18.0 mm; Th: 9.0 mm; Wt: 3 g
606302.715 E; 4527996.741 N; 173.051 m

KG-023-0084 (obsidian flake)
L: 20.0 mm; W: 13.0 mm; Th: 7.0 mm; Wt: 1 g
606302.790 E; 4527996.550 N; 173.080 m

KG-023-0088 (obsidian flake)
L: 29.0 mm; W: 16.0 mm; Th: 8.0 mm; Wt: 2 g
606302.399 E; 4527996.976 N; 172.999 m

KG-023-0092 (obsidian flake)
L: 28.0 mm; W: 21.0 mm; Th: 5.0 mm; Wt: 2 g

KG-023-0093 (obsidian flake)
L: 24.0 mm; W: 23.0 mm; Th: 6.0 mm; Wt: 4 g
606301.094 E; 4527997.699 N; 173.056 m

KG-023-0094 (obsidian flake)
L: 31.0 mm; W: 20.0 mm; Th: 8.0 mm; Wt: 5 g
606300.859 E; 4527997.779 N; 173.088 m

KG-023-0095 (obsidian flake)
L: 74.0 mm; W: 48.0 mm; Th: 19.0 mm; Wt: 47 g
606301.262 E; 4527998.092 N; 173.090 m

KG-023-0096 (obsidian flake)
L: 43.0 mm; W: 42.0 mm; Th: 10.0 mm; Wt: 16 g
606301.267 E; 4527998.511 N; 173.114 m

KG-023-0097 (obsidian flake)
L: 47.0 mm; W: 38.0 mm; Th: 10.0 mm; Wt: 15 g
606301.487 E; 4527998.779 N; 172.989 m

KG-023-0098 (obsidian flake)
L: 35.0 mm; W: 14.0 mm; Th: 9.0 mm; Wt: 3 g
606302.140 E; 4527998.741 N; 173.033 m

KG-023-0099 (obsidian flake)
L: 33.0 mm; W: 20.0 mm; Th: 10.0 mm; Wt: 6 g
606302.579 E; 4527997.967 N; 172.957 m

KG-023-0107 (obsidian flake)
L: 16.0 mm; W: 10.0 mm; Th: 2.0 mm; Wt: 1 g
606302.383 E; 4527996.948 N; 172.941 m

KG-056-0229-01 (rim)
Rim diam.: 200 mm (3 %)
Fabric: completely oxidizing atmosphere, soft, coarse temper (214)
Surface: ext. and int. smoothed
Colour: ext. 15YR 6/6 (reddish yellow); core 15YR 6/6 (reddish yellow); int. 5YR 8/4 (pink)
Decoration: below the rim round impressions on the inside

KG-056-0229-01 (rim)
Rim diam.: 200 mm (3 %)
Fabric: completely oxidizing atmosphere, soft, coarse temper (214)
Surface: ext. and int. smoothed
Colour: ext. 15YR 6/6 (reddish yellow); core 15YR 6/6 (reddish yellow); int. 5YR 8/4 (pink)
Decoration: below the rim round impressions on the inside

KG-056-0229-05 (rim)
Rim diam.: 200 mm (8 %)
Fabric: ext. oxidizing, int. reducing atmosphere, hard, medium fine temper (333)
Surface: ext. and int. smoothed
Colour: ext. 7.5YR 5/4 (brown); core 2.5Y 4/1 (dark grey); int. 2.5Y 5/1 (grey)

KG-056-0229-06 (rim)
Rim diam.: 190 mm (12 %)
Fabric: irregular firing atmosphere, hard, medium fine temper (733)
Surface: ext. burnished; int. smoothed
Colour: ext. 5YR 5/6 (yellowish red); core Gley 1 3/N (very dark grey); int. 5YR 6/6 (reddish yellow)

KG-056-0229-07 (base)
Base diam.: 90 mm (35 %)
Fabric: not fully oxidized core, hard, medium fine temper (533)
Surface: ext. burnished, int. smoothed
Colour: ext. 7.5YR 6/6 (reddish yellow); core Gley 1 2.5/N (black); int. 7.5YR 6/4 (light brown)

Selected Chalcolithic sherds from topsoil and subsoil layers

KG-054-0220-07 (rim)
Rim diam.: 140 mm (25 %)
Fabric: completely oxidizing atmosphere, soft, coarse temper (214)
Surface: ext. and int. smoothed
Colour: ext. 5YR 5/6 (yellowish red); core 5YR 5/6 (yellowish red); int. 5YR 5/6 (yellowish red)
Decoration: on the inside below the rim a row of round impressions

KG-033-0127-01 (rim)
Rim diam.: 200 mm (3 %)
Fabric: completely oxidizing atmosphere, medium hard, medium fine temper (223)
Surface: ext. smoothed; int. smoothed and slipped
Colour: ext. 52.5YR 6/6 (light red); core 2.5YR 5/3 (reddish brown); int. 10YR 8/3 (very pale brown)

KG-033-0127-02 (rim)
Rim diam.: 200 mm (3 %)
Fabric: completely oxidizing atmosphere, medium hard, medium fine temper (223)
Surface: ext. smoothed/slipped; int. smoothed/slipped

vessel type	KG-016 KG-019	KG-018	KG-022	KG-023	KG-049
jar	17	3			
bowl	9	1	1	2	
mangal	13	4	1		1
flat base	19	6		2	2
round base	3			1	
other (n. d.)	9	1			2
total	70	15	2	5	5

Table 1. Types of vessels attested in each of the Chalcolithic contexts

Colour: ext. 10YR 8/3 (very pale brown); core 2.5YR 6/4 (light reddish brown); int. 10YR 8/3 (very pale brown)

KG-033-0127-03 (base)
Base diam.: 70 mm (25 %)
Fabric: not fully oxidized core, medium hard, medium fine temper (523)
Surface: ext. and int. smoothed/slipped
Colour: ext. n. d.; core 10YR 4/1 (dark grey); int. 10YR 8/3 (very pale brown)

KG-033-0127-04 (rim)
Rim diam.: 140 mm (8 %)
Fabric: not fully oxidized core, hard, medium fine temper (533)
Surface: ext. and int. smoothed
Colour: ext. 7.5YR 4/3 (brown); core Gley 1 4/N (dark grey); int. 7.5YR 4/3 (brown)
Decoration: some irregular scratches on the surface

KG-033-0127-05 (rim)
Rim diam.: n. d.
Fabric: completely oxidizing atmosphere, medium hard, very fine temper (221)
Surface: ext. smoothed/slipped; int. smoothed/slipped
Colour: ext. and int. darkened by secondary fire; core 5YR 4/6 (yellowish red)

KG-033-0127-06 (base)
Base diam.: 60 mm (20 %)
Fabric: not fully oxidized core, medium hard, medium fine temper (523)
Surface: ext. and int. smoothed
Colour: ext. n. d.; core 5YR 3/1 (very dark grey), int. 5YR 6/4 (light reddish brown)

III.4 Dating

The reassessment of old excavations and various new projects conducted in the last decades contributed significantly to a better understanding of the Chalcolithic Period in the Southern Caucasus, which lasted from c. 5000/4800 to c. 3500 BC. A tentative internal periodization has been proposed, that defines an Early Chalcolithic (c. 5000–4000 BC) – possibly further divisible into an Early (c. 5000–4500 BC) and Middle (c. 4500–4000 BC) Chalcolithic period (Lyonnet et al. 2012: 87) – and a Late Chalcolithic period (c. 4000–3500 BC). The latter in Azerbaijan mainly corresponds to the Leilatepe Culture (Müseyibli 2014a; 2014b 2015; 2016).

According to the current state of research, recently summarized by A. Sagona (2018: 182–212), the pottery assemblages of the Chalcolithic period can be divided into two different, but closely related, chronologically and geographically overlapping horizons: Chaff-Faced Ware and Sioni Ware.

Chaff-Faced Ware in the Southern Caucasus forms part of the wider distribution range of chaff-tempered wares that included Eastern Anatolia and the northern regions of Syria, Mesopotamia and Iran. It is above all the technical properties, in particular the eponymous abundant use of chaff temper, that form a connecting element across the different regional pottery assemblages (Sagona 2014: 29–30; 2018: 184–189). It has been argued that Chaff-Faced Ware was an intrusive pottery tradition and reached the Southern Caucasus as a result of the increasing contacts between these regions. However, this assumption has recently been challenged in favour of a possible local genesis and direct development from the Neolithic (Marro 2010; 2012).

Sioni Ware or the ›Sioni Cultural Complex‹ is still somewhat elusive, but it appears to have been a local tradition, geographically confined to the Southern Caucasus (Sagona 2018: 134 Fig. 4.1; Lyonnet 2018: 563). Mineral and obsidian temper predominate. The fabric is usually of a pale brown, red or yellow colour (Sagona 2014: 30; 2018: 207–208). The repertoire of shapes seems to be restricted to a few types – the most prominent hallmark being ovoid-necked jars with incised or impressed decoration on the rim (Менабде/Кигурадзе 1981: 13–14 Fig. 2–3). At Mentesh Tepe they first appeared in Period III and were considered kitchen ware, as they were frequently blackened and bore traces of soot (Lyonnet 2018: 558–560). Some were chaff tempered, but most of them had obsidian temper, which might be related to their proposed use as cooking containers (Palumbi 2015).[7] The surface was often combed. Besides ovoid-necked jars, mangals and pans were the most typical forms among the kitchen ware assemblage at Mentesh Tepe (Lyonnet et al. 2012: 101; Lyonnet 2017: 145–147; 2018). Both types were attested throughout Periods II and III – though with

7 The sole attestation of obsidian temper at Tepe 5 was a body sherd found loose in a topsoil context (KG-054-0220-14).

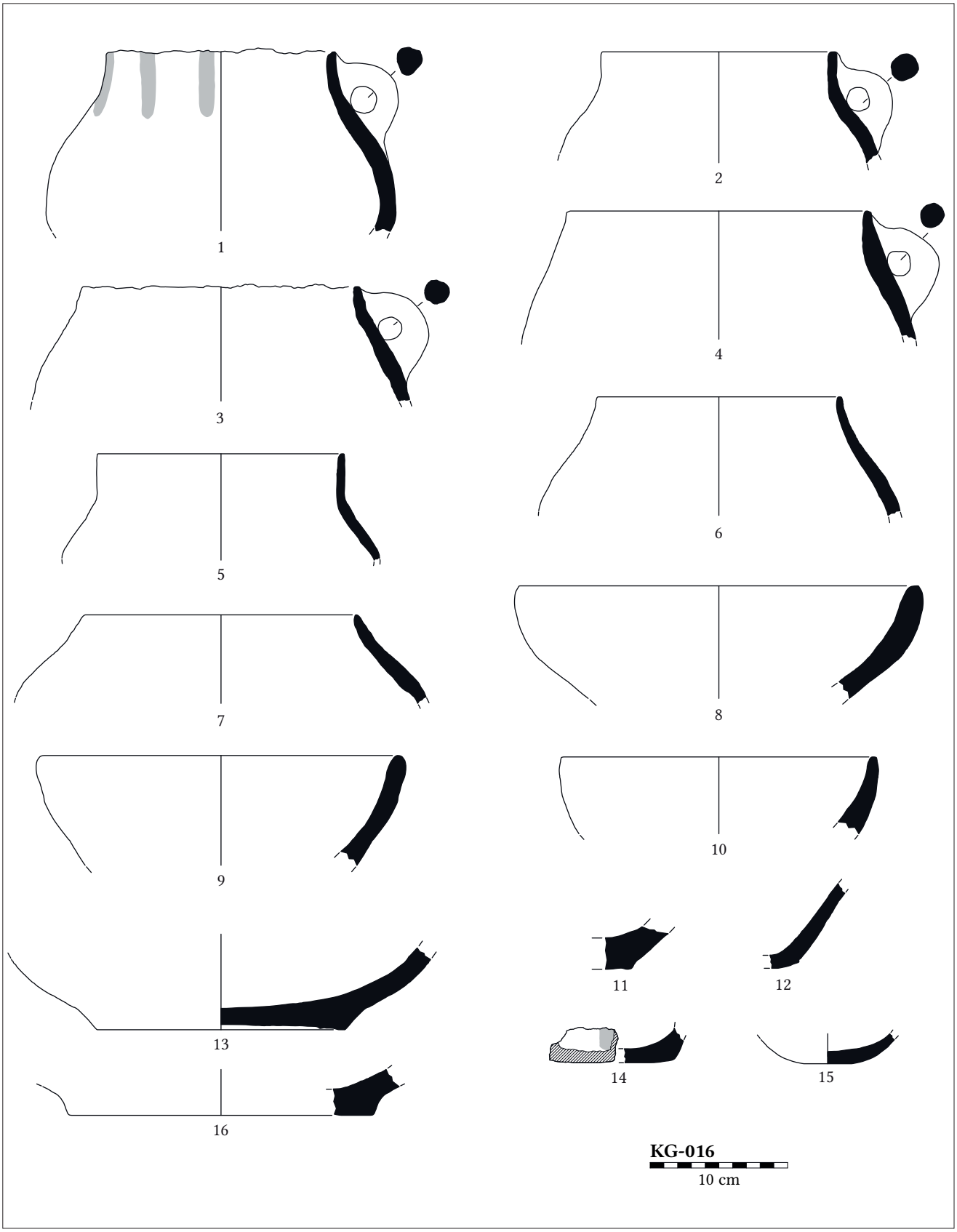

Fig. 15. Selected pottery from pit KG-016: 1 – handled jar (0045-01); 2 – handled jar (0045-06); 3 – handled jar (0045-05); 4 – handled jar (0045-04); 5 – jar (0045-10); 6 – jar (0045-03); 7 – jar (0045-11); 8 – bowl (0045-41); 9 – bowl (0045-42); 10 – bowl (0045-35); 11 – base (0045-59); 12 – base (0045-60); 13 – base (0045-49); 14 – base (0045-50); 15 – base (0045-64); 16 – base (0045-47)

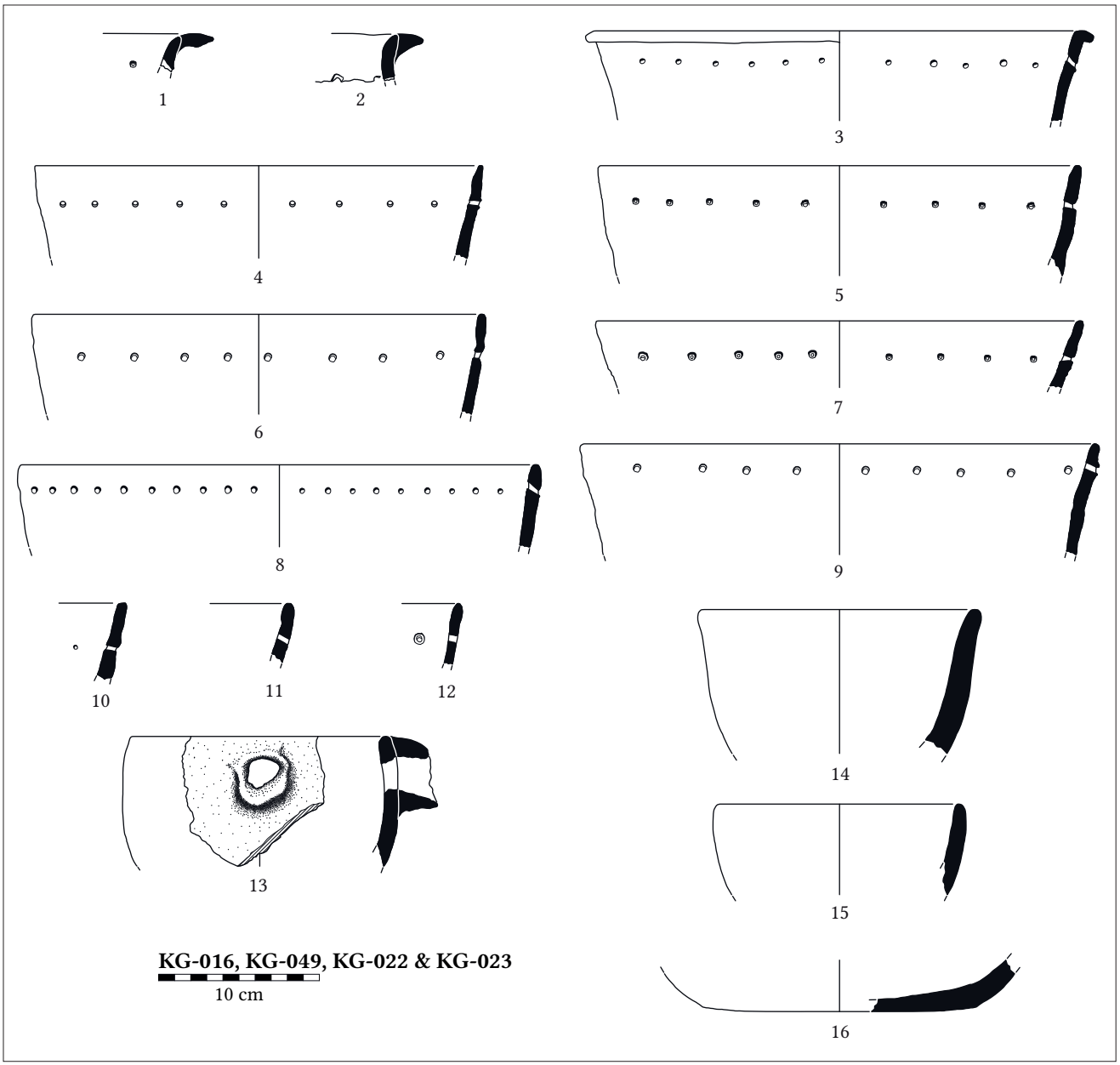

Fig. 16. Selected pottery from Chalcolithic contexts (KG-016-0045, KG-049-0196, KG-022-0073 and KG-023–0082): 1 – mangal (0045-15); 2 – mangal (0045-16); 3 – mangal (0049-08); 4 – mangal (0196-04); 5 – mangal (0045-17); 6 – mangal (0045-19); 7 – mangal (0045-18); 8 – mangal (0049-04); 9 – mangal (0073-01); 10 – mangal (0045-22); 11 – mangal (0045-25); 12 – mangal (0045-20); 13 – spouted vessel (0196-01); 14 – bowl (0073-02); 15 – bowl (0082-05); 16 – base (0082-03)

various changes – and mangals continued to be used in the Leilatepe Culture (Müseyibli 2007: Pl. 18, 9).

In terms of its technological and morphological features the pottery from the Chalcolithic contexts at Tepe 5 was very homogeneous and is therefore treated here as a unit. The formal repertoire was limited to jars, bowls/beakers and mangals and a couple of unique pieces (Table 1), of which the spouted vessel from pit KG-049 is the most noteworthy (Fig. 16, 13).

Jars were particularly well attested in pit KG-016 (Table 1). All of them were hand-made. As indicated by the linear pattern of the cracks and by their visual appearance, they were certainly built by using the slab technique (Fig. 17, 1–2 and Fig. 20). The fabric was of light red to reddish-brown colour, suggesting an oxidizing firing atmosphere, while darker, reddish-grey spots imply irregular firing conditions. In most cases the firing was insufficient to burn out all the carbon, resulting in a light pale to dark grey coloured core. The clay matrix was predominantly tempered with medium fine to coarse mineral particles and to a small extent with vegetal temper. The surface was smoothed and revealed trac-

Fig. 17. Selected pottery from pit KG-016: 1 – handled jar (0045-01); 2 – handled jar (0045-05)

es of burnishing, but no combed decoration. Although sometimes substantial parts of the body and rim were preserved, none of the jars was preserved well enough to determine the shape of the lower body and base. Judging by some of the profiles, however, their body was either of globular or ovoid shape. Although the considerable number of flat bases found along with the jars (Table 1) might argue against round bases, the high fragmentation and the general difficulty to distinguish round bases from body sherds certainly qualifies this assumption. Moreover, considering the fabric and surface treatment, some of the base sherds likely belonged to mangals or bowls. Similar to Mentesh Tepe none of the bases bore mat impressions, as they were frequently attested at sites attributed to the Sioni Cultural Complex in the Alazani valley (Варазашвили 1992: Pl. 25, 14–18. 27, 1–6. 28, 4–7; see however Lyonnet 2018: 562 for the potential earlier date of these examples).

Some of the jars were hole-mouthed (Fig. 15, 7), while others either had a slightly sinuous rim profile (Fig. 15, 1) or a pronounced shoulder with an upright neck (Fig. 15, 2. 5). Although they were predominantly tempered with minerals, and in particular the jars with upright neck are comparable to ovoid-necked jars of the Sioni Ware, e. g., from Sioni (Kiguradze/Sagona 2003: 51 Fig. 3.6, 1) or Mentesh Tepe (Lyonnet et al. 2012: 104 Fig. 148, 4. 6), they lack the typical incised or impressed decoration on the rim as well as the combed surface decoration. Moreover, in contrast to the ovoid-necked jars from Mentesh Tepe, the examples from Tepe 5 were presuma-

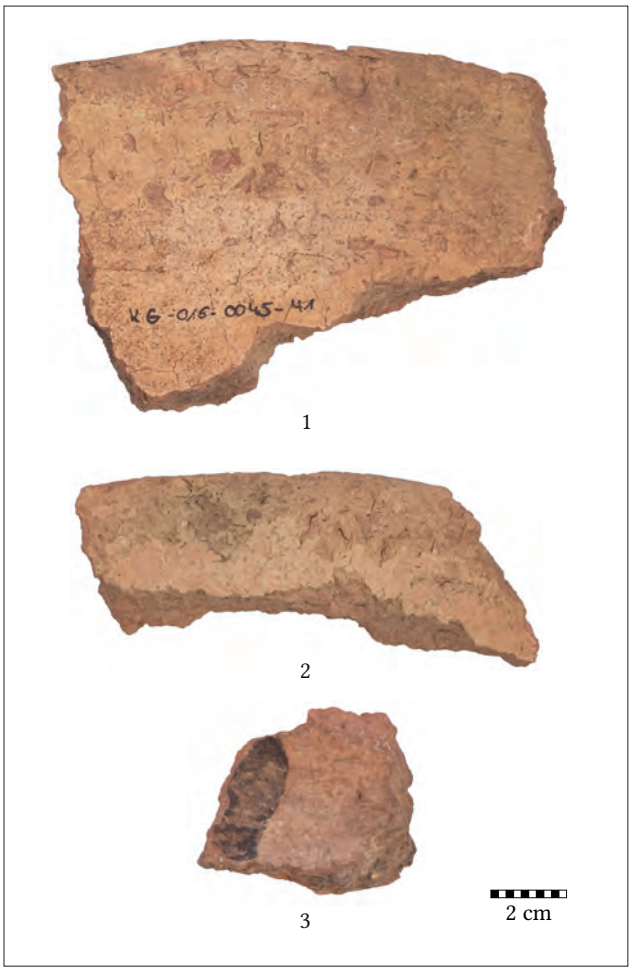

Fig. 18. Selected pottery from pit KG-016: 1 – bowl (0045-41); 2 – bowl (0045-43); 3 – bowl (0045-50)

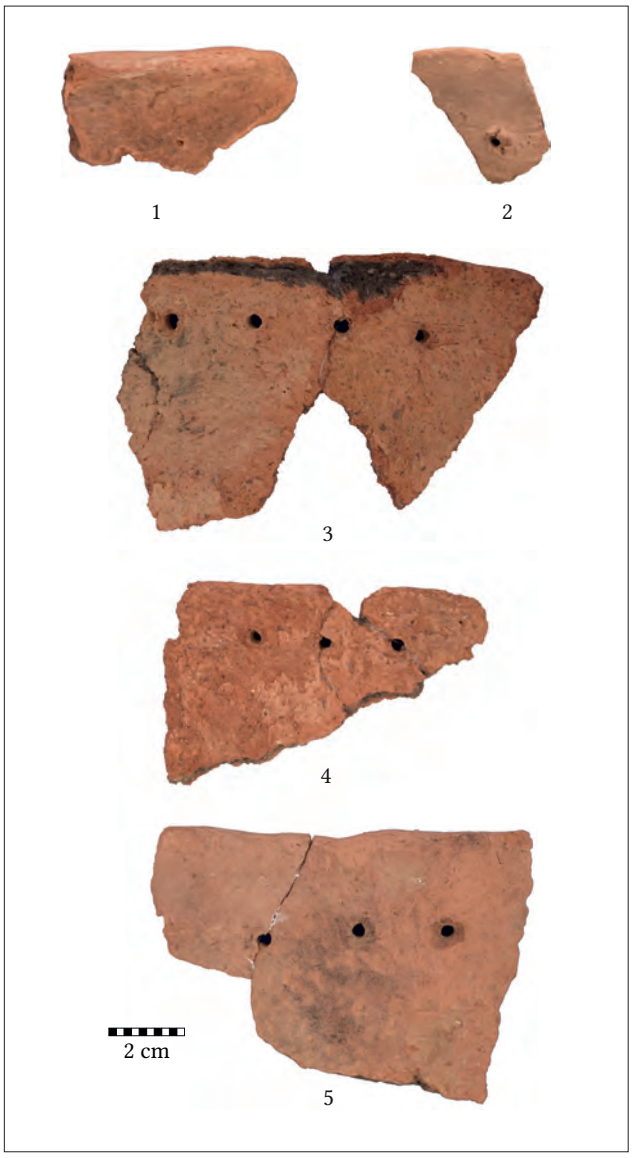

Fig. 19. Selected pottery from contexts KG-016 and KG-018: 1 – mangal (0045-16); 2 – mangal (0045-28); 3 – mangal (0049-08); 4 – mangal (0049-04); 5 – mangal (0045-17)

Fig. 20. Cross-section of a sherd (0045-01) revealing the impressions of two jointed slabs

bly not used for cooking, since they showed no traces of blackening or soot. Against this background and despite the mineral temper it may be more plausible to associate these jars with morphologically similar jars of the Mentesh III common ware (e. g. Lyonnet et al. 2012: 100 Fig. 144, 4–5 and possibly Lyonnet 2017: Fig. 14 top and 15 bottom). Vertical bands painted with bitumen(?) from the rim down to the shoulder of jar 0045-01 (Fig. 15, 1 and Fig. 17, 1) further substantiate this assumption, as similar painted decorations appeared on various vessels of the Mentesh III common ware (Lyonnet et al. 2012: Fig. 143, 1. 144, 4).

What remains peculiar, are the loop handles applied below the rim of at least eight jars from Tepe 5. Unfortunately, the state of preservation prevented us from determining whether they were single-handled or double-handled and whether handles represent an integral or occasional component of this vessel type. Although handles are occasionally attested, e. g., at Damtsvari Gora in the Alazani valley (Варазашвили 1992: Pl. XIII), on various vessels at Ovchular Tepesi (Marro et al. 2009: 52 Pl. 11. 13, 1; 2011: 56 Pl. I; Gülçur/Marro 2012: 320 Fig. 11, 5. 12, 7) and at least once at Mentesh Tepe Period II (Lyonnet 2017: 145 Fig. 11), they are not a common feature of Chalcolithic pottery and only become more frequent

after the mid-4th mill. BC, during the onset of the Early Bronze Age. The overall technological and morphological characteristics of the jars, however, make such a late date unlikely, because they do neither comply with the distinctive traits of the Late Chalcolithic Leilatepe Culture pottery, which produced different jars mostly with a pronounced shoulder and an everted neck described as wheel-thrown (Müseyibli 2007: 69; 2015: 58), nor with Early Bronze Age material.

Fragments of bowls and beakers were found in each of the Chalcolithic contexts (Table 1). They were thick-walled and of hemispherical shape (Fig. 15, 8–10 and Fig. 16, 14–15). No complete profiles were preserved, but their fabric and surface treatment corresponded with some of the thick, flat bases (e. g. Fig. 15, 11. 13. 16). The clay was tempered with chaff that was superficially burnt out, as is typical for the Chaff-Faced Ware. There was some medium fine mineral temper present, as well. The paste was of light reddish-brown colour, and the cores were not fully oxidized and coloured dark-grey. The interior and in some instances also the exterior surfaces were covered with a buff slip (Fig. 18, 1–2). Comparisons can be drawn with »table ware« bowls of Mentesh III, most of which were painted with bitumen designs of chevrons and dots (Lyonnet et al. 2012: 101 Fig. 146; 2017: 147 Fig. 13). Traces of bitumen painting were attested only on a single fragment of what appears to be the bottom of a bowl (Fig. 15, 14 and Fig. 18, 3).

Mangals are easily identifiable by their thin, almost vertical profile and a row of perforations below the rim (Fig. 16, 1–12 and Fig. 19). Their fabric was tempered with a mixture of chaff and medium fine minerals (no obsidian), though the amount of chaff can vary considerably. The core was regularly of a very dark grey colour. In most cases the surface was simply smoothed, but a few fragments showed traces of a scratched or combed surface (Fig. 19, 2). No complete vessels were preserved. Two or possibly three mangals had a horizontal, semi-circular lug applied to the rim (Fig. 16, 1–3 and Fig. 19, 1. 3). According to the typological development observed at Mentesh Tepe, such horizontal lugs are more typical for Period II, whereas in Period III lugs were either applied vertically or completely absent (Lyonnet et al. 2012: 98. 101 Fig. 142. 149; Lyonnet 2018: 554. 560 Fig. 7. 11).

Selected pottery from Chalcolithic contexts

KG-016-0045-01 (handled jar) Fig. 15, 1; Fig. 17, 1
Rim diam.: 165 mm (50 %)
Fabric: not fully oxidized core, soft, medium fine temper (513)
Surface: ext. and int. smoothed (sparely burnished exterior)
Colour: ext. 10R 6/6 (light red); core 10R 6/3 (pale red); int. 10R 6/6 (light red)
Decoration: painted vertical bands from the rim down to the shoulder

KG-016-0045-03 (jar) Fig. 15, 6
Rim diam.: ~160 mm (5 %)
Fabric: fully oxidized, soft, coarse temper (214)
Surface: ext. and int. smoothed
Colour: ext. 2.5YR 6/8 (light red); core 10R 6/3 (pale red); int. 2.5YR 6/8 (light red)

KG-016-0045-04 (handled jar) Fig. 15, 4
Rim diam.: 110 mm (10 %)
Fabric: oxidizing atmosphere, soft, medium fine temper (213)
Surface: ext. and int. smoothed (sparely burnished exterior)
Colour: ext. 5YR 6/6 (reddish yellow); core 2.5YR 5/6 (red); int. 2.5YR 6/6 (light red)

KG-016-0045-05 (handled jar) Fig. 15, 3; Fig. 17, 2
Rim diam.: 200 mm (37 %)
Fabric: exterior oxidized, interior not fully oxidized, soft, coarse temper (514)
Surface: ext. and int. smoothed (sparely burnished exterior)
Colour: ext. 5YR 4/2 (dark reddish grey); core 5YR 5/4 (reddish brown); int. 5YR 4/1 (dark grey)

KG-016-0045-06 (handled jar) Fig. 15, 2
Rim diam.: 140 mm (25 %)
Fabric: not fully oxidized core, soft, coarse temper (514)
Surface: ext. and int. smoothed (sparely burnished exterior)
Colour: ext. 5YR 6/4 (light reddish brown); core 5YR 4/1 (dark grey); int. 5YR 5/4 (reddish brown)

KG-016-0049-08 (mangal) Fig. 16, 3; Fig. 19, 3
Rim diam.: 305 mm (10 %)
Fabric: not fully oxidized core, medium hard, medium fine temper (523)
Surface: ext. and int. smoothed
Colour: ext. 5YR 6/4 (reddish brown); core 5YR 3/1 (very dark grey); int. 5YR 6/4 (light reddish brown)

KG-016-0045-10 (jar) Fig. 15, 5
Rim diam.: ~180 mm (5 %)
Fabric: not fully oxidized core, medium hard, coarse temper (524)
Surface: ext. and int. smoothed
Colour: ext. 2.5YR 6/6 (light red); core 2.5YR 3/1 (dark reddish grey); int. 2.5YR 5/3 (reddish brown)

KG-016-0045-11 (jar) Fig. 15, 7
Rim diam.: 180 mm (12 %)
Fabric: not fully oxidized core, medium hard, coarse temper (524)
Surface: ext. and int. smoothed
Colour: ext. 5YR 5/6 (yellowish red); core 5YR 3/1 (very dark grey); int. 5YR 5/6 (yellowish red)

KG-016-0045-15 (mangal) Fig. 16, 1
Rim diam.: n. d.
Fabric: not fully oxidized core, medium hard, medium fine temper (523)

Surface: ext. and int. smoothed
Colour: ext. 7.5YR 5/4 (brown); core 7.5YR 5/3 (brown); int. 2.5YR 6/4 (light reddish brown)

KG-016-0045-16 (mangal) Fig. 16, 2; Fig. 19, 1
Rim diam.: n. d.
Fabric: not fully oxidized core, soft, coarse temper (514)
Surface: ext. and int. smoothed
Colour: ext. 5YR 7/4 (pink); core 5YR 4/2 (dark reddish grey); int. 5YR 6/4 (light reddish brown)

KG-016-0045-17 (mangal) Fig. 16, 5; Fig. 19, 5
Rim diam.: 220 mm (15 %)
Fabric: not fully oxidized core, medium hard, medium fine temper (523)
Surface: ext. and int. smoothed
Colour: ext. 5YR 5/4 (reddish brown); core 5YR 3/1 (very dark grey); int. 5YR 6/4 (light reddish brown)

KG-016-0045-18 (mangal) Fig. 16, 7
Rim diam.: 300 mm (12 %)
Fabric: not fully oxidized core, medium hard, medium fine temper (523)
Surface: ext. and int. smoothed
Colour: ext. 5YR 5/4 (reddish brown); core 5YR 3/1 (very dark grey); int. 5YR 6/4 (light reddish brown)

KG-016-0045-19 (mangal) Fig. 16, 6
Rim diam.: 280 mm (15 %)
Fabric: not fully oxidized core, medium hard, medium fine temper (523)
Surface: ext. and int. smoothed
Colour: ext. 5YR 5/4 (reddish brown); core 5YR 3/1 (very dark grey); int. 5YR 6/4 (light reddish brown)

KG-016-0045-20 (mangal) Fig. 16, 12
Rim diam.: n. d.
Fabric: not fully oxidized core, medium hard, medium fine temper (523)
Surface: ext. and int. smoothed
Colour: ext. 5YR 5/4 (reddish brown); core 5YR 3/1 (very dark grey); int. 5YR 6/4 (light reddish brown)

KG-016-0045-22 (mangal) Fig. 16, 10
Rim diam.: n. d.
Fabric: not fully oxidized core, medium hard, medium fine temper (523)
Surface: ext. and int. smoothed
Colour: ext. 5YR 5/4 (reddish brown); core 5YR 3/1 (very dark grey); int. 5YR 6/4 (light reddish brown)

KG-016-0045-25 (mangal) Fig. 16, 11
Rim diam.: n. d.
Fabric: not fully oxidized core, medium hard, medium fine temper (523)
Surface: ext. and int. smoothed
Colour: ext. 5YR 5/4 (reddish brown); core 5YR 3/1 (very dark grey); int. 5YR 6/4 (light reddish brown)

KG-016-0045-35 (bowl) Fig. 15, 10
Rim diam.: 230 mm (10 %)
Fabric: fully oxidized, medium hard, medium fine temper (223)
Surface: ext. and int. smoothed, interior with buff slip (7.5YR 6/8)
Colour: ext. 10YR 6/3 (pale brown); core 10YR 6/3 (pale brown); int. 10YR 6/2 (light brownish grey)

KG-016-0045-41 (bowl) Fig. 15, 8; Fig. 18, 1
Rim diam.: 290 mm (13 %)
Fabric: not fully oxidized core, medium hard, medium fine temper (523)
Surface: ext. and int. smoothed, buff slip
Colour: ext. 2.5YR 7/4 (light reddish brown); core 2.5YR 7/4 (light reddish brown); int. 5YR 6/4 (light reddish brown)

KG-016-0045-42 (bowl) Fig. 15, 9
Rim diam.: 260 mm (7 %)
Fabric: not fully oxidized core, medium hard, medium fine temper (523)
Surface: ext. and int. smoothed, buff slip
Colour: ext. 2.5YR 7/4 (light reddish brown); core 10YR 4/1 (dark grey); int. 5YR 6/4 (light reddish brown)

KG-016-0045-47 (base) Fig. 15, 16
Base diam.: 220 mm (11 %)
Fabric: not fully oxidized core, medium hard, medium fine temper (523)
Surface: ext. and int. smoothed, interior with buff slip
Colour: ext. 5YR 6/6 (reddish yellow); core 10YR 4/1 (dark grey); int. 2.5YR 6/4 (light reddish brown)

KG-016-0045-49 (base) Fig. 15, 13
Base diam.: 180 mm (27 %)
Fabric: fully oxidized, medium hard, coarse temper (224)
Surface: ext. and int. smoothed, interior with buff slip
Colour: ext. 10R 7/4 (very pale brown); core 10YR 5/6 (yellowish brown); int. 2.5YR 6/8 (light red)

KG-016-0045-50 (base) Fig. 15, 14; Fig. 18, 3
Base diam.: n. d.
Fabric: not fully oxidized core (irregular), medium hard, coarse temper (724)
Surface: ext. and int. smoothed and with buff slip
Colour: ext. 2.5YR 6/6 (light red); core 10R 6/6 (light red); int. 2.5YR 5/1 (reddish grey)
Decoration: Black paint (Gley1 2,5/N) on the interior surface

KG-016-0045-59 (base) Fig. 15, 11
Base diam.: n. d.
Fabric: not fully oxidized core, medium hard, coarse temper (524)
Surface: ext. and int. smoothed, interior with buff slip
Colour: ext. 2.5YR 6/6 (light red); core 2.5YR 5/4 (reddish brown); int. 10YR 7/2 (light grey)

KG-016-0045-60 (base) Fig. 15, 12
Base diam.: n. d.
Fabric: not fully oxidized core, medium hard, coarse temper (524)
Surface: ext. and int. smoothed, interior with buff slip
Colour: ext. 5YR 6/4 (light reddish brown); core 5YR 5/1 (grey); int. 5YR 5/4 (reddish brown)

KG-016-0045-64 (round base) Fig. 15, 15
Fabric: not fully oxidized core, medium hard, medium fine temper (523)
Surface: ext. and int. smoothed

Colour: ext. 5YR 6/6 (reddish yellow); core 5YR 6/6 (reddish yellow); int. 5YR 3/1 (very dark grey)

KG-018-0049-03 (mangal)
Rim diam.: 300 mm (4 %)
Fabric: not fully oxidized core, medium hard, coarse temper (524)
Surface: ext. and int. smoothed
Colour: ext. 5YR 6/4 (reddish brown); core 5YR 3/1 (very dark grey); int. 5YR 6/4 (light reddish brown)

KG-018-0049-04 (mangal) Fig. 16, 8; Fig. 19, 4
Rim diam.: 220 mm (15 %)
Fabric: not fully oxidized core, medium hard, medium fine temper (523)
Surface: ext. and int. smoothed
Colour: ext. 5YR 6/4 (reddish brown); core 5YR 3/1 (very dark grey); int. 5YR 6/4 (light reddish brown)

KG-018-0049-05 (rim)
Rim diam.: 220 mm (8 %)
Fabric: not fully oxidized core, medium hard, medium fine temper (523)
Surface: ext. and int. smoothed
Colour: ext. 5YR 6/4 (reddish brown); core 5YR 3/1 (very dark grey); int. 5YR 6/4 (light reddish brown)

KG-018-0049-09 (base)
Base diam.: ~150 mm (15 %)
Fabric: not fully oxidized core, medium hard, coarse temper (524)
Surface: ext. and int. smoothed
Colour: ext. 5YR 6/4 (reddish brown); core 5YR 3/1 (very dark grey); int. 2.5YR 4/6 (red)

KG-022-0073-01 (mangal) Fig. 16, 9
Rim diam.: 320 mm (8 %)
Fabric: not fully oxidized core, medium hard, medium fine temper (523)
Surface: ext. and int. smoothed
Colour: ext. 5YR 6/4 (reddish brown); core 5YR 3/1 (very dark grey); int. 5YR 6/4 (light reddish brown)

KG-022-0073-02 (beaker) Fig. 16, 14
Rim diam.: 170 mm (8 %)
Fabric: fully oxidized, medium hard, medium fine temper (223)
Surface: ext. and int. smoothed and slipped with buff colour
Colour: ext. 10YR 7/3 (very pale brown); core 7.5YR 5/3 (brown); int. 10YR 7/3 (very pale brown)

KG-023-0082-05 (beaker) Fig. 16, 15
Rim diam.: 150 mm (20 %)
Fabric: not fully oxidized core, medium hard, medium fine temper (523)
Surface: ext. and int. smoothed and slipped
Colour: ext. 5YR 5/4 (reddish brown); core Gley 1 3/N (very dark grey); int. 5YR 5/3 (reddish brown)

KG-023-0082-03 (base) Fig. 16, 16
Base diam.: 170 mm (15 %)
Fabric: not fully oxidized core, medium hard, coarse temper (524)
Surface: ext. and int. smoothed
Colour: ext. 5YR 6/4 (reddish brown); core 5YR 3/1 (very dark grey); int. 5YR 6/4 (light reddish brown)

KG-049-0196-01 (spouted vessel) Fig. 16, 13
Rim diam.: 160 mm
Fabric: not fully oxidized core, medium hard, medium fine temper (523)
Surface: ext. and int. smoothed
Colour: ext. 10YR 7/3 (very pale brown); core 10YR 4/1 (dark grey); int. 10YR 7/3 (very pale brown)

KG-049-0196-02 (handle)
Diam.: n. d.
Fabric: not fully oxidized core, medium hard, coarse temper (524)
Surface: ext. and int. smoothed
Colour: ext. 2.5YR 6/6 (light red); core 10R 6/2 (pale red); int. 2.5YR 7/4 (light reddish brown)

KG-049-0196-04 (mangal) Fig. 16, 4
Rim diam.: 280 mm
Fabric: not fully oxidized core, medium hard, medium fine temper (523)
Surface: ext. and int. smoothed
Colour: ext. 5YR 6/4 (light reddish brown); core 5YR 3/1 (very dark grey); int. 5YR 6/4 (light reddish brown)

KG-049-0196-05 (base)
Base Diam.: 180 mm
Fabric: not fully oxidized core, medium hard, medium fine temper (523)
Surface: ext. and int. smoothed
Colour: ext. 5YR 6/4 (light reddish brown); core 5YR 3/1 (very dark grey); int. 5YR 6/4 (light reddish brown)

III.5 Conclusions

The limited number of Chalcolithic finds at Tepe 5, their isolated deposition in pits and the lack of radiocarbon-datable material, make a more accurate assessment difficult. Fortunately, the recent excavations at Mentesh Tepe provided valuable information into the pottery development in north-western Azerbaijan during that period and the site therefore served as a reference point for the material from Tepe 5.

Jars were the most elusive vessel type, as they combine certain traits of the chaff-tempered common ware and Sioni Ware. Moreover, the many loop handles are relatively uncommon in the Chalcolithic period, and rarely attested elsewhere. Although so far no exact comparison is possible, the specific morphological and technological characteristics of these jars indicate typological links with similar vessels from Mentesh Tepe Period III and perhaps Period II, even though the pottery assemblage of the latter is still not well known.

The bowls and beakers from Tepe 5 are comparable to similar pieces from Mentesh Tepe Period III, in particular the fragment of a painted bowl.

The mangals provide another indication of the dating of the Tepe 5 assemblage. This vessel type is associated

with the local pottery of the Chalcolithic period at the latest from Mentesh Period II until the Late Chalcolithic period (Leilatepe Culture). Especially the morphological development of their lugs from a horizontal, semi-circular shape in Period II to a vertical application to the rim or the total absence of a lug in Period III. The attestation of horizontal lugs among the mangals at Tepe 5 therefore suggests a chronological proximity to Mentesh Tepe Period II.

To sum up, the pottery from Tepe 5 provides links to both Mentesh Tepe Periods II (first half of the 5th mill. BC) and III (second half of the 5th mill. BC). A general date within the Early Chalcolithic Period is, therefore, very likely. Some traits of the pottery suggest a somewhat greater proximity to Period II. However, this proposed dating is necessarily preliminary, as future ceramic studies will certainly improve our understanding of the development of the Chalcolithic pottery in the region.

IV. The Tepe 5 Cemetery

Martin Gruber

IV.1 Introductory remarks

The excavation extended over almost the entire surface of Tepe 5, for a total of 312.5 sqm (Fig. 21). In the first year (Babaev et al. in print), an additional test trench was opened on the eastern slope to explore the extension of the burial ground as well as to investigate two anomalies visible in the magnetogram which enclose the hill (see ch. II.2, Fig. 11). The test trench extended from 6310.50–6322.00 E and 7997.50–7999.50 N, covering a further 23 sqm (Fig. 46). Apart from a bronze dagger found loose in the subsoil layer (see ch. IV.8) and some obsidi-

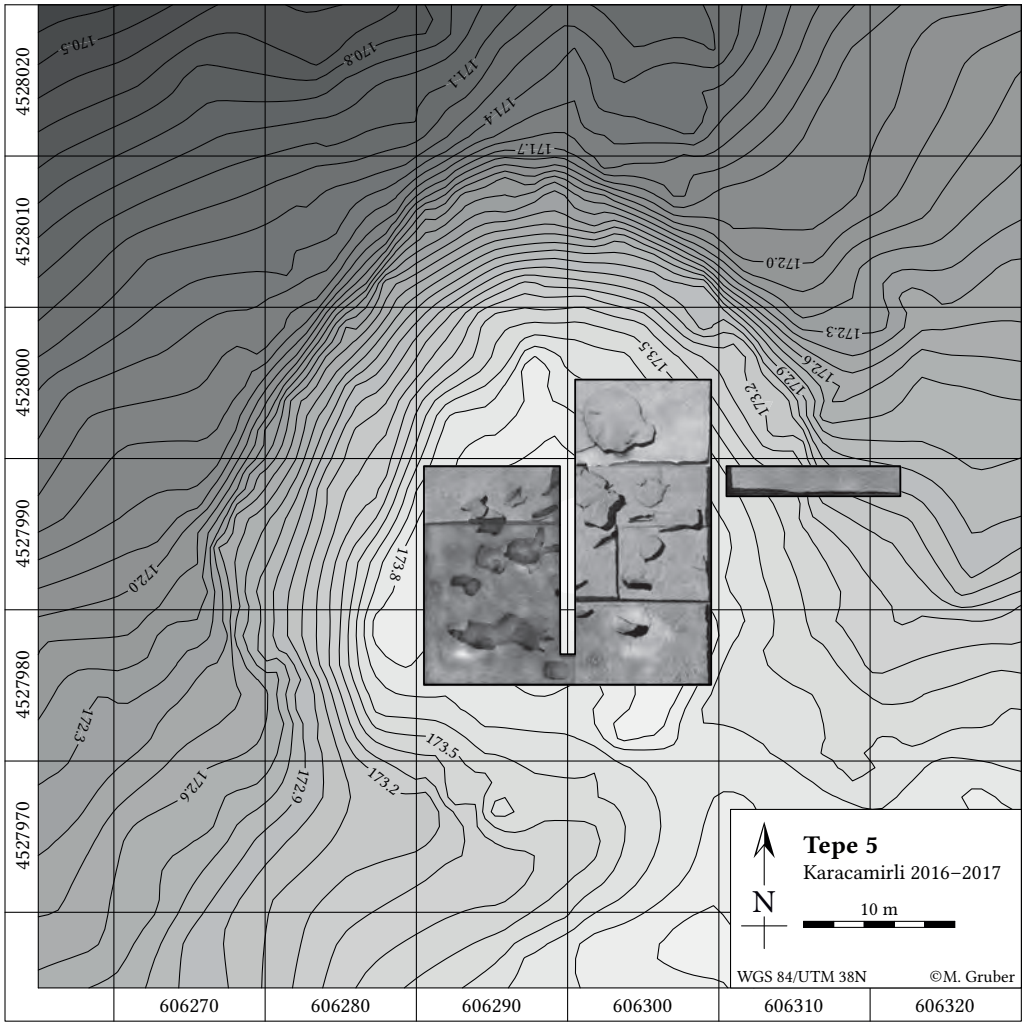

Fig. 21. Contour map of Tepe 5 with orthophotos of the excavated area

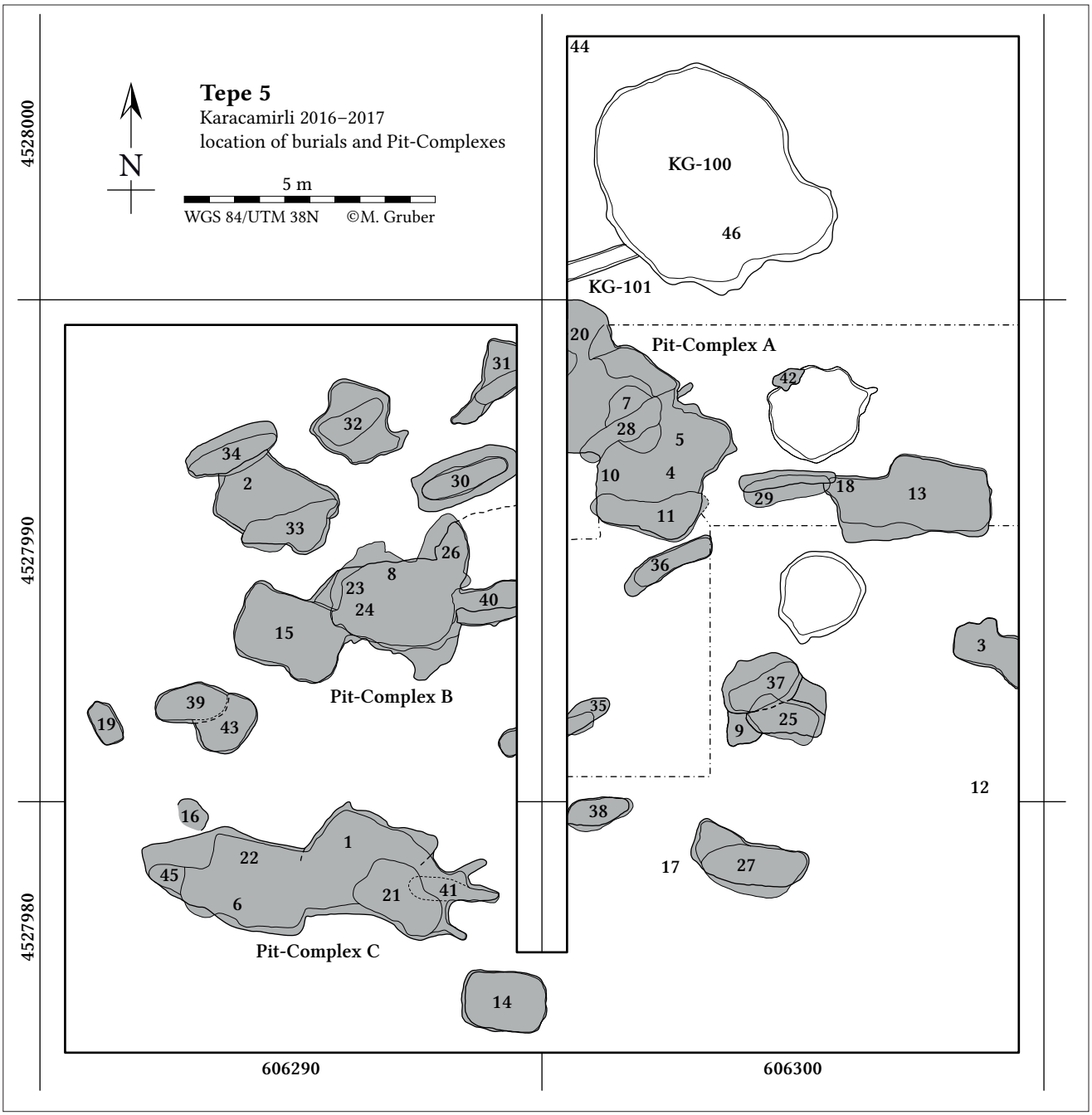

Fig. 22. Location of burials and Pit-Complexes on Tepe 5

an flakes no further finds or features were discovered in this trench, which either implies that the burial ground did not extend much beyond the centre of the hill or all features at the slopes were eroded. The two anomalies in the magnetogram are most likely shallow irrigation ditches of recent date channelling the irrigation water for the fields around the hill.

The sections at various points of Tepe 5 all showed a largely identical sequence of three layers: The uppermost layer was c. 20 cm thick and consisted of the mixed material of the topsoil. Below was a c. 20 cm thick subsoil layer of soft loam with many chalk inclusions, which gave the soil a whitish colour. Both layers showed no signs of anthropogenic activities. The second layer rested on considerably harder, coarse brown clay, impermeable to water. This lowest layer did not reveal any anthropogenic traces as well and can be considered as virgin soil. Except for the shallower pottery deposits of the Late Bronze/Early Iron Age (see ch. IV.2.3), all grave-pits penetrated the calcareous layer and were dug down into virgin soil (Fig. 23). The uppermost level of the virgin soil therefore provided an ideal planum to facilitate

Fig. 23. Temporary southern section of the south-western quadrant of square 6300/7990 showing the three natural layers on Tepe 5; the eastern part (right side) was disturbed by the grave-pit of the Medieval Burial 38

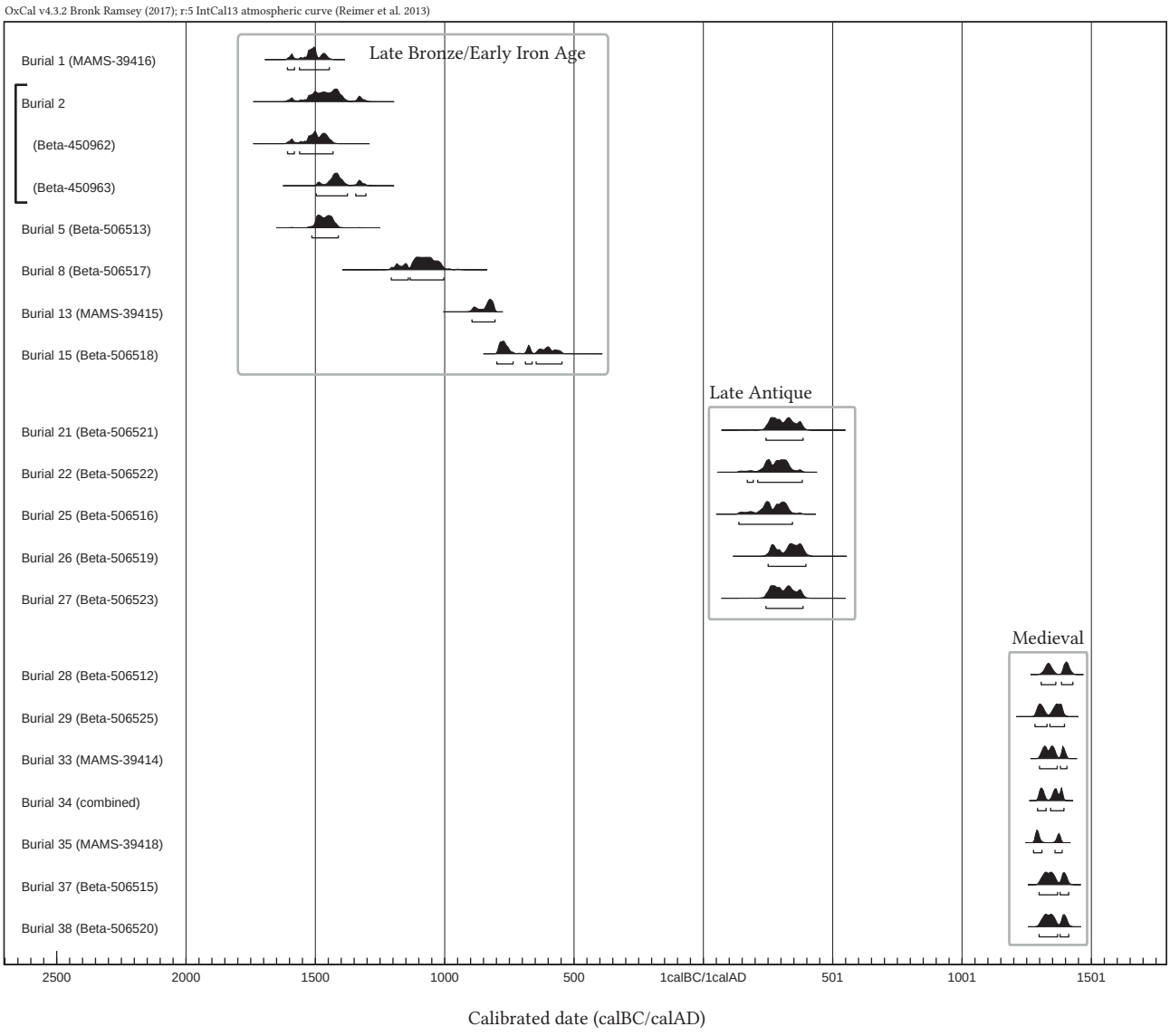

Fig. 24. Radiocarbon dates showing the three occupation phases of the cemetery

the detection and excavation of the sometimes very deep grave-pits. The original levels, from which the burials were dug, were eroded.

Regardless of the occupation phase, all grave-pits were filled with very homogeneous, light brown-coloured soil. It had a softer consistency and a finer texture

than the surrounding sediment, but did not differ much visually. During excavation the edges of the grave-pits were in most cases detectable only for a short period of time before the ground dried out in the summer heat of the Kura valley. The homogeneous fillings posed particular problems in recognizing later disturbances or cuts in the Pit-Complexes (see ch. IV.6), because they left no visible traces in the soil.

In total 46 burials were excavated. Through radiocarbon analyses, typological comparisons of the grave contents, stratigraphic relations and to some extant through their overall characteristics, the chronology of the cemetery was clarified, and three distinct occupation phases were recognized (Fig. 24):

The first occupation phase included Burials 1–20, spanning the period from the beginning of the Late Bronze Age to the Early Iron Age (late 16th–8th/7th cent. BC).

The second occupation phase was represented by seven burials (Burials 21–27) datable to the Late Antique period (mid-3rd to the end of the 4th cent. AD).

The third occupation phase consisted of 14 Medieval burials (Burials 28–41). The results of the radiocarbon analyses revealed a possible time span between AD 1280 and AD 1420.

Five burials remained undated (Burials 42–46), due to a lack of datable material.

IV.2 Late Bronze/Early Iron Age

IV.2.1 A short history of research

The scientific exploration of the Late Bronze/Early Iron Age of Azerbaijan began in the last decades of the 19th century, when German and Russian scholars initiated excavations at various sites in north-western Azerbaijan. One of the key figures was the renowned polymath R. Virchow who had developed an early interest in the Archaeology of the Caucasus. He had established contact with G. Radde, since 1867 director of the Caucasus Museum in Tbilisi (Plontke-Lüning 2015), and provided financial support for the excavations of F. Bayern, one of the pioneers of the archaeology in the Caucasus, and W. Belck, an employee of the Siemens & Halske copper mining company at Gadabay. Between 1888 and 1891 W. Belck excavated more than 250 cist graves of the Late Bronze/Early Iron Age near the smelting plants at Gadabay and Kalakent (Belck 1893; Kohlmeyer/Saherwala 1983: 17–22; Nagel/Strommenger 1985; Nawroth 2011: 88–90; Gruber 2019: 36–38).

In 1896 the Imperial Russian Archaeological Society sent A. A. Ivanovsky to the Gadabay region where he investigated further burial grounds (Ивановский 1911). From the mid-1890s until 1913 E. Rösler and later G. Rosendorf, on behalf of the Russian Imperial Archaeological Commission, conducted several excavations in the area of *Helenendorf* (Hanlar/Göygöl) and along the upper course of the Qoshqarchay as well as in Nagorno-Karabakh. Their results were published either in the Proceedings of the Imperial Archaeological Commission in Saint Petersburg (Отчетъ Императорской Археологической Комиссии) or in the *Zeitschrift für Ethnologie* in Berlin.

In the 1930s J. Hummel, schoolteacher at *Helenendorf*, explored various archaeological sites in the vicinity of his hometown (see in particular Гуммель 1940). During the course of the construction of the Mingachevir dam across the Kura river from 1945 to 1953 archaeological sites of various periods were discovered, among them a large cemetery of the Late Bronze/Early Iron Age that is still an important reference point for the material culture of this region and period (Асланов et al. 1959). In the following decades the Academy of Sciences of the Soviet Republic of Azerbaijan undertook regular expeditions into the foothills of the Lesser Caucasus that aimed to investigate burial grounds (e. g. Абилова 1960; Кесаманлы/Гусейнова 1986; Кесаманлы 1999), but also cyclopean structures, a widespread but still poorly studied architectural phenomenon of the Late Bronze/Early Iron Age in the region (Мещанинов 1932; Джафарзаде 1938; Расулоглы 1993; Reinhold 2009).

In the 1970s and 1980s the construction of the Shamkir reservoir, and later on the smaller Yenikand reservoir, led to a series of rescue excavations along the Kura river, during which six Bronze Age kurgans were discovered not far north-east of modern Qaracamirli, hereafter designated as »Karacamirli kurgans« (Асланов 1986; Сурхаев 2005; Гусейнова/Алиев 2008; Surkhayev 2012; Гусейнова 2011: 108–144). Between 2001 and 2005 a massive rescue archaeology programme was organized ahead of the Baku-Tbilisi-Ceyhan (BTC) and South-Caspian Baku-Erzurum (SCP) pipeline constructions. The excavations revealed a large number of sites and artefacts from the Chalcolithic to the Medieval period (Taylor/Maynard 2011; Taylor et al. 2011; Taylor 2018). Although the results are mostly available only in short preliminary reports (Maynard 2011), some of the larger sites have been studied in more detail. Of particular importance are the extensive excavations at the cemeteries at Tovuzchay (Müseyibli et al. 2008; Hacili 2010; 2012) and Zayamchay (Müseyibli 2004; 2009; Müseyibli et al. 2008; Nəcəfov 2008a; 2008b; 2018; Квачидзе 2008; Müseyibli/Nəcəfov 2019). Both sites are comparatively well documented and contribute significantly to the under-

standing of the burials at Tepe 5 as well as of the material culture of the Late Bronze/Early Iron Age as a whole.

IV.2.2 The Khojaly-Gadabay-Culture

One of the first to attempt a definition of the Late Bronze/Early Iron Age of the Southern Caucasus was F. Hančar (1932; 1934), who coined the term »Ganca-Karabagh-Culture«. Today, the term »Khojaly-Gadabay-Culture«, used by scholars in Azerbaijan since the mid-20th century, has gained greater popularity and will be used here as well.

Despite the long history of research on the Khojaly-Gadabay-Culture, its chronological and regional subdivisions are up to now debated. Not only the age of many excavations and the methodology employed at the time, but also language and political boundaries and the difficult accessibility of reports impede a thorough analysis of the material and its contextualisation within the culture-historical development of neighbouring and in parts better researched regions of the Southern Caucasus. It must first be emphasized that the somewhat unsatisfactory designation »Khojaly-Gadabay-Culture« should not be understood as a cultural (or ethnic or linguistic) entity, but merely as an archaeological complex or group (*Formenkreis*) within the considerably larger cultural environment of the region. This is maybe best illustrated by the many and distant links between the material culture of Tepe 5 and that of sites in the Armenian Highlands (this is particularly true for the earliest burials) and Eastern Georgia.

The first attempt to establish a chronological framework was made by N. V. Minkevich-Mustafaeva (Минкевич-Мустафаева 1962). Chiefly on the basis of metal objects, she divided the Khojaly-Gadabay-Culture into three chronological stages (Fig. 25): The early stage lasted from the 13th to the 11th cent. BC and was characterized by a paucity of bronze objects. The developed stage (11th–9th cent. BC) was characterized by a large quantity and considerable variety of bronze weapons and ornaments. In the last stage (9th–7th cent. BC) iron objects appeared in greater numbers. Minkevich-Mustafaeva also distinguished three regional groups within the Khojaly-Gadabay-Culture, named Karabakh, Gadabay and Ganja/Kirovabad-Hanlar. The Karabakh group is roughly located in the Nagorno-Karabakh region as far north as the Tartar River. The Ganja-Hanlar group comprises sites in the Kura valley, especially to the south of the modern Mingachevir reservoir. The Gadabay group extents over the northern part of the Lesser Caucasus and its eastern foothills down to the Kura Valley. The regional differentiation, as Minkevich-Mustafaeva noted

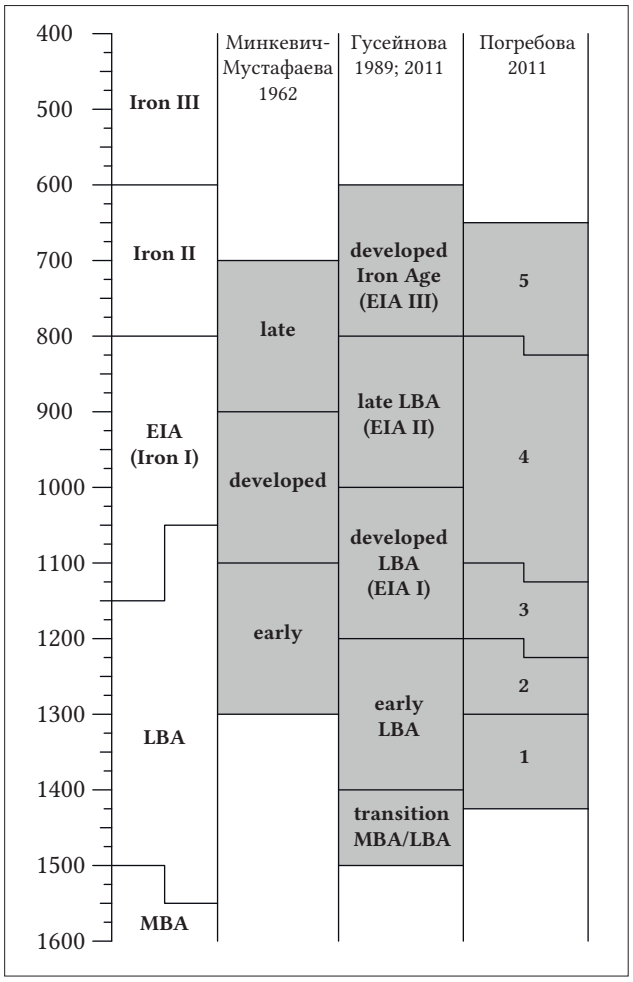

Fig. 25. Proposed subdivision of the Late Bronze/Early Iron Age (Khojaly-Gadabay-Culture) in north-western Azerbaijan after Минкевич-Мустафаева 1962, Гусейнова 1989; 2011 and Погребова 2011. The archaeological periodization in the left column combines the original (Smith et al. 2009) and revised version (Manning et al. 2018) of the chronological model established by the ArAGATS-project

herself, should not obscure the fact that there are substantial formal similarities between all three regions, in particular with respect to their metal objects.

In 1989 M. A. Gusejnova proposed a different subdivision of the Khojaly-Gadabay-Culture based on pottery studies (Гусейнова 1989; 2011). The earliest part of the Late Bronze Age (15th cent. BC) was considered as transitional between the Middle and Late Bronze Ages. The Late Bronze Age was then divided into an early (14th–13th cent. BC), a developed (12th–11th cent. BC) and a late (10th–9th cent. BC) stage (Fig. 25). The last two »Late Bronze« stages were at the same time termed (Early) Iron I and (Early) Iron II and were followed by the developed Iron Age (EIA III) between the 8th–6th cent. BC (Гусейнова 1989: 10; 2011: 20). This confusing terminology was likely caused by the attempt to merge various

chronological systems known at the time. The division of the Late Bronze Age – though in M. A. Gusejnova's work not explicitly mentioned – might have been to some extent influenced by the chronological studies of A. A. Martirosyan in Armenia (Мартиросян 1964). The designations for the Iron Age, however, were adapted from the terminology of northern Iran (Гусейнова 1989: 10; 2011: 51). Both systems of periodization have since been re-evaluated regarding their terminology and absolute time ranges (for a brief overview of the research history see Smith et al. 2009: 39–40 and Piller 2012: 305–307). M. A. Gusejnova's terminology should therefore be considered with some caution.

The most recent chronological study of the Khojaly-Gadabay-Culture is owed to M. N. Pogrebova (Погребова 2011) who proposed a completely new chronological division of the material culture into five phases (Fig. 25), with the following durations: First phase – end of the 15th to the 14th cent. BC, second phase – 13th cent. BC, third phase – end of the 13th to the 12th cent. BC, fourth phase – end of the 12th to the 9th cent. BC and fifth phase – end of the 9th to the first half of 7thcent. BC.

Despite these efforts to structure the material culture of the Late Bronze/Early Iron Age chronologically, the lack of detailed documentation of archaeological data (and the objects themselves) makes it difficult to evaluate the consistency of the proposals. Furthermore, the same lack of sufficiently accurate publications frequently obstructs the assessment of newly excavated archaeological finds. The typological comparisons suggested for the Tepe 5 material are therefore limited to a few better published sites in north-western Azerbaijan (see below). Of considerable importance has been the revision of the Armenian evidence in recent decades (e. g. Badalyan/Avetisyan 2007; Avetisyan/Bobokhyan 2008; Smith et al. 2009; Manning et al. 2018). However, unlike the region west of the Lesser Caucasus, where the formation of Urartu in the 9th/8th cent. BC had a significant impact on the local material culture (Smith et al. 2009: 91–92), the regions east of the Lesser Caucasus appear largely untroubled by these changes and experienced a continuous development, at least until the late 8th cent. BC, when incursions of Scythian tribes were felt in the entire region. Significant comparisons can be drawn also with well-published Early Iron Age site in Eastern Georgia (Ludwig 2010; Brodbeck-Jucker 2019).

For the earliest burials at Tepe 5 a group of kurgans discovered c. 120 m from the right bank of the Kura river (Сурхаев 2005: 235), in an area now part of the Yenikand reservoir, is particularly relevant: Between 1985 and 1989 six of these Middle to Late Bronze Age burials were excavated (Асланов 1986; Сурхаев 2005; Гусейнова/Алиев 2008; Surkhayev 2012; Гусейнова 2011: 108–144). The kurgans contained a rich inventory of pottery, bronze weapons, jewellery as well as skeletons of horses with their harnesses and traces of wagons. For Kurgans 1 and 2 a date at the beginning of the Late Bronze Age (15th–14th cent. BC) was suggested (Сурхаев 2005). The earliest barrow, Kurgan 6, was dated to the 16th cent. BC (Гусейнова/Алиев 2008: 137–138; Гусейнова 2011: 125–126). The black-polished pottery in Kurgans 4 and 5 indicated links to both, the Middle Bronze Age and the Late Bronze Age, and was thus considered to mark a transitional phase lasting from the 16th to the 15th cent. BC (Гусейнова/Алиев 2008: 133–136; Гусейнова 2011: 120–121). Many vessels were ornamented with geometric patterns using a stamp- or comb-like tool that was rolled over the surface creating regular dashed lines of small rectangular or oval-shaped impressions that were filled with white paste (Гусейнова 2011: 109). In the case of Tepe 5 similar impressions regularly consisted of two parallel lines (Fig. 26). M. M. Surkhayev (2012: 253) used the term »triangular stamped ornament« and distinguished it from the later »engraved« or incised ceramics. Vessels of identical shape and decoration also appeared in the Armenian Highlands where this type of decoration is referred to as »punctate ornamentation« (Smith et al. 2009: 66), a term adapted in the present study. This particular decoration technique appears to represent a distinctive feature of the transitional period between the Middle and Late Bronze Ages (Smith et al. 2009: 30; Гусейнова 2011: 109).

Fig. 26. Punctate ornamentation on pot 0200-03 from Burial 2

The most important reference points for the later periods are the cemeteries of Mingachevir, Zayamchay and Tovuzchay.

At Mingachevir the excavators initially divided the more than 100 pit burials and five larger barrows into two chronological groups: The earlier group was supposed to cover the timespan from the 13th to 11th cent. BC; for the second group, including the barrows, a date between the 11th and 9th cent. BC was brought forward (Асланов et al. 1959: 119–120). The relative sequence and date of the Mingachevir burials are, however, still under debate. M. A. Gusejnova assigned the Mingachevir burials mainly to her latest stage (Гусейнова 1989). Some critical issues of the dating were recently summarized by M. N. Pogrebova who proposed to date the entire burial ground within her fifth stage of the Khojaly-Gadabay-Culture, more precisely the 8th cent. and first half of the 7th cent. BC (Погребова 2011: 181–194). Both scholars assumed a period of 150–200 years during which all individuals had supposedly been buried. In contrast, the recent excavations at Zayamchay and Tovuzchay as well as at Tepe 5 (see below) revealed rather long occupations lasting throughout the entire Late Bronze/Early Iron Age. This prompts the question, if a re-examination of Mingachevir might reveal a similarly long-lasting occupation, as was originally suggested by the excavators. That some of the Mingachevir burials belong to an earlier part of the Late Bronze/Early Iron Age is indicated, for example, through ceramic vessels in Tepe 5 Burial 6 (15th and mid-12th cent. BC) which have close parallels at Mingachevir (see below).

The cemeteries at Zayamchay and Tovuzchay were both excavated during the construction of the BTC-pipeline. The time range proposed for the 130 burials of Zayamchay lasts from the 14th to the 10th/9th cent. BC, but burials from the earliest and latest occupation phases of the cemetery are rare, so the bulk of the graves was dated to the 12th and 11th cent. BC (Nəcəfov 2008a: 59–60; Müseyibli/Nəcəfov 2019: 190–193). The earliest burials in the Tovuzchay cemetery were dated slightly later, to the 13th cent. BC, but the site continued to be used as a burial ground until the 9th cent. BC (Nəcəfov 2018: 70).

The end of the Khojaly-Gadabay-Culture is not well defined. According to M. A. Gusejnova it is marked by the widespread use of iron in the 8th cent. BC (Гусейнова 2011: 27). N. V. Minkevich-Mustafaeva and M. N. Pogrebova placed it in the 7th cent. BC. The end has been associated with the penetration of the Scythians into the Caucasus region and the appearance of Scythian elements in burials (Есаян/Погребова 1985; Погребова 2011: 167–168). It has, however, been argued by G. Mehnert that when considering the individual contexts of these Scythian elements (weapons, horse harnesses and objects of animal style) they do not necessarily attest to the presence of an ethnic group, but might only reflect the adoption of new elements in the local material culture (Mehnert 2008). The movements of the Scythians into and through the Caucasus region, therefore, need not be considered a dominant factor for the local material culture, in particular for the pottery which underwent a continuous development until the appearance of the Achaemenids in the mid-1st millennium BC when new vessel shapes and fabrics were introduced (Ludwig 2010: 90–92). The Achaemenids permeated the local material culture on a larger scale than all their predecessors and caused the most radical change in the material culture since a thousand years.

IV.2.3 General description of burials and grave contents

The burials of the Late Bronze/Early Iron Age were spread over the entire cemetery (Fig. 27). There are two types of mortuary structures: On the one hand grave-pits that contained an inhumation accompanied by different burial gifts, on the other hand pottery deposits without any traces of skeletal remains. Even though the preservation of bones depends on soil conditions and possible post-depositional disturbances, the latter group of burials differs also in size and depth from the first group. It is unlikely, that these pits were ever meant to contain a corpse, and they can therefore be considered either as a possible form of cenotaphs or as funerary deposits related to one or more of the other graves. Burials 3, 12 and 16–18 belong to this group. Burial 10 could be possibly a pottery deposit as well, however, due to the repeated interments in Pit-Complex A the character of this context is not conclusive. Although Burial 19 also did not contain skeletal remains, it is not considered part of this group, because the size of the grave-pit and the discovery of a small bronze fragment and at least 15 beads suggest that we are dealing with the inhumation of an adorned infant whose bones have completely decayed. All other burials of this group did not or only barely penetrate virgin soil and were found at heights between 173.30 m and 173.70 m, i. e., only c. 20–60 cm below the surface. The grave-pits were therefore difficult to distinguish from the surrounding soil and could only be determined for Burials 3 and 16. The individual pits contained up to three ceramic vessels. Attested are bowls (Burial 3), small pots (Burials 3 and 18), jugs (Burial 16) and a small beaker in Burial 12 that contained also two frit beads.

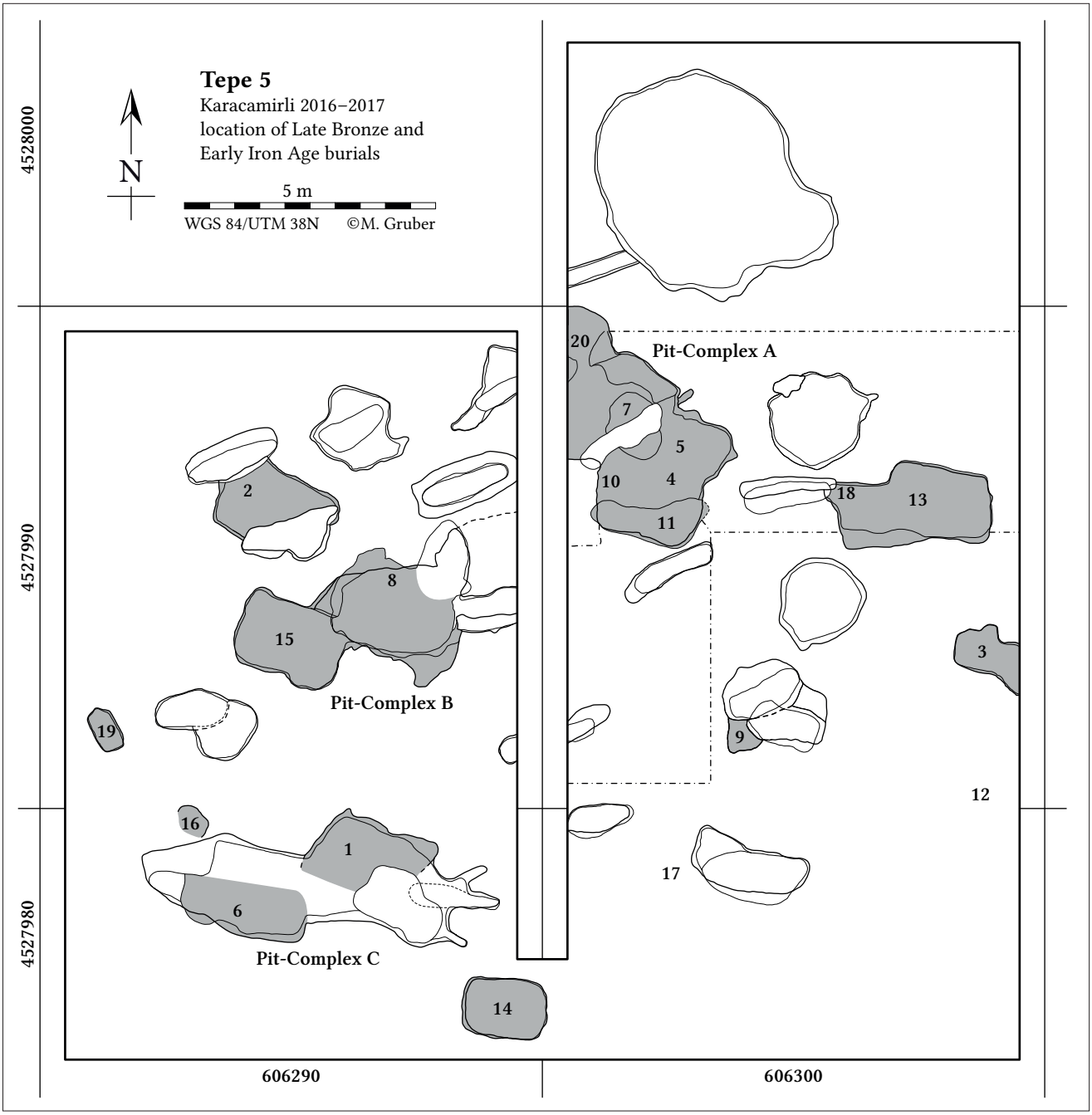

Fig. 27. Location of Late Bronze/Early Iron Age burials

The custom to bury objects without a human body is not unknown in the Late Bronze/Early Iron Age. Among the 130 burials at Zayamchay, for example, 90 did not contain skeletons (Müseyibli/Nəcəfov 2019: 175–180 Table 2). Although bad bone preservation or other factors might bias these numbers, depositions in burial contexts appear to be a common practice.

Burials with inhumations are more frequent at Tepe 5, numbering 14. The size and shape of the grave-pits varied in detail, though in general the rectangular form dominated (Table 2). The grave-pits were all filled with the same light brown soft material. The only exception was Burial 2, the filling of which contained large amounts of ashy material and pieces of charcoal and was therefore of much darker colour.

The orientation of the grave-pits and skeletons (Table 2) was calculated on the basis of their longest axis, which in the case of the skeletons was either defined by the orientation of the spinal column or the general position of the bones towards the head. To be sure, all measurements represent only approximate values. Eleven grave-pits were preserved sufficiently to determine their orien-

burial	shape of grave-pit	orientation of grave-pit	position of skeleton	position of head	orientation of skeleton
1	rectangular (?)	118°–298°	n. d.	SE	n. d.
2	rectangular (?)	120°–300°	n. d.	n. d.	n. d.
3	oblong/irregular	113°–293°	–	–	–
4	n. d.	n. d.	left side, flexed	NW	~310°
5	rectangular (?)	111°–291°	left side, flexed	NW	303°
6	rectangular (?)	106°–286°	left side, flexed	W	284°
7	oval	150°–330°	n. d.	SE	n. d.
8	n. d.	n. d.	n. d.	n. d.	n. d.
9	n. d.	n. d.	n. d.	W/SW	n. d.
10	n. d.	n. d.	–	–	–
11	oblong	94°–274°	n. d.	n. d.	n. d.
12	n. d.	n. d.	–	–	–
13	rectangular	87°–267°	n. d.	n. d.	n. d.
14	rectangular	93°–273°	n. d.	W(?)	n. d.
15	rectangular	110°–290°	n. d.	n. d.	n. d.
16	n. d.	n. d.	–	–	–
17	n. d.	n. d.	–	–	–
18	n. d.	n. d.	–	–	–
19	rectangular	150°–330°	n. d.	n. d.	n. d.
20	n. d.	n. d.	right side, flexed	W(?)	n. d.

Table 2. General features and orientation of grave-pits and skeletons of Late Bronze/Early Iron Age burials

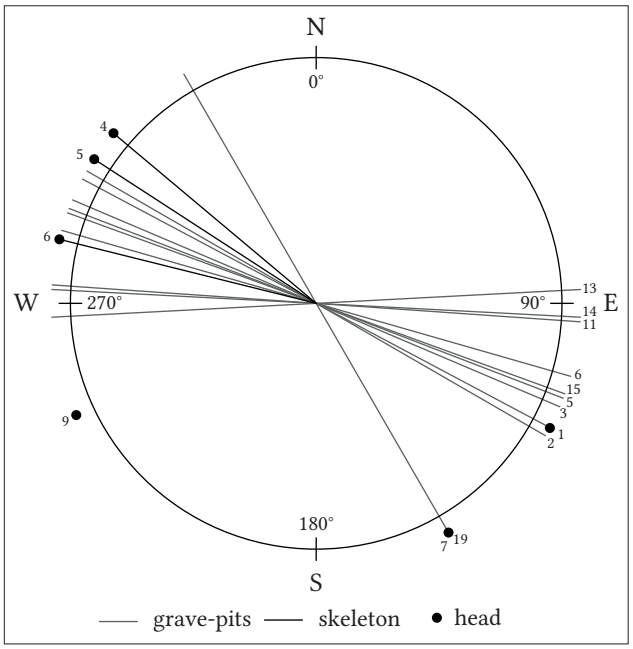

Fig. 28. Orientation of the grave-pits and skeletons in the Late Bronze/Early Iron Age

tation. Except for Burials 7 and 19, which were oriented north-north-west to south-south-east, all other burials ranged between west-east and north-west to south-east (Fig. 28). Whenever determinable the skeletons were placed on their left side in a flexed position (Burials 4–6) and only in one case probably on the right side (Burial 20). In Burials 4–6 the deceased was oriented north-west to south-east with the head in the north-west. In Burial 1 the body was probably laid down with the head in the south-east, as was the case in Burial 7. The few remains in Burial 9 might indicate that the head was in the west or south-west of the grave-pit.

Almost all burials contained ceramic vessels. In contrast to Burials 9 and 20, where the lack of pottery is likely explained by secondary disturbance and incomplete excavation, Burials 4, 5 and 19 contained no pottery, but, in turn, were richly equipped with large sets of frit, carnelian, bone and bronze beads (Table 3). Clay beads were less common and attested only in Burials 13 and 14, as were cowry shells or molluscs (Burials 4 and 14). The highest number and largest variety of bronze objects

burial	sex	grave contents												fill						
		human skeleton	animal bones	ceramic vessels	frit beads	carnelian beads	bronze beads	bone beads	clay beads	cowry shell/mollusc	bronze objects	obsidian arrowhead	obsidian flakes	obsidian flakes	ceramic sherds	human bones	frit beads	carnelian beads	bronze objects	iron fragments
1	n. d.	1	2	4										7	10		14	1		
2				7										1	1					
3				2																
4	n. d.	1			3	27	2	57		3										
5	(♂)	1				1	57				1(2)			4	1					
6	n. d.	1		6								1		17		1	2		1	
7	(♂)	1		4									2	1	5					
8	n. d.	1		2																
9	n. d.	1					3				14(23)									
10				2										1						
11				2										5		1				
12				1																
13	n. d.	1	1	5		2			1					7						
14	n. d.	1		2	122	21	18		1	1	5(45)			4			1			
15	n. d.	1		5	2	3								5	1					1
16				2	2															
17				1																
18				1																
19					4			11			(1)									
20	n. d.	1												1						

Table 3. Type and number of objects found in Late Bronze/Early Iron Age burials and in their fill (the number of fragments is written in brackets); if the sex was determined only by probability, the results are shown in brackets

was encountered in Burial 9, even though it was largely destroyed by later interments. Bronze adornments were also attested in Burial 14 and in Burial 5. In addition, a bronze fragment was found in Burial 19. Only two burials contained animal bones (Burials 1 and 13). Obsidian objects as burial gifts were limited to a single obsidian arrowhead in Burial 6. A second arrowhead was found re-used in Burial 21, but originally probably belonged to Burial 1. In Burial 7 two obsidian flakes were found inside of vessels and are therefore considered as intentionally placed there. All other obsidian flakes in the fill are most likely accidental intrusions. The frequent occurrence of obsidian flakes in the Chalcolithic pits suggests that the flakes found in burials, in topsoil and subsoil layers (see ch. IV.8) are probably remnants of this earlier occupation episode (see ch. III).

Although there is a marked focus on beads and bronze adornments in certain burials, this can not be conclusively explained through the sex of the buried individuals. The bad preservation of the bones severely reduced the number of skeletons whose sex could be anthropologically determined. Only the individuals in Burial 5 and Burial 7 could be identified as probably male (see ch. V.3 and Table 16). Burial 5 is of particular interest, because it contained many beads and a bronze adornment, which disproves an exclusive association of women with jewellery.

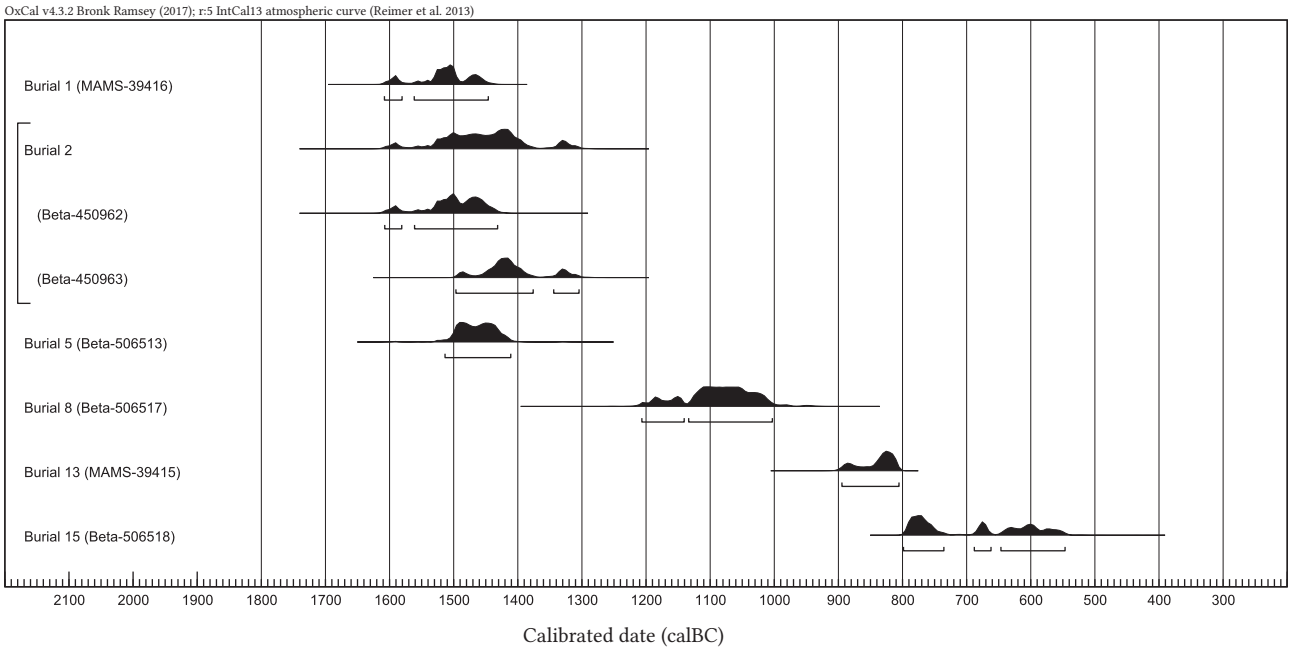

Fig. 29. Radiocarbon dates of Late Bronze/Early Iron Age burials

burial	laboratory-nos.	individual	material	conv. ^{14}C age (BP)	cal. age 2σ (95.4%)	cal. age 1σ (68.2%)
1	MAMS-39416	KG-094-0474	bone	3242 ± 23	(11.9%) cal BC 1609–1581 (83.5%) cal BC 1562–1447	(3.7%) cal BC 1594–1589 (50.3%) cal BC 1531–1496 (14.3%) cal BC 1477–1459
2	Beta-450962	KG-044-0189	charcoal	3230 ± 30	cal BC 1525–1495 cal BC 1480–1455	cal BC 1605–1585 cal BC 1545–1435
2	Beta-450963	KG-044-0195	charcoal	3140 ± 30	cal BC 1435–1405	cal BC 1495–1480 cal BC 1455–1385 cal BC 1340–1315
5	Beta-506513	KG-038-0146	bone	3190 ± 30	(95.4%) cal BC 1514–1412	(36.3%) cal BC 1464–1435 (31.9%) cal BC 1497–1472
8	Beta-506517	KG-057-0247	bone	2900 ± 30	(78.8%) cal BC 1134–1004 (16.6%) cal BC 1207–1141	(68.2%) cal BC 1123–1024
13	MAMS-39415	KG-032-0137	bone	2688 ± 22	(95.4%) cal BC 895–806	(6.4%) cal BC 889–881 (61.8%) cal BC 844–808
15	Beta-506518	KG-058-0243	bone	2540 ± 30	(44.4%) cal BC 799–736 (38.9%) cal BC 647–547 (12.2%) cal BC 689–663	(40.3%) cal BC 795–751 (13.3%) cal BC 615–591 (9.5%) cal BC 683–668 (5.1%) cal BC 637–625

Table 4. Radiocarbon dates of Late Bronze/Early Iron Age burials

IV.2.4 Radiocarbon dates

Five skeletons of the Late Bronze/Early Iron Age were sampled for radiocarbon dating (Burials 1, 5, 8, 13 and 15). The bone samples were analysed by *Beta Analytic Inc.*, Miami (Beta), and the *Curt-Engelhorn-Zentrum für Archäometrie GmbH* at Mannheim (MAMS). In addition to the skeletons, two charcoal samples from the filling of Burial 2 were analysed by *Beta Analytic* (Fig. 29; Table 4).

The calibrated dates of Burials 1 and 2 reveal their close proximity in time and confirm the archaeological

dating to the transitional period between the Middle and Late Bronze Ages, in absolute terms at the end of the 16th and the beginning of the 15th cent. BC. Burial 2 appears to be only slightly later, as one of the analysed charcoal samples makes an interment and backfilling of the grave-pit with burnt material after 1500 BC more likely. Burial 5 can be dated to the 15th cent. BC, which is also in accordance with the archaeological dating. Burial 8 was of later date (12th–11th cent. BC) and represents the transition from the Late Bronze Age to the Early Iron Age. The radiocarbon date of Burial 13 in the 9th cent. BC matches the archaeological comparisons of the pottery with contemporary Early Iron Age material from Eastern Georgia. The latest radiocarbon date of the Early Iron Age (Burial 15) is already at the fringe of the Hallstatt plateau (c. 800–400 calBC) and therefore results in a calibrated age range between 800 and 550 calBC. However, considering the slightly higher probabilities for the 8th cent. BC and the archaeological data from Burial 15, a date early in this timeframe seems more plausible.

IV.2.5 The sequence of Late Bronze/Early Iron Age burials at Tepe 5

To establish a relative sequence of the Late Bronze/Early Iron Age burials several obstacles must be overcome. Foremost, it is challenging to assess the multiple existing periodizations of the Khojaly-Gadabay-Culture, both in terms of its relative sequence and absolute dates (see ch. IV.2.4). In particular, detailed pottery sequences that could provide more information about chronological and regional differentiation through the investigation of specific vessel type sequences, fabrics or decorations and the composition of pottery assemblages in a particular period of time, are lacking. Currently typological comparisons between finds from Tepe 5 and other sites regularly lead to ambiguous results from which rather long timeframes for the suggested dating of a particular burial may ensue. It was therefore decided to use radiocarbon dating as a primary means to establish the chronological backbone of the proposed sequence of the Late Bronze/Early Iron Age burials on Tepe 5 (Table 4). With the aid of typological, stratigraphical and to some extent also chemical data (ch. VII) all other burials were included in this sequence. In view of the aforementioned restrictions – when relying on typological comparisons – the possible timespan for an interment is in many cases quite long (Fig. 30). Therefore, the sequence presented here remains to a certain degree conjectural; future research into the Khojaly-Gadabay-Culture will undoubtedly further clarify the issue and necessitate alternations.

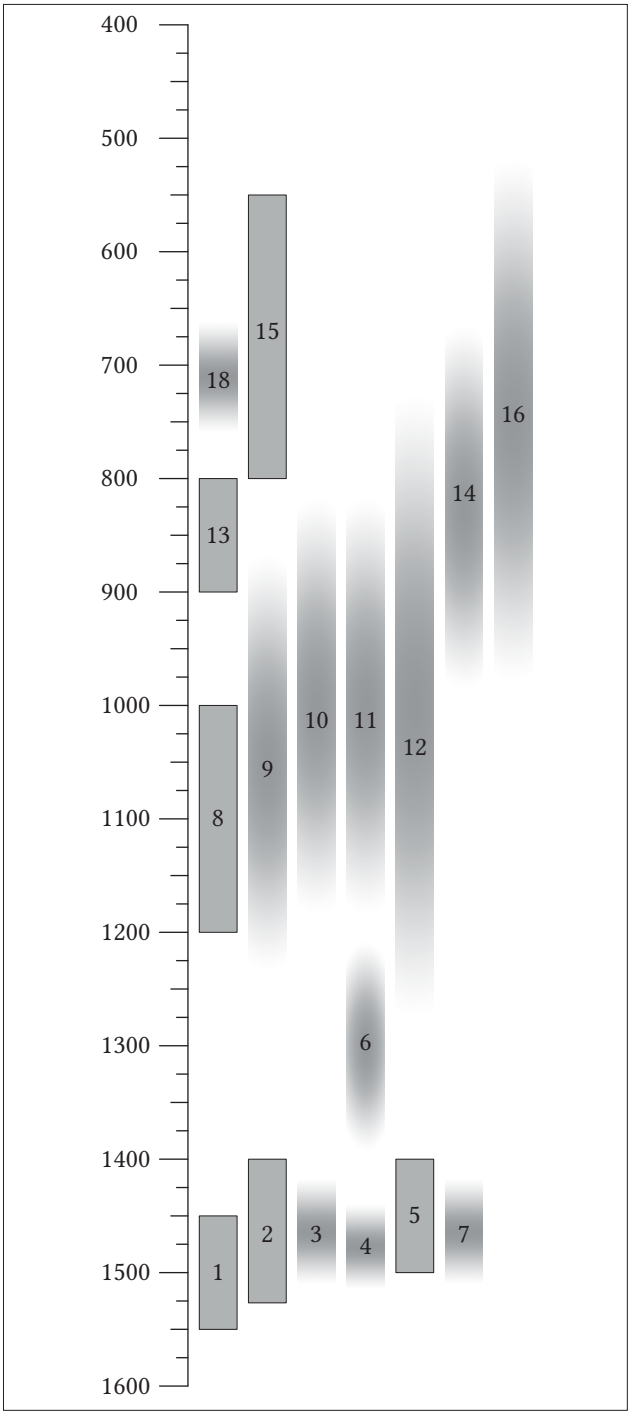

Fig. 30. Proposed chronological sequence of Late Bronze/Early Iron Age burials; radiocarbon-dated burials are marked by their solid frame

Burials 1–5 and 7 form a distinct group datable to the onset of the Late Bronze Age between the end of the 16th cent. BC through the 15th cent. BC. The ceramic inventories of these burials showed close morphological similarities among each other as well as with the Karacamirli Kurgans 4 and 5 and with burials at Harich, Armenia (see ch. IV.9). The comparisons with Harich at-

test to the wide diffusion of these pottery types beyond the mountain ridges of the Lesser Caucasus as far west as the Tsaghkahovit Plain. Moreover, the proposed archaeological dating of the Karacamirli kurgans to the transitional period between the Middle Bronze Age and Late Bronze Age (Гусейнова 2011) and of the Harich pottery to the final Middle Bronze Age period (Smith et al. 2009: 68–77) is now further supported by the radiocarbon dates published here. Burial 4 did not contain pottery, but was included in this group because of its stratigraphic relation with the radiocarbon-dated Burial 5. The latter appears to have caused damage to Burial 4 and should therefore be of later date.

The mature part of the Late Bronze Age is not well attested at Tepe 5. The only burial that can be dated tentatively to this period is Burial 6. The archaeological comparisons of the pottery in this burial set a possible timeframe between the 15th cent. BC and the mid-12th cent. BC for the interment, and also the typological differences in the pottery assemblages between the early group of Late Bronze Age burials and the Early Iron Age burials (see below) make a dating in between these two groups likely.

The Early Iron Age is represented by the radiocarbon-dated Burials 8, 13 and 15 and at least seven more burials which can be assigned to this period on the basis of typological considerations. Because of the already mentioned difficulties to distinguish the specific typological feature within a long period of time, the proposed chronological range of most Early Iron Age burials is considerable. Therefore, their relative sequence – in particular in the case of Burials 9–12 – remains tentative. This equally applies to Burials 14 and 16. Typological links between Burials 14, 15 and possibly Burial 13 support the dating of Burial 14 to a similar timeframe in the first centuries of the 1st mill. BC. For Burial 16 a date within the first half of the 1st mill. BC was suggested on the basis of typological comparisons. The Early Iron Age date of Burial 18 is solely based on its stratigraphic relation with Burial 13, which must be of earlier date. Burials 17, 19 and 20 can be dated only in general terms to the Late Bronze/Early Iron Age and are therefore not listed in Fig. 30.

IV.3 Late Antique Period

IV.3.1 Historical background

In the Late Antique period Tepe 5 was located in the border area between the kingdoms of Armenia and Caucasian Albania. In Roman texts of the 1st and 2nd cent. AD the Kura river is mentioned as border between these two kingdoms (Bais 2001: 169). Although in these centuries Albania advanced several times to the Arax river in the west, the extension and permanence of these military efforts remain controversial (Dudwick 1990). In general, the borders of the Caucasian kingdoms were not sharply defined, as the ruling families »were not neatly confined to the jurisdiction of a particular realm« (Rapp 2014a: 18).

The Late Antique occupation of Tepe 5 as a burial ground lasted for no longer than 150 years from the mid-3rd to the end of the 4th cent. AD (see the radiocarbon dates in ch. IV.3.4). This period of time was characterized by the advance of the Sasanians into the Caucasus, who attempted to re-establish the previous extent of the Achaemenid empire (Braund 1994: 238; Bais 2001: 97–98).

In the course of military campaigns against the Roman Empire from at the latest AD 253 onwards (Kettenhofen 1982) Shapur I, Sasanian king of Persia, occupied the kingdom of Armenia. With or shortly after the devastating defeat and the capture of the Roman Emperor Valerian in AD 260 Shapur I had also established overlordship over the kingdoms of Iberia and Albania. This is suggested by the trilingual inscription placed by him at Naqsh-e Rostam in about AD 262, which listed Albania as one of the new possessions of the Sasanian empire (Rapp 2014b: 28). In contrast to the Iberian king Amazaspus, the Albanian king was not mentioned by name in the inscription, possibly indicating his minor political importance to the Sasanians (Braund 1994: 239–240; Bias 2001: 99). A further glimpse into the political constellation of the last quarter of the 3rd cent. AD in the Caucasus provides the high *magus* Kirdir, who listed, inter alia, Albania, Iberia and Armenia among the non-Iranian lands under Sasanian hegemony (Braund 1994: 243–244; Bais 2001: 100; Rapp 2014b: 29). In the last two decades of the 3rd cent. AD Rome strove to regain the lost provinces and advanced several times against the Sasanian Empire, which at that time was weakened by internal political unrest. The conflict ultimately led to the treaty of Nisibis (AD 298) between the Sasanian king Narseh, a son of Shapur I, and the Roman Tetrarchic Emperors Galerius and Diocletian. As a consequence, Narseh lost control over Armenia, Iberia and its territories in northern Mesopotamia. Albania was not considered in the treaty and remained under Sasanian influence for the following centuries (Chaumont 1985; Bais 2001: 103–148). After the 3rd cent. AD Albania has virtually disappeared from Greek and Latin sources, implying that it was beyond the political horizon of Rome (Bais 2001: 101). The few sources for the 4th cent. AD suggest an increasing rapprochement with the Sasanian Empire under Shapur II (Bais 2001: 110).

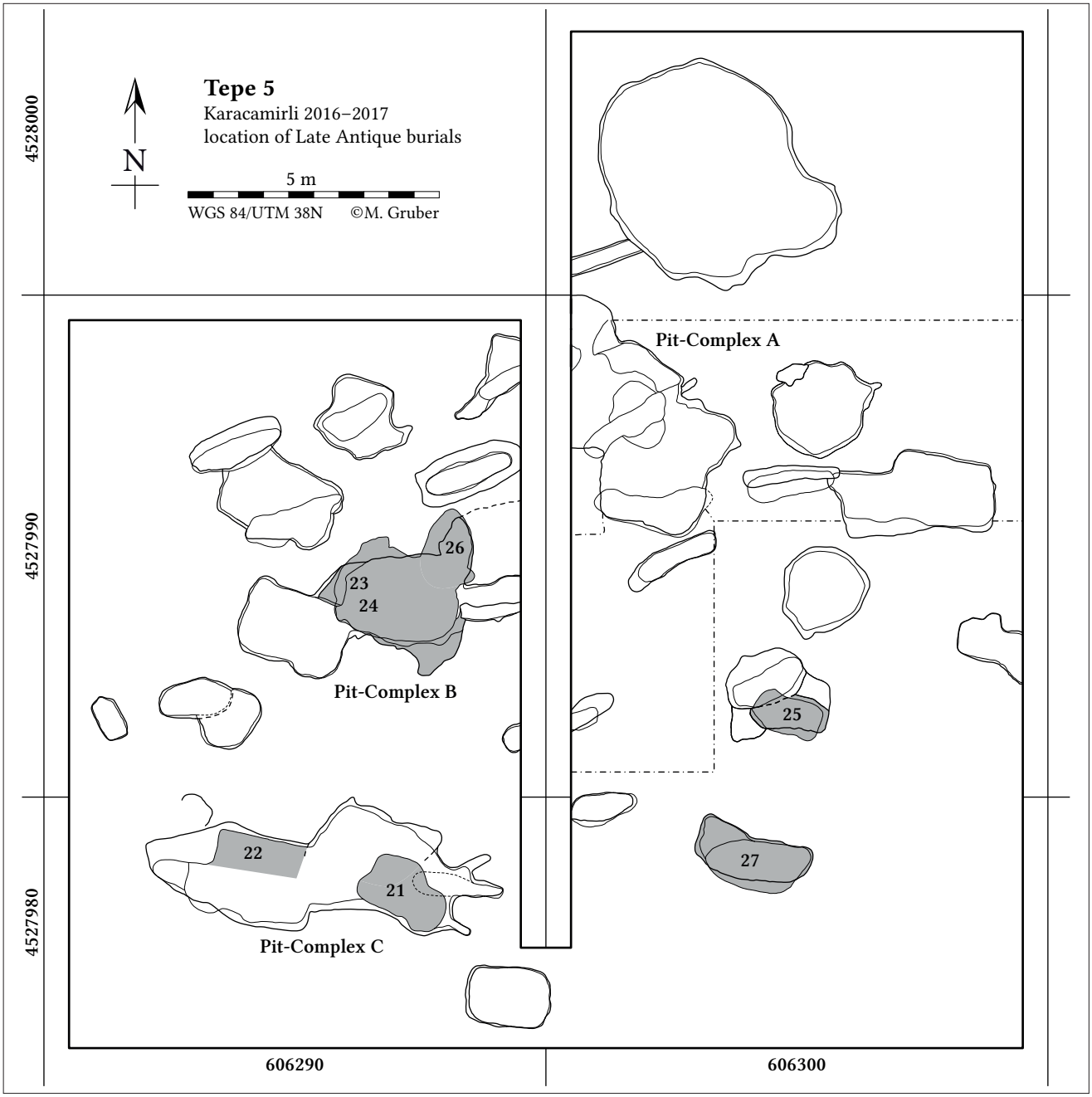

Fig. 31. Location of Late Antique burials

The first half of the 4th cent. AD marks another fundamental change in the Caucasus: the Christianization. Even though the roots of Christianity in the southern Caucasus are supposed to date back to the Age of the Apostles (Bais 2001: 104–105), the successive conversion of the ruling families in Armenia, Iberia and Albania were of particular importance for its persistent diffusion (Rapp 2014a: 2). By the middle of the 4th cent. AD Urnayr, ruler of Albania at the time of Shapur II, was baptised (Bais 2001: 106), providing an incisive impetus for the gradual progress of Christianization in Albania.

IV.3.2 Regional Context

In Azerbaijan the 3rd and 4th cent. AD is understood as part of the »Early Medieval« period, which ranges from the 3rd to the 10th cent. AD (Ахундов 1986; Məmmədov 2006). The material culture of the Late Antique period in north-western Azerbaijan is insufficiently studied, and it is therefore still difficult to distinguish finer chronological stages between the Antique and the Medieval periods solely on the basis of archaeological finds (for an overview of relevant sites see Xəlilov 2008).

Worth mentioning are the excavations of a settlement (Sudaghilan or Settlement no. 2) at Mingachevir, the earliest occupation level of which was dated to the 3rd–5th cent. AD (Ваидов 1954; 1961: 151). In the course of the construction of the BTC/SCP pipelines some possible remains from the Late Antique period were detected in the wider surroundings of Karacamirli: At the sites Lak I and Lak II pottery indicates occupation in the 2nd–5th cent. AD and in the 4th–8th cent. AD (Dostiyev 2007a; Agayev 2007). Various burials were discovered at Hajialili III (Dostiyev/Mammadov 2008) and Dashbulag (Nəcəfov et al. 2007). More substantial were the finds at Chaparli, where several burials were discovered which were dated either to the 2nd–3rd cent. AD (Aşurov 2008a: 201) or to the 3rd–4th cent. AD (Aşurov 2008b). These burials were sumperimposed by a building that is believed to be a Christian Albanian chapel of the 4th–5th cent. AD.

In the immediate vicinity of Tepe 5 possible Late Antique settlement remains were discovered at Uzumlu Tepe, near Bitdili, 6 km west-south-west of Tepe 5. Limited excavations there revealed the remains of an »Early Medieval« settlement with a possible earlier occupation in the Antique period (Кесаманлы et al. 1978a: 499; 1980: 8). A similar occupational sequence is suggested for Qanli Tepe, a part of the Bulaqbashi excavation north of Yeniabad and Kür on the right bank of the Kura river (Кесаманлы/Джафаров 1979: 11; Кецушов/Аббасова 1987; Abbasova 2003). Noteworthy is the attestation of sherds decorated with parallel thin white lines (Кецушов/Аббасова 1987: 12 Pl. 5, 3; Аббасова 1988: Pl. 7, 4; Abbasova 2003: 66 Pl. 55, 4), identical to ceramic material found in the post-Achaemenid occupation levels at Ideal Tepe and Gurban Tepe (Babaev et al. 2006: 317 Fig. 36). Contrary to the dating of the excavators, who proposed a date in the 7th–9th cent. AD, this pottery decoration is typical for the final 4th and 3rd–2nd cent. BC (Ludwig 2010: 98–100. 113). The »Early Medieval« occupation at Qanli Tepe, for which a date from the 1st to the 4th cent. AD was proposed, was heavily destroyed by later burials. A third site with a possible occupation during the »Early Medieval« period was discovered at Ali-Godja II in the now flooded area immediately west of the Yenikand dam (Гусейнова/Алиев 1992).

IV.3.3 General description of burials and grave contents

Seven burials at Tepe 5 can be attributed to the Late Antique period either through their radiocarbon dates (see ch. IV.3.4) or their grave contents (see below). The location of the burials (Fig. 31) did not reveal any particular pattern, except for the fact that six of them were cut into Late Bronze/Early Iron Age burials and caused substantial damage to them. This seemingly regular pattern might indicate, that the Late Bronze/Early Iron Age burials were marked at the surface – perhaps with stones or small embankments as it was, for example, observed at Zayamchay (Müseyibli/Nəcəfov 2019: 175–180), so that the people in the Late Antique period were still able to recognize their location. Although this practice had destructive effects on the Late Bronze/Early Iron Age burials, it could emphasize at the same time an awareness of the Late Antique population for these earlier interments. Moreover, the significance and appreciation of earlier artefacts – though apparently selective – is exemplified by the re-used obsidian arrowhead (0502) in Burial 21 that most likely originated from the disturbed adjacent Late Bronze Age Burial 1.

The Late Antique grave-pits were rectangular or oblong oval in shape (Table 5). The orientation of the grave-pits varied (Fig. 32): Burials 21, 25 and 27 were within the range from east-west and north-west to south-east. The outline of the Burials 23 and 24 in the Pit-Complex B could

burial	sex	shape of grave-pit	orientation of grave-pit	position of skeleton	position of head and line of sight	orientation of skeleton
21	(♂)	rectangular (?)	126°–306°	left side, flexed	NW	~318°
22	n. d.	rectangular (?)	n. d.	n. d.	n. d.	n. d.
23	(♂)	n. d.	n. d.	left side, flexed	NE (facing SSE)	64°
24	n. d.	n. d.	n. d.	back(?), flexed	S(?)	169°(?)
25	♂	rectangular	104°–284°	left side, flexed	NW (facing NE)	280°
26	(♀)	oblong oval	7°–187°	right side, flexed	S	~190°
27	(♂)	oblong oval	98°–278°	left side, flexed	W (facing N)	287°

Table 5. General features and orientation of grave-pits and skeletons of Late Antique burials (see also Table 2)

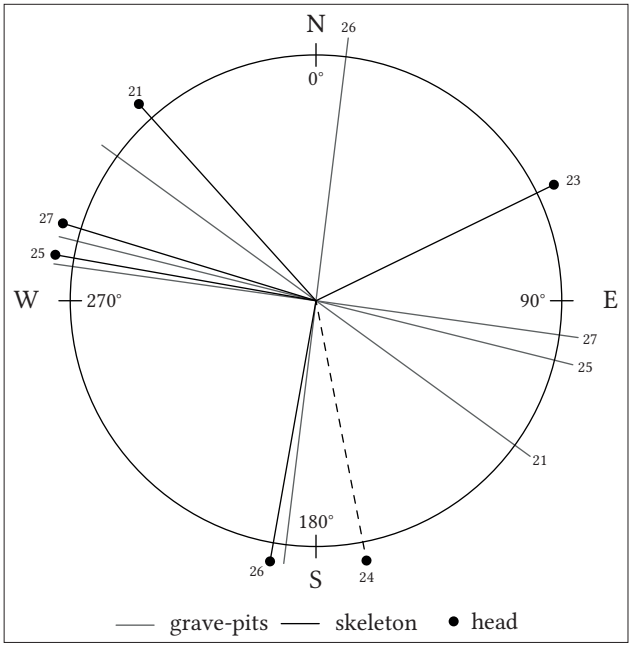

Fig. 32. Orientation of the grave-pits and skeletons in the Late Antique period

Fig. 33. Typical black coloured stains on a Late Antique vessel from Burial 25 (0209-01)

not be determined. The skeleton of the former was placed with its head in the south-east, facing south-south-east. Burial 26 differed significantly in its orientation and was possibly only comparable to Burial 24, which, however, was not preserved well enough to determine the exact position of the upper body. Whether the orientation of Burial 26 is associated with the probably female sex of the buried individual remains speculative, as the number of burials is small. However, Burial 26 also held the only individual placed on the right side with flexed legs. The individuals in Burials 21, 23, 25 and 27 all rested on the left side with their legs flexed. The position of the skeleton in Burial 24 was inconclusive, even though the pelvic area suggested it was placed on its back.

burial	sex	grave contents							fill							
		human skeleton	animal bones	ceramic vessels	iron objects	finger ring	bronze objects	obsidian arrowhead	obsidian flakes	ceramic sherds	spindle whorl	frit beads	carnelian beads	bronze objects	iron fragments	mollusc
21	(♂)	1	1	1	1			1	4			9	1	1		
22	?	1														
23	(♂)	1	1	1					12	4	1	1			11	1
24	?	1														
25	♂	1		1	2	1								3		
26	(♀)	1		1					3							
27	(♂)	1		1	1	1	1									

Table 6. Type and number of objects found in Late Antique burials and in their fill (see also Table 3)

Regarding their grave contents the Late Antique burials present a coherent picture (Table 6). Three or four burials contained a trefoil jug (Burials 21, 25(?), 26, 27). Besides some minor difference in their fabric, all vessels had more or less the same general appearance, i. e., the same reddish coloured fabric and in particular the distinctive black colour stains on the surface (Fig. 33). The same features applied to the large, two-handled pot in Burial 23 and allowed the attribution of this burial to the Late Antique period. Both vessel types and the reddish colour are, for example, attested at the more or less contemporary site of Sudaghilan at Mingachevir (Ваидов 1954: 129 Fig. 58. 62; 1961: 152–153). Burial 24 was dated to the Late Antique period due to its stratigraphic relation with Burial 23 (see the detailed description). Burials 21 and 23 contained bones of a sheep or goat – in case of the former in direct association with an iron blade (0514). The handle of an iron knife or dagger was also found in Burial 27 (0471). Further iron fragments were discovered in Burial 25 and a large amount in the fill of Burial 23. Particularly noteworthy are two finger rings worn by the individuals in Burials 25 and 27. The bronze finger ring in Burial 25 bore an undecorated stone (0211), whereas the finger ring in Burial 27 was made of silver and had the half of a frit bead as inlay (0470). The obsidian arrowhead in Burial 21 was re-used as a burial gift and originated probably from Burial 1 (see above).

In the fill of the grave-pits numerous obsidian flakes were encountered, which are probably related to the Chalcolithic pits (ch. III). The many beads found in the fill of Burial 21 can be explained by the disturbance of the adjacent Burial 1. This also applies to the bronze objects found in Burial 25 which certainly originated from the Late Bronze/Early Iron Age Burial 9 that was almost

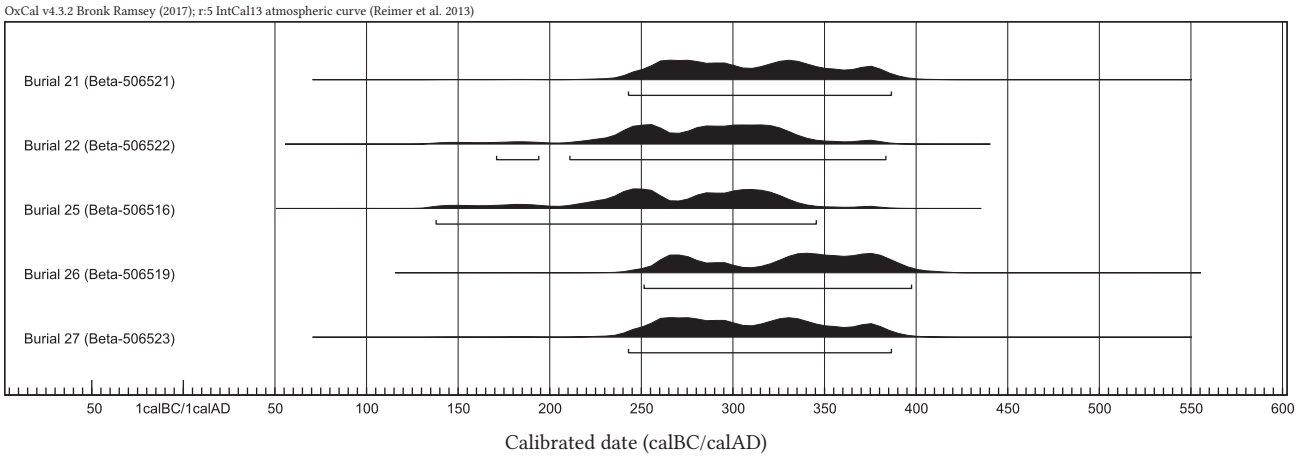

Fig. 34. Radiocarbon dates of Late Antique burials

burial	laboratory-nos.	Individual	material	conv. ^{14}C age (BP)	cal. age 2σ (95.4%)	cal. age 1σ (68.2%)
21	Beta-506521	KG-074-0507	bone	1730 ± 30	(95.4%) cal AD 242–386	(41%) cal AD 254–302 (25%) cal AD 314–346 (2.2%) cal AD 372–376
22	Beta-506522	KG-095-0496	bone	1760 ± 30	(93.1%) cal AD 210–383 (2.3%) cal AD 170–194	(47.7%) cal AD 274–330 (20.5%) cal AD 239–264
25	Beta-506516	KG-053-0208	bone	1770 ± 30	(95.4%) cal AD 138–345	(42.3%) cal AD 274–330 (25.9%) cal AD 230–264
26	Beta-506519	KG-066-0392	bone	1710 ± 30	(95.4%) cal AD 251–397	(52.7%) cal AD 325–386 (15.5%) cal AD 260–280
27	Beta-506523	KG-097-0455	bone	1730 ± 30	(95.4%) cal AD 242–386	(41%) cal AD 254–302 (25%) cal AD 314–346 (2.2%) cal AD 372–376

Table 7. Radiocarbon dates of Late Antique burials

completely destroyed by the Late Antique burial. The successive interments in the pit KG-057 (Pit-Complex B) created a similarly mixed fill that prevented the secure attribution of the artefacts to one of the three individuals (Burial 8, 23, 24), so all finds are assigned merely by convention to Burial 23.

IV.3.4 Radiocarbon dates

The radiocarbon dates from the five Late Antique burials revealed a maximum duration of c. 150 years between the mid-3rd and the late 4th cent. AD (Fig. 34; Table 7). The calibrated dates of Burials 21, 26 and 27 range within almost the same period of time, only Burials 22 and 25 appear to be of a slightly earlier date. Overall, it seems that in the Late Antique period Tepe 5 was used as a burial ground only for a rather short period of time. The chronological proximity of the burials is further reflected in their uniform characteristics, in particular of the ceramic vessels.

IV.4 Medieval Period

IV.4.1 Historical Background

The ruins of the medieval city of Shamkir are located c. 9 km east of the modern city of Shamkir and 14 km south-west of Tepe 5 on the left bank of the Shamkirchay. The fortified city of 28 ha consisted of a walled domestic quarter in the west and a citadel at its eastern end, controlling a bridge that spanned the river. The proximity of Tepe 5 to Shamkir is fortunate, because the city is mentioned in numerous historical documents, that shed some light on the historical circumstances in its vicinity for the period 1280–1420 AD, when the Tepe 5 cemetery was in use. For much of this period, Shamkir was a border town between the predominantly Christian kingdom of Georgia and the Muslim dominions to the south and east.

In the closing years of the 12th cent. AD, Georgian forces under Queen Tamar (r. 1184–1213) were in the offensive against Ildegizids and Seljuks, winning Shamkir in 1195 and Ganja in c. 1205 AD. The year 1220 marked the first of a series of Mongol raids, following up on their devastation of Khwarezmia (Rayfield 2012: 112–119). The region of Ganja played an important role as Mongol base. In the following volatile situation, a temporary retreat of the Mongol army beyond the Amu Darya offered the Khwarezmian ruler Jalal ad-Din (r. 1221–1231) an opportunity to invade Georgia himself and capture Tbilisi in 1226 under great losses to the population (Fähnrich 2010: 234; Rayfield 2012: 123–124). The final Mongol conquest took place in 1235, when Chormaqan Noyan set up camp in the Mughan Plain in Azerbaijan and besieged and destroyed Ganja in 1235 (the dates follow May 2010; see there on pp. 132, 134 and 139 for a discussion; Dashdondog 2011: 53). In 1239 a part of Chormaqan's army besieged Shamkir, destroyed the city and put all inhabitants to death (Kirakos Gandzaketsi 1986: 203–205; Bedrosian 1979: 22–27; Fähnrich 2010: 236). In 1240, the Caucasus was in Mongol hands or bound by treaties.

After the death of the Georgian queen Rusudan (1243) the succession to the throne was contested and the Mongols installed Rusudan's son Davit Narin (Davit VI, r. 1245–1293) and at the same time her nephew Davit Ulu (Davit VII, r. 1246–1270) as legitimate kings and both ruled Georgia together for a short period of time (Fähnrich 2010: 239; Rayfield 2012: 127–128), before they joined the repeated revolts of Georgian nobles against the Mongol rule (Fähnrich 2010: 240–241). Nevertheless, due to disagreements between the two Georgian kings, Davit Ulu decided to negotiate with the Mongols of the newly established Ilkhanate and despite his previous insubordination was reinstalled as vassal king of Eastern Georgia, while Western Georgia remained in the hands of Davit Narin and became increasingly independent from the Mongol suzerainty. The Caucasian regions contributed actively to the Ilkhanate's wars, in the Levant, in Mesopotamia as against the Golden Horde, thereby gaining greater autarchy. Hand in hand with the disintegration of the Ilkhanate local powers reasserted themselves. In 1334, a Georgian kingdom was reunited under Giorgi V, the Brilliant (r. 1299–1302 and 1314–1346), who ushered in a short period of consolidation and stability (Lang 1955; Fähnrich 2010: 249–252; Rayfield 2012: 139–145). In the year of his death the plague, which spread probably along the Mongol trade routes over Asia, Middle East, Europe and Northern Africa, reached Georgia and drastically decimated its population (May 2017: (vol. 2) 8–10). Little is known from the years of Davit IX's reign (r. 1346–1360). The plague continued into the early years of Bagrat V (r. 1360–1393), who allied himself in 1385 with the Golden Horde to face a new threat, that was to bring yet more misery to the Southern Caucasus: the invasion of Timur.

From 1386 until 1404 the region suffered eight invasions by Timur (Fähnrich 2010: 252–256; Rayfield 2012: 147–152). In the Southern Caucasus states, only Shirvan, bordering the Ganja region in the east, appears to have emerged largely unscathed, thanks to diplomatic manoeuvring under Shah Ibrahim I (r. 1382–1418). In 1401, Giorgi VII (1393–1407) desperately negotiated the truce

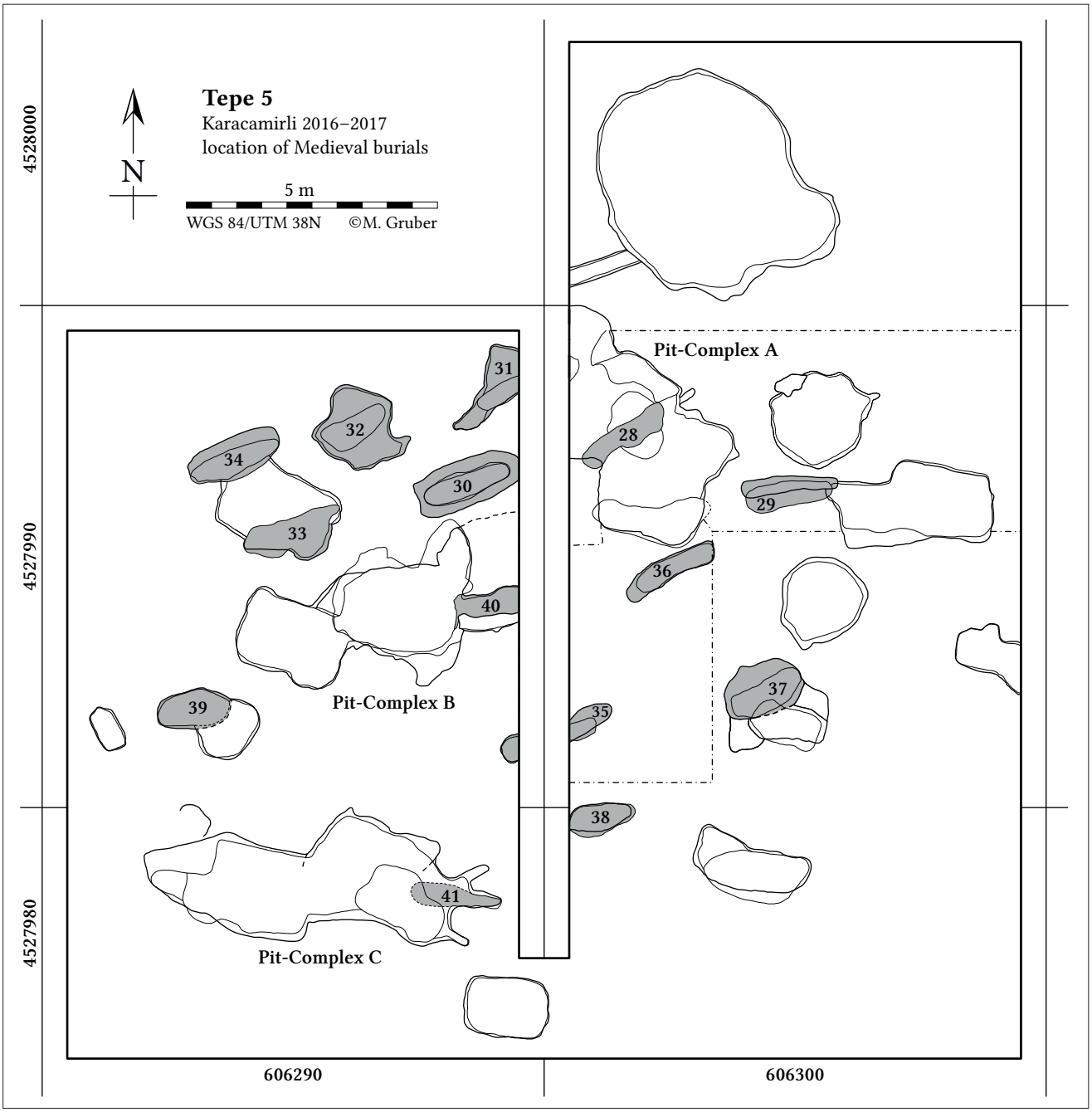

Fig. 35. Location of Medieval burials

of Shamkir, which again appears as a frontier town, with Timur, who agreed to guarantee the safety of Georgia and its ruler in exchange for an annual tribute, troops, and free transit for Timurid armies. Nevertheless, Timur invaded Georgia two more times before he left the Caucasus in 1404. Not more than six years later, in 1410, another advancing power beckoned from the south, the Qara Qoyunlu (Black Sheep Turcomens) who had captured Armenia and threatened the settlements in the Kura valley. Thanks mostly to another energetic Georgian monarch, Alexander I, the Great (r. 1412–1442), their excursions were limited in extent to the provinces of Samtskhe and Kartli.

IV.4.2 Regional Context

Besides Shamkir, the main centre of the Medieval period in the region (Авалов 2008; Dostiyev 2008; 2009; 2012), a number of contemporaneous smaller settlements were

burial	sex	shape of grave-pit	orient. of grave-pit	position of skeleton	position of arms	position of head and line of sight	orient. of skeleton
28	♂	narrow, oblong	55°–235°	back, straight	n. d.	(SW)	215°
29	♂	narrow, oblong	80°–260°	right side, straight	crossed in front of stomach	WSW (facing S)	260°
30	♀	narrow, oblong	69°–249°	back, straight	n. d.	SW (facing E)	249°
31	(♀)	narrow, oblong	54°–234°	right side, straight	flexed in front of face	SW (facing SSE)	234°
32	n. d.	oval, oblong	48°–228°	right side, straight	placed in front of stomach	SW (facing SE)	228°
33	♂	narrow, oblong	68°–248°	right side, straight (one leg flexed)	placed in front of stomach	SW (facing SE)	248°
34	♂	narrow, oblong	63°–243°	right side, slightly flexed	placed in front of stomach	SW (facing SE)	243°
35	(♂)	narrow, oblong	67°–247°	n. d., straight	n. d.	SW (facing SE)	247°
36	♂	narrow, oblong	63°–243°	right side, slightly flexed	placed in front of stomach	SW (facing SE)	243°
37	(♂)	oval, oblong	61°–241°	back, straight	crossed in front of chest	SW (facing E)	241°
38	(♀)	oval, oblong	74°–255°	back (slightly turned right), slightly flexed	placed in front of chest	SW (facing SE)	255°
39	♂	oval, oblong	83°–263°	back (slightly turned right), straight	placed in front of chest	W (facing SE)	263°
40	n. d.	narrow, oblong	86°–266°	n. d., straight	n. d.	W (facing SE)	266°
41	♂	narrow, oblong	101°–281°	right side, slightly flexed	placed in front of stomach	WNW (facing SW)	281°

Table 8. General features and orientation of grave-pits and skeletons of Late Antique burials (see also Table 2)

discovered in its surroundings. The most substantial settlement remains in the vicinity of Tepe 5 are located c. 2.5 km north at Muncuqlu Tepe, in the now flooded area immediately west of the Yenikand dam. Muncuqlu Tepe was a fortified settlement at the right bank of the Kura river, presumably founded in the 9th cent. AD and – as suggested by thick ash layers – destroyed by the Mongols in the 14th cent. AD (Алиев 1987; Алиев/Велиев 1985: 63; Abbasova 2003: 91). Domestic structures constructed of stone and burnt bricks, tandirs, brick paved floors and storage pits indicate a sophisticated settlement structure. An Arabic stone inscription, seemingly found at the site, was dated to the mid-11th cent. AD (Nemətova 2008). The nearby settlement of Ali-Godja II also revealed remains of the 12th and 13th cent. BC (Кәсәмәнлы/Чәфәров 1977: 17; Кесаманлы et al. 1980: 9; Алиев n. d.: 2).

Another Medieval settlement was detected during the work on the BTC-pipeline at Dashbulaq, c. 16 km west of Qaracamirli. The site was characterized primarily by numerous tandirs and storage pits. The pottery appears to be slightly earlier than the burials at Tepe 5, and was dated tentatively to the 9th–12th cent. AD (Nəcəfov et al. 2007; Hüseynov/Cəlilov 2008).

A number of other Medieval sites were excavated along the pipeline corridor between Ganja and Tovuz (Maynard 2011). In most cases, however, the archaeological remains consisted only of pottery layers or stray finds. This group of sites includes Hajialili I (Dostiyev 2006), Hajialili II (Mammadov/Agayev 2007) and c. 5 km south-east of Tepe 5 the site of Seyidlar (Huseynov et al. 2007). At Garajamirli II, south-east of the modern village, a coin of the 9th cent. and pottery of the 11th and 12th cent. AD were found (Dostiyev 2007b). More substantial were the excavations at Fakhrali (Jalilov/Kvachidze 2007) and Hajialili III (Dostiyev/Mammadov 2008), where tandirs, storage pits and pottery of the 9th

to 12th cent. AD have been discovered. In addition, excavations in 1976, c. 800–900 m north of the Early Iron Age site of Bitdili (Yeniabad) revealed a small settlement with remains of tandirs and a stone wall. The glazed and unglazed pottery was dated to the 13th and 14th cent. AD (Кесаманлы/Джафаров 1979: 11).

Traces of a Medieval settlement were located just c. 650 m north of Tepe 5 during our survey in the Karacamirli area between 2013 and 2017 and referred to as Tepe 6 (Babaev et al. 2016; Babaev et al. in print). The hill covered an area of c. 230 × 100 m and the surface pottery dates to the Medieval period.

Cemeteries of the Medieval period comparable to, but slightly earlier than Tepe 5 were excavated at Zayamchay and Chaparli. At Zayamchay, near a Medieval bridge, 74 burials were excavated. The deceased were placed according to Muslim funerary practice with their head facing towards Mecca. Although it is difficult to provide a secure date, the occurrence of beads in two graves might indicate an early date, perhaps within the 8th–10th cent. AD (Müseyibli/Kvachidze 2006: 7–8).

The burials at Chaparli were interred within the remains of an Albanian chapel (Aşurov 2008a; 2008b). Of particular interest are some differences in the placement of the bodies that might be linked with different religious practices (see below). Two radiocarbon dates allow to date the cemetery to a minimum timespan between the late 9th and the mid-12th cent. AD. In the southern area, above the burials, a stone structure was found associated with glazed pottery dated to the 11th and 12th cent. AD.

IV.4.3 General description of the burials

The burials of the Medieval period were arranged in a consistent pattern that was superimposed on the earlier burials without respect to their position (Fig. 35). All burials were characterized by a uniform orientation and shape of the grave-pit (Table 8; Fig. 38). The latter was regularly oblong and very narrow. Only in a few instances (Burials 30, 31, 32, 37) was the outline of the grave-pit enlarged on a higher level, perhaps to facilitate the placement of the body. In the narrow grave-pits the orientation of the skeletons, with their heads in the south-west, matched the orientation of the pits; they all ranged between west/south-west to east/north-east. The sole exception was Burial 41, the skeleton of which had a west-north-west to east-south-east orientation. Noteworthy are the grave-pits of Burials 29 and 35, as they were not dug vertically into the ground, but with a slanting axis towards the south (see Fig. 154).

Fig. 36. Burial 29 (KG-031) with an individual placed on its right side (first group)

Considering the position of the skeletons, arms and the placement of the head, some internal distinctions allow to define two different groups:

In seven instances the body was placed on the right side (Burials 29, 31–34, 36, 41) and in two more it was at least slightly turned towards the right (Burials 38 and 39). The legs were either straight or slightly flexed – in Burials 33 and 38 the left leg was straight and the right leg slightly flexed. In this first group of burials, the heads of the deceased were turned sideways to allow for a line of sight towards the south-east. The arms were crossed or – if it cannot be determined more precisely – placed in front of the abdomen or, in one case (Burial 39), on the chest (Fig. 36). Similar body positions were observed in the cemeteries in Zayamchay and Chaparli, where they

Fig. 37. Burial 37 (KG-052) with an individual laying on its back with stretched legs (second group)

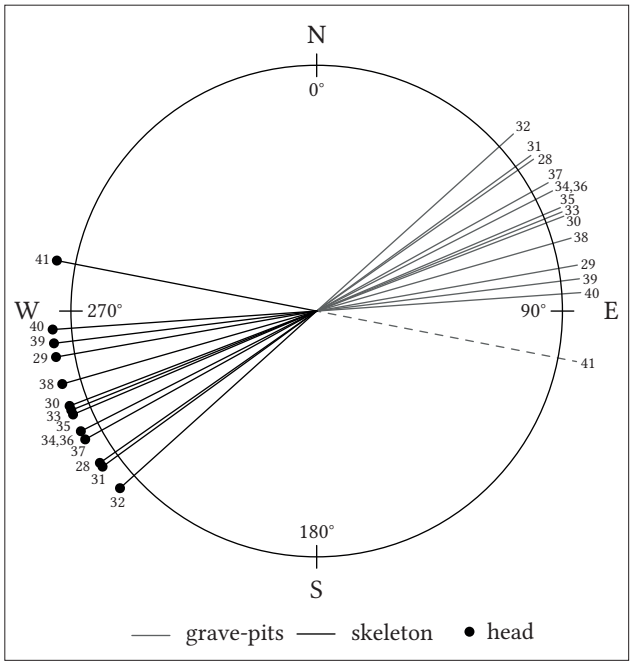

Fig. 38. Orientation of the grave-pits and skeletons in the Medieval period

were associated with Muslim funerary practices (Müseyibli/Kvachidze 2006: 6; Taylor/Maynard 2011).

The second group was considerably smaller and consisted of Burials 30 and 37. In these two instances the deceased were placed on their backs with stretched legs (Fig. 37). In both burials the head was supported and slightly bent upwards, so that it faced towards the east. This body position is comparable to some burials at Chaparli, which were tentatively interpreted as Christian (Aşurov 2008b: 6. 8; Taylor/Maynard 2011).

The skeletons in Burials 28, 35 and 40 were only partially preserved, but the lateral position of the skull in Burials 35 and 40 suggests that they belong to the first group, whereas the straight position of the legs in Burial 28 would place it closer to the second group.

Although, at first, it is tempting to assume that each burial group represents a different chronological period, the radiocarbon dates taken from both groups (Table 10) confirm they were interred within the same timespan. A similar chronological proximity between potentially Muslim and Christian burials was suggested by radiocarbon dates at Chaparli, even though the entire cemetery is one to four centuries earlier than the one on Tepe 5 (Taylor/Maynard 2011). It is therefore conceivable, that members of both religions were buried side by side at Tepe 5. Given the historical circumstances of the Shamkir region between the Muslim Ildegizids and Khwarezmia in the south and the Christian Kingdom of Georgia in the north, the coexistence of both faiths is not surprising. At Shamkir, for example, the existence of an Albanian Christian community in the city and

burial	sex	grave contents				fill		
		human skeleton	beads	bronze disc	silver earring	obsidian flakes	burnt mud-brick	bronze objects
28	♂	1				1		1
29	♂	1		1		2		
30	♀	1						
31	(♀)	1						
32	n. d.	1				1		
33	♂	1				2		
34	♂	1						
35	(♂)	1					1	
36	♂	1				1		
37	(♂)	1				1		1
38	(♀)	1	24			1		
39	♂	1			1	1		
40	n. d.	1						
41	♂	1						

Table 9. Burials of the Medieval period with burial gifts (see also Table 2)

the continuation of their tradition is historically and archaeologically attested (Dostiyev 2016: 56–57). It is doubtful, whether the invasion of the Mongols changed the religions landscape, as they followed a policy of religious neutrality (May 2018). Even after the formation of the Muslim Ilkhanate various other religious groups continued to exist and wielded influence, including Caucasian Christians. At last, the truce between King Giorgi VII and Timur signed at Shamkir in AD 1401 (see ch. IV.4.1) calls for equal treatment of Muslims and Christians, even though another clause prohibited practicing of Christian religion on Muslim territory, suggesting a separation of both religious practices – the mere existence of this paragraph in the treaty might well imply that such a separation was up to that date not in effect.

The burials did contain only few finds (Table 9), which is in accordance with Muslim funerary practice. Nevertheless, burial gifts are occasionally attested, for example, at the Muslim cemetery at Zayamchay, where two burials contained beads. These occurrences might be related to pre-Muslim traditions or the influence of other religious practices (Müseyibli/Kvachidze 2006: 7–8).

At Tepe 5 adornments are attested in three burials of the first (potentially Muslim) group: The male individual in Burial 29 was accompanied by a small bronze disc (Fig. 154), the female individual in Burial 38 had a string of beads around her arms (Fig. 170) and the male individual in Burial 39 wore a silver earring on its right side (Fig. 172). The sex determination did not reveal any specific pattern in the presence of adornments between male or female individuals.

As with all other burials at Tepe 5, the fill contained obsidian flakes. The two bronze objects found in the fill of Burials 28 and 37 were likely displaced objects from the Late Bronze/Early Iron Age Burials 7 and 9, which were disturbed by the Medieval interments. A unique find was the fragment of a burnt mud-brick that was found high up in the fill of Burial 35.

IV.4.4 Radiocarbon dates

In total seven burials of the Medieval occupation phase were sampled for radiocarbon dating, with Burial 34 being dated twice. Six of the analysed burials belong to the first, potentially Muslim group. Burial 37 was assigned to the second, potentially Christian group. The results demonstrate that all burials were interred within a maximum span of time between AD 1280 and AD 1420 (Fig. 39; Table 10), suggesting that all burials, regardless of the

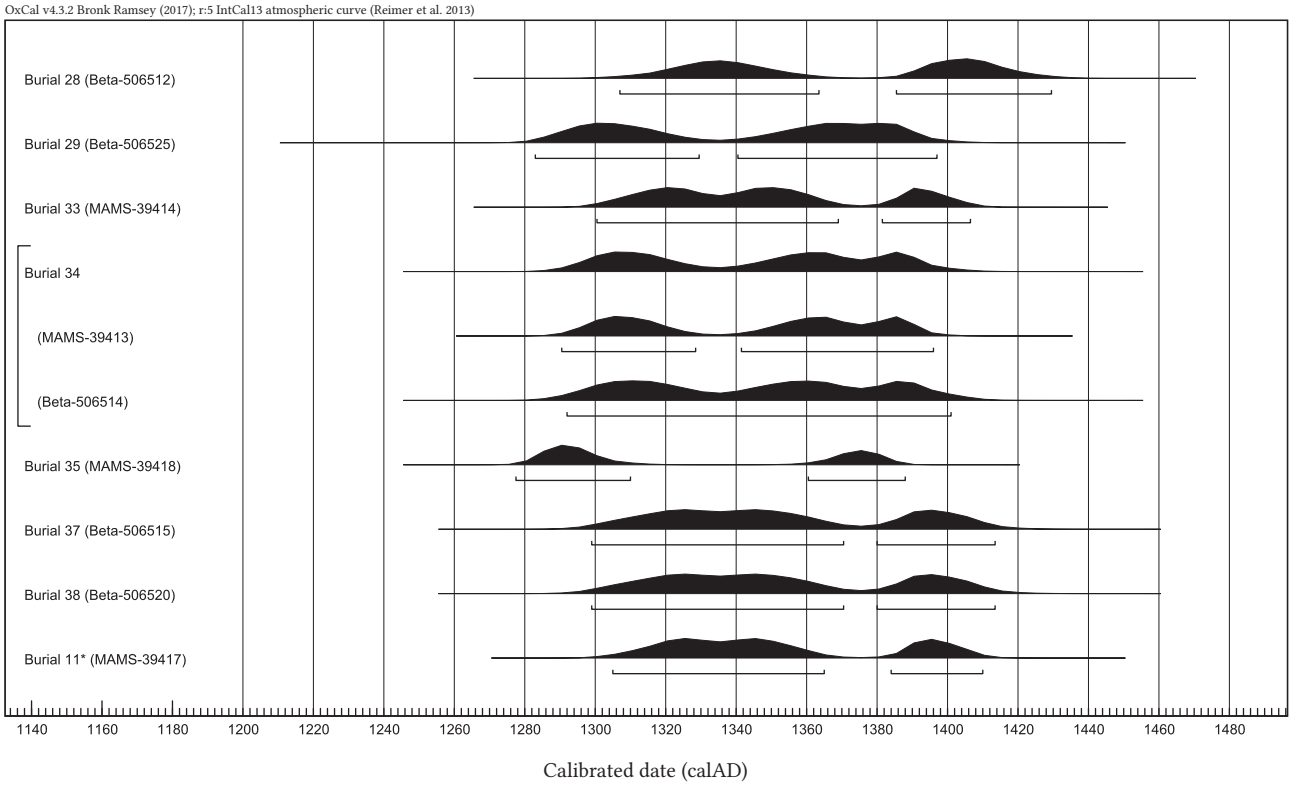

Fig. 39. Radiocarbon dates of Medieval burials; the sample MAMS-39417 was taken from a single human bone found loose in the fill of Burial 11

burial	laboratory-nos.	Individual	material	conv. ^{14}C age (BP)	cal. age 2σ (95.4%)	cal. age 1σ (68.2%)
28	Beta-506512	KG-027-0106	bone	560 ± 30	(50.1%) cal AD 1306–1363 (45.3%) cal AD 1385–1429	(34.3%) cal AD 1392–1416 (33.9%) cal AD 1322–1347
29	Beta-506525	KG-031-0120	bone	640 ± 30	(54.4%) cal AD 1340–1396 (41%) cal AD 1282–1329	(40.7%) cal AD 1355–1388 (27.5%) cal AD 1292–1316
33	MAMS-39414	KG-046-0192	bone	599 ± 20	(73.3%) cal AD 1300–1369 (22.1%) cal AD 1381–1406	(55.3%) cal AD 1310–1360 (12.9%) cal AD 1387–1398
34	Beta-506514	KG-048-0197	bone	620 ± 30	(95.4%) cal AD 1292–1400	(26.6%) cal AD 1298–1324 (26.5%) cal AD 1346–1372 (15%) cal AD 1378–1393
34	MAMS-39413	KG-048-0197	bone	628 ± 20	(38.0%) cal AD 1290–1328 (57.4%) cal AD 1341–1396	(27.3%) cal AD 1298–1317 (25.6%) cal AD 1354–1372 (15.3%) cal AD 1378–1389
35	MAMS-39418	KG-098-0467	bone	671 ± 20	(57.2%) cal AD 1277–1310 (38.2%) cal AD 1360–1388	(44.6%) cal AD 1284–1299 (23.6%) cal AD 1370–1380
37	Beta-506515	KG-052-0205	bone	590 ± 30	(67.9%) cal AD 1298–1370 (27.5%) cal AD 1380–1413	(51.5%) cal AD 1313–1358 (16.7%) cal AD 1388–1403
38	Beta-506520	KG-073-0508	bone	590 ± 30	(67.9%) cal AD 1298–1370 (27.5%) cal AD 1380–1413	(51.5%) cal AD 1313–1358 (16.7%) cal AD 1388–1403
11*	MAMS-39417	KG-029-0115	bone	589 ± 20	(69.7%) cal AD 1305–1365 (25.7%) cal AD 1384–1410	(53.6%) cal AD 1318–1353 (14.6%) cal AD 1390–1400

Table 10. Radiocarbon dates of Medieval burials

group to which they belong, are more or less contemporary.

In addition, a single vertebral arch (0115) found in the fill of the Late Bronze/Early Iron Age Burial 11 was analysed (marked with an asterisk). The calibrated radiocarbon date of the bone showed that it was not an integral part of the original burial, but belonged to a Medieval individual and is, therefore, a later intrusion of unknown origin.

IV.5 Undated burials

Five burials could not be assigned to one of the three occupation phases of the Tepe 5 cemetery, either because of their bad state of preservation or the lack of datable material (Fig. 41). Because of their low significance, no radiocarbon dating was attempted.

Burial 42 was cut into the edge of the Chalcolithic pit KG-016 and contained the badly preserved remains of an infant individual (Fig. 40).

Burial 43 had a substantial grave-pit, which, however, contained only few bones. Although it was apparently cut by the Medieval Burial 39, the lack of datable material prevented a secure dating.

Burial 44 was detected immediately below the modern surface in the topsoil and hence the preservation of bones was very poor. The deceased appears to have been placed in a west-east direction with the head in the west. This might indicate a Medieval date, but that remains speculative.

Fig. 40. Undated Burial 42 (KG-035) with an infant individual

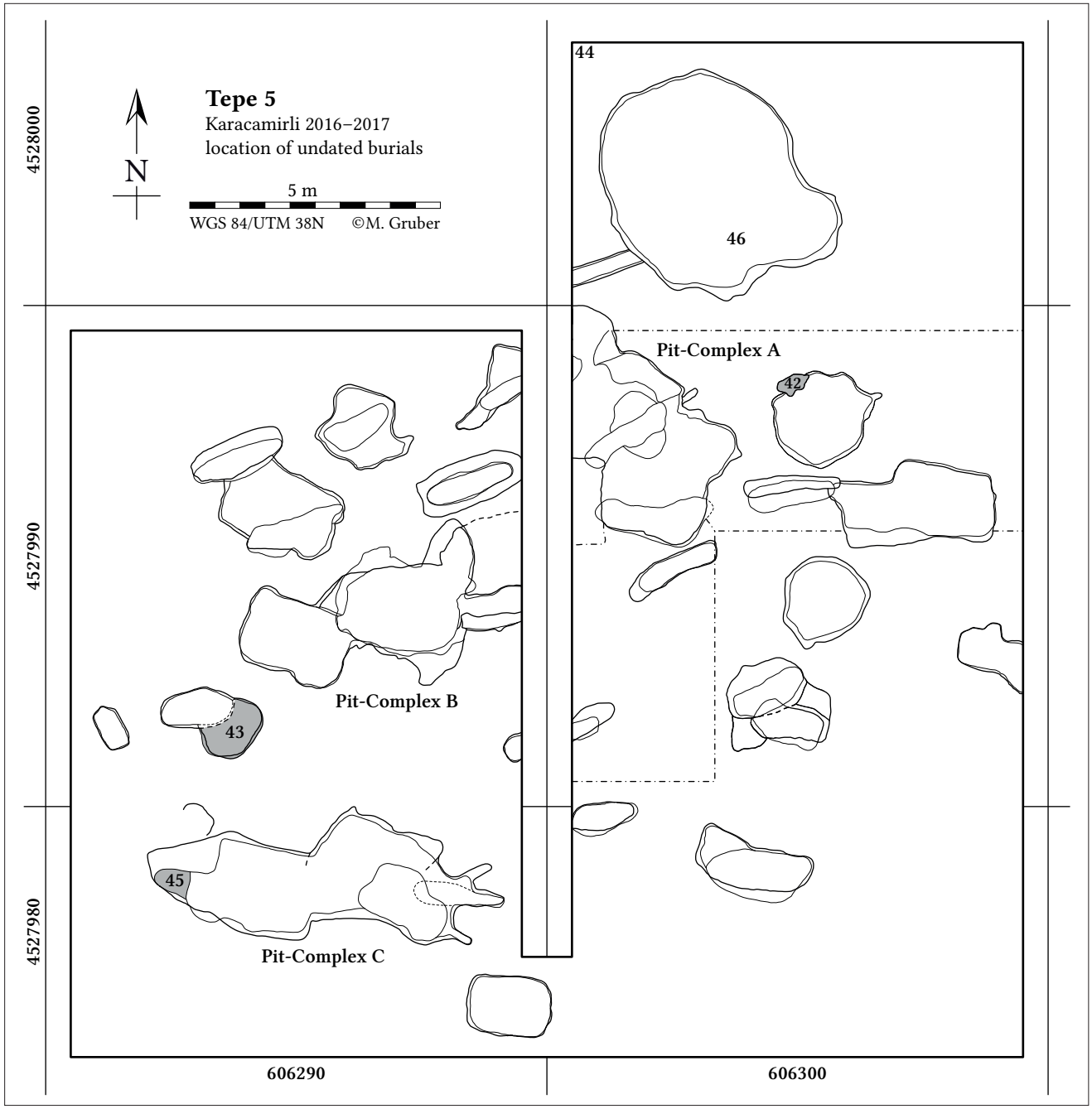

Fig. 41. Location of undated burials

Burial 45 was interred at the western end of Pit-Complex C and contained only some rib fragments and two teeth. The narrow width of the grave-pit might indicate a date after the Late Bronze/Early Iron Age, presumable a Medieval date, but the dating criteria are not conclusive.

Burial 46 subsumes a few dislocated bones found in the fill of the large pit KG-100. It is possible that these bones originate from a burial completely destroyed by the large pit (see ch. IV.7).

IV.6 Pit-Complexes

In the course of our excavations three large, irregularly shaped pits came to light that dominated the layout of the entire burial ground and contained several inhumations (Fig. 22). Although the on average larger grave-pits of the Late Bronze/Early Iron Age certainly formed the starting point of these pits, they were not multiple burials, but resulted from the successive interment of different burials very close together or intersecting each other

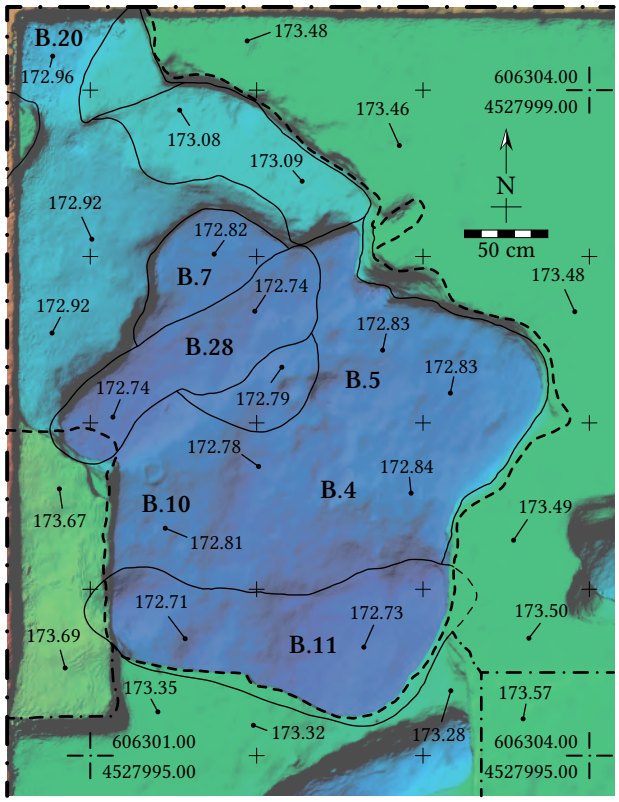

Fig. 42. Plan of Pit-Complex A

during all three periods of the cemetery. To distinguish them terminologically from grave-pits with multiple burials, we used the designation »Pit-Complex« for them.

All Pit-Complexes were filled with the identical homogeneous material as all other burials. In many cases it was therefore difficult to recognize the edges of later grave-pits that were cut into the fill of already existing burials.

IV.6.1 Pit-Complex A

Pit-Complex A occupied almost the entire north-west quadrant of square 6300/7990 (Fig. 42) and extended further west beyond the limits of the excavation (perhaps as far west as Burial 31). It comprised at least seven interments of different periods. In the central and eastern area of the pit were Burials 7, 4 and 5 of the Late Bronze Age. The grave-pit of Burial 5 caused the orthogonal edge in the east of Pit-Complex A, which suggests an originally rectangular outline of that grave-pit. The curved southern edge of Pit-Complex A resulted from the grave-pit of Burial 11 which slightly undercut the surrounding soil. Less well definable was the outline of Burial 10 along the south-western edge of the pit. The medieval Burial 28 was most likely the latest interment in Pit-Complex A. It disturbed Burial 7 in the central part. Burial 20 in the northernmost corner of the area is of unknown date. In contrast to all other burials it was delimited from the main part of Pit-Complex A by shallow elevations. The stratigraphic relation between this burial and the Pit-Complex is, however, equivocal. It might either have been cut through the northern corner of the existing northern part of Pit-Complex A or was disturbed by the latter. In the area between Burial 20 and Burials 7 and 28 no traces of interments were discovered. A peculiarity in that area worth mentioning is a shallow bench-like elevation along the north-eastern section. It is very likely that this part of the pit was never intended as a burial ground but resulted from a rubbish-pit of the Chalcolithic period that was completely destroyed by the repeated deposition of bodies in the surrounding burials. The existence of such a trash-pit is substantiated by several sherds that were found predominantly in the northern part of the fill of Pit-Complex A (contexts KG-018, KG-022 and KG-023) and are identical to the contents of the two excavated Chalcolithic pits nearby (see ch. III).

IV.6.2 Pit-Complex B

Pit-Complex B consisted of a series of interments in the south-eastern quadrant of square 6290/7990 (Fig. 43). The overall complex extended c. 5.5 m from west to east and varied between 1.5 m and 2.1 m in width. Its eastern part was occupied by the rectangular grave-pit of the Iron Age Burial 16. The bottom of that grave-pit was on a level c. 50 cm higher than that of the adjacent Burials 8, 23 and 24. These three burials constituted the central part of Pit-Complex B. The earliest of them was the Early Iron Age Burial 8, of which only few remains were left, because it was destroyed and pushed aside by the Late Antique Burial 23. In the course of this latter interment apparently also Burial 16 was disturbed, since joining fragments of a bowl were found scattered in both grave-pits. Probably very shortly afterwards, a second interment (Burial 24) was laid down directly atop the body of Burial 23. The outlines of the individual grave-pits could not be distinguished and therefore the following description is limited to the general layout of the entire pit (KG-057). It had a regular oval shape that was only interrupted in the north-east by the grave-pits of Burials 26 and 40. Noteworthy is a long, undercut section along its north-western edge right behind the skeleton of Burial 23, where displaced bones and sherds of Burial 8 were found. At a height of 173.25 m – c. 70 cm above the bottom of the grave – the outline of the grave-pit changed and was enlarged by irregular projections in the north-west

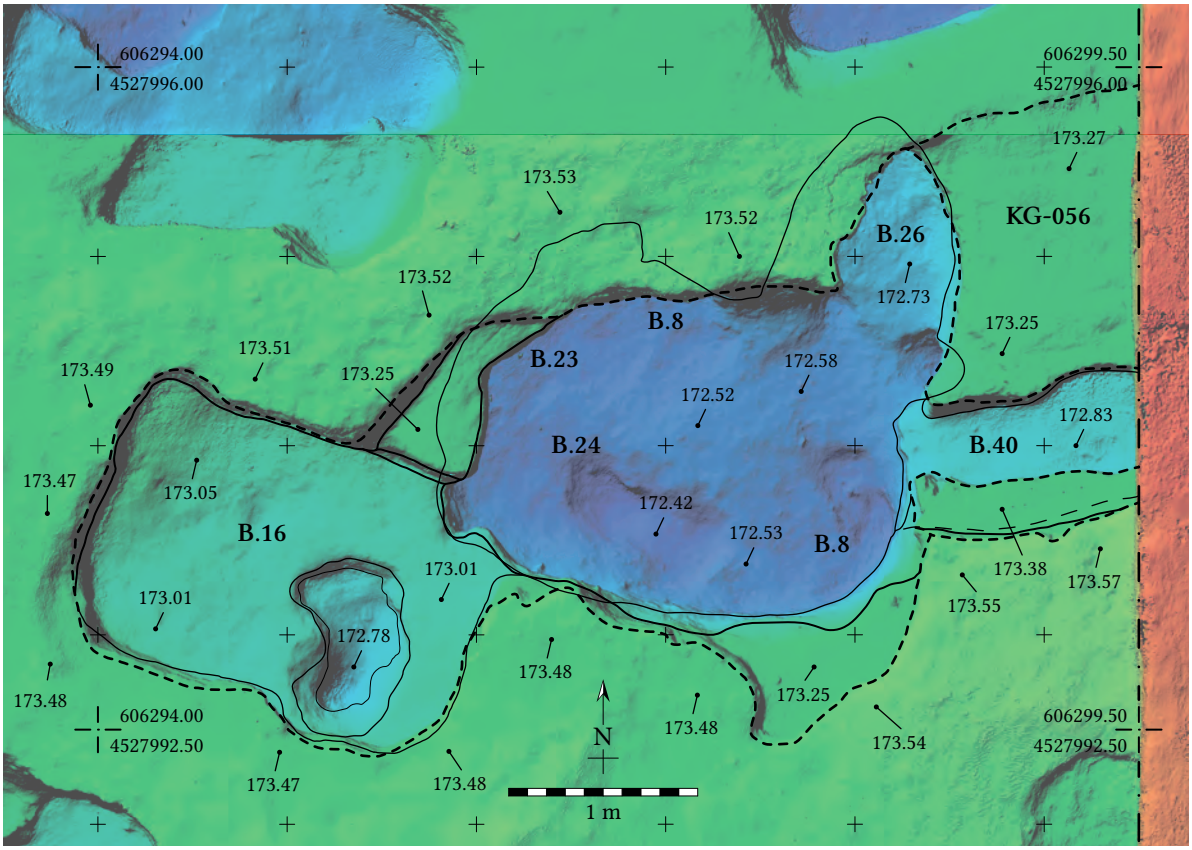

Fig. 43. Plan of Pit-Complex B

and south-east. These extensions might be connected with the process of digging the original pit or re-opening the area for the subsequent interments (see also Pit-Complex C-1). This might also be the case with the area between Burials 26 and 40 at the north-eastern end of Pit-Complex B that was dug down to a similar height of 173.25 cm but never used as a burial space. However, the filling material of that area (KG-056) contained a mixed assemblage with sherds that are similar to the pottery of the Early Iron Age and others to the Chalcolithic period, perhaps indicating another destroyed Chalcolitic pit in that area, which would also explain the high amount of obsidian in that area.

IV.6.3 Pit-Complex C

Pit-Complex C was located in the northern half of square 6290/7980 (Fig. 44 and Fig. 45). It had an irregular oblong shape and measured c. 7.1 m from west to east and 1.8–2.0 m from north to south. For the sake of clarity, the entire Pit-Complex was divided into four sections:

Section C-1 comprised the westernmost end of the Pit-Complex with the undated Burial 45. North of that burial a 1.3 m long and 45 cm wide part of the Pit-Complex was dug down only to a level of c. 173.13 m and thus c. 40–60 cm above the bottom of the adjacent burials. The reasons for this are unknown, but one might speculate if this was some sort of a working pit to facilitate the process of digging the actual grave-pit. Nevertheless, even in this case, it is not possible to determine to which burial such a working pit might have belonged.

Section C-2 contained the Late Bronze Age Burial 6 and the Late Antique Burial 22. The former occupied the southern part of this rectangular-shaped part of the Pit-Complex. Close to the northern edge were the remains of the Late Antique interment.

Section C-3 was shifted towards the north, creating a break in the alignment between Sections C-2 and C-3. It contained Burial 1, the oldest interment of Pit-Complex C, as well as of the entire cemetery, and the western half of the Late Antique Burial 21 that caused severe damage to the earlier interment. Because of this disturbance of Burial 1, many objects originating from it ended up in the fill of Burial 21 or – as can be shown in at least one instance – were reused as burial gifts.

The boundary between Sections C-3 and C-4 is less clearly defined due to the amorphous outline of that part of the Pit-Complex. Section C-4 includes the eastern part of Burial 21 and the Medieval Burial 41 that was at the

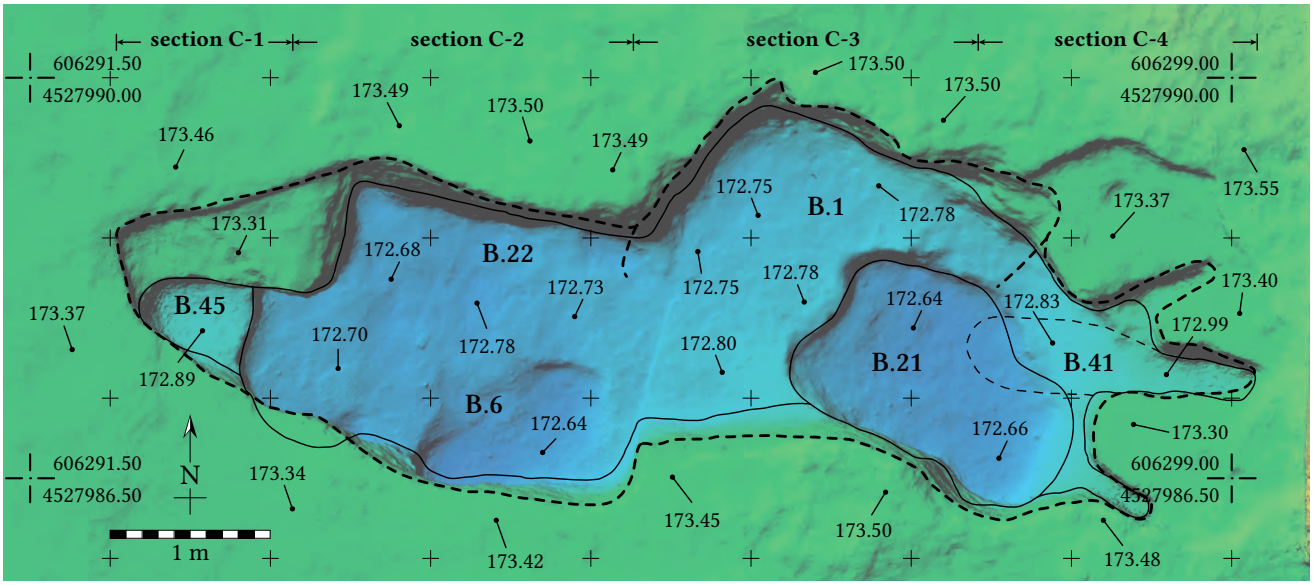

Fig. 44. Plan of Pit-Complex C

Fig. 45. Pit-Complex C with Burial 21 (KG-074) and remains of Burial 1 (KG-094)

same time the latest interment of the entire Pit-Complex. Burial 21 occupied the southern part of the section and was overlapped in parts by the Medieval interment that was placed in a very narrow grave-pit at the eastern edge of the Pit-Complex. Together with two more small oblong, but empty pits Burial 41 contributed to the finger-like appearance of the eastern end of Section C-4.

In total, the Pit-Complex C contained burials of all three occupation phases of the cemetery: Two of the earliest burials at Tepe 5 (Burials 1 and 6), two burials that can be assigned to the Late Antique period (Burials 21 and 22), the Medieval Burial 41 and the undated Burial 45.

IV.7 KG-100 and KG-101

In the southern half of square 6300/8000 a large roundish pit (KG-100) with a diameter between c. 3.8 and 4.3 m was excavated (Fig. 22). The perimeter had a protrusion in the south-east. The pit had been cut from an eroded surface down into the soil to a level at 172.78 m. Its bottom was virtually flat, with only a few irregular and deeper spots (down to 172.65 m). The filling was homogeneous and slightly softer than the surrounding soil. It contained a few pieces of burnt clay, 26 highly fragmented pottery sherds of unknown date (0479) and three obsidian flakes (0446, 0478, 0482). In the fill, c. 70 cm above the bottom, two displaced human bones were found (Burial 46). The general character is not that of a grave-pit, but rather of a more recently opened pit, perhaps in order to extract raw material. It is possible, that one or more burials of the cemetery have been destroyed during the digging of the pit and that some of the dispersed bones ended up in the fill. If this was true, the round protrusion at the south-eastern side of the pit could be the remaining original outline of one of those grave-pits, but this

remains speculation. Another possible source for the bones is the narrow pit KG-101 (Fig. 22) that appears to have been cut by the larger pit KG-100. Its bottom was reached at c. 173.30 m. The narrow pit was completely empty, though its shape and orientation somewhat resembled the other Medieval grave-pits and therefore it might originally have been one.

List of finds

KG-100-0446 (obsidian flake)
L: 28.5 mm; W: 18.0 mm; Th: 6.0 mm; Wt: 1 g
606305.098 E; 4528002.343 N; 173.146 m

KG-100-0478 (obsidian flake)
L: 15.5 mm; W: 13.0 mm; Th: 7.0 mm; Wt: <1 g
606305.206 E; 4528001.195 N; 172.952 m

KG-100-0482 (obsidian flake)
L: 19.5 mm; W: 11.0 mm; Th: 7.0 mm; Wt: 1 g
606301.585 E; 4528001.926 N; 173.062 m

IV.8 Stray finds

Totalling 192 examples, obsidian flakes were the most frequent category of small finds. Only a small fraction of them was retouched, however (e. g. 0413, Fig. 141, 6), and the majority were unworked splinters, perhaps production waste. Fig. 46 illustrates their distribution within the excavated area (the following finds are not shown in the map due to missing coordinates: 0037, 0044, 0063, 0069, 0092, 0190, 0457, 0481, 0500, 0505). Of the overall number of obsidian flakes, only two pieces can with some certainty be interpreted as intentional burial gifts, as they were found inside two pottery vessels in Burial 7 (0108, 0161 – both are not shown in Fig. 46). The remaining were all found loose in the fill of grave-pits or in the topsoil and subsoil layers.

The blue dots in Fig. 46 represent obsidian flakes found in the fill of grave-pits. These pieces are listed in the corresponding burial contexts. Orange dots indicate obsidian flakes found in topsoil or subsoil layers, as well as in contexts not assignable to a specific burial. The latter includes in particular, the contexts KG-018, KG-022 and KG-023 with Chalcolithic material in Pit-Complex A and KG-056 at the eastern end of Pit-Complex B (listed in ch. III). The distribution pattern demonstrates the correlation between obsidian flakes and grave-pits (in particular of the Late Bronze/Early Iron Age). Even the examples uncovered in the topsoil and subsoil layers, where the outline of burial pits was not yet distinguish-

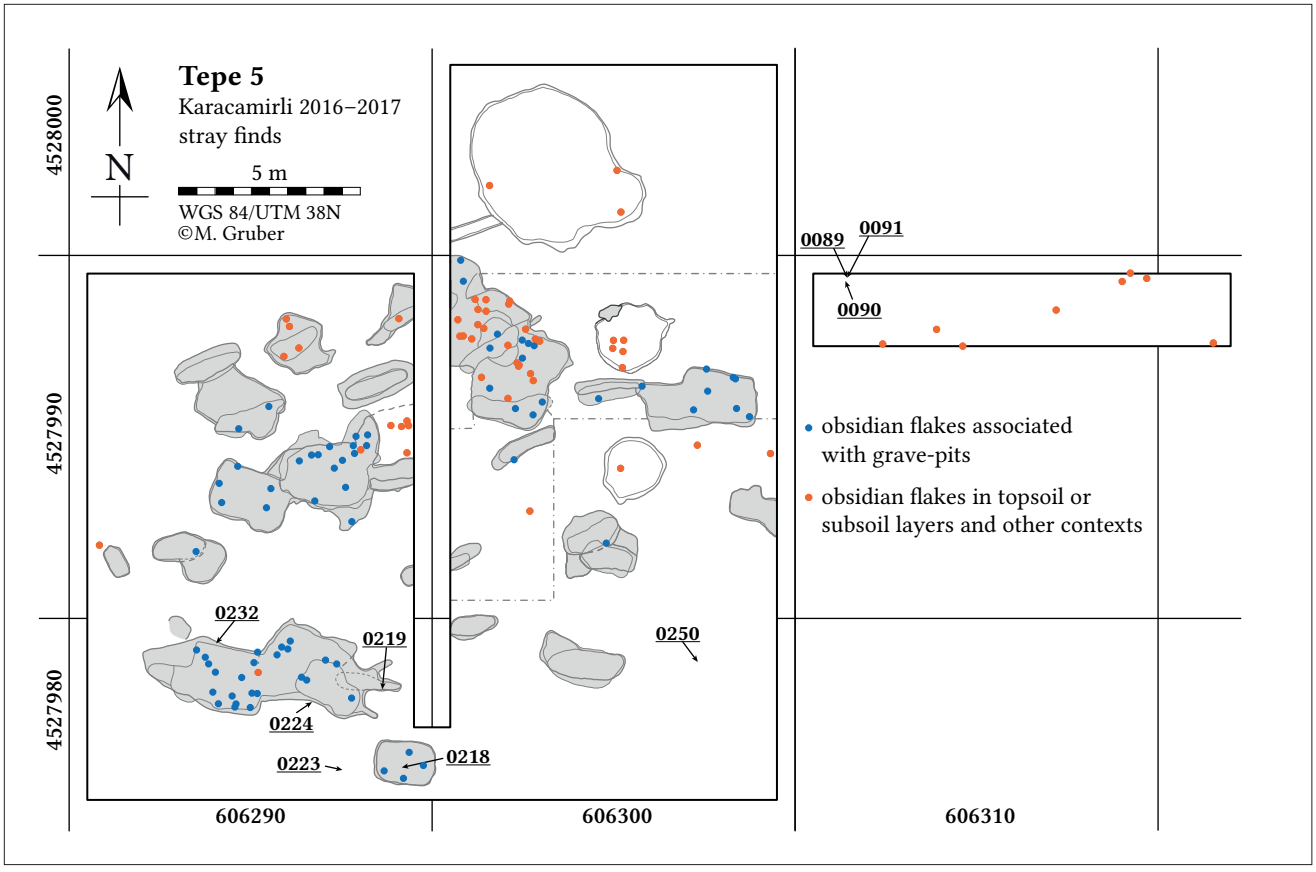

Fig. 46. Distribution of stray finds

able from the surrounding soil, were located above the burials. Only the trench at the eastern slope revealed a random distribution of obsidian flakes.

To better assess the nature of this distribution pattern and the taphonomy of the obsidian flakes, it is necessary to recall the character of the Chalcolithic occupation on Tepe 5 (ch. III). Considering the high density of obsidian in the Chalcolithic pits (40.6 % of the total amount), the material appears to have been in frequent use during this period and we can conclude, that the high overall density of obsidian flakes on Tepe 5 is likely related to the now eroded Chalcolithic level, from which the rubbish pits were dug. The stray finds in the trench on the eastern slope (Fig. 46) might well be displaced pieces from this eroded level.

At the time the Late Bronze/Early Iron Age burials were interred, the Chalcolithic settlement debris on the top of the hill may have been more substantial and it seems that it was here, that many of the obsidian flakes accidentally ended up in the grave-pit refill. While we cannot exclude, that the obsidian splinters were placed in the grave-pits deliberately, as is actually attested in Burial 7, we consider it unlikely, in the light of their unworked shapes, that they were specifically prepared for the funeral or brought to the burial site elsewhere. In all probability, the obsidian flakes therefore originate from the eroded deposits of the Chalcolithic occupation of Tepe 5.

Besides the obsidian flakes only few artefacts were discovered out of context in the topsoil and subsoil layers (Fig. 46). Most of them were located in the vicinity of Pit-Complex C and at least two bluish frit beads with applied knobs (0223, 0224) are probably linked with the disturbance of the Late Bronze Age Burial 1 by the Late Antique Burial 21 (for more details see Burial 1).

Similarly, two fragments of a bronze sheet (0218) found in the topsoil above the grave-pit of Burial 14 (Fig. 46) likely originate from this burial, as it contained many such bronze fragments (see Burial 14).

Two more finds originate from the area of the Pit-Complex C: a shapeless bronze fragment (0232) and the piece of a thick bronze wire (0219). Both finds could be related with the repeated interments and disturbances in the Pit-Complex C.

In the topsoil east of the Late Antique Burial 27 the fragment of a burnt mud-brick (0250) was discovered. Its fabric and colour were very similar to the mud-brick found in the fill of Burial 35 and therefore the piece is likely of Medieval date.

In the test trench at the eastern slope of Tepe 5 a tanged dagger (0089) with a separate fenestrated pommel (0091) was found loose in the subsoil (Fig. 47, 1–2).

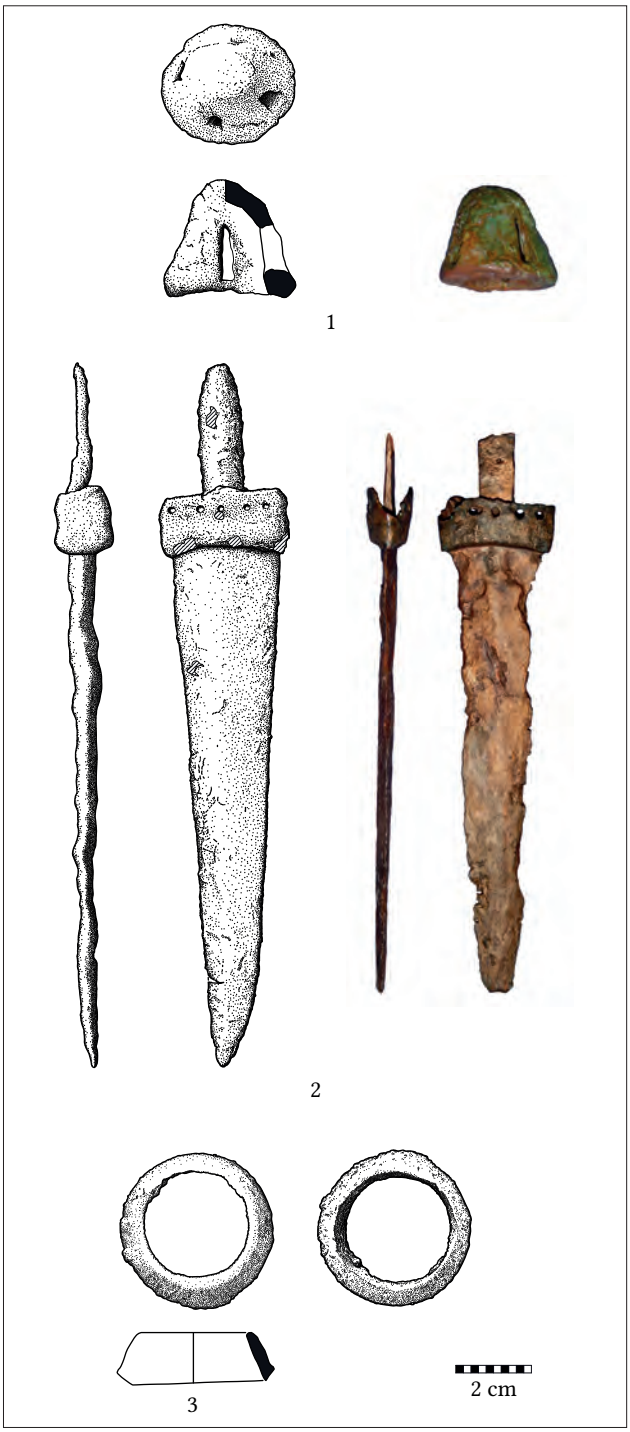

Fig. 47. Stray finds (KG-024): 1 – bronze pommel (0091; 2 – bronze dagger (0089); 3 – bronze ring (0090); the drawings represent the appearance of the dagger before its restoration (note that the tip of the blade and the tang were broken off and are not shown in the photographs)

The dagger was made of tin bronze (ch. VII). The blade was heavily corroded, but appears to have been lentoid or perhaps even slightly rhomboid in section. The tang was flat and thinning at its end. During restoration on

one side, a small hole was visible that wasn't completely drilled through the tang. Around the shoulders and tang an oval socket for the hilt was mounted that slightly protruded from the blade. The sockets' upper edge was pierced several times on both side by rivet-holes, which certainly served to fasten the handle, probably made of wood, to the dagger. The hilt was capped by a fenestrated pommel cast of bronze.

Right next to the dagger and pommel, a solid bronze ring of conical shape was discovered (0090, Fig. 47, 3). The proximity to the dagger suggests a direct connection between these objects, even though it is unclear whether it is an integral part of the dagger (e. g., around the wooden hilt) or perhaps a part of a scabbard or holster.

According to N. V. Minkevich-Mustafaeva such daggers appeared frequently in the developed stage of the Khojaly-Gadabay-Culture in all three sub-regions (Минкевич-Мустафаева 1962: 120. 125. 130). Hence, it is likely that the dagger belonged to a completely eroded Late Bronze Age/Early Iron Age burial on the eastern edge of the hill. Comparable daggers are, for example, known from Mingachevir (Асланов et al. 1959: Pl. 14), the Kalakent region (Nagel/Strommenger 1985: Pl. 48 (2702a). 54 2758a. 63 (2418a). 71 (2556a)) or from burials at Zayamchay (Müseyibli/Nəcəfov 2019: Pl. 113, 4. 115, 6).

M. N. Pogrebova conducted a comprehensive study of this type of bronze daggers; on the basis of a combination of various metrical and morphological characteristics, she distinguished seven variants and tried to determine their possible chronological and geographical distribution (Погребова 2011: 263–267). They first appeared in her second chronological group, but became frequent only in the following three stages. Judging by the general morphological similarities between the dagger from Tepe 5 and the exemplary daggers presented for each of her variants (Погребова 2011: Pl. 54, 1–10), it is tempting to assign the dagger to Pogrebova's variants VI or VII. The proposed typology, however, is in many aspects problematic, as some characteristics are based on subtle morphological differences, in particular the shape of the blade, that often depends on the state of preservation. The viability of the proposed typology for chronological issues is also questionable when considering her results, according to which three variants (II, III and IV) are attested throughout all of the last three stages of Pogrebova's chronological system. Only variant I appears to be limited to the third stage. The variants V, VI and VII seem more frequent in the last two stages and, therefore would suggest a date between the end of the 12th and the first half of the 7th cent. BC. Again, without the possibility to consider any further associated objects, this remains conjectural.

List of stray finds

KG-024-0089 (bronze dagger) Fig. 47, 2
(all measurements refer to the unrestored object)
L: 147.0 mm; W: 34.0 mm; Th: 15.0 mm; Wt: 80 g
606311.357 E; 4527999.296 N; 172.978 m

KG-024-0090 (bronze ring) Fig. 47, 3
Diam: 41.0 mm; inner diam: 28.0 mm; H: 13.0 mm; Wt: 25 g; 606311.426 E; 4527999.356 N; 172.996 m

KG-024-0091 (bronze pommel) Fig. 47, 1
Diam: 30.0–25.0 mm; H: 36.0 mm; Wt: 43 g
606311.426 E; 4527999.358 N; 172.996 m

KG-054-0218 (fragments of bronze sheet)
L: 11.0 mm; W: 9.0 mm; Th: 1.0 mm; Wt: < 1 g
606299.167 E; 4527985.893 N; 173.692 m

KG-054-0218 (fragments of bronze sheet)
L: 11.0 mm; W: 9.0 mm; Th: 1.0 mm; Wt: < 1 g
606299.167 E; 4527985.893 N; 173.692 m

KG-054-0219 (fragments of thick bronze wire)
L: 8.7 mm; Th: 2.3 mm; Wt: < 1 g
606298.631 E; 4527988.055 N; 173.732 m

KG-054-0223 (bluish frit bead with knobs) Fig. 53, 11
H: 1.9 mm; Diam.: 1.9–3.0 mm; Hole diam.: 0.9 mm
606297.514 E; 4527985.810 N; 173.426 m
probably displaced from Burial 1

KG-054-0224 (bluish frit bead with knobs) Fig. 53, 12
H: 2.9 mm; Diam.: 2–2.3 mm; Hole diam.: 0.9 mm
606296.675 E; 4527987.679 N; 173.465 m
probably displaced from Burial 1

KG-054-0232 (fragments of bronze object)
L: 6.5 mm; W: 5.0 mm; Th: 4.0 mm; Wt: < 1 g
606294.034 E; 4527989.333 N; 173.400 m

KG-061-0250 (fragments of burnt mud-brick)
L: 154.0 mm; W: 133.0 mm; Th: 47.0 mm; Wt: 1427 g
606307.306 E; 4527988.783 N; 173.675 m

KG-011-0034 (obsidian flake)
L: 28.0 mm; W: 15.0 mm; Th: 8.0 mm; Wt: 2 g
606305.247 E; 4527996.909 N; 173.707 m

KG-015-0037 (obsidian flake)
L: 27.0 mm

KG-017-0048 (obsidian flake)
L: 18.0 mm; W: 10.0 mm; Th: 7.0 mm; Wt: 1 g
606299.087 E; 4527998.257 N; 173.740 m

KG-017-0052 (obsidian flake)
L: 38.0 mm; W: 36.0 mm; Th: 10.0 mm; Wt: 12 g
606296.071 E; 4527998.042 N; 173.652 m

KG-017-0061 (obsidian flake)
L: 39.0 mm; W: 23.0 mm; Th: 11.0 mm; Wt: 13 g
606295.985 E; 4527998.249 N; 173.54 m

KG-020-0065 (obsidian flake)
L: 38.0 mm; W: 24.0 mm; Th: 26.0 mm; Wt: 8 g
606302.343 E; 4527997.039 N; 173.420 m

KG-021-0070 (obsidian flake)
L: 23.0 mm; W: 19.0 mm; Th: 4.0 mm; Wt: 2 g
606317.200 E; 4527998.494 N; 172.673 m

KG-021-0078 (obsidian flake)
L: 21.0 mm; W: 19.0 mm; Th: 6.0 mm; Wt: 1 g
606313.905 E; 4527997.961 N; 172.87 m

KG-024-0085 (obsidian flake)
L: 50.0 mm; W: 31.0 mm; Th: 16.0 mm; Wt: 20 g
606301.491 E; 4527998.463 N; 173.135 m

KG-024-0087 (obsidian flake)
L: 17.0 mm; W: 15.0 mm; Th: 5.0 mm; Wt: 1 g
606312.420 E; 4527997.559 N; 173.208 m

KG-024-0129 (two obsidian flakes)
L: 19.0 mm; W: 17.0 mm; Th: 3.0 mm; Wt: 1 g
606321.532 E; 4527997.587 N; 172.441 m

KG-024-0130 (obsidian flake)
L: 40.0 mm; W: 32.0 mm; Th: 14.0 mm; Wt: 12 g
606314.626 E; 4527997.500 N; 172.713 m

KG-024-0131 (obsidian flake)
L: 24.0 mm; W: 21.0 mm; Th: 6.0 mm; Wt: 3 g
606319.020 E; 4527999.281 N; 172.461 m

KG-024-0132 (obsidian flake)
L: 27.0 mm; W: 21.0 mm; Th: 6.0 mm; Wt: 3 g
606319.246 E; 4527999.511 N; 172.545 m

KG-024-0133 (obsidian flake)
L: 29.0 mm; W: 25.0 mm; Th: 9.0 mm; Wt: 7 g
606319.697 E; 4527999.366 N; 172.443 m

KG-024-0135 (obsidian flake)
L: 15.0 mm; W: 13.0 mm; Th: 2.0 mm; Wt: 1 g
606302.696 E; 4527992.954 N; 173.287 m

KG-033-0126 (obsidian flake)
L: 53.0 mm; W: 37.0 mm; Th: 12.0 mm; Wt: 25 g
606295.917 E; 4527997.217 N; 173.385 m

KG-033-0128 (obsidian flake)
L: 42.0 mm; W: 20.0 mm; Th: 8.0 mm; Wt: 5 g
606296.331 E; 4527997.448 N; 173.436 m

KG-037-0176 (obsidian flake)
L: 43.3 mm; W: 20.7 mm; Th: 10.0 mm; Wt: 7 g
606305.197 E; 4527994.132 N; 173.592 m

KG-037-0178 (obsidian flake)
L: 24.1 mm; W: 26.2 mm; Th: 4.3 mm; Wt: 2 g
606307.312 E; 4527994.770 N; 173.453 m

KG-054-0246 (obsidian flake)
L: 15.0 mm; W: 8.5 mm; Th: 1.5 mm; Wt: 0.5 g
606295.209 E; 4527988.507 N; 173.420 m

KG-054-0248 (obsidian flake)
L: 38.0 mm; W: 22.0 mm; Th: 11.0 mm; Wt: 6 g
606290.834 E; 4527992.015 N; 173.515 m

KG-056-0230 (obsidian flake)
L: 18.0 mm; W: 15.0 mm; Th: 5.0 mm; Wt: 1 g
606298.036 E; 4527994.643 N; 173.401 m

KG-056-0231 (obsidian flake)
L: 22.0 mm; W: 13.5 mm; Th: 5.0 mm; Wt: 1 g
606299.354 E; 4527995.309 N; 173.365 m

KG-056-0233 (obsidian flake)
L: 20.0 mm; W: 7.0 mm; Th: 3.0 mm; Wt: 1 g
606298.865 E; 4527995.313 N; 173.360 m

KG-056-0234 (obsidian flake)
L: 22.0 mm; W: 17.5 mm; Th: 4.0 mm; Wt: 1 g
606299.310 E; 4527994.560 N; 173.377 m

KG-056-0236 (obsidian flake)
L: 22.0 mm; W: 19.5 mm; Th: 6.0 mm; Wt: 1 g
606309.327 E; 4527994.540 N; 173.329 m

KG-056-0238 (obsidian flake)
L: 24.0 mm; W: 10.0 mm; Th: 4.0 mm; Wt: 1 g
606299.310 E; 4527995.438 N; 173.343 m

KG-056-0242 (two obsidian flakes)
L: 26.0 mm; W: 20.5 mm; Th: 6.5 mm; Wt: 1 g
606299.159 E; 4527995.285 N; 173.306 m

IV.9 Detailed description of the burials

The following catalogue describes each burial in detail and provides lists of the grave contents and all objects found in the fill. The latter do not necessarily originate from the burial and might have ended up in the fill either by accidental intrusions or by the interment of later burials. In several cases – in particular among the burials in the Pit-Complexes – the contents of two or more burials of different periods were mixed. Apart from pit KG-057 (Burials 8, 23 and 24) most finds could be re-assigned to their original burial context, nevertheless, for the sake of clarity, all displaced objects are listed as part of the burial context they were discovered in. References to these objects, however, are provided in the description of all related burials. The information on sex and age class is based on the anthropological analyses of the human bones, treated in more detail in chapter V.

Burial 1 (KG-094)

Burial 1 was located in the northern half of square 6290/7980 (Fig. 27). It was the earliest interment of Pit-Complex C. The original outline of the grave-pit was securely detectable only at its northern end where it formed a rectangular corner and followed for at least 1.85 m a straight line towards the south-south-east (Fig. 48). The entire southern and eastern part of the pit was disturbed by the later Burials 21 (Late Antique period) and 41 (Medieval period) and, therefore, the original limits were impossible to define. The grave-pit's current pentagonal appearance is caused by the straight east-west oriented southern edge of the Pit-Complex C-3 (at 4527987.80 N). However, this extension is very likely not original, but resulted from the disturbance of the burial that appears to have taken place when the adjacent Burial 21 was interred. The original southern edge might

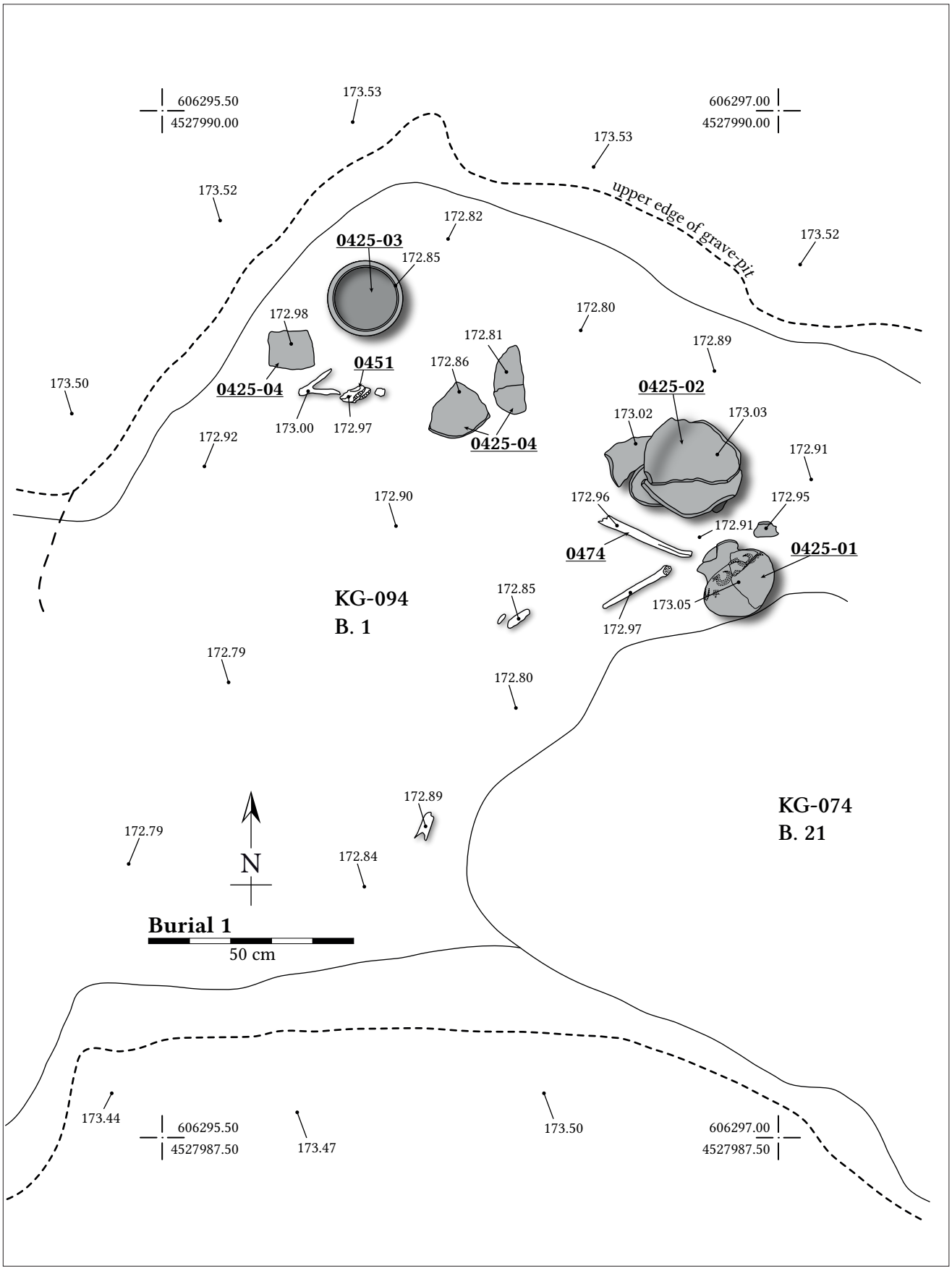

Fig. 48. Plan of Burial 1 (KG-094); Pit-Complex C-3

Fig. 49. Black-polished pot KG-094-0425-01 from Burial 1 with punctate ornamentation

well have been somewhere parallel to its north-eastern counterpart and thus the entire pit might originally have had a rectangular shape. The robbing seems to have destroyed the entire southern part of the burial. Most of the skeleton was removed. Besides a few loose human bone fragments in the fill only parts of the humerus and radius of the right arm were still found *in situ* at the eastern end of the pit. The position of these bones makes it likely that the head of the deceased was originally in the south-east. North of the skeleton at least four vessels were lined up. They seem to have lain at the margin of the most severe disturbances and were consequently less damaged or displaced. Fragments of different vessels found in the fill, however, indicate that originally the number of vessels might have been higher (Fig. 52).

Next to the right arm was a black-polished pot (0425-01). It was tipped over and a quarter of its body was missing (it was probably cut off when the grave-pit of Burial 21 was dug). The vessel bore a punctate ornamentation on its shoulder. The decoration consisted of an alternating pattern of hanging hooks and upwards pointing double-angles (Fig. 49 and Fig. 51, 1). Shape and fabric of the pot are similar to the vessels found in Burial 2 and thus share the same comparisons with Karacamirli Kurgans 4 and 5 (Гусейнова/Алиев 2008) as well as with burials in the Armenian highlands. Most noteworthy are two small black-polished pots with a similar shape and decoration from Lchashen Tomb 254 (Smith et al. 2009: 72 Fig. 22r) and from the Tomb of Sevanges (Smith et al. 2009: 72 Fig. 22s). Both burials were attributed to the Sevan-Uzerlik 2 ceramic group and dated accordingly to the Middle

Fig. 50. Black-polished bowl KG-094-0425-03 from Burial 1

Bronze Age III period. The connection of pot 0425-01 to the final Middle Bronze Age period is further supported by the applied hook motif. This decorative element is particularly well attested on different vessels in Karacamirli Kurgan 5 (Гусейнова/Алиев 2008: Fig. VI, 1. 4–6. VII, 3. 7. VIII, 5–6) and was considered as a reminiscence of Middle Bronze Age ornamentation, suggesting a transitional date of the kurgan between the Middle and Late Bronze Age periods (Гусейнова 2011: 118–121).

North of pot 0425-01 – only a few centimetres away – were the remains of a wide-mouthed pot (0425-02, Fig. 51, 2). Its large-sized fragments were stacked. Their position does not appear to be the result of a mere collapse of the vessel but of the disturbance, especially since a substantial part of the pot was missing. The fabric was coarse and of a dark greyish colour. Its surface was badly preserved, but seems to have been originally burnished. It had a flat base, conical lower body and a pronounced but not carinated shoulder with a short neck and an outrolled rim. Two pairs of four shallow knobs arranged in a rectangular pattern were applied on opposite sides on the shoulder. The closest comparison of that type of decoration was found on a similar pot in Burial 7 (see 0100-01).

The bowl 0425-03 was the only vessel still perfectly *in situ* and untouched (Fig. 50 and Fig. 51, 3). It was situated at the north-western end of the grave-pit on a height slightly below the level of the skeleton – perhaps the reason why it was overlooked by the robbers. It was black-polished and undecorated. Morphologically it is very similar to the bowls found in Burial 2 (see below), although its rim is a little longer and more upright.

The last vessel that can be assigned to the original grave contents of Burial 1 is a large pot (0425-04, Fig. 51, 4). Its fragments were scattered over the north-western half of the grave-pit and only parts of the shoulder and neck were preserved. Most of the surface was flaked off, but in some places the original black-polished surface with remains of a punctate ornamentation was visible.

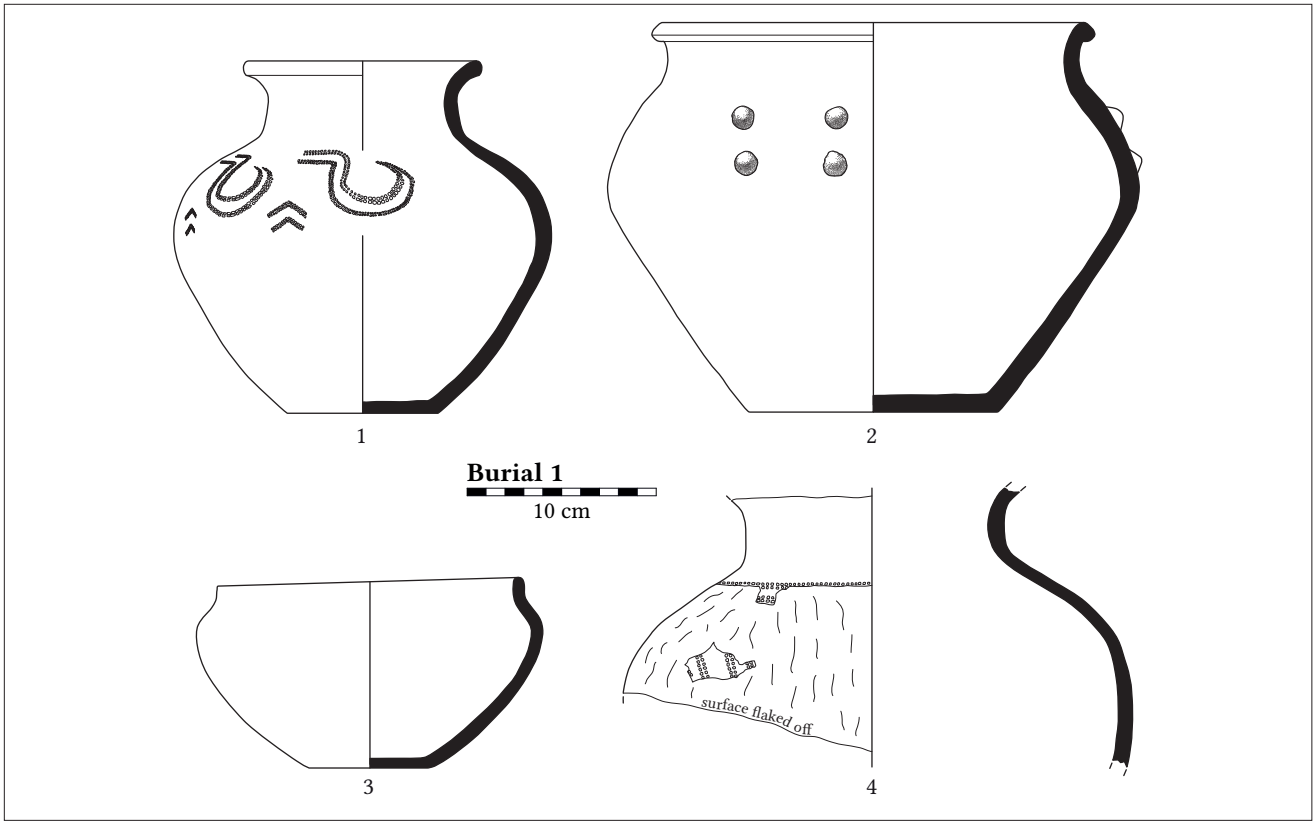

Fig. 51. Pottery from Burial 1 (KG-094): 1 – pot (0425-01); 2 – pot (0425-02); 3 – bowl (0425-03); 4 – pot (0425-04)

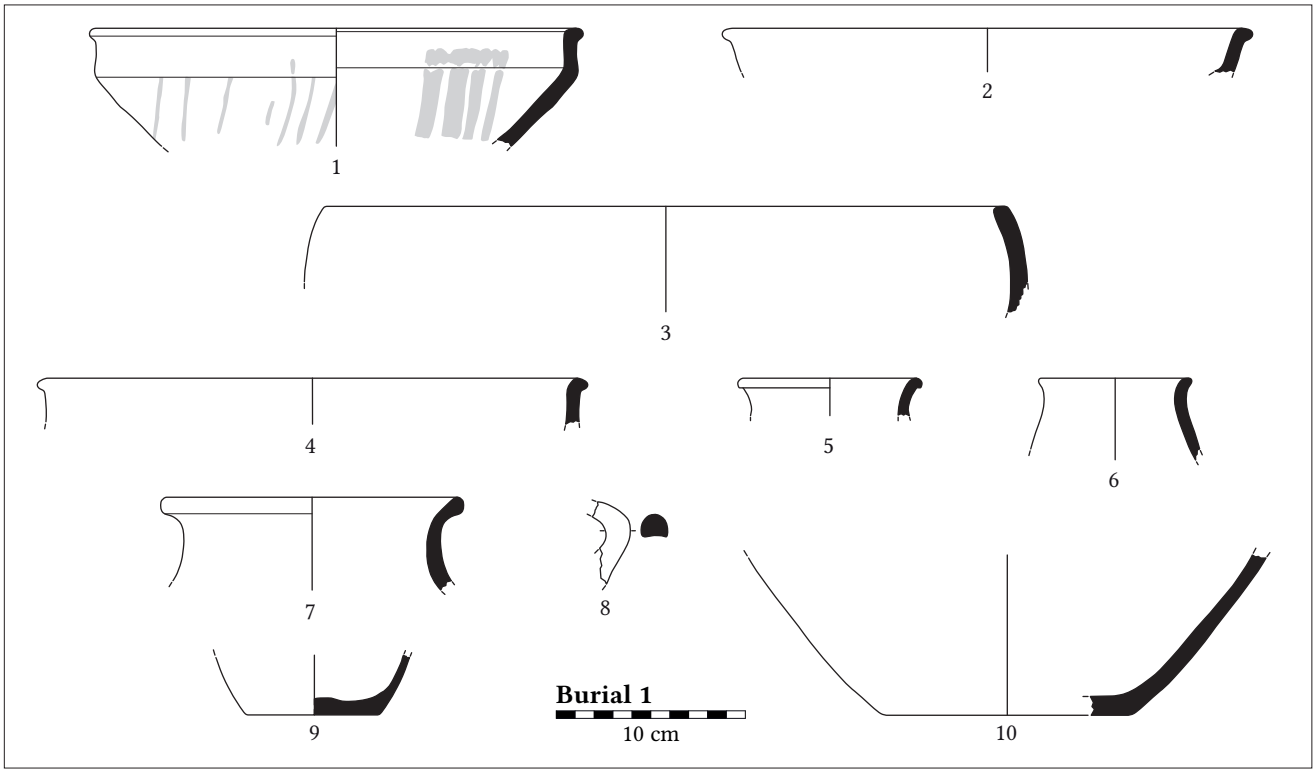

Fig. 52. Pottery from the fill of Burial 1 (KG-094): 1 – bowl (0425-05); 2 – bowl (0425-06); 3 – bowl (0425-07); 4 – bowl (0425-08); 5 – pot (0425-09); 6 – pot (0425-10); 7 – pot (0425-11); 8 – handle (0425-12); 9 – base (0425-14); 10 – base (0425-13)

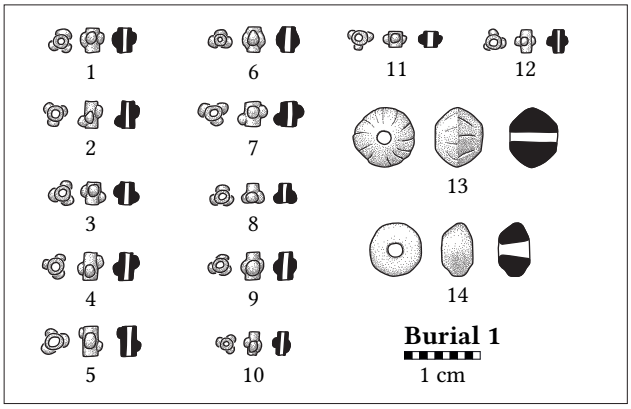

Fig. 53. Finds from the fill of Burial 1 (KG-094): 1 – frit bead (0423); 2 – frit bead (0427); 3 – frit bead (0428); 4 – frit bead (0436); 5 – frit bead (0437); 6 – frit bead (0439); 7 – frit bead (0440); 8 – frit bead (0453); 9 – frit bead (0458); 10 – frit bead (0464); 13 – frit bead (0452); 14 – carnelian bead (0456); finds in context KG-054: 11 – frit bead (0223); 12 – frit bead (0224)

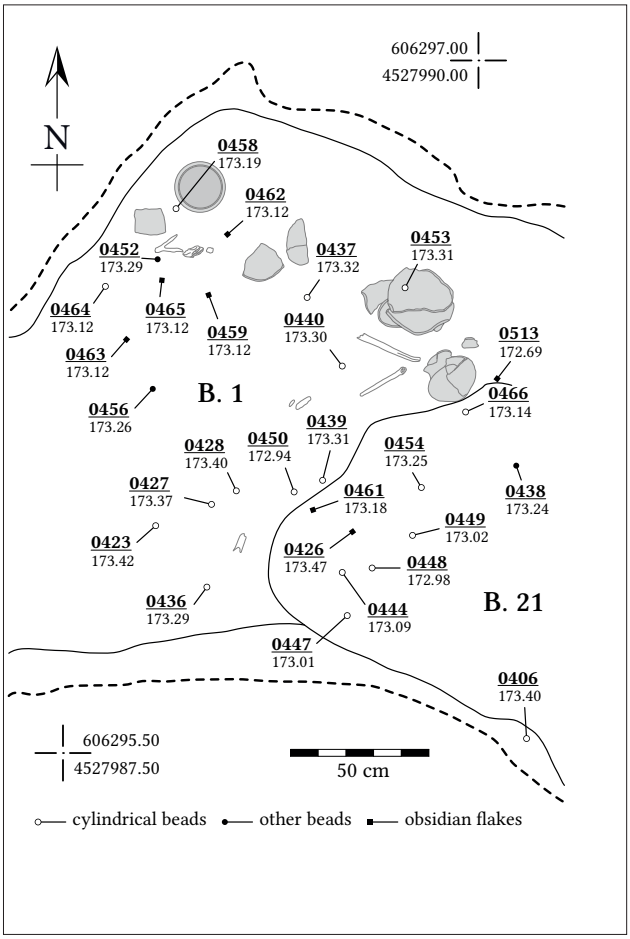

Fig. 54. Distribution of beads and obsidian flakes in the fill of Burials 1 (KG-094) and 21 (KG-074)

South of bowl 0425-03 and in the area of the fragments of 0425-04 a small cluster of animal bones was found (0451) that included the remains of a sheep or goat, the humerus of a wild bird as well as the tooth of a mouse. While the sheep/goat and presumably also the bird bone can be considered as burial gifts, the mouse tooth may be an accidental inclusion, perhaps through a burrowing animal.

In the fill some 10–15 cm above the animal bones was a loose cluster of four obsidian flakes (0459, 0462, 0463, 0465). All flakes lay at exactly the same height of 173.12 m (Fig. 54). This level also marks the lowest level of five identical frit beads (0437, 0440, 0453, 0458, 0464) that were found scattered throughout the fill of the northern part of the burial. Six similar beads were located in the southern part of the pit and ten more in the area disturbed by Burial 21 on different heights between 172.98 m and 173.42 m (Fig. 54). All beads were made of a light blue frit paste and had a cylindrical body with three knobs applied around its longitudinal side (Fig. 55). Their uniformity suggests that they once belonged to the same necklace (Fig. 53, 1–10).

The lack of detailed publications of beads in West-Azerbaijan makes it difficult to find significant comparisons. There is some evidence of similar beads in burials near the *Paradiesfestung* at Kalakent: Burial 86 contained eight cylindrical frit beads of blue colour with »warts« (Nagel/Strommenger 1985: 105–106, no. 2673, Fig. 73); also in Burial 82 (Nagel/Strommenger 1985: 103–104, no. 2669o, Fig. 69) and Burial 149 (Nagel/Strommenger 1985: 128–129, no. 2728c, Fig. 99) beads of a similar type were found. In addition, Burial 6a at *Helenendorf* is worth mentioning, since the deceased was accompanied by a similar bead, but with five knobs and of unclear material (Rösler 1901: 116 Fig. 37n). Interesting is the attestation of a very similar bead made of blue paste in Kurgan 3 at Tetri Kvebi near Udabno in Kakheti (Georgia). The kurgan was linked to the Middle Bronze Age Trialeti Culture (Bertram/Picchelauri 2005: 348–354 Fig. 46, 9), more precisely to its second and third phase (according to Гогадзе 1972), the absolute dates of which, however, are still debated and vary between the final centuries of the 3rd millennium and the second quarter of the 2nd millennium BC (summarized in Rubinson 1976; Zischow 2004: 70–73; Narimanishvili et al. 2018: 206).

Notwithstanding the imprecise absolute range of the different stages of the Trialeti-Culture, the general attribution of the finds to the Middle Bronze Age implies an early date for such beads and makes it very likely that the cylindrical frit beads originally belonged to Burial 1 and not to the adjacent Late Antique Burial 21. Therefore, their distribution in the fill of both burials (Fig. 54) permits the reconstruction of the taphonomic process and the extent of the disturbance through Burial 21: It seems

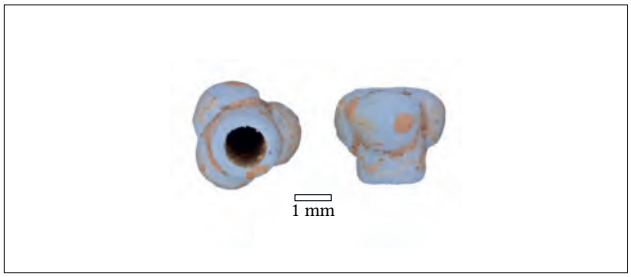

Fig. 55. Light blue frit bead (0453) with a cylindrical body and three applied knobs

likely that the beads (or a string of beads) were originally deposited near the deceased of Burial 1. When this burial was disturbed, the beads were removed from their primary position and spread over the re-opened grave-pit, ending up in the fill of the newly opened pit of Burial 21 as well. Against this backdrop, the uniform height of the beads just above the bottom of the burial in the northern part of Burial 1 may therefore well indicate a specific level reached during the course of the robbery on which several artefacts fell. Moreover, the beads in the southern part of the pit and in the fill of Burial 21 were deposited at different altitudes, which in turn implies that the material there was mixed to a higher degree.

In addition to the cylindrical beads found directly in the grave-pits, two more beads of identical type were found in the surface context KG-054 immediately south of Pit-Complex C-4 (0224, Fig. 53, 12) and at a distance of c. 1.5 m to the pit (0223, Fig. 53, 11). Their location could mark the area where the extracted soil was heaped up in the course of the interment of Burial 21 and makes it plausible to assign them to the same group of beads from Burial 1 and the fill of Burial 21 (see also ch. IV.8). A third bead (0381) was found inside the nearby Burial 14 (Fig. 114, 29), however, this bead, too, might well originate from Burial 1. It can at least not be excluded, that it ended up in the adjacent grave-pit due to some later disturbances (perhaps by animals) of the residual quantities of the extracted soil after the interment of Burial 21.

Besides these cylindrical beads with knobs some other objects were apparently relocated from Burial 1: A biconical frit bead of a bluish colour with radial grooves (0452) found loose in the fill in the northern part of the pit (Fig. 53, 13). Some 20 cm south of that bead and on the same level was a roughly disc-shaped bead made of carnelian (0456, Fig. 53, 14). A similar carnelian bead (0438, Fig. 133, 3), a small frit bead (0501, Fig. 133, 7) and the fragment of a bronze bracelet (0512, Fig. 133, 2) were found displaced in the fill of Burial 21 – all very likely belonged originally to the content of Burial 1. Most noteworthy, however, is an obsidian arrowhead (0502, Fig. 133, 1) that – considering the predominantly Bronze Age date of such weapons (Picchelauri 1997: 29–30) – very likely originates from Burial 1. In this instance we apparently witness the intentional deposition and reuse of a Bronze Age object as a burial gift close to the body of a Late Antique burial.

Considering the typological conclusions drawn from the pottery Burial 1 can be attributed to the final stage of the Middle Bronze Age period or to the transitional phase between the Middle and Late Bronze Age period. The proposed dating for the transition from the Middle to the Late Bronze Age period around 1500 BC (Гусейнова 2011) is now also supported by a radiocarbon date of the collagen sample (MAMS-39416) taken from the skeleton that sets a similar time span for Burial 1 (see Table 4).

Grave contents

KG-094-0474 (human bones) Table 4
Sex and age could not be determined Table 16

KG-094-0451 (animal bone)
remains of sheep/goat and bird

KG-094-0425-01 (pot) Fig. 49; Fig. 51, 1
Rim diam.: 160 mm (75%)
H: 100 mm
Base diam.: 65 mm
Fabric: exterior reducing, interior oxidizing atmosphere, medium hard, coarse temper (424)
Surface: ext. polished; int. smoothed
Colour: ext. Gley 1 2.5/N (black); core Gley 1 2.5/N (black); int. Gley 1 2.5/N (black)
Decoration: punctate ornamentation on the shoulder (row of hanging hooks with a short horizontal section on the upper end; between the hooks separate upward-pointing angles)
Condition: a quarter of the vessel body and rim is missing, most likely due to the disturbance by Burial 21
Comparanda:
Lchashen, Burial 254, MBA III (Smith et al. 2009: 72 Fig. 22r; Avetisyan/Bobokhyan 2008: 164 Fig. 27, 1)
Tomb of Sevanges, MBA III (Smith et al. 2009: 72 Fig. 22s)

KG-094-0425-02 (pot) Fig. 51, 2
Rim diam.: 215 mm (64%)
H: 205 mm
Base diam.: 130 mm
Fabric: exterior reducing, interior oxidizing atmosphere, medium hard, fine temper (422)
Surface: ext. and int. wash
Colour: ext. Gley 1 2.5/N (black); core Gley 1 4/N (dark grey); int. Gley 1 3/N (very dark grey)
Decoration: four shallow knobs in a rectangular arrangement on opposite sides
Condition: half the vessel is missing; rim partially broken off; surface flaked off
Comparanda:
Tepe 5, Burial 7 (see pot KG-026-0100-01)

KG-094-0425-03 (bowl) Fig. 50; Fig. 51, 3
Rim diam.: 160 mm (100%)

H: 99 mm
Base diam.: 65 mm
Fabric: completely reducing atmosphere, hard, medium coarse temper (133)
Surface: ext. and int. polished
Colour: ext. Gley 1 2.5/N (black); core Gley 1 4/N (dark grey); int. Gley 1 2.5/N (black)
Condition: complete
Comparanda:
Tepe 5, Burial 2 (see bowls KG-044-0200-06 and KG-044-0200-07)

KG-094-0425-04 (pot) Fig. 51, 4
Rim diam.: ~120 mm (15%)
H: only 170 mm preserved
Base diam.: not preserved
Fabric: completely reducing atmosphere, hard, fine temper (132)
Surface: ext. polished; int. smoothed
Colour: ext. Gley 1 2.5/N (black); core 10YR 6/1 (grey); int. 10YR 6/3 (pale brown)
Decoration: Punctate ornamentation on the shoulder (at least two horizontal lines and below four diagonal lines of unknown pattern)
Condition: only about three quarters of the shoulder and neck preserved; surface in most parts flaked off

Fill

KG-094-0423 (bluish frit bead with knobs) Fig. 53, 1
H: 3.1 mm; Diam.: 1.7–3.1 mm; Hole diam.: 0.8 mm
606295.834 E; 4527988.319 N; 173.415 m

KG-094-0427 (bluish frit bead with knobs) Fig. 53, 2
H: 3.2 mm; Diam.: 1.7–3.1 mm; Hole diam.: 1.0 mm
606296.036 E; 4527988.398 N; 173.371 m

KG-094-0428 (bluish frit bead with knobs) Fig. 53, 3
H: 3.0 mm; Diam.: 2.0–3.4 mm; Hole diam.: 1.0 mm
606296.126 E; 4527988.445 N; 173.396 m

KG-094-0436 (bluish frit bead with knobs) Fig. 53, 4
H: 3.5 mm; Diam.: 2.2–3.1 mm; Hole diam.: 1.0 mm
606296.019 E; 4527988.097 N; 173.287 m

KG-094-0437 (bluish frit bead with knobs) Fig. 53, 5
H: 3.9 mm; Diam.: 2.5–3.9 mm; Hole diam.: 1.1 mm
606296.382 E; 4527989.144 N; 173.320 m

KG-094-0439 (bluish frit bead with knobs) Fig. 53, 6
H: 3.3 mm; Diam.: 1.6–3.2 mm; Hole diam.: 0.8 mm
606296.438 E; 4527988.483 N; 173.310 m

KG-094-0440 (bluish frit bead with knobs) Fig. 53, 7
H: 3.1 mm; Diam.: 2.2–4.0 mm; Hole diam.: 1.0 mm
606296.509 E; 4527988.896 N; 173.301 m

KG-094-0450 (bluish frit bead with knobs)
H: 2.7 mm; Diam.: 1.4–2.1 mm; Hole diam.: 0.8 mm
606296.335 E; 4527988.441 N; 172.935 m

KG-094-0453 (bluish frit bead with knobs) Fig. 55; Fig. 53, 8
H: 2.8 mm; Diam.: 1.8–3.0 mm; Hole diam.: 0.9 mm
606296.736 E; 4527989.179 N; 173.310 m

KG-094-0458 (bluish frit bead with knobs) Fig. 53, 9
H: 3.5 mm; Diam.: 1.9–3.0 mm; Hole diam.: 0.9 mm
606295.908 E; 4527989.465 N; 173.188 m

KG-094-0464 (bluish frit bead with knobs) Fig. 53, 10
H: 3.0 mm; Diam.: 1.4–2.8 mm; Hole diam.: 0.7 mm
606295.653 E; 4527989.184 N; 173.115 m

KG-094-0452 (bluish biconical frit bead) Fig. 53, 13
H: 6.1 mm; Diam.: 8.0 mm; Hole diam.: 1.9 mm
606295.841 E; 4527989.282 N; 173.293 m

KG-094-0456 (disc-shaped carnelian bead) Fig. 53, 14
Th: 4.1 mm; Diam.: 7 mm; Hole diam.: 1.9 mm
606295.824 E; 4527988.814 N; 173.255 m

KG-094-0457 (obsidian flake)
L: 22.5 mm; W: 18 mm; Th: 5 mm; Wt: 2 g
found loose in fill

KG-094-0459 (obsidian flake)
L: 13 mm; W: 8 mm; Th: 3 mm; Wt: 4 g
606296.026 E; 4527989.153 N; 173.116 m

KG-094-0462 (obsidian flake)
L: 12 mm; W: 10 mm; Th: 1.2 mm; Wt: <1 g
606296.094 E; 4527989.372 N; 173.124 m

KG-094-0463 (obsidian flake)
L: 18.5 mm; W: 8 mm; Th: 8 mm; Wt: 1 g
606295.729 E; 4527988.992 N; 173.122 m

KG-094-0465 (obsidian flake)
L: 11 mm; W: 8 mm; Th: 2 mm; Wt: <1 g
606295.857 E; 4527989.206 N; 173.120 m

KG-093-0476 (obsidian flake)
L: 24.0 mm; W: 18.0 mm; Th: 7.5 mm; Wt: 1 g
606297.373 E; 4527988.741 N; 173.026 m

KG-094-0513 (obsidian flake)
L: 22.0 mm; W: 19.0 mm; Th: 4.0 mm; Wt: 2 g
606297.065 E; 4527988.847 N; 172.690 m

KG-094-0425-05 (bowl) Fig. 52, 1
Rim diam.: 270 mm (15%)
H: 56 mm preserved
Fabric: completely reducing atmosphere, hard, medium fine temper (133)
Surface: ext. smoothed; int. smoothed
Colour: ext. 7.5YR 4/1 (dark grey); core 7.5YR 5/2 (brown); int. 7.5YR 4/1 (dark grey)
Decoration: polished ornamentation on the exterior and interior surface (vertical lines)
Condition: only parts of the rim and the carinated shoulder preserved

KG-094-0425-06 (rim sherd of bowl) Fig. 52, 2
Rim diam.: 280 mm
H: 23 mm preserved
Fabric: reducing atmosphere with oxidized core, medium hard, fine temper (622)
Surface: ext. and int. smoothed
Colour: ext. Gley 1 3/N (very dark grey); core 7.5YR 5/4 (brown); int. Gley 1 3/N (very dark grey)

KG-094-0425-07 (rim sherd of bowl) Fig. 52, 3
Rim diam.: 280 mm
H: 23 mm preserved
Fabric: reducing atmosphere with oxidized core, medium hard, fine temper (132)
Surface: ext. and int. smoothed
Colour: ext. Gley 1 3/N (very dark grey); core 7.5YR 5/4 (brown); int. Gley 1 3/N (very dark grey)

KG-094-0425-08 (rim sherd of bowl) Fig. 52, 4
Rim diam.: 260 mm
H: 22 mm preserved
Fabric: reducing atmosphere with oxidized core, medium hard, medium fine temper (623)
Surface: ext. and int. smoothed
Colour: ext. Gley 1 3/N (very dark grey); core 7.5YR 5/4 (brown); int. Gley 1 3/N (very dark grey)

KG-094-0425-09 (rim sherd of pot) Fig. 52, 5
Rim diam.: 90 mm
H: 18 mm preserved
Fabric: completely reducing atmosphere, hard, medium fine temper (133)
Surface: ext. and int. smoothed
Colour: ext. 2.5Y 4/1 (dark grey); core 2.5Y 4/1 (dark grey); int. 2.5Y 4/1 (dark grey)

KG-094-0425-10 (rim sherd of pot) Fig. 52, 6
Rim diam.: 80 mm
H: 42 mm preserved
Fabric: completely reducing atmosphere, medium hard, medium fine temper (123)
Surface: ext. and int. smoothed
Colour: ext. Gley 1 2.5/N (black); core Gley 1 4/N (dark grey); int. Gley 1 4/N (dark grey)

KG-094-0425-11 (rim sherd of pot) Fig. 52, 7
Rim diam.: 160 mm
H: 41 mm preserved
Fabric: ext. reducing and int. oxidizing atmosphere, medium hard, fine temper (422)
Surface: ext. and int. smoothed
Colour: ext. Gley 1 2.5/N (black); core 5Y 4/1 (dark grey); int. 10YR 4/1 (dark grey)

KG-094-0425-12 (handle) Fig. 52, 8
Diam.: 8–12 mm
L: 42 mm preserved
Fabric: reducing atmosphere with oxidized core, hard, medium fine temper (633)
Surface: ext. and int. smoothed
Colour: ext. 10YR 4/1 (dark grey); core 2.5YR 6/4 (light reddish brown); int. 10YR 4/1 (dark grey)

KG-094-0425-13 (base sherd) Fig. 52, 10
Base diam.: 130 mm
H: 125 mm preserved
Fabric: ext. reducing and int. oxidizing atmosphere, hard, fine temper (432)
Surface: ext. polished; int. smoothed
Colour: ext. Gley 1 2.5/N (black); core Gley 1 4/N (dark grey); int. 10YR 5/2 (greyish brown)

KG-094-0425-14 (base sherd) Fig. 52 9
Base diam.: 70 mm
H: 31 mm preserved
Fabric: completely reducing atmosphere, hard, fine temper (132)
Surface: ext. burnished; int. smoothed
Colour: ext. Gley 1 2.5/N (black); core Gley 1 5/N (grey); int. Gley 1 5/N (grey)

Burial 2 (KG-044)

The grave-pit was located in the northern half of square 6290/7990 (Fig. 27). Its south-eastern and north-western edges were cut by the Medieval Burials 33 and 34. The latter interments caused damage to vessel 0200-06. The original outline of the pit appears to have been of rectangular shape (Fig. 58). Unlike all other burials this pit fill was heavily intermixed with ashy material and pieces of charcoal. It contained a loose sherd (0191-01) and high up in the eastern corner of the pit – near the disturbance by Burial 33 – an obsidian flake (0188). No skeleton was detected. The layout of the grave-pit, however, suggests that it was placed in the southern part of the pit and either had vanished or was disturbed by the interment of

Fig. 56. Black-polished pot with punctate ornamentation (0200-04) from Burial 2 (KG-044)

Fig. 57. Black-polished bowl (0200-07) from Burial 2 (KG-044)

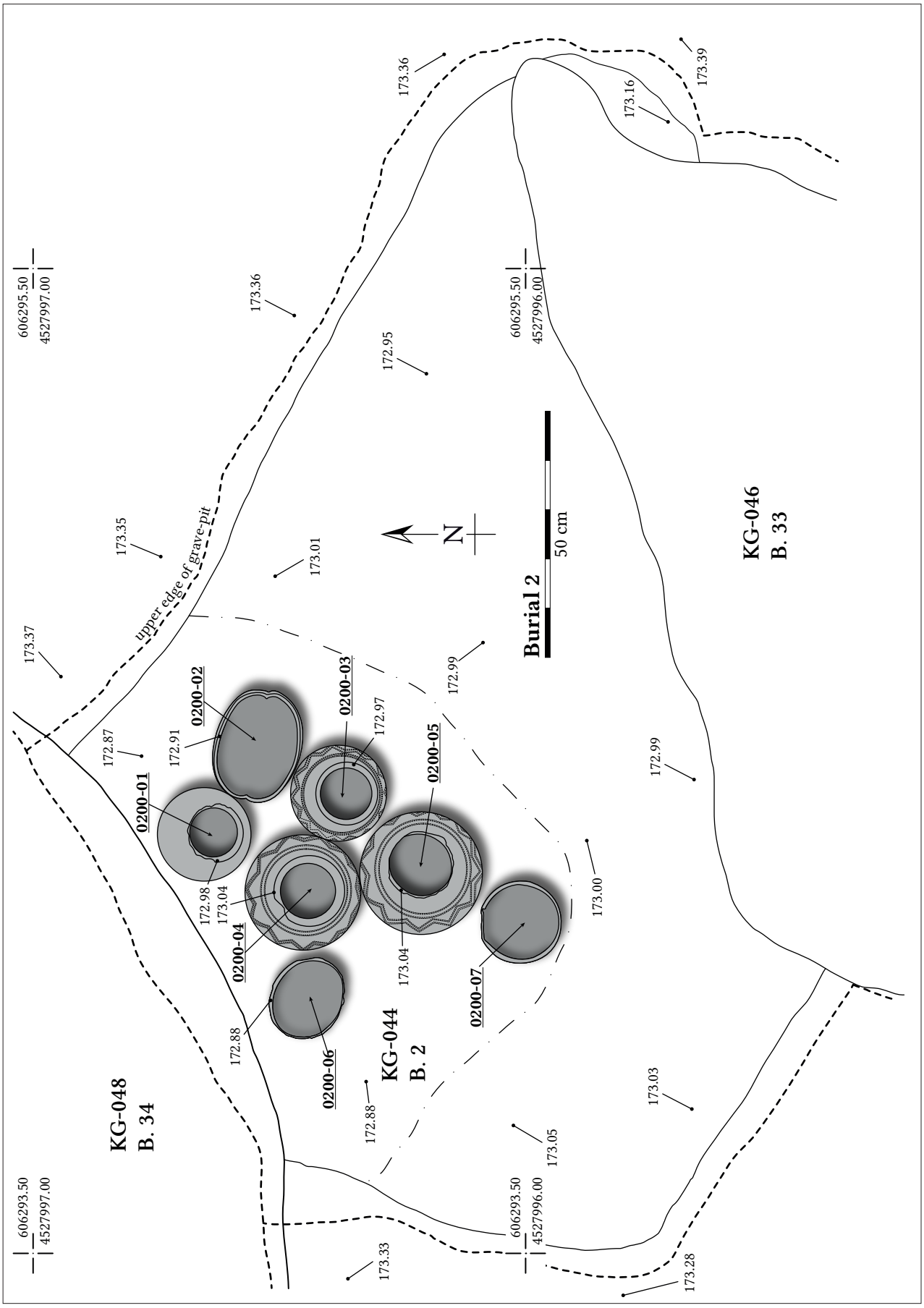

Fig. 58. Plan of Burial 2 (KG-044)

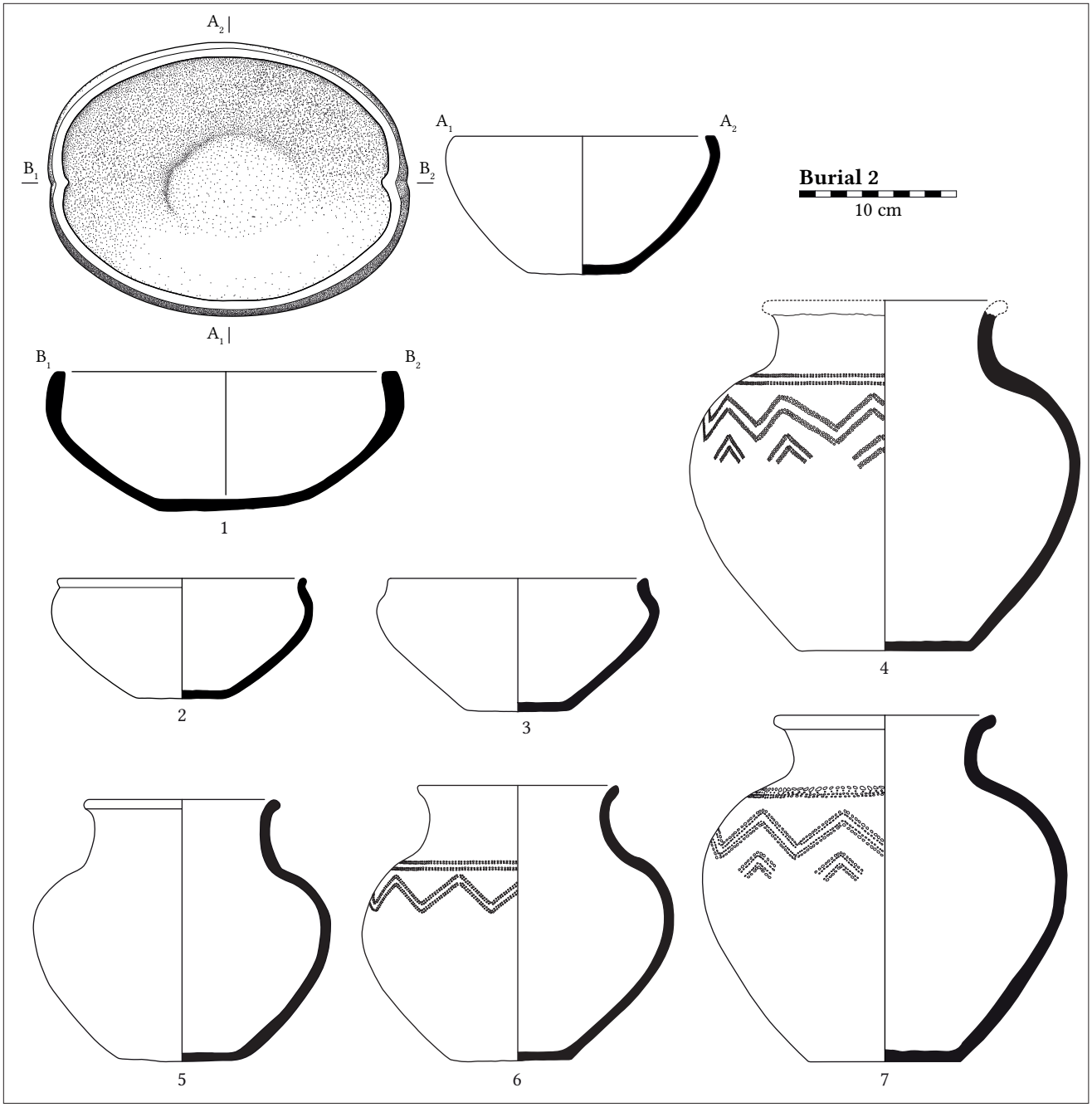

Fig. 59. Pottery from Burial 2 (KG-044): 1 – bowl (0200-02); 2 – bowl (0200-07); 3 – bowl (0200-06); 4 – pot (0200-05); 5 – pot (0200-01); 6 – pot (0200-03); 7 – pot (0200-04)

Burial 33. A group of seven vessels was arranged in two rows at the north-western end of the pit close to the pit of Burial 34. It consisted of four pots, two small bowls and a walnut-shaped bowl. All vessels were made of a very dark grey fabric with a black-polished surface.

Close typological comparisons can be drawn between the pottery of Burial 2 and the Karacamirli Kurgans 4 and 5 (Гусейнова/Алиев 2008). Although the pottery assemblage of the kurgans included several exceptional types and almost all vessels bore a more or less sophisticated geometric or figurative decoration, morphologically only two dominant vessel types can be identified that determine the entire repertoire of all three burials: on the one hand spherical pots with constricted neck and slightly everted rim and on the other hand bowls with a spheroid body and short upright or slightly everted rim. Walnut-shaped bowls and vessels with figurative applications, spouts, handles or foots can enrich the assemblage, but in essence even these exceptional forms are in

Fig. 60. Walnut-shaped bowl (0200-02) from Burial 2 (KG-044)

themselves only extensions or variations of the basic pot and bowl forms.

Three of the pots from Burial 2 were decorated with punctate ornamentation on their shoulder that is reminiscent of a transitional Middle/Late Bronze Age date. All of them had two horizontal lines close to the neck and below a double-lined zigzag pattern (Fig. 49 and Fig. 56). Each line actually consisted of two exactly parallel rows of impressions. Unlike in the Karacamirli kurgans none of the punctate ornamentations was filled with white paste. Two of the pots (0200-05 and 0200-06, Fig. 59, 4. 7 and Fig. 56) had additional angles below the zigzag lines – a virtually identical pot is attested in Karacamirli Kurgan 4 (Гусейнова/Алиев 2008: Fig. I, 9). The undecorated pot 0200-01 (Fig. 59, 5) was slightly smaller but nevertheless morphologically identical to the other pots in the burial. Comparisons of that vessel's type and decoration are found also further west, beyond the Lesser Caucasus in Armenia: Pot 0200-03 (Fig. 26 and Fig. 59, 6), for example, is almost identical to a piece found in Tomb 10 at Harich (Avetisyan/Bobokhyan 2008: 160 Fig. 23, 3). Furthermore, vessels of similar shape and with similar decoration are attested in Harich Tombs 13, 29, 41 (see below). The burials at Harich were assigned to the Middle Bronze Age III period, the Karmir-Berd ceramic horizon, which is contemporary with the complexes of Karmir-Vank, Sevan-Uzerlik and Trialeti-Vanadzor 3 (Smith et al. 2009: 66–68). Only Harich Tomb 41 was dated to the subsequent Lchashen-Metsamor 1 pottery group, defined as the earliest stage of the Late Bronze Age in Armenia and at the same time a transitional phase between the Middle and Late Bronze Ages. This period sees the emergence of new pottery types, but still includes forms and ornamentations typical of the preceding Middle Bronze Age complexes (Avetisyan/Bobokhyan 2008: 126; Smith et al. 2009: 68–77).

Another vessel type that links Burial 2 with Harich and other sites in the Armenian highlands (e. g. Karashamb, Lchashen and Verin-Naver) is the walnut-shaped bowl 0200-02 (Fig. 59, 1 and Fig. 60). It is characterized by an ellipsoid body and by pressing the vertex points of the rim inwards it resembles the shell of a walnut. In Armenia this vessel type is well attested in the Middle Bronze Age III pottery assemblages, but it continues with some morphological variations and increasingly less ornamentation into the Late Bronze Age I and II phases (Smith et al. 2009: 66–67. 73. 79). Painted walnut-shaped bowls with geometric patterns from Middle Bronze Age levels at sites in Nakhchivan (e. g. Kültepe II, Kizilvank and Culfa) confirm their widespread occurrence before the onset of the Late Bronze Age (Bahşaliyev 1997: 109). The closest comparison, however, can again be drawn with a black-polished walnut-shaped bowl found in Karacamirli Kurgan 5 (Гусейнова/Алиев 2008: Fig. VI, 6). Its surface was decorated with horizontal lines and a punctate hook ornament. As mentioned above, the punctate ornamentation is considered characteristic for a transitional phase between the Middle and Late Bronze Age, whereas the hook-motif is reminiscent of the Middle Bronze Age period. The bowl from Burial 2, however, was undecorated, indicative of a Late Bronze Age date.

The two undecorated bowls 0200-06 (Fig. 59, 3) and 0200-07 (Fig. 57 and Fig. 59, 2) complete the pottery assemblage of Burial 2. They follow the same typological connections as the previously described pieces and invite comparison with spheroid bowls with upright rims of the Lchashen-Metsamor 1 group (Smith et al. 2009: 73 sub 5a), even though those vessels are generally decorated on the outside and had more pronounced shoulders. Comparisons to bowls in the Karacamirli kurgans, which are all decorated as well, are limited to a few fragments in Kurgan 5 that show similar rim profiles (Гусейнова/Алиев 2008: Fig. VII, 5. 7).

In order to provide a corrective for our typological dating, two radiocarbon samples of charcoal (0189 and 0195) from the fill were analysed. They indicate a date for the filling between the very end of the 16th cent. BC and the beginning of the 15th cent. BC (Table 4, Beta-450962 and Beta-450963). This supports the conclusions drawn from the typological comparisons of the pottery, placing Burial 2 in the transitional phase between the Middle and Late Bronze Age or at the very beginning of the Late Bronze Age.

Grave contents

KG-044-0200-01 (pot) Fig. 59, 5
Rim diam.: 120 mm (100%)
H: 168 mm

Base diam.: 80 mm
Fabric: completely reducing atmosphere, hard, fine temper (132)
Surface: ext. polished; int. smoothed
Colour: ext. Gley 1 2.5/N (black); core Gley 1 4/N (dark grey); int. Gley 1 2.5/N (black)
Condition: part of rim broken off, surface partially flaked off, otherwise complete
Comparanda:
Apart from the missing decoration and its smaller size, the pot is typologically similar to KG-044-0200-03, KG-044-0200-04 and KG-044-0200-05

KG-044-0200-02 (bowl) Fig. 59, 1; Fig. 60
Rim diam.: 166–217 mm (100%)
H: 88 mm
Base diam.: 65–82 mm
Fabric: completely reducing atmosphere, hard, fine temper (132)
Surface: ext. and int. polished
Colour: ext. Gley 1 2.5/N (black); core Gley 1 4/N (dark grey); int. Gley 1 2.5/N (black)
Condition: along the rim surface partially flaking off, otherwise complete
Comparanda:
Karacamirli, Kurgan 5, MBA/LBA (Гусейнова/Алиев 2008: Fig. VI, 6)
Kültepe II, MBA levels (Алиев 1991: 110 Fig. XII, 1. Pl. 28, 8; Bahşaliyev 1997: Pl. XII, 6. 8)
Kizilvank, MBA (Алиев 1991: 108–110 Pl. 24, 7; Bahşaliyev 1997: 109 Pl. XIV, 4–5)
Culfa, MBA (Bahşaliyev 1997: 109; Алиев 1991: 108–110 Fig. XII, 2)
Lori Berd (Деведжян 1981, Pl. XI, 3–6)
Harich, Tomb 41, LBA I (Avetisyan/Bobokhyan 2008: 168 Fig. 31, 6; Smith et al. 2009: 75 Fig. 24o)
Karashamb, Burial 46, LBA I (Avetisyan/Bobokhyan 2008: 173 Fig. 36, 7)
Lchashen, Burial 200, LBA I (Avetisyan/Bobokhyan 2008: 174 Fig. 37, 4)
Lchashen, Burial 97, LBA II (Avetisyan/Bobokhyan 2008: 178 Fig. 41, 11–12; Smith et al. 2009: 80 Fig. 27a).
Verin-Naver, Burial 4, MBA (Kushnareva 1997: Fig. 54, 15)

KG-044-0200-03 (pot) Fig. 26; Fig. 59, 6
Rim diam.: 125 mm (100%)
H: 185 mm
Base diam.: 77 mm
Fabric: completely reducing atmosphere, hard, fine temper (132)
Surface: ext. and int. polished
Colour: ext. Gley 1 2.5/N (black); core Gley 1 4/N (dark grey); int. Gley 1 2.5/N (black)
Decoration: punctate ornamentation on the shoulder (two horizontal lines above a zigzag pattern)
Condition: complete
Comparanda:
Typological similarities to pots in Karacamirli Kurgan 4 and Kurgan 5, MBA/LBA (Гусейнова/Алиев 2008: Fig. I. V–VI)
Harich, Tomb 10, MBA III (Avetisyan 2003: 59 Pl. 1, 5; Avetisyan/Bobokhyan 2008: 160 Fig. 23, 3)
Harich, Tomb 13, MBA III (Avetisyan 2003: 59 Pl. 1, 7; Avetisyan/Bobokhyan 2008: 159 Fig. 22, 2; Smith et al. 2009: 70 Fig. 20g) – this pot has a more pronounced break between shoulder and neck
Harich, Tomb 29, MBA III (Хачатрян 1975: 105 Fig. 60; Avetisyan/Bobokhyan 2008: 158 Fig. 21, 3. 5; Smith et al. 2009: 70 Fig. 20k)
Harich, Tomb 41, LBA I (Avetisyan 2003: 59 Pl. 1, 9; Avetisyan/Bobokhyan 2008: 168 Fig. 31, 1)

KG-044-0200-04 (pot) Fig. 56; Fig. 59, 7
Rim diam.: 139 mm (100%)
H: 221 mm
Base diam.: 97 mm
Fabric: completely reducing atmosphere, hard, fine temper (132)
Surface: ext. polished; int. smoothed
Colour: ext. Gley 1 2.5/N (black); core Gley 1 4/N (dark grey); int. Gley 1 2.5/N (black)
Decoration: punctate ornamentation on the shoulder (two horizontal lines above a zigzag pattern, below each upwards pointing angle an additional angle)
Condition: complete, except for a notch in the rim
Comparanda:
Karacamirli, Kurgan 4, MBA/LBA (Гусейнова/Алиев 2008: Fig. I, 9); see also KG-044-0200-03

KG-044-0200-05 (pot) Fig. 59, 4
Rim diam.: ~150 mm (100%)
H: 224 mm
Base diam.: 120 mm
Fabric: completely reducing atmosphere, hard, fine temper (132)
Surface: ext. and int. polished
Colour: ext. Gley 1 2.5/N (black); core Gley 1 4/N (dark grey); int. Gley 1 2.5/N (black)
Decoration: see KG-044-0200-04
Condition: most part of the rim broken off; surface flaked off; base fragmented
Comparanda: see KG-044-0200-04

KG-044-0200-06 (bowl) Fig. 59, 3
Rim diam.: 162 mm (55%)
H: 85 mm
Base diam.: 68 mm
Fabric: completely reducing atmosphere, hard, fine temper (132)
Surface: ext. and int. polished
Colour: ext. Gley 1 2.5/N (black); core Gley 1 4/N (dark grey); int. Gley 1 2.5/N (black)
Condition: only the base and one side up to the rim were preserved; the damage was probably caused by disturbances during the interment of the adjacent Burial 34
Comparanda: Karacamirli, Kurgan 5, MBA/LBA (Гусейнова/Алиев 2008: Fig. VII, 5. 7)
Harich, Tomb 41, LBA I (Avetisyan 2003: 59 Pl. 1, 10. 12. 14; Avetisyan/Bobokhyan 2008: 168 Fig. 31, 2. 4–5; Smith et al. 2009: 75 Fig. 24b)

KG-044-0200-07 (bowl) Fig. 57; Fig. 59, 2
Rim diam.: 155 mm (100%)
H: 77 mm
Base diam.: 55 mm
Fabric: completely reducing atmosphere, hard, fine

temper (132)
Surface: ext. and int. polished
Colour: ext. Gley 1 2.5/N (black); core Gley 1 4/N (dark grey); int. Gley 1 2.5/N (black)
Condition: a quarter of the rim was flaked off (this side was shattered)
Comparanda: see KG-044-0200-06 and KG-051-0201-02

Fill

KG-044-0191-01 (body-sherd)
Fabric: completely reducing atmosphere, hard, fine temper (132)

KG-044-0188 (obsidian flake)
L: 36 mm; W: 22 mm; H: 6 mm; Wt: 4 g
606295.503 E; 4527995.836 N; 173.251 m

KG-044-0189 (charcoal sample) Table 4

KG-044-0195 (charcoal sample) Table 4

Burial 3 (KG-051)

Burial 3 was located in the south-eastern quadrant of square 6300/7990 (Fig. 27). The pit was of irregular shape and measured c. 80 cm from south-west to north-east and c. 1.5 m from north-west to south-east, where it extended further into the eastern baulk (Fig. 61). Its base

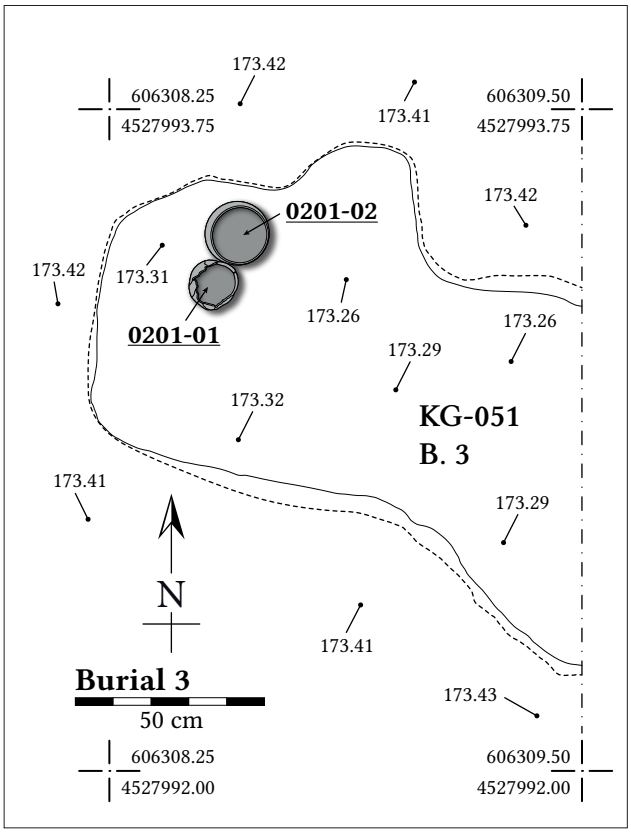

Fig. 61. Plan of Burial 3 (KG-051)

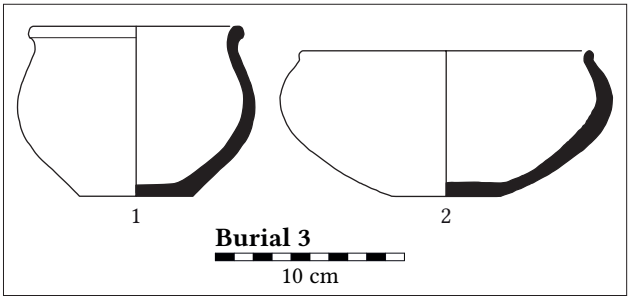

Fig. 62. Pottery from Burial 3 (KG-051): 1 – pot (0201-01); 2 – bowl (0201-02)

was reached already at a height of 173.25 m and thus considerably higher than in the case of most other burials. No skeletal remains were found and it is questionable whether Burial 3 ever contained an inhumation but belonged to the group of burial deposits or cenotaphs instead (see ch. IV.2.3).

Near the western edge of the pit, two pottery vessels were placed next to each other. The southern one (0201-01) was damaged and almost a third of the vessel's body was missing; nevertheless, the profile could be reconstructed, and it proved to be a small wide-mouthed pot with a flat base, a slightly curved body and a flaring thickened rim (Fig. 62, 1). Its clay was coarse and of black colour.

North of the small pot was a black-polished bowl (0201-02, Fig. 62, 2). Its fabric, surface treatment and morphological features were virtually identical to the spheroid bowls with short upright rim known from Burial 2 (in particular bowl 0200-07). It can therefore be assumed that there is no significant chronological distance between these two burials. Hence, the comparison with Burial 2, that was dated on the basis of radiocarbon analyses and typological comparisons to the transitional phase between the Middle Bronze Age and Late Bronze Age (end of the 16th cent. BC and the beginning of the 15th cent. BC), allows for a dating of Burial 3 no later than the early stage of the Late Bronze Age.

Grave contents

KG-051-0201-01 (pot) Fig. 62, 1
Rim diam.: 110 mm (55%)
H: 89 mm
Base diam.: 60 mm
Fabric: completely reducing atmosphere, medium hard, coarse temper (124)
Surface: ext. and int. smoothed
Colour: ext. Gley 1 2.5/N (black); core Gley 1 2.5/N (black); int. Gley 1 2.5/N (black)
Condition: one third of the upper vessel's body missing, highly fragmented

KG-051-0201-02 (bowl) Fig. 62, 2
Rim diam.: 154 mm (100%)
H: 77 mm

Base diam.: 57 mm
Fabric: completely reducing atmosphere, hard, fine temper (132)
Surface: ext. and int. polished
Colour: ext. Gley 1 2.5/N (black); core Gley 1 2.5/N (black); int. Gley 1 2.5/N (black)
Condition: a small portion of the rim was broken off
Comparanda: see KG-044-0200-06 and KG-044-0200-07

Burial 4 (KG-039 and KG-040)

Burial 4 was probably the earliest interment of Pit-Complex A (Fig. 42). This is implied by its poor state of preservation which is related to the subsequent interment of Burial 5 close to its northern side and of Burial 11 further south. Similarities in terms of body-orientation and altitude between Burials 4 and 5 indicate a chronological proximity between those two interments (see Burial 5). The outline of the grave-pit could not be determined (Fig. 63).

Of the skeleton, only the right radius, a single phalanx (0165) and parts of the lower legs (0163) were preserved (Fig. 64). The position of the bones suggests that the body was placed on its left side with its head in the north-west and with its legs flexed in a similar fashion as it was observed for Burial 5. Surrounding the radius was a dense cluster of different beads which probably adorned the head or upper part of the deceased's body. In total 27 carnelian beads of different sizes (0149a) were found spread over a small area south-east of the radius; their forms vary from large roundish beads to small disc-shaped beads (Fig. 65, 1–6). A second, very dense cluster of at least 57 tiny disc-shaped bone beads (0162) was located at the northern side of the radius. Most of them had an average diameter of 2 mm and a thickness of only 1–2 mm (Fig. 65, 12–13). Only two examples were larger and had diameters of 3 mm and 4 mm, respectively. These two larger beads had an additional perforation from side to side, that crossed the slightly larger main drill hole (Fig. 65, 10–11). Such double-perforated beads are, for instance, attested in Burial 19 at Khojaly (Rösler 1898b: 441 Fig.

Fig. 63. Pit-Complex A with Burials 4 (KG-039 & KG-040) and 5 (KG-038); the pot west of Burial 5 belongs to the already removed Burial 7; the two vessels at the western end of the Pit-Complex mark the location of Burial 10 (KG-041)

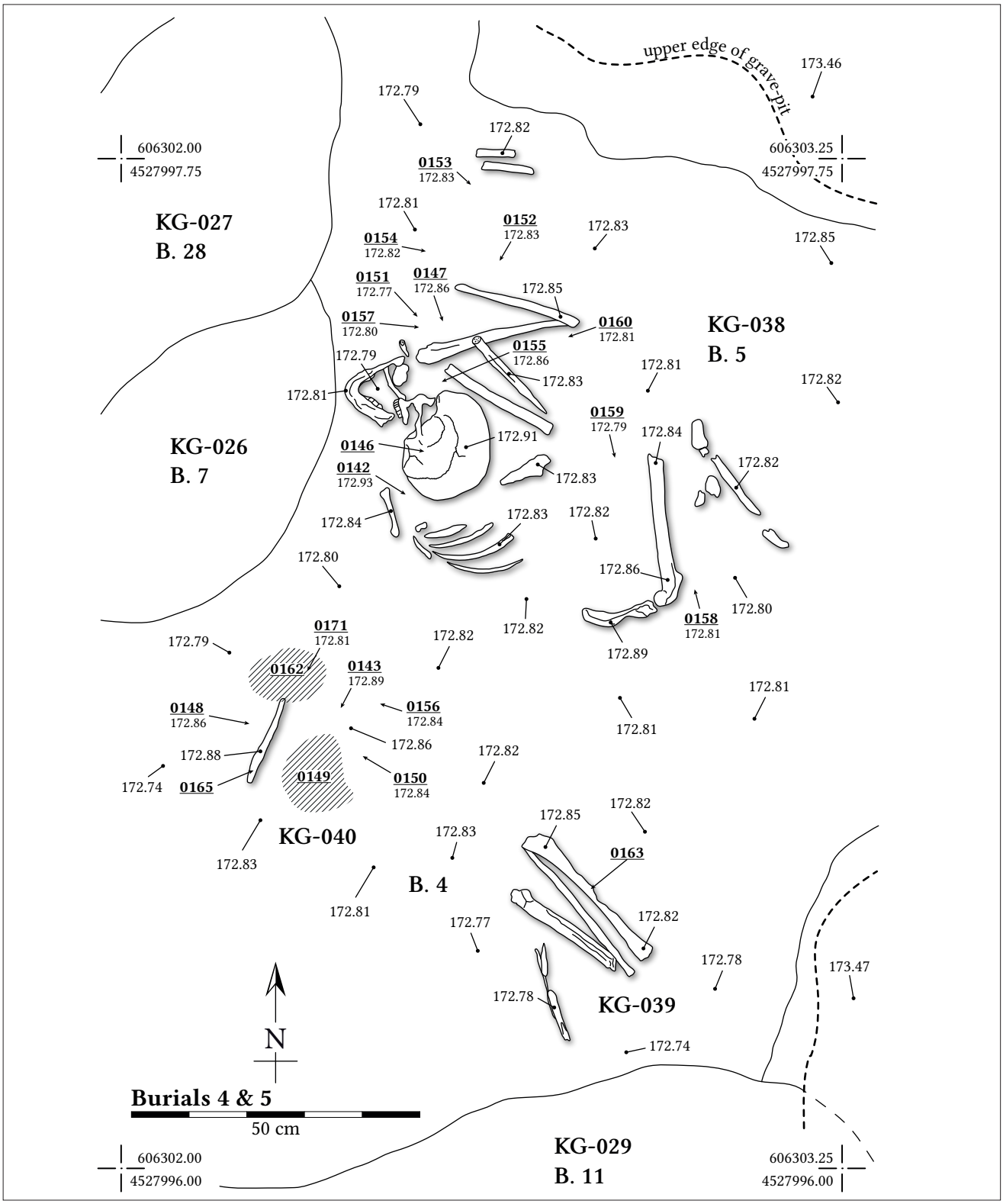

Fig. 64. Plan of Burials 4 (KG-039 & KG-040) and 5 (KG-038); Pit-Complex A

51u). In the area around the many carnelian and bone beads were also three frit beads of a light blue colour. Two of them (0148; 0156) had the shape of a rice grain with a lengthwise perforation and were decorated with short grooves arranged in a regular pattern around their surface (Fig. 65, 7–8). The third one (0143) had an irregular rhombic form and a biconical section; all over its surface were incised parallel grooves (Fig. 65, 9). The only bronze

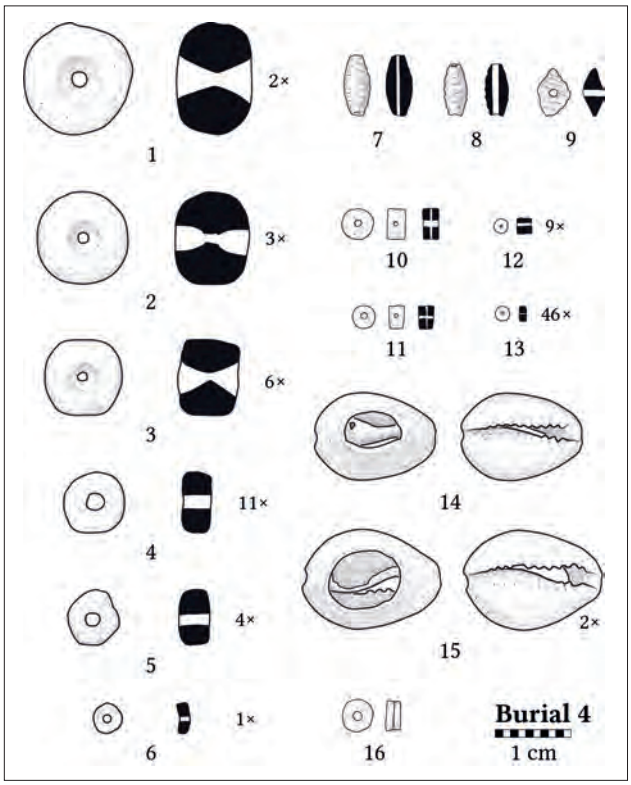

Fig. 65. Finds from Burial 4 (KG-039 & KG-040): 1–6 – carnelian beads (0149a); 7 – frit bead (0156); 8 – frit bead (0148); 9 – frit bead (0143); 10–13 – bone beads (0162); 14 – cowry shell (0150); 15 – cowry shell (0171); 16 – bronze bead (0149b)

objects found in Burial 4 were two small disc-shaped beads (0149b) that were discovered among the carnelian beads. The beads were fused by corrosion (Fig. 65, 16) and their form corresponds well with the many bronze beads of the adjacent Burial 5. Three cowrie shells (0150; 0171) add to the diversity of the adornment of the deceased in Burial 4 (Fig. 65, 14–15). Their back sides were cut off and the resulting hole made it easy to thread the shell or fix it to an object. Although no further shell items were found in the burials of Tepe 5, cowries and other molluscs appear regularly in various quantities as burial gifts throughout the Caucasus region (Reinhold 2007: 110) – as is the case, for example, in the burials at Mingachevir (Асланов et al. 1959: 154) or at Shusha (Rösler 1892: 566–567 Fig. 1).

Grave contents

KG-039-0163 & KG-040-0165 (human bones) Table 16
Sex: could not be determined
Age class: Adultas–Maturitas

KG-040-0143 (rhombic frit bead, light blue) Fig. 65, 9
L: 6.0 mm; W: 4.0 mm; Th: 2.5 mm;
Hole diam.: 0.9 mm; Wt: <1 g
606302.380 E; 4527996.799 N; 172.887 m

KG-040-0148 (grain-shaped frit bead, light blue) Fig. 65, 8
L: 7.7 mm; Diam: 3.2 mm; Hole diam.: 0.9 mm; Wt: <1 g
606302.222 E; 4527996.771 N; 172.862 m

KG-040-0156 (grain-shaped frit bead, light blue) Fig. 65, 7
L: 8.8 mm; Diam: 3.7 mm; Hole diam.: 0.5 mm; Wt: <1 g
606302.448 E; 4527996.806 N; 172.837 m

KG-040-0149a (27 carnelian beads) Fig. 65, 1–6
Diam: 4.0–12.0 mm; Th: 1.3–9.8 mm;
Hole diam.: 0.7–3.5 mm
scattered in the area:
606302.316 E; 4527996.640, N; 172.830 m
606302.367 E; 4527996.672, N; 172.849 m
606302.345 E; 4527996.734, N; 172.860 m

KG-040-0149b (two disc-shaped bronze beads) Fig. 65, 16
Diam: 4.2 mm; Th: 1.0 mm; Hole diam.: 1.2 mm
found in the area of KG-040-0149a

KG-040-0162 (57 disc-shaped bone beads, 2 of them with double perforation) Fig. 65, 10–13
Diam: 1.9–4.0 mm; Th: 1.0–2.0 mm; Hole diam.: 0.2–0.8 mm
scattered around the coordinates:
606302.288 E; 4527996.860, N; 172.822 m

KG-040-0150 (cowry shell) Fig. 65, 14
L: 15.8 mm; W: 11.4 mm; Th. 6.3 mm; Wt: 5 g
606302.418 E; 4527996.715 N; 172.844 m

KG-040-0171 (2 cowry shells) Fig. 65, 15
L: 18.0 mm; W: 13.0 mm; Th. 1.7 mm; Wt: 5.1 g
L: 19.0 mm; W: 17.0 mm; Th. 1.8 mm; Wt: 5.1 g
606302.323 E; 4527996.863 N; 172.805 m

Burial 5 (KG-038)

Burial 5 was located in the eastern section of Pit-Complex A (Fig. 42 and Fig. 63). In the north and east the outline of its grave-pit is identical with the edge of the Pit-Complex itself and formed a right-angled corner, so the grave-pit may originally have been of rectangular shape, with a north-west to south-east orientation. Its southern end could not be determined, although it should be expected somewhere very close to Burial 4, since the latter might have sustained some damage by the interment of Burial 5. The western edge of the grave-pit was completely destroyed by Burials 7 and 28 (Fig. 64).

The deceased had been interred on his left side with its legs and arms in a flexed position. The skull was only half preserved and not in its original position. It had fallen onto the chest, and the lower jaw was turned upside down. The secondary position of the skull was probably due to the proximity of the adjacent Burial 7, the grave-pit of which extended as far as the skeletal remains of Burial 5. The disarticulation of the skull might have been caused either unintentionally by the earth movements and changed conditions of the soil density during the interment of Burial 7 or, more likely, the skull of Burial 5

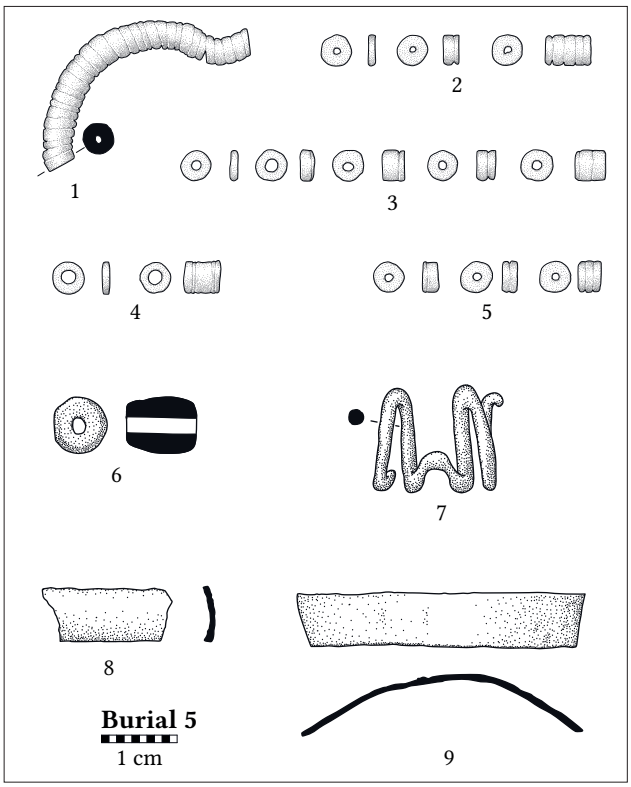

Fig. 66. Finds from Burial 5 (KG-038): 1 – bronze beads (0157); 2 – bronze beads (0155); 3 – bronze beads (0151); 4 – bronze beads (0147); 5 – bronze beads (0154); 6 – carnelian bead (0153); 7 – temporal bronze ornament (0158); 8 – bronze strip (0160); 9 – bronze strip (0159)

was uncovered, damaged and intentionally pushed back into the side wall of the grave-pit. The latter possibility, however, would imply that there was still an open or at least loosely filled cavity or burial chamber above the deceased of Burial 5 at the time.

The relation of two fragmented long bones 20–25 cm north of the left forearm with the actual skeleton remains unclear; their proximity and identical heights suggest that they are an integral but displaced part of the burial. In that area a single barrel-shaped carnelian bead (0153, Fig. 66, 6) and an obsidian flake were found (0152).

The body or garment of the deceased was adorned mainly with bronze objects. Most noteworthy are 58 tiny disc-shaped bronze beads discovered near the left shoulder (0147; 0151; 0154; 0155; 0157). They measured 4 mm in diameter with a perforation of 0.7–1.8 mm (Fig. 66, 1–5). Their thickness varied between 1 and 1.5 mm. Many beads were corroded – a set of 30 beads (0157) still reproduced the form of the thread on which they were strung (Fig. 66, 1). Next to the left elbow was the fragment of a thin strip of bronze (Fig. 66, 8). It could be part of a second, but longer piece of a bent bronze strip that was detected between the right elbow and the right knee (Fig. 66, 9). Near the joint between pelvis and right femur a spiral-shaped artefact made of a thick bronze wire was found (Fig. 66, 7). It resembles two similarly twisted objects – so called temporal curls or rings – found in Tomb 65 at Harich that was assigned to the Trialeti-Vanadzor 3 ceramic style of the Middle Bronze Age III period (Хачатрян 1975: 116–117 Fig. 71; Kushnareva 1997: 143 Fig. 67, 4; Smith et al. 2009: 67). This type of jewellery – though often made of gold – can be traced back to the late Kura-Araxes culture (Lordkipanidze 1991: 51; Stöllner 2018: 125) and is well attested in the kurgans of the Middle Bronze Age Trialeti culture (Куфтин 1941: 94; Lordkipanidze 1991: 68). Various forms, however, also continued in use throughout the Late Bronze Age/Early Iron Age and beyond (Reinhold 2007: 77–78).

The link with Harich Tomb 65 relates Burial 5 with the earliest group of burials at Tepe 5, in particular with Burials 1 and 2, the pottery of which already displayed great similarities with Middle Bronze Age III burials at Harich. The early date is confirmed by a radiocarbon date (Beta-506513) taken from the skeleton that makes an interment of the deceased within the 15th cent. BC probable (Table 4).

Grave contents

KG-038-0146 (human bones) Table 4
Sex: probably male Table 16
Age class: Adultas

KG-038-0147 (4 disc-shaped bronze beads) Fig. 66, 4
Diam: 4.0 mm; Th: 1.0 mm;
Hole diam.: 1.8 mm; Wt: <1 g
606302.557 E; 4527997.469 N; 172.859 m

KG-038-0151 (8 disc-shaped bronze beads) Fig. 66, 3
Diam: 4.0 mm; Th: 1.0–1.5 mm;
Hole diam.: 1.3–1.7 mm; Wt: <1 g
606302.513 E; 4527997.477 N; 172.773 m

KG-038-0153 (barrel-shaped carnelian bead) Fig. 66, 6
L: 8.4 mm; Diam: 7.1 mm; Hole diam.: 1.4 mm; Wt: <1 g
606302.606 E; 4527997.706 N; 172.833 m

KG-038-0154 (7 disc-shaped bronze beads) Fig. 66, 5
Diam: 4.0 mm; Th: 1.0 mm;
Hole diam.: 1.1 mm; Wt: <1 g
606302.528 E; 4527997.589 N; 172.821 m

KG-038-0155 (8 disc-shaped bronze beads) Fig. 66, 2
Diam: 4.0 mm; Th: 1.0 mm;
Hole diam.: 0.7 mm; Wt: <1 g
606302.557 E; 4527997.363 N; 172.855 m

KG-038-0157 (30 disc-shaped bronze beads) Fig. 66, 1
L: 36.5 mm (string); Diam: 4.0 mm; Th: 1.0 mm;
Hole diam.: 0.8 mm; Wt: <1 g
606302.516 E; 4527997.458 N; 172.797 m

KG-038-0158 (temporal bronze ornament) Fig. 66, 7
L: 16.7 mm; Diam: 15.0 mm; Diam (wire): 2.0–3.00 mm
606302.994 E; 4527997.004 N; 172.805 m

Comparanda:
Harich, Tomb 10, MBA III (Хачатрян 1975: 116–117 Fig. 71; Kushnareva 1997: 143 Fig. 67, 4)

KG-038-0159 (fragment of bronze strip) Fig. 66, 9
L: 20.0 mm; W: 6.8 mm; Th: 1.2 mm; Wt: <1 g
606302.856 E; 4527997.232 N; 172.786 m

KG-038-0160 (fragment of bronze strip) Fig. 66, 8
L: 16.3 mm; W: 7.00 mm; Th: 1.3 mm; Wt: <1 g
606302.775 E; 4527997.441 N; 172.806 m

Fill

KG-038-0141-01 (rim sherd)
Fabric: not fully oxidized, medium hard, medium fine temper (523)
Surface: ext. and int. smoothed
Colour: ext. 5YR 6/4 (reddish brown); core 5YR 3/1 (very dark grey); int. 5YR 6/4 (light reddish brown)
perforated just below the rim (Chalcolithic mangal)

KG-038-0101 (obsidian flake)
L: 15.0 mm; W: 7.0 mm; Th: 2.0 mm; Wt: 1 g
606302.486 E; 4527997.666 N; 172.910 m

KG-038-0140 (obsidian flake)
L: 35.0 mm; W: 28.0 mm; Th: 5.9 mm; Wt: 6 g
606302.815 E; 4527997.512 N; 173.025 m

KG-038-0142 (obsidian flake)
L: 14.1 mm; W: 12.9 mm; Th: 5.2 mm; Wt: 1 g
606302.492 E; 4527997.168 N; 172.929 m

KG-038-0152 (obsidian flake)
L: 25.1 mm; W: 11.2 mm; Th: 4.8 mm; Wt: 1 g
606302.656 E; 4527997.574 N; 172.826 m

Burial 6 (KG-095-0497)

Burial 6 was located in the southern half of Pit-Complex C-2 (Fig. 44). The grave-pit had a rectangular outline and extended c. 2.5 m from west to east (Fig. 67 and Fig. 68). The northern edge was for the most part removed by the Late Antique Burial 22. Only in the westernmost area, adjacent to Burial 45, was the original width of the grave-pit preserved. It measured c. 0.8–1.0 m but might well have been wider on the eastern side. The burial contained a badly preserved skeleton that occupied the south-eastern part of the pit. This area was further distinguished by a noticeable density of obsidian flakes. Judging by the position of the leg bones, the body was placed on its left side with flexed legs. Its head was in the west and rested in a large bowl (0498-01). Examples for the intentional positioning of the head in a bowl are known from Tovuzchay, e. g. Burials 28 and 69, and Zayamchay, e. g. Burial 71 (Maynard 2011; Taylor et al.

Fig. 67. Pit-Complex C-1 and 2 with Burial 6 (KG-095-0497) in the south, Burial 45 (KG-096) in the west and Burial 22 (KG-095-0496) in the north

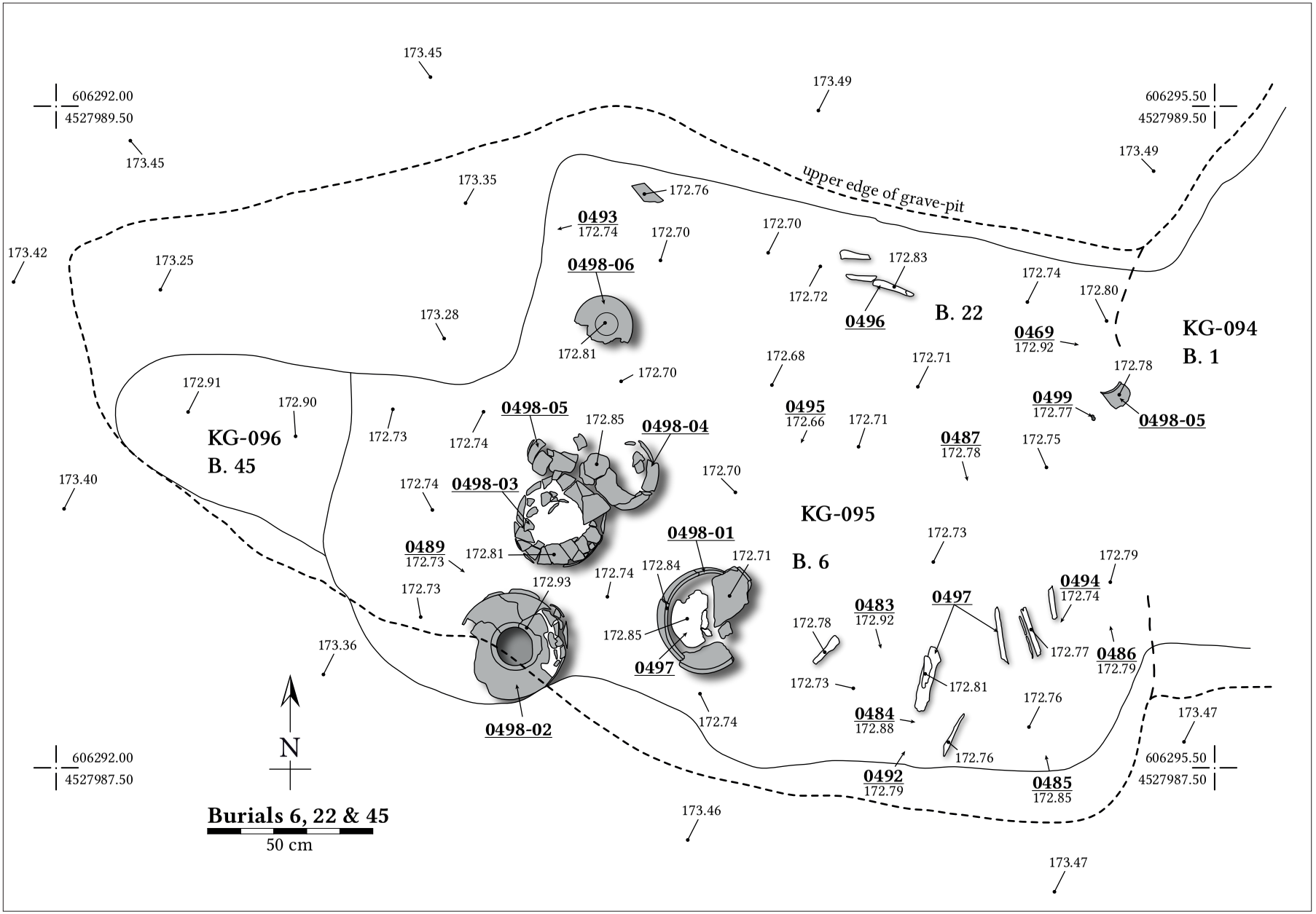

Fig. 68. Plan of Burials 6 (KG-095-0497), 22 (KG-095-0496) and 45 (KG-096); Pit Complex C-1–2

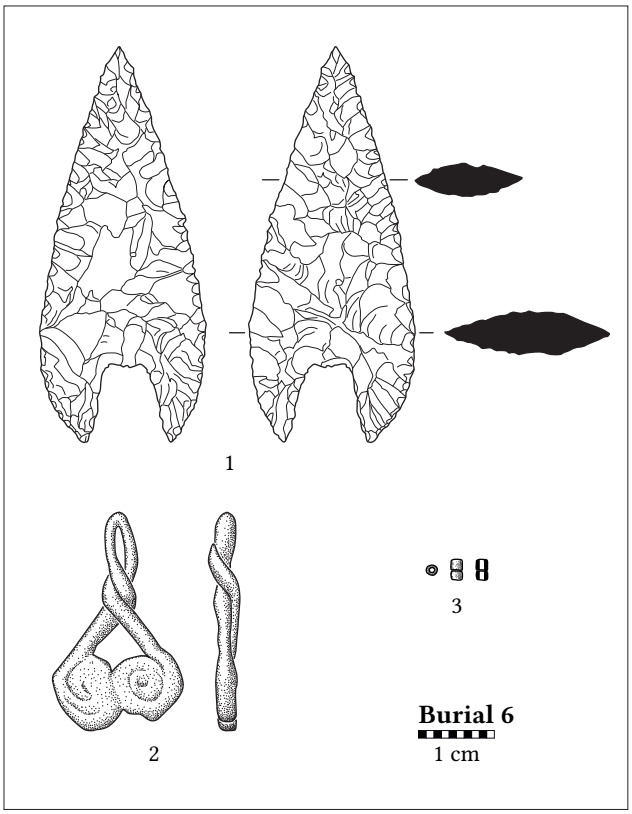

Fig. 69. Finds from Burial 6 (KG-095-0497): 1 – obsidian arrowhead (0489); 2 – bronze pendant (0499); 3 – frit beads (0490)

Fig. 70. Bowl 0498-01 from Burial 6 (KG-095-0497)

Fig. 71. Pot 0498-02 with decorated lug from Burial 6

2011: 148; Müseyibli/Nəcəfov 2019: 402 Fig. 167, 2). Five more vessels were placed at some distance west of the deceased. Between the two pots 0498-02 and 0498-03 we found a carefully retouched obsidian arrowhead (0489, Fig. 69,1). The three northernmost vessels (0498-04, 0498-05 and 0498-06) all suffered damage from the interment of Burial 22. The pot 0498-06 was displaced from its original position and lay upside down slightly off the other vessels. The extension of the disturbance is best illustrated by a single rim-sherd of bowl 0498-05 found at the eastern end of the Late Antique grave-pit (Fig. 68). Next to it an object made of bronze wire (0499) was found that seems to have been dislocated from Burial 6 as well. Both ends of the wire were bent into spirals, and the middle part was twisted to form an eye (Fig. 69, 2). This type of jewellery resembles the double-spiral pendants known, for example, from Kurgan 3 near Killik-Dagh (Реслер 1902: 74 Fig. 150), Kurgan 1 near *Helenendorf* (Погребова 2011: Pl. XXXIV, 4), *Paradiesfestung* Burial 142 (Nagel/Strommenger 1985: 131 Fig. 101, 1) or from Burial 102 at Mingachevir (Асланов et al. 1959: 80 XVII, 33–34). In the fill of the same area were two bluish cylindrical frit beads fused together (0490, Fig. 69, 3). Since none of the other Late Antique burials contained beads, they are more likely to be associated with the Late Bronze Age burial. In addition, a single human tooth (0468) was found loose in the fill c. 30 cm above the ground of the pit. It was either displaced from one of the two skeletons or more likely originated from Burial 45.

The bowl holding the skull (0498-01, Fig. 70 and Fig. 72, 6) had a flat base and a spheroid body with a carination that pronounced the convex collar. Such profiles are attested in several burials excavated near Kalakent, e. g., in Burial 11 and a smaller variant in Burial 55 (Ивановский 1911: 93. 126 Pl. XI, 3. XII, 11). Noteworthy is a similar bowl found in Kurgan 3 of the so-called Steppe Kurgans near Ganja that was dated to the 13th cent. BC (Погребова 2011: 95–96 Pl. XXVIII, 3).

The egg-shaped pot at the southern edge of the pit (0498-02, Fig. 71 and Fig. 72, 2) was made of grey fabric, and the lower body was covered with polished vertical lines down to the round base. On the shoulder and just below the rim run two combed horizontal lines. The short rim was bent outwards to form a horizontal lip.

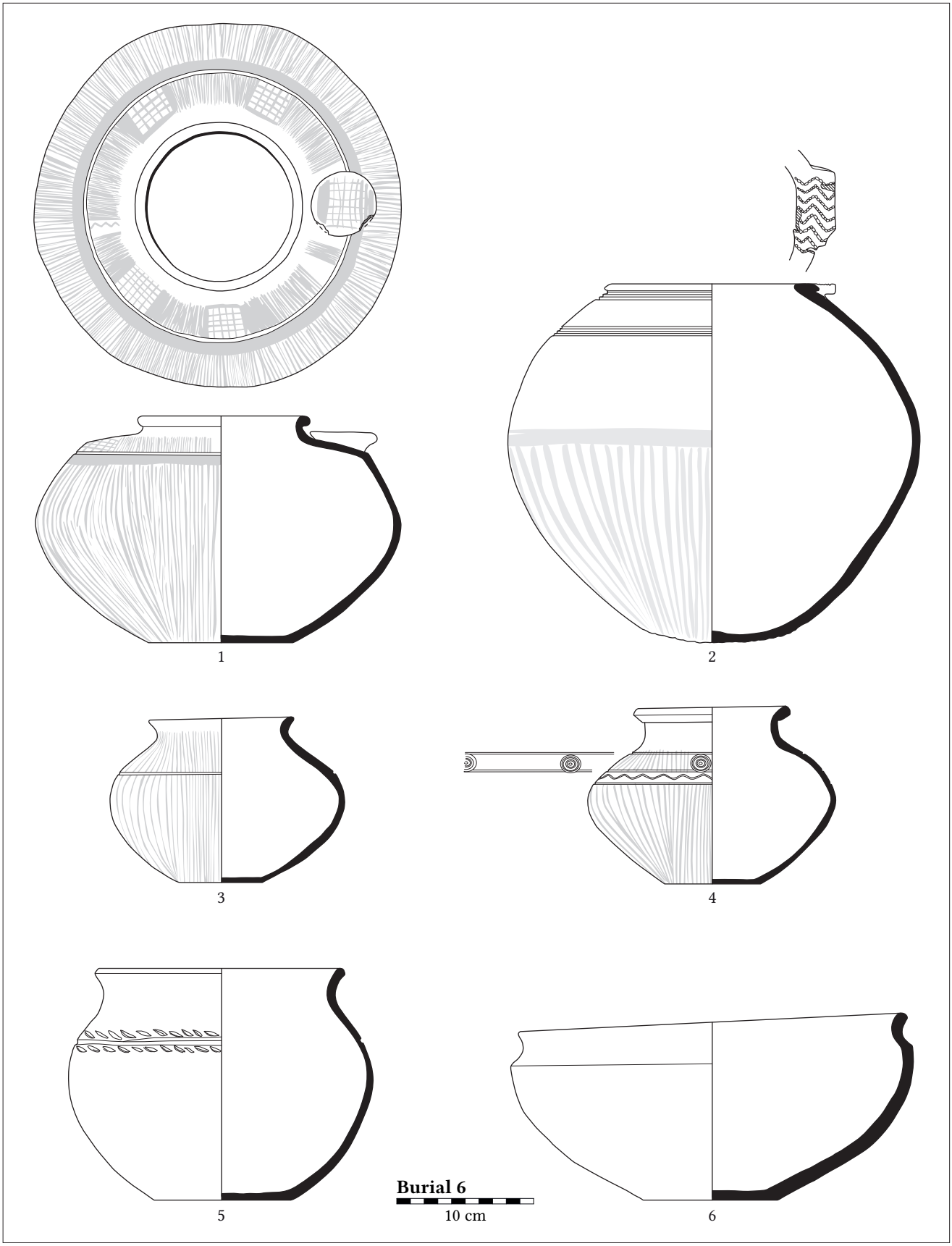

Fig. 72. Pottery from Burial 6 (KG-095-0497): 1 – pot (0498-03); 2 – pot (0498-02); 3 – pot (0498-05); 4 – pot (0498-06); 5 – pot (0498-04); 6 – bowl (0498-01)

Fig. 73. Pot 0498-03 with polished decoration and disc-shaped lug from Burial 6 (KG-095-0497)

Fig. 74. Pot 0498-06 from Burial 6 (KG-095-0497) with circular impressions on the shoulder

On one side protruded a rectangular lug decorated on top with eight zigzag lines made with the same punctate ornamentation technique as it was observed on the pottery in Burials 1 and 2. A similar vessel is known from the Zayamchay cemetery in Burial 44, although in that case the vessel carried an additional line of diagonal notches around the shoulder and the flat upper side of the rim was ribbed and the zigzag pattern on the horizontal lug was incised (Müseyibli/Nəcəfov 2019: 296 Fig. 61, 4). This vessel type is attested also in burials at Mingachevir (Асланов et al. 1959: Pl. XXIX, 4) or in the area of Kalakent (Ивановский 1911: Pl. X, 1).

The chronologically most significant vessel is the richly decorated pot 0498-03 (Fig. 72, 1 and Fig. 73). It had a flat base and a spheroid body with an angular transition to the shoulder which gives the vessel a stocky appearance. The neck is short, and the rim is thickened externally. The shoulder is further pronounced by a single incised groove with a polished band right below. The body was completely covered with polished vertical lines, and the shoulder was decorated with alternating fields of dense vertical lines and cross-hatchings that were interrupted on one side by a disc-shaped lug resting on the shoulder. The flat surface of the lug was decorated with cross-hatching as well. On the opposite side of the lug, the regular pattern was changed and a field with cross-hatching was exchanged for a vertical wavy line. A morphologically similar vessel with polished decoration is known from Burial 78b at Mingachevir: (Асланов 1959: 62 Fig. 43 Pl. XXIX, 11). Comparisons can also be drawn with several vessels from Khojaly Kurgan 5, dated by M. A. Gusejnova to the 14th–13th cent. BC (Гусейнова 1989: 11–12 Pl. I, 5. 8–10; 2011: 96). Slightly earlier is the proposed dating brought forward by M. N. Pogrebova who assigned the same kurgan to her first chronological stage that covers the 15th and 14th cent. BC (Погребова 2011: Pl. XXIII, 1–2. 4).

Two completely damaged small pots sat next to pot 0498-03; of both vessel sherds were missing or displaced during the interment of the Late Antique Burial 22. Only half of the medium fine tempered pot 0498-04 was recovered, though its morphological features could be fully restored (Fig. 72, 5). It had a flat base, a sinuous profile with a slightly flaring neck and wide opening. The shoulder was decorated with two rows of diagonal notches and a single groove in between. Similar shaped pots with a wide opening are known, for example, from Kurgan 34 (Гусейнова 1989: Pl. IV, 17) or Kurgan 8 near *Helenendorf* (Гуммель 1940: 40–41 Fig. 16, II-4), whereby the shoulder of the latter was incised with a more complex pattern. Both complexes were dated either to the 14th–13th cent. BC (Гусейнова 1989: 16) or to the 15th–14th cent. BC (Погребова 2011: 64–68). In addition, some wide mouthed and decorated pots from Mingachevir resemble our vessel (Асланов 1959: Pl. XXXIII, 2. 4).

The second pot (0498-05, Fig. 72, 3) was better preserved, although some of its sherds were spread over a large area. The dark-coloured surface was covered from the rim down to the base by vertical polished lines. The shoulder was emphasized by a single incised groove. The pot was smaller than 0498-04 and had a more pronounced curvature of the body and a narrower neck, however, the typological comparisons point into the same direction (see below). Most noteworthy is a similarly decorated piece – though with a more pronounced carination – from Kurgan 34 near *Helenendorf* (Гусейнова 1989: 16 Pl. IV, 14).

The last pot (0498-06) was situated further north of the other vessels (Fig. 72, 4 and Fig. 74). It had a pronounced, almost biconical profile with a flat base, a short upright neck and an externally thickened rim that was slightly bent outwards. The surface was covered with polished vertical lines up to three horizontal grooves that divided the shoulder into two circumferential strips, the lower of which contained an incised wavy line and the upper an alternating pattern of polished vertical lines and five circular impressions. Comparisons can be drawn again with Kurgan 8 near *Helenendorf*, in particular with a morphologically similar but undecorated vessel (Гуммель 1940: 41 Fig. 16. II-3). The same kurgan, as well as Kurgan 14, contained different ceramic types with identical circular impressions as on the pot in Burial 6 (Гуммель 1940: 41. 55–56 Fig. 16–17, III-1. 22–23, III-4; Гусейнова 1989: Pl. VI, 3. 31). As already pointed out by M. N. Pogrebova (Погребова 2011: 66), a similar circular ornament is known also on a vessel from Burial 437 in the Artik necropolis in Armenia (Хачатрян 1975: 226 Fig. 139; 1979: 305). The Artik burials are dated predominantly to the Late Bronze Age II/Lchashen-Metsamor 2 pottery horizon which was previously dated roughly to the mid-15th through the late 14th cent. BC (Smith et al. 2009: 77–81), but recently a revised date from the early 13th to the mid-12th cent. BC was proposed for the Late Bronze Age II period on the Tsaghkahovit Plain (Manning et al. 2018: 1539–1542). Another characteristic feature of the Lchashen-Metsamor 2 pottery in Armenia is the frequent use of polished decoration that appears remarkable often also on the vessels from Burial 6. These comparisons with Artik and the kurgans near *Helenendorf* make it possible to assign Burial 6 to the Late Bronze Age. The various chronological proposals for comparable archaeological material from Azerbaijan and Armenia do not allow for a more precise dating between the 15th cent. BC and mid-12th cent. BC. However, considering the characteristics of the pottery, which differs from the early group of Tepe 5 burials (Burials 1–5) on the one hand and from the Early Iron Age burials on the other hand, we tentatively date Burial 6 from the 14th to the mid-12th cent. BC.

Grave contents

KG-095-0497 (human bones)
Sex and age could not be determined — Table 16

KG-095-0498-01 (bowl) — Fig. 70; Fig. 72, 6
Rim diam.: 280 mm (100%)
H: 135 mm
Base diam.: 100 mm
Fabric: completely reducing atmosphere, medium hard, fine temper (122)
Surface: ext. burnished; int. smoothed
Colour: ext. Gley 1 2.5/N (black); core 2.5Y 5/2 (greyish brown); int. 2.5Y 5/2 (greyish brown)
Condition: broken into larger sherds, but otherwise complete
Comparanda:
Kalakent, e. g. Burials 11 and 55, LBA/EIA (Ивановский 1911: 93. 126 Pl. XI, 3. XII, 11)
Steppe Kurgans, Kurgan 3, LBA (Погребова 2011: 95–96 Pl. XXVIII, 3)

KG-095-0498-02 (pot) — Fig. 71; Fig. 72, 2
Rim diam.: 120 mm (100%)
H: 245 mm
Base diam.: ~70 mm
Fabric: exterior reducing, interior oxidizing atmosphere, medium hard, medium fine temper (423)
Surface: ext. burnished; int. smoothed
Colour: ext. Gley 1 3/N (very dark grey); core Gley 1 5/N (grey); int. 10YR 5/1 (grey)
Decoration: the lower body was covered with polished decoration (vertical lines and horizontal band around the largest circumference); on the shoulder and below the rim were two incised combed lines; the horizontal lug was decorated with punctate ornamentation in form of eight zigzag lines
Condition: broken into sherds, but complete; to ensure stability base and body were kept separate
Comparanda:
Zayamchay, Burial 44, LBA/EIA (Müseyibli/Nəcəfov 2019: 296 Fig. 61, 4)
Mingachevir, e. g. Burial 63, LBA/EIA (Асланов et al. 1959: Pl. XXIX, 4)
area of Kalakent, Burials 26 and 38, LBA/EIA (Ивановский 1911: Pl. X, 1)

KG-095-0498-03 (pot) — Fig. 72, 1; Fig. 73
Rim diam.: 120 mm (100%)
H: 165 mm
Base diam.: 105 mm
Fabric: completely reducing atmosphere, medium hard, coarse temper (124)
Surface: ext. burnished; int. smoothed
Colour: ext. Gley 1 2.5/N (black); core 5Y 4/1 (dark grey); int. 5Y 4/1 (dark grey)
Decoration: incised groove and polished band around the shoulder; the lower body was covered with polished vertical lines; the shoulder carried a polished decoration of vertical lines and cross-hatchings (in one case a vertical wavy line); the lug was covered with a polished cross-hatching
Condition: broken into many sherds, but completely reassembled
Comparanda: Mingachevir, Burial 78b, LBA/EIA (Асланов 1959: 62 Pl. XXIX, 11)

KG-095-0498-04 (pot) — Fig. 72, 5
Rim diam.: 160 mm (50%)
H: 175 mm
Base diam.: 90 mm
Fabric: irregular atmosphere, medium hard, medium fine temper (723)
Surface: ext. and int. smoothed
Colour: ext. Gley 1 2.5/N (black); core 10YR 5/3

(brown); int. 10YR 4/1 (dark grey)
Decoration: one or two incised grooves around the shoulder that was bordered on both sides by single rows of diagonally impressed notches
Condition: fragmented, half of the vessel is missing
Comparanda:
Helenendorf, Kurgan 34, LBA (Гусейнова 1989: 16 Pl. IV, 17)
Helenendorf, Kurgan 8, LBA (Гуммель 1940: 41 Fig. 16, II-4. 17 II-4; Гусейнова 1989: Pl. VI, 10)
Mingachevir, e. g Burials 81 and 135, LBA/EIA (Асланов 1959: Pl. XXXIII, 2. 4)

KG-095-0498-05 (pot) Fig. 72, 3
Rim diam.: 105 mm (100%)
H: 118 mm
Base diam.: 63 mm
Fabric: completely reducing atmosphere, hard, fine temper (132)
Surface: ext. burnished; int. smoothed
Colour: ext. Gley 1 2.5/N (black); core 5Y 5/1 (grey); int. Gley 1 5/1 (greenish grey)
Decoration: a single incised groove around the shoulder, the remaining body was completely covered by polished vertical lines
Condition: some of the body-sherds are missing
Comparanda:
Helenendorf, Kurgan 34, LBA (Гусейнова 1989: 16 Pl. IV, 14)
Mingachevir, Burials 23 and 78a, LBA/EIA (Асланов 1959: Pl. XXXIV, 1)

KG-095-0498-06 (pot) Fig. 72, 4; Fig. 74
Rim diam.: 110 mm (100%)
H: 125 mm
Base diam.: 70 mm
Fabric: completely reducing atmosphere, medium hard, fine temper (122)
Surface: ext. burnished; int. smoothed
Colour: ext. Gley 2 2.5/5PB (bluish black); core Gley 1 4/N (dark grey); int. Gley 1 2.5/N (black)
Decoration: three incised grooves divided the shoulder into two stripes with alternating patterns of circular impressions and polished vertical lines as well as a single wavy line; the lower body was completely covered with polished vertical lines
Condition: approximately a quarter of the vessel's body was missing
Comparanda:
Helenendorf, Kurgan 8, LBA (Гуммель 1940: 41 Fig. 16. II-3; Гусейнова 1989: Pl. VI, 2)

KG-095-0489 (obsidian arrowhead) Fig. 69, 1
L: 52.0 mm; W: 22.0 mm; Th: 5.2 mm; Wt: 4 g
606293.232 E; 4527988.088 N; 172.730 m

Fill

KG-095-0468 (human tooth)
Single tooth (I1)

KG-095-0499 (bronze pendant) Fig. 69, 2
L: 29.0 mm; W: 17.1 mm; Th: 4.2 mm; Wt: 1 g
606295.131 E; 4527988.559 N; 172.766 m

KG-095-0490 (two bluish cylindrical frit beads) Fig. 69, 3
Diam: 1.5 mm; Th: 3.0 mm; Hole diam.: 0.8 mm

KG-095-0429 (obsidian flake)
L: 21.0 mm; W: 11.0 mm; Th: 4.0 mm; Wt: 1 g
606295.192 E; 4527989.066 N; 173.397 m

KG-095-0430 (obsidian flake)
L: 18.0 mm; W: 12.0 mm; Th: 3.0 mm; Wt: 1 g
606293.751 E; 4527988.926 N; 173.298 m

KG-095-0431 (obsidian flake)
L: 22.0 mm; W: 21.0 mm; Th: 4.0 mm; Wt: 1 g
606293.843 E; 4527988.743 N; 173.284 m

KG-095-0432 (obsidian flake)
L: 18.0 mm; W: 8.0 mm; Th: 4.2 mm; Wt: <1 g
606294.030 E; 4527988.514 N; 173.351 m

KG-095-0433 (obsidian flake)
L: 23.0 mm; W: 18.0 mm; Th: 5.0 mm; Wt: 2 g
606293.959 E; 4527987.964 N; 173.383 m

KG-095-0434 (obsidian flake)
L: 21.0 mm; W: 14.5 mm; Th: 5.0 mm; Wt: 1 g
606294.113 E; 4527987.644 N; 173.363 m

KG-095-0469 (obsidian flake)
L: 25.0 mm; W: 10.0 mm; Th: 8.0 mm; Wt: 1 g
606295.093 E; 4527988.778 N; 172.924 m

KG-095-0481 (obsidian flake)
L: 15.0 mm; W: 6.5 mm; Th: 5.5 mm; Wt: <1 g

KG-095-0483 (obsidian flake)
L: 41.0 mm; W: 26.0 mm; Th: 8.0 mm; Wt: 6 g
606294.492 E; 4527987.858 N; 172.919 m

KG-095-0484 (obsidian flake)
L: 15.0 mm; W: 13.0 mm; Th: 5.0 mm; Wt: <1 g
606294.598 E; 4527987.640 N; 172.877 m

KG-095-0485 (obsidian flake)
L: 29.0 mm; W: 17.2 mm; Th: 8.5 mm; Wt: 3 g
606294.991 E; 4527987.541 N; 172.850 m

KG-095-0486 (obsidian flake)
L: 32.5 mm; W: 25.5 mm; Th: 4.0 mm; Wt: 4 g
606295.184 E; 4527987.927 N; 172.786 m

KG-095-0487 (obsidian flake)
L: 36.0 mm; W: 29.0 mm; Th: 5.5 mm; Wt: 3 g
606294.755 E; 4527988.368 N; 172.775 m

KG-095-0492 (obsidian flake)
L: 22.0 mm; W: 13.5 mm; Th: 5.0 mm; Wt: <1 g
606294.567 E; 4527987.553 N; 172.793 m

KG-095-0493 (obsidian flake)
L: 42.5 mm; W: 31.0 mm; Th: 20.0 mm; Wt: 15 g
606293.511 E; 4527989.126 N; 172.743 m

KG-095-0494 (obsidian flake)
L: 19.0 mm; W: 11.5 mm; Th: 6.0 mm; Wt: <1 g
606295.037 E; 4527987.937 N; 172.736 m

KG-095-0487 (silex flake with cortex)
L: 40.0 mm; W: 31.5 mm; Th: 11.5 mm; Wt: 13 g
606294.250 E; 4527988.480 N; 172.655 m

Fig. 75. Pit-Complex A with Burial 7 (KG-026) and the Medieval Burial 28 (KG-027); at the time the foto was taken, the pot 0100-09 east of the skull was not yet exposed (see Fig. 63).

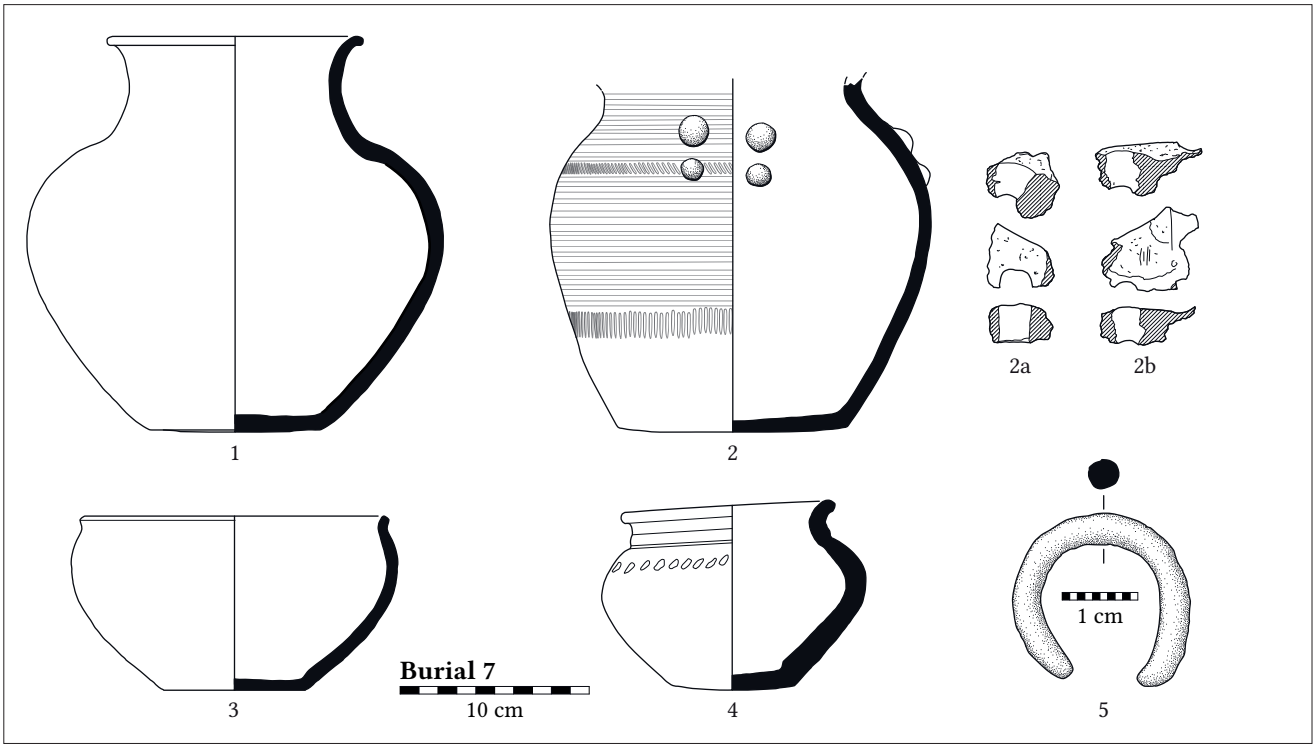

Fig. 76. Pottery from Burial 7 (KG-026): 1 – pot (0100-03); 2 – pot (0100-01); 3 – bowl (0100-02); 4 – pot (0100-09); 5 – bronze ring found in fill of Burial 28 (0103)

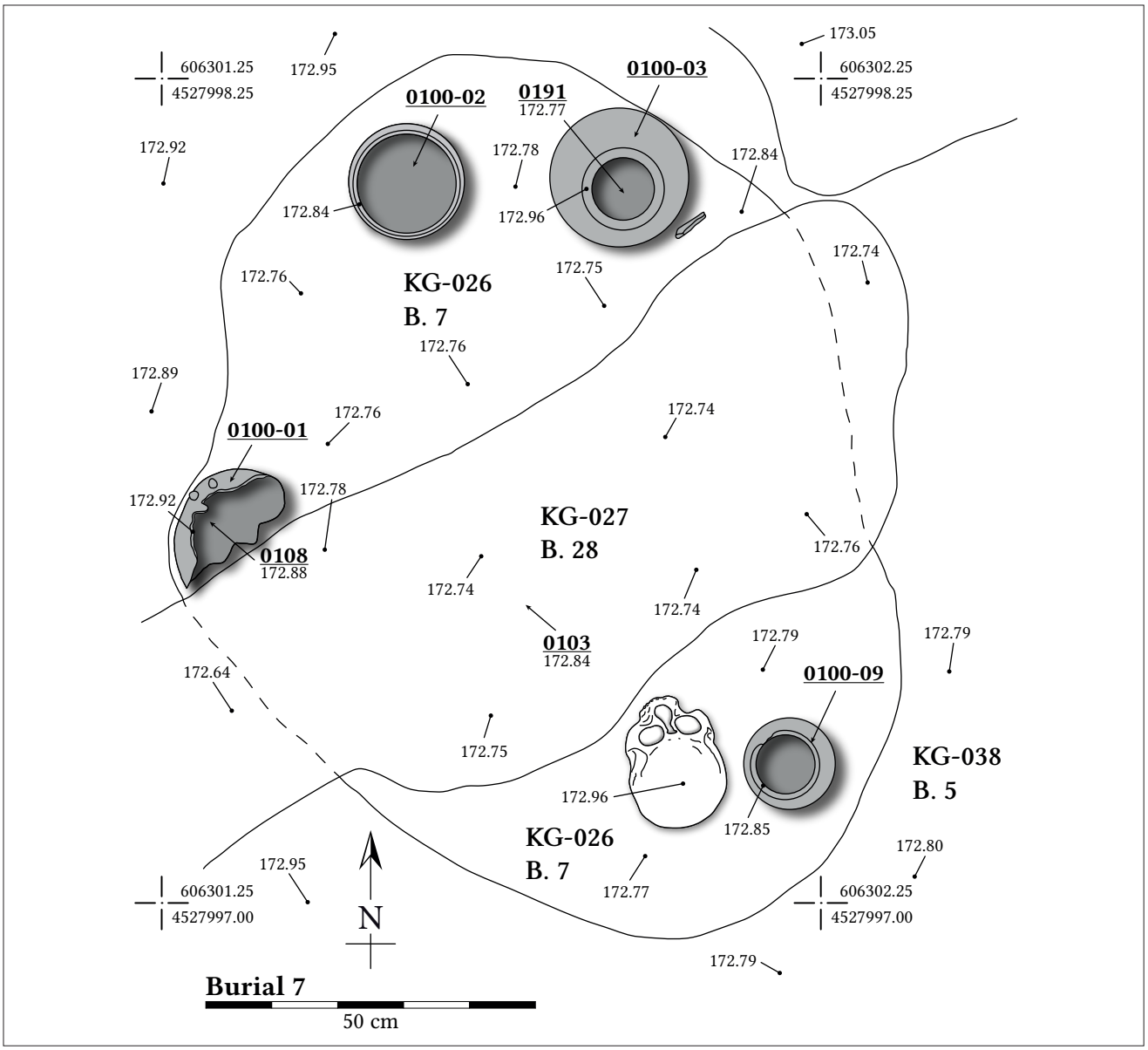

Fig. 77. Plan of Burial 7 (KG-026); Pit-Complex A

Burial 7 (KG-026)

Burial 7 occupied the northern part of Pit-Complex A (Fig. 42). Since this interment probably caused the displacement of the skull in Burial 5 (see above), it is considered younger. As the following analysis of the pottery implies, however, the chronological interval between both burials can not have been long.

The grave-pit had an oval shape and was cut in its central part by the medieval Burial 28 (Fig. 73 and Fig. 77). The intact southern portion of the grave-pit still contained the skull and a single vessel next to it (0100-09); the lower jaw, however, and all other skeletal parts were lost due to the later disturbance. In the northern portion two complete vessels (0100-02; 0100-03) were standing at the edge of the pit. One half of a third one (0100-01) remained at the western end, immediately north of the disturbance.

The black-polished pot 0100-03 (Fig. 76, 1 and Fig. 78) is slightly larger but otherwise virtually identical to the undecorated pot 0200-01 in Burial 2 (Fig. 59, 5) and – apart from the decoration – also to the other pots in Burial 2 (Fig. 59, 4. 6–7). Morphological comparisons can also be drawn with Burial 1, in particular with vessel 0425-01 (Fig. 51, 1). Another similarity between Burials 7 and 1 is the application of four knobs on pots 0100-01 (Fig. 76, 2 and Fig. 79) and 0425-02 (Fig. 51, 2), even though their shapes are different. Pot 0100-01 had a wide flat base and an oval body. The rim was lost, and two fragments

Fig. 78. Black-polished pot 0100-03 from Burial 7 (KG-026)

Fig. 79. Fragment of pot 0100-01 from Burial 7 (KG-026)

with a large hole (Fig. 76, 2a–b) could not be joined to the preserved vessel parts. The thickness of the fragments as well as the hole might indicate that the pot originally had some sort of spout. The body of the pot was decorated with shallow horizontal grooves that were bordered at the lower end, c. 6 cm above the base, by a row of vertical, similarly shallow notches. A second row of diagonal shallow notches marked the shoulder. Bowl 0100-02 (Fig. 76, 3 and Fig. 80) is comparable to other bowls with spheroid bodies and short upright rims found in Burials 1 and 2. The small, stocky pot 0100-09 had a pronounced belly, a carinated neck with an everted rounded rim and a row

Fig. 80. Black-polished bowl 0100-02 from Burial 7 (KG-026)

Fig. 81. Pot 0100-09 from Burial 7 (KG-026)

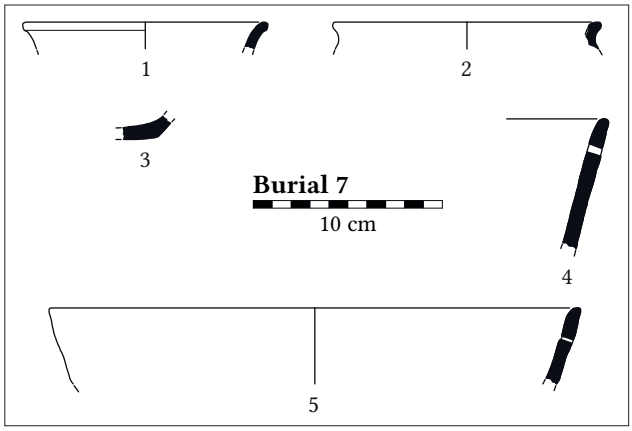

Fig. 82. Pottery from the fill of Burial 7 (KG-026): 1 – pot (0100-04); 2 – pot (0100-06); 3 – base (0100-05); 4 – rim sherd (0100-07); 5 – rim sherd (0100-08)

of diagonally incised notches on the shoulder (Fig. 76, 4 and Fig. 81). It is similar to the smallest of three vessels in Karacamirli Kurgan 4 that were decorated in the same way on the shoulder (Гусейнова/Алиев 2008: Fig. III, 2).

Noteworthy are two obsidian flakes found inside two of the vessels. One flake (0161) was deposited at the bottom of pot 0100-03 and the second one (0108) lay at the bottom of the still intact half of pot 0100-01. Throughout the Tepe 5 cemetery this is the only evidence for a seemingly intentional deposition of unworked obsidian flakes inside of vessels.

The only adornment that most likely can be attributed to the deceased in Burial 7 was an open ring of thick bronze wire (0103; Fig. 76, 5) found some 25 cm northwest of the skull in the area disturbed by Burial 28. Although from the fill above the skeleton of the medieval burial, it seems very likely that it was originally part of Burial 7.

In sum, the vessels in Burial 7 resemble the pottery inventories of Burial 1 and Burial 2 and therefore share the same typological connections with the Karacamirli Kurgans 4 and 5 as well as with the Armenian highlands. Consequently, Burial 7 can be grouped among the earliest burials on Tepe 5.

Grave contents

KG-026-0105 (human bones)
Sex: probably male — Table 16
Age class: Adultas

KG-026-0100-01 (pot) — Fig. 76, 2; Fig. 79
Base diam.: 120 mm
Fabric: completely reducing atmosphere, medium hard, medium fine temper (123)
Surface: ext. and int. smoothed
Colour: ext. Gley 1 4/N (dark grey); core Gley 1 2.5/N (black); int. Gley 1 4/N (dark grey)
Decoration: shallow horizontal lines covering body and shoulder, bordered at the lower end by a row of shallow vertical notches; around the shoulder a line of diagonal notches. Four applied knobs in a rectangular arrangement on the shoulder
Condition: rim not preserved; half of the body missing; two fragments do not join
Comparanda: see KG-094-0425-02 in Burial 1

KG-026-0100-02 (bowl) — Fig. 76, 3; Fig. 80
Rim diam.: 165 mm (100%)
H: 97 mm
Base diam.: 78 mm
Fabric: completely reducing atmosphere, hard, fine temper (131)
Surface: ext. and int. polished
Colour: ext. Gley 1 2.5/N (black); int. Gley 1 2.5/N (black)
Condition: complete
Comparanda: see bowls in Burial 1 and Burial 2

KG-026-0100-03 (pot) — Fig. 76, 1; Fig. 78
Rim diam.: 129 mm (100%)
H: 209 mm
Base diam.: 89 mm
Fabric: completely reducing atmosphere, hard, fine temper (132)
Surface: ext. and int. polished
Colour: ext. Gley 1 2.5/N (black); int. Gley 1 2.5/N (black)
Condition: complete
Comparanda: morphologically identical to KG-044-0200-01 and the other pots from Burial 2

KG-026-0100-09 (pot) — Fig. 76, 4; Fig. 81
Rim diam.: 94 mm (100%)
H: 98 mm
Base diam.: 64 mm
Fabric: completely reducing atmosphere, soft, medium fine temper (113)
Surface: ext. burnished; int. smoothed
Colour: ext. Gley 1 2.5/N (black); core Gley 1 2.5/N (black); int. Gley 1 2.5/N (black)
Decoration: row of diagonal notches around the shoulder
Condition: small part of rim broken off, otherwise complete
Comparanda:
Karacamirli, Kurgan 4, MBA/LBA (Гусейнова/Алиев 2008: Fig. III, 2)

KG-026-0108 (obsidian flake)
L: 24.0 mm; W: 18.0 mm; Th: 10.0 mm; Wt: 5 g
606301.323 E; 4527997.578 N; 172.882 m
found inside of pot KG-026-0100-01

KG-026-0161 (obsidian flake)
L: 57.4 mm; W: 37.7 mm; Th: 9.1 mm; Wt: 15 g
found at the bottom inside of pot KG-026-0100-03

Fill

KG-026-0100-04 (rim sherd) — Fig. 82, 1
Rim diam.: 130 mm (8 %)
Fabric: completely reducing atmosphere, hard, very fine temper (131)
Surface: ext. and int. polished
Colour: ext. Gley 1 2.5/N (black); core Gley 1 4/N (dark grey); int. Gley 1 2.5/N (black)

KG-026-0100-05 (base sherd) — Fig. 82, 3
Fabric: completely reducing atmosphere, hard, very fine temper (131)
Surface: ext. polished; int. burnished
Colour: ext. Gley 1 2.5/N (black); core Gley 1 4/N (dark grey); int. Gley 1 4/N (dark grey)

KG-026-0100-06 (rim sherd) — Fig. 82, 2
Rim diam.: 140 mm (5 %)
Fabric: completely reducing atmosphere, hard, very fine temper (131)
Surface: ext. burnished
Colour: ext. Gley 1 4/N (dark grey); core Gley 1 4/N (dark grey); int. Gley 1 4/N (dark grey)

KG-026-0100-07 (rim sherd) — Fig. 82, 4
Rim diam.: n. d. (1 %)
Fabric: not fully oxidized, medium hard, coarse temper (524)
Surface: ext. and int. smoothed
Colour: ext. 5YR 6/4 (reddish brown); core 5YR 3/1

(very dark grey); int. 5YR 6/4 (light reddish brown)
perforated just below the rim (Chalcolithic mangal)

KG-026-0100-08 (rim sherd) Fig. 82, 5
Rim diam.: 280 mm (4 %)
Fabric: not fully oxidized, medium hard, coarse temper (524)
Surface: ext. and int. smoothed
Colour: ext. 5YR 6/4 (reddish brown); core 5YR 3/1 (very dark grey); int. 5YR 6/4 (light reddish brown)
perforated just below the rim (Chalcolithic mangal)

KG-026-0104 (obsidian flake)
L: 18.0 mm; W: 11.0 mm; Th: 3.0 mm; Wt: 1 g
606301.803 E; 4527997.80 N; 172.753 m

Burial 8 (KG-057-0247 and KG-057-0404)

Burial 8 was the earliest interment of the pit KG-057 in the central part of Pit-Complex B (Fig. 43). It was heavily disturbed by two later interments of the Late Antique period (Burials 23 and 24). The only intact part of the original grave-pit may have been the grey-coloured pot

Fig. 83. Grey coloured pot 0417-01 from Burial 8 (KG-057-0247 and KG-057-0404)

Fig. 84. Pit KG-057 with remains of Burial 8 in the south-eastern (pot 0417-01) and north-western corner (KG-057-0247 and KG-057-0404 with one half of bowl 0418-01), and the Late Antique Burials 23 (KG-057-0415) and 24 (KG-057-0414)

Fig. 85. The rejoined halves of bowl 0418-01 (Burial 8) and 0241-02 (fill of Burial 15)

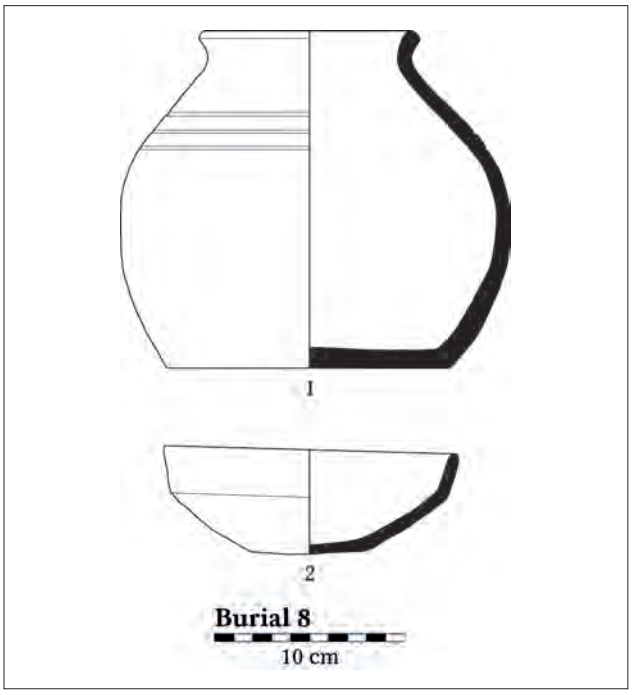

Fig. 86. Pottery from Burial 8 (KG-057-0247 & KG-057-0404): 1 – pot (0417-01); 2 – bowl (0418-01 and 0241-02)

0417-01, discovered *in situ* at the south-eastern end of what must have been a very large grave-pit (Fig. 84 and Fig. 138). It had a very wide flat base, a spherical body and a short neck with a slightly thickened rim (Fig. 83 and Fig. 86, 1). The shoulder was decorated with three incised lines. Similar pots are known from the Mingachevir cemetery (Асланов et al. 1959: Pl. XXXIV, 7–8). The only other vessel that most likely formed part of the original inventory was a fragmented carinated bowl (0418-01) of which one half (0241-02) was dislocated to the fill of the adjacent Burial 15 (Fig. 115). The dark grey-coloured bowl had a flat base, a conical lower body and an almost vertical collar with a plain rim (Fig. 85 and Fig. 86, 2). Comparisons can again be drawn with Mingachevir (Асланов et al. 1959: Pl. XXXIII, 8). The bowl was located in an undercut section at the northern side of the grave-pit (Fig. 138) and was found together with fragments of a long bone and part of a human skull (0404). These bones and additional remains of a skull, a right clavicle and long bones (0247), deposited immediately east of the skeleton of Burial 23, as well as a pelvis fragment that was found loose in the fill at the southern edge of the pit very likely all belonged to Burial 8. It seems that the skeleton was completely dispersed when Burial 23 was interred. As indicated by the two dislocated joining parts of bowl 0418-01/0241-02, also pottery vessels were taken out of the burial and ended up in the probably simultaneously disturbed adjacent Burial 15. In the course of this disturbance all other objects of the original inventory were scattered and mixed with the contents of the later burials (Fig. 140). Noteworthy is a cluster of sherds in the central area of the pit (0416). Besides red coloured sherds probably of the Late Antique period it also included some dark grey-coloured body-sherds that might have belonged to the original Burial 8. The same cluster contained a biconical spindle whorl made of burnt clay (0420, Fig. 141, 7). It was, however, not possible to assign this object securely to one of the three interments. By definition these objects are listed together with all the other finds from the fill of the pit KG-057 in the section dealing with Burial 23 that appears to have caused most of the damage to Burial 8.

The general dating of Burial 8 into the Late Bronze/Early Iron Age occupation phase is indicated by the pottery inventory which is comparable to material from Mingachevir. A radiocarbon date of the bones allows for a more precise dating between the 12th and 11th cent. BC (Beta-506517) and hence to a time period which saw the transition between the Late Bronze to the Early Iron Age.

Grave contents

KG-057-0247 and KG-057-0404 (human bones) — Table 4
- Sex: could not be determined — Table 16
- Age class: Maturitas–Senilis

KG-057-0417-01 (pot) — Fig. 83; Fig. 86, 1
- Rim diam.: 100 mm (100%)
- H: 117 mm
- Base diam.: 150 mm
- Fabric: completely reducing atmosphere, hard, medium fine temper (133)
- Surface: ext. burnished; int. smoothed
- Colour: ext. Gley 1 6/N (grey); core Gley 1 2.5/N (black); int. Gley 1 6/10Y (greenish grey)
- Decoration: three grooves are running around the shoulder; faint traces of lighter coloured vertical stripes that, however, might as well be just traces of the manufacturing process
- Condition: complete

Comparanda:
Mingachevir, e. g. Burials 2, 53, 86, 106, 131, 165, LBA/EIA (Асланов et al. 1959: Pl. XXXIV, 7–8)

KG-057-0418-01 and KG-058-0241-02 (bowl) Fig. 85; Fig. 86, 2
Rim diam.: 155 mm (950%)
H: 55 mm
Base diam.: 60 mm
Fabric: not completely reduced core, medium hard, medium fine temper (623)
Surface: ext. and int. burnished
Colour: ext. Gley 1 3/N (very dark grey); core 5Y 4/1 (dark grey); int. Gley 1 2.5/N (black)
Condition: part of the rim broken off, otherwise complete
Comparanda:
Mingachevir, LBA/EIA (Асланов et al. 1959: Pl. XXXIII, 8)

Burial 9 (KG-043)

Burial 9 was located in the southern part of square 6300/7990 (Fig. 27). Only the south-western corner of a presumably rectangular grave-pit was preserved (Fig. 87). The remaining parts were completely destroyed by the Late Antique Burial 25 and the Medieval Burial 37. The various bronze objects found in the undisturbed area suggest a richly adorned individual of the Late Bronze/Early Iron Age (Fig. 88). Although except for some teeth and fragments of the mandible the skeleton was completely decayed, the specific position of the bones and pieces of jewellery indicate that the head was in the west or south-west of the grave-pit and rested on his left side. Two large circular bronze discs with identical embossed ornamentation (0178 and 0180) and with their backsides facing each other were found below and on top of the bone fragments suggesting that they were worn as a headdress on both sides of the head (see also Асланов et al. 1959: 81). The same position of one such disc was, for example, observed in a burial near Dashkasan (Реслер 1905: 13 Fig. 8–9). The discs were made of a 1 mm thick bronze sheet and measured 13.5 cm in diameter (Fig. 89 and Fig. 90, 1–2). Into the upper edge a keyhole-shaped opening was cut which, together with a pair of small perforations next to it, probably served to fasten the discs on the head. Along the edge ran a row of elongated dents and an embossed line. The central field was decorated with six knobs some of which were connected by

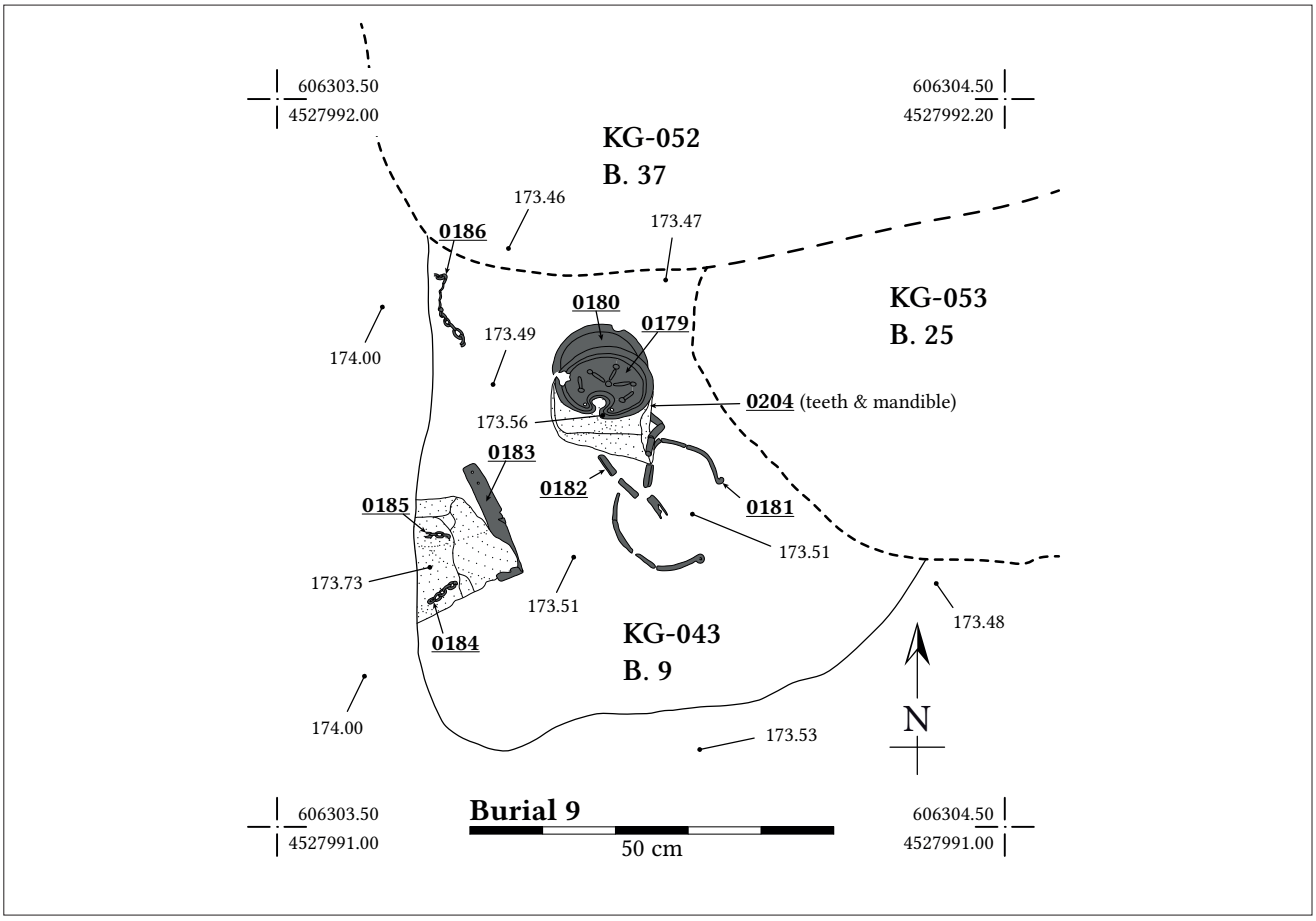

Fig. 87. Plan of the remains of Burial 9 (KG-043)

Fig. 88. Bronze objects and adornment of the individual in Burial 9 (KG-043)

Fig. 89. Ornamented bronze discs (0179 and 0180) *in situ* with remains of a human skull in between

embossed bars. Similar discs with varying ornamentation are known, for example, from burials at *Helenendorf*, Kachbulag, Chovdar, Qaramurad, *Paradiesfestung*/Kalakent, Mingachevir and Zayamchay (see below). One of the earliest examples of such ornamental discs is known from Kurgan 3 near Killik-Dagh (Реслер 1902: 73–77 Fig. 149), dated to the 13th cent. BC (Погребова 2011: 104); they continue to appear throughout the 12th to 9th cent. BC, for example in Burial 11 at Kushchu (Гуммель 1940: 133–135 Fig. 3 no. 4; Погребова 2011: 141). Already N. V. Minkevich-Mustafaeva considered burials with a large number of bronze artefacts typical for her developed phase of the Khojaly-Gadabay-Culture which was supposed to last from the 11th cent. BC to the 9th cent. BC (Минкевич-Мустафаева 1962: 114–115). The proposed dates set a chronological frame for Burial 9 but do not allow for a more precise dating within the final stage of the Late Bronze Age and the first centuries of the Early Iron Age.

As in Burial 9 the discs are often accompanied by a bronze headband. On Tepe 5 it was made from a thin undecorated sheet of bronze (0183) narrowing towards the ends where two perforations facilitated the fastening (Fig. 90, 3). That such bronze stripes were used as headbands is indicated by their usual position near the head of the deceased (and in at least one case still in place on the skull – Rösler 1901: 102. 113 Fig. 25a). Similar headbands were found at Bayan, Kachbulag, Chovdar, Kalakent and Mingachevir (see below).

Near the bronze discs were several small cylindrical tubes, c. 3 cm long and 0.8–1 cm in diameter (0182, Fig. 90, 4). They were probably part of a necklace or a similar piece of jewellery worn near the head. Similar tubes at Mingachevir and Zayamchay were, for example, interpreted as hair ornaments (Асланов et al. 1959: 111 Pl. XVII, 22–24; Müseyibli/Nəcəfov 2019: 185–186). Considering size and shape the tubes from Burial 9 are best compared to examples from Shusha (Rösler 1898a: 293 Fig. 10) and *Helenendorf* (Rösler 1902: 168. 178–179 Fig. 126. 179). Partially superimposed by some of the bronze tubes was a large torc (0181, Fig. 90, 5). It measured c. 17 cm in diameter and was made of a thick bronze wire with curled ends. An almost identical plain torc is known from Burial 10 at Mingachevir (Асланов et al. 1959: 70 Fig. 53), however, the twisted variant appears to be more widespread (e. g. Асланов et al. 1959: 81 Pl. XVIII, 17–18; Nagel/Strommenger 1985: Pl. 5–6).

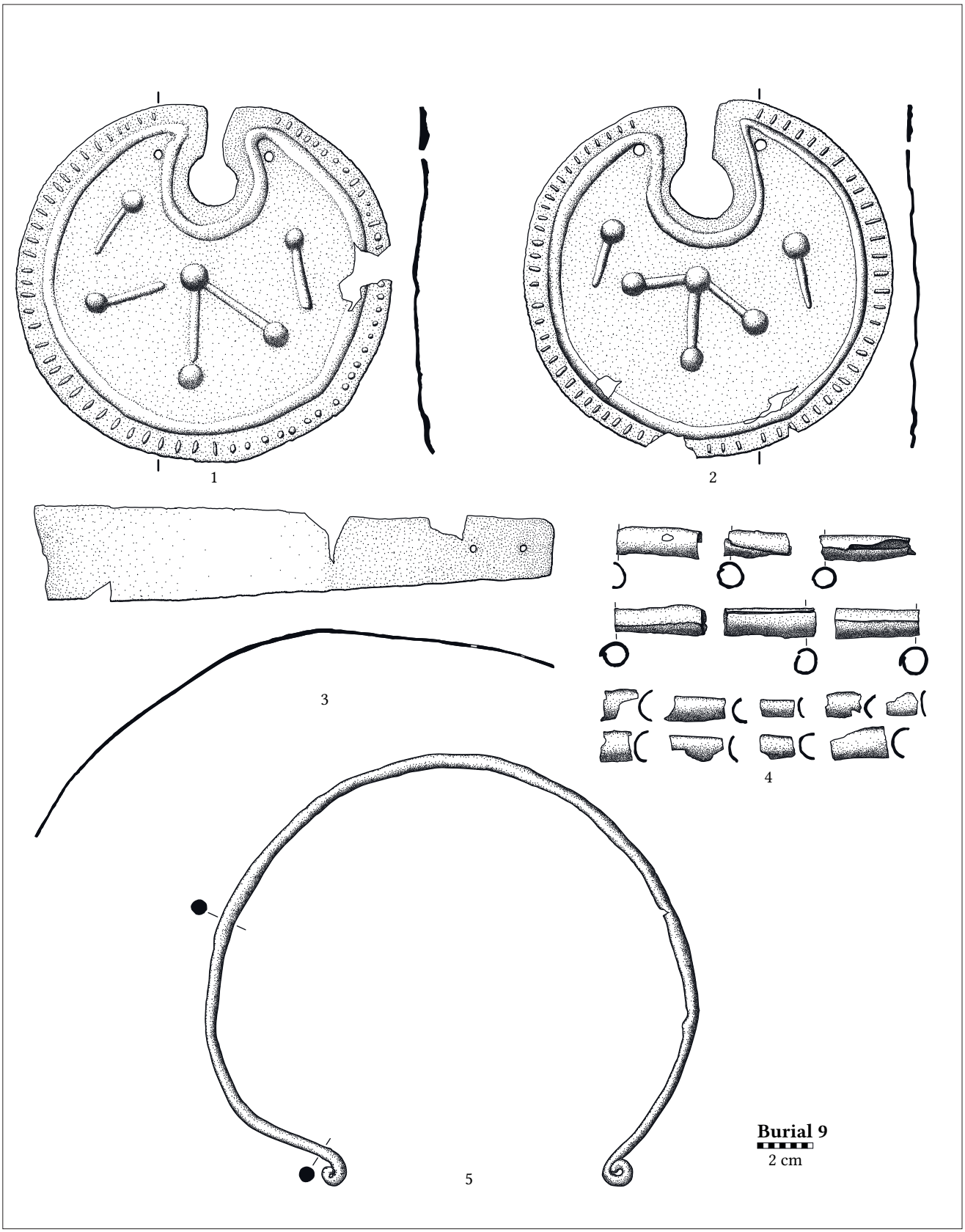

Fig. 90. Finds from Burial 9 (KG-043): 1 – bronze disc (0179); 2 – bronze disc (0180); 3 – bronze headband (0183); 4 – bronze tubes (0182); 5 – bronze torc (0181)

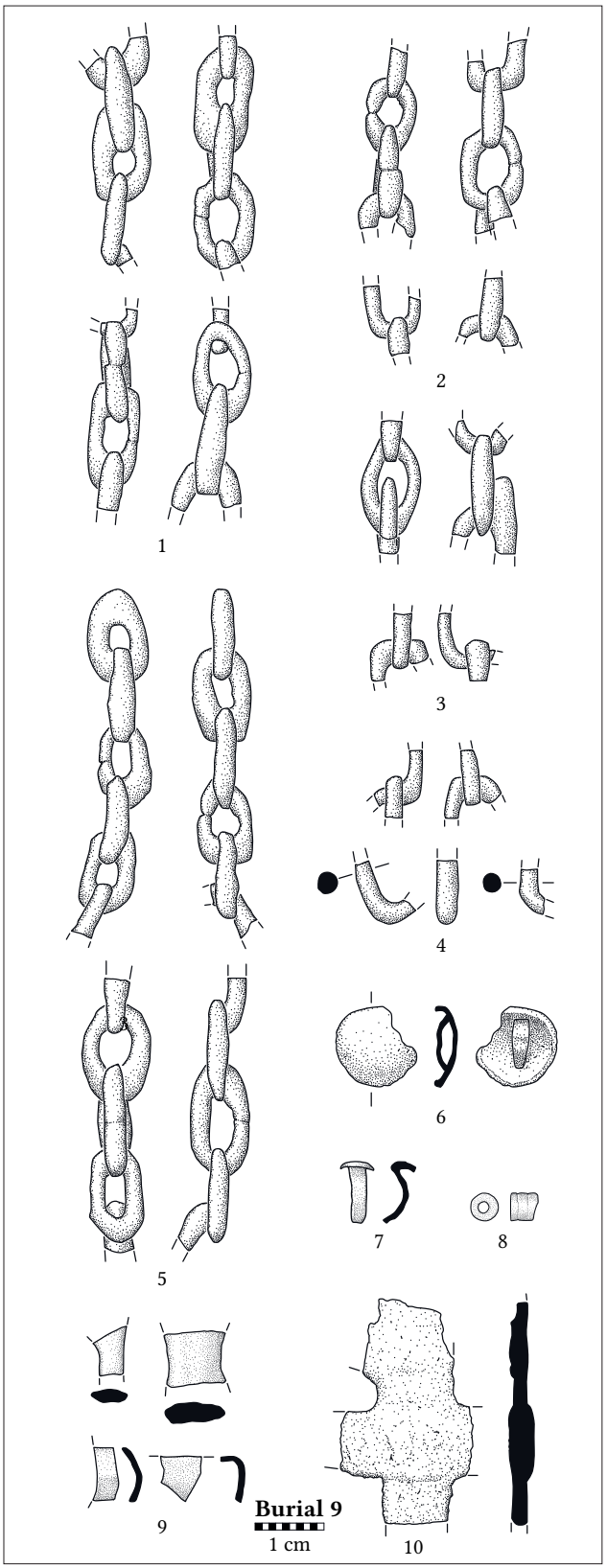

Fig. 91. Finds from Burial 9 (KG-043): 1 – bronze chain (0184); 2 – bronze chain (0185); 3–4 – bronze chain links (0187a); 5 – bronze chain (0186); 6 – bronze button/rivet (0187d); 7 – bronze object (0187e); 8 – bronze beads (0198); 9 – bronze fragments (0187b); 10 – bronze object (0187c)

In various places at the eastern edge of the grave-pit lay parts of bronze chains (0184–0187a, Fig. 91, 1–5). Three longer sections of those chains (0184–0186) ran horizontally on a level c. 20 cm above the other finds before they bent and followed a vertical line down to the bottom of the pit (Fig. 88). Chains were used to hold pendants or other objects, but in this case, their large number and peculiar position could be an indication that they belonged to a single piece of jewellery (e. g. Rösler 1901: 102; Nagel/Strommenger 1985: 113 Pl. 70). Due to the later disturbances some chain links ended up in the fill of the later Burials 25 and 37 (0206, 0210, 0215, Fig. 144, 3–4).

The adornment of the deceased also included a small button or rivet (0187d, Fig. 91, 6), several bronze fragments (0187b, 0187c, 0187e; Fig. 91, 7. 9–10) and three disc-shaped bronze beads that were corroded together (0198, Fig. 91, 8). All these finds were found scattered near the larger bronze objects. A small cylindrical bronze bead discovered in Burial 25 (0212, Fig. 144, 5) probably also originated from Burial 9.

Grave contents

KG-043-0204 (human bones)
crowns of teeth and fragments of mandible — Table 16

KG-043-0179 (bronze disc with embossed ornamentation) — Fig. 89; Fig. 90, 1
Diam: 13.3 mm; Th: 1 mm; Wt: 81 g
606303.946 E; 4527991.560 N; 173.558 m
Comparanda:
Ashaghi Dashkasan, Burial 2, LBA (Реслер 1905: 13 Fig. 8–9; Погребова 2011: 129)
Killik-Dagh, Kurgan 3, LBA (Реслер 1902: 73–77 Fig. 149; Погребова 2011: 104)
Helenendorf, Kurgan 6a, LBA/EIA (Rösler 1901: 113 Fig. 36a)
Kachbulag, Kurgan 1 interment 30, LBA/EIA (Кесаманлы 1999: 51 Pl. 18, 1–2)
Chovdar, Burials 11, 12, 16 and 19, LBA/EIA (Шарифов 1929: 252–253. 256. 258 Fig. 12–13)
Qaramurad, Burial 11 (Nagel/Strommenger 1985: 95 Pl. 64, 3)
Paradiesfestung/Kalakent, Burials 27, 42 and 75, LBA/EIA (Nagel/Strommenger 1985: 70. 75. 106–107 Fig. 40d. 41, 5. 41, 7. 47. 74, 5) and Burials 28, 48 and 69, LBA/EIA (Ивановский 1911: Pl. VI, 3. 9–10)
Mingachevir, e. g. Burial 63, LBA/EIA (Асланов et al. 1959: Fig. 115)
Zayamchay, Burial 60, LBA/EIA (Müseyibli/Nəcəfov 2019: Pl. 76, 1)

KG-043-0180 (bronze disc with embossed ornamentation) — Fig. 90, 2
Diam: 13.4 mm; Th: 1 mm; Wt: 61 g
606303.946 E; 4527991.589 N; 173.486 m
Comparanda: see KG-043-0179

KG-043-0181 (bronze torc) — Fig. 90, 5
Diam: 17.7 mm; Th: 5.5 mm
606304.028 E; 4527991.448 N; 173.500 m

Comparanda:
Mingachevir, Burial 10 (Асланов et al. 1959: 70. Fig. 53)

KG-043-0182 (six bronze sheet tubes plus fragments) Fig. 90, 4
L: 30.0–33.0 mm; Diam: 9.0–10.0 mm; Th: 1 mm
606304.002 E; 4527991.482 N; 173.512 m
Comparanda:
Mingachevir, e. g. Burials 26, 43, 63, 102, 107, 114, LBA/EIA (Асланов et al. 1959: 111 Pl. XVII, 22–24)
Shusha, Burial 10, LBA/EIA (Rösler 1898a: 293 Fig. 10)
Helenendorf, Kurgans 48a and 50b, LBA/EIA (Rösler 1902: 168. 178–179 Fig. 126. 179)
Zayamchay, Burials 27 and 72, LBA/EIA (Müseyibli/Nəcəfov 2019: Pl. 41, 11. 43. 89, 8–9)

KG-043-0183 (bronze headband) Fig. 90, 3
L: 232.0 mm; W: 22.0–33.0 mm; Th: 1 mm; Wt: 32 g
606303.795 E; 4527991.426 N; 173.513 m
Comparanda:
Helenendorf, Burials 6a and 19, LBA/EIA (Rösler 1901: 102. 113 Fig. 25a)
Bayan, Kurgan 4 *Parssegahoch* interment 5, LBA/EIA (Rösler 1905: 135 Fig. 63; Кесаманлы 1999: 63)
Kachbulag, Kurgan 1 interments 30 and 35, Burial 27, LBA/EIA (Кесаманлы 1999: 51. 53. 110 Pl. 14, 9. 18, 5)
Chovdar, Burials 11, 16 and 19, LBA/EIA (Шарифов 1929: 252. 256. 258 Fig. 12–13)
Kalakent, Burial 28, LBA/EIA (Nagel/Strommenger 1985: 70 Nr. 2621c; Ивановский 1911: 100 Pl. VIII, 3)
Mingachevir, e. g. Burial 63 and Kurgan II interment 9, LBA/EIA (Асланов et al. 1959: Pl. XVII, 20)
Kushchu, Burial 11, EIA (Гуммель 1940: 133–135 Fig. 3, no. 4)

KG-043-0184 (bronze chain) Fig. 91, 1
L: 190.0 mm; W: 8.0 mm; Wt: 45 g
606303.741 E; 4527991.332 N; 173.719 m

KG-043-0185 (bronze chain) Fig. 91, 2
L: 37.0 mm; W: 8.0 mm; Wt: 34 g
606303.730 E; 4527991.398 N; 173.707 m

KG-043-0186 (bronze chain) Fig. 91, 5
L: 230.0 mm; W: 8.0 mm; Wt: 266 g
606303.742 E; 4527991.692 N; 173.562 m

KG-043-0187a (bronze chain links) Fig. 91, 3–4

KG-043-0187b (four bronze fragments) Fig. 91, 9
L: 6.5–8.0 mm; W: 2.5–7.5 mm

KG-043-0187c (bronze object with broken off protrusions) Fig. 91, 10
L: 32.5 mm; W: 1.2–1.9 mm

KG-043-0187d (bronze button or rivet) Fig. 91, 6
Diam: 1.2 mm; Th: 3.0 mm

KG-043-0187e (bronze object) Fig. 91, 7
L: 9.0 mm; W: 2.0–5.0 mm

KG-043-0198 (three bronze beads) Fig. 91, 8
Diam: 4.0 mm; Th: 1.0 mm; Wt: 1 g
found near torc KG-043-0181

Fig. 92. Grey coloured pot (0164-02) from Burial 10 (KG-041)

Fig. 93. Grey coloured cup (0164-01) from Burial 10 (KG-041)

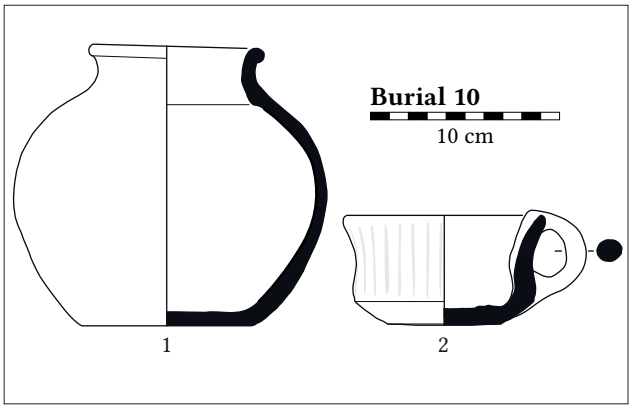

Fig. 94. Pottery from Burial 10 (KG-041): 1 – pot (0164-02); 2 – cup (0164-01)

Burial 10 (KG-041)

Burial 10 was located north of Burial 11 in the western part of Pit-Complex A (Fig. 42). It seems that the burial comprised only two vessels, a small cup (0164-01) and c. 40 cm north of it a pot (0164-02), but no skeleton. It is unknown, whether these decayed completely or whether the vessels were not accompanied by a body in the first place. Except for the western edge, which corresponded to the edge of the entire Pit-Complex, the outline of the grave-pit was not traceable (Fig. 95). Its southern and northern ends might well have been destroyed by the later interments of Burial 11 and the Medieval Burial 28.

Both vessels were made of the same medium fine and grey-coloured fabric as the vessels in the adjacent Burial 11 which suggests a certain chronological proximity. The pot (Fig. 92 and Fig. 94, 1) had a wide opening, short neck and a spherical body with a wide base. Its surface was somewhat carelessly burnished, as was the small cup (Fig. 93 and Fig. 94, 2). The latter had a concave body with a conical indented flat base. The handle protruded from the slightly pointed rim and joined the body again at the carination between body and base. Above the carination the surface was polished with vertical lines.

Comparisons for both vessels can be found at Mingachevir (Асланов et al. 1959: type VI, Pl. XXV, 1 and type XVI, Pl. XXXIV, 5). A similarly shaped but taller cup was recovered from Burial 11 at Kushchu (Гуммель 1940: 136 Fig. 5, no. 78), dated to the 12th–11th cent. BC (Гусейнова 1989: 38–39) or to the 12th–9th cent. BC (Погребова 2011: 141), respectively.

Grave contents

KG-041-0164-01 (cup) Fig. 93; Fig. 94, 2
- Rim diam.: 103 mm (100%)
- H: 57 mm
- Base diam.: 58 mm
- Fabric: completely reduced, hard, medium fine temper (133)
- Surface: ext. burnished; int. smoothed
- Colour: ext. Gley 1 5/N (grey); int. 10YR 5/1 (grey)
- Condition: complete
- Comparanda:
- Mingachevir, Burials 35, 159, MBA/EIA (Асланов et al. 1959: Pl. XXV, 1)
- Kushchu, Burial 11, EIA (Гуммель 1940: 136 Fig. 5, no. 78)

KG-041-0164-02 (pot) Fig. 92; Fig. 94, 1
- Rim diam.: 86 mm (100%)
- H: 147 mm
- Base diam.: 90 mm
- Fabric: completely reduced, hard, medium fine temper (133)
- Surface: ext. burnished; int. smoothed
- Colour: ext. Gley 1 5/N (grey); int. 10YR 5/1 (grey)
- Condition: complete
- Comparanda:
- Mingachevir, Burials 102, 131, MBA/EIA (Асланов et al. 1959: Pl. XXXIV, 5)

Fill

KG-041-0170 (obsidian flake)
- L: 36.7 mm; W: 14.2 mm; Th: 7.3 mm; Wt: 5 g
- 606301.590 E: 4527996.339 N; 172.792 m

Burial 11 (KG-029)

The southernmost edge of Pit-Complex A (Fig. 42) was occupied by a west-east oriented oblong grave-pit (Fig. 95). Both its western and eastern ends undercut the surrounding soil. It appears to be the latest burial of the Late Bronze Age/Early Iron Age within Pit-Complex A. The late date is not only suggested by the ceramic inventory, but also by the proposed stratigraphic relation to Burial 4 and perhaps to Burial 10, as it seems possible that the disturbance of the latter was partially caused by the digging of a large pit for Burial 11.

No skeletal remains were preserved. A single human vertebral arch was found loose in the fill, but its radiocarbon-determined age (Table 10, MAMS-39417) proves that it dates to the Medieval period and, therefore, is most likely an intrusion due to animal burrowing that might have caused the complete decay of the skeleton as well.

In the middle of the grave-pit were two intact vessels: a single-handled jug with a wide base (0112-01, Fig. 96 and Fig. 98, 2) and a churn (0112-02, Fig. 97 and Fig. 98, 1). Both vessels were made of grey fabric and decorated with five rows of incised horizontal lines on the shoulder. In addition, the jug had a polished ornamentation of vertical stripes on the neck and body.

Churns (маслобойкы/nehrə) generally have an oval body and are characterized by a single short and narrow spout on the shoulder that is usually accompanied by a horizontal handle. Vessels of this form were used until the 20th cent. AD to produce butter or cheese (Brodbeck-Jucker 2019: 63–64). The frequent attestation of churns in burials supports the results of the isotopic analysis (ch. VI.3.1) that demonstrated the importance of milk products to the diet. In Armenia handleless churns with wavy or linear decorations are attested for the first time in the Late Bronze Age III/Lchashen-Metsamor 3 pottery group (Smith et al. 2009: 81 Fig. 28q). By the Lchashen-Metsamor 5 (Iron Age IB) they occur frequently and are usually decorated with incised horizontal lines (Smith et al. 2009: 91 Fig. 33q), just like the churn from Burial 11. In Kakheti (Eastern Georgia) they also

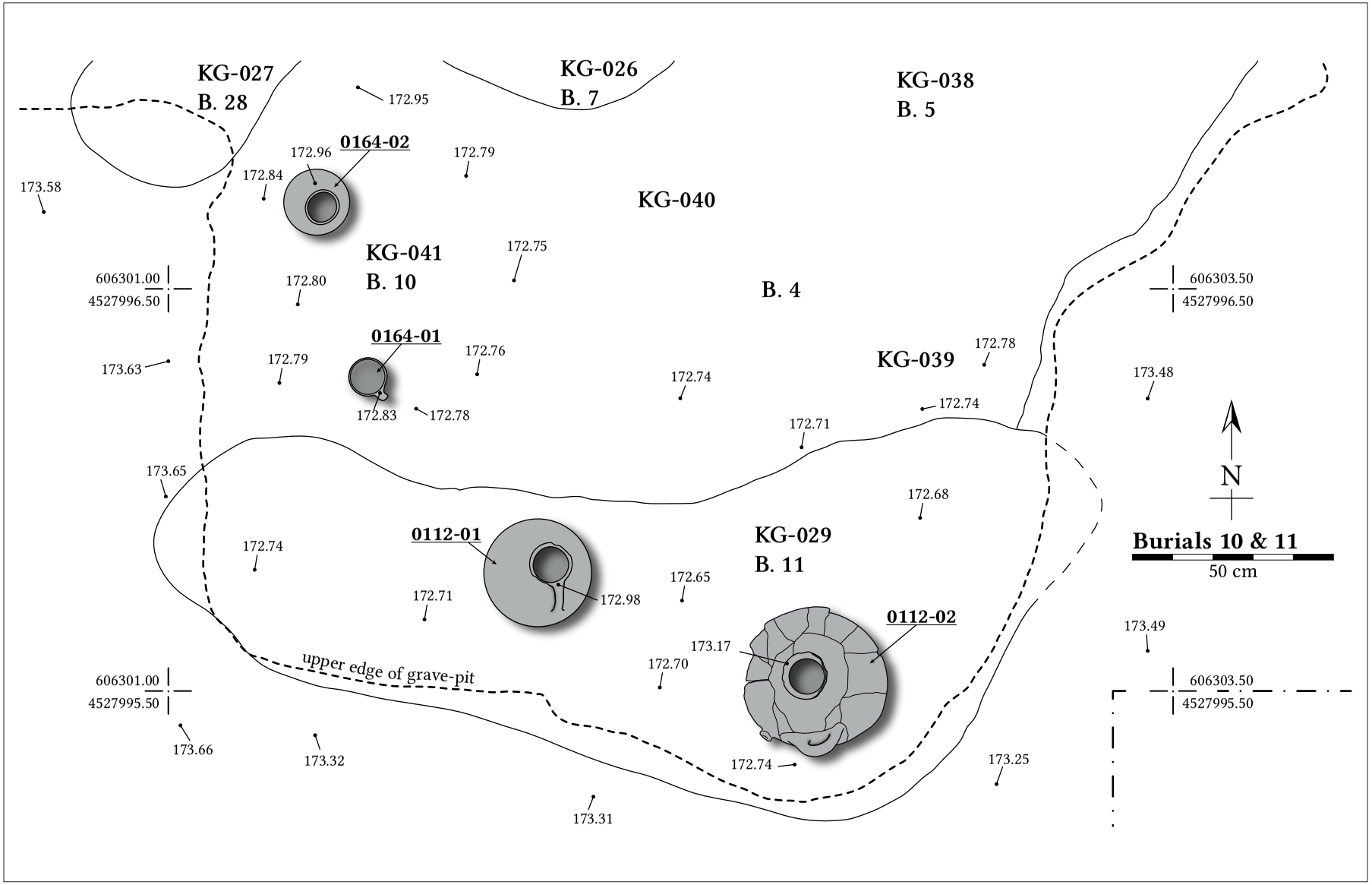

Fig. 95. Plan of Burials 10 (KG-041) and 11 (KG-029); Pit-Complex A

Fig. 96. Grey coloured jug (0112-01) from Burial 11 (KG-029)

Fig. 97. Grey coloured churn (0112-02) from Burial 11 (KG-029)

appear in the Late Bronze Age and continue to appear throughout the Early Iron Age (Ludwig 2010: 105–106; Brodbeck-Jucker 2019: 65; Ludwig-Egermann 2012: 161–163).

In Azerbaijan it is still difficult to describe the genesis of this pottery type in more detail. According to M. A. Gusejnova churns appeared in the ›developed stage‹ of the Khojaly-Gadabay-Culture, between the 12th and 11th cent. BC (Гусейнова 1989: 33. 39). Recent excavations at the Zayamchay cemetery have, however, produced an earlier example: Zayamchay Burial 72 contained a churn that on the basis of radiocarbon dates (Beta-220987, conv. ^{14}C age 3050 ± 40 BP: 2σ cal BC 1410–1200; 1σ cal BC 1390–1270) was placed in the burial between the 14th and the mid-13th cent. BC (Nəcəfov 2008a: 58; Müseyibli/Nəcəfov 2019: 324 Fig. 89, 2). The churn in this burial was of grey fabric and ornamented with incised lines around body and shoulder with a polished decoration in between. Similar churns of grey fabric were also found in Zayamchay Burials 19, 22 and 88 (Müseyibli/Nəcəfov 2019: 267 Fig. 32, 6–7. 269 Fig. 34, 4. 334 Fig. 99, 3) and even more often in the contemporary Tovuzchay cemetery (Müseyibli et al. 2008). Both cemeteries were in use from the 14th/13th to the 10th/9th cent. BC (see ch. IV.2.2), i. e. throughout most of the Late Bronze and Early Iron Ages. Churns remained part of the grave inventories until the end of their occupation sequences, as demonstrated by a similar grey-coloured churn in Zayamchay Burial 8, dated on the basis of a collagen radiocarbon sample to the 9th cent. BC (Nəcəfov 2008a: 58; Beta-220992, conv. ^{14}C age 2660 ± 40 BP: 2σ cal BC 880–790; 1σ cal BC 830–800).

Churns are also well attested among the grave inventories at the Mingachevir burial ground (Асланов et al. 1959: 88 type XIII Pl. XXXII, 1–3). The appearance of churns – together with other pottery types – led the excavators to assign those burials to their second chronological group initially dated from the 11th to the 9th cent. BC (Асланов et al. 1959: 119). The various chronological proposals for the dating of the Mingachevir burials (see ch. IV.2.2), however, still limit the significance of this cemetery for establishing a more differentiated chronology of individual vessel types. Furthermore, the morphological uniformity of churns makes any (chrono-)typological division difficult. Interesting is a specific surface decoration observed on at least three churns from the Zayamchay cemetery: The first example was found in Burial 19 and was made of a grey fabric. The entire vessel was decorated with a polished ornamentation that consisted of a dense pattern of vertical lines from the base up to almost the maximum diameter of the body; the upper part of the body was covered at regular intervals with wide vertical stripes and two incised horizontal lines framing a wavy line encircling

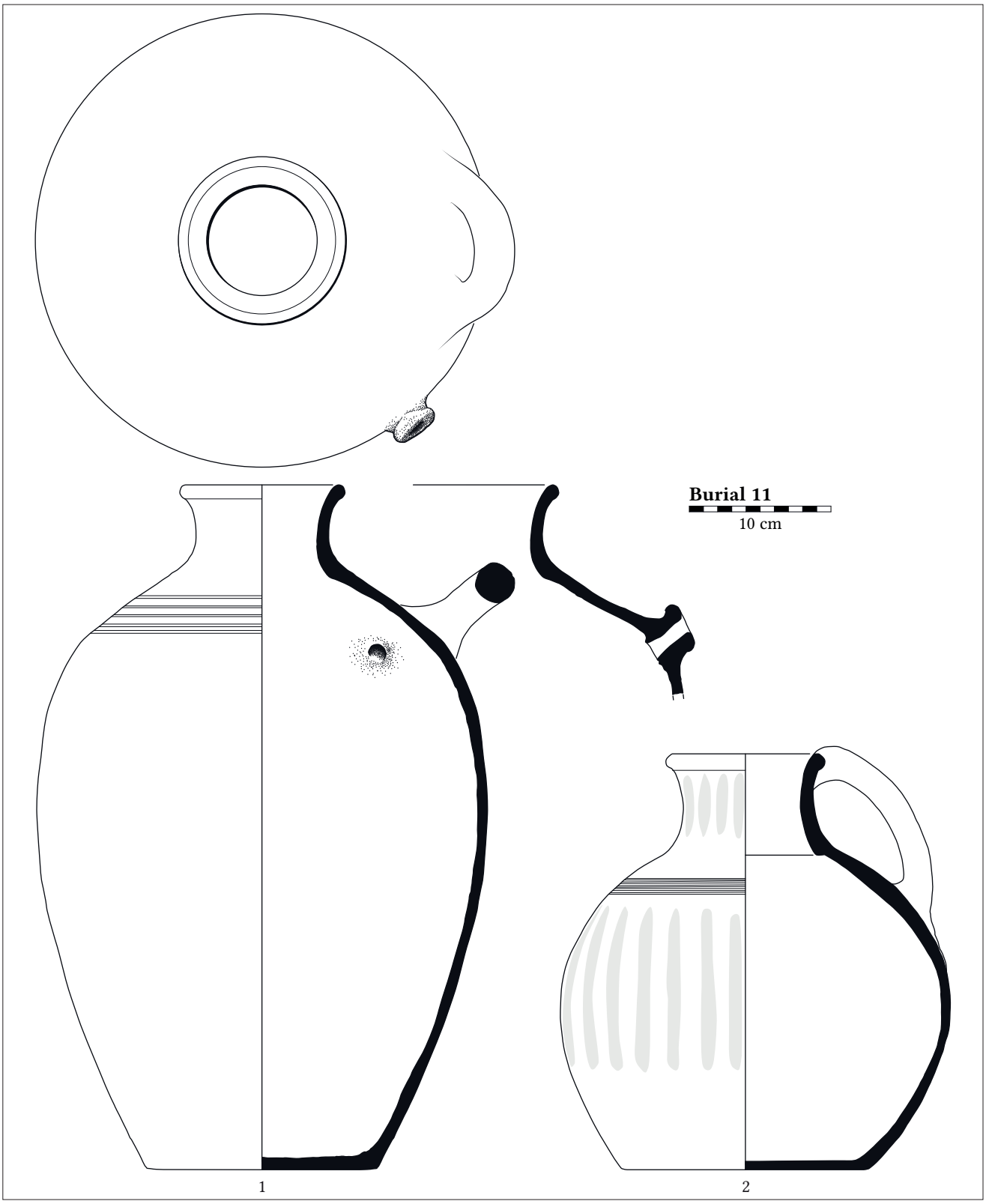

Fig. 98. Pottery from Burial 11 (KG-029): 1 – churn (0112-02); 3 – jug (0112-01)

the shoulder (Müseyibli 2004: Pl. IV, 1; Taylor et al. 2011: 149). The two other churns can not be attributed securely to particular burials (Müseyibli 2004: Pl. IV, 2–3). One of them was similarly decorated with a duplicate version of the incised horizontal and wavy lines, while the other churn had only single wavy lines running around the

shoulder and neck. Comparisons for this type of decoration can be drawn again with the Armenian Highland, where such decorations are well attested from the Late Bronze III (Lchashen-Metsamor 3) onwards (Smith et al. 2009: 81 Fig. 28q–r), as well as with Kakheti, where they seem to appear slightly earlier during the Late Bronze Age (Brodbeck-Jucker 2019: 47). Most noteworthy are several churns with such decoration from Burials 2, 3, 7 and 10 at Sagarejo (Мамиашвили 1988: Pl. XXXV, 16. XXXVI, 31. XLI, 128. XLIII, 159; Ludwig 2010: 47. 218–225) and in the roughly contemporary settlement of Udabno, which was occupied from the turn of the 2nd millennium until the late 9th cent. BC (Korfmann et al. 2003/2004: 200. 203–208 Fig. 29, 9; Brodbeck-Jucker 2012: 125 Fig. 2, 2; 2015: 17. 19; 2019: 47. 85–87).

Considering the long chronological sequence of churns throughout the Late Bronze and Early Iron Ages and despite many comparisons with churns found in the cemeteries of Mingachevir, Zayamchay and Tovuzchay, no accurate date within this period can be suggested for the churn from Burial 11 at Tepe 5. The horizontal lines on the shoulder, which resemble similar churns found in Udabno and seem to correspond to churns found in Armenia, make a deposition at the end of the 2nd or in the first two centuries of the 1st millennium BC most likely. The same holds for the jug. Comparable vessels appeared in particular in burials at Mingachevir (Асланов et al. 1959: type XII-4 Pl. XXXII, 4. 6. 8–9), but also at Zayamchay (e. g. Müseyibli 2004: Pl. III, 10), Tovuzchay (e. g. Müseyibli et al. 2008: Fig. 39, 3), in Sagarejo (Мамиашвили 1988: Pl. XXXVIII, 65) and Udabno (Brodbeck-Jucker 2012: 137 Fig. 7, 2).

Grave contents

KG-029-0112-01 (single-handled jug) Fig. 96; Fig. 98, 2
Rim diam.: 104 mm (100%)
H: 293 mm
Base diam.: 172 mm
Fabric: completely reducing atmosphere, hard, medium fine temper (133)
Surface: ext. burnished; int. smoothed
Colour: ext. 10YR 6/1 (grey); core 7.5YR 5/3 (brown); int. Gley 1 5/N (grey)
Decoration: polished decoration of vertical stripes around the neck and body; five incised horizontal lines around the shoulder
Condition: body cracked and part of rim broken off
Comparanda:
Mingachevir, e. g. Burials 18, 40, 45, 65, 101, 111, 118, LBA/EIA (Асланов et al. 1959: Pl. XXXII, 4. 6. 8–9)
Sagarejo, Burial 4, EIA (Мамиашвили 1988: Pl. XXXVIII, 65)
Udabno, house U I-F, EIA (Brodbeck-Jucker 2012: 137 Fig. 2)

KG-029-0112-02 (churn) Fig. 97; Fig. 98, 1
Rim diam.: 112 mm (100%)
H: 486 mm
Base diam.: 163 mm
Fabric: completely reducing atmosphere, hard, medium fine temper (133)
Surface: ext. burnished; int. smoothed
Colour: ext. 10YR 6/1 (grey); core Gley 1 5/N (grey); int. Gley 1 5/N (grey)
Decoration: five incised horizontal lines around the shoulder
Condition: body cracked (one missing body-sherd), otherwise complete
Comparanda:
Mingachevir, Burials 2, 45, 140, 151 and burials 5 and 10 in Burrow II, LBA/EIA (Асланов et al. 1959: Pl. XXXII, 1–3)
Sagarejo, Burial 3, EIA (Мамиашвили 1988: 79 Pl. XXXVI, 31; Ludwig 2010: 220 no. 1543)
Udabno I, house U I-K, EIA (Brodbeck-Jucker 2012: 132 Fig. 2, 2; 2019: Pl. 26–28. 32, 1)
Tovuzchay, Burials 1, 24, 46, 47, 59, 63, 67, 76, 79, LBA/EIA (Müseyibli et al. 2008: 67 Fig. 40, 3; Maynard 2011)
Zayamchay, Burials 8, 22, 70, 72, 76, LBA/EIA (Maynard 2011)

Fill

KG-029-0115 (human bone) Table 4
Single vertebral arch

KG-029-0110 (flint flake)
L: 16 mm; W: 13 mm; Th: 6 mm; Wt: 1 g
606301.539 E; 4527995.903 N; 172.894 m

KG-029-0114 (obsidian flake)
L: 28 mm; W: 21 mm; Th: 7 mm; Wt: 4 g
606303.039 E; 4527995.959 N; 172.871 m

KG-029-0116 (obsidian flake)
L: 28 mm; W: 17 mm; Th: 7 mm; Wt: 4 g
606300.863 E; 4527999.288 N; 172.992 m

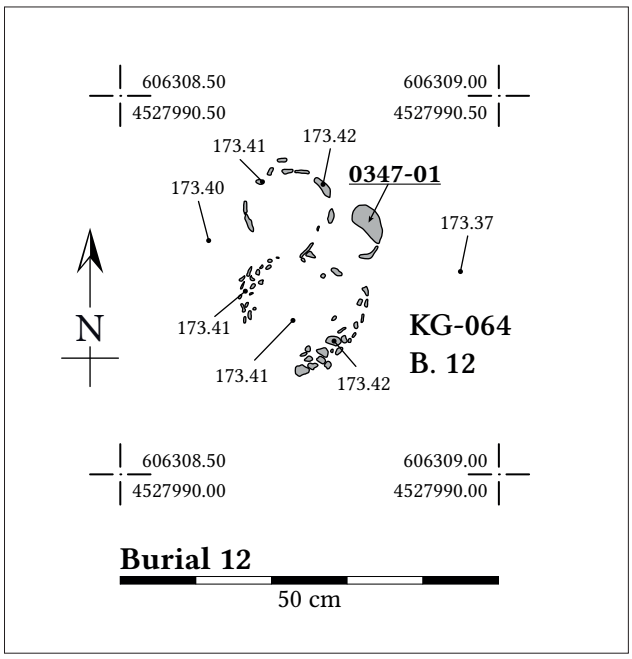

Fig. 99. Plan of Burial 12 (KG-064)

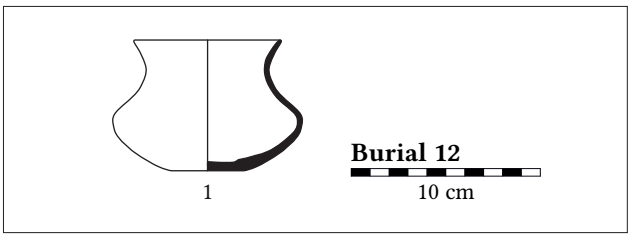

Fig. 100. Pottery from Burial 12 (KG-064): 1 – beaker (0347-01)

KG-029-0118 (obsidian flake)
L: 30 mm; W: 21 mm; Th: 14 mm; Wt: 4 g
606302.299 E; 4527995.780 N; 172.729 m

KG-029-0119 (obsidian flake)
L: 22 mm; W: 17 mm; Th: 5 mm; Wt: 1 g
606302.785 E; 4527995.606 N; 172.809 m

Burial 12 (KG-064)

Burial 12 was discovered already 10–15 cm below the modern surface of the hill in the north-eastern corner of square 6300/7980 (Fig. 27). The outline of the pit could not be distinguished from the surrounding soil. No skeletal remains were preserved. The only evidence for a burial was a cluster of highly fragmented sherds of probably three vessels (Fig. 99), of which, however, only the smallest one could be reconstructed (0347-01, Fig. 100, 1). It appears to have been a miniature jar or beaker with a biconical body and a wide flaring rim. The fabric was fine and of very dark grey to grey colour. Considering the present state of research, this vessel type is not common in Azerbaijan. It must be emphasized that the bad state of preservation does not allow for a definite typological determination, and the possibility of an applied handle can not be excluded. Nevertheless, some morphological comparisons can be drawn with miniature beakers in Kakheti that appeared in the Late Bronze Age and lasted at least until the 7th cent. BC (Ludwig 2010: 50–51 Pl. 144–145; Brodbeck-Jucker 2019: 61. Pl. 7–8. 233). Similar beakers are also known from Armenia and Nakhchivan (Brodbeck-Jucker 2019: 78–79 Pl. 233).

The considerable timespan suggested for this type of beakers and the lack of further means of dating makes a more precise placement within the chronological sequence of the burials at Tepe 5 difficult. Therefore, the proposed placement between Burials 11 and 13 remains highly tentative.

Grave contents

KG-064-0347-01 (beaker) Fig. 100, 1
Rim diam.: 80 mm (5%)
H: 59 mm
Base diam.: 40 mm
Fabric: completely reducing atmosphere, hard, fine temper (132)

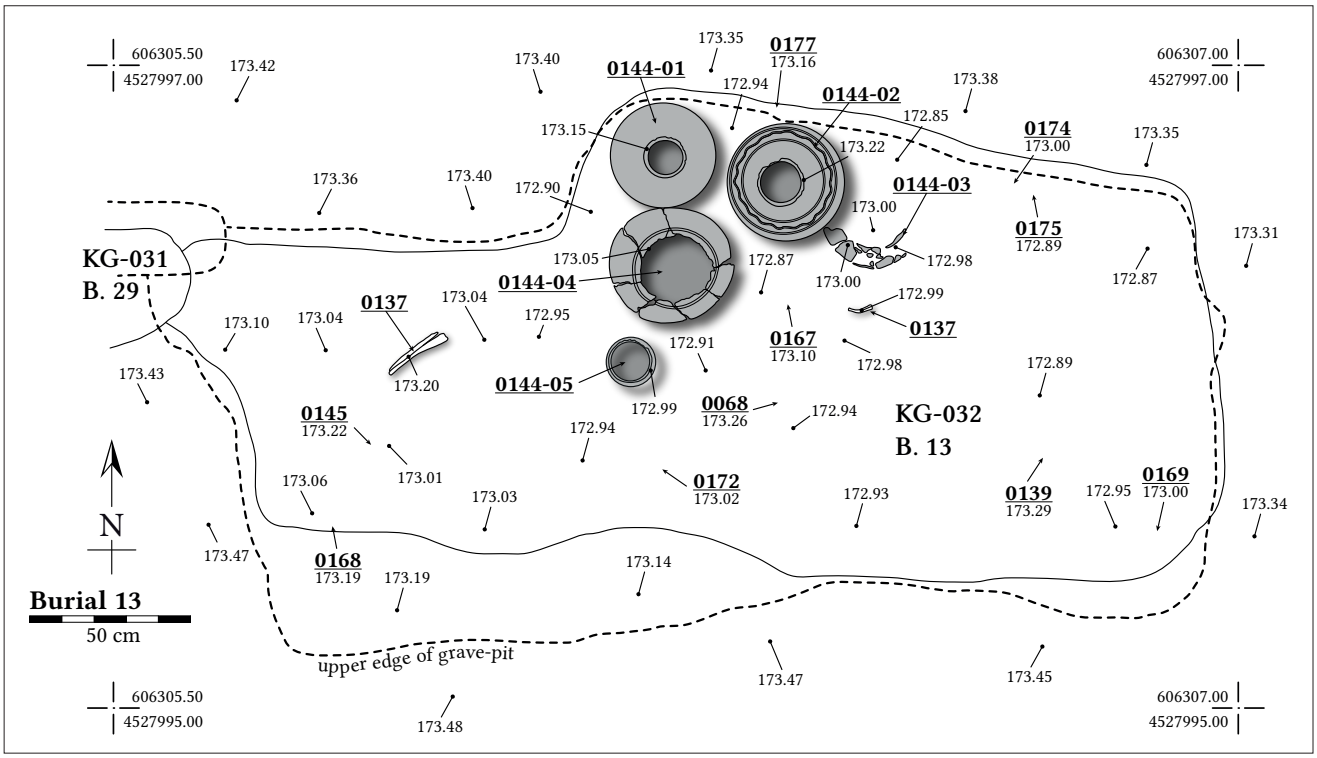

Fig. 101. Plan of Burial 13 (KG-032)

Fig. 102. Burial 13 (KG-032)

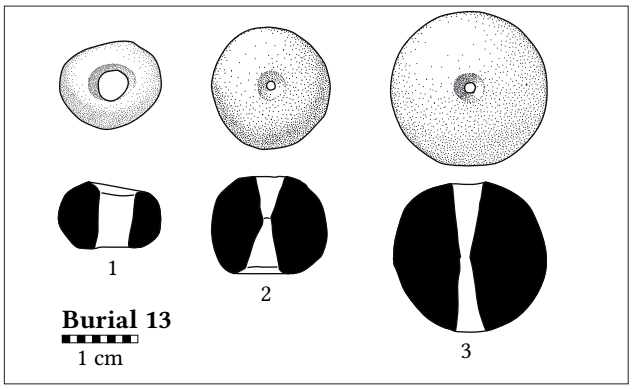

Fig. 103. Finds from Burial 13 (KG-032): 1 – carnelian bead (0145); 2 – carnelian bead (0168); 3 – carnelian bead (0068)

Fig. 104. Pot 0144-01 from Burial 13 (KG-032)

Surface: ext. polished; int. smoothed
Colour: ext. Gley 1 2.5/N (black); core 5YR 5/1 (grey); int. 5YR 5/1 (grey)
Condition: heavily fragmented; most of the vessel is missing

Burial 13 (KG-032)

Burial 13 was located in the north-eastern quadrant of square 6300/7990 (Fig. 27). The grave-pit was rather large and measured more than 3 m in west-east direction and 1.3–1.5 m from north to south (Fig. 101 and Fig. 102). Its outline was rectangular, except for the north-western corner that protruded inwards and narrowed the width of the western half. The north-westernmost edge of the pit was cut by the Medieval Burial 29 and immediately east of that area a single vessel (0036-01, Fig. 128, 1) was found high up in the fill of the grave-pit. This vessel was very likely not part of Burial 13, but marked a later burial or pottery deposit (see Burial 18).

Right in the corner of the protruding northern edge of the grave-pit were three intact large pots (0144-01, 0144-02, 0144-04) that were accompanied by a completely damaged pot (0144-03) to the east of 0144-02 and a small beaker (0144-05) south of 0144-04. Of the skeleton only few remains were left, among them fragments of femoral bones in the western half of the pit and some rib fragments near the pottery as well as parts of the skull and of the right tibia and fibula (0137, 0166). Two large circular carnelian beads (0068, 0168) and a small ring-shaped bead made of a dark brown burnt clay (0145) were found loose in the soil approximately in the same area (Fig. 103, 1–3). If they were part of the deceased's adornment, their location would suggest that the body was laid down somewhere south or south-west of the pottery. However, since none of the objects and bones was *in situ*, they do not allow for a more precise reconstruction of the body's position. In fact, it seems that the entire southern side of the grave-pit was disturbed, but without causing any damage to the pottery. Some bones of a small rodent found in the fill of the pit indi-

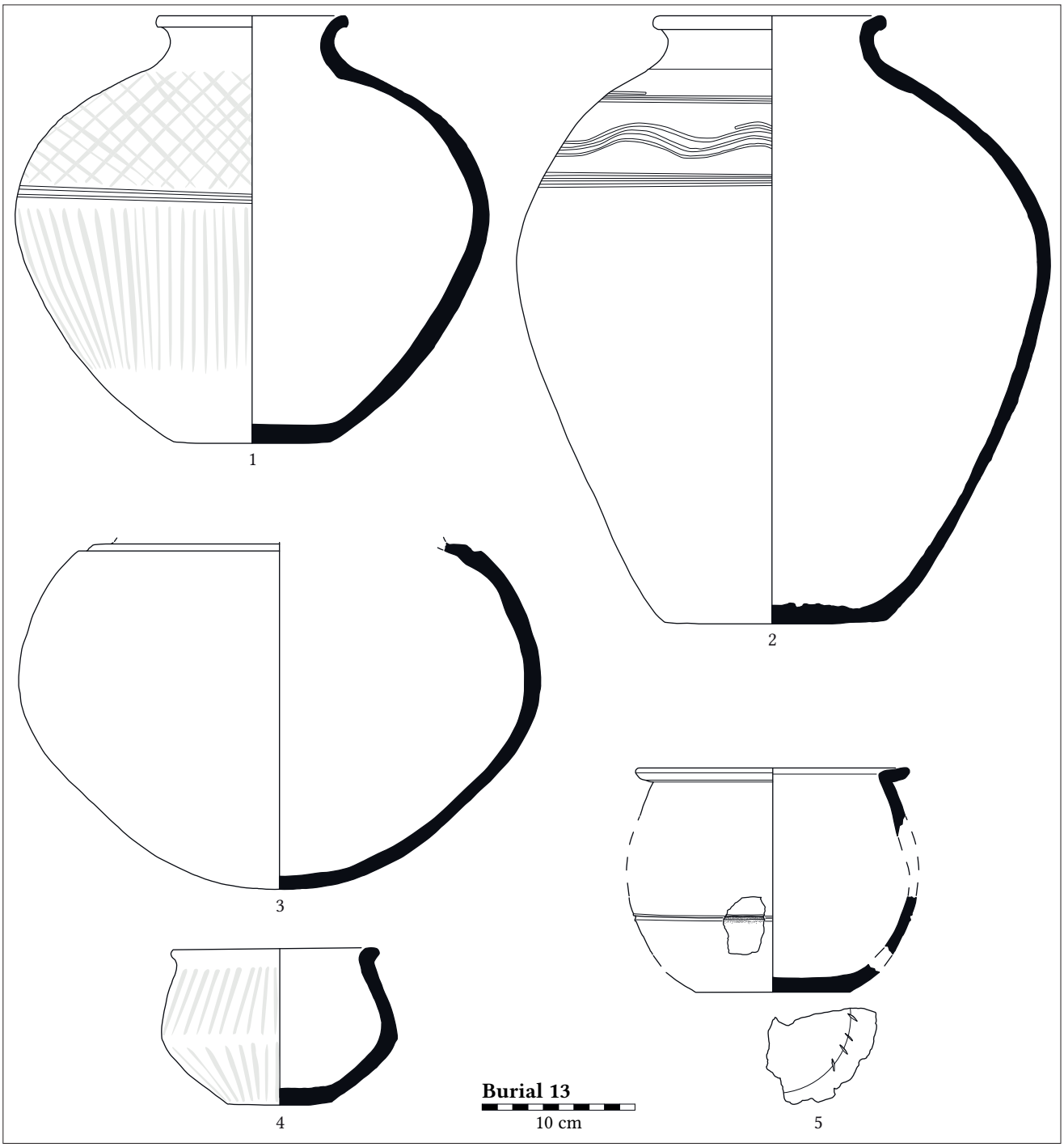

Fig. 105. Pottery from Burial 13 (KG-032): 1 – pot (0144-01); 2 – pot (0144-02); 3 – pot (0144-04); 4 – pot (0144-05); 5 – pot (0144-03)

cate animal activity that could have caused the damage to the skeletal remains and explain the difference in the state of preservation between the northern and southern parts. Only a humerus of a sheep or goat (0553) found loose in the fill might be considered as a burial gift. The eastern half of the grave-pit was virtually empty – only four obsidian flakes were found on different levels loose in the fill; three more obsidian flakes were collected in the central part of the grave-pit.

A radiocarbon sample taken from a femoral bone fragment (MAMS-39415) enables us to date the burial to the 9th cent. BC (Table 4). The typological comparisons of the pottery support this date by showing links to the Early Iron Age material from Udabno.

The pot 0144-01 (Fig. 104 and Fig. 105, 1) was made of a black-dark-greyish fabric, it had a wide spherical body with a flat base and short neck. Around the widest circumference two incised horizontal lines divided

Fig. 106. Pot 0144-02 from Burial 13 (KG-032)

Fig. 107. Pot 0144-04 from Burial 13 (KG-032)

the surface into two sections with different patterns of a polished decoration: The shoulder carried cross-hatching and the surface of the lower body was covered with vertical lines. Shape and decoration of the pot are comparable to some pots from Kachbulag (Гусейнова 1989: 56 Pl. XXIII, 13–14), however, so far nothing secure can be said about their dating. In Tovuzchay similarly shaped vessels are attested, but without decoration (Müseyibli et al. 2008: Fig. 44, 2. 48). The vessel is similar to double-handled jars from Udabno (Brodbeck-Jucker 2019: 66–68. 87–90 Pl. 43–52). Although the pot 0144-01 is missing the opposing handles, the vessel's profile is comparable. In addition, the jars from Udabno often carry polished decoration that was divided between shoulder and body by horizontal lines. This resembles the division on

Fig. 108. Small beaker 0144-05 from Burial 13 (KG-032)

the pot in Burial 13, although due to the missing handles it is lower on the vessel's body. Both types of polished decoration pattern are attested on various double-handled jars in various combinations with other motives (Brodbeck-Jucker 2019: Pl. 43. 50. 52). Comparisons with the Armenian Highlands can be drawn with storage jars of the Lchashen-Metsamor 5 horizon (Iron Age IB), that sometimes carry an incised decoration (Smith et al. 2009: 87 Fig. 31a).

The tall jar 0144-02 was made of a grey fabric (Fig. 105, 2 and Fig. 106). It was decorated with an incised multiple wavy line around the shoulder that was framed by horizontal lines. Comparable vessels are known again from houses dated to the 10th and 9th cent. BC at Udabno (Brodbeck-Jucker 2019: 203–204. 214 Pl. 93. 95) and from the Tovuzchay cemetery (Müseyibli et al. 2008: Fig. 40, 2).

East of the tall jar 0144-02 lay the remains of a highly fragmented small pot (0144-03), the shape of which could not be fully reconstructed. The drawing in Fig. 105, 5 should, therefore, be considered tentative, in particular the position of the body-sherd with a horizontally incised groove. Noteworthy are the rim, bent at almost right angle, and several notches that were incised along the edge of the flat base. The material from Udabno provides us with an idea of such pots in different sizes and with sometimes more elaborate surface decorations (Brodbeck-Jucker 2019: Pl. 61–70).

The large pot 0144-04 had a wide spheroid body with a rounded base (Fig. 105, 3 and Fig. 107). The shoulder was marked by a pronounced ridge. The rim was missing and seems to have been broken off already before the vessel was deposited in the grave. The damage makes it difficult to determine its type. However, it might be connected with a group of hole-mouthed vessels found, for example, at Mingachevir or in the area of Kalakent, even though

these vessels usually have an additional disc-shaped or flat rectangular application near the opening (see vessel 0498-03 in Burial 6), of which there was no evidence on pot 0144-04. Its coarse fabric had for the most part a black or dark-greyish colour suggesting a reducing atmosphere, however, above the ridge on the shoulder the fabric changed to a brownish-red colour indicating that the firing process was controlled to achieve a distinct colour pattern on the vessel's surface.

Pot 0144-04 stood next to the grey-coloured small pot or beaker 0144-05 (Fig. 105, 4 and Fig. 108). It had a biconical profile and a short outward bent rim. Its surface was covered with a polished decoration of vertical lines. It is difficult to find good comparisons for this vessel type; some links point again to Udabno where a similar small biconical vessel was found (Brodbeck-Jucker 2019: Kat. 141 Pl. 81, 1), on the other hand there are some examples of the same size and morphology excavated by A. A. Ivanovsky in the region of Kalakent (Ивановский 1911: Pl. XII, 8).

Grave contents

KG-032-0137 and KG-032-0166 (human bones) Table 4
Sex: could not be determined Table 16
Age class: Maturitas–Senilis

KG-032-0553 (animal bones)
humerus of a sheep

KG-032-0144-01 (pot) Fig. 104; Fig. 105, 1
Rim diam.: 122 mm (100%)
H: 280 mm
Base diam.: 105 mm
Fabric: completely reducing atmosphere, hard, medium fine temper (133)
Surface: ext. burnished; int. smoothed
Colour: ext. Gley 1 2.5/N (black); int. Gley 1 2.5/N (black)
Decoration: polished decoration of vertical stripes on the lower body; two incised horizontal lines around the widest circumference and a polished cross-hatching on the shoulder
Condition: complete
Comparanda:
Kachbulag, burials (Гусейнова 1989: 56 Pl. XXIX, 13–14)
Tovuzchay, Burials 76 and 82, EIA? (Müseyibli et al. 2008: Fig. 44, 2. 48)
Mastara, Tomb 17, Iron IB (Smith et al. 2009: 87 Fig. 31a)
Udabno, various houses, EIA, double-handled pots (Brodbeck-Jucker 2019: Pl. 43–52)

KG-032-0144-02 (pot) Fig. 105, 2; Fig. 106
Rim diam.: 145 mm (100%)
H: 395 mm
Base diam.: 145 mm
Fabric: exterior reducing, interior oxidizing atmosphere, hard, coarse temper (434)
Surface: ext. burnished; int. smoothed
Colour: ext. Gley 1 2.5/N (black); core 5Y 5/1 (grey); int. 5Y 5/1 (grey)
Decoration: incised horizontal lines on the shoulder, separated by a multiple-lined wavy band
Condition: complete
Comparanda:
Udabno, U III-D and U I-K, EIA (Brodbeck-Jucker 2019: Kat. 142 and 267, Pl. 93. 95. 166. 168)
Tovuzchay, Burial 76, LBA/EIA (Müseyibli et al. 2008: Fig. 40, 2)

KG-032-0144-03 (pot) Fig. 105, 5
Rim diam.: 178 mm
H: c. 130 mm
Base diam.: 100 mm
Fabric: completely reducing atmosphere, medium hard, medium fine temper (123)
Surface: ext. and int. smoothed
Colour: ext. 10YR 3/1 (very dark grey); core 10YR 5/1 (grey); int. 10YR 5/1 (grey)
Decoration: at least a single incised line around the body
Condition: heavily fragmented
Comparanda:
Udabno, EIA (Brodbeck-Jucker 2019: Pl. 61–70)

KG-032-0144-04 (pot) Fig. 105, 3; Fig. 107
H: 239 mm preserved
Base diam.: 100 mm
Fabric: irregular atmosphere (parts above the shoulder ridge oxidized, otherwise mostly reducing atmosphere), hard, coarse temper (434)
Surface: ext. burnished; int. smoothed
Colour: ext. 2.5Y 3/1 (very dark grey); core 5YR 5/4 (reddish brown); int. 10YR 6/4 (light yellowish brown)
Decoration: distinctive change of colour between body and shoulder by controlled firing atmosphere
Condition: the body is fragmented and the coarse fabric prevented a complete reconstruction; rim probably already broken in antiquity

KG-032-0144-05 (beaker) Fig. 105, 4; Fig. 108
Rim diam.: 138 mm (100%)
H: 100 mm
Base diam.: 64 mm
Fabric: completely reducing atmosphere, hard, medium fine temper (133)
Surface: ext. burnished; int. smoothed
Colour: ext. Gley 1 5/N (grey); int. Gley 1 5/N (grey)
Decoration: polished vertical lines above and below the carination
Condition: complete
Comparanda:
Udabno, U I-K, EIA (Brodbeck-Jucker 2019: Kat. 141, Pl. 81)
area of Kalakent, Burials 11, 47, 56, LBA/EIA (Ивановский 1911: Pl. XII, 8)

KG-032-0068 (circular carnelian bead) Fig. 103, 3
Diam: 19.0–20.0 mm; Hole diam.: 4.0 mm; Wt: 11 g
606307.568 E; 4527995.949 N; 173.262 m

KG-032-0168 (circular carnelian bead) Fig. 103, 2
Diam: 15.3 mm; Th: 12.8 mm; Hole diam.: 3.8–4.4 mm; Wt: 5 g
606306.181 E; 4527995.569 N; 173.190 m

KG-032-0145 (ring-shaped clay bead) Fig. 103, 1
Diam: 13.3 mm; Th: 8.9 mm;
Hole diam.: 4.7 mm; Wt: 1 g
606306.302 E; 4527995.820 N; 173.222 m

Fill

KG-032-0139 (obsidian flake)
L: 22.0 mm; W: 14.7 mm; Th: 4.5 mm; Wt: 1 g
606308.392 E; 4527995.781 N; 173.286 m

KG-032-0167 (obsidian flake)
L: 30.0 mm; W: 21.0 mm; Th: 7.9 mm; Wt: 7 g
606307.567 E; 4527996.259 N; 173.101 m

KG-032-0169 (obsidian flake)
L: 25.8 mm; W: 22.5 mm; Th: 9.4 mm; Wt: 3 g
606308.748 E; 4527995.556 N; 172.998 m

KG-032-0172 (obsidian flake)
L: 12.2 mm; W: 11.6 mm; Th: 2.0 mm; Wt: 1 g
606307.208 E; 4527995.744 N; 173.023 m

KG-032-0174 (obsidian flake)
L: 31.9 mm; W: 22.5 mm; Th: 8.6 mm; Wt: 5 g
606308.302 E; 4527996.636 N; 172.998 m

KG-032-0175 (obsidian flake)
L: 19.9 mm; W: 17.8 mm; Th: 6.5 mm; Wt: 2 g
606308.362 E; 4527995.598 N; 172.892 m

KG-032-0177 (obsidian flake)
L: 32.1 mm; W: 22.0 mm; Th: 7.9 mm; Wt: 6 g
606307.564 E; 4527996.868 N; 173.159 m

KG-032-0144-06 (body-sherd)
Fabric: not completely reduced core, medium hard, fine temper (622)

KG-032-0144-07 (body-sherd)
Fabric: not completely reduced core, hard, medium fine temper (633)

Burial 14 (KG-059)

Burial 14 was located in the south-eastern corner of the north-eastern quadrant of square 6290/7980 (Fig. 27). To expose the entire outline of the grave-pit a 2 m long section of the baulk between squares 6290/7980 and 6300/7980 was removed (KG-062). The grave-pit was oriented west-east and had a very regular rectangular shape (1.65 × 1.2 m) with rounded corners (Fig. 110). Apart from obsidian flakes (0255, 0251, 0257, 0273) found loose in the fill, all finds were concentrated in the western half of the burial.

Along the western edge of the grave-pit two ceramic vessels were placed, a double-handled jar and a pot. The grey-coloured jar (0252-01) had a very regular oval shape with a lenticular base, a narrow, but tall, slightly flaring neck and a horizontally outrolled rim (Fig. 109, 1 and Fig. 111). Two round handles sat on opposite sides of the body, and each of them carried an incised decoration of four rows of notches on the upper joint. Around the shoulder ran an incised wavy line. Morphologically the jar comes closest to double-handled jars that are known from the Late Bronze Age onwards in Eastern Georgia (Brodbeck-Jucker 2019: 66) and appear frequently since the Lchashen-Metsamor 4 pottery horizon (Iron Ia) in the Armenian highlands (Smith et al. 2009: 83 Fig. 29m). In Azerbaijan this vessel type is less widespread and the few known examples listed by S. Brodbeck-Jucker (2019: 66 note 477) seem to be of larger size than the jar from Burial 14. This is also true for the double-handled jars

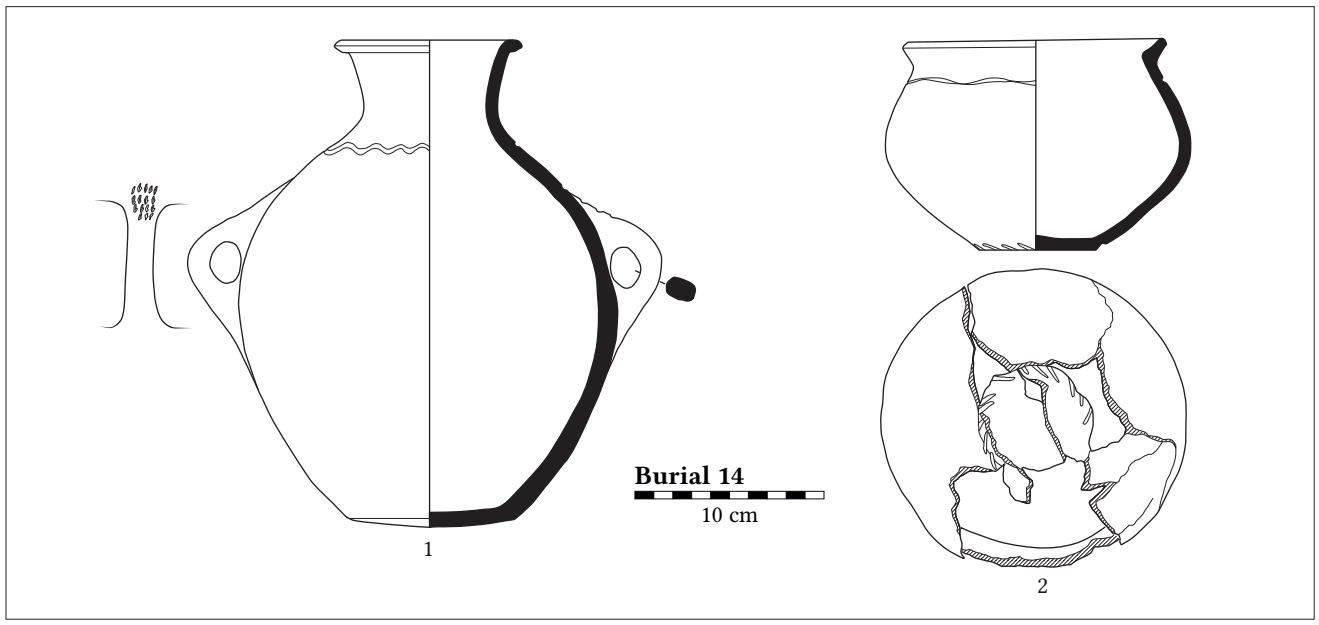

Fig. 109. Pottery from Burial 14 (KG-059): 1 – jar (0252-01); 2 – pot (0252-02)

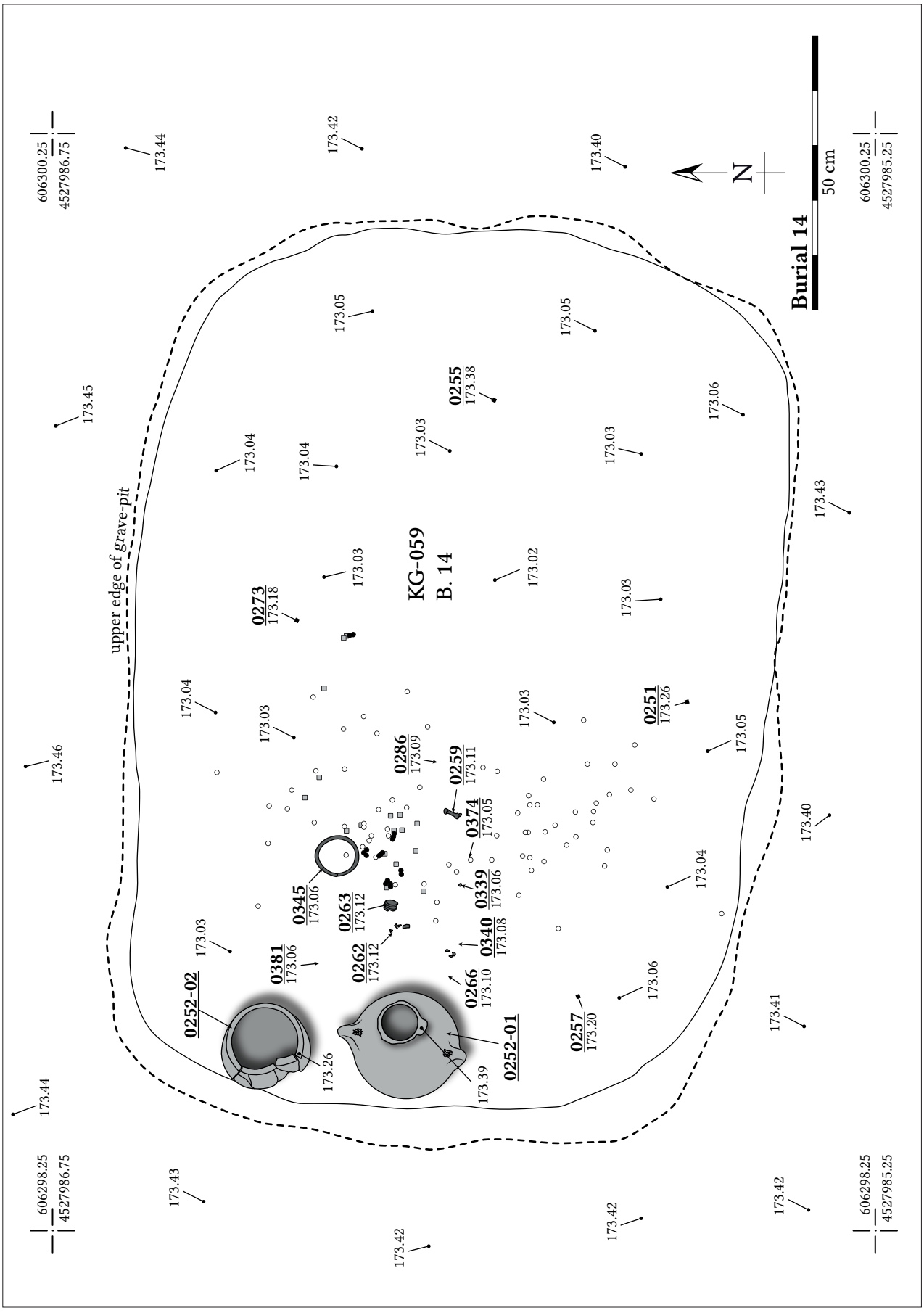

Fig. 110. Plan of Burial 14 (KG-059)

Fig. 111. Pot 0252-01 from Burial 14 (KG-059)

from Armenia and Georgia that were usually taller, had a wider body diameter and a shorter neck. Only a small jar in house U III-C at Udabno was of comparable size (Brodbeck-Jucker 2019: Kat. 247 Pl. 38. 136, 1). Noteworthy, however, is the lenticular base that is a common feature of double-handled jars in Udabno (Brodbeck-Jucker 2019: 87).

The pot (0252-02) was made of a similar grey fabric, but most of its surface was blackened (Fig. 109, 2). Its flat base was decorated with a row of notches around the circumference, and the shoulder carried an incised wavy line. The rounded body ended in a sharply bent flaring rim. Ornamentation and morphological features are comparable to pot 0241-07 in Burial 15 which, in turn, provides links to the Early Iron Age material from Udabno (Brodbeck-Jucker 2019: Pl. 61–71), to similar pottery vessels in various burials (e. g. Burials 10, 24, 32, 39, 116) at Zayamchay (Müseyibli 2004: Pl. I, 9; Müseyibli 2009: 57 Pl. X, 7; Müseyibli/Nəcəfov 2019: Pl. 19, 3. 36, 5. 51, 1. 53, 2. 118, 2) and to earlier material of the Lchashen-Metsamor 3 (LBA III) horizon in the Armenian highland (Smith et al. 2009: 81 Fig. 28p).

Of the skeleton (0346) nothing was preserved, except for a single finger bone that had been protected by a bronze finger ring (0263, Fig. 112, 2). It was found 15 cm east of jar 0252-01 (Fig. 110). The ring was made of a c. 1.5 mm thick bronze wire that was twisted four times to form a cylinder with a diameter of c. 19 mm. Two similar spiral finger rings were found at Tovuzchay: One was made of a thin bronze wire and was still in place on the finger bone of one of the two skeletons in Burial 46 (Mü-

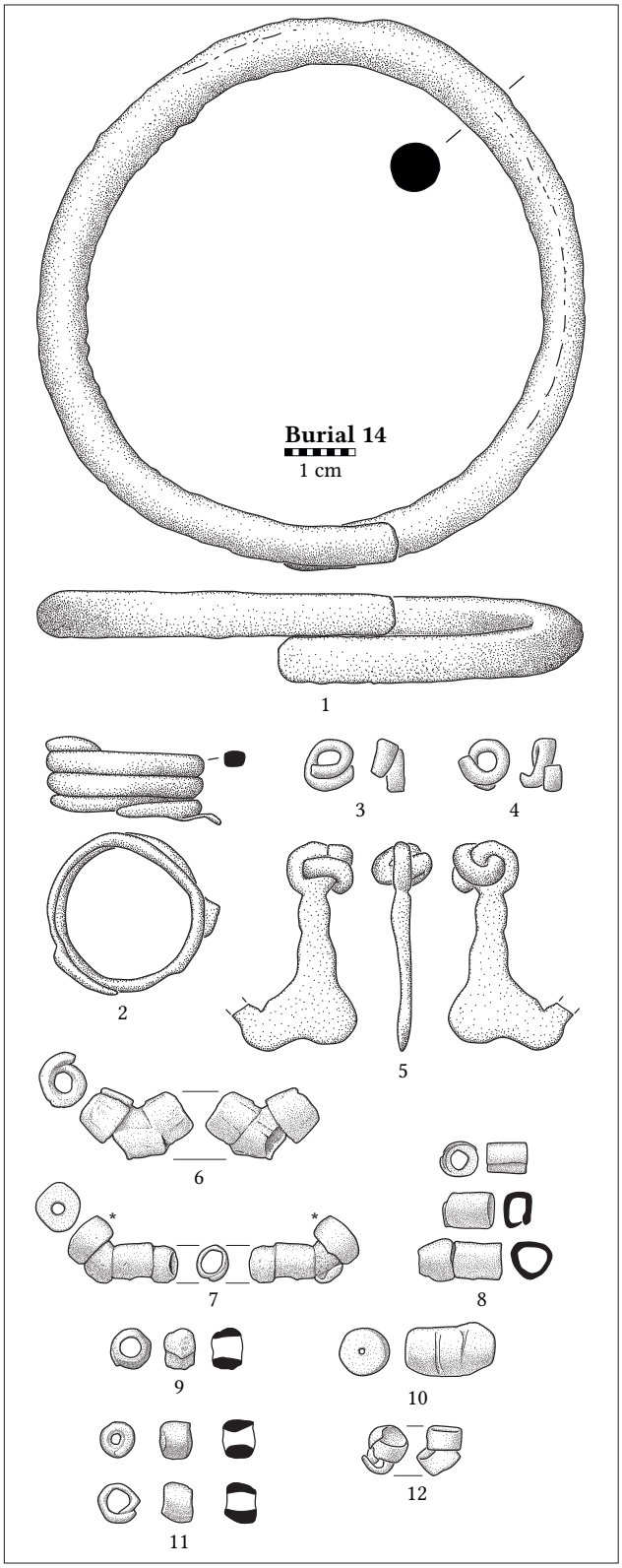

Fig. 112. Finds from Burial 14 (KG-059): 1 – bronze bracelet (0345); 2 – bronze finger ring (0263); 3 – bronze eyelet (0374a); 4 – bronze eyelet (0279); 5 – bronze pendant (0259); 6 – bronze beads (0344); 7 – bronze and carnelian (*) bead (0271); 8 – bronze beads (0341a); 9 – bronze bead (0302a); 10 – bronze beads (0343a); 11 – bronze beads (0338a); 12 – bronze beads (0342a)

seyibli et al. 2008: Pl. 53, 9) and another accompanied the deceased in Burial 76, though it had only one and a half twists (Müseyibli et al. 2008: Fig. 29, 6). Similar spiral finger rings are also known from Mingachevir, where a ring with seven twists was discovered in Burial 150 (Асланов et al. 1959: 174 Pl. XX, 4), and in the area of Kalakent, e. g. in *Paradiesfestung* Burial 2 (Nagel/Strommenger 1985: 53 Pl. 4, 3–5) or Qaramurad Burial 11 (Nagel/Strommenger 1985: 95 Pl. 64, 6).

The finger ring in Burial 14 belonged to a larger set of bronze adornments that included a bracelet (0345, Fig. 112, 1). The 6–7 mm thick round bronze rod was curved into a ring with an inner diameter of 6.5 cm and overlapping ends. The surface remained undecorated. This type of body adornment is frequently attested, for example, in burials in Zayamchay, Tovuzchay, Mingachevir and in the area of Kalakent (see below). Further southeast lay a pendant (0259) made of a 1–2 mm thick and 3 cm long bronze band (Fig. 112, 5). The upper end was perforated, and a small bronze eyelet or chain link was attached to it. The lower end of the pendant was widened and at least at one side broken. Two similar eyelets were found not far from the pendant (0279, 0374a, Fig. 112, 3–4).

South of the spiral finger ring and east of the jar 0252-01 more than 40 small fragments of bronze sheet were found (0262, 0266, 0276d, 0285, 0339, 0340) that might have belonged to one or more pieces of adornment, however, their original shape could not be determined (Fig. 110).

Spread over a limited area south of the bracelet and east of the finger ring (Fig. 110) were 18 bronze beads (0271a, 0302a, 0338a, 0341a, 0342a, 0343a, 0344). The beads were all made by rolling a thin bronze sheet to a short tube of varying length between 3 and 7 mm (Fig. 112, 6–12). In the same area of the bronze beads and in one case further east (0338b) a total of 21 carnelian beads were found (Fig. 110). The majority were disc-shaped, only one was cylindrical (0333, Fig. 113, 15) and a second one had a lenticular shape (0311, Fig. 113, 16). Six carnelian beads (0271b, 0338b, 0341b, 0342b, 0343b) were placed right next to or even corroded to bronze beads (see Fig. 112, 7) which implies that bronze and carnelian beads may have been part of the same necklace.

The by far largest number of finds were frit beads that formed a 70 × 40 cm large cluster in the western half of the grave-pit (Fig. 110). In total at least 122 beads were recovered, not including many fragments of decayed frit beads. They were for the most part ring-shaped, only a few were cylindrical (Fig. 114, 23–25). The colours varied from whitish/yellowish-buff to brown-buff. In two instances two frit beads were fused together, probably during the production process (0335, 0371 Fig. 114, 26–27). A striking exception was a bluish cylindrical bead with

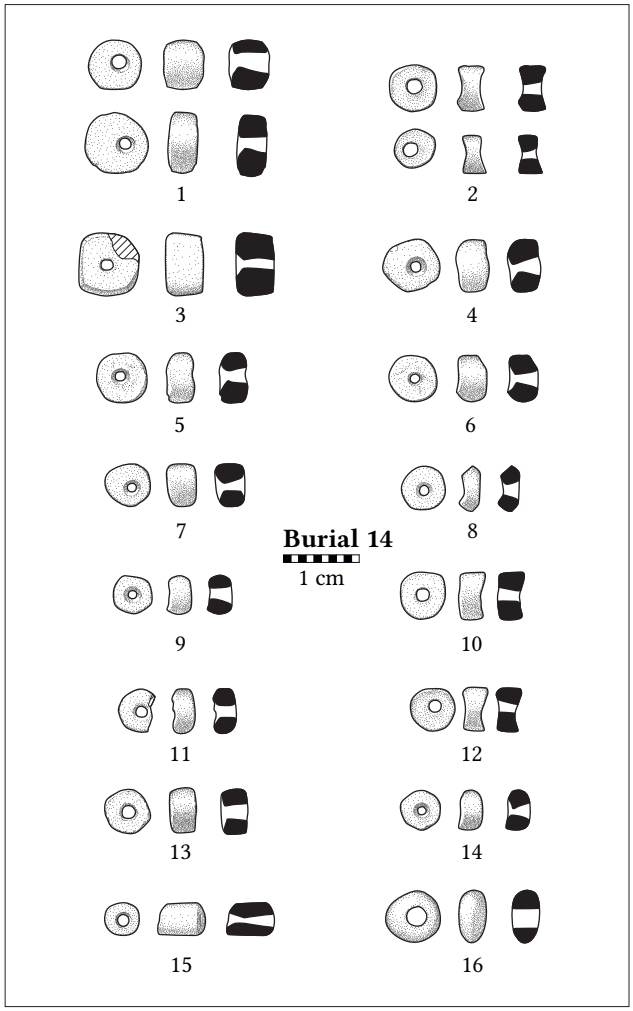

Fig. 113. Carnelian beads from Burial 14 (KG-059): 1 – (0338b); 2 – (0276b); 3 – (0343b); 4 – (0306); 5 – (0366); 6 – (0269); 7 – (0272); 8 – (0336); 9 – (0316); 10 – (0342b); 11 – (0300); 12 – (0341b); 13 – (0337a); 14 – (0361); 15 – (0333); 16 – (0311)

three applied knobs (0381, Fig. 114, 29) that was found off the main cluster of the frit beads further west close to pot 0252-02 (Fig. 110). In terms of morphology, material and colour, this bead was identical to the large number of beads found in Burial 1 and in the fill of Burial 21 that disturbed the former. Two beads of the same type were found in the topsoil layer (KG-054) south of the grave-pit of these two burials and were interpreted as objects originally from Burial 1 that were scattered in the course of its disturbance by Burial 21 (see Burial 1). One of those beads (0223) was found not far west of Burial 14 raising the possibility that bead 0381 might be assigned to the original grave contents of Burial 1 as well and should therefore be interpreted as an accidental intrusion, perhaps due to an animal burrowing. That some minor disturbances might have happened is further suggested by two small joining fragments of bronze sheet (0218) found

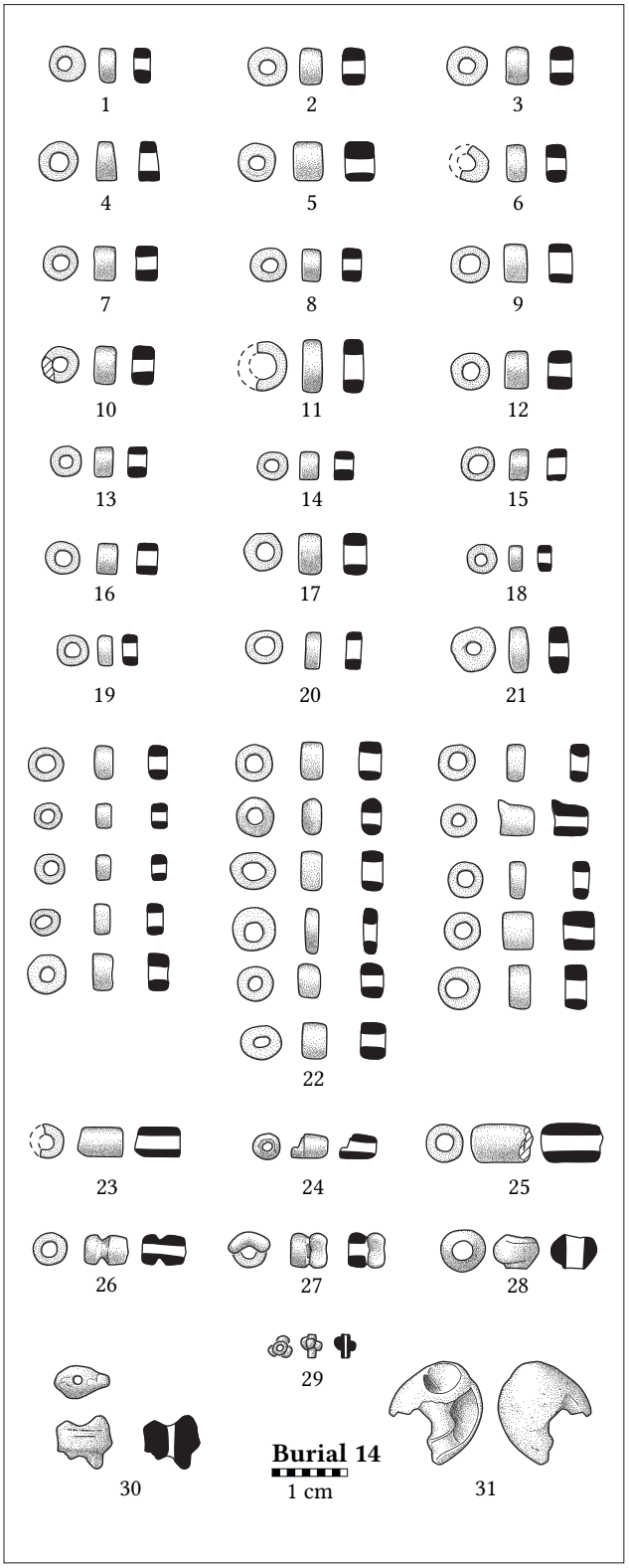

Fig. 114. Frit beads and other finds from Burial 14 (KG-059): 1 – (0274); 2 – (0275); 3 – (0268); 4 – (0313); 5 – (0267); 6 – (0270); 7 – (0307); 8 – (0310); 9 – (0284); 10 – (0329); 11 – (0331); 12 – (0330); 13 – (0264); 14 – (0261); 15 – (0370); 16 (0334); 17 – (0304); 18 – (0352); 19 – (0341c); 20 – (0359); 21 – (0337b); 22 – (0276a); 23 – (0368); 24 – (0357); 25 – (0302b); 26 – (0335); 27 – (0371); 28 – (0375); 29 – (0381); 30 – (0276c); 31 – (0286)

higher up in the topsoil layer KG-054, but still within the outline of the grave-pit (ch. IV.8). As they are similar to the many bronze sheet fragments found at the bottom of the pit, these two bronze pieces might well be displaced fragments of burial gifts.

In addition to the bronze, carnelian and frit beads, a single clay bead was found in the grave-pit (0276c, Fig. 114, 30). Its surface was damaged and in parts broken off, so its original shape could not be determined. The fragment of a mollusc (0286, Fig. 114, 31) completes the diverse range of materials found in Burial 14. Unfortunately, the damage to the shell prevented any further specification of its possible use as an adornment.

All finds were found within a layer between 173.03 m and 173.16 m in the western half of the grave-pit. The many beads and adornments, but in particular the position of the finger bone and the bracelet, indicate that the body was placed with its upper body in that area.

The dating of the burial is mainly based on the ceramic vessels. The pot with notched base points to an Early Iron Age date in the first half of the 1st millennium BC, as it closely resembled pot 0241-07 in Burial 15 that was dated to the 8th–7th cent. BC and might be related to pot 0144-03 in Burial 13 of the 9th cent. BC. Despite some differences in size and shape, also the double-handled jar 0252-01 allows an attribution to typical jars of the Early Iron Age which further supports the proposed date of Burial 14 to the first centuries of the 1st millennium BC.

Grave contents

KG-059-0346 (human phalanx)
Sex and age class could not be determined — Table 16

KG-059-0252-01 (pot) — Fig. 109, 1; Fig. 111
Rim diam.: 257 mm (100%)
H: 257 mm
Base diam.: 90 mm
Fabric: completely reducing atmosphere, hard, fine temper (132)
Surface: ext. burnished; int. smoothed
Colour: ext. 2.5Y 5/1 (grey); core 2.5Y 6/1 (grey); int. 2.5Y 5/1 (grey)
Decoration: four rows of notches atop the handles and an incised wavy line around the shoulder
Condition: some parts of the rim broken off, otherwise complete
Comparanda:
Udabno, U III-C, EIA (Brodbeck-Jucker 2019: Kat. 247 Pl. 38. 136, 1)

KG-059-0252-02 (pot) — Fig. 109, 2
Rim diam.: 135 mm (85%)
H: 111 mm
Base diam.: 60 mm
Fabric: exterior reducing, interior oxidizing atmosphere, medium hard, medium fine temper (423)
Surface: ext. burnished; int. smoothed

Colour: ext. Gley 1 2.5/N (black); core 2.5Y 7/2 (light grey); int. 2.5Y 7/2 (light grey)
Decoration: row of notches along the circumference of the base and incised wavy line around the shoulder
Condition: body was heavily fragmented and not all sherds could be reassembled
Comparanda:
Zayamchay, Burials 10, 24, 32, 39, 116, LBA/EIA (Müseyibli 2004: Pl. I, 9; Müseyibli 2009: 57 Pl. X, 7; Müseyibli/Nəcəfov 2019: Pl. 19, 3. 36, 5. 51, 1. 53, 2. 118, 2)
Udabno, EIA (Brodbeck-Jucker 2019: Pl. 61–71)
Oshakan, Burial 100, LBA III (Smith et al. 2009: 81 Fig. 28p)

KG-059-0345 (bronze bracelet) Fig. 112, 1
Diam: 72.0 mm; Inner diam.: 65.0 mm;
Th: 6.0–7.0 mm; Wt: 44 g
606298.940 E; 4527986.235 N; 173.056 m
Comparanda:
Zayamchay, Burials 26 and 27, LBA/EIA (Müseyibli 2004: 63 Pl. VI, 13. 15; Müseyibli/Nəcəfov 2019: Pl. 38, 8. 42, 2)
Tovuzchay, e. g. Burials 6, 16, 19, 53, 69, 77, 79, 84 LBA/EIA (Müseyibli et al. 2008: Fig. 23, 8–9. 25, 4–5. 29, 1–2. 30, 14. 32, 6–7. 33, 15)
Mingachevir, LBA/EIA (Асланов et al. 1959: Pl. XX, 13–15. 18. 22–23)
Paradiesfestung, e. g. Burials 45, 95, LBA/EIA (Nagel/Strommenger 1985: Pl. 18, 3. 39, 4)
Gogdaja, Burial 10, LBA/EIA (Nagel/Strommenger 1985: Pl. 68, 4)

KG-059-0263 (bronze spiral finger ring) Fig. 112, 2
Diam: 23.0 mm; Inner diam.: 18.0 mm;
Th: 12.0 mm; Wt: 3 g
606298.834 E; 4527986.139 N; 173.120 m
Comparanda:
Tovuzchay, Burials 16, 46, 76, LBA/EIA (Müseyibli et al. 2008: Pl. 53, 9. Fig. 29, 6. 33, 14)
Mingachevir, Burial 150, LBA/EIA (Асланов et al. 1959: Pl. XX, 4)
Kalakent, Burial 28, LBA/EIA (Nagel/Strommenger 1985: 91 Pl. 60, 6)
Paradiesfestung, Burials 2, 73, 82, LBA/EIA (Nagel/Strommenger 1985: Pl. 4, 3–5. 34, 9. 35, 10)
Qaramurad, Burial 11, LBA/EIA (Nagel/Strommenger 1985: 95 Pl. 64, 6)
Gogdaja, Burial 22, LBA/EIA (Nagel/Strommenger 1985: 114 Pl. 72, 5)
Kushchu, Burial 24, EIA (Гуммель 1940: 138 Fig. 4, no. 30)

KG-059-0259 (bronze pendant with attached eyelet) Fig. 112, 5
L: 30.0 mm; W: 16.0 mm; Th: 2.5 mm; Wt: 2 g
606299.027 E; 4527986.018 N; 173.114 m

KG-059-0374a (bronze eyelet) Fig. 112, 3
Diam: 7.0 mm; Th: 4.7 mm;
Hole diam.: 2.0–3.0 mm; Wt: <1 g
606298.927 E; 4527985.990 N; 173.044 m

KG-059-0279 (bronze eyelet) Fig. 112, 4
Diam: 7.5 mm; Th: 6.0 mm;
Hole diam.: 2.5 mm; Wt: <1g

KG-059-0266 (c. 20 fragments of bronze sheet)
Th: 0.5 mm; Wt: 1 g
606298.714 E; 4527986.030 N; 173.095 m

KG-059-0262 (c. 20 fragments of bronze sheet)
Th: 0.5 mm; Wt: 1 g
606298.792 E; 4527986.131 N; 173.119 m

KG-059-0339 (fragment of bronze sheet)
L: 4.0 mm; W: 2.0 mm; Th: 2.0 mm; Wt: <1 g
606298.869 E; 4527986.006 N; 173.060 m

KG-059-0340 (fragment of bronze sheet)
L: 4.0 mm; W: 3.5 mm; Th: 1.0 mm; Wt: <1 g
606298.772 E; 4527986.012 N; 173.075 m

KG-059-0285 (fragment of bronze sheet)
L: 4.0 mm; W: 3.0 mm; Th: 1.0 mm; Wt: <1 g

KG-059-0276d (two fragments of bronze sheet)

KG-059-0271a (three bronze beads) Fig. 112, 7
Diam: 9.4 mm; L: 4.0–5.8 mm;
Hole diam.: 2.7 mm; Wt: 1 g
606298.974 E; 4527986.130 N; 173.070 m
found together with one carnelian bead

KG-059-0302a (bronze bead) Fig. 112, 9
Diam: 6.0 mm; Th: 4.0 mm;
Hole diam.: 3.6 mm; Wt: <1 g
606298.827 E; 4527985.533 N; 173.114 m

KG-059-0338a (two bronze beads) Fig. 112, 11
Diam: 5.2–5.8 mm; Th: 4.3–4.5 mm;
Hole diam.: 2.4–3.1 mm; Wt: 1 g
606299.333 E; 4527986.211 N; 173.066 m

KG-059-0341a (four bronze beads) Fig. 112, 8
Diam: 4.0–6.2 mm; L: 5.5–7.0 mm;
Hole diam.: 1.2–3.2 mm; Wt: 1 g
606298.879 E; 4527986.139 N; 173.070 m

KG-059-0342a (two bronze beads) Fig. 112, 12
Diam: 4.0–5.5 mm; Th: 4.0–4.7 mm;
Hole diam.: 2.5–3.8 mm; Wt: <1 g
606298.911 E; 4527986.124 N; 173.068 m

KG-059-0343a (three bronze beads) Fig. 112, 10
Diam: 6.8–7.0 mm; Th: 3.1–4.5 mm;
Hole diam.: 0.4–0.8 mm; Wt: <1 g
606298.936 E; 4527986.157 N; 173.070 m

KG-059-0344 (three bronze beads) Fig. 112, 6
Diam: 7.0–7.3 mm; Th: 5.3–5.5 mm;
Hole diam.: 2.7–3.0 mm; Wt: 1 g
606298.938 E; 4527986.183 N; 173.080 m

KG-059-0269 (disc-shaped carnelian bead) Fig. 113, 6
Diam: 6.2 mm; Th: 4.0 mm;
Hole diam.: 2.0 mm; Wt: <1 g
606299.237 E; 4527986.256 N; 173.156 m

KG-059-0271b (disc-shaped carnelian bead)
Diam: 6.3–7.1 mm; Th: 5.0 mm;
Hole diam.: 1.6 mm; Wt: <1 g
606298.974 E; 4527986.130 N; 173.070 m

KG-059-0272 (disc-shaped carnelian bead) Fig. 113, 7
Diam: 5.5–6.0 mm; Th: 4.0 mm;
Hole diam.: 2.0 mm; Wt: <1 g
606299.007 E; 4527986.118 N; 173.087 m

KG-059-0276b (four disc-shaped carnelian beads) Fig. 113, 2
Diam: 5.0–6.0 mm; Th: 3.1–3.5 mm;
Hole diam.: 1.8–2.0 mm; Wt: <1 g

KG-059-0300 (disc-shaped carnelian bead) Fig. 113, 11
Diam: 5.8 mm; Th: 3.0 mm;
Hole diam.: 1.4 mm; Wt: <1 g
606298.868 E; 4527986.075 N; 173.084 m

KG-059-0306 (disc-shaped carnelian bead) Fig. 113, 4
Diam: 6.5–7.8 mm; Th: 4.4 mm;
Hole diam.: 2.7 mm; Wt: <1 g
606298.941 E; 4527986.089 N; 173.073 m

KG-059-0311 (lenticular carnelian bead) Fig. 113, 16
Diam: 6.9–7.1 mm; Th: 3.9 mm;
Hole diam.: 2.3 mm; Wt: <1 g
606299.038 E; 4527986.291 N; 173.072 m

KG-059-0316 (disc-shaped carnelian bead) Fig. 113, 9
Diam: 5.1 mm; Th: 3.1 mm;
Hole diam.: 2.0 mm; Wt: <1 g
606299.075 E; 4527986.265 N; 173.056 m

KG-059-0333 (cylindrical carnelian bead) Fig. 113, 15
Diam: 4.5 mm; L: 6.5 mm;
Hole diam.: 1.5 mm; Wt: <1 g
606298.991 E; 4527986.087 N; 173.064 m

KG-059-0336 (disc-shaped carnelian bead) Fig. 113, 8
Diam: 5.9 mm; Th: 2.9 mm;
Hole diam.: 2.0 mm; Wt: <1 g
606298.979 E; 4527986.214 N; 173.059 m

KG-059-0337a (disc-shaped carnelian bead) Fig. 113, 13
Diam: 6.0 mm; Th: 3.5 mm; Hole diam.: 2.0 mm; Wt: 1 g
606298.988 E; 4527986.184 N; 173.073 m

KG-059-0338b (two disc-shaped carnelian bead) Fig. 113, 1
Diam: 6.4–8.3 mm; Th: 4.0–5.2 mm;
Hole diam.: 2.1–2.4 mm; Wt: 2 g
606299.333 E; 4527986.211 N; 173.066 m

KG-059-0341b (disc-shaped carnelian bead) Fig. 113, 12
Diam: 4.0 mm; Th: 2.0 mm;
Hole diam.: 2.0 mm; Wt: <1 g
606298.879 E; 4527986.139 N; 173.070 m

KG-059-0342b (disc-shaped carnelian bead) Fig. 113, 10
Diam: 6.0 mm; Th: 3.1 mm;
Hole diam.: 1.6 mm; Wt: <1 g
606298.911 E; 4527986.124 N; 173.068 m

KG-059-0343b (roughly disc-shaped carnelian bead) Fig. 113, 3
Diam: 8.0 mm; Th: 5.0 mm; Hole diam.: 1.6 mm; Wt: 1 g
606298.936 E; 4527986.157 N; 173.070 m

KG-059-0361 (disc-shaped carnelian bead) Fig. 113, 14
Diam: 5.2 mm; Th: 3.2 mm;
Hole diam.: 2.1 mm; Wt: <1 g
606298.979 E; 4527986.114 N; 173.071 m

KG-059-0366 (disc-shaped carnelian bead) Fig. 113, 5
Diam: 6.7 mm; Th: 3.5 mm;
Hole diam.: 2.0 mm; Wt: <1 g
606299.005 E; 4527986.135 N; 173.073 m

KG-059-0276c (clay bead) Fig. 114, 30
L: 7.2 mm; W: 7.0 mm; Th: 4.1 mm;
Hole diam.: 1.0 mm; Wt: <1 g

KG-059-0286 (mollusc) Fig. 114, 31
L: 13.0 mm; W: 12.0 mm; Th: 9.0 mm; Wt: <1 g
606299.102 E; 4527986.050 N; 173.091 m

KG-059-0261 (fragments of a buff frit bead) Fig. 114, 14
Diam: 3.9 mm; Th: 2.3 mm;
Hole diam.: 2.0 mm; Wt: <1 g
606298.814 E; 4527986.053 N; 173.113 m

KG-059-0264 (buff ring-shaped frit bead) Fig. 114, 13
Diam: 4.0 mm; Th: 2.5 mm;
Hole diam.: 1.7 mm; Wt: <1 g
606298.943 E; 4527985.741 N; 173.119 m

KG-059-0265 (fragments of yellowish-buff frit bead)
606298.800 E; 4527985.830 N; 173.097 m

KG-059-0267 (whitish-buff ring-shaped frit bead) Fig. 114, 5
Diam: 5.0 mm; Th: 4.0 mm;
Hole diam.: 1.9 mm; Wt: <1 g
606298.841 E; 4527986.376 N; 173.092 m

KG-059-0268 (whitish-buff ring-shaped frit bead) Fig. 114, 3
Diam: 5.2 mm; Th: 3.0 mm;
Hole diam.: 2.1 mm; Wt: <1 g
606299.221 E; 4527986.276 N; 173.159 m

KG-059-0270 (half of whitish-buff ring-shaped frit bead) Fig. 114, 6
Diam: 4.8 mm; Th: 2.5 mm;
Hole diam.: 1.9 mm; Wt: <1 g
606299.025 E; 4527985.882 N; 173.095 m

KG-059-0274 (whitish-buff ring-shaped frit bead) Fig. 114, 1
Diam: 4.8 mm; Th: 2.1 mm;
Hole diam.: 1.9 mm; Wt: <1 g
606298.967 E; 4527985.798 N; 173.076 m

KG-059-0275 (brown-buff ring-shaped frit bead) Fig. 114, 2
Diam: 5.0 mm; Th: 3.0 mm;
Hole diam.: 2.0 mm; Wt: <1 g
606298.949 E; 4527986.186 N; 173.081 m

KG-059-0276a (42 yellowish/buff disc- or ring-shaped frit beads plus fragments) Fig. 114, 22
Diam: 3.5–5.5 mm; Th: 1.9–4.0 mm;
Hole diam.: 1.7–2.8 mm; Wt: 3 g

KG-059-0281 (fragments of yellowish-buff frit bead)
606299.052 E; 4527985.698 N; 173.125 m

KG-059-0283 (fragments of yellowish-buff frit bead)
606299.167 E; 4527986.068 N; 173.084 m

KG-059-0284 (whitish-buff ring-shaped frit bead) Fig. 114, 9
Diam: 5.0 mm; Th: 3.0 mm;
Hole diam.: 2.7 mm; Wt: <1 g
606298.914 E; 4527985.746 N; 173.087 m

KG-059-0298 (whitish-buff ring-shaped frit bead)
Diam: 5.0 mm; Th: 2.5 mm;
Hole diam.: 2.0 mm; Wt: <1 g
606299.016 E; 4527986.157 N; 173.089 m

KG-059-0299 (fragments of yellowish-buff frit bead)
606298.848 E; 4527986.051 N; 173.085 m

KG-059-0301 (fragments of yellowish-buff frit bead)
606299.023 E; 4527986.356 N; 173.072 m

KG-059-0302b (whitish cylindrical frit bead) Fig. 114, 25
Diam: 5.0 mm; L: 8.0 mm; Hole diam.: 1.9 mm; Wt: <1 g
606298.827 E; 4527985.533 N; 173.114 m

KG-059-0303 (fragments of yellowish-buff frit bead)
606298.916 E; 4527986.029 N; 173.078 m

KG-059-0304 (whitish-buff ring-shaped frit bead) Fig. 114, 17
Diam: 5.0 mm; Th: 3.0 mm;
Hole diam.: 2.0 mm; Wt: <1 g
606299.084 E; 4527986.451 N; 173.085 m

KG-059-0307 (yellowish-buff ring-shaped frit bead) Fig. 114, 7
Diam: 4.8 mm; Th: 2.9 mm;
Hole diam.: 2.0 mm; Wt: <1 g
606299.034 E; 4527986.132 N; 173.063 m

KG-059-0308 (yellowish-buff ring-shaped frit bead)
Diam: 4.0 mm; Th: 2.0 mm;
Hole diam.: 2.0 mm; Wt: <1 g
606299.057 E; 4527986.082 N; 173.068 m

KG-059-0309 (fragments of yellowish-buff frit bead)
606299.163 E; 4527986.221 N; 173.076 m

KG-059-0310 (whitish-buff ring-shaped frit bead) Fig. 114, 8
Diam: 4.1 mm; Th: 2.2 mm;
Hole diam.: 1.9 mm; Wt: <1 g
606299.087 E; 4527986.271 N; 173.058 m

KG-059-0312 (fragments of yellowish-buff frit bead)
606299.018 E; 4527986.323 N; 173.075 m

KG-059-0313 (brown-buff ring-shaped frit bead) Fig. 114, 4
Diam: 5.0 mm; Th: 2.5 mm; Hole diam.: 2.1 mm; Wt: 1 g
606299.231 E; 4527986.105 N; 173.079 m

KG-059-0314 (whitish-buff ring-shaped frit bead)
Diam: 4.0 mm; Th: 2.0 mm;
Hole diam.: 2.0 mm; Wt: <1 g
606299.155 E; 4527986.160 N; 173.068 m

KG-059-0315 (whitish-buff ring-shaped frit bead)
Diam: 4.0 mm; Th: 2.0 mm;
Hole diam.: 2.0 mm; Wt: <1 g
606299.186 E; 4527986.184 N; 173.085 m

KG-059-0318 (fragments of yellowish-buff frit bead)
606299.044 E; 4527985.737 N; 173.074 m

KG-059-0319 (fragments of yellowish-buff frit bead)
606299.012 E; 4527985.799 N; 173.089 m

KG-059-0320 (fragments of yellowish-buff frit bead)
606298.993 E; 4527985.767 N; 173.084 m

KG-059-0321 (whitish-buff ring-shaped frit bead)
606299.025 E; 4527985.868 N; 173.078 m

KG-059-0322 (whitish-buff ring-shaped frit bead)
Diam: 5.0 mm; Th: 2.0 mm;
Hole diam.: 3.0 mm; Wt: <1 g
606298.975 E; 4527985.885 N; 173.074 m

KG-059-0323 (half of brown-buff ring-shaped frit bead)
Diam: 5.5 mm; Th: 2.5 mm;
Hole diam.: 2.5 mm; Wt: <1 g
606298.932 E; 4527985.895 N; 173.057 m

KG-059-0324 (fragments of brown-buff frit bead)
606299.086 E; 4527985.941 N; 173.072 m

KG-059-0325 (brown-buff ring-shaped frit bead)
Diam: 5.0 mm; Th: 2.5 mm;
Hole diam.: 2.2 mm; Wt: <1 g
606298.903 E; 4527986.015 N; 173.064 m

KG-059-0326 (fragments of yellowish-buff frit bead)
606299.020 E; 4527986.106 N; 173.065 m

KG-059-0327 (brown-buff ring-shaped frit bead)
Diam: 5.0 mm; Th: 3.8 mm;
Hole diam.: 1.6 mm; Wt: <1 g
606299.090 E; 4527986.219 N; 173.062 m

KG-059-0328 (whitish-buff ring-shaped frit bead)
Diam: 4.0 mm; Th: 2.0 mm;
Hole diam.: 2.0 mm; Wt: <1 g
606299.052 E; 4527986.315 N; 173.072 m

KG-059-0329 (whitish-buff ring-shaped frit bead) Fig. 114, 10
Diam: 4.9 mm; Th: 2.9 mm;
Hole diam.: 1.9 mm; Wt: <1 g
606298.955 E; 4527986.358 N; 173.058 m

KG-059-0330 (whitish-buff ring-shaped frit bead) Fig. 114, 12
Diam: 3.0 mm; Th: 3.0 mm;
Hole diam.: 2.0 mm; Wt: <1 g
606298.952 E; 4527985.815 N; 173.088 m

KG-059-0331 (half of whitish-buff frit bead) Fig. 114, 11
Diam: 7.0 mm; Th: 2.6 mm;
Hole diam.: 3.2 mm; Wt: <1 g
606298.976 E; 4527985.854 N; 173.074 m

KG-059-0332 (whitish-buff ring-shaped frit beads and fragments of second bead)
Diam: 3.1 mm; Th: 2.0 mm;
Hole diam.: 1.9 mm; Wt: <1 g
606298.929 E; 4527985.882 N; 173.079 m

KG-059-0334 (brown-buff ring-shaped frit bead) Fig. 114, 16
Diam: 4.5 mm; Th: 2.8 mm;
Hole diam.: 2.0 mm; Wt: <1 g
606298.881 E; 4527986.074 N; 173.066 m

KG-059-0335 (two fused whitish-buff ring-shaped frit bead) Fig. 114, 26
Diam: 5.1 mm; L (both): 6.9 mm;
Hole diam.: 1.9 mm; Wt: <1 g
606298.993 E; 4527986.274 N; 173.064 m

KG-059-0337b (two buff disc-shaped frit beads) Fig. 114, 21
Diam: 5.0 mm; Th: 2.2 mm;
Hole diam.: 1.7 mm; Wt: <1 g
606298.988 E; 4527986.184 N; 173.073 m

KG-059-0341c (whitish-buff ring-shaped frit bead) Fig. 114, 19
Diam: 4.0 mm; Th: 2.0 mm;
Hole diam.: 2.0 mm; Wt: <1 g
606298.879 E; 4527986.139 N; 173.070 m

KG-059-0349 (half of whitish-buff frit bead)
Diam: 4.5 mm; Th: 2.4 mm;
Hole diam.: 1.9 mm; Wt: <1 g
606299.036 E; 4527985.656 N; 173.077 m

KG-059-0350 (whitish-buff ring-shaped frit bead)
Diam: 3.9 mm; Th: 2.0 mm;
Hole diam.: 1.6 mm; Wt: <1 g
606299.134 E; 4527985.691 N; 173.097 m

KG-059-0351 (whitish-buff ring-shaped frit bead)
Diam: 3.5 mm; Th: 2.0 mm;
Hole diam.: 1.5 mm; Wt: <1 g
606299.099 E; 4527985.727 N; 173.072 m

KG-059-0352 (whitish-buff frit bead) Fig. 114, 18
Diam: 4.0 mm; Th: 1.7 mm;
Hole diam.: 1.5 mm; Wt: <1 g
606299.099 E; 4527985.777 N; 173.049 m

KG-059-0353 (whitish-buff ring-shaped frit bead)
Diam: 4.0 mm; Th: 2.0 mm;
Hole diam.: 2.9 mm; Wt: <1 g
606299.179 E; 4527985.784 N; 173.049 m

KG-059-0354 (yellowish-buff ring-shaped frit bead)
Diam: 4.0 mm; Th: 2.0 mm;
Hole diam.: 2.0 mm; Wt: <1 g
606299.072 E; 4527985.857 N; 173.069 m

KG-059-0355 (two whitish-buff ring-shaped frit beads)
Diam: 3.9 mm; Th: 2.0 mm;
Hole diam.: 1.1 mm; Wt: <1 g
Diam: 4.0 mm; Th: 3.1 mm;
Hole diam.: 1.5 mm; Wt: <1 g
606298.988 E; 4527985.836 N; 173.087 m

KG-059-0356 (whitish-buff ring-shaped frit bead)
Diam: 4.1 mm; Th: 2.0 mm;
Hole diam.: 2.0 mm; Wt: <1 g
606298.922 E; 4527985.856 N; 173.059 m

KG-059-0357 (whitish-buff ring-shaped frit bead and yellowish cylindrical frit bead) Fig. 114, 24
Diam: 3.9 mm; Th: 4.5 mm;
Hole diam.: 1.8 mm; Wt: <1 g
606298.906 E; 4527985.879 N; 173.054 m

KG-059-0358 (fragment of whitish-buff ring-shaped frit bead)
606298.861 E; 4527985.902 N; 173.056 m

KG-059-0359 (brown-buff ring-shaped frit bead and fragments of second bead) Fig. 114, 20
606298.925 E; 4527985.951 N; 173.057 m

KG-059-0360 (whitish-buff ring-shaped frit bead)
Diam: 4.0 mm; Th: 2.0 mm;
Hole diam.: 2.0 mm; Wt: <1 g
606299.093 E; 4527985.967 N; 173.046 m

KG-059-0362 (fragments of whitish-buff frit bead)
606298.930 E; 4527986.162 N; 173.090 m

KG-059-0363 (whitish-buff ring-shaped frit bead)
Diam: 3.5 mm; Th: 2.1 mm;
Hole diam.: 1.9 mm; Wt: <1 g
606298.934 E; 4527986.216 N; 173.060 m

KG-059-0364 (half of whitish-buff ring-shaped frit bead)
Diam: 5.0 mm; Th: 2.5 mm;
Hole diam.: 2.5 mm; Wt: <1 g
606298.986 E; 4527986.219 N; 173.074 m

KG-059-0365 (brown-buff frit bead)
Diam: 5.0 mm; Th: 2.5 mm;
Hole diam.: 3.0 mm; Wt: <1 g
606298.969 E; 4527986.170 N; 173.080 m

KG-059-0367 (whitish-buff ring-shaped frit bead)
Diam: 5.0 mm; Th: 2.8 mm;
Hole diam.: 3.0 mm; Wt: <1 g
606298.969 E; 4527986.139 N; 173.073 m

KG-059-0368 (fragments of whitish-buff cylindrical frit bead) Fig. 114, 23
606298.960 E; 4527986.174 N; 173.076 m

KG-059-0369 (whitish-buff ring-shaped frit bead)
Diam: 4.0 mm; Th: 2.0 mm;
Hole diam.: 2.0 mm; Wt: <1 g
606299.028 E; 4527985.761 N; 173.043 m

KG-059-0370 (whitish-buff ring-shaped frit bead) Fig. 114, 15
Diam: 4.5 mm; Th: 2.1 mm;
Hole diam.: 2.5 mm; Wt: <1 g
606299.042 E; 4527985.884 N; 173.052 m

KG-059-0371 (two fused whitish-buff ring-shaped frit bead) Fig. 114, 27
Diam: 6.2 mm; L (both): 5.0 mm;
Hole diam.: 1.9 mm; Wt: <1 g
606298.975 E; 4527985.889 N; 173.054 m

KG-059-0372 (half of whitish-buff ring-shaped frit bead)
Diam: 4.5 mm; Th: 2.0 mm;
Hole diam.: 2.5 mm; Wt: <1 g
606298.969 E; 4527985.942 N; 173.057 m

KG-059-0373 (brown-buff ring-shaped frit bead)
Diam: 4.0 mm; Th: 1.8 mm;
Hole diam.: 1.8 mm; Wt: <1 g
606298.927 E; 4527985.990 N; 173.044 m

KG-059-0374b (fragments of a white frit bead)
606298.927 E; 4527985.990 N; 173.044 m

KG-059-0375 (dark brown-buff ring-shaped frit bead) Fig. 114, 28
Diam: 6.0 mm; Th: 4.1 mm;
Hole diam.: 2.9 mm; Wt: <1 g
606298.981 E; 4527986.141 N; 173.063 m

KG-059-0376 (fragments of whitish-buff frit bead)
606299.013 E; 4527985.766 N; 173.049 m

KG-059-0377 (fragments of whitish-buff frit bead)

KG-059-0378 (fragments of brown-buff frit bead)
Diam: 5.8 mm; Th: 4.1 mm;
Hole diam.: 2.0 mm; Wt: <1 g
606299.010 E; 4527985.904 N; 173.038 m

Fill

KG-059-0381 (bluish frit bead with knobs) Fig. 114, 29
Diam: 2.9 mm; L: 3 mm; Hole diam.: 0.7 mm; Wt: <1 g
606298.737 E; 4527986.265 N; 173.060 m

KG-059-0251 (obsidian flake)
L: 19.0 mm; W: 11.0 mm; Th: 9.0 mm; Wt: 1 g
606299.213 E; 4527985.590 N; 173.264 m

KG-059-0255 (obsidian flake)
L: 26.0 mm; W: 17.0 mm; Th: 5.0 mm; Wt: 2 g
606299.762 E; 4527985.944 N; 173.375 m

KG-059-0257 (obsidian flake)
L: 22.0 mm; W: 19.0 mm; Th: 7.0 mm; Wt: 3 g
606298.680 E; 4527985.795 N; 173.204 m

KG-059-0273 (obsidian flake)
L: 17.0 mm; W: 15.0 mm; Th: 2.0 mm; Wt: 1 g
606299.370 E; 4527986.306 N; 173.176 m

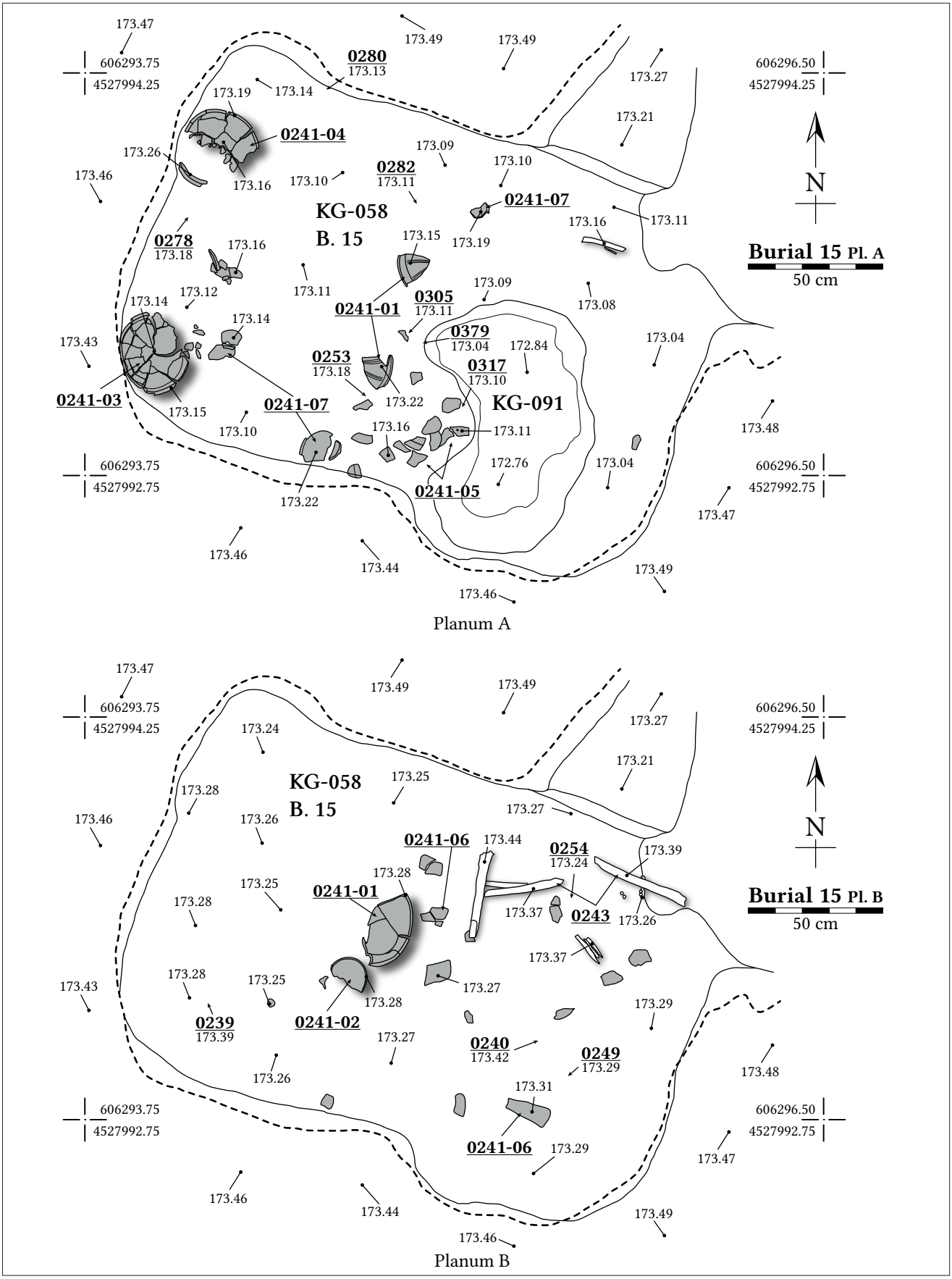

Fig. 115. Plana A and B of Burial 15 (KG-058); Pit-Complex B

Fig. 116. Bowl 0241-03 from Burial 15 (KG-058)

Fig. 117. Bowl 0241-04 from Burial 15 (KG-058)

Fig. 118. Bowl 0241-01 from Burial 15 (KG-058)

Burial 15 (KG-058)

Burial 15 was located in the southern half of square 6290/7990 and formed the western part of Pit-Complex B (Fig. 43). Its grave-pit was rectangular (2.1 × 1.5 m) and oriented north-west to south-east (Fig. 115). After clearing out the grave-pit, an irregular depression was detected in its eastern part (KG-091). It was c. 20–30 cm deep and filled with soft soil, but did not contain any archaeological material. Whether this was a later disturbance or an original part of the grave-pit, remained unclear. In general, the burial showed significant post-depositional disturbances. To reconstruct the taphonomic processes a dark-grey coloured bowl was essential (Fig. 85 and Fig. 86, 2) of which one half (0241-02) was found in the fill of Burial 15, whereas the other half (0418-01) was located at the bottom of the adjacent pit KG-057. The position of the bowl indicated that it originally belonged to the Early Iron Age Burial 8 that was almost completely destroyed by the two Late Antique Burials 23 and 24 that thus appear to be responsible for the damage in Burial 15 as well. In order to exclude the possibility that the scattered skeletal remains found in the fill of Burial 15 were dislocated from the earlier Burial 8, radiocarbon dates were taken from both bone collections (Beta-506517 and Beta-506518). The analysis revealed a considerably later date of the bones in Burial 15 and allowed their attribution to that interment. The radiocarbon date sets a timeframe from the 8th through the mid-6th cent. BC for Burial 15, however, in view of the probabilities of the calibrated dates and the archaeological comparisons a date within the 8th cent. BC seems likely.

For the sake of clarity, the distribution of the grave content is presented in two plans (Fig. 115): Planum A defines the actual burial with some vessels still *in situ* and others damaged and scattered all over the place. Planum B is an artificially defined level approximately 15 cm above Planum A. It comprised scattered sherds of vessels from Planum A (in particular of bowl 0241-01), the displaced half of bowl 0241-02 and most of the human bones (0243).

The only two vessels still *in situ* were the two large carinated bowls along the west side of the pit. The bowls were virtually identical in shape (Fig. 116, Fig. 117, and Fig. 119, 2–3). They had a flat or rounded base and a conical body with a straight vertical collar above the carination. The rim was outrolled and slightly pointed. The southern bowl (0241-03) was highly fragmented but almost complete. It had a dark-grey colour and carried a polished decoration at the bottom side, however, almost the entire outer surface was flaked off, so that only few parts of the pattern were preserved. As shown in Fig. 119, 2 the polished ornament consisted of two crossing lines at the base and rays of multiple lines that ascend from the base to the carination. Traces of polished horizontal lines below the rim indicate that the collar, too, was probably decorated with a wide polished stripe. The northern carinated bowl (0241-04, Fig. 119, 3) was of similar shape and fabric but less well preserved. The bottom side was

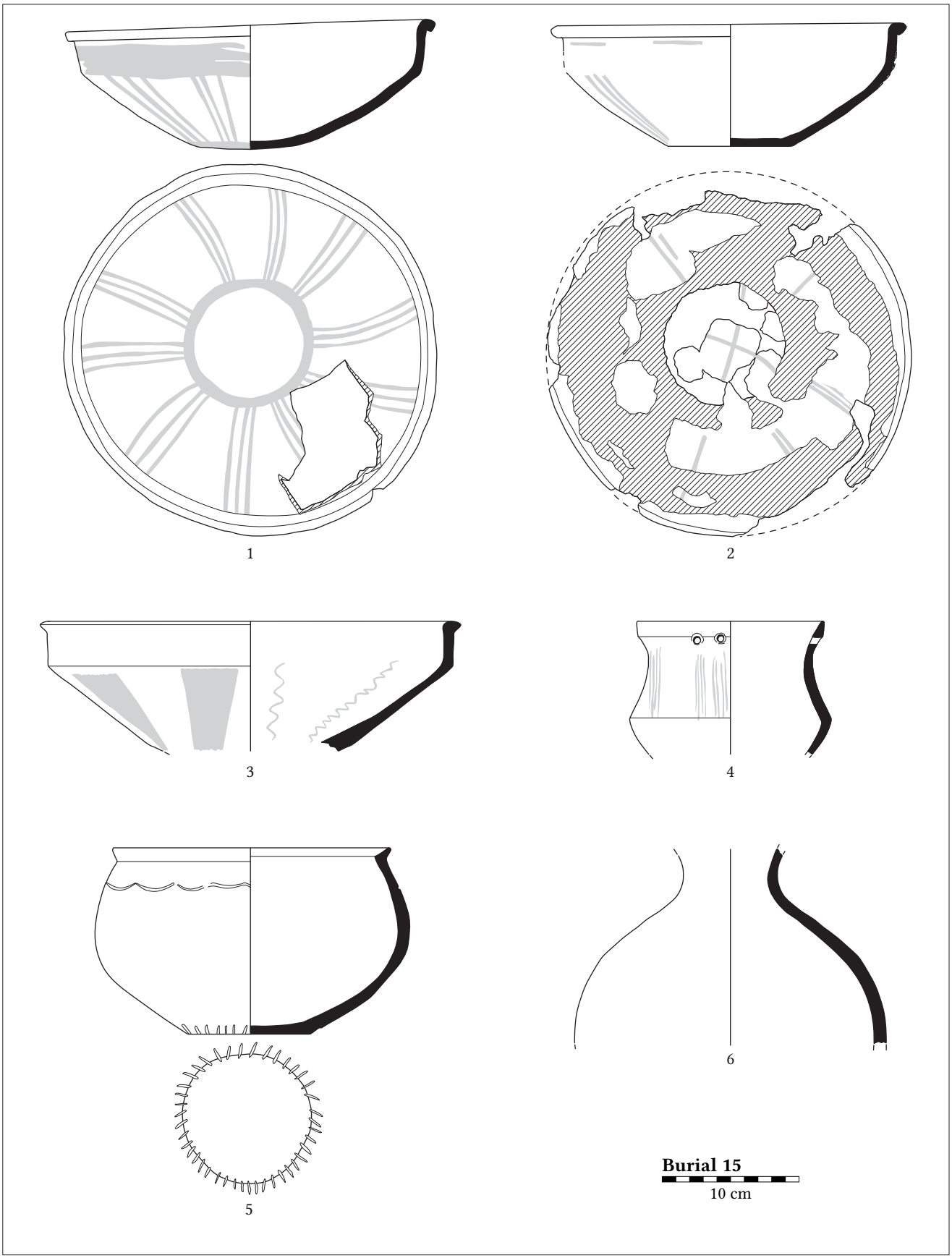

Fig. 119. Pottery from Burial 15 (KG-059): 1 – bowl (0241-01); 2 – bowl (0241-03); 3 – bowl (0241-04); 4 – pot (0241-05); 5 – pot (0241-07); 6 – bottle (0241-06)

Fig. 120. Small pot 0241-05 from Burial 15 (KG-058)

Fig. 121. Pot 0241-07 from Burial 15 (KG-058)

decorated with radially arranged wide polished stripes. The collar was left blank. On the inside polished wavy lines were running at regular intervals from below the rim down towards the centre of the bowl. A third morphologically identical bowl was found in the central area of the grave-pit (0241-01, Fig. 118 and Fig. 119, 1). Because some of its sherds were found scattered in both plana, the original position of the vessel is unknown. Like the other two examples, also this bowl carried a polished decoration. The base was delimited from the lower body by a thick polished line which at same time served as border line for ten polished, slightly curved triple lines running up to the carination. The collar was covered with a solid polished stripe. Comparisons for this type of carinated bowl can be drawn in particular from the pottery of the cemeteries discovered at Tovuzchay (e. g. Müseyibli et al. 2008: Fig. 35–37 Pl. 49, 1–4. 51, 3), Zayamchay (e. g. Müseyibli 2004: 60–61 Pl. I, 8; Müseyibli/Nəcəfov 2019: Pl. 19, 1. 71, 4–5) and Mingachevir (Асланов et al. 1959: Pl. XXIII). At Tovuzchay at least one burial that contained such carinated bowls (Burial 78) was radiocarbon-dated through an animal bone found in the grave-pit to the 11th cent. or 10th cent. BC (Beta-232333; cal BC 1130–920; cal BC 1080–980 (1σ); Müseyibli et al. 2008: 72 Fig. 45, 1–2). Of earlier date were the carinated bowls in Burial 72 at Zayamchay that was radiocarbon-dated to the 14th–13th cent. BC (Beta-220989; cal BC 1420–1250; Nəcəfov 2008a: 58; Müseyibli/Nəcəfov 2019: 323 Fig. 88, 7). In contrast to the examples from Tepe 5 the carinated bowls in Tovuzchay and Zayamchay often have one or more vertically or horizontally pierced lugs applied to the collar. Remarkable, however, are the similarities in the patterns used for the polished decoration. The radial ornament on bowl 0241-01 is almost identical to two examples from Zayamchay (Müseyibli 2004: 68 Pl. I, 2, 8; Müseyibli/Nəcəfov 2019: Pl. 71, 5) and to a bowl from Burial 33 in Kushchu (Гуммель 1940: 136. 143 Fig. 5, no. 85) of which a date between the end of the 12th and 9th cent. BC was proposed (Погребова 2011: 141). The wavy lines on the inside of bowl 0241-04 resemble a bowl from Burial 85 at Tovuzchay (Müseyibli et al. 2008: 78 Fig. 51, 2) and are also attested in combination with vertical lines on the inside and outside of two bowls from Zayamchay (Müseyibli 2004: 68 Pl. I, 7; Müseyibli/Nəcəfov 2019: Pl. 19, 2. 71, 4–5). Moreover, wavy lines inside of similar bowls appeared also among the pottery material from Udabno and were dated there to the second half of the 9th cent. BC (Brodbeck-Jucker 2019: 211–213 Pl. 117). In Eastern Georgia carinated bowls of this type (S1) appeared until the mid-1st millennium BC (Ludwig 2010: 52). Examples of the 8th–7th cent. BC are known from period E at Ciskaraant-Gora, that was dated from the last third of the 8th to the first third of the 7th cent. BC (Furtwängler/Knauss 1997: 369 Fig. 16, 3; Furtwängler et al. 1998: 352–354).

Although the available radiocarbon dates and the proposed dates for the comparable material in north-western Azerbaijan as well as Eastern Georgia suggest an Early Iron Age date for this type of carinated bowls, they first appeared in the Late Bronze Age period. This is further substantiated by two examples of carinated bowls – one of them with a polished decoration – from the Burials IX and X of Kurgan 21 near *Helenendorf*, that were dated to the 15th–14th cent. BC or 14th–13th cent. BC, respectively (Гуммель 1940: 22–25 Fig. 9, IX-5. X-5a–b; Гусейнова 1989: 16 Pl. III, 24–25; Погребова 2011: 64–68), as well as by the above-mentioned Burial 72 at Zayamchay.

In the central southern part of the grave-pit of Burial 15 lay a cluster of sherds that resulted from the damage of a small spherical pot (0241-07) and a second pot with

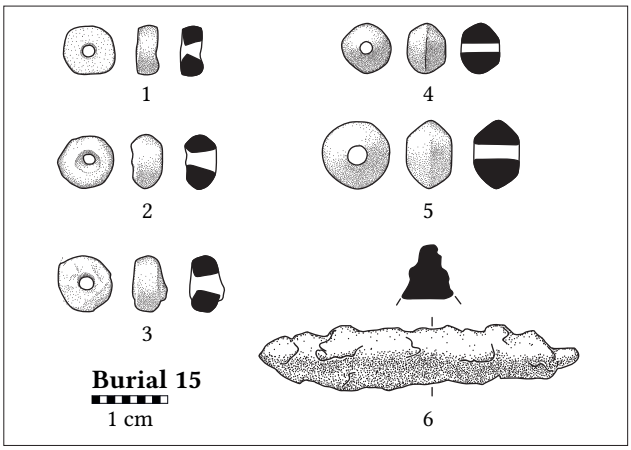

Fig. 122. Finds from Burial 15 (KG-059): 1 – carnelian bead (0253); 2 – carnelian bead (0305); 3 – carnelian bead (0317); 4 – bead of white material (0282); 5 – bead of white material (0379); 6 – iron fragment (0249)

a tall convex collar (0241-05). Both vessels were incompletely preserved. Some of the sherds of 0241-07 were found scattered near the northern edge of the grave-pit (Fig. 115). Pot 0241-05 was made of dark-grey fabric. The profile had a pronounced carination that separated the conical lower body from the high convex collar which ended in a band-rim (Fig. 119, 4 and Fig. 121). Just below the rim the vessel was perforated before firing two times on opposite sides (hole diameter c. 5 mm). In addition, the collar was decorated with at least five bundles of thin vertical polished lines. The base was missing but judging by a similar vessel – though with an applied handle – found in the area of Kalakent it was probably flat (Ивановский 1911: 159 Pl. XI, 22). The base of the dark-grey coloured spherical pot 0241-07 was decorated around the edge with notches (Fig. 119, 5 and Fig. 121). Its profile was curved, and the rim was flaring with a pronounced carination on the inside. Generally speaking, the typological features of this vessel type are related to pot 0252-02 (Fig. 109, 2) in Burial 14 as well as perhaps to the badly preserved pot 0144-03 from Burial 13 (Fig. 105, 5) and thus to a similar array of Early Iron Age pots found at Udabno (Brodbeck-Jucker 2019: Pl. 61–71). Comparisons can also be drawn with earlier, similarly shaped and decorated pots of the Lchashen-Metsamor 3 (LBA III) horizon on the Armenian highland (Smith et al. 2009: 81 Fig. 28p). The pot from Burial 15 carried a row of incised curved notches on the shoulder that resemble a wavy line. This decorative technique was observed on a morphologically similar but larger vessel at Zayamchay (Müseyibli 2004: Pl. I, 9; Müseyibli/Nəcəfov 2019: Pl. 19, 3), in particular on vessels from Burials 24 and 32 (Müseyibli 2009: 57 Pl. X, 7; Müseyibli/Nəcəfov 2019: Pl. 36, 5. 51, 1). These two burials contained a bottle (Müseyibli 2009: 57 Pl. X, 4; Müseyibli/Nəcəfov 2019: Pl. 36, 6. 50, 3) that is attested in several other burials at Zayamchay as well (Müseyibli 2004: 70 Pl. III, 1–5). The pottery inventory of Burial 15 seems to have included a similar bottle (0241-06), the sherds of which were scattered all over Planum B (Fig. 119, 6). Although the rim and most of the lower body were missing, the characteristic transition from the shoulder to the neck permits a general typological classification as bottle or jug.

In the same area of the pottery cluster four beads were found (Fig. 115). Three of them (0253, 0305, 0317) were roughly disc-shaped carnelian beads (Fig. 122, 1–3) and the fourth (0379) was of biconical shape and was made of a white (frit or chalk?) material (Fig. 122, 5). A similarly shaped bead also made of the same material (0282) was found north of the sherds of bowl 0241-01 (Fig. 122, 4). The only noteworthy find from Planum B was a heavily corroded oblong iron object with a triangular form in section (Fig. 122, 6).

Grave contents

KG-058-0243 (human bones) Table 4
Sex: could not be determined Table 16
Age class: Maturitas–Senilis

KG-058-0241-01 (bowl) Fig. 118; Fig. 119, 1
Rim diam.: 275 mm (90%)
H: 90 mm
Base diam.: 80 mm
Fabric: completely reducing atmosphere, medium hard, medium fine temper (123)
Surface: ext. burnished; int. smoothed
Colour: ext. Gley 1 2.5/N (black); core 10YR 5/1 (grey); int. Gley 1 4/N (dark grey)
Decoration: polished decoration that formed a circle around the base and radial lines running from the base to the carination; the collar was completely covered with a polished stripe
Condition: some body-sherds are missing
Comparanda:
Zayamchay, e. g. Burials 10, 32, 60, 72. 116, EIA (Müseyibli 2004: Pl. I, 2. 8; Müseyibli 2009: 49. 57 Pl. II, 5. X, 3; Müseyibli/Axundova 2013: 24 Pl. V, 2; Müseyibli/Nəcəfov 2019: Pl. 19, 1. 71, 5. 72, 2. 73. 88, 1. 90, 4)
Tovuzchay, Burials 46 and 77, EIA (Müseyibli et al. 2008: Fig. 37, 2. 41, 8)
Kushchu, Burial 33, EIA (Гуммель 1940: 136. 143 Fig. 5, no. 85; Гусейнова 1989: Pl. XXII, 11)
Udabno, EIA (Brodbeck-Jucker 2019: Pl. 116)

KG-058-0241-03 (bowl) Fig. 116; Fig. 119, 2
Rim diam.: 260 mm (80%)
H: 89 mm
Base diam.: 90 mm
Fabric: not completely reduced core, medium hard, medium fine temper (623)
Surface: ext. and int. burnished
Colour: ext. Gley 1 2.5/N (black); core 7.5YR 6/1 (grey);

int. Gley 1 4/N (dark grey)
Decoration: cross of polished lines at the base; on the lower body vertical polished lines and horizontal lines on the collar
Condition: heavily fragmented; some parts of the rim and body missing; outside surface for the most part flaked off
Comparanda: see above bowl KG-058-0241-01

KG-058-0241-04 (bowl) Fig. 117; Fig. 119, 3
Rim diam.: 300 mm (40%)
H: 94 mm
Fabric: not completely reduced core, medium hard, medium fine temper (623)
Surface: ext. burnished; int. smoothed
Colour: ext. Gley 1 2.5/N (black); core 2.5YR 6/2 (pale red); int. Gley 1 3/N (very dark grey)
Decoration: polished decoration of wide vertical stripes at the outside and wavy lines at the inside
Condition: more than half of the vessel (including the entire base) is missing
Comparanda:
see above the comparanda for bowl KG-058-0241-01; for the wavy lines see in particular:
Zayamchay, Burials 10 and 60, EIA (Müseyibli 2004: Pl. I, 7; Müseyibli/Nəcəfov 2019: Pl. 19, 2. 71, 4–5)
Tovuzchay, Burial 85, EIA (Müseyibli et al. 2008: Fig. 51, 2)
Udabno, U I-C and U I-D, EIA (Brodbeck-Jucker 2019: Pl. 117. 193–194)

KG-058-0241-05 (pot) Fig. 120; Fig. 119, 4
Rim diam.: 140 mm (40%)
H: 96 mm
Fabric: not completely reduced core, medium hard, medium fine temper (623)
Surface: ext. and int. burnished
Colour: ext. Gley 1 2.5/N (black); core 10YR 6/2 (light brownish grey); int. Gley 1 2.5/N (black)
Decoration: two pairs of perforations at opposite sides below the rim; bundles of vertical polished lines on the high collar
Condition: the rim is complete; at least one third of the body and the complete base are missing
Comparanda:
area of Kalakent, Burial 91, LBA/EIA (Ивановский 1911: 159 Pl. XI, 22)

KG-058-0241-07 (pot) Fig. 121; Fig. 119, 5
Rim diam.: 200 mm (45%)
H: 135 mm
Base diam.: 90 mm
Fabric: not completely reduced core, hard, coarse temper (634)
Surface: ext. and int. burnished
Colour: ext. Gley 1 3/N (very dark grey); core 10YR 5/1 (grey); int. Gley 1 4/N (dark grey)
Decoration: row of notches along the circumference of the base and a row of incised hanging lines around the shoulder
Condition: heavily fragmented; parts of the rim and body are missing
Comparanda:
Zayamchay, Burials 24 and 32, EIA (Müseyibli 2004: Pl. I, 9. 12; Müseyibli 2009: 57 Pl. X, 7; Müseyibli/Nəcəfov 2019: Pl. 19, 3. 36, 5. 51, 1)
Udabno, EIA (Brodbeck-Jucker 2019: Pl. 61–71)
Oshakan, Burial 100, LBA III (Smith et al. 2009: 81 Fig. 28p)

KG-058-0253 (disc-shaped carnelian bead) Fig. 122, 1
Diam: 6.1–6.9 mm; Th: 2.8 mm;
Hole diam.: 2.2 mm; Wt: <1 g
606294.795 E; 4527993.047 N; 173.179 m

KG-058-0305 (disc-shaped carnelian bead) Fig. 122, 2
Diam: 7.5 mm; Th: 4.0 mm;
Hole diam.: 3.0 mm; Wt: <1 g
606294.952 E; 4527993.280 N; 173.109 m

KG-058-0317 (disc-shaped carnelian bead) Fig. 122, 3
Diam: 7.0 mm; Th: 5.0 mm;
Hole diam.: 2.1 mm; Wt: <1 g
606295.152 E; 4527993.004 N; 173.095 m

KG-058-0282 (biconical white bead) Fig. 122, 4
Diam: 6.5 mm; Th: 5.0 mm;
Hole diam.: 1.3 mm; Wt: <1 g
606294.983 E; 4527993.763 N; 173.113 m

KG-058-0379 (biconical white bead) Fig. 122, 5
Diam: 9.0 mm; Th: 6.0 mm;
Hole diam.: 2.2 mm; Wt: <1 g
606295.009 E; 4527993.244 N; 173.040 m

Fill

KG-058-0241-06 (bottle) Fig. 119, 6
Fabric: not completely reduced core, medium hard, medium fine temper (623)
Surface: ext. burnished(?); int. smoothed
Colour: ext. 2.5Y 3/2 (very dark greyish brown); core 2.5Y 5/1 (grey); int. Gley 1 2.5/N (black)
Condition: only shoulder and parts of the neck preserved; outer surface porous and flaking off
Comparanda:
Zayamchay, Burial 32 and others, LBA/EIA (Müseyibli 2004: Pl. III, 3–5; Müseyibli 2009: 57 Pl. X, 4

KG-058-0249 (iron fragment) Fig. 122, 6
L: 42.0 mm; W: 8.5 mm; Th: 7.0 mm; Wt: 4 g
606295.546 E; 4527992.913 N; 173.288 m

KG-058-0239 (obsidian flake)
L: 21.0 mm; W: 6.0 mm; Th: 2.0 mm; Wt: 1 g
606294.203 E; 4527993.189 N; 173.389 m

KG-058-0240 (obsidian flake)
L: 30.0 mm; W: 30.0 mm; Th: 5.5 mm; Wt: 2 g
606295.437 E; 4527993.047 N; 173.418 m

KG-058-0254 (obsidian flake)
L: 32.5 mm; W: 30.5 mm; Th: 11.5 mm; Wt: 9 g
606295.559 E; 4527993.575 N; 173.241 m

KG-058-0278 (obsidian flake)
L: 21.0 mm; W: 17.0 mm; Th: 6.0 mm; Wt: 2 g
606294.135 E; 4527993.719 N; 173.176 m

KG-058-0280 (obsidian flake)
L: 25.0 mm; W: 21.0 mm; Th: 6.0 mm; Wt: 4 g
606294.645 E; 4527994.189 N; 173.128 m

Burial 16 (KG-055)

Burial 16 consisted of two ceramic vessels that were deposited side by side in a small pit in the north-western quadrant of square 6290/7980, immediately north of Pit-Complex C-1 (Fig. 27). The bottom of the pit was reached already c. 20–25 cm below the modern surface. Near-surface disturbances and probably also recent agricultural activities obscured the outline of the pit which is why it could only be determined with some certainty along its north-eastern side (Fig. 123). The pottery had suffered damage as well and the upper parts of both vessels were cut off.

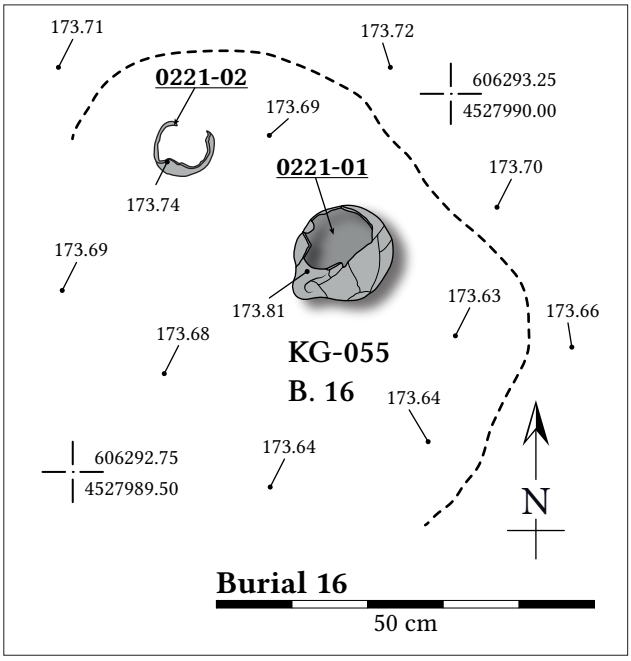

Fig. 123. Plan of Burial 16 (KG-055)

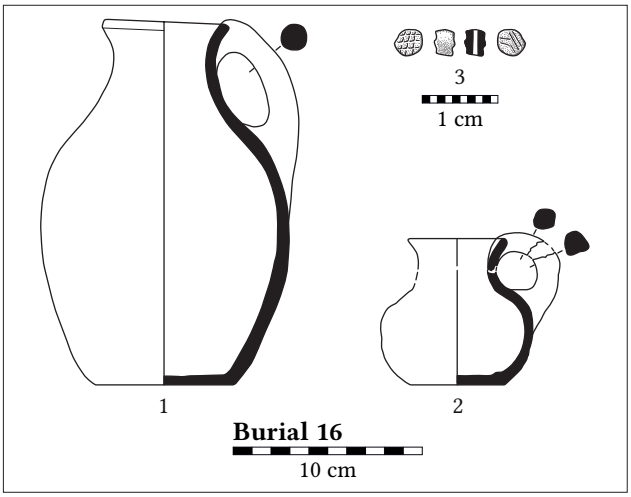

Fig. 124. Pottery and finds from Burial 16 (KG-065): 1 – jug (0221-01); 2 – jug (0221-02); 3 – frit bead (0222)

The larger jug in the south (0221-01) was made of a grey fabric. It had a flat base and an oblong egg-shaped body. The thick, round handle protruded from the rim and ended on the shoulder (Fig. 124, 1 and Fig. 125). The simple shape of such jugs and their long-lasting use makes it difficult to draw chronological conclusions. However, comparisons with similarly shaped but larger jugs, e. g., in Burial 25 at Kushchu (Гуммель 1940: Fig. 5, no. 81; Гусейнова 1989: Pl. XXII, 6), dated by M. N. Pogrebova (Погребова 2011: 141) to her fourth stage of the Khojaly-Gadabay-Culture (end of the 12th to the 9th cent. BC), or with examples at Saritepe and Babadervish (Гусейнова 1989: Pl. XXVII, 2–3, 5. 9. 11), of which a date in the 11th–9th cent. BC was proposed (Гусейнова 1989: 53), imply an Early Iron Age date. This can be further substantiated by considering the date of similar jugs in Kakheti, in particular of jug types K7b and K7c that have been dated from the 7th–6th cent. BC to the middle of the 1st millennium BC (Ludwig 2010: 59).

The second, smaller jug (0221-02) was placed at a distance of c. 15 cm north-west of the larger jug. It was made of a finer grey clay, and its surface showed traces of burnishing. It had a stocky, globular body with a short neck and rim (Fig. 124, 2). The lower end of the handle was applied on the shoulder, and the upper end joined the rim. It is difficult to find viable comparisons for this vessel; a

Fig. 125. Jug 0221-01 from Burial 16 (KG-055)

possible typological link exists in the form of a jug from Burial 8 at Sagarejo in Kakheti (Мамиашвили 1988: Pl. XLII, 138; Ludwig 2010: 223–224 Pl. 221) of which recently a date not later than the 9th cent. BC was suggested (Ludwig 2010: 47). The pottery comparisons suggest an Early Iron Age date for Burial 16 with a wide timeframe covering the entire first half of the 1st millennium BC.

Besides the two jugs a disc-shaped, bluish frit bead with lateral perforation (0222) was found near jug 0221-01 (Fig. 124, 3). One side of the bead was decorated with an impressed rhombic pattern, while the other side carried an irregular pattern of lines. Fragments of a second frit bead of yellowish colour (0228) were detected nearby.

Grave contents

KG-055-0221-01 (jug) Fig. 124, 1; Fig. 125
Rim diam.: 65 mm (80%)
H: 19 mm
Base diam.: 75 mm
Fabric: completely reducing atmosphere, hard, medium fine temper (133)
Surface: ext. and int. smoothed
Colour: ext. 2.5Y 5/1 (grey); core 2.5Y 5/1 (grey); int. 2.5Y 5/1 (grey)
Conditions: the upper part was heavily fragmented, some parts of shoulder, neck and rim were missing
Comparanda:
Kushchu, Burial 25, EIA (Гуммель 1940: Fig. 5, no. 81; Гусейнова 1989: Pl. XXII, 6)
Kakheti, various sites, EIA (Ludwig 2010: 59 Pl. 217)

KG-055-0221-02 (jug) Fig. 124, 2
Rim diam.: 50 mm (70%)
H: 61 mm
Base diam.: 50 mm
Fabric: exterior reducing, interior oxidizing atmosphere, medium hard, fine temper (422)
Surface: ext. burnished; int. smoothed
Colour: ext. 2.5Y 3/1 (very dark grey); core 2.5Y 6/1 (grey); int. 2.5YR 3/1 (dark reddish grey)
Conditions: heavily fragmented, a quarter of the body and the upper part were missing
Comparanda:
Sagarejo, Burial 8, EIA (Мамиашвили 1988: Pl. XLII, 138; Ludwig 2010: 223–224 Pl. 221)

KG-055-0222 (disc-shaped frit bead) Fig. 124, 3
Diam: 3.6 mm; Th: 2.6 mm;
Hole diam.: 1.0 mm; Wt: <1 g

KG-055-0228 (fragments of yellowish frit bead)

Burial 17 (KG-065)

Between Burials 38 and 27 in the north-western quadrant of square 6300/7980 the base of a jar (0348-01, Fig. 126, 1) was found still *in situ* at a height of 173.69 m and thus only c. 20 cm below the modern surface (Fig. 27). Although no pit, skeletal remains or any other finds were associated with the vessel, the latter was clearly placed there intentionally and therefore recorded as a burial or pottery deposit. The upper part of the vessel was completely missing, probably due to agricultural activities that penetrated the topsoil. The near-surface position also prevented the detection of a possible pit.

The jar was made of fine grey fabric with a slightly darker surface that resembled the pottery more typical for the later burials of the first occupation phase of the cemetery, which is why Burial 17 can – generally speaking – be attributed to the Early Iron Age.

Grave contents

KG-065-0348-01 (base) Fig. 126, 1
Base diam.: 75 mm
Fabric: completely reducing atmosphere, hard, fine temper (132)
Surface: ext. and int. smoothed
Colour: ext. 10YR 2/1 (black); core 10YR 4/1 (dark grey);

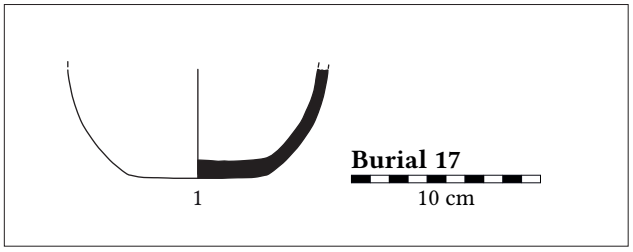

Fig. 126. Pottery from Burial 17 (KG-065): 1 – base (0348-01)

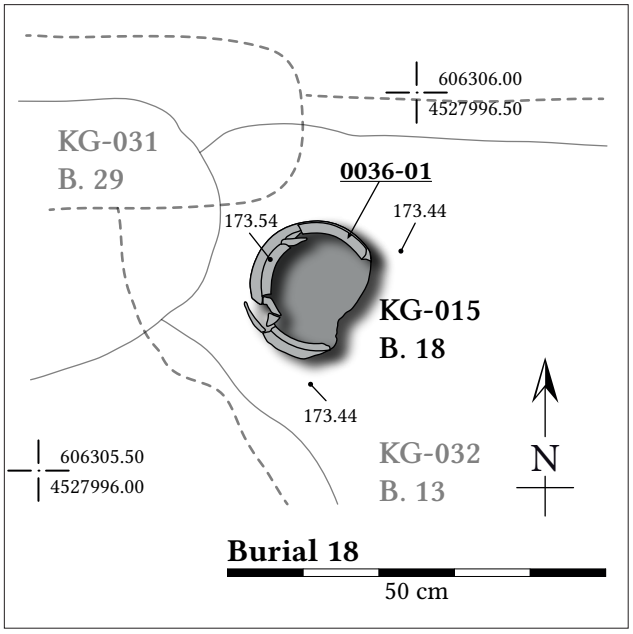

Fig. 127. Plan of Burial 18 (KG-015)

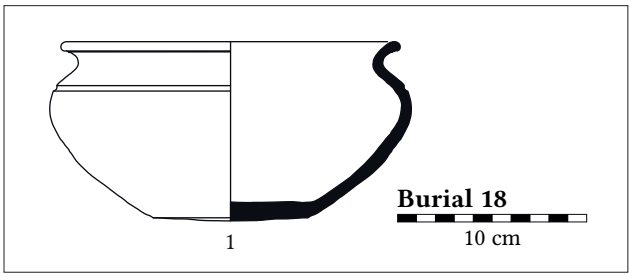

Fig. 128. Pottery from Burial 18 (KG-015): 1 – pot (0036-01)

int. 10YR 4/1 (dark grey)
Conditions: only the base up to height of 6 cm was preserved

Burial 18 (KG-015)

In the north-eastern quadrant of square 6300/7990 (Fig. 27), close to the intersection between the Early Iron Age Burial 13 and the Medieval Burial 29, an almost intact vessel was found in the subsoil layer KG-015 (Fig. 127). It was partially placed in the fill of Burial 13 (c. 40 cm above the bottom of the pit in that area), but most likely was not a part of that burial, but of a later intrusion, the extent of which could not be determined. No traces of a skeleton or any other finds could be discerned, which is why Burial 18 most likely belongs to the group of pottery deposits or cenotaphs.

The vessel (0036-01) was made of a dark-grey coloured clay with a black surface (Fig. 128, 1). It had a slightly lenticular base, a curved profile with a flaring rim and wide mouth. The shoulder was decorated with a groove and along the lower side of the rim three thin lines were incised. So far, no conclusive typological comparisons can be suggested. As regards the dating, however, the already mentioned stratigraphic relationship between Burial 18 and the radiocarbon-dated Early Iron Age Burial 13 points to a relatively late date within the Early Iron Age period.

Grave contents

KG-015-0036-01 (pot) Fig. 128, 1
Rim diam.: 170 mm (60%)
H: 95 mm
Base diam.: 80 mm
Fabric: completely reducing atmosphere, hard, medium fine temper (133)
Surface: ext. burnished; int. smoothed
Colour: ext. Gley 1 2.5/N (black); core Gley 1 4/N (dark grey); int. Gley 1 4/N (dark grey)
Conditions: one third of the vessel was missing and considerable parts of the surface were flaked off

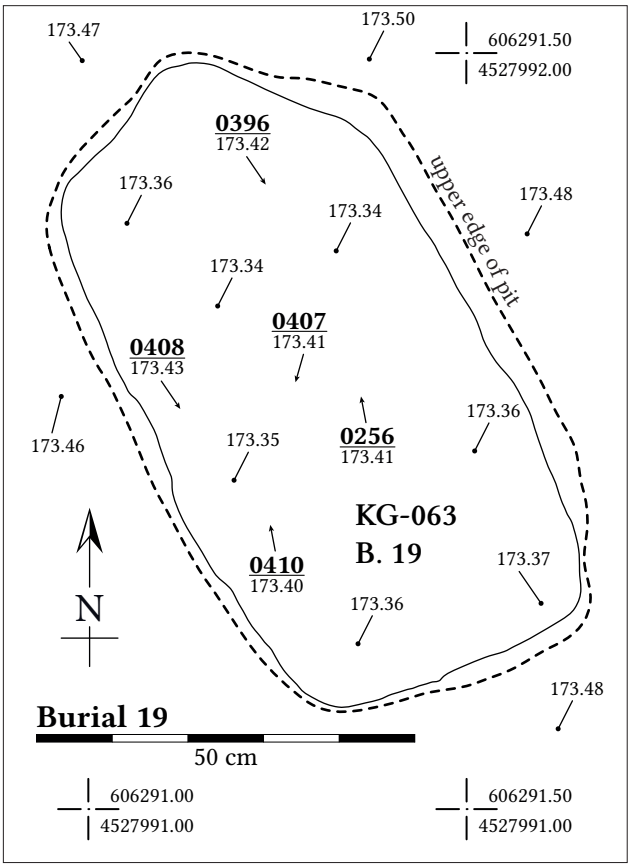

Fig. 129. Plan of Burial 19 (KG-063)

Burial 19 (KG-063)

Burial 19 was located in the south-western quadrant of square 6290/7990 (Fig. 27). The small size of the grave-pit (90 × 50 cm) and its shallow depth (Fig. 129) suggested at first a deposition or cenotaph, however, the beads found in the pit rather support the possibility of an adorned infant body that had completely vanished. In total 15 beads were discovered. Eleven beads were made of bone and were disc-shaped or cylindrical with a diameter not exceeding 2 mm (0409, Fig. 130, 2). They were found throughout the pit. Two small cylindrical beads were made of bluish frit (0396, 0407, Fig. 130, 3–4). One bead was of biconical shape and made of whitish frit (0408, Fig. 130, 5) and in the southern half of the pit were the fragments of a yellowish disc-shaped frit bead (0410). The distribution of the beads did not show a coherent pattern, offering no clues towards their original position on the body.

In the centre of the pit was the fragment of a bronze object (0256, Fig. 130, 1). It was made of a curved bronze sheet, of which one end was rounded and perforated. The other end was broken off.

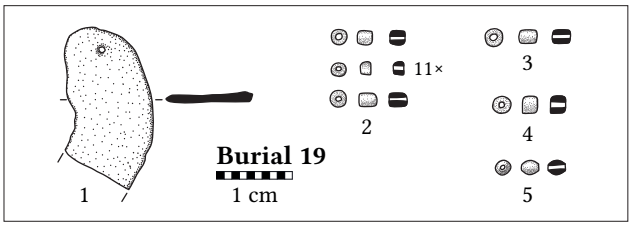

Fig. 130. Finds from Burial 19 (KG-063): 1 – bronze object (0256); 2 – bone beads (0409); 3 – frit bead (0407); 4 – frit bead (0396); 5 – frit bead (0408)

The find contributes little to a precise dating, however, at least the beads compare with similar ones found in Burial 4 or Burial 14. For Burial 19, therefore, a general date within the Late Bronze Age/Early Iron Age occupation of the cemetery is proposed.

Grave contents

KG-063-0256 (bronze object) Fig. 130, 1
L: 21.0 mm; W: 11.0 mm; Th: 0.8 mm; Wt: <1 g
606291.360 E; 4527991.549 N; 173.410 m

KG-063-0396 (bluish cylindrical frit bead) Fig. 130, 4
Diam: 2.2 mm; Th: 2.0 mm;
Hole diam.: 0.7 mm; Wt: <1 g
606291.234 E; 4527991.826 N; 173.418 m

KG-063-0407 (bluish cylindrical frit bead) Fig. 130, 3
Diam: 2.4 mm; L: 2.4 mm; Hole diam.: 0.7 mm; Wt: <1 g
606291.273 E; 4527991.563 N; 173.413 m

KG-063-0408 (white biconical frit bead) Fig. 130, 5
Diam: 2.0 mm; Th: 1.9 mm;
Hole diam.: 0.7 mm; Wt: <1 g
606291.121 E; 4527991.529 N; 173.432 m

KG-063-0409 (11 white bone beads) Fig. 130, 2
Diam: 2.0 mm; Th: 1.2–2.0 mm;
Hole diam.: 0.7 mm; Wt: <1 g

KG-063-0410 (fragments of white frit bead)
Wt: <1 g

Burial 20 (KG-030 and KG-102)

Burial 20 was excavated in two campaigns (Fig. 27): Its southern half was excavated during the campaign of 2016 (context KG-030) and the northern half in 2017 (context KG-102). This artificial division is indicated in Fig. 131 by a dashed line that corresponds to the northern limit of square 6300/7990 in 2016 (at 4527999.50 N). In the west a considerable part of the grave-pit was covered by the baulk between squares 6290/7990 and 6300/7990 and remained unexcavated. The eastern outline of the grave-pit was roundish. In the south it joined Pit-Complex A (Fig. 42), but remained delimited from it by shallow elevations that projected from the eastern and presumably

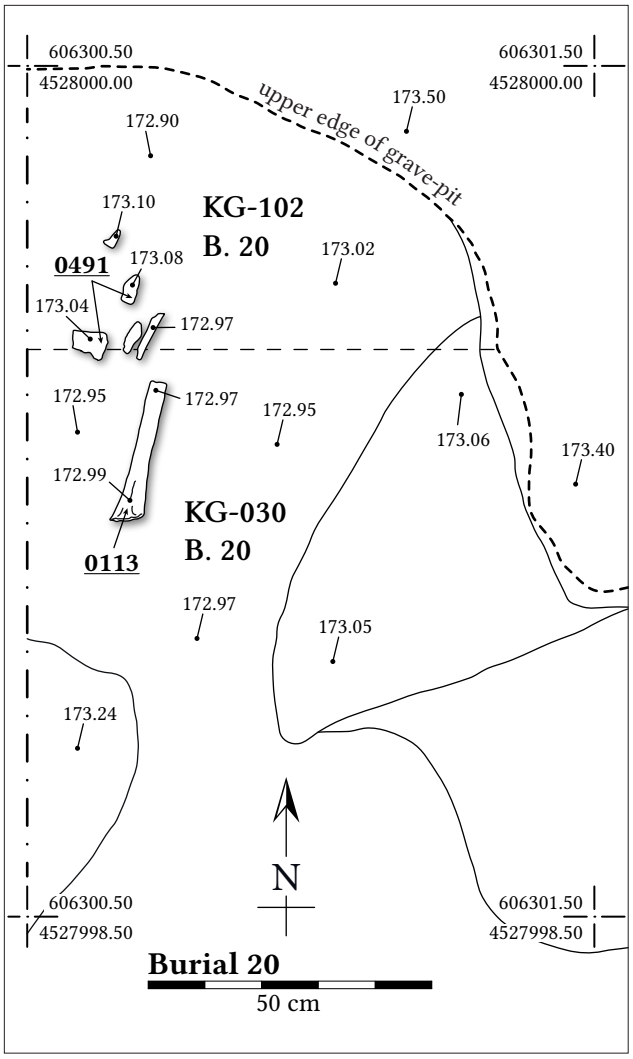

Fig. 131. Plan of Burial 20 (KG-030 & KG-102); Pit-Complex A

also from the unexcavated western edge of the grave-pit, leaving only a narrow gap of c. 25 cm in between. The stratigraphic relation between Burial 20 and Pit-Complex A remained inconclusive, because it could not be determined, whether the southern edge of Burial 20 was cut by Pit-Complex A or vice versa.

Only a few remains of the skeleton were preserved. They were identified as parts of the left femoral bone with fragments of a fibula found directly below it (0113) and parts of the sacrum immediately north of it (0491). Classification and position of the bones in the eastern part of the pit (Fig. 131) suggest, that the deceased had been interred on his right side in a flexed position and the upper part of the body should be expected further west.

The burial contained no burial objects. The only noteworthy find was an obsidian flake found loose in the fill. The date of Burial 20 is unknown, although the as-

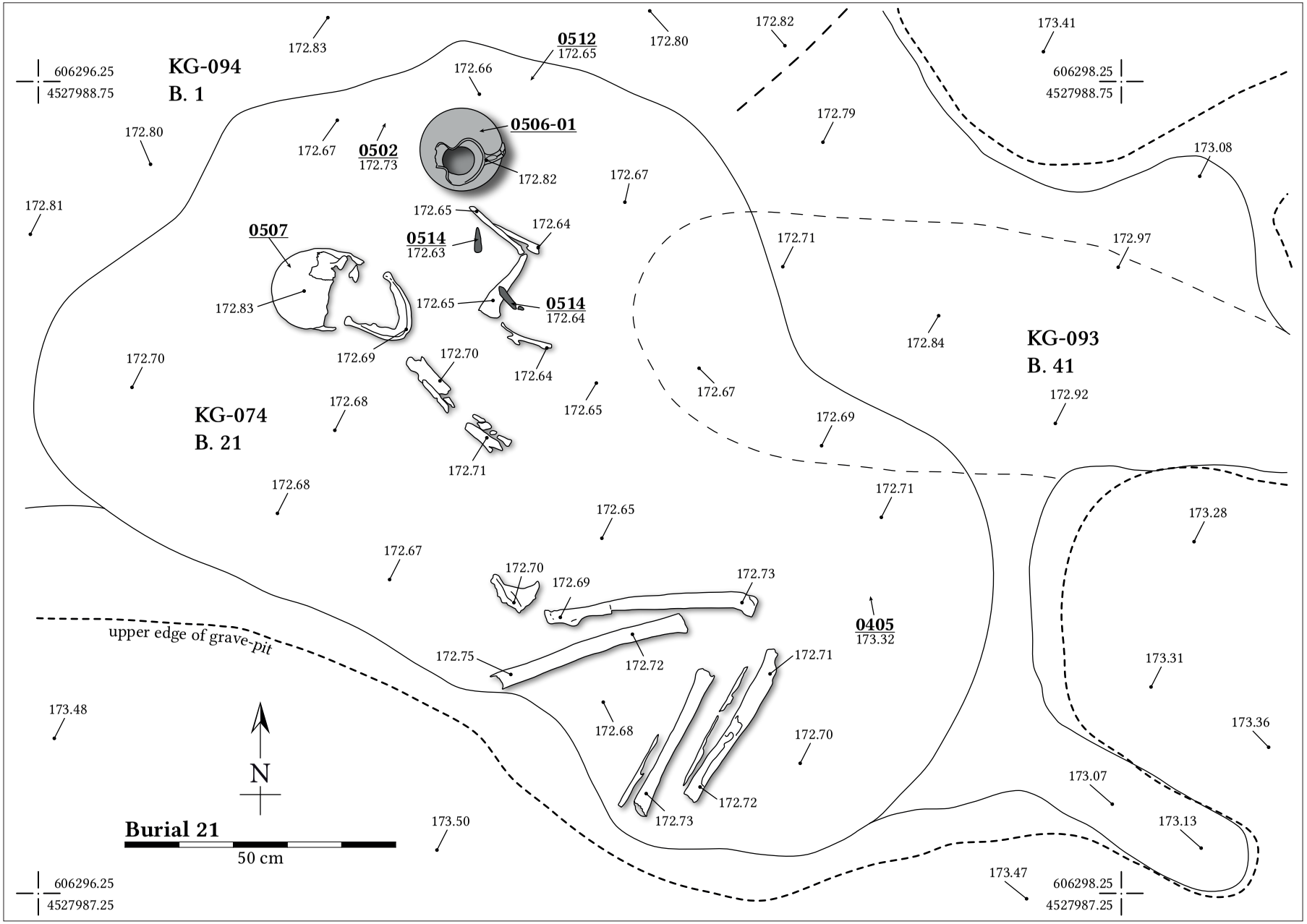

Fig. 132. Plan of Burial 21 (KG-074); Pit-Complex C-3–4

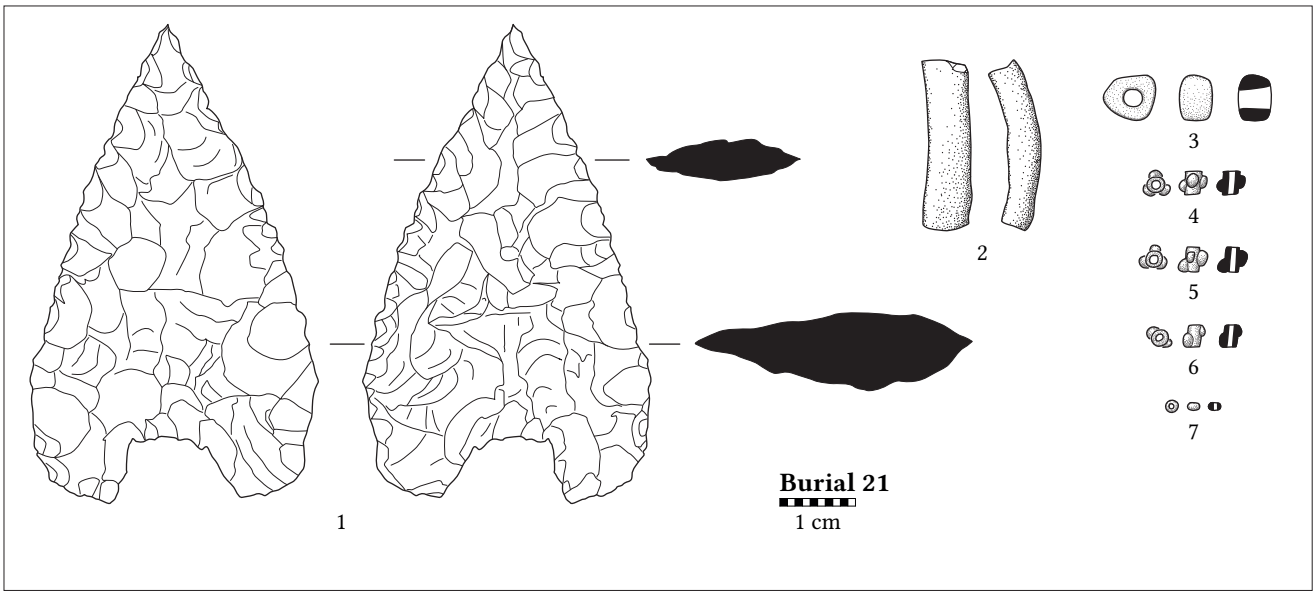

Fig. 133. Finds from Burial 21 (KG-074) that probably originate from Burial 1 (KG-094): 1 – obsidian arrowhead (0502); 2 – bronze bracelet (0512); 3 – carnelian bead (0438); 4 – frit bead (0466); 5 – frit bead (0454); 6 – frit bead (0406); 7 – frit bead (0501)

Fig. 134. Trefoil jug 0506-01 from Burial 21 (KG-074)

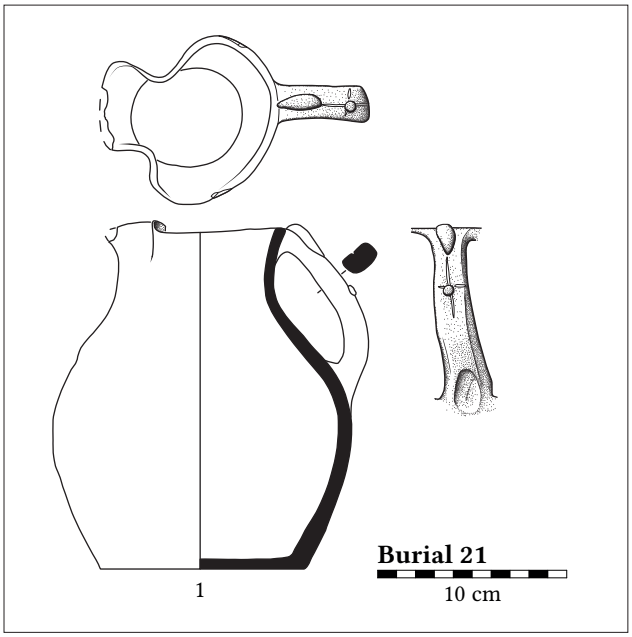

Fig. 135. Pottery from Burial 21 (KG-074): 1 – jug (0506-01)

sumed flexed body position and the bad preservation of the bones indicate a date at least prior to the Medieval period, perhaps as early as the Late Bronze/Early Iron Age period.

Grave contents

KG-030-0113 and KG-102-0491 (human bones)
Sex: could not be determined
Age class: Maturitas–Senilis

Table 16

Fill

KG-102-0488 (obsidian flake)
L: 25.0 mm; W: 19.0 mm; Th: 7.0 mm; Wt: 2 g
606300.790 E; 4527999.866 N; 173.374 m

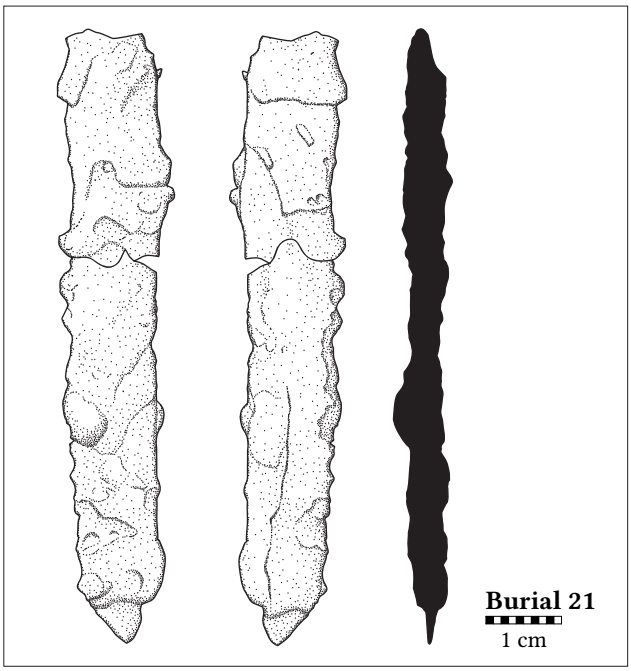

Fig. 136. Find from Burial 21 (KG-074): 1 – iron blade (0514)

Burial 21 (KG-074)

Burial 21 was located in the southern part of Pit-Complex C-3 and C-4 (Fig. 44 and Fig. 45). The grave-pit had an irregular shape and extended towards the north-west into the grave-pit of the Late Bronze Age Burial 1 (Fig. 132). The extensive disturbance of that burial and the entire southern part of Pit-Complex C-3 probably happened during the construction of Burial 21. This is suggested by ten cylindrical frit beads with applied knobs that were found in the fill of both burials (Fig. 54) and probably originated all from Burial 1. This applies as well to a small ring-shaped frit bead (0501, Fig. 133, 7), a disc-shaped carnelian bead (0438, Fig. 133, 3) and the fragment of a bronze bracelet (0512, Fig. 133, 2). Remarkable, however, is the apparent reuse of an obsidian arrowhead (0502, Fig. 133, 1) typical for the Bronze Age that was very likely found during the robbing of Burial 1 and afterwards deposited as a burial gift in the Burial 21. While all the other objects were found loose in the fill, the arrowhead appears to have been intentionally placed close to the jug of the later interment (Fig. 132).

The position of the leg bones suggests that the deceased was laid down on his left side with flexed legs. The body was oriented north-west to south-east orientated, even though almost nothing of the torso and arms was preserved. The skull had fallen over, so that the back of the skull and the bottom side of the mandibula were facing upwards. The anthropological analysis of the skull points to a rather male individual of at least adult age. A trefoil jug (0506-01), typical for the Late Antique period, was placed some 20 cm north-east of the skull (Fig. 134 and Fig. 135, 1). It was made of a reddish-brown fabric, and the surface was covered with many small black stains. It had a wide flat base and a wide neck. The handle was incised with two lines forming a cross, in the middle of which a small knob was applied. A second oval-shaped knob was applied to the top of the handle, and the lower end of the handle was decorated with a thumb-like impression. South-east of the vessel we discovered parts of the front leg of a sheep or goat still in its anatomical position (0551). Atop the humerus was one part of an iron blade, of which the second joining part was c. 7 cm away closer to the jug (0514, Fig. 136). Furthermore, animal bones of a rodent and an individual of the family of leporidae were found in the fill, but are very likely accidental intrusions.

A radiocarbon sample taken from the skeleton (Beta-506521) revealed the Late Antique date of the burial as between the mid-3rd and the late 4th cent. AD, which is in accordance with the suggested dating of the jug and the presence of an iron blade.

Grave contents

KG-074-0507 (human bones) Table 7
Sex: probably male Table 16
Age class: Maturitas–Senilis

KG-074-0551 (animal bones)
leg of a sheep or goat

KG-074-0506-01 (pot) Fig. 135, 1
Rim diam.: 95 mm (100%)
H: 184 mm
Base diam.: 110 mm
Fabric: completely oxidizing atmosphere, hard, medium fine temper (233)
Surface: ext. and int. smoothed
Colour: ext. 5YR 5/6 (yellowish red); core 5YR 5/6 (yellowish red); int. 5YR 5/6 (yellowish red)
Decoration: on the handle were two crosswise incised lines, two knob-like applications and a thumb-like impression
Condition: small part of the rim broken off, otherwise complete

KG-074-0514 (iron blade) Fig. 136L: 80.0 mm; W: 10.0 mm; Th.: 3.0 mm; Wt: 11 g
606297.115 E; 4527988.351 N; 172.644 m

KG-074-0502 (obsidian arrowhead) Fig. 133, 1
L: 31.5 mm; W: 17.7 mm; Th.: 5.0 mm
606296.888 E; 4527988.674 N; 172.730 m

Fill

KG-074-0512 (fragment of bracelet) Fig. 133, 2
H: 22.0 mm; Diam.: 5.0 mm
606297.156 E; 4527988.753 N; 172.654 m

KG-074-0406 (bluish frit bead with knobs) Fig. 133, 6
H: 2.9 mm; Diam.: 2.1–3.8 mm; Hole diam.: 1.1 mm
606297.175 E; 4527987.550 N; 173.401 m
with only two knobs

KG-074-0444 (bluish frit bead with knobs)
H: 2.0 mm; Diam.: 3.4 mm; Hole diam.: 0.8 mm
606296.509 E; 4527988.150 N; 173.094 m

KG-074-0447 (bluish frit bead with knobs)
three identical beads
H: 3.2 mm; Diam.: 3.0 mm; Hole diam.: 0.7 mm
606296.527 E; 4527987.994 N; 173.012 m

KG-074-0448 (bluish frit bead with knobs)
H: 3.5 mm; Diam.: 2.2 mm; Hole diam.: 0.9 mm
606296.617 E; 4527988.166 N; 172.977 m

KG-074-0449 (bluish frit bead with knobs)
H: 3.0 mm; Diam.: 3.0 mm; Hole diam.: 0.8 mm
606296.763 E; 4527988.284 N; 173.018 m

KG-074-0454 (bluish frit bead with knobs) Fig. 133, 5
H: 3.1 mm; Diam.: 2.2–3.9 mm; Hole diam.: 0.9 mm
606296.795 E; 4527988.457 N; 173.254 m

KG-074-0466 (bluish frit bead with knobs) Fig. 133, 4
H: 3.0 mm; Diam.: 2.3–3.9 mm; Hole diam.: 1.0 mm
606296.955 E; 4527988.730 N; 173.138 m

KG-074-0503 (bluish frit bead with knobs)
H: 3.8 mm; Diam.: 2.9 mm; Hole diam.: 0.6 mm

KG-074-0501 (bluish frit bead) Fig. 133, 7
H: 1.0 mm; Diam.: 1.6 mm; Hole diam.: 07 mm

KG-074-0438 (disc-shaped carnelian bead) Fig. 133, 3
Th: 4.7 mm; Diam.: 6.5–7.5 mm; Hole diam.: 2.9 mm
606297.138 E; 4527988.536 N; 173.244 m

KG-074-0405 (obsidian flake)
L: 30.0 mm; W: 33.0 mm; Th: 6.0 mm; Wt: 4 g
606297.783 E; 4527987.801 N; 173.320 m

KG-074-0426 (obsidian flake)
L: 19.0 mm; W: 8.0 mm; Th: 5.0 mm; Wt: 4 g
606296.546 E; 4527988.297 N; 173.468 m

KG-074-0461 (obsidian flake)
L: 20 mm; W: 11.0 mm; Th: 5.0 mm; Wt: 1 g
606296.403 E; 4527988.376 N; 173.184 m

KG-074-0505 (obsidian flake)
L: 20.5 mm; W: 9.0 mm; Th: 4.5 mm; Wt: 1 g

Burial 22
(KG-095-0496)

The grave-pit of Burial 22 was located in the northern half of Pit-Complex C-2 (Fig. 44). It measured 1.9 m from west to east and was approximately 1 m wide (Fig. 68), although the southern extent can only be estimated on the basis of the damage caused to the pottery inventory of the adjacent Late Bronze Age Burial 6. Only scarce remains of the skeleton were preserved along the northern edge of the grave-pit. The anthropological analysis suggests a young age of the deceased (Infans I or II). Besides some displaced objects and sherds of the disturbed Burial 6 that were scattered in the area of the later interment no objects accompanied the deceased (all objects found in the fill are listed with Burial 6).

The dating to the Late Antique period is based on a radiocarbon sample taken from one of the bones (Beta-506522) that allows a more precise placement between the final 3rd cent. AD and the end of the 4th cent. AD.

Fig. 137. Two-handled pot (0419-01) from Burial 23

Grave contents

KG-095-0496 (human bones) Table 7
Sex: could not be determined Table 16
Age class: Infans I–II

Burial 23
(KG-057-0415)

Burial 23 was interred in the north-western part of pit KG-057 which itself forms the central part of Pit-Complex B (Fig. 43). The original outline of the grave-pit was not preserved, but it seems to have caused severe damage to the Early Iron Age Burial 8 and thus should have been of considerable size. The deceased was placed in a flexed position on its left side with the head in the north-east and the legs in the south-west (Fig. 84 and Fig. 138). The analysis of the bones showed the individual to be rather male. Directly on top of the skeleton rested the bent knees of the subsequent Burial 24. The proximity of the

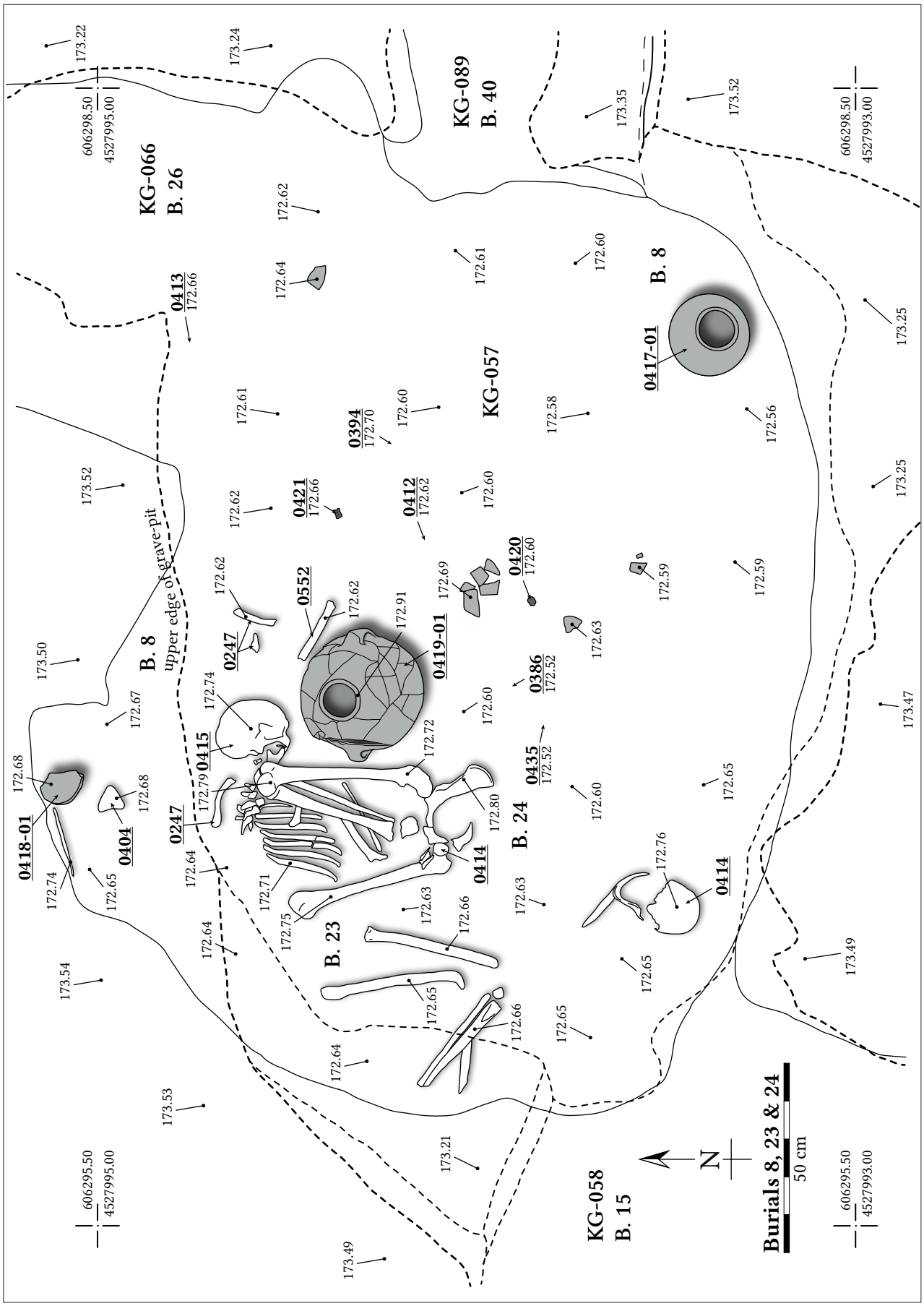

Fig. 138. Plan of Burials 8 (KG-057-0247 & KG-057-0404), 23 (KG-057-0415) and 24 (KG-057-0414); Pit-Complex B

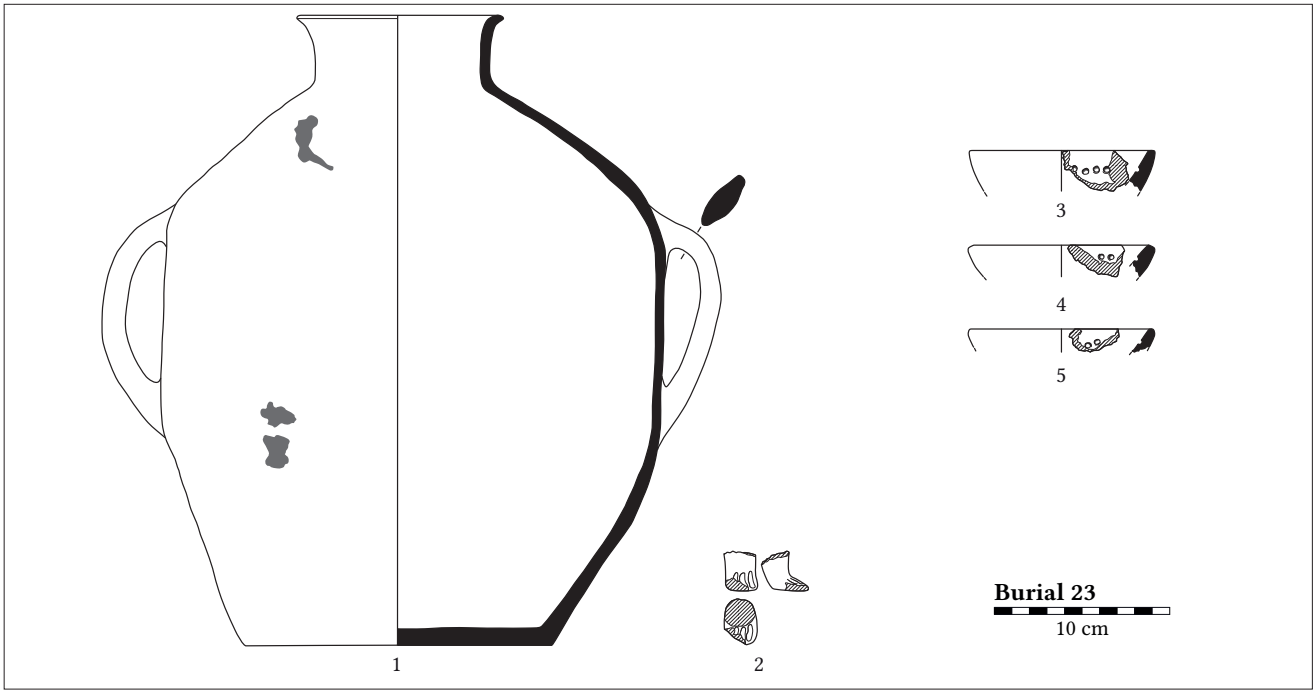

Fig. 139. Pottery from Burial 23 (KG-057-0415): 1 – pot (0419-01); 2 – ceramic object (0416-06); 3 – bowl (0416-08); 4 – bowl (0244-01); 5 – bowl (0244-02)

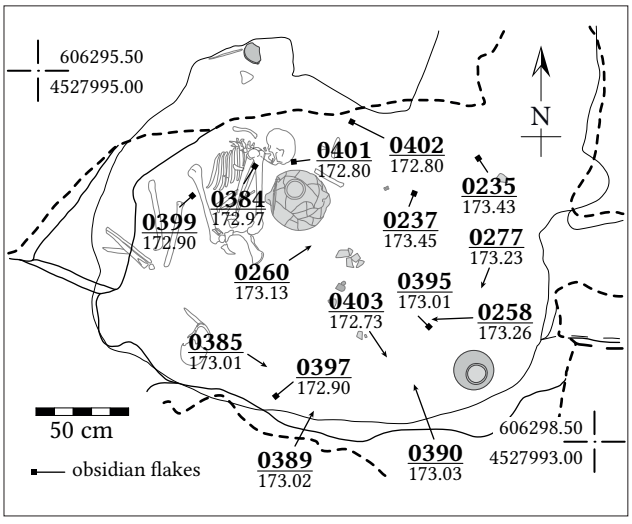

Fig. 140. Distribution of finds in the fill of pit KG-057 (Pit-Complex B)

two bodies without significant traces of disturbance indicates a short interval between both interments.

In front of the head of the deceased a large red-coloured pot (0419-01) with two handles on opposite sides was placed (Fig. 137 and Fig. 139, 1). Its reddish fabric and the black colour stains on the surface are in line with the typical pottery found in the other Late Antique burials at Tepe 5. It had a wide flat base and an oval profile that flattened where the handles were applied. The neck was vertical and ended in a short flaring rim. Although judging by its proximity to Burial 23 as well as to Burial 24 the vessel could be attributed to both burials, it appears more likely to assign it to Burial 23, because in the other Late Antique burials at Tepe 5 pottery vessels tend to be placed near the head of the deceased.

East of the pot was a single tibia of sheep (0552) and at some distance also an astragalus bone (0421) that both could have belonged to Burial 23. Besides the pottery and animal bones, no other objects could be securely attributed to this inhumation. This is partially due to the overall mixed character of the fill of the pit KG-057 (Fig. 140) that prevents any viable division of the material. In the catalogue (see below) all these finds are by definition listed as part of the fill of Burial 23, but it should be kept in mind that certain finds could belong to each of the three inhumations. This applies especially to the many iron fragments that were found on different levels and in different parts of the pit (0258, 0260, 0277, 0382, 0386, 0435, Fig. 141, 1–5). The only exception might be a group of three iron fragments that were found on the bottom of the pit not far east of the skeleton of Burial 24. Apart from a biconical spindle whorl (0420, Fig. 141, 7), already mentioned in connection with Burial 8, the fragment of a bracelet (0390, Fig. 141, 8) and of a bronze needle or wire (0394, Fig. 141, 9), an orange cylindrical frit bead with two yellow applied knobs (0389, Fig. 141, 10) and a retouched obsidian flake (0413, Fig. 141, 6) were found loose in the fill. Two additional finds are worth mentioning: Firstly, a small pottery object that resembles a small foot or

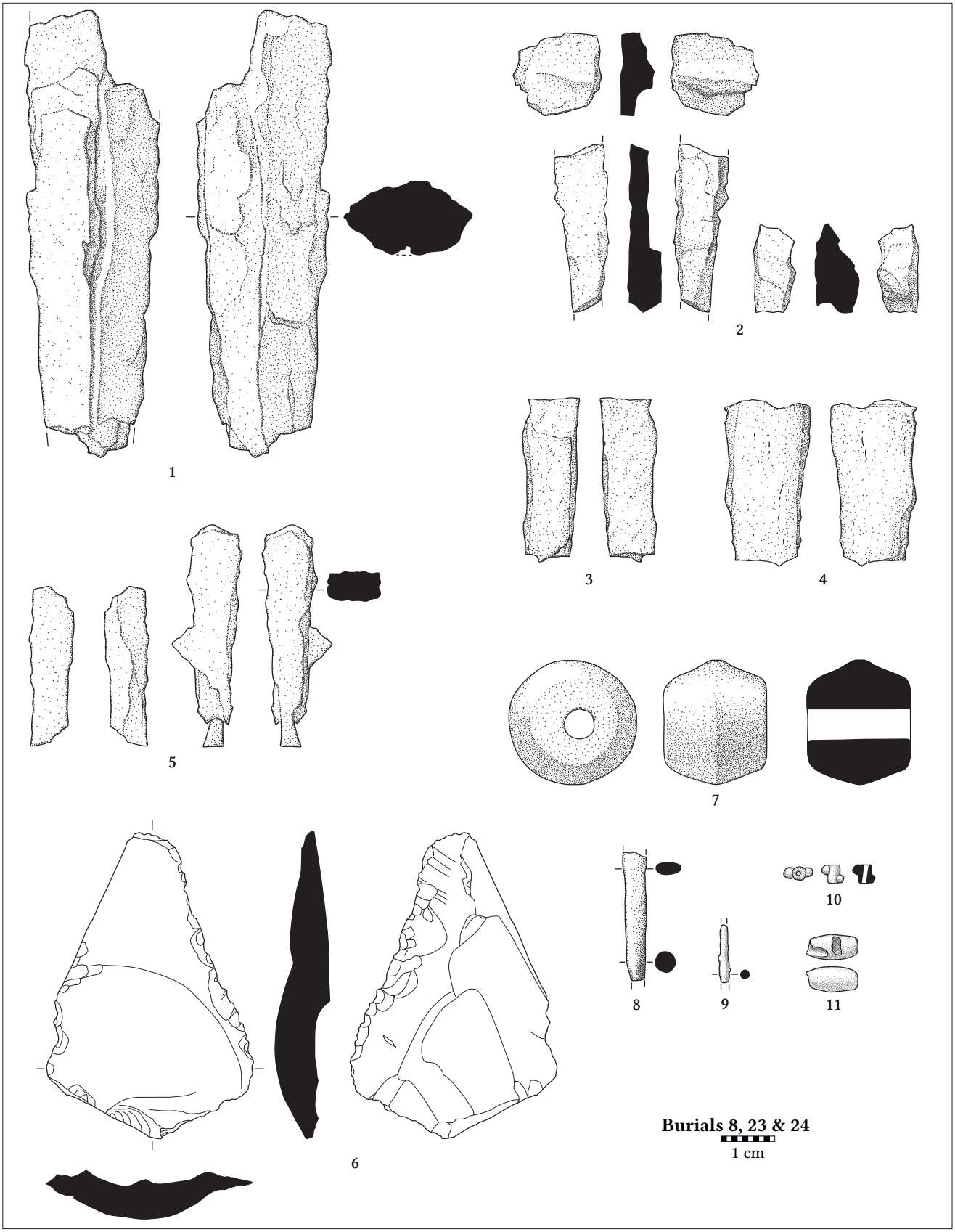

Fig. 141. Finds from the fill of pit KG-057 (Pit-Complex B): 1 – iron fragment (0277); 2 – iron fragments (0435); 3 – iron fragment (0382); 4 – iron fragment (0260); 5 – iron fragment (0258); 6 – retouched obsidian (0413); 7 – clay spindle whorl (0420); 8 – iron/copper bracelet (0390); 9 – bronze fragment (0394); 10 – frit bead (0389); 11 – mollusc (0385)

paw with vertical impressions (0416-06, Fig. 139, 2). It was made of the same red fabric as the pottery of Late Antique period and thus might belong either to Burial 23 or Burial 24. Secondly, three fragments of perhaps the same bowl with a row of circular impressions on the inside below the rim (0244-01, 0244-02, 0416-08, Fig. 139, 3–5). The latter are similar to sherds from KG-056 datable to the Chalcolithic period and probably ended up in the fill as accidental intrusions.

Grave contents

KG-057-0415 (human bones)
Sex: probably male — Table 16
Age class: Maturitas–Senilis

KG-057-0552 (animal bones)
tibia of a sheep

KG-057-0419-01 (pot) — Fig. 137; Fig. 139, 1
Rim diam.: 115 mm (100%)
H: 360 mm
Base diam.: 175 mm
Fabric: completely oxidizing atmosphere, very hard, fine temper (242)
Surface: ext. burnished; int. smoothed
Colour: ext. 7.5YR 6/4 (light brown); core 5YR 6/4 (light reddish brown); int. 5YR 6/6 (reddish yellow)
Decoration: some black coloured stains on the surface
Condition: few sherds missing, otherwise complete

Fill

KG-057-0244-01 (rim-sherd) — Fig. 139, 4
Rim diam.: 100 mm (10%)
Fabric: completely oxidizing atmosphere, medium hard, coarse temper (224)
Surface: ext. and int. smoothed
Colour: ext. 5YR 5/6 (yellowish red); core 5YR 5/6 (yellowish red); int. 5YR 5/6 (yellowish red)
Decoration: row of circular impressions at the inside below the rim

KG-057-0244-02 (rim-sherd) — Fig. 139, 5
Rim diam.: 100 mm (11%)
Fabric: completely oxidizing atmosphere, medium hard, coarse temper (224)
Surface: ext. and int. smoothed
Colour: ext. 5YR 5/6 (yellowish red); core 5YR 5/6 (yellowish red); int. 5YR 5/6 (yellowish red)
Decoration: row of circular impressions at the inside below the rim

KG-057-0416-08 (rim-sherd) — Fig. 139, 3
Rim diam.: 100 mm (10%)
Fabric: completely oxidizing atmosphere, medium hard, medium fine temper (223)
Surface: ext. and int. smoothed
Colour: ext. 5YR 6/6 (reddish yellow); core 5YR 6/6 (reddish-yellow); int. 5YR 6/6 (reddish yellow)
Decoration: row of circular impressions at the inside below the rim

KG-057-0416-06 (pottery object/foot?) — Fig. 139, 2
Fabric: completely oxidizing atmosphere, medium hard, medium fine temper (223)
Surface: ext. and int. smoothed
Colour: ext. 5YR 5/6 (yellowish red); core 5YR 5/6 (yellowish red); int. 5YR 5/6 (yellowish red)
Decoration: three parallel impressions

KG-057-0416-01 (body-sherd)
Fabric: not completely reduced core, hard, fine temper (632)

KG-057-0420 (clay spindle whorl) — Fig. 141, 7
H: 19.0 mm; Diam.: 23.0 mm; Hole diam.: 5.2 mm
606297.172 E; 4527993.874 N; 172.599 m

KG-057-0389 (orange frit bead with knobs) — Fig. 141 10
H: 3.5 mm; Diam.: 2.3–5.4 mm; Hole diam.: 0.9 mm
606296.986 E; 4527993.167 N; 173.022 m

KG-057-0390 (fragment of an iron/copper bracelet) — Fig. 141, 8
L: 24.0 mm; Diam: 3.8 mm; Wt: 2 g
606297.525 E; 4527993.314 N; 173.031 m

KG-057-0394 (fragment of a bronze wire or needle) — Fig. 141, 9
L: 10.8 mm; Diam: 1.7 mm; Wt: 1 g
606297.561 E; 4527994.224 N; 172.701 m

KG-057-0421 (astragalus bone)
606297.379 E; 4527994.367 N; 172.660 m

KG-057-0258 (two fragments of an iron object) — Fig. 141, 5
L: 41.0 mm; W: 11.0 mm; Th: 5.0; Wt: 5 g
606297.619 E; 4527993.658 N; 173.257 m

KG-057-0260 (fragment of an iron object) — Fig. 141, 4
L: 30.5 mm; W: 16.0 mm; Th: 2.5; Wt: 2 g
606296.974 E; 4527994.063 N; 173.130 m

KG-057-0277 (fragment of an iron object) — Fig. 141, 1
L: 83.0 mm; W: 24.0 mm; Th: 14.0; Wt: 30 g
606297.888 E; 4527993.825 N; 173.230 m

KG-057-0382 (fragment of an iron object) — Fig. 141, 3
L: 31.0 mm; W: 10.0 mm; Th: 4.0; Wt: 2 g

KG-057-0386 (amorph lumps of iron)
606296.921 E; 4527993.904 N; 173.034 m

KG-057-0435 (three fragments of an iron object) — Fig. 141, 2
606296.821 E; 4527993.824 N; 172.519 m

KG-057-0385 (small mollusc) — Fig. 141, 11
Diam: 4.9 mm; L: 9.3 mm; Wt: <1 g
606296.737 E; 4527993.400 N; 173.007 m

KG-057-0235 (obsidian flake)
L: 19.0 mm; W: 10.0 mm; Th: 2.0 mm; Wt: 1 g
606297.864 E; 4527994.543 N; 173.426 m

KG-057-0237 (obsidian flake)
L: 14.0 mm; W: 8.0 mm; Th: 5.0 mm; Wt: 1 g
606297.532 E; 4527994.353 N; 173.449 m

KG-057-0245 (obsidian flake)
L: 22.0 mm; W: 19.0 mm; Th: 6.0 mm; Wt: 2 g
606297.790 E; 4527992.664 N; 173.365 m

KG-057-0384 (obsidian flake)
L: 14.5 mm; W: 13.5 mm; Th: 3.0 mm; Wt: <1 g
606296.680 E; 4527994.499 N; 172.972 m

KG-057-0395 (obsidian flake)
L: 36.0 mm; W: 21.0 mm; Th: 7.0 mm; Wt: 4 g
606297.618 E; 4527993.609 N; 172.614 m

KG-057-0397 (obsidian flake)
L: 23.0 mm; W: 11.0 mm; Th: 6.0 mm; Wt: <1 g
606296.769 E; 4527993.234 N; 172.897 m

KG-057-0399 (obsidian flake)
L: 12.0 mm; W: 11.0 mm; Th: 4.0 mm; Wt: 1 g
606296.343 E; 4527994.337 N; 172.904 m

KG-057-0401 (obsidian flake)
L: 25.0 mm; W: 14.0 mm; Th: 9.0 mm; Wt: 3 g
606296.863 E; 4527994.507 N; 172.802 m

KG-057-0402 (obsidian flake)
L: 12.0 mm; W: 12.0 mm; Th: 3.0 mm; Wt: <1 g
606297.178 E; 4527994.730 N; 172.799 m

KG-057-0412 (obsidian flake)
L: 12.0 mm; W: 9.0 mm; Th: 5.0 mm; Wt: 1 g
606297.307 E; 4527994.137 N; 172.615 m

KG-057-0413 (retouched obsidian flake) Fig. 141, 6
L: 56.5 mm; W: 38.5 mm; Th: 8.5 mm; Wt: 14 g
606297.830 E; 4527994.756 N; 172.662 m

KG-057-0403 (flint flake)
L: 42.0 mm; W: 18.0 mm; Th: 9.0 mm; Wt: 7 g
606297.381 E; 4527993.452 N; 172.732 m

Burial 24 (KG-057-0414)

Burial 24 was the last inhumation in the central part of Pit-Complex B (Fig. 43). It occupied the western part of pit KG-057, but the outline of the grave-pit was not distinguishable any more from the surrounding fill of the earlier burials interred in the same spot (Fig. 84 and Fig. 138). The skeleton was orientated north-south. The lower legs were tightly flexed in a kneeling position and rested directly on the ribcage of Burial 23 but without disturbing the latter's anatomical arrangement. This peculiar placing and the lack of damage to the earlier burial suggest a temporal proximity between the two interments, which is why Burial 24 was dated to the Late Antique period as well. From the pelvis upwards, the entire torso was missing. It was impossible to determine, if these parts of the skeleton were completely decayed or whether there was a later disturbance in that area. In the south, at a distance of c. 40 cm to the pelvis, were fragments of the skull and the mandible were discovered both facing downwards.

The only find that was possibly associated with Burial 24 are three fragments of an iron object (0435, Fig. 141, 2) that were placed not far east of the skeleton. However, because this attribution is far from assured, the object is listed together with all the other finds from the fill (see Burial 23)

Grave contents

KG-057-0414 (human bones)
Sex: could not be determined Table 16
Age class: Maturitas–Senilis

Burial 25 (KG-053)

Burial 25 was located in the southern half of square 6300/7990 (Fig. 31). Its grave-pit cut an earlier burial of the Late Bronze/Early Iron Age (Burial 9) and was itself cut by the Medieval Burial 37. It had an almost rectangular shape and was oriented west-northwest to east-southeast (Fig. 142 and Fig. 143). The southern edge was slightly undercut. The burial contained a male individual of 40–70 years of age. The body was laid down on its left side with the head in the north-west, facing north-east. The legs were flexed. The left arm was placed next to the shoulder of the pottery vessel 0209-01 that was placed in the north-western corner of the grave-pit. The finger bones had collapsed and were fallen onto the level of the

Fig. 142. Burial 25 (KG-053)

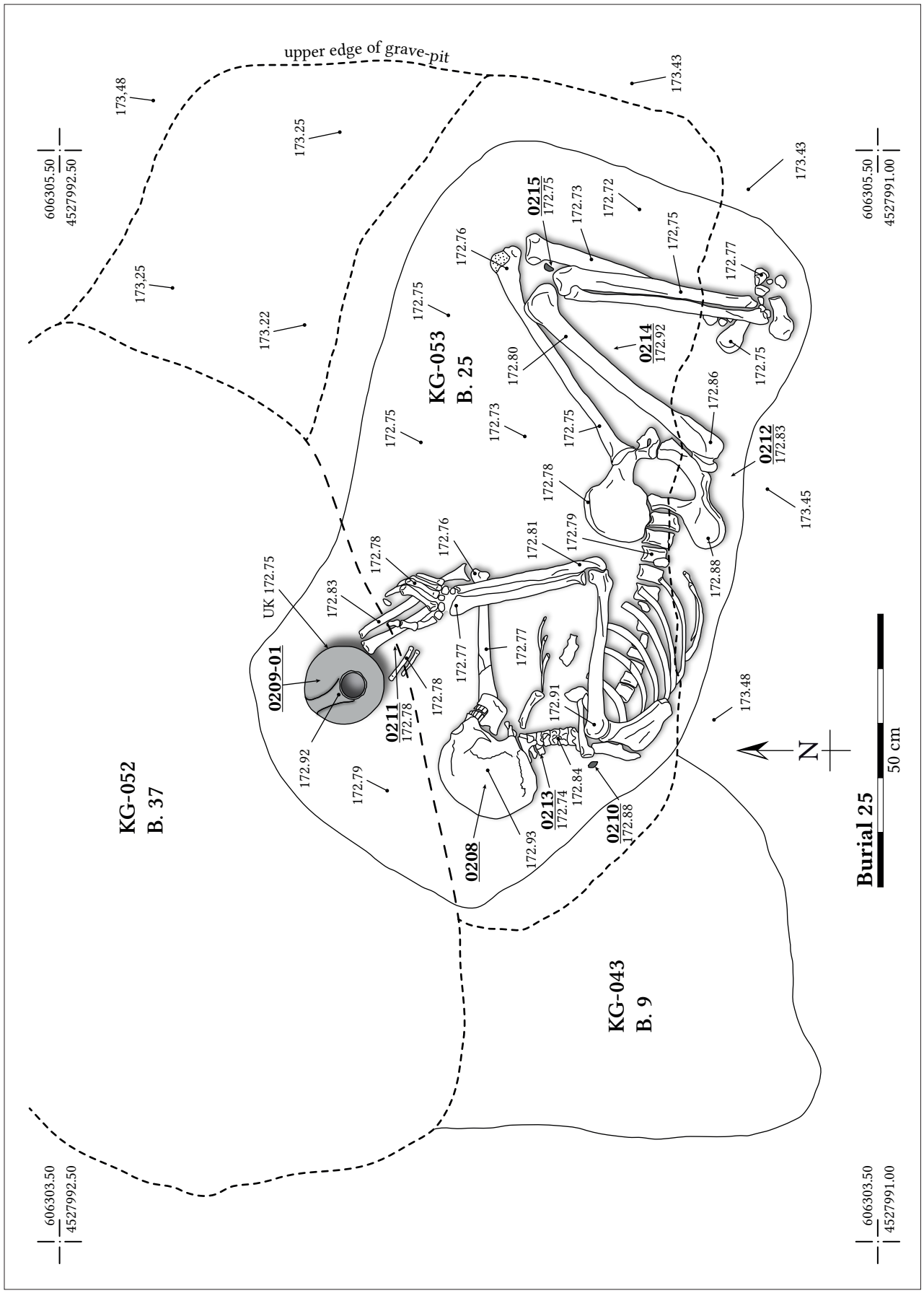

Fig. 143. Plan of Burial 25 (KG-053)

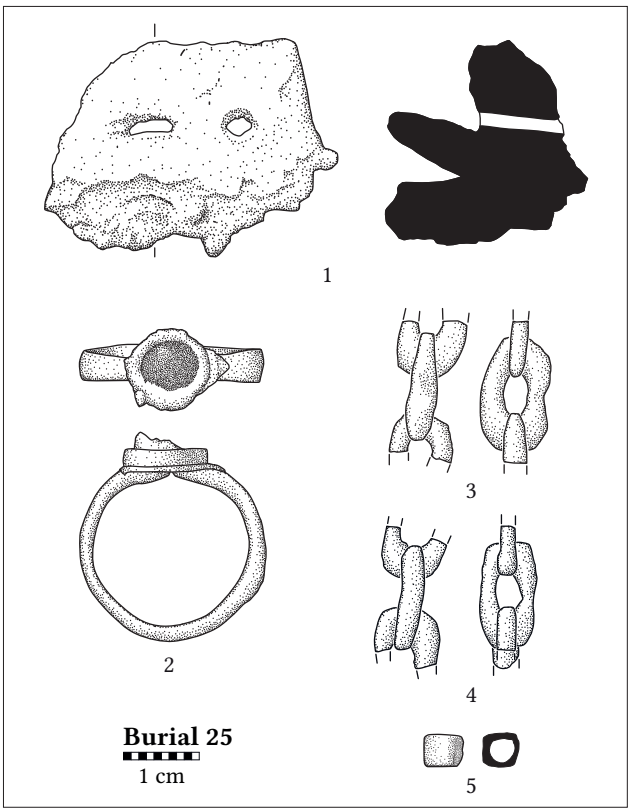

Fig. 144. Finds from Burial 25 (KG-053): 1 – iron object (0213); 2 – finger ring (0211); 3 – bronze chain (0210); 4 – bronze chain (0215); 5 – bronze chain (0212)

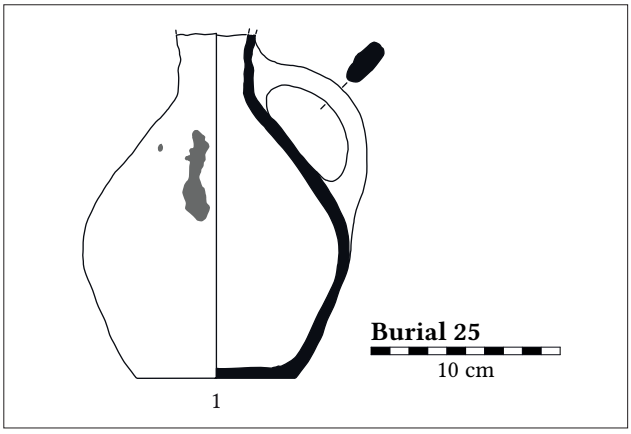

Fig. 145. Pottery from Burial 25 (KG-053): 1 – jug (0209-01)

vessel's base. One finger still carried a bronze ring with a round stone inlay (0211, Fig. 144, 2). The right hand rested on the left forearm. The pottery vessel was made of a reddish clay and the surface showed black colour stains typical for the Late Antique pottery at Tepe 5 (Fig. 33 and Fig. 145). Its body was pear-shaped with a large handle applied to it. The neck was narrow and tall. Although the rim was completely cut off when the grave-pit of the Medieval Burial 37 was dug, it was very likely a trefoil jug as in the other Late Antique period burials. The proposed dating for the vessel is confirmed by a radiocarbon date (Beta-506516) that brackets the time of the interment between the mid-3rd to the mid-4th cent. AD.

Behind the neck of the skeleton was an iron object of irregular shape with an oblong protrusion on one side and two small holes (0213, Fig. 144, 1). Small amorphous iron fragments were also found in the bend between the thighs and lower legs (0214). Two links of a bronze chain found behind the shoulder (0210, Fig. 144, 3) and at the knees (0215, Fig. 144, 4), as well as a cylindrical bronze bead near the pelvis (0212, Fig. 144, 5) very likely originate from Burial 9 and in the course of its disturbance ended up in the Burial 25.

Grave contents

KG-053-0208 (human bones) Table 7
Sex: male Table 16
Age class: Maturitas–Senilis

KG-053-0209-01 (jug) Fig. 33; Fig. 145, 1
H: 182 mm
Base diam.: 83 mm
Fabric: ext. oxidizing atmosphere, int. reducing atmosphere, hard, fine temper (332)
Surface: ext. and int. smoothed
Colour: ext. 7.5YR 5/6 (strong brown); core 7.5YR 7/8 (reddish yellow); int. 10YR 3/1 (very dark grey)
Decoration: some black colour stains on the surface
Condition: entire rim broken off

KG-053-0211 (bronze finger ring with stone inlay) Fig. 144, 2
Diam: 25.0 mm; W: 5.0 mm; Wt: 36 g
606304.586 E; 4527991.885 N; 172.780 m

KG-053-0213 (iron object) Fig. 144, 1
L: 29.0 mm; W: 23.0 mm; Th: 32.0 mm; Wt: 156 g
606304.388 E; 4527991.616 N; 172.739 m

KG-053-0214 (amorph iron fragments)
606305.138 E; 4527991.478 N; 172.924 m

Fill

KG-053-0210 (bronze chain) Fig. 144, 3
L: 20.0 mm; W: 8.0 mm; Wt: 18 g
606304.374 E; 4527991.522 N; 172.882 m

KG-053-0215 (bronze chain) Fig. 144, 4
L: 19.0 mm; W: 8.0 mm
606305.284 E; 4527991.604 N; 172.748 m

KG-043-0212 (cylindrical bronze bead) Fig. 144, 5
Diam: 4.0 mm; L: 4.0 mm;
Hole diam.: 3.0 mm; Wt: 1.7 g
606304.906 E; 4527991.264 N; 172.830 m

Burial 26 (KG-066)

Burial 26 was located in the easternmost part of Pit-Complex B (Fig. 43). The grave-pit was oblong and north-south oriented (Fig. 146 and Fig. 147). The upper edge of

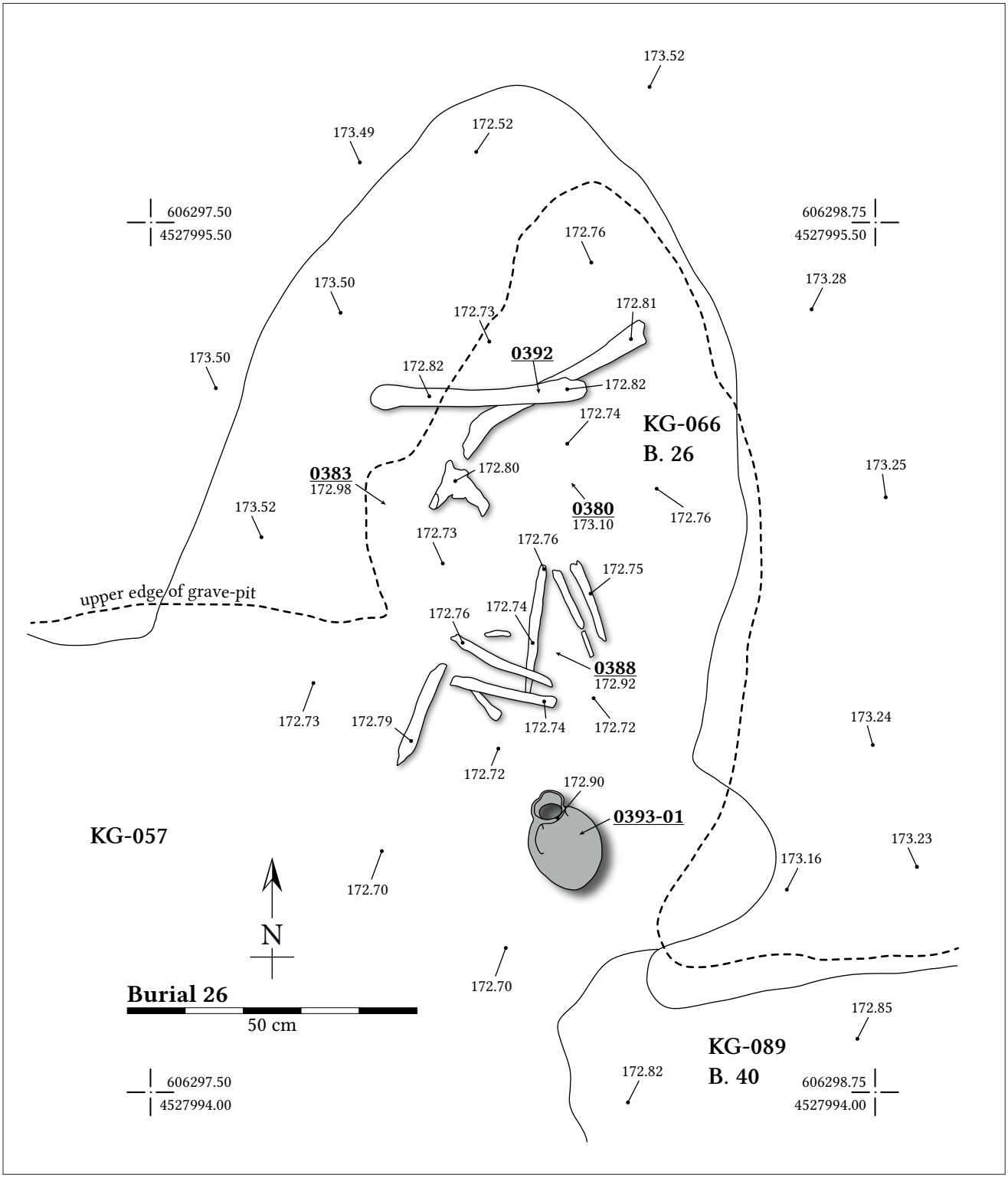

Fig. 146. Plan of Burial 26 (KG-066)

the grave-pit was considerably narrower (60–65 cm) than the bottom of the pit which was cut into the western section (85–100 cm). It seems that the pit was initially dug down vertically and then enlarged at the bottom to give enough room for the deceased. The southern end joined with the large pit KG-057 (with the Burials 8, 23 and 24). In this area the outline of the grave-pit could only be estimated.

The burial contained the skeleton of a rather female individual. Only some of the long bones and parts of the pelvis were preserved and revealed a flexed position on the right side with the head in the south. Next to the head a very tall and slander trefoil jug was placed (0393-01, Fig. 148, 1). The reddish fabric and the black-coloured stains on the surface clearly indicate a Late Antique date for this burial. This is also confirmed by a radiocarbon date (Beta-506519) that puts the interment into the time-frame from the mid-3rd cent. AD through the end of the 4th cent. BC. In the course of the anthropological analysis, the bone of a fetal or neonatal non-human mammal was identified. The question, if this was an actual burial gift or a later intrusion, remains unanswered.

Fig. 147. Burial 26 (KG-066)

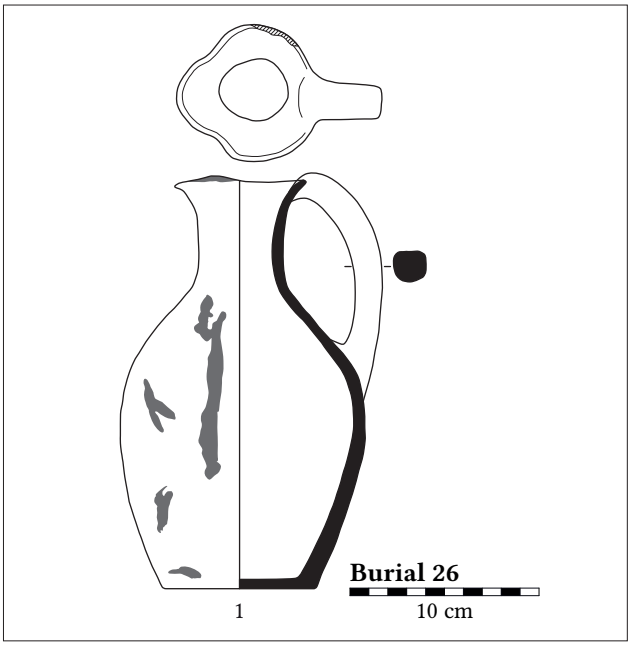

Fig. 148. Pottery from Burial 26 (KG-066): 1 – jug (0393-01)

Grave contents

KG-066-0392 (human bones) Table 7
Sex: probably female Table 16
Age class: Maturitas–Senilis

KG-066-0393-01 (pot) Fig. 148, 1
Rim diam.: 70 mm (100%)
H: 212 mm
Base diam.: 80 mm
Fabric: completely oxidizing atmosphere, hard, medium fine temper (233)
Surface: ext. and int. smoothed
Colour: ext. 5YR 6/6 (reddish yellow); core 5YR 6/6 (reddish yellow); int. 5YR 6/6 (reddish yellow)
Decoration: irregular black stains on the surface
Condition: complete

Fill

KG-066-0383 (obsidian flake)
L: 32.0 mm; W: 22.0 mm; Th: 6.0 mm; Wt: 3 g
606297.905 E; 4527995.014 N; 172.976 m

KG-066-0388 (obsidian flake)
L: 22.0 mm; W: 22.0 mm; Th: 6.0 mm; Wt: 3 g
606298.198 E; 4527994.759 N; 172.916 m

KG-066-0380 (obsidian flake)
L: 19.0 mm; W: 9.0 mm; Th: 8.0 mm; Wt: 2 g
606298.225 E; 4527995.054 N; 173.101 m

Burial 27 (KG-097)

Burial 27 was located in the northern quadrants of square 6300/7980 (Fig. 31). The grave-pit was oriented east-west and of an oblong oval shape (Fig. 150 and Fig.

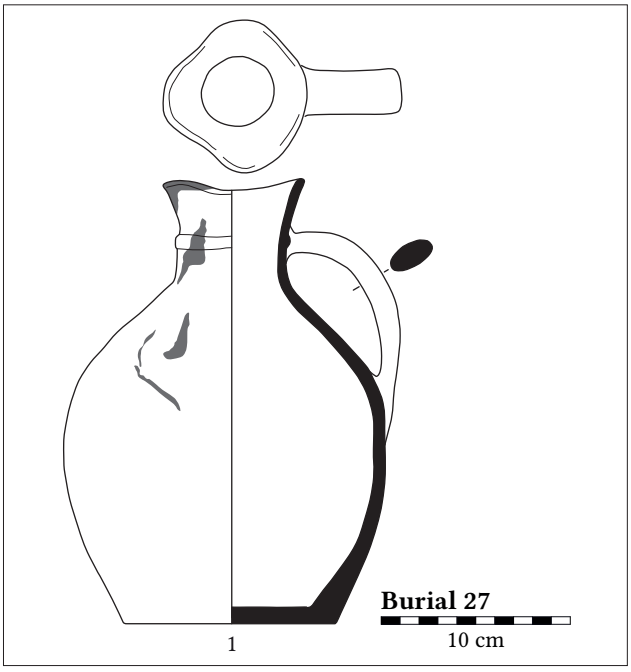

Fig. 149. Pottery from Burial 27 (KG-097): 1 – jug (0472-01)

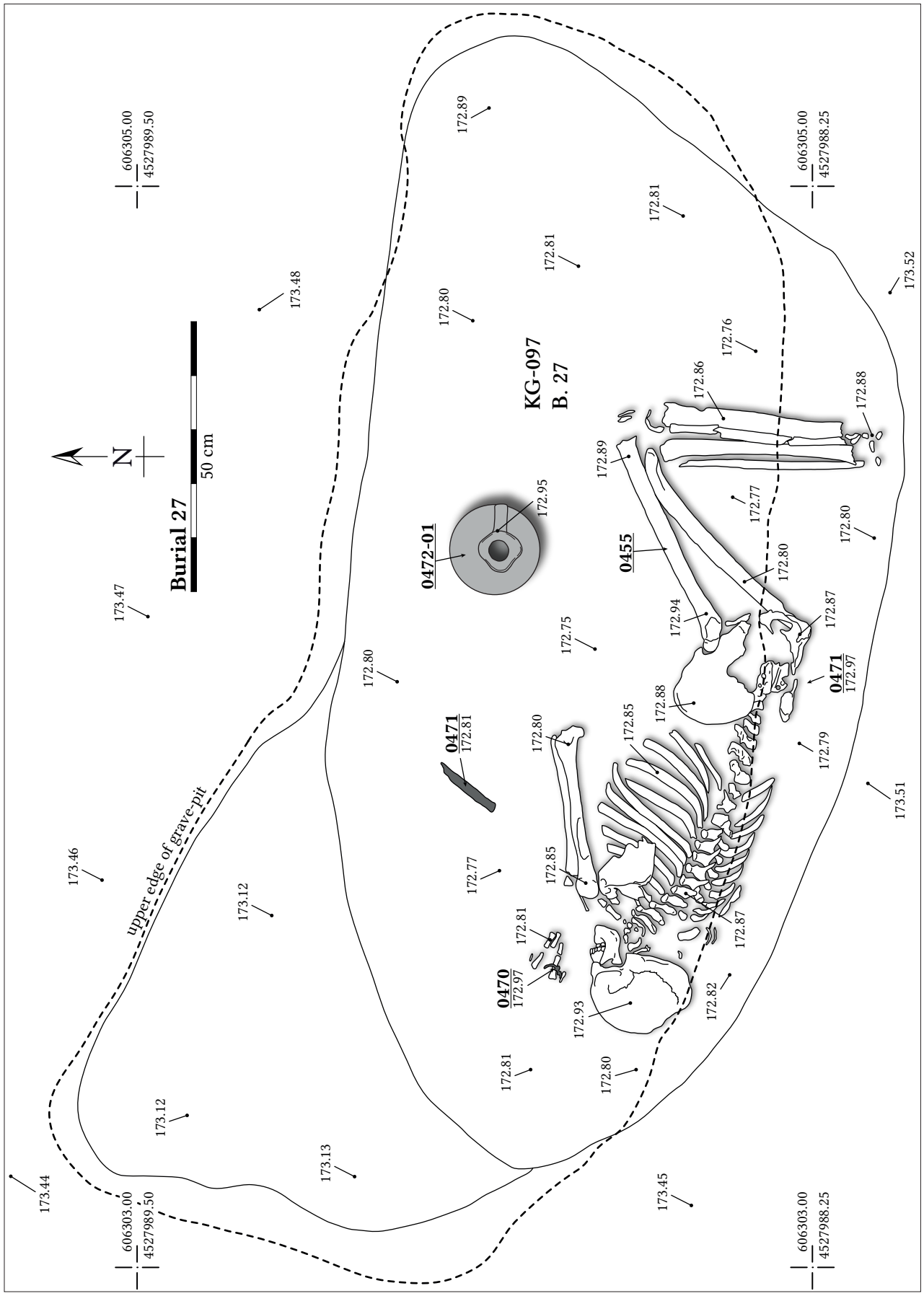

Fig. 150. Plan of Burial 27 (KG-097)

Fig. 151. Burial 27 (KG-097)

151). On a level c. 35 cm above the actual bottom of the pit the upper edge of the grave-pit was enlarged towards the north-west and formed an angular extension that might have been some kind of step or working pit to facilitate the excavation of the deep pit and the placement of the body. The rather male individual was placed on its left side along the southern edge of the grave-pit that was cut 20–25 cm into the section. The head was in the west-north-west, facing north-north-east. The legs were bent, and the arms were placed in front of the slightly tilted torso with the hands in front of the face. The deceased wore a silver finger ring on the right hand (0470), on which one half of a yellowish-brown frit bead was mounted (Fig. 152, 2). Next to the back side of the pelvis, a small bronze ring was found (0473, Fig. 152, 3). North of the arms was a c. 13 cm long iron object (0471) that appears to have been the hilt of a knife or dagger. The blade and what might have been a pommel were heavily corroded, whereas the c. 8 cm long section of the hilt in between was much better preserved, probably because it was originally covered by wood or another organic material (Fig. 152, 1). Two irregular holes that were visible

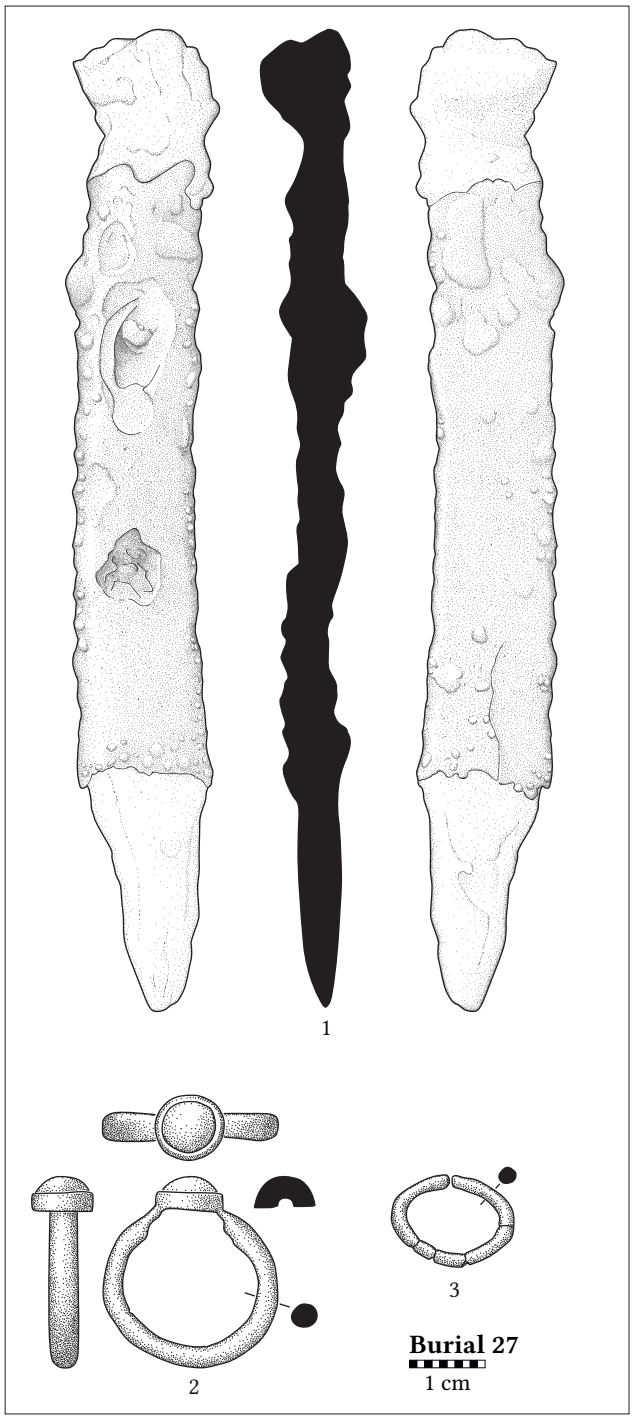

Fig. 152. Burial 27 Finds from Burial 27 (KG-097): 1 – handle of iron knife or dagger (0471); 2 – silver finger ring with frit bead inlay (0470); 3 – bronze ring (0473) (KG-097)

only on one side of the object might be the remains of the fasting of the hilt's cover by rivets or nails.

At some distance north of the skeleton a trefoil jug was placed (0472-01, Fig. 149, 1) that repeats the general typological features of the Late Antique pottery found in the burials at Tepe 5. In addition, a radiocarbon date

(Beta-506523) of the bones confirms the Late Antique date of Burial 27 and again sets a timeframe between the mid-3rd cent. AD and the late 4th cent. AD.

Grave contents

KG-097-0455 (human bones) Table 7
Sex: probably male Table 16
Age class: Adultas–Maturitas

KG-097-0472-01 (jug) Fig. 149, 1
Rim diam.: 75 mm (100%)
H: 235 mm
Base diam.: 110 mm
Fabric: completely oxidizing atmosphere, hard, fine temper (232)
Surface: ext. and int. smoothed
Colour: ext. 7.5YR 6/6 (reddish yellow); core 7.5YR 6/6 (reddish yellow); int. 7.5YR 6/6 (reddish yellow)
Decoration: a slight bead around the neck and various black colour stains on the surface
Condition: complete

KG-097-0470 (silver finger ring with frit bead inlay) Fig. 152, 2
Diam: 22.0–23.0 mm; Diam. wire: 3.0 mm; Diam. bead: 7.0 mm; Wt: 3 g
606303.554 E; 4527988.727 N; 172.969 m

KG-097-0473 (bronze ring) Fig. 152, 3
Diam: 12.0–16.0 mm; Diam. wire: 2.0 mm; Wt: <1g
606304.081 E; 4527988.261 N; 172.969 m

KG-097-0471 (handle of iron knife or dagger) Fig. 152, 1
L: 130.0 mm; W: 18.0 mm; Th.: 6.0–12.0 mm; Wt: 26 g
606303.891 E; 4527988.896 N; 172.805 m

Burial 28 (KG-027)

Burial 28 was located in the central area of Pit-Complex A (Fig. 42). The grave-pit was oriented south-west/north-east, c. 1.85 m long and only c. 35–45 cm wide (Fig. 75 and Fig. 153). Its western end undercut the edge of Pit-Complex A. The deceased was found to be a young male. He was placed on his back in a straight position with his head in the south-west. The skeleton was only preserved from the pelvis downwards; the torso, upper extremities and skull were completely missing. Although no apparent traces of a disturbance were discovered, the clear distinction between the preserved and vanished parts makes it probable that a man-made disturbance had occurred that caused the complete dislocation or decomposition of the upper part of the skeleton.

The eastern part of the grave-pit cut through the Late Bronze Age Burial 7 and divided it into two halves. It is very likely that due to this disturbance the bronze ring 0103 (Fig. 76, 5), that probably originated from Burial 7, ended up in the fill above the skeleton of Burial 28. The

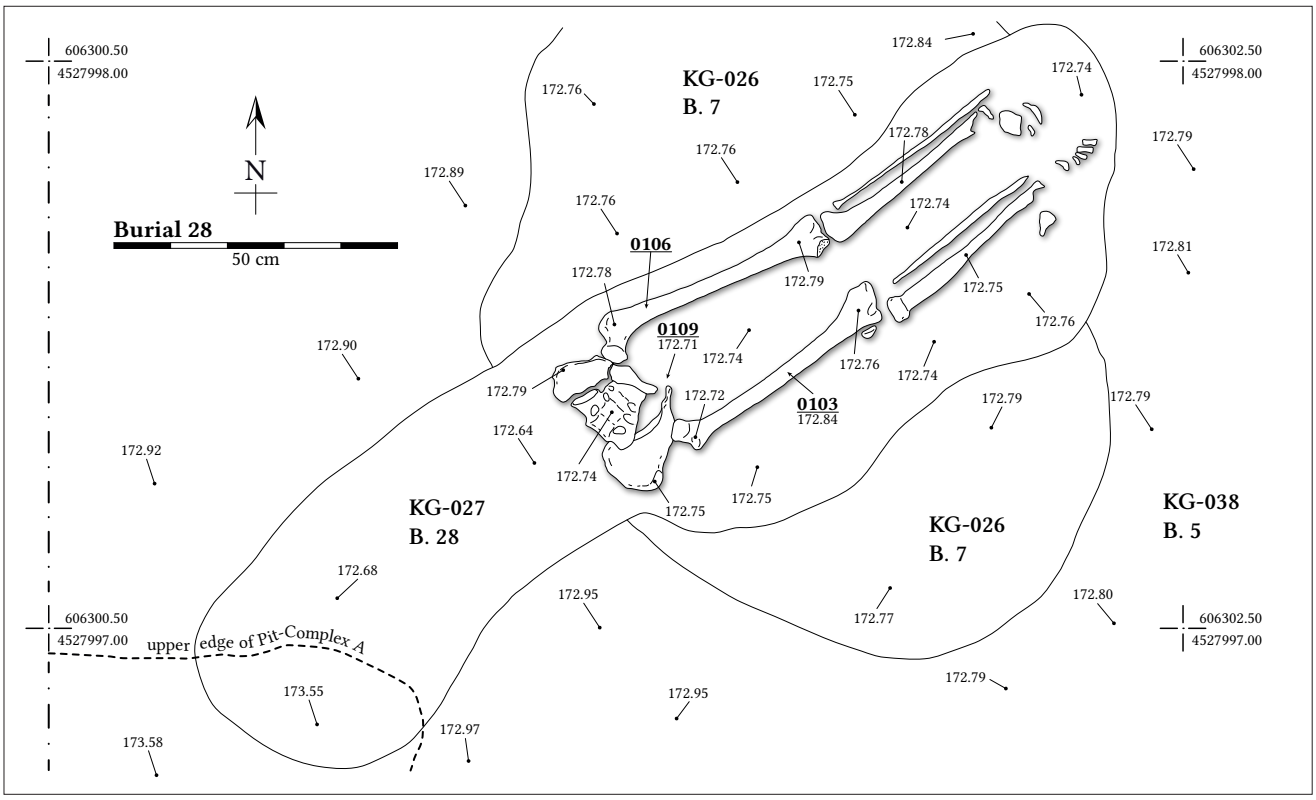

Fig. 153. Plan of Burial 28 (KG-027); Pit-Complex A

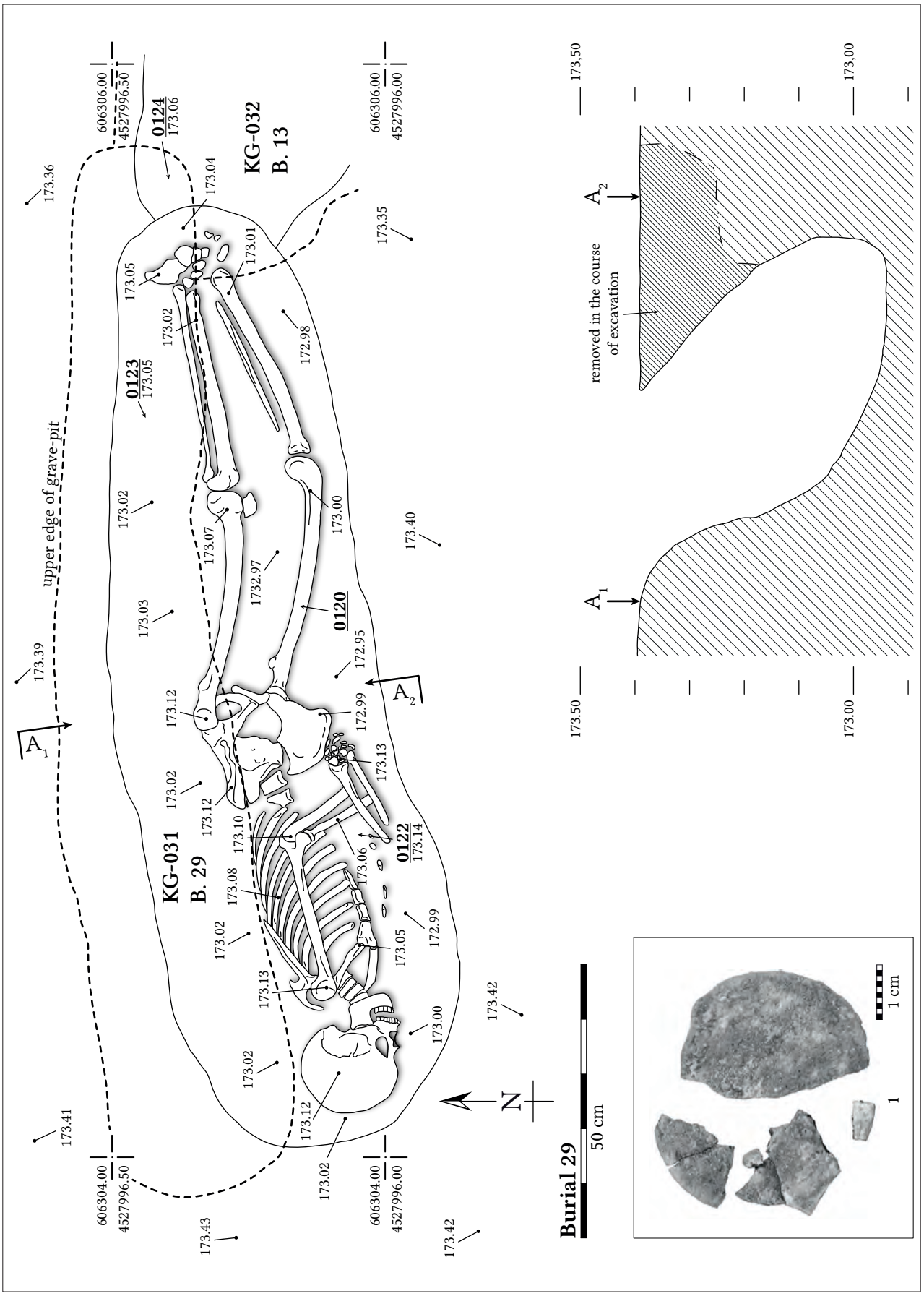

Fig. 154. Plan of Burial 29 (KG-031) with bronze object (0123)

obsidian flake 0109 found near the pelvis can be considered an accidental intrusion as well.

A radiocarbon sample (Beta-506512) taken from the phalanx bone of a foot dates Burial 28 to the Medieval period (Table 10). It is, therefore, the latest interment in Pit-Complex A.

Grave contents

KG-027-0106 (human bones) Table 10
Sex: male Table 16
Age class: Juvenis

Fill

KG-027-0103 (bronze ring) Fig. 76, 5
Diam: 22.0–25.0 mm; Diam wire: 4 mm; Wt: 3 g
606301.802 E; 4527997.452 N; 172.838 m
probably displaced from Burial 7

KG-027-0109 (obsidian flake)
L: 18.0 mm; W: 15.0 mm; Th: 9.0 mm; Wt: 2 g
606301.597 E; 4527997.445 N; 172.712 m

Burial 29 (KG-031)

The oblong grave-pit of Burial 29 was located in the northern half of square 6300/7990 (Fig. 35). It was oriented west-east. The eastern end cut though the corner of the adjacent Burial 13. The grave-pit was very narrow and at its uppermost detected outline the opening measured only 23–34 cm in width and 1.92 m in length (Fig. 36 and Fig. 154). The pit itself had a peculiar shape as well. It was not dug straight down into the soil, but followed a 50° incline sideways, creating a steep slope towards the south. To reach the skeleton a part of the southern edge of the original grave-pit had to be removed in the course of the excavation (section in Fig. 154). The deceased was laid down at the end of that slope on its left side with straight legs and its head in the west, facing south. The arms were crossed in front of the belly. The preservation of the bones was excellent and thus it was possible to securely determine sex and age. According to the anthropological analysis the deceased was a 20–25-year-old male.

Besides two obsidian flakes in the fill (0122, 0124), fragments of a small bronze disc (0123) were found c. 10 cm north of the left lower leg (Fig. 154, 1). Its original form could not be entirely reconstructed but the disc seems to have had a slight curvature on one side. It is the only object that can be considered as a burial gift or rather a part of the deceased's adornment.

A collagen sample was taken from the skeleton for radiocarbon-dating (Beta-506525) that allowed the attribution of Burial 29 to the 14th cent. AD.

Grave contents

KG-031-0120 (human bones) Table 10
Sex: male Table 16
Age class: Adultas

KG-031-0123 (bronze disc) Fig. 154, 1
Diam: c. 40.0 mm; Th: 2.0 mm; Wt: 5 g
606305.352 E; 4527996.439 N; 173.048 m

Fill

KG-031-0122 (obsidian flake)
L: 33.0 mm; W: 29.0 mm; Th: 7.0 mm; Wt: 4 g
606304.591 E; 4527996.052 N; 173.138 m

KG-031-0124 (obsidian flake)
L: 27.0 mm; W: 12.0 mm; Th: 7.0 mm; Wt: 2 g
606305.789 E; 4527996.396 N; 173.064 m

Burial 30 (KG-036)

The grave-pit of Burial 30 was found in the north-eastern quadrant of square 6290/7990 (Fig. 35); it was oriented south-west to north-east. The uppermost detected edge of the pit measured c. 2.15 × 0.90 m. At a level c. 45–55 cm above the bottom the pit was narrowed, leaving a step of c. 20 cm width on all sides, so that the actual grave-pit was only 1.80 m long and 0.50 m wide (Fig. 155 and Fig. 156). The additional step might have helped to position the deceased at the bottom of the pit. The skeleton was poorly preserved – both lower legs, most arm bones and the torso were missing. The upper part of the spine was only indicated by roots that had penetrated the verte-

Fig. 155. Burial 30 (KG-036)

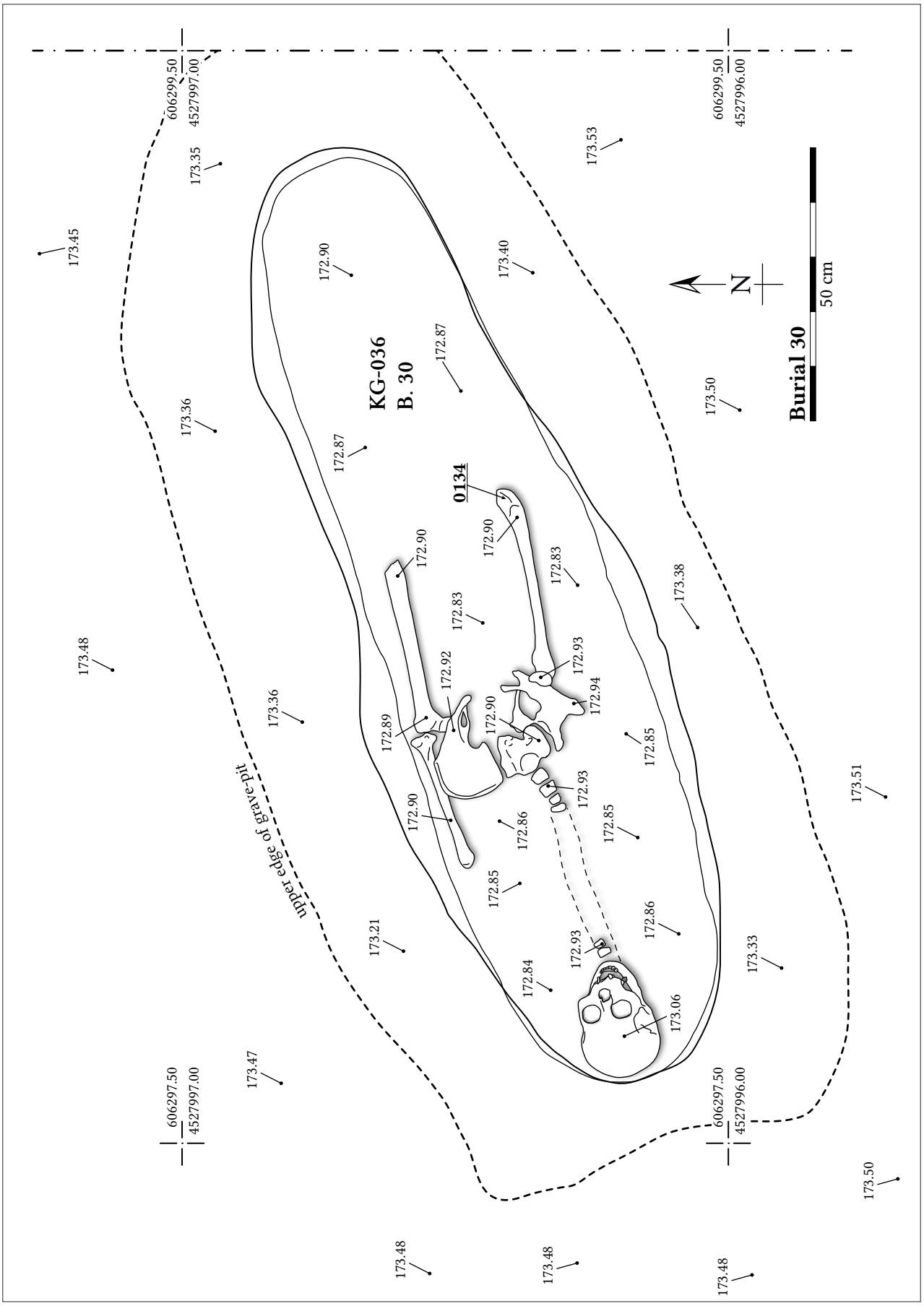

Fig. 156. Plan of Burial 30 (KG-036)

brae and had turned them into a solid mass of organic matter. Nevertheless, the preserved bone characteristics revealed a female individual that was placed on its back with stretched legs and the head in the south-west. Some undefined animal bones indicated animal burrowing, that might have caused also the secondary position of the left humerus next to the pelvis. No objects accompanied the burial. The body posture on the back and the orientation of the grave-pit suggest a Medieval date for Burial 30.

Grave contents

KG-036-0134 (human bones)
Sex: female
Age class: Maturitas
Table 16

Burial 31 (KG-042)

Burial 31 was located in the north-eastern quadrant of square 6290/7990 (Fig. 35). The grave-pit was of a peculiar shape (Fig. 157 and Fig. 158). The main part of the pit was only c. 40 cm wide and extended over a length of 1.6 m from south-west to north-east, where it was partially covered by the unexcavated baulk between squares 6290/7990 and 6300/7990. The skeleton, however, occupied only the north-eastern part, while the slightly higher ground in the south-west was empty. The reasons behind the angular extension of the grave-pit in the north remain unclear. Although described here in connection with Burial 31, it can not be excluded that this part of the grave-pit belonged to another burial or even marked the western extension of Pit-Complex A.

The skeleton was of a young, rather female individual that was laid down on its right side with the head in the south-west, facing south-east (Fig. 157). The right and probably also the left arm were bent and the hands were placed in front of her face. The lower legs and feet were not excavated, because they extended into the section.

Body position, preservation, and shape of the main grave-pit are comparable, for example, to Burials 33 and 34, so Burial 31 very likely is of Medieval date, too.

Grave contents

KG-042-0173 (human bones)
Sex: probably female
Age class: Infans I–Infans II
Table 16

Fig. 157. Burial 31 (KG-042)

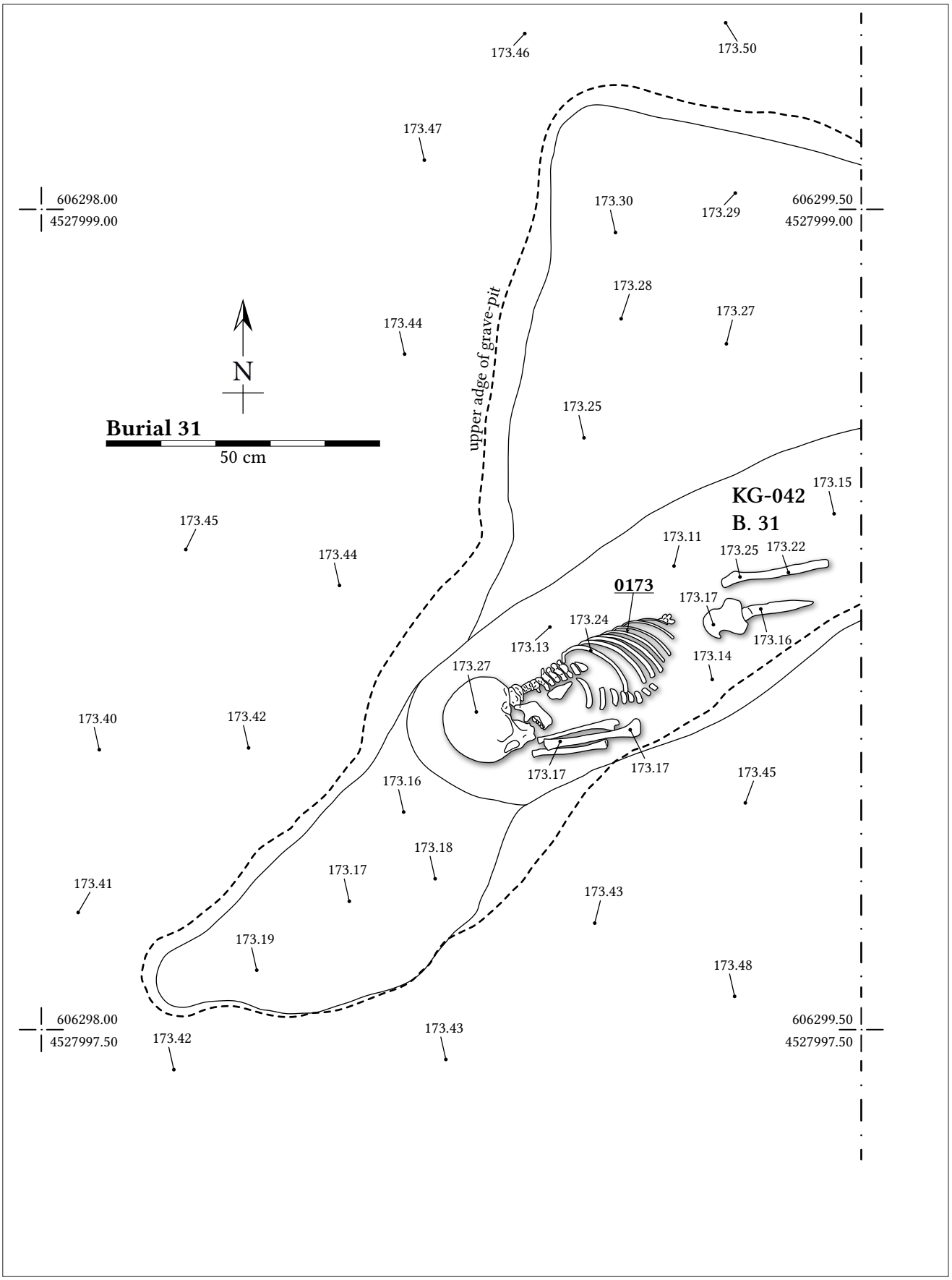

Fig. 158. Plan of Burial 31 (KG-042)

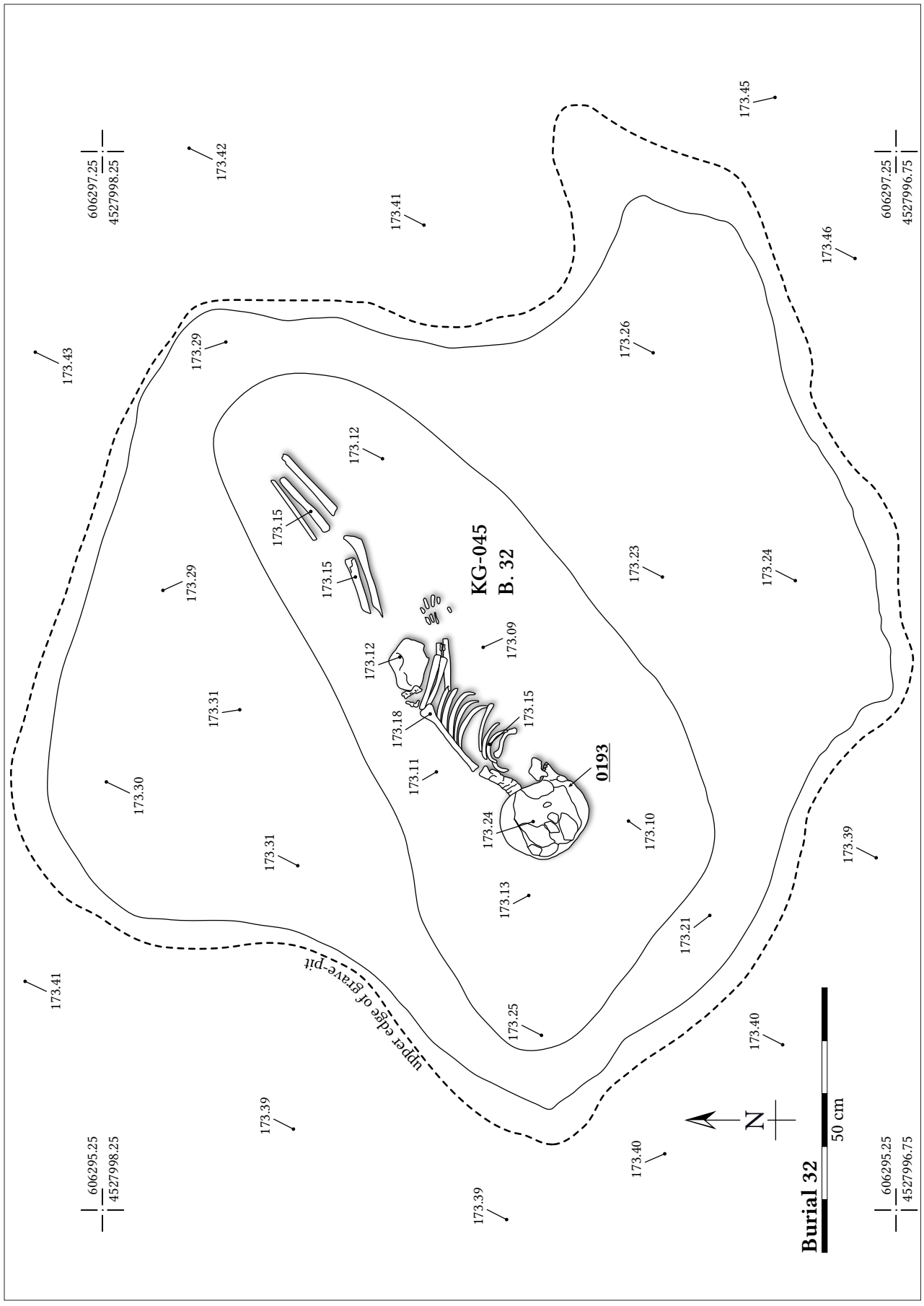

Fig. 159. Plan of Burial 32 (KG-045)

Burial 32 (KG-045)

Burial 32 was located in the north-eastern quadrant of square 6290/7990 (Fig. 35). The deceased had been placed in an oblong (1.30 × 0.5 m), south-west to north-east orientated grave-pit (Fig. 159). At a level c. 10–20 cm above the bottom the pit was getting larger and covered more than twice the area of the actual grave-pit in the centre. The upper edge was irregular in shape and reached a maximum length of 1.6 m and a width of between 1.3 m and 1.7 m.

The deceased was laid down on its right side with the head in the south-west. The legs were stretched, and the lower arms were placed in front of the pelvis. Judging from the anthropological analyses, the deceased was of rather young age. The sex could not be determined.

The arrangement of the body as well as the shape and orientation of the (central) grave-pit conforms with burials of the Medieval period.

Grave contents

KG-045-0193 (human bones)
Sex: could not be determined
Age class: Infans I
Table 16

Fill

KG-045-0190 (obsidian flake)
L: 30.7 mm; W: 20.4 mm; Th: 8.1 mm; Wt: 2 g

Burial 33 (KG-046)

Burial 33 was located in the central area of square 6290/7990 (Fig. 35). The grave-pit had been cut into the south-eastern portion of the grave-pit of Burial 2. The northern edge of the grave-pit (including the left leg and the right foot) was excavated during 2016, the remaining parts of the grave-pit in 2017. It was of oblong shape with two round protrusions along the southern edge, of which the western one undercut the surrounding soil (Fig. 160 and Fig. 161). Grave-pit and skeleton were orientated south-west to north-east. The deceased was laid down on its right side with the head in the south-west facing south. The left leg was stretched, while the right leg was slightly bent. The hands were placed in front of the torso. According to the anthropological analysis, the individual was male and of adult age.

Besides an obsidian (0225) and silex (0226) flake in the fill, no objects were found in the burial. Shape and ori-

Fig. 160. The southern part of Burial 33 (KG-046) in 2017; the left leg and right foot were excavated in the previous campaign and are therefore not shown in the picture

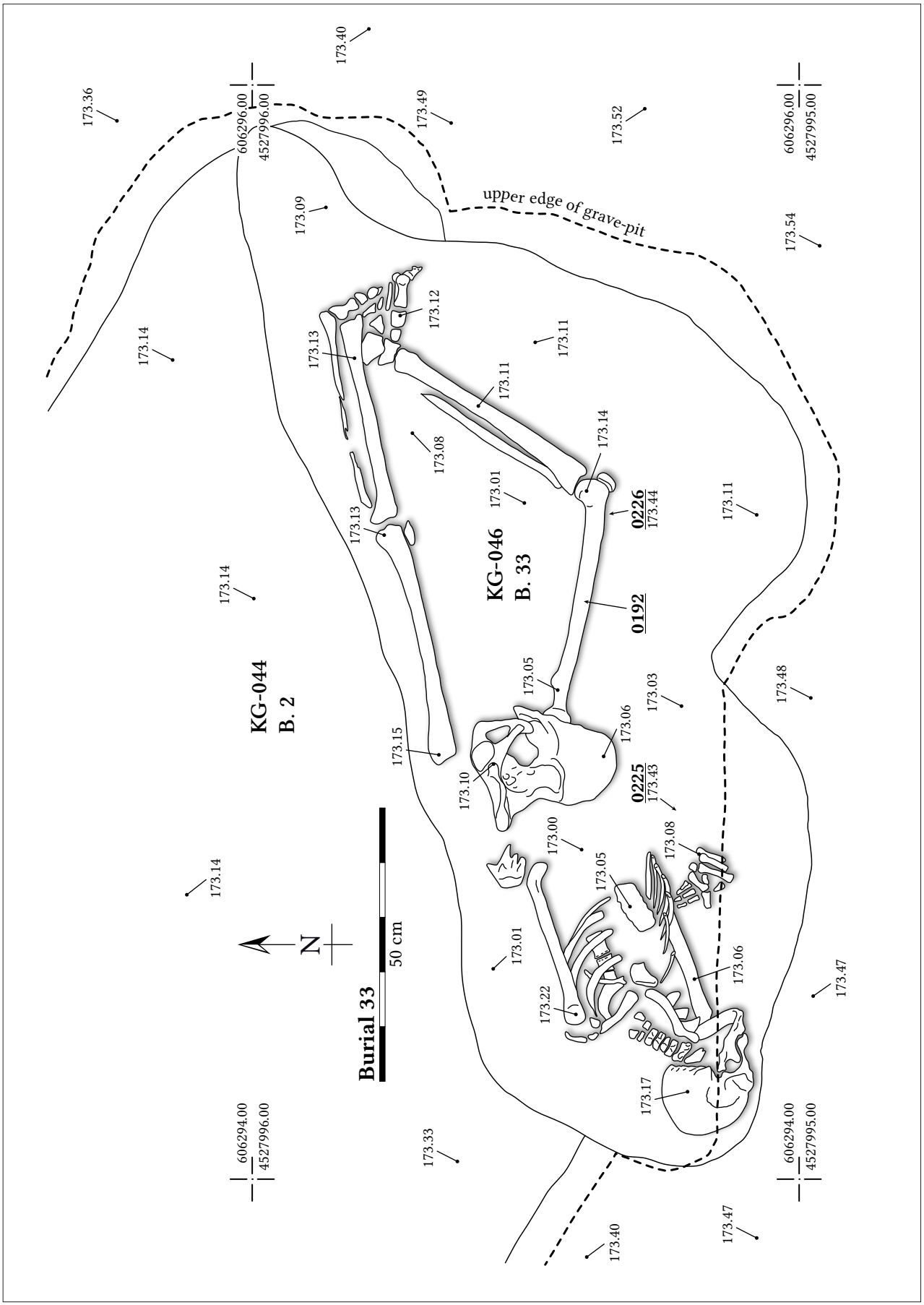

Fig. 161. Plan of Burial 33 (KG-046)

entation of the grave-pit as well as the posture of the body are very similar to the nearby Burial 34. A radiocarbon-dated sample from the bones (MAMS-39414) gave a Medieval date (14th cent. AD).

Grave contents

KG-046-0192 (human bones) Table 10
Sex: male Table 16
Age class: Adultas

Fill

KG-046-0225 (obsidian flake)
L: 32.0 mm; W: 29.0 mm; Th: 3.0 mm; Wt: 2 g
606294.673 E; 4527995.224 N; 173.432 m

KG-046-0226 (silex flake)
L: 31.0 mm; W: 26.0 mm; Th: 10.0 mm; Wt: 6 g
606295.215 E; 4527995.348 N; 173.440 m

Burial 34 (KG-048)

The grave-pit of Burial 33 was located in the north-western quadrant of square 6290/7990 (Fig. 35). It had been cut into the north-western corner of the Late Bronze Age Burial 2 and caused some damage to its pottery inventory. The grave-pit was oriented south-west to north-east and contained the exceptionally preserved skeleton of a male individual of high age (Fig. 162 and Fig. 163). The deceased was placed on his right side with the head in the south-west. The legs were slightly bent, and the arms were placed in front of the torso. No objects were found in the grave-pit. Unlike all other burials, the fill was noticeably harder and crumblier. The reasons for this difference remain unknown.

In many respects Burial 34 mirrors the nearby Burial 33. On the basis of radiocarbon analyses both can be

Fig. 162. Burial 34 (KG-048) and parts of the pottery inventory of Burial 2 (KG-044)

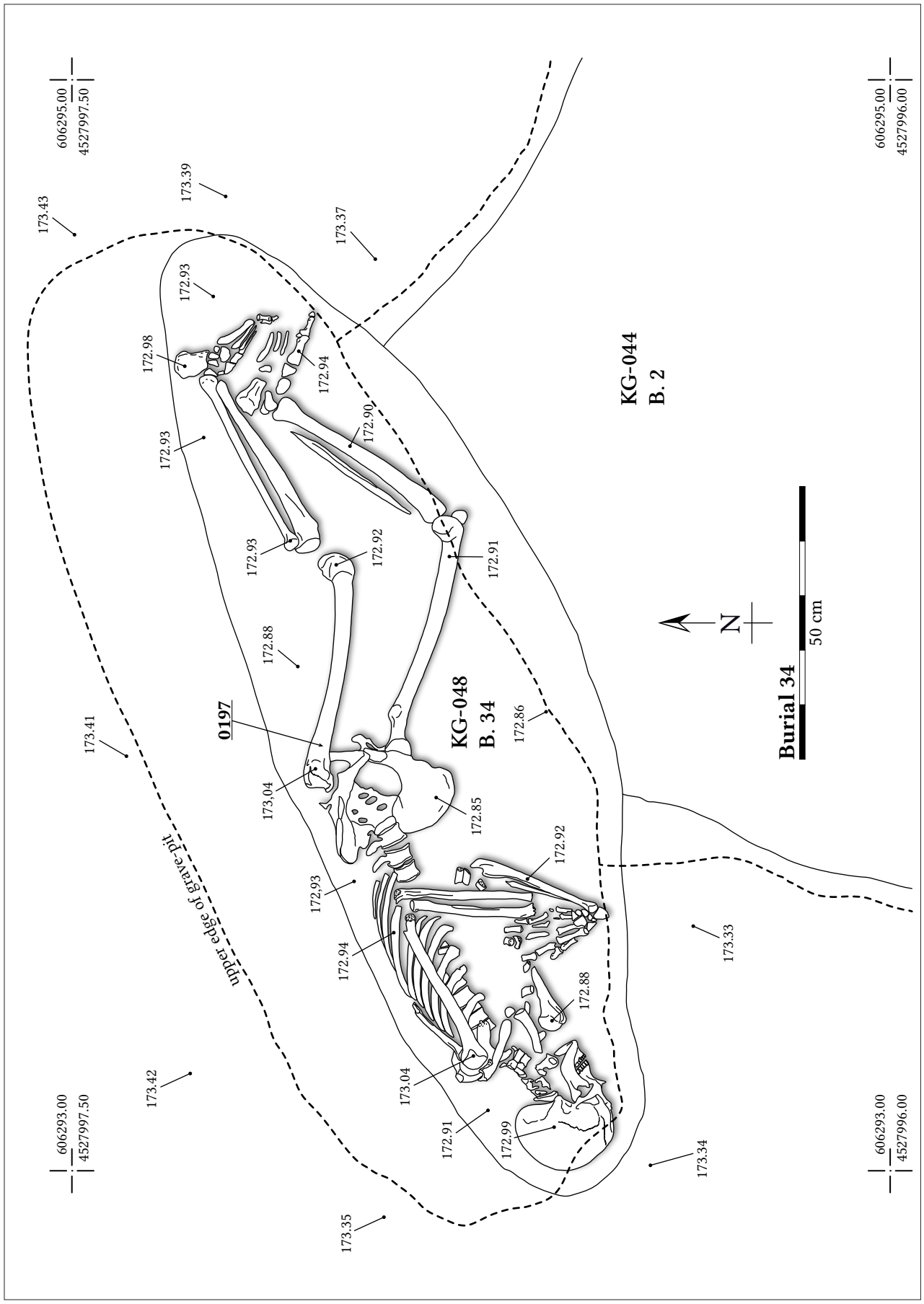

Fig. 163. Plan of Burial 34 (KG-048)

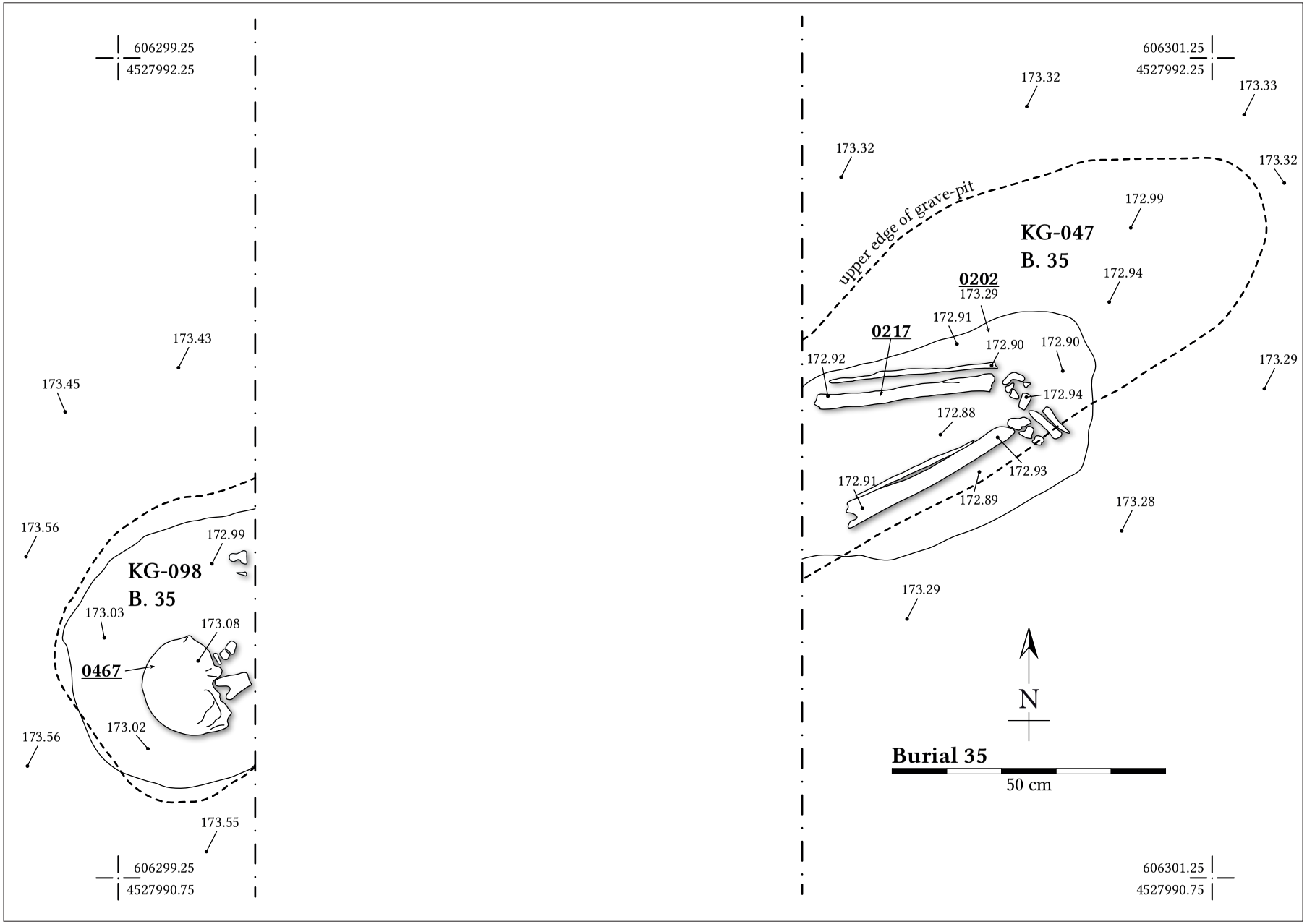

Fig. 164. Plan of Burial 35 (KG-047 & KG-098)

securely dated to the Medieval period. The sample from Burial 34 (MAMS-39413) gave a date in the 14th cent. AD.

Grave contents

KG-048-0197 (human bones) Table 10
Sex: male Table 16
Age class: Senilis

Burial 35 (KG-047 and KG-098)

Burial 35 was excavated in two steps: The eastern part (KG-047) in the south-western quadrant of square 6300/7990 (Fig. 35) was excavated in 2016. The grave-pit was oriented south-west to north-east and got considerably narrower towards the bottom (Fig. 164). Only the lower legs and feet of a skeleton (0217) could be excavated. The remaining body parts extended further south-west into the baulk between squares 6290/7990 and 6300/7990 and were not excavated. In 2017 the westernmost edge of the grave-pit of Burial 35 (KG-098) was located west of the baulk in square 6300/7990 (Fig. 164). The entire grave-pit was thus c. 2.35 m long (measured at the upper edge) and c. 0.5 m wide. At the western end, the skull and few vertebrae were found. Parts of the shoulder blade and left humerus were visible in the section of the baulk, but were not removed. Their position suggested that the deceased was laid down on its back.

The only object associated with Burial 35 was a broken brick (0202) that was found high up in the fill of the grave-pit. The date of the skeleton to the Medieval period (late 13th to the late 14th cent. AD) is based on a radiocarbon date (MAMS-39418).

Grave contents

KG-047-0217 & KG-098-0467 (human bones) Table 10
Sex: probably male Table 16
Age class: Adultas–Maturitas

Fill

KG-047-0202 (burnt mud-brick)
L: 150.0 mm; W: 100.0 mm; Th: 50.0 mm; Wt: 1094 g
606300.842 E; 4527991.745 N; 173.29 m

Fig. 165. Burial 36 (KG-050)

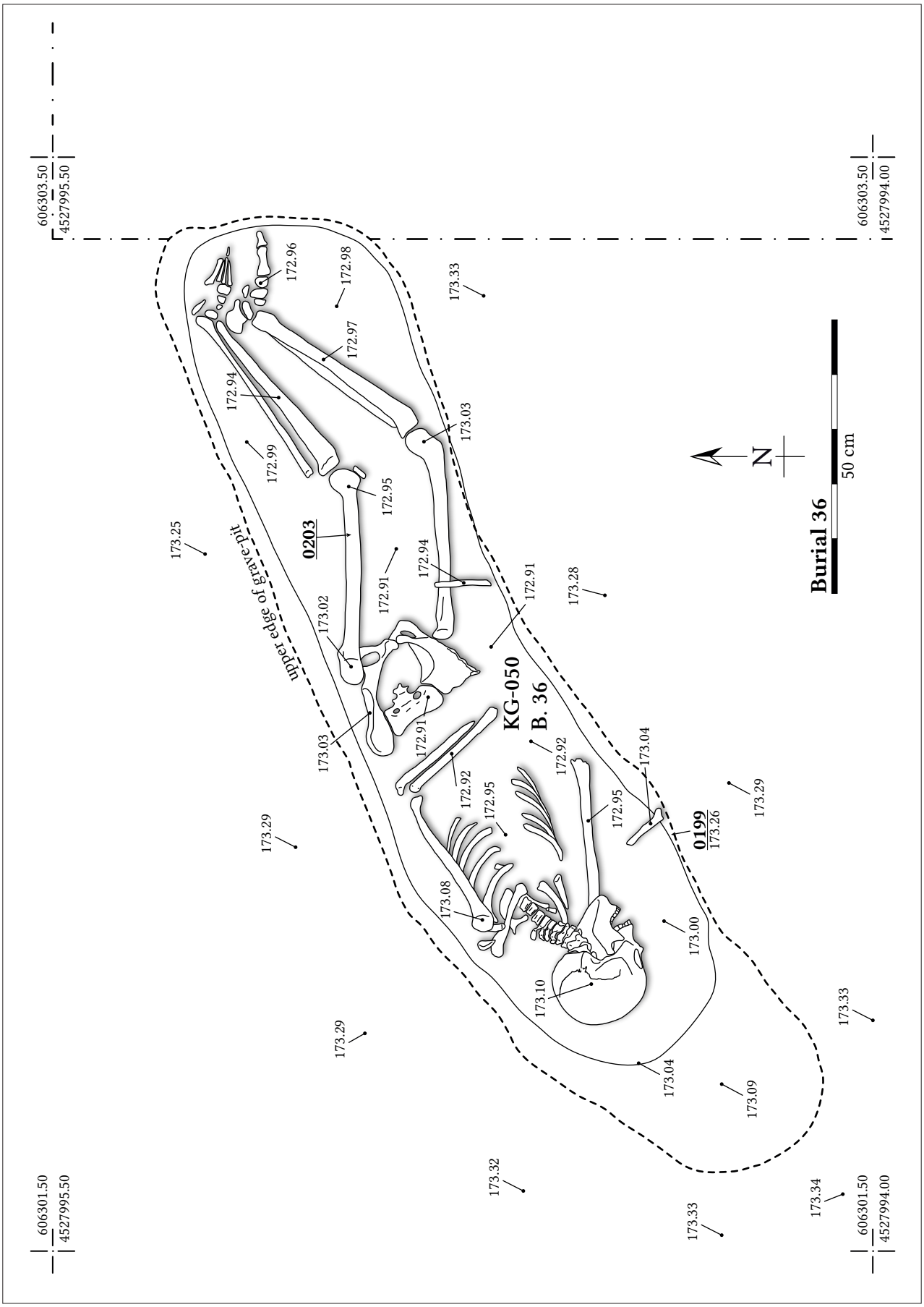

Fig. 166. Plan of Burial 36 (KG-050)

Burial 36 (KG-050)

Burial 36 was located in the south-western quadrant of square 6300/7990 immediately south of Pit-Complex A (Fig. 35). The grave-pit was narrow and oblong (c. 0.45 × 2 m), the ends were pointing towards south-west and north-east. The burial contained a skeleton with its head in the south-west, and the face was looking towards south-east (Fig. 165 and Fig. 166). The body was placed on his back, turned just a little bit to its right side. The legs were only slightly flexed. The left arm rested on the belly, the right lower arm was displaced probably by an animal and its radius was found on top of the right femur. The anthropological analysis of the bones showed that the deceased was male and buried at an age of 50 to 70 years. With the exception of a loose obsidian flake in the fill, that can be considered accidental, no burial gifts accompanied the body.

Although no radiocarbon sample was taken from that burial, the typical oblong shape of the grave-pit and the position of the body strongly resemble the other interments of the Medieval period, so that Burial 36 can quite safely be attributed to that phase.

Grave contents

KG-050-0203 (human bones)
Sex: male — Table 16
Age class: Maturitas–Senilis

Fill

KG-050-0199 (obsidian flake)
L: 33.2 mm; W: 30.4 mm; Th: 9.1 mm; Wt: 8 g
606302.261 E; 4527994.369 N; 173.256 m

Burial 37 (KG-052)

The grave-pit of Burial 37 cut through the northern parts of Burial 9 and caused damage to Burial 25 (square 6300/7990; Fig. 35). The burial was oriented south-west to north-east (Fig. 37 and Fig. 168). The upper edge of the grave-pit was of oval shape and much wider than the deeper portions of the pit at the southern side which contained the actual interment. The step created that way along the northern side might have served to facilitate the placement of the deceased. The body was laid down on his back in a stretched position. The head was in the south-west. The arms were tightly flexed and rested on the chest and on the right shoulder. No burial gifts accompanied the deceased. The fill contained an obsidian flake (0207) and a single bronze chain link (0206) identical to the examples found in the Late Bronze Age Burial 9. Considering the sequence of interments at this particular spot, it was clearly an accidental intrusion in the course of the disturbance of Burial 9.

The dating of Burial 37 to the Medieval period is based on a radiocarbon analysis (Beta-506515), revealing that the interment took place in the 14th cent. AD.

Grave contents

KG-052-0205 (human bones) — Table 10
Sex: probably male — Table 16
Age class: Infans II–Juvenis

Fill

KG-052-0206 (bronze chain)
L: 20.0 mm; W: 8.0 mm; Wt: 47 g

KG-052-0207 (obsidian flake)
L: 54.8 mm; W: 33.4 mm; Th: 3.4 mm; Wt: 21 g
606304.802 E; 4527992.071 N; 173.100 m

Burial 38 (KG-073)

The grave-pit of Burial 38 was located in the north-western corner of square 6300/7980 (Fig. 35). It had an oblong outline and was oriented east-west (Fig. 167 and Fig. 169). It contained a rather female individual that was laid down on its back with the head in the west, facing south. Arms and legs, too, were placed to the right of the body. Apart from the skull, the skeleton was not well preserved, e. g., the entire pelvic region was missing. Near the left arm in total 23 beads and a stone pendant were found that probably were part of a single necklace or bracelet that adorned the deceased. Except for a single bead (0504), that was made of carnelian and resembled

Fig. 167. Burial 38 (KG-073)

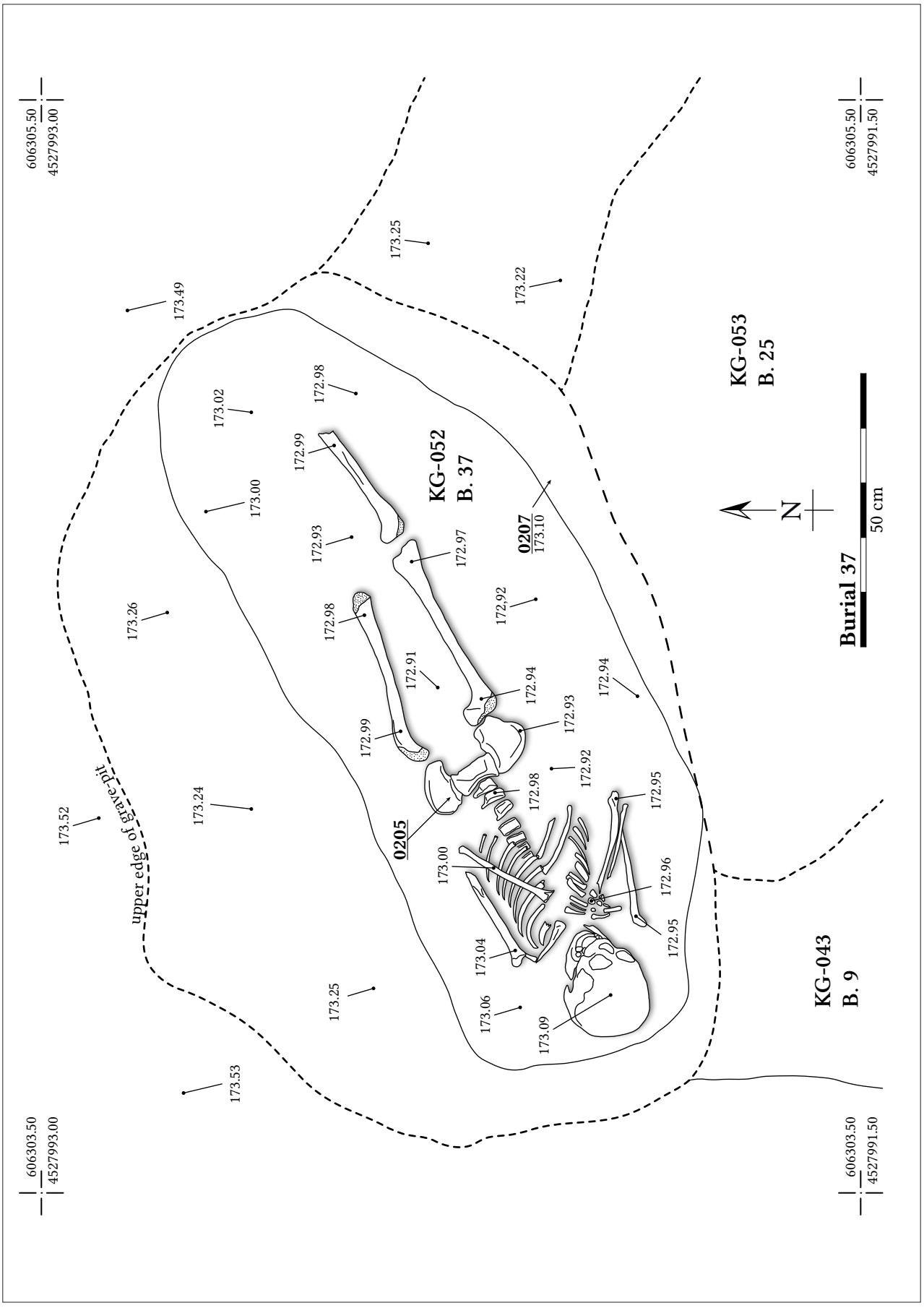

Fig. 168. Plan of Burial 37 (KG-052)

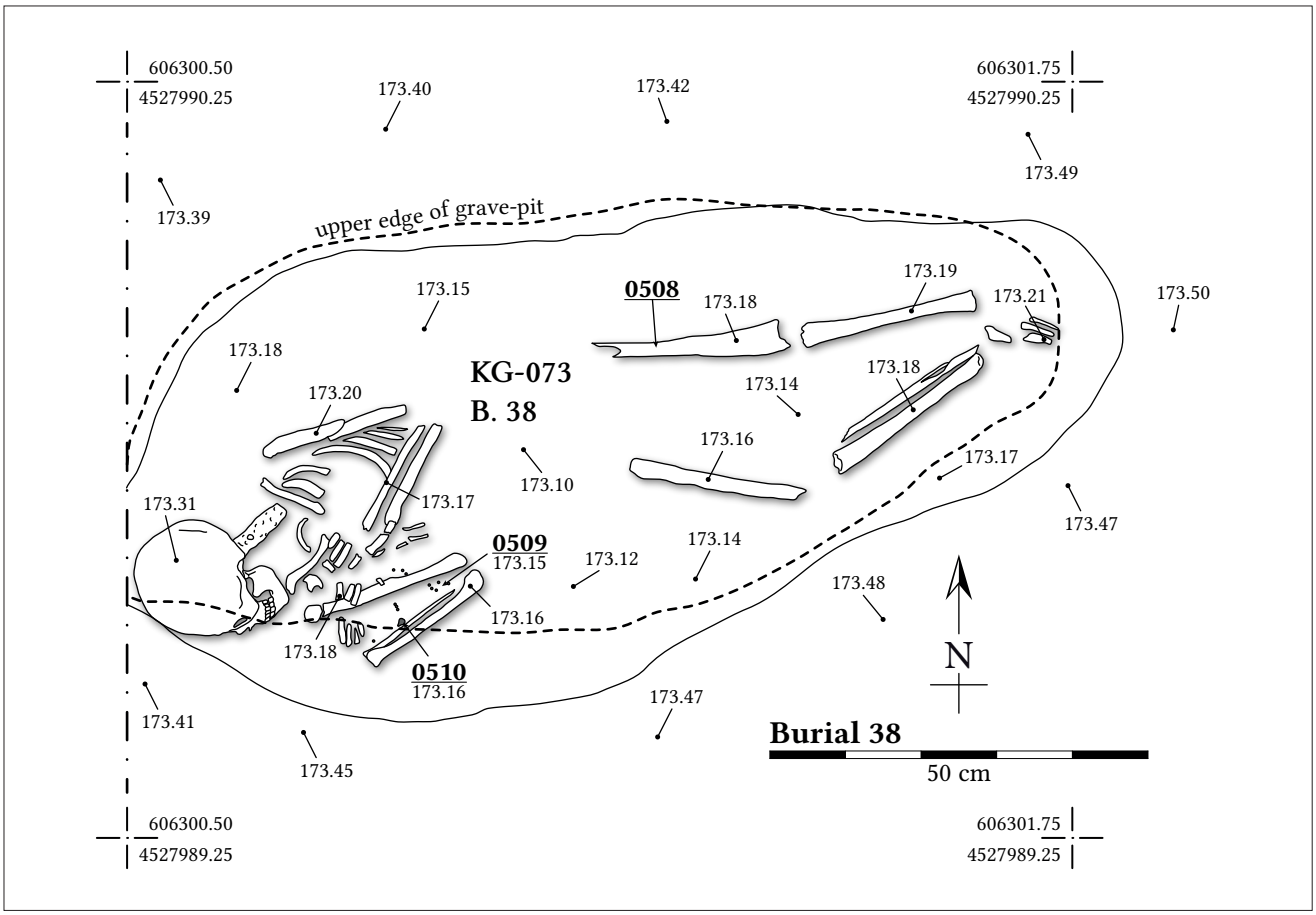

Fig. 169. Plan of Burial 38 (KG-073)

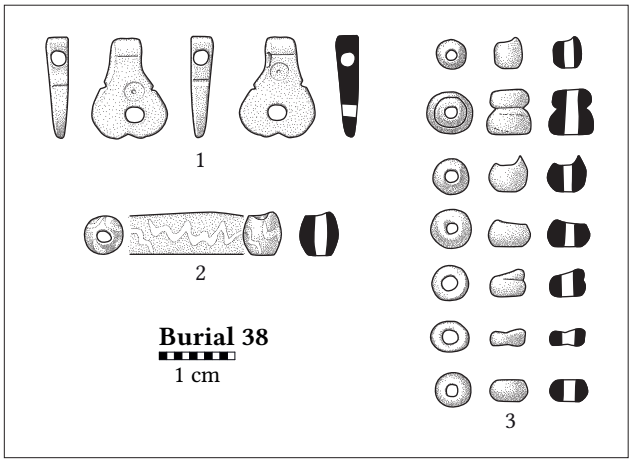

Fig. 170. Finds from Burial 38 (KG-073): 1 – stone pendant (0510); 2 – frit bead (0509a); 3 – frit beads (0509b)

beads, for example, from Burial 14, all other 22 beads (0509) were uniformly made of yellowish-white, at some places greenish frit and were ring- or barrel-shaped (Fig. 170, 2–3). Two pairs of those beads were fused by corrosion. Another, particularly large barrel-shaped bead was decorated with an inwrought oscillating line pattern (0509a, Fig. 170, 2). The drop-shaped pendant (0510) was made of a hard, dark stone (Fig. 170, 1). The narrow end was laterally perforated, so that a string could easily have been threaded through the hole. Two incised lines on both sides of the pendant indicated the direction of the perforation. The wide lower part of the pendant was perforated as well, but this seems to have been for decorative purposes only. On each side at different places was a circular incision with a point in the centre that might have been cut into the stone with the very same drill the actual perforations were executed. Two notches cut into the otherwise round edges on both sides and the bottom of the pendant.

The posture of the body and the shape of the grave-pit indicate a Medieval date. This assumption is confirmed by a radiocarbon date of the bones (Beta-506520) that puts Burial 38 into the 14th cent. AD.

Grave contents

KG-073-0508 (human bones)	Table 10
Sex: probably female	Table 16
Age class: Maturitas–Senilis	

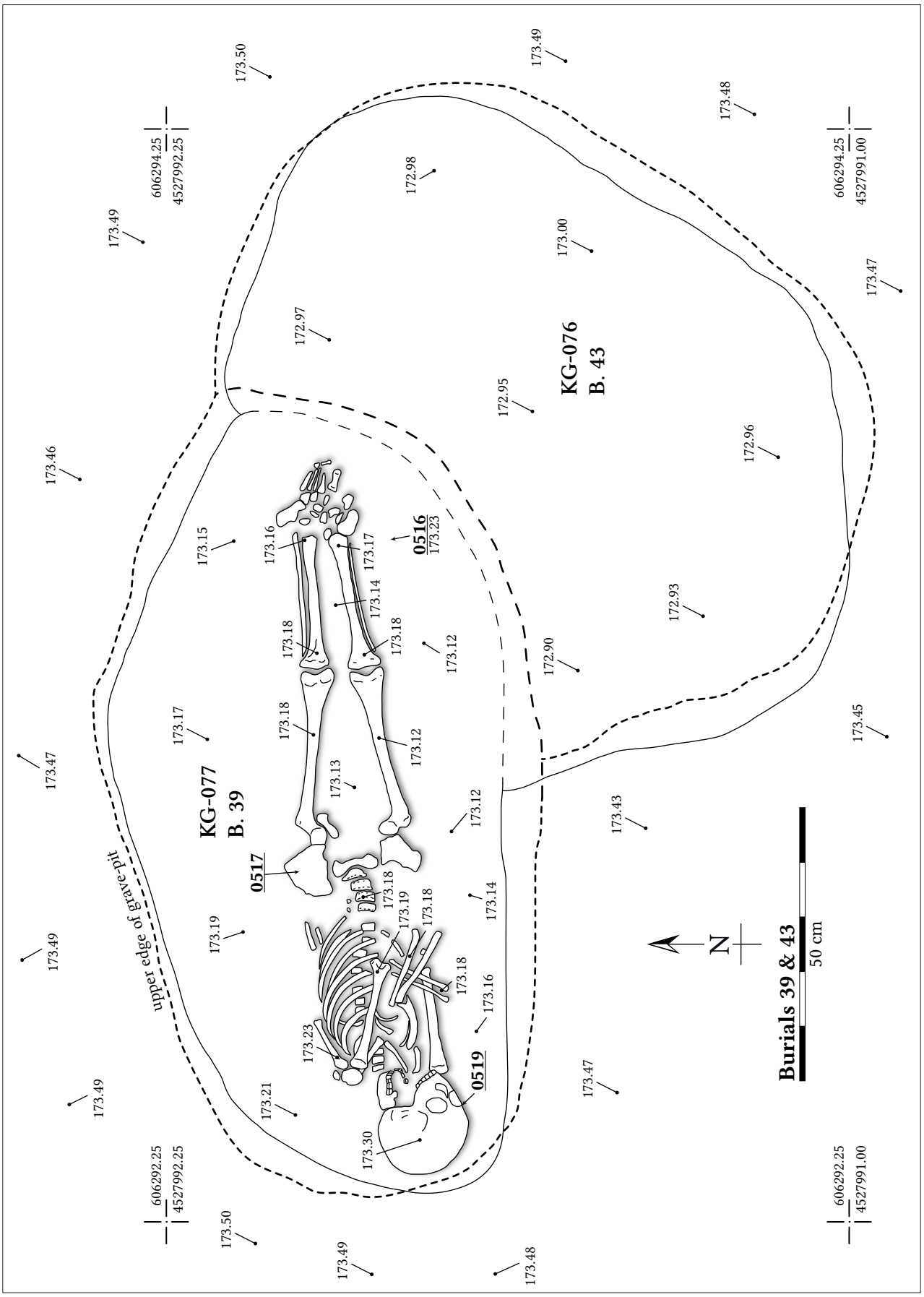

Fig. 171. Plan of Burials 39 (KG-077) and 43 (KG-076)

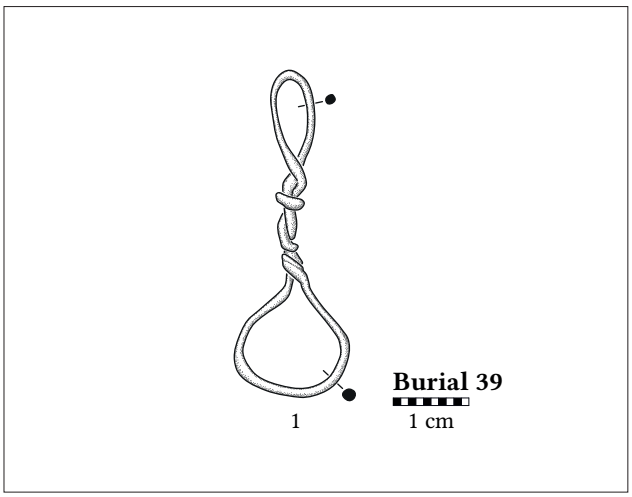

Fig. 172. Find from Burial 39 (KG-077): 1 – silver earring (0519)

KG-073-0504 (disc-shaped carnelian bead)
Diam: 5.7 mm; Th: 3.6 mm;
Hole. diam.: 1.6 mm; Wt: <1 g

KG-073-0510 (stone pendant) Fig. 170, 1
L: 13.0 mm; W: 10.0 mm; Th: 3.4 mm; Wt: <1 g
606300.861 E; 4527989.535 N; 173.159 m

KG-073-0509a (yellowish-white frit bead with oscillating decoration) Fig. 170, 2
Diam: 5.1 mm; H: 5.7 mm; Diam. hole: 1.6 mm; Wt: <1 g

KG-073-0509b (21 yellowish-white frit beads) Fig. 170, 3
Diam: 4.0–5.7 mm; Th: 2.0–4.4 mm;
Hole. diam.: 1.4–1.9 mm; Wt: 3 g

Fill

KG-073-0500 (obsidian flake)
L: 15.0 mm; W: 12.5 mm; Th: 5.0 mm; Wt: 1 g

Burial 39 (KG-077)

The grave-pit of Burial 39 was located in the south-western quadrant of square 6290/7990 (Fig. 35) and cut the north-western edge of Burial 43 (Fig. 171 and Fig. 173). The c. 1.5 m long and c. 0.75 m wide pit was oriented west-east. It contained a male individual of young age (Infans II) that was laid down in a stretched position on its back with the head in the west. The skull rested on its right side as did the arms that were crossed in front of the torso. This position of the body is particularly similar to Burial 37 that was dated on the basis of radiocarbon analyses to the 14th cent. BC. It is therefore likely that Burial 39 was also interred during the Medieval period.

While recovering the skull for anthropological analysis a silver wire was found still attached to the right side

Fig. 173. Burials 39 (KG-077) and 43 (KG-076)

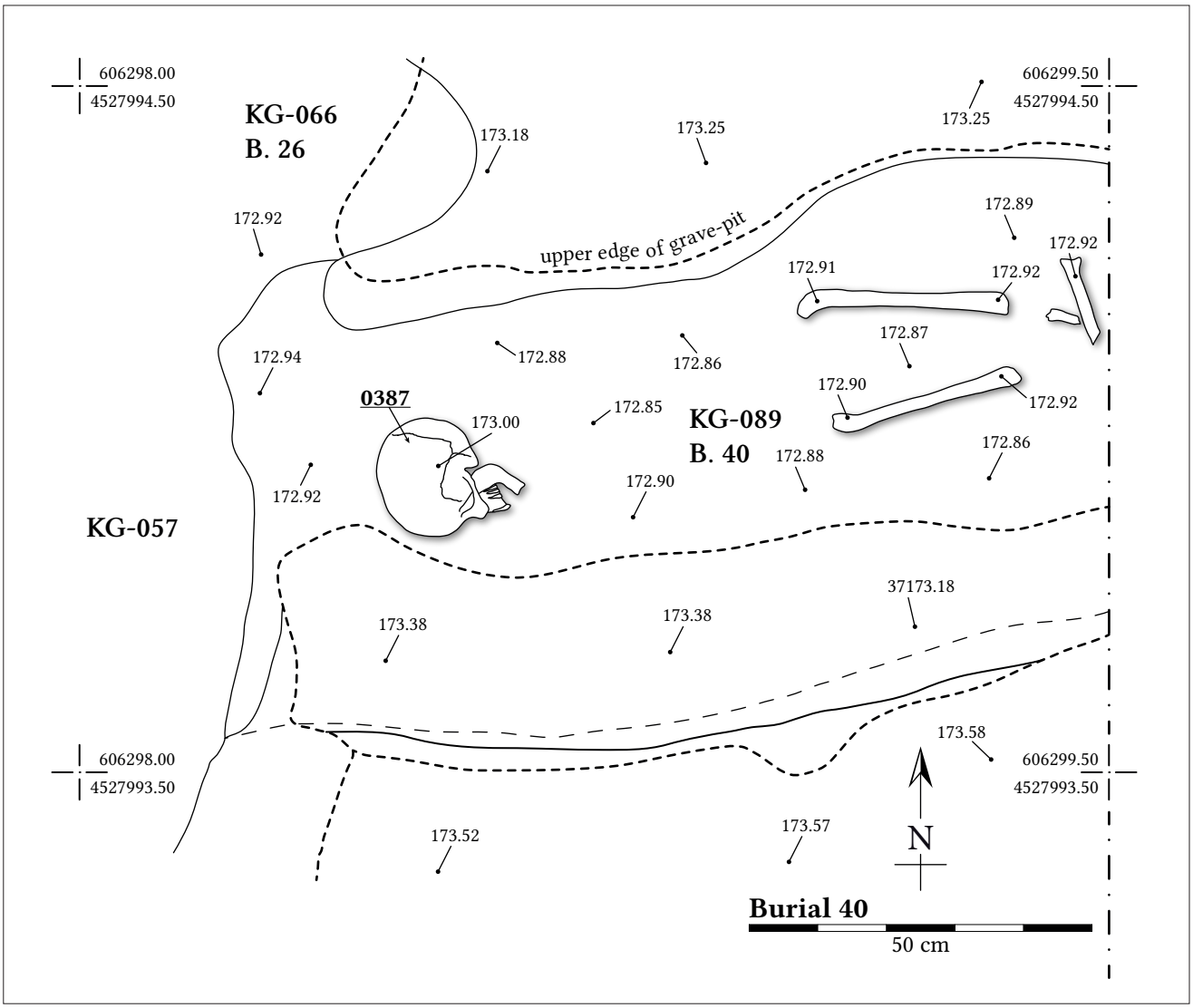

Fig. 174. Plan of Burial 40 (KG-089)

of the skull (0519). It was bent and twisted in the middle to form two loops at both ends (Fig. 172, 1). The position of the object suggests its use as earring or temporal ornament.

Grave contents

KG-077-0517 (human bones)
Sex: male
Age class: Infans II
Table 16

KG-077-0519 (silver earring)
L: 43.0 mm; W: 15.0 mm; Diam. wire: 1.0 mm; Wt: 1 g
found at the right side of the skull
Fig. 172, 1

Fill

KG-077-0516 (obsidian flake)
L: 29.0 mm; W: 23.0 mm; Th: 10.0 mm; Wt: 5 g
606293.497 E; 4527991.839 N; 173.228 m

Burial 40 (KG-089)

Burial 40 was located in the eastern part of Pit-Complex B (Fig. 43). The grave-pit was oblong and oriented west-east (Fig. 174). Only c. 1.2 m of the grave-pit could be excavated, because the eastern end extended beyond the limits of the excavation and was covered by the baulk between the squares 6290/7990 and 6300/7990. The width of the grave-pit varied between 40–50 cm at the upper edge and c. 65 cm at the bottom, where it was enlarged towards the south and undercut the surrounding soil. The burial contained a skeleton of unknown sex that could be assigned to the age class Infans II or Juvenis. Only half of the skull and some long bones could be recovered from the grave (parts of the lower extremities might be still concealed below the baulk). The skull was lying in

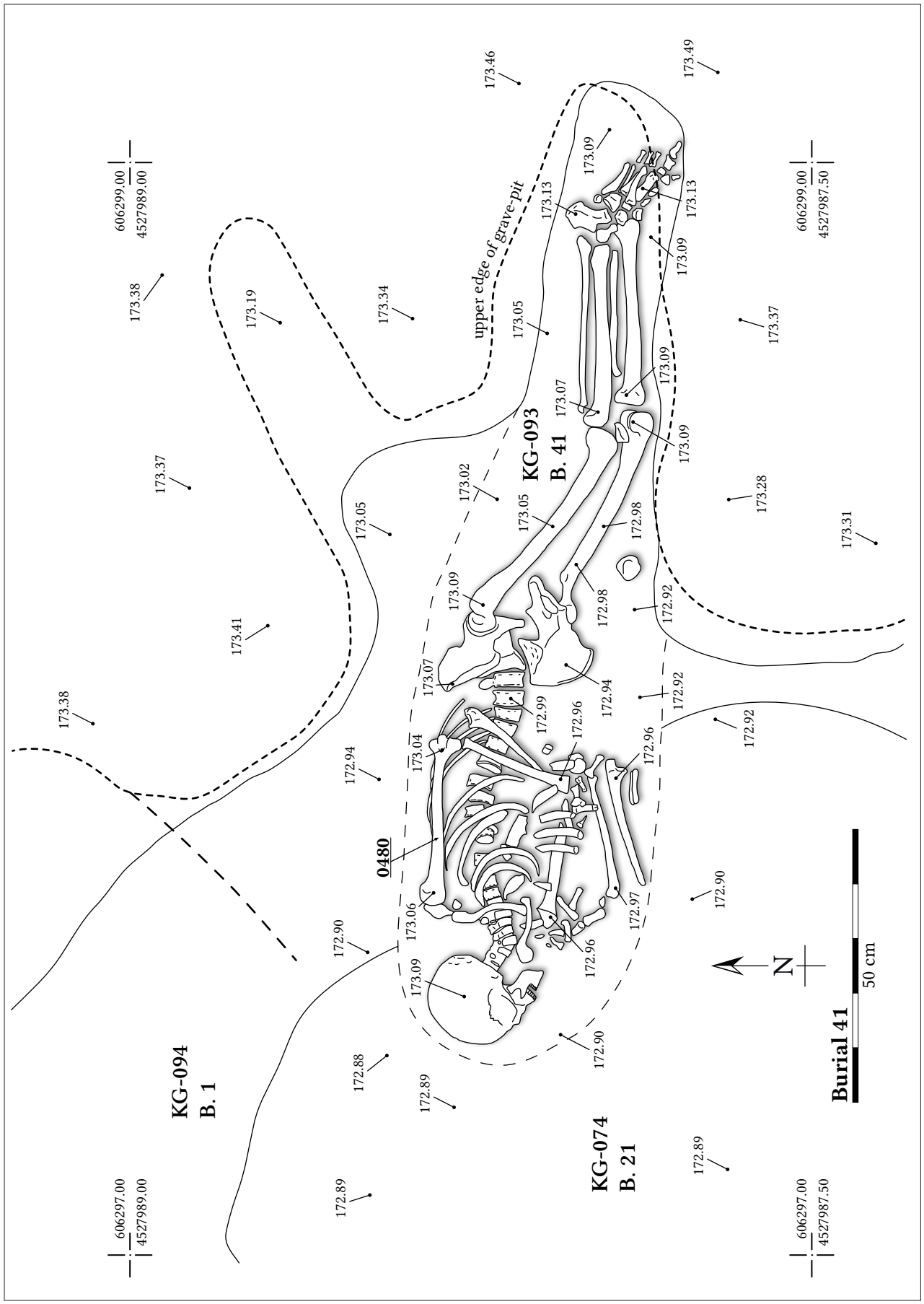

Fig. 175. Plan of Burial 41 (KG-093)

Fig. 176. Burial 41 (KG-093)

the west on its right side. The parallel alignment of the two femoral bones indicates a stretched position. Shape and orientation of the grave-pit comply with the burials of the Medieval period.

Grave contents

KG-089-0387 (human bones)
Sex: could not be determined
Age class: Infans II–Juvenis

Table 16

Burial 41 (KG-093)

Burial 41 was dug into the easternmost portion of Pit-Complex C-4 (Fig. 44). The edge of the grave-pit could only be securely detected at its eastern end, where it was 20–25 cm wide, just enough to enable the placement of the legs of the deceased (Fig. 175 and Fig. 176). Although the outline of the pit in the west, where it overlapped the Late Antique Burial 21, was not distinguishable from the surrounding fill, it was probably just big enough to place the body. The skeleton was oriented west-east with its head in the west, facing south. The body was laid down in a stretched position in its right side. The left arm was bent at a right angle and rested on the belly. The right

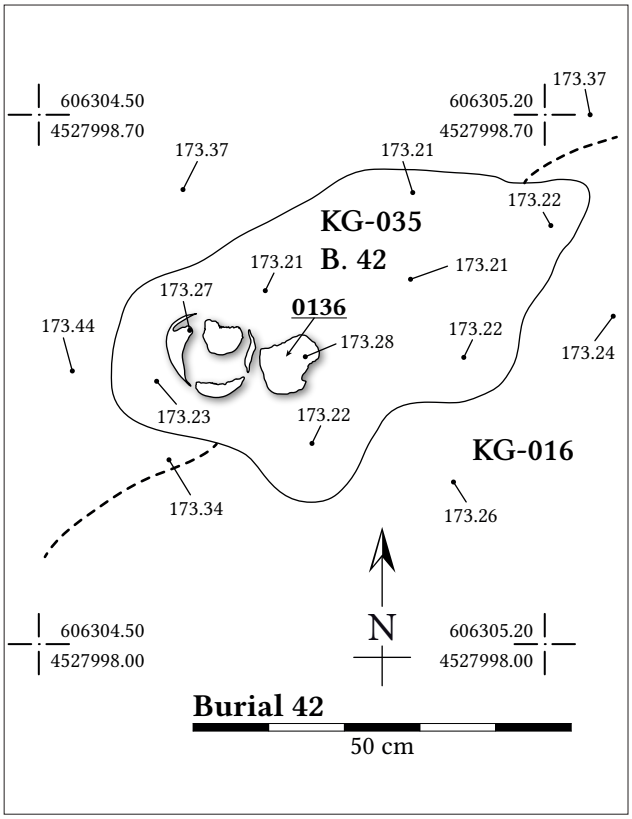

Fig. 177. Plan of Burial 42 (KG-035)

arm was tightly flexed, so that the hand was close to the left shoulder. Judging from the anthropological features, it was a 50–60-year-old male individual. No burial gifts were placed aside the deceased.

The narrow, oblong shape of the grave-pit and the position of the body suggests a Medieval date for Burial 41.

Grave contents

KG-093-0480 (human bones)
Sex: male — Table 16
Age class: Maturitas

Burial 42 (KG-035)

Burial 42 was cut through the north-western edge of the Chalcolithic trash-pit KG-016 in square 6300/7990 (Fig. 41). The grave-pit had an irregular outline and measured c. 35 × 65 cm (Fig. 40 and Fig. 177). In its western half were parts of the skull and two vertebral arches of an infant of about 3–9 months of age. No objects accompanied the body.

It is not possible to place Burial 42 securely within one of the three chronological stages of the cemetery.

Grave contents

KG-035-0136 (human bones)
Sex: could not be determined — Table 16
Age class: Infans I

Burial 43 (KG-076)

Burial 43 was located in the south-western quadrant of square 6290/7990 (Fig. 41). Although the grave-pit was of considerable size and depth, no coherent remains of an inhumation could be detected. The interpretation as a burial, however, is justified by the presence of a few finger bones and a vertebra scattered throughout the fill of the pit. Since the north-western edge of Burial 43 was cut by the Medieval Burial 39 (Fig. 171 and Fig. 173), it is possible that the interment of the latter was responsible for the disturbance. Because of the lack of any datable archaeological material in Burial 43, however, the stratigraphic connection between these two burials alone, does not allow for a secure attribution to any of the three occupation phases.

Grave contents

KG-076-0515 (human bones)
Sex and age class could not be determined — Table 16

Burial 44 (KG-092)

The remains of Burial 44 were found in the north-western corner of the south-western quadrant of square 6300/8000 (Fig. 41), only a few centimetres below the modern surface. Therefore, no grave-pit could be discerned, and the bones were in a very bad condition and highly fragmented. Nevertheless, the general alignment of the bones suggests a west-east oriented burial with the head in the west and presumably stretched legs (Fig. 178). The sex could not be determined, but the individual appears to have been of rather high age (Maturitas–Senilis). The bad state of preservation and the lack of further evidence do not permit a dating of the burial.

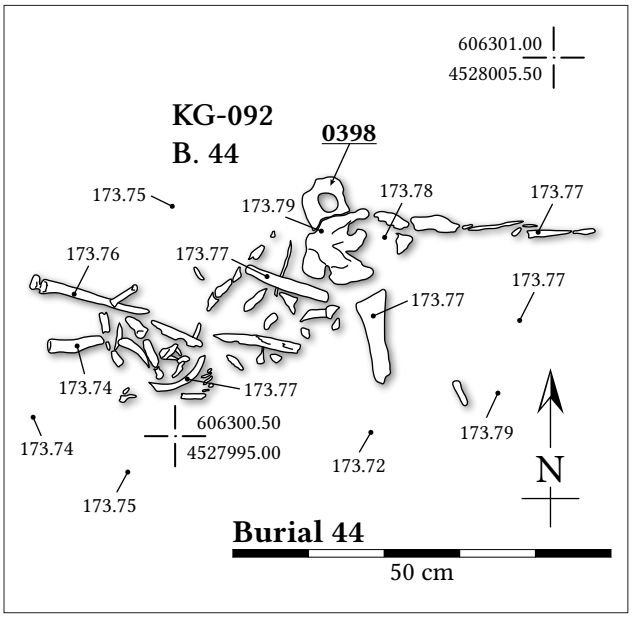

Fig. 178. Plan of Burial 44 (KG-092)

Grave contents

KG-092-0398 (human bones)
Sex: not determined — Table 16
Age class: Maturitas–Senilis

Burial 45 (KG-096)

Burial 45 was located in Section 1 of Pit-Complex C (Fig. 44). Only its western half (c. 70 cm long) was clearly delimited from the surrounding soil (Fig. 67 and Fig. 68). There, the grave-pit was only c. 55 cm wide and appears to have been oblong with a west-north-west/east-south-east orientation. In this part of the grave-pit, some rib

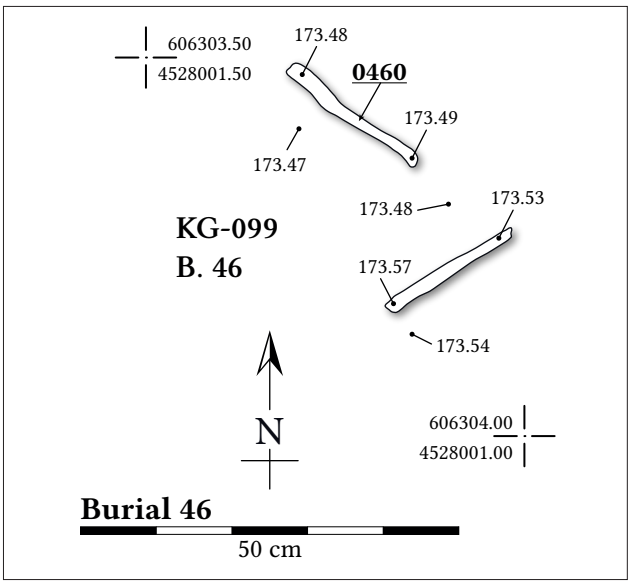

Fig. 179. Plan of Burial 46 (KG-099)

fragments and two teeth were found which suggest that the body was laid down with its head in the west. The eastern half of the grave-pit extended into the fill of Burial 6, where a single tooth (0468) was found that might originate from Burial 45. It could, however, not be determined, if the grave-pit was cut into the fill of Burial 6 or vice versa. Although the former appears more likely, because the narrow, oblong shape of the preserved portion of the grave-pit corresponds to burials of the Late Antique period and even more to the Medieval period, the evidence does not allow for a secure dating.

Grave contents

KG-096-0445 (human bones)
Sex and age class could not be determined Table 16

Burial 46 (KG-099)

In the south-western quadrant of square 6300/8000 (Fig. 41), in the fill of the pit KG-100, but c. 75 cm above its bottom, the radius and ulna of a human left arm were found close together (Fig. 179). These bones were not *in situ* anymore and they probably originate from a burial nearby that was destroyed by the large pit KG-100. The latter has caused a substantial disturbance in the southern half of square 6300/8000, at a time very likely long after the use of Tepe 5 as a burial ground.

Grave contents

KG-099-0460 (human bones)
Sex and age class could not be determined Table 16

V. Morphological and histological survey of human remains from Tepe 5

Andrea Göhring

V.1 Introduction

Anthropological analyses of human skeletal remains provide an indispensable insight into life in previous times. Written reports are often rare and usually only forceful personalities got a chance to speak, while the remaining majority of a population remains silent. However, human skeletal remains give a variety of information, not only on sex and age, but also on past living conditions and diseases. Similar studies on human remains from archaeological burials in Azerbaijan are rare. Thus, the aim of this anthropological survey was to investigate the human remains from the graveyard at Tepe 5 (Karacamirli) in order to gather information about the life and death of the people buried there. This survey supplies necessary primary data for the archaeological interpretation.

V.2 Methods

V.2.1 Morphological analysis

The skeletons were morphologically examined by this author in the field season of 2017. The human remains of the previous year's campaign had been stored locally and were included in the analysis.

Bones were only partially cleaned with water, where necessary. The morphological survey included the state of preservation, the inventory of preserved bones, sex and age determination, the examination of the joints, the bone surface, and the teeth, cranial and postcranial measurements, the examination of diseases or pathologies manifested on the skeleton, and the documentation of both epigenetic and acquired variations of bones and teeth.

Sex was determined on a variety of skeletal criteria of the pelvis, the skull, and the femur listed in Table 11 (see e. g. Cunningham et al. 2016; Grupe et al. 2015; Herrmann et al. 1990; Schaefer et al. 2009; White/Folkens 2005). Depending on the age of the individual different criteria were used (see Table 11). Sex-specific criteria of the pelvis are more informative than criteria of both the skull and the femur. This can be easily explained by the functional sex-specific difference in the pelvis, while both skull and femur reflect the overall robustness of the skeleton. Individuals were classified as »probably male« and »probably female«, respectively, if the pelvic features could not be examined. If too little or no criteria could be examined the sex remained indetermined (»nd«).

Age at death of adult individuals was determined using the epiphyseal and apophyseal closure of bones after Schaefer et al. (2009), the state of the Facies symphysialis (Acsádi/Nemeskéri 1970), the state of the Facies auricularis (Buckberry/Chamberlain 2002), the closure of the cranial sutures (Herrmann et al. 1990), as well as the dental chart (e. g. intravital tooth loss, abrasion, third molar). In the case of non-adult individuals epiphyseal and apophyseal closure (Schaefer et al. 2009), tooth development (AlQahtani et al. 2010), and coalescence of parts of the skull (e. g. fontanel, mandible), the vertebral column, and the pelvis were examined (see Herrmann et al. 1990; Schaefer et al. 2009). In addition, long bone measures can provide information on the age at death (see Stloukal/Hanakova 1978).

Individuals are grouped into six different age classes: Infans I (0–6 years), Infans II (7–12 years), Juvenis (13–19 years), Adultas (20–39 years), Maturitas (40–59 years), and Senilis (60–x years) (see e. g. Herrmann et al. 1990).

Long bones and vertebrae were investigated with respect to changes to the joints due to age, work load, and

ADULTS	criterium	male	female
pelvis	Overall appearance	high, narrow	low, broad
	Pelvic inlet	heart-shaped	oval
	Incisura ischiadica major	narrow	wide
	Sulcus praeauricularis	flat/missing	deeply grooved
	Arc composé	one arc	two arcs
	Angulus subpubicus	narrow	wide
	Linea arcuata	does not cross Facies auricularis	crosses Facies auricularis
	Crista iliaca	S-curvature	slight curvature
	Fossa iliaca	deep, narrow	low, broad
	Subpubic concavity	linear, convex	concave
	Ramus ischio-pubicus	rounded	sharp edge
	Arcus ventralis	missing	present
	Index ischiopubicus	52–71	68–91
skull	Forehead	sloping	steep
	Glabella	distinct	bland
	Processus mastoideus	big	small
	Crista supramastoidea	distinct	bland
	Arcus superciliaris	strong	bland
	Orbita	rather rectangular	rather rounded
	Margo supraorbitalis	rounded	sharp-edged
	Thickness of Protuberantia occipitalis externa	> 1.1 cm	< 1.1 cm
	Lineae nuchae	thick cortical bone	thin cortical bone
	Tuber frontale	missing	present
	Tuber parietale	missing	present
mandible	Mentum region	broad, square chin	narrow, pointed chin
	Incisor region	U-shaped	parabolic
	Gonion region	everted	not everted
	Gonion angle	strongly everted	hardly everted
femur	Diameter of Caput femoris	> 4.45	< 4.35
NON-ADULTS	criterium	male	female
pelvis	Incisura ischiadica major	< 90°	> 90°
	Depth of Incisura ischiadica major	rather deep	rather flat
	Arc composé	one arc	two arcs
	Crista iliaca	S-curvature	slight curvature
mandible	Mentum region	broad, square chin	narrow, pointed chin
	Incisor region	U-shaped	parabolic
	Gonion region	everted	not everted

Table 11. Criteria for sex determination of adult and non-adult skeletons

trauma, respectively (long bones: 0 = nd; 1 = no changes; 2 = minor rim, osteophytes < 3 mm; 3 = major rim, osteophytes > 3 mm; 4 = 80 % of the joint is damaged, stiffened joint; 5 = synostosis; vertebrae: 0 = nd; 1 = no changes; 2 = minor changes; 3 = major changes). Furthermore, bone surfaces were examined. This allows the detection of periostitis of different severity (0 = nd; 1 = no changes; 2 = longitudinal stripes; 3 = single and separate locations, less than 25 % of the long bone affected; 4 = moderate periostitis, less than 50 % of the long bone affected; 5 = more than 50 % of the long bone affected, deformation; 6 = osteomyelitis; 7 = associated with a fracture).

In addition, a tooth chart was created for each individual examining the tooth status (e. g. intra-vital tooth loss, post-vital tooth loss, dental germ), the state of calculus (0 = nd; 1 = no calculus; 2 = minor calculus; 3 = moderate calculus; 4 = major calculus; after Brothwell 1981), caries (0 = nd; 1 = no caries; 2 = chalky white, isolated brownish discoloration; 3 = clear lesion of the enamel, dentin not affected; 4 = pulp cavity infected, dental alveolus not affected; 5 = tooth and paradontium infected; after Grupe et al. 2015), abrasion (state 0 to 8; after Smith 1984), and linear enamel hypoplasia (LEH; 0 = nd; 1 = no hypoplasia; 2 = thin line visible, however not tangible; 3 = clearly tangible line at tooth surface; 4 = severe damage, visible and tangible; after Schultz 1988; see Massler et al. (1941) for the estimation of age at LEH formation).

Cranial and postcranial measurements were conducted according to Herrmann et al. (1990) (see Table 12 and Table 14) This permits the calculation of a variety of indices (see Table 13 and Table 15), which can help to identify different groups of individuals. Furthermore, body height was estimated after Trotter and Gleser (1958) for

	cranial measure	section	tool
1	Maximum Cranial Length	g-op	sp. c.
2	Cranial Base Length	n-ba	sp. c.
8	Maximum Cranial Breadth	eu-eu	sp. c.
9	Minimum Frontal Breadth	ft-ft	sl. c.
10	Maximum Frontal Breadth	co-co	sp./sl. c.
12	Biasterionic Breadth	ast-ast	sl. c.
17	Basion–Bregma Height	ba-b	sp. c.
20	Auricular–Bregmatic Height	po-b	sl. c.
23	Horizontal Glabella Diameter		t. m.
24	Transverse Arc	po-po	t. m.
25	Nasion–Opisthion Arc	n-o	t. m.
26	Frontal Arc	n-b	t. m.
27	Parietal Arc	b-l	t. m.
28	Occipital Arc	l-o	t. m.
29	Frontal Chord	n-b	sl. c.
40	Basion–Prosthion Length	ba-pr	sp./sl. c.
45	Bizygomatic Breadth	zy-zy	sp./sl. c.
47	Morphological Facial Height	n-gn	sl. c.
48	Nasion–Prosthion Height	n-pr	sl. c.
51	Orbital Breadth	mf-ek	sl. c.
52	Orbital Height		sl. c.
54	Nasal Breadth (max. breadth)		sl. c.
55	Nasal Height	n-ns	sl. c.
66	Bigonial Height	go-go	sl. c.
69	Chin Height	id-gn	sl. c.
70	Maximum Ramus Height		sl. c.

Table 12. Overview of the cranial measures including sections of measurement and measurement tools (after Herrmann et al. 1990). Abbreviations: traditional cranial landmarks: ast = asterion, b = bregma, ba = basion, co = coronale, eu = euryon, ft = frontotemporale, g = glabella, gn = gnathion, go = gonion, id = infradentale, l = lambda, mf = maxillofrontale, ec = ectoconchion, n = nasion, ns = nasospinale, o = opisthion, op = opisthocranion, po = porion, pr = prosthion, zy = zygion; measurement tools: sp. c. = spreading caliper; sl. c. = sliding caliper; t. m. = tape measure (see e. g. Herrmann et al. 1990; Martin 1914; Martin/Saller 1957; 1959; Steele/Bramblett 1988)

Cranial Index	**8***100/**1**
Basio-Bregmatic Longitudinal Index	**17***100/**1**
Basio-Bregmatic Transversal Index	**17***100/**8**
Porio-Bregmatic Longitudinal Index	**20***100/**1**
Transverse Frontal Index	**9***100/**10**
Transverse Fronto-Parietal Index	**9***100/**8**
Sagittal Fronto-Parietal Index	**27***100/**26**
Sagittal Frontal Index	**29***100/**26**
Jugo-Frontal Index	**9***100/**45**
Jugo-Mandibular Index	**66***100/**45**
Transverse Cranio-Facial Index	**45***100/**8**
Total Facial Index	**47***100/**45**
Superior Facial Index	**48***100/**45**
Orbital Index	**52***100/**51**
Nasal Index	**54***100/**55**

Table 13. Cranial indices calculated from cranial measures (after Herrmann et al. 1990; Martin 1914; Martin/Saller 1957; 1959). Numbers in bold indicate cranial measures (see Table 12)

	postcranial measure	measurement tool
	humerus	
1	Maximum Humerus Length	sliding caliper
2	Total Humerus Length	sliding caliper
5	Maximum Diameter of humerus diaphysis at midshaft	sliding caliper
6	Minimum Diameter of humerus diaphysis at midshaft	sliding caliper
7	Minimum Diameter of humerus diaphysis	tape measure
9	Transverse Diameter of humeral head	sliding caliper
10	Sagittal Diameter of humeral head	sliding caliper
	radius	
1	Maximum Radius Length	sliding caliper
1b	Parallel Radius Length	sliding caliper
2	Functional Radius Length	sliding caliper
3	Minimum Diameter of radius diaphysis	tape measure
	ulna	
1	Maximum Ulna Length	sliding caliper
2	Functional Ulna Length	sliding caliper
3	Minimum Diameter of ulna diaphysis	tape measure
	femur	
1	Maximum Femur Length	sliding caliper
2	Total Femur Length	sliding caliper
7	Transversal Diameter of the femur diaphysis at midshaft	sliding caliper
6	Sagittal Diameter of the femur diaphysis at midshaft	sliding caliper
9	Transversal Diameter of femur diaphysis at upper femoral shaft	sliding caliper
10	Sagittal Diameter of femur diaphysis at upper femoral shaft	sliding caliper
18	Vertical Diameter of Caput femoris	sliding caliper
19	Transversal/Sagittal Diameter of Caput femoris	sliding caliper
	tibia	
1	Total Tibia Length	sliding caliper
1b	Length	sliding caliper
8a	Maximum Diameter of tibia diaphysis at midshaft	sliding caliper
9a	Transversal Diameter of tibia diaphysis at midshaft	sliding caliper
10b	Minimum Diameter of tibia diaphysis	tape measure

Table 14. Overview of the postcranial measures including measurement tools for humerus, radius, ulna, femur, and tibia (after Herrmann et al. 1990; Martin 1914; Martin/Saller 1957; 1959)

adults and after Telkkä et al. (1962) for non-adult individuals.

In the past craniometry was largely used by typologists who attempted to define human »races« on the basis of cranial measurements (for a historical review see e. g. Hefner et al. 2016; von Cramon-Taubadel 2014). Due to this abuse of the method, craniometry is still under debate today. However, craniometry can be used, when stripped of its »racial« connotations, to consider cranial variation between groups. From a population genetic

point of view the morphological appearance of several cranial regions is genetically influenced (e. g. Harvati/Weaver 2006; Manica et al. 2007; Smith 2009). Several studies showed that some cranial measures are also correlated with both geographical and climatic variables, i. e. latitude or temperature (e. g. Beals et al. 1983; Beals et al. 1984; Harvati/Weaver 2006; Hubbe et al. 2009; Manica et al. 2007; Roseman 2004). For example, populations adapted to colder climates show a smaller nasal breadth, a higher nasal height, a smaller facial height, a shorter head, and a broader braincase in accordance with the rules of Bergman and Allen (Hubbe et al. 2009; Roseman 2004).

In the following, an overview of the classification of relevant cranial and postcranial indices is given: The cranial index (Table 13) indicates the size of the head classified as dolichocephalic (70.0–74.9, long head), mesocephalic (75.0–79.9), and brachycephalic (80.0–84.9, short head). The braincase is described using the basio-bregmatic longitudinal, the basio-bregmatic transversal index, and the porio-bregmatic longitudinal index, respectively (Table 13). The braincase can be classified as chamaecranic (≤ 69.9; low braincase), orthocranic (70.0–74.9), or hypsicranic (≥ 75.0; high braincase) according to the basio-bregmatic longitudinal index, while the braincase can also be tapeinocranic (≤ 91.9; broad braincase), metriocranic (92.0–97.9) or acrocranic (≥ 98.0; narrow braincase) with respect to the basio-bregmatic transversal index. The porio-bregmatic longitudinal index classifies the braincase as chamaecranic (≤ 57.9; low braincase), orthocranic (58.0–62.9), and hypsicranic (≥ 63.0; high braincase). The facial skull can be described mainly using four indices, namely the total facial index, the superior facial index, the orbital index, and the nasal index (Table 13). The face can be classified as euryprosopic (80.0–84.9; short face), mesoprosopic (85.0–89.9), and leptoprosopic (90.0–94.9; long face), respectively, according to the total facial index. With respect to the superior facial index the forehead is classified as euryene (45.0–49.9; broad upper face), mesene (50.0–54.9), and leptene (55.0–59.9; narrow upper face). Furthermore, the orbital index describes the position of the orbits as chamaeconch (≤ 75.9; low orbits), mesoconch (76.0–84.9), and hypsiconch (≥ 85.0; high orbits). The nose is classified as leptorrhine (≤ 46.9; narrow nose), mesorrhine (47.0–50.9), or chamaerrhine (51.0–57.9; broad nose). In addition, the forehead can be more closely described using the transverse frontal index as well as the transverse fronto-parietal index (Table 13). According to the transverse frontal index the forehead can be described as rather spherical (< 80) or more oval (> 100). The transverse fronto-parietal index classifies the forehead as stenometopic (≤ 65.9; narrow forehead), metriometopic (66.0–68.9), and eurymetopic (≥ 69.0; broad forehead). Both the sagittal fronto-parietal index and the sagittal frontal index describe the appearance of the frontal bone (Table 13). The forehead is described as orthometopic (< 90; steep (spherical) forehead) or chamaemetopic (> 90; flat forehead). Finally, the facial appearance is described by the jugo-frontal index as well as the jugo-mandibular index (Table 13). The jugo-frontal index shows a striking sex-specific difference. The face is classified as narrow to broad according to both the jugo-frontal index (narrow: ♂: 70.0–74.9, ♀: 72.0–76.9; medium: ♂: 75.0–79.9, ♀: 77.0–81.9; broad: ♂: 80.0–84.5, ♀: 82.0–86.9) and the jugo-mandibular index (narrow: ♂: 70.0–74.9, ♀: 68.0–72.9; medium: ♂: 75.0–79.9, ♀: 73.0–77.9; broad: ♂: 80.0–84.5, ♀: 78.0–82.9). If these two indices are very similar to each other and at the same time show high values, the contour of the face becomes quadratic and angular (Herrmann et al. 1990; Martin 1914; Martin/Saller 1957; 1959; Steele/Bramblett 1988).

humerus	robustness index	**7***100/**1**
radius	robustness index	**3***100/**2**
ulna	robustness index	**3***100/**2**
femur	index platymericus	**10***100/**9**
	robustness index	**(6+7)***100/**2**
tibia	index cnemicus	**9a***100/**8a**
	robustness index	**10b***100/**1**

Table 15. Postcranial indices calculated from postcranial measures (after Herrmann et al. 1990). Numbers in bold indicate cranial measures (see Table 14)

The postcranial index platymericus (Table 15) is used in order to classify a femur as platymeric (75.0–84.9), eurymeric (85.0–99.9), and stenomeric (≥ 100.0). In case of the index cnemicus (Table 15) the tibiae are classified as platycnemic (≤ 64.9), mesocnemic (65.0–69.9), and eurycnemic (≥ 70.0), respectively (Herrmann et al. 1990). Furthermore, robustness indices of femur, tibia, humerus, radius, and ulna (Table 15) give hints on muscular activity as well as right- or left-handedness.

Finally, the skeletons were examined with respect to pathological skeletal changes (e. g. trauma, infection, deficiency) as well as both acquired and epigenetic (non-metric) variants.

Only few diseases are visible on the human skeleton. The skeleton is often only affected in case of chronic diseases (Ortner 2008), while heavy diseases usually cause the death of an individual before the disease will be manifested on the skeleton. In addition, slight diseases might not cause any visible sign on the skeleton at all.

This has to be kept in mind when analysing pathologies on past human remains.

Skeletal variants can be either epigenetic (inherent) or acquired. A variety of cranial and postcranial variants is known (see e. g. Berry/Berry 1967; Finnegan 1978; Finnegan/Faust 1974; Perizonius 1979; Saunders/Rainey 2008). Bone variants can be classified into ten different categories (hyperostotic, hypostotic, supernumerary vault sutures, foramina/canals/grooves for blood vessels and nerves, variations at the craniovertebral border, spinal variant, prominent bony processes, facet variations, field defects, other; for more details see, for example, Saunders/Rainey 2008). Some variants may, however, fall into several categories dependent on their definition, thus also varying between different authors (Saunders/Rainey 2008). In order to avoid confusion, in the following bone variants are classified as acquired or epigenetic. Furthermore, epigenetic variants are categorized as cranial variants, variants of vertebrae or ribs, and other postcranial variants. Similarly, tooth variants can be divided into different categories (lobes, marginal ridges, tuberculum projections, occlusal tubercles, cervical enamel line, supernumerary occlusal cusps, accessory ridges, socket orientation, root cones, supernumerary radicular structures; for more details see, e. g., Scott/Pilloud 2019).

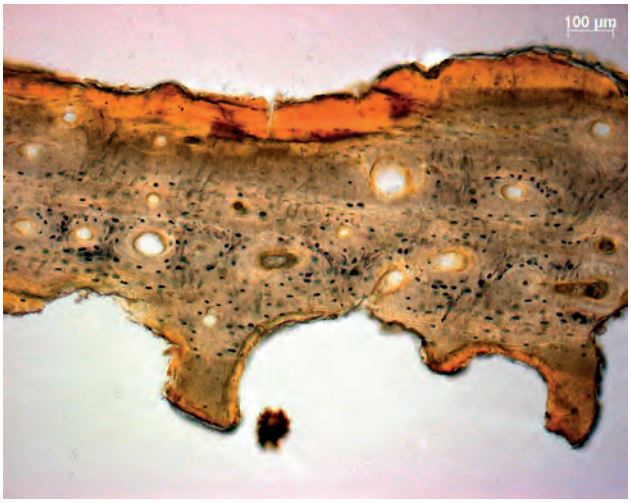

Fig. 180. Example of the histological composition of bone in a young individual. Histological thin section of a femur diaphysis sample of individual KG-095-0496, Burial 22 (histological age: Infans I, photograph by A. Alesi)

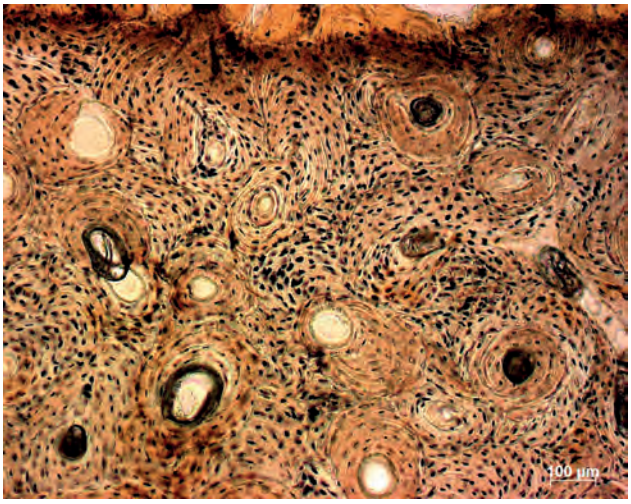

Fig. 181. Example of the histological composition of bone in a young individual. Histological thin section of a femur diaphysis sample of individual KG-095-0496, Burial 35 (histological age: Infans I, photograph by A. Alesi)

V.2.2 Histological analysis

In addition to the morphological determination, histology can be used to estimate the age at death. This is of special importance if the age at death could not be determined morphologically due to a poor and incomplete preservation. However, it can also be understood as a complement to morphology.

Both bones and teeth can be used for histological determination of the age at death.

Histological analyses were conducted at the Biocenter of Ludwig Maximilian University Munich, Germany. Bone and tooth samples were washed and air-dried. Afterwards, the samples were embedded into epoxy resin (Biodur E12, *Biodur Products GmbH*, Heidelberg, Germany) and mixed with hardener (Biodur E1, *Biodur Products GmbH*, Heidelberg, Germany) in a ratio of 100 to 28. The embedded samples were placed in a desiccator at about 100 mbar for 24 h. On the next day, the desiccator was aerated and samples remained at room pressure and

age (combined) = $67.43 + 1.11x_1 + 2.46x_2 + 0.20x_3 - 1.57x_5 - 0.30x_6 - 0.39x_7$ (± 10.08) (Ericksen 1991) (Eq. 1)

age (males) = $57.98 + 1.36x_1 + 1.90x_2 + 0.32x_3 - 1.62x_5 - 0.17x_6 - 0.33x_7$ (± 10.05) (Ericksen 1991) (Eq. 2)

age (females) = $63.39 + 0.55x_1 + 3.12x_2 + 0.20x_3 + 0.92x_4 - 1.57x_5 - 0.31x_6 - 0.24x_7$ (± 10.00) (Ericksen 1991) (Eq. 3)

age (combined) = $23.22 + 1.285x_1$ (± 8.5) (Thompson/Galvin 1983) (Eq. 4)

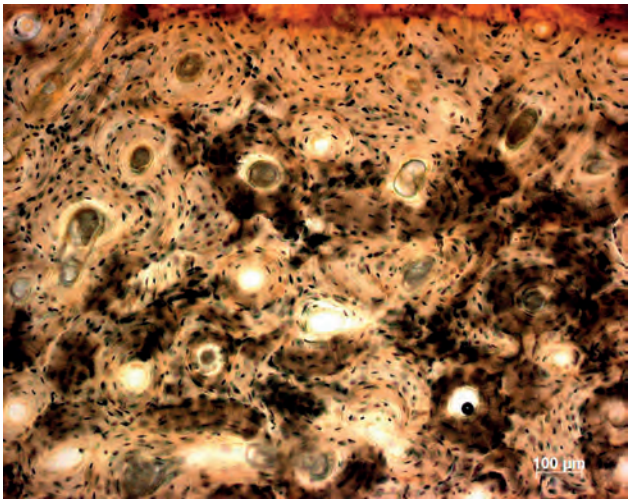

Fig. 182. Example of the histological composition of bone in a mature or senile individual. Histological thin section of a femur diaphysis sample (periosteal part) of individual KG-092-0398, Burial 44 (histological age: 56–76 years, photograph by A. Alesi)

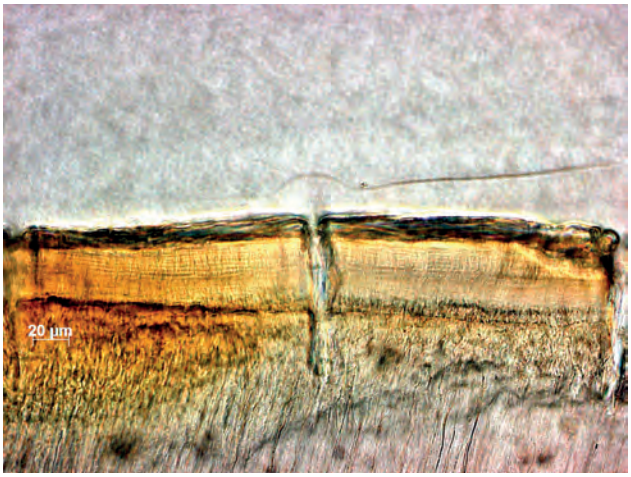

Fig. 183. Example of the TCA analysis of a tooth in an adult or mature individual. Histological thin section of an upper premolar sample of individual KG-097-0455, Burial 27 (TCA age: 42–46 years, photograph by A. Alesi)

room temperature for 48 h. Finally, the samples were heated at 30°C for another 24 h. Histological thin sections were prepared using a Leica 1600 saw microtome equipped with a diamond-coated blade. Slices of 60 µm to 100 µm were prepared. After being fixed on object slides, the bone samples were ground in case of rather thick sections. The sections were covered with cover slips. Microscopic images were produced using a transmitted light microscope (Axioskop 2 plus, Zeiss) and a CCD camera (AxioCam Mrc color, Zeiss). A square grid (1 × 1 mm) was placed on the images of the bone sample for microstructural analyses (see Ericksen 1991).

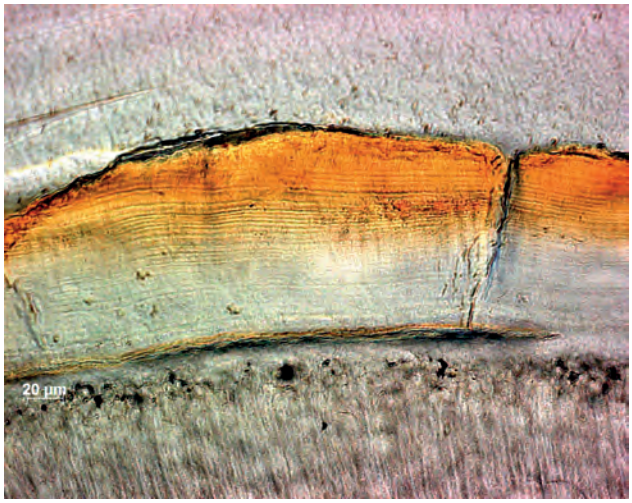

Fig. 184. Example of the TCA analysis of a tooth in a mature or senile individual. Histological thin section of a lower premolar sample of individual KG-090-0398, Burial 44 (TCA age: 59–64 years, photograph by A. Alesi)

The histological appearance of bones changes with time (see Fig. 180, Fig. 181 and Fig. 182). With increasing age, the number of osteons as well as osteon fragments increases, while the number of Haversian canals and the percentage of unremodeled bone decrease with age (see, e. g., Robling/Stout 2007). Consequently, the histomorphometrical investigation of bone microstructures, namely secondary osteons/mm^2 (x_1), type II osteons/mm^2 (x_2), fragments/mm^2 (x_3), resorption spaces/mm^2 (x_4), non-Haversian canals/mm^2 (x_5), percentage of unremodeled circumferential bone (x_6), and percentage of osteonal bone (x_7) can be used to examine the (biological) age of an individual (see Ericksen 1991; Thompson/Galvin 1983). The biological age at death was estimated using the regression equations of Ericksen (1991) in the case of femur samples (see Eqs. 1–3 for combined sexes, males, and females; in years) and the regression equation of Thompson and Galvin (1983) for tibia samples (see Eq. 4; in years).

The prepared images of the tooth samples were evaluated according to Kagerer and Grupe (2001) using TCA (Tooth Cementum Annulation). Age estimation is based on the series of annual hypo- and hypermineralized incremental lines (see Fig. 183 and Fig. 184), which can be counted. Each pair of hypo- and hypermineralized lines counts for one year of age. The number of counted annual lines is added to the time of eruption of the respective tooth resulting in an estimated chronological age at death – in contrast to the biological age in morphological and histomorphometrical analyses (Kagerer/Grupe 2001).

V.2.3 X-ray analysis

Radiographs are a noninvasive method for the examination of bones. The absorption of X-radiation by the irradiated sample results in an X-ray image. Radiation energy (in kV), beam current (in mA), exposure time (in s), and the distance between the radiographic film and the focal spot of the X-ray apparatus (focus-film distance) have an impact on the quality of the radiation (kVp = peak kilovoltage) as well as the intensity, i. e. the amount of X-ray photons produced (mAs = milliampere-seconds).

X-ray analysis was conducted at the Biocenter of Ludwig-Maximilians-University in Munich, Germany. An Eickmeyer Innovit 300 X-ray apparatus in combination with an automatic developer (Dürr Dental AC 245 E) was used for the analysis.

V.2.4 Data analysis and software

For cluster analysis a Gaussian Mixture Model (GMM) clustering approach was chosen. As shown previously, GMM clustering is a useful tool for the application on multi-isotope data in order to extract additional information beyond the common bivariate plots (see, e. g., Göhring et al. 2016; Göhring et al. 2018; Grupe et al. 2018; Mauder et al. 2016). The main goal of cluster analyses is the identification of groups which are clearly separated from each other (Fraley/Raftery 2002). As a consequence, samples clustered together are similar to each other, but distinct from samples which are grouped together in another cluster (Xiong/Li 2014).

GMM clustering is based on multivariate normal (Gaussian) distributions. Thus, Gaussian curves are placed on all different (isotopic) dimensions in order to cluster the data. A model-based clustering approach – as GMM cluster analysis – aims to optimize the fitting between the observed data and the mathematical model (here: multivariate Gaussian distribution) using a probabilistic approach. This is based on the assumption that the data result from an underlying probability distribution. As a consequence, a probability can be assigned to each data point (Aggarwal 2014; Deng/Han 2014). The modeling quality is validated using the Bayesian Information criterion (BIC; Schwarz 1978). In addition, the expectation maximization (EM) algorithm chooses the clustering model with maximum likelihood (Fraley/Raftery 1998) resulting in the optimal model parameters (Reynolds 2009). This includes the optimal cluster number as well as geometric cluster features (e. g. volume, shape, and orientation; Scrucca et al. 2016). The »R« package »mclust« (version 5.4.1; Scrucca et al. 2016) was used for clustering. For more details see Göhring et al. (2016) and references therein.

Photographs as well as skeletal schemes were edited with Adobe Photoshop CS3 Extended. Graphs were produced with the statistic software »R« (R Core Team 2018).

V.3 Catalogue of human remains

The burials are sorted by their chronological order. Burials 1–20 are dated to the Late Bronze Age/Early Iron Age (LBA/EIA, see ch. V.3.1), Burials 21–27 are dated to the Late Antique period (ANT, see ch. V.3.2), and Burials 28–41 are dated to the Medieval period (MA; see ch. V.3.3). Burials 42–46 could not be dated (UD; see ch. V.3.4). Eight burials (Burials 2, 3, 10, 12, 16, 17, 18, and 19) did not contain any human skeletal remains and were consequently not considered in the following. See chapter IV for more information on the dating. Detailed descriptions and discussions on resulting osteometry and craniometry, detected non-metric variants and pathologies are given in chapters V.4.3 to V.4.6.

V.3.1 Late Bronze Age/Early Iron Age burials

Burial 1 (KG-094-0474)

The skeleton of individual KG-094-0474 was only partially preserved (Fig. 185) with slight taphonomic damages to the bone surfaces. Due to the poor state of preservation neither sex nor age at death could be determined.

Some animal remains were detected in the grave, namely a tooth of a mouse (KG-094-0451b), phalanx I and II, Os carpi radiale, and Os intermedium of a sheep or goat (KG-094-0451c) with a relatively high age at death (>> 1 a), as well as a humerus of a wild bird.

Burial 4 (KG-039-0163 and KG-040-0165)

In the case of individual KG-039-0163 only parts of the lower legs, the diaphyseal part of the right radius, and a proximal phalanx of the hand were preserved (Fig. 186). It was therefore not possible to morphologically determine the sex and age of this individual. According to histological age determination after Thompson and Galvin (1983) the biological age at death was estimated at about 43 years (± 9 years).

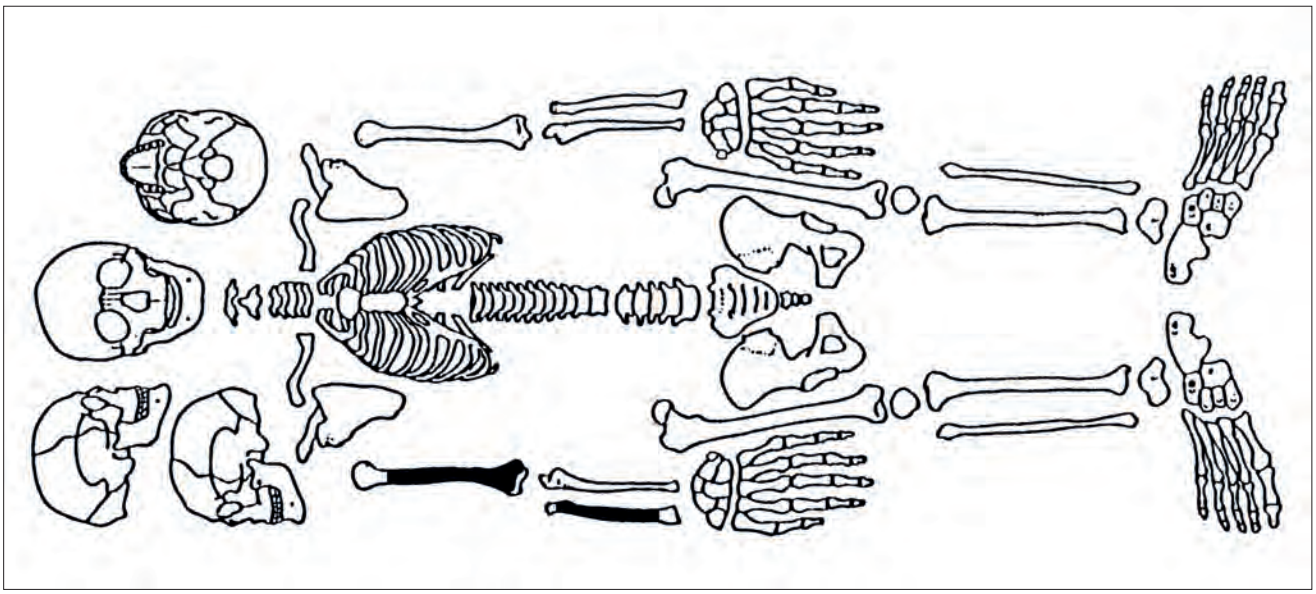

Fig. 185. Skeletal scheme of KG-094-0474 (Burial 1)

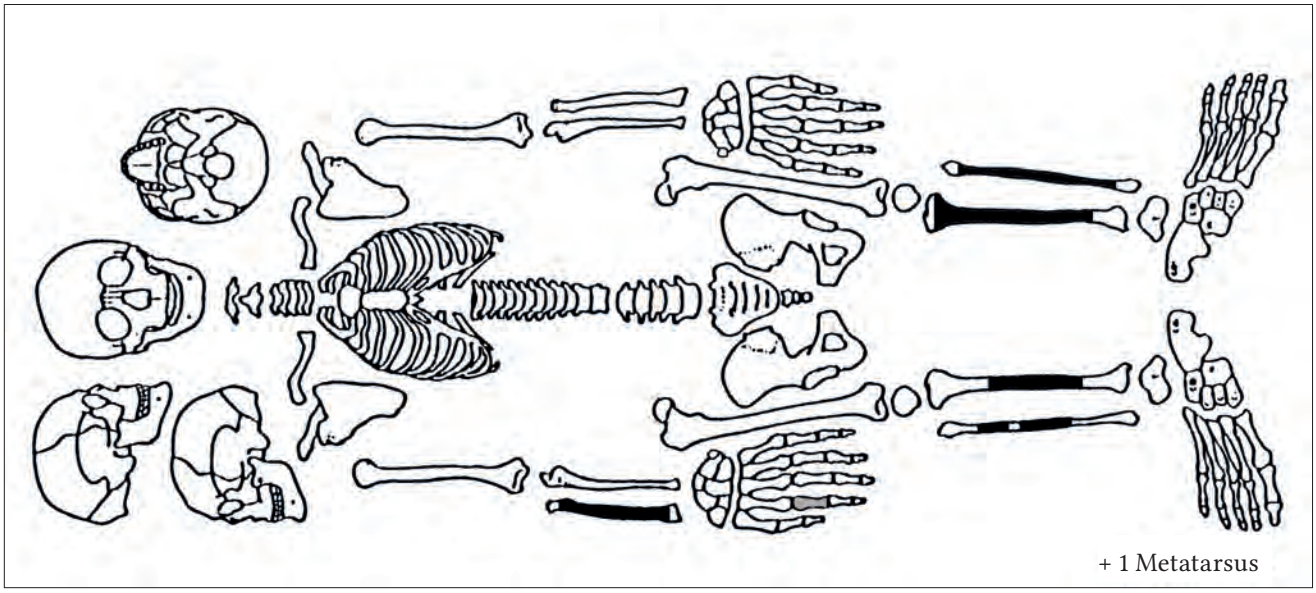

Fig. 186. Skeletal scheme of KG-039-0163 and KG-040-0165 (Burial 4)

Burial 5 (KG-038-0146)

Only parts of the cranium, upper body, and pelvic girdle of individual KG-038-0146 were preserved (Fig. 187). It was determined as a probably male individual. Sex determination on the pelvis was only possible with respect to the Crista iliaca, which was classified as probably male. Features of both the mandible and the cranium were typical for a male or probably male individual. The age at death was determined as c. 20–30 years. The age determination was based on the completely closed epiphysis at the proximal (left) humerus (right nd), which indicates an age above 20–25 years. Furthermore, according to the cranial sutures, the individual was younger than 30 years. The state of abrasion of the teeth was rather low, indicating an even younger age at death.

Animal remains were identified as radius, tibia, humerus, and mandible of the puppy of a fox or a domesticated dog (KG-023-0554). These animal bones probably came from a burrow and cannot be seen as burial gifts.

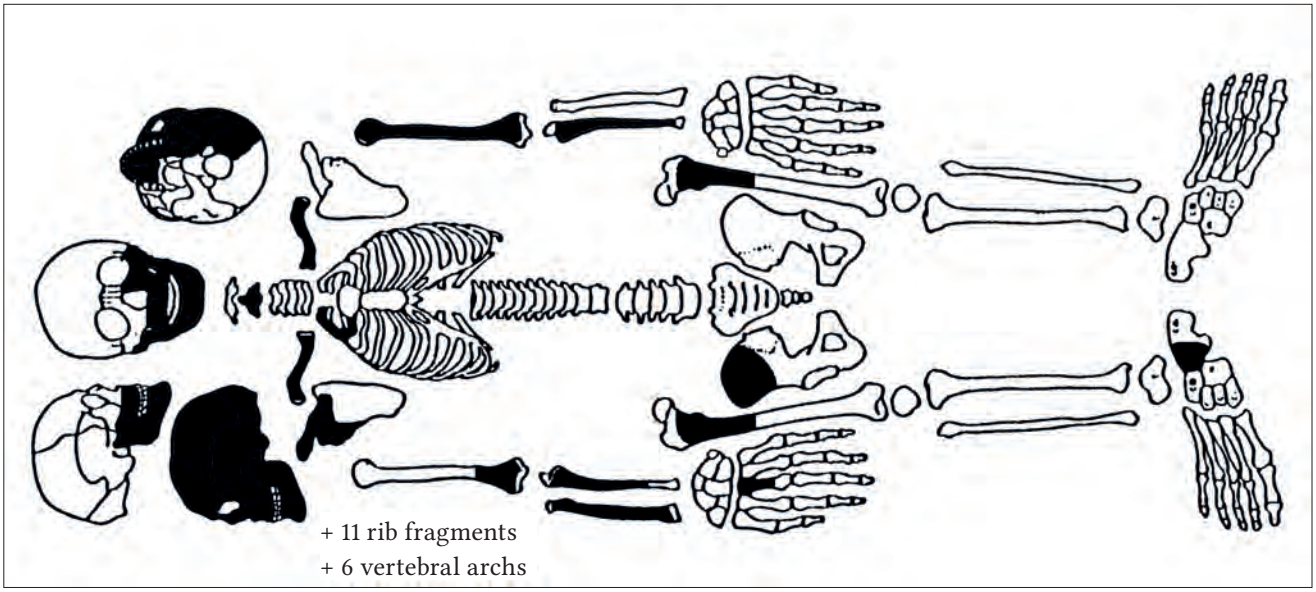

Fig. 187. Skeletal scheme of KG-038-0146 (Burial 5)

Burial 6 (KG-095-0497)

The skeleton of individual KG-095-0497 was poorly preserved (Fig. 190) and highly fragmented. Only a single tooth (I1) was preserved (0468). The bone surfaces showed strong taphonomic damages. Sex and age determinations were not possible due to the poor state of preservation.

Burial 7 (KG-026-0105)

In Burial 7 the incomplete adult skeleton of individual KG-026-0105, of which mainly cranial bones remained, was found (Fig. 191). With respect to the sexual dimor-

Fig. 188. Norma frontalis of the skull of individual KG-026-0105 (Burial 7)

Fig. 189. Norma lateralis of the skull of individual KG-026-0105 (Burial 7)

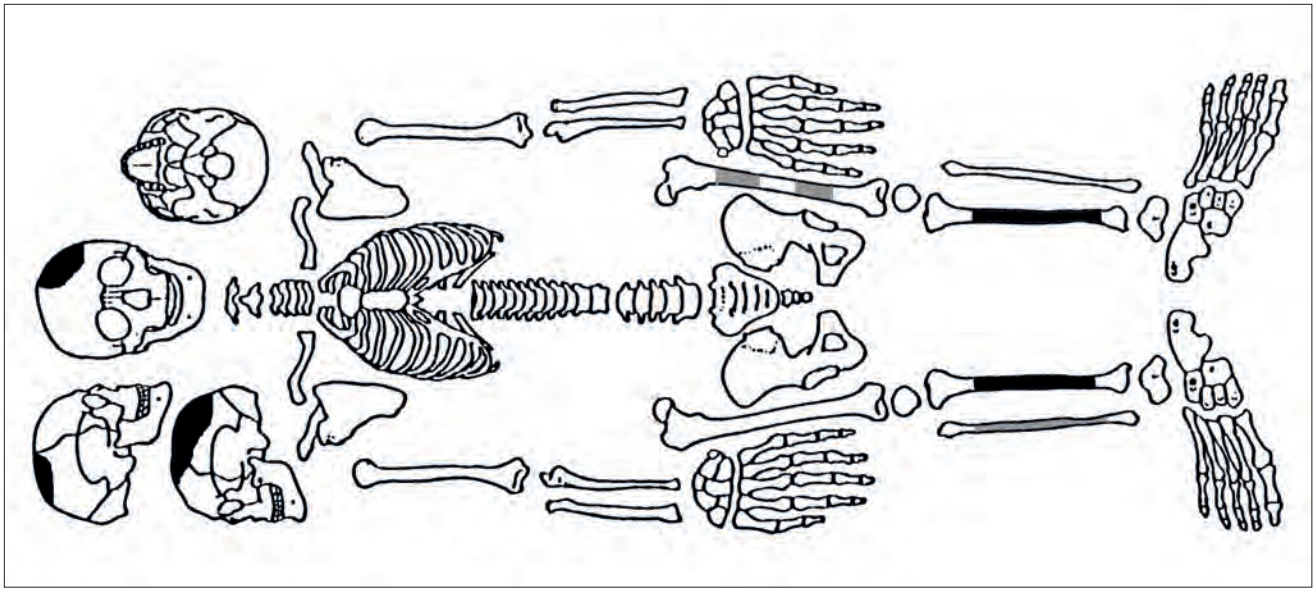

Fig. 190. Skeletal scheme of individual KG-095-0497 (Burial 6). Bones of indeterminable siding and/or position are shown in grey

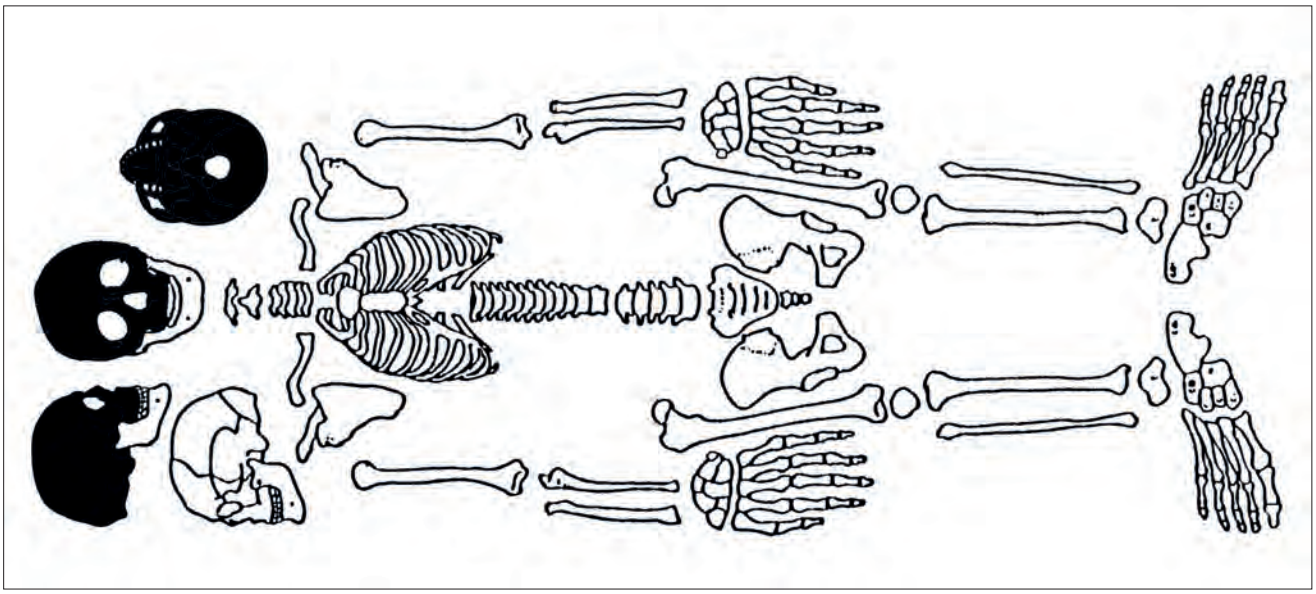

Fig. 191. Skeletal scheme of individual KG-026-0105 (Burial 7). Bones of indeterminable siding and/or Position are shown in grey

phism of the skull this individual was determined as probably male. Cranial sutures showed an age at death of about 20 to 30 years, which is in agreement with the tooth statue which shows almost no abrasion.

According to the cranial measurements the skull of the individual was brachycephalic (82.6), hypsicranic (80.2), metriocranic (97.1), hypereuryene (43.7), hypsiconch (86.8), and chamaerrhine (54.3). Thus, the individual had a short head, with a high, narrow braincase, a very broad upperface, high orbits, and a broad nose (Fig. 188 and Fig. 189; see also Table 17 and ch. V.4.3.1).

Burial 8 (KG-057-0247 and KG-057-0404)

The skeleton of individual KG-057-0247/KG-057-0404 was highly fragmented and incompletely preserved (Fig. 192) with strong taphonomic damages on the bone surface. Sex determination was not possible due to the lack of informative bones. However, the left Facies symphysialis could be used for age determination. State 3–4 indicates an age at death of about 40 to 70 years.

A tibia of a sheep was found in the grave (0455).

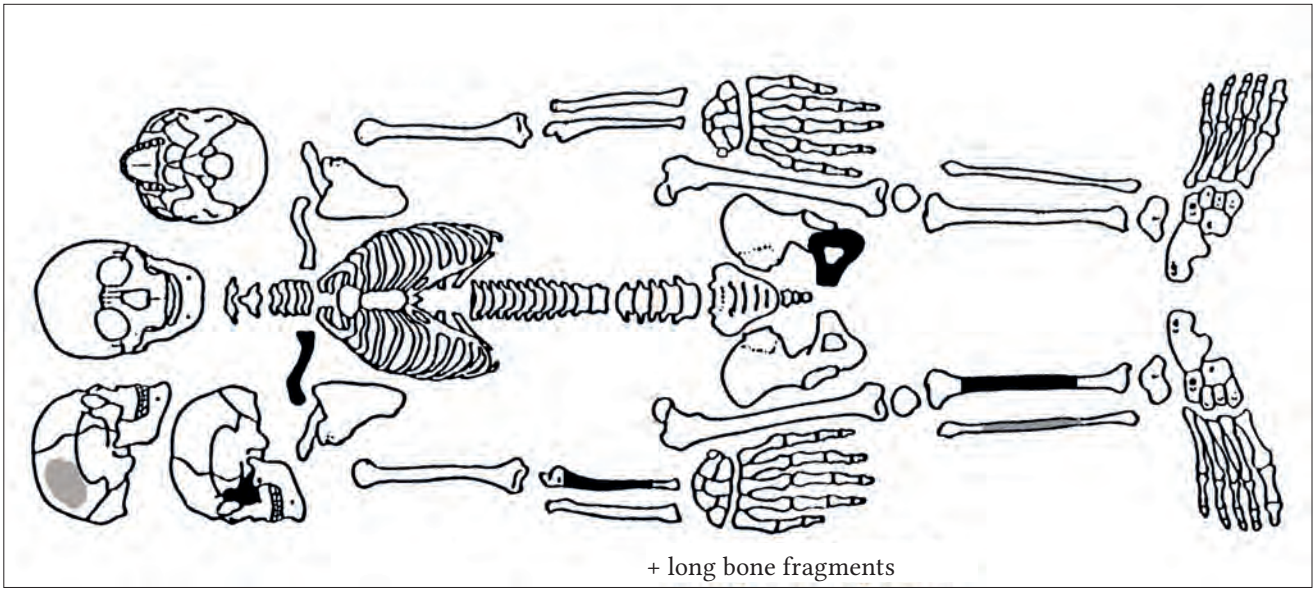

Fig. 192. Skeletal scheme of KG-057-0247 and KG-057-0404 (Burial 8). Bones of indeterminable siding and/or position are shown in grey

Burial 9 (KG-043-0204)

Only the crowns (enamel) of 15 permanent teeth of individual KG-043-0204 were preserved. Neither age nor sex determination was possible.

Burial 11 (KG-029-0115)

Loose in the fill of Burial 11 a displaced single vertebral arch (KG-029-0115) was preserved that, however, did not belong to the original Early Iron Age interment, but to an individual of the Medieval period (see ch. IV.9).

Burial 13 (KG-032-0166)

The skeleton KG-032-0166 was highly fragmented and incomplete with only some long bone and rib fragments preserved (Fig. 193).

According to the poor state of preservation neither sex nor age could be morphologically determined. However, histological age determination was possible using histomorphometrical analysis after Ericksen (1991) as well as TCA (see Kagerer/Grupe 2001). The age at death was estimated at about 65 years (± 10 years) and 54 years (± 2 years) for histological age determination and TCA, respectively. The teeth preserved in the lower right jaw showed a quite high state of abrasion (see V.4.5). This could be indicative of a rather high age at death. However, even diet could explain the abrasion.

A fragment of a right rib showed a healed fracture on the anterior side (Fig. 194, see ch. V.4.5).

The grave also contained animal remains, which were determined as bones and teeth of a small rodent, a metapodium of a neonatal rabbit or hare (Leporidae sp.), an ulna of a wild bird, and a humerus of a sheep or goat (KG-032-0553).

Burial 14 (KG-059-0346)

Only a phalanx of individual KG-059-0346 was preserved.

Burial 15 (KG-058-0243)

The incomplete and fragmented skeleton of individual KG-058-0243 (Fig. 195) showed strong taphonomic damages. Due to the poor state of preservation neither sex nor age at death could be morphologically determined; only histomorphometrical age determination was possible. According to this determination, the biological age could be estimated at about 63 years (± 10 years) using the method of Ericksen (1991).

Postcranial measurements were only possible on the femoral bones with an index platymericus of 81.3 and

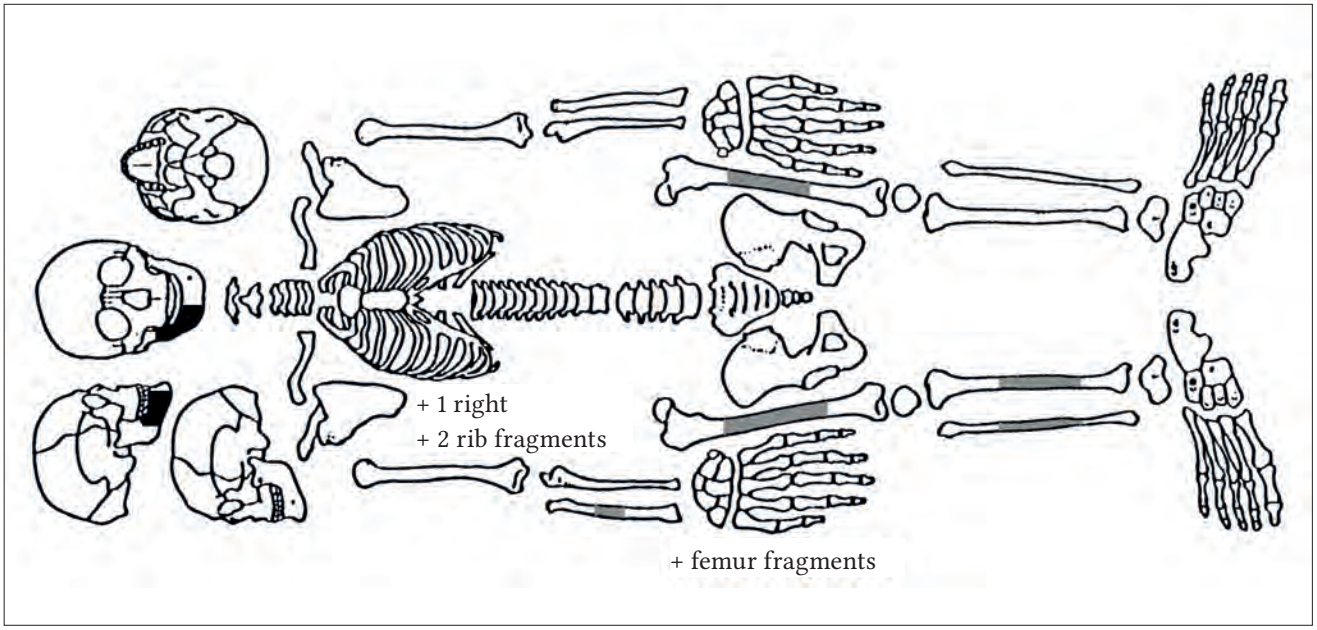

Fig. 193. Skeletal scheme of KG-032-0166 (Burial 13). Bones of indeterminable siding and/or position are shown in grey

Fig. 194. Healed rib fracture (see arrows) on a right rib of individual KG-032-0166 (Burial 13)

74.4 at the right and left femur, respectively. This indicates a platymeric right and a hyperplatymeric left femoral bone (see ch. V.4.3.2).

Burial 20 (KG-030-0113 and KG-102-0491)

The incomplete skeleton of individual KG-030-0113/KG-102-0491 only included the diaphyseal part of the left femoral bone and a fibula fragment, as well as a small

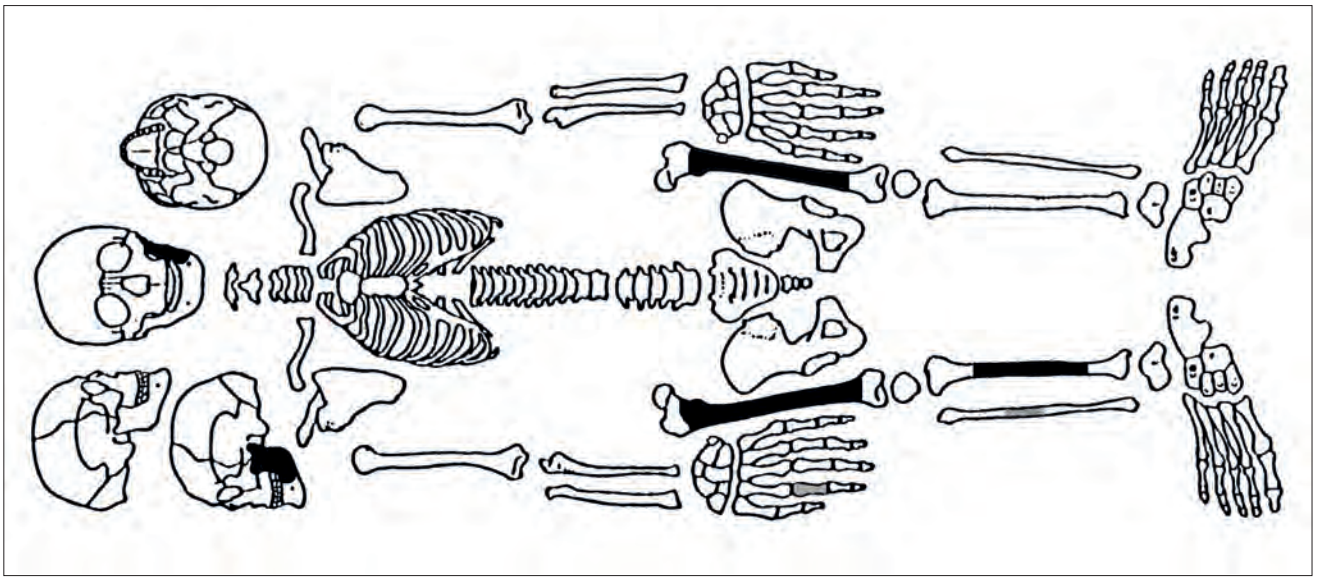

Fig. 195. Skeletal scheme of KG-058-0243 (Burial 15). Bones of indeterminable siding and/or position are shown in grey

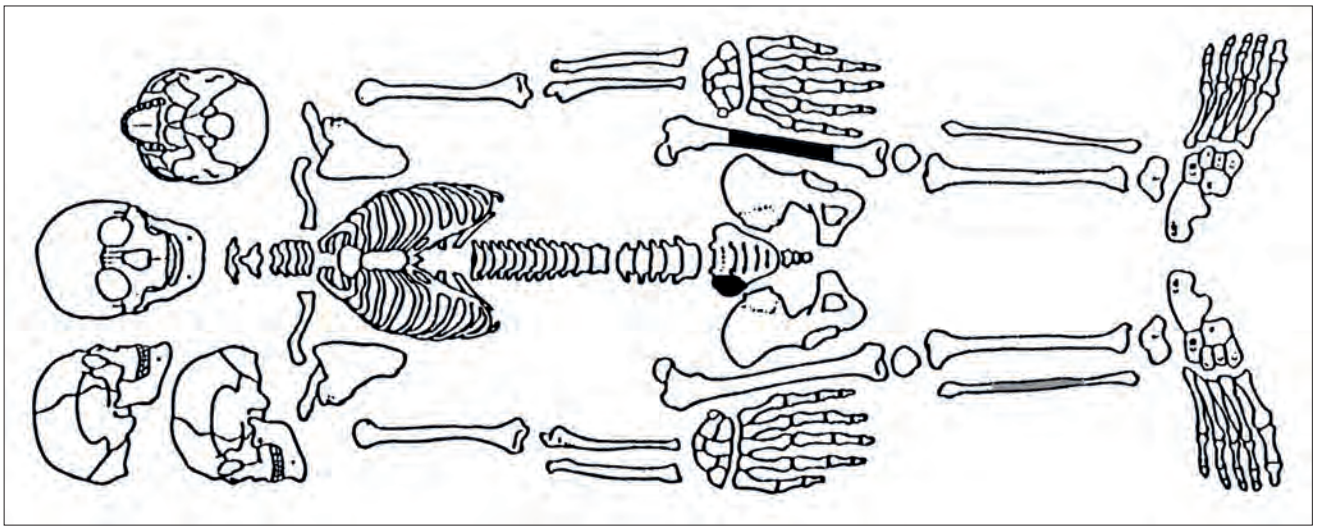

Fig. 196. Skeletal scheme of KG-030-0113 and KG-102-0491 (Burial 20). Bones of indeterminable siding and/or position are shown in grey

part of the sacrum (Fig. 196). With this state of preservation neither morphological sex nor age determination was possible. However, histomorphometrical age determination after Ericksen (1991) revealed a biological age at death of about 63 years (± 10 years). Due to the poor conservation other descriptive parameters could not be determined.

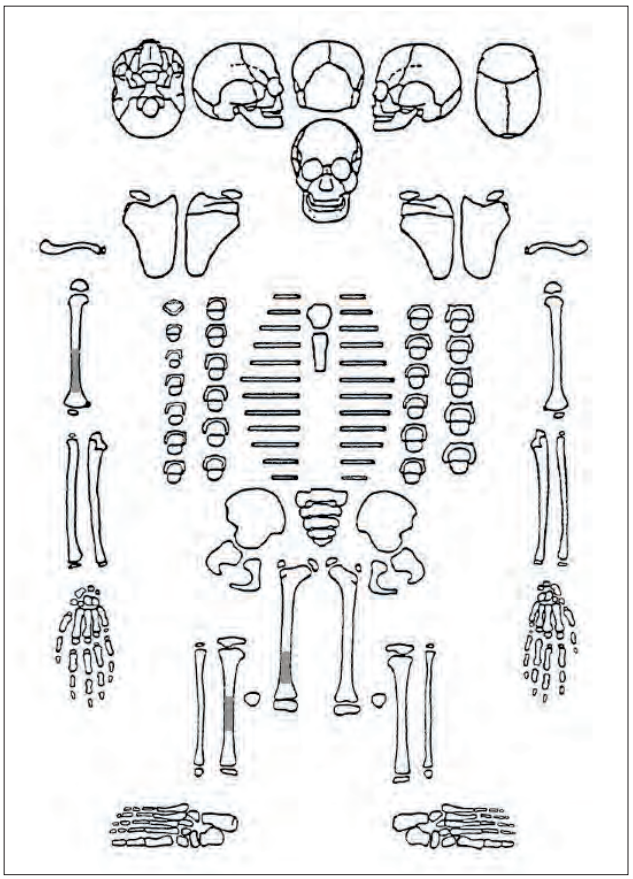

Fig. 197. Skeletal scheme of KG-095-0496 (Burial 22). Bones of indeterminable siding and/or position are shown in grey

V.3.2 Late Antique burials

Burial 21 (KG-074-0507)

The skeleton of individual KG-074-0507 was only partly preserved (Fig. 198) and highly fragmented. Bone surfaces showed strong taphonomic damages. Sex determination on specific features of the skull showed the individual to be probably male. The morphological age at death could only be determined as at least adult. According to histological analyses the biological age at death was estimated at 65 years (± 10 years) if the sex was not considered and as about 58 years (± 10 years) in case of a male individual (see Ericksen 1991).

Several animal bones were detected in the grave. These include the humerus, fused ulna and radius, and Os carpi radiale of a sheep or goat (0551) as well as the metapodium of an individual of the family of Leporidae, possibly Lepus timidus.

Burial 22 (KG-095-0496)

The skeleton of the child KG-095-0496 was partially preserved (Fig. 197). The bone surfaces showed slight taphonomic damages. Neither sex nor age determination was

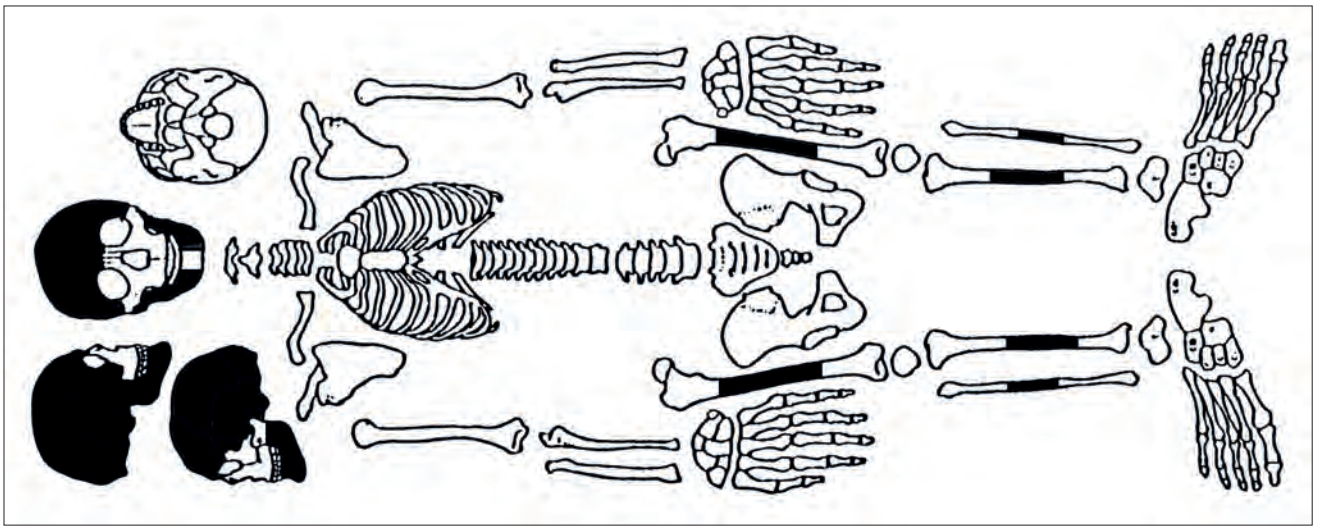

Fig. 198. Skeletal scheme of KG-074-0507 (Burial 21)

possible due to the poor state of preservation. Bone size might, however, indicate an individual of late Infans I or Infans II. Histologically, no regression formula could be used for an age determination. However, due to the presence of a huge amount of circumferential lamellae, only few secondary osteons, and the lack of interstitial lamellae the age at death was subjectively estimated at age class Infans I, which is in agreement with the bone lengths.

Burial 23 (KG-057-0415)

The skeleton of individual KG-057-0415 was incompletely preserved (Fig. 199). Bones showed strong taphonomic damages. Sex determination was only possible on features of the skull indicating a probably male individual. Morphological age determination was not possible, but the individual was at least adult. The individual showed an ossicle at the lambda as well as some lambdoid ossicles at the lambdoid suture (Fig. 200 and Fig. 201). Therefore, cranial sutures could not be used for age determination. However, tooth loss (IV 5) and a rather high abrasion of the teeth might indicate a rather high age at death. Histomorphometrical age estimation of a femur sample revealed a biological age at death of 63 years (± 10 years) in case of unknown sex and of 59 years (± 10 years) in case of a male individual (see Ericksen 1991). According to TCA (see Kagerer/Grupe 2001), the individual died at a chronological age of about 52 years (± 3 years).

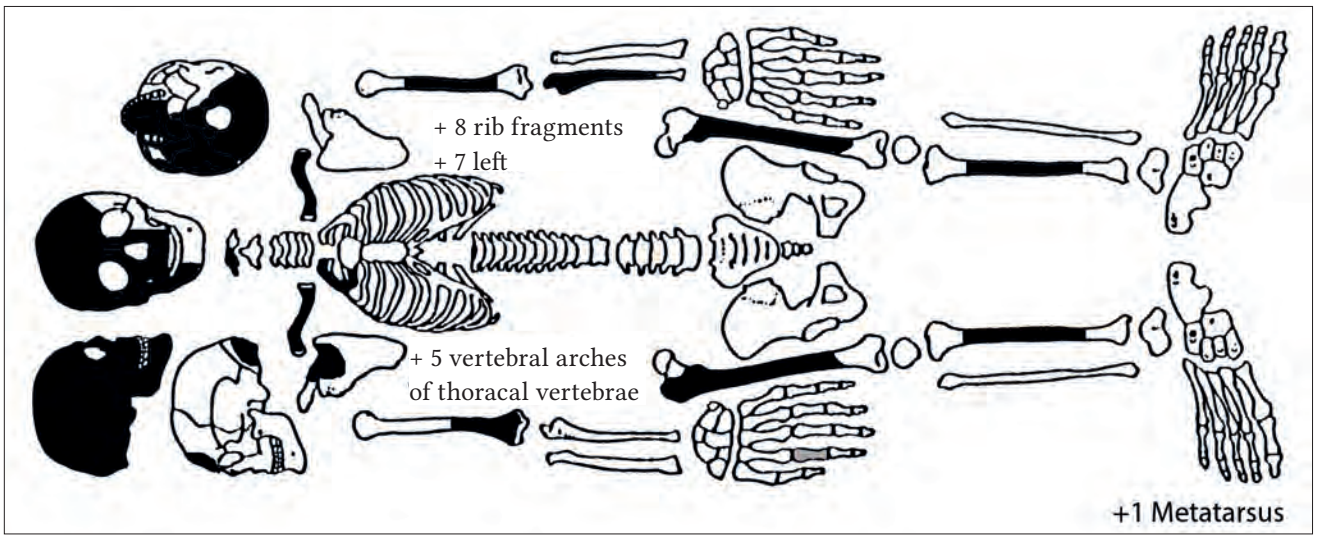

Fig. 199. Skeletal scheme of KG-057-0415 (Burial 23). Bones of indeterminable siding and/or position are shown in grey

Fig. 200. Lambdoid ossicles (see arrows) at the Sutura lambdoidea of individual KG-057-0415 (Burial 23)

Fig. 201. Ossicle at the lambda and lambdoid ossicles (see arrows) at the Sutura lambdoidea of individual KG-057-0415

Apart from the rather high abrasion level of the teeth, caries was detected on two teeth of the upper right jaw (I 3, I 4). Caries of level 5 was accompanied with an infected pulp cavity (see ch. V.4.5). An ossicle at the lambda and lambdoid ossicles have already been mentioned (Fig. 200 and Fig. 201). In addition, the individual showed a patent Canalis condylaris at the right side of the foramen magnum (Fig. 202). The left side could not be determined (see ch. V.4.6).

Fig. 202. Canalis condylaris patent at the right side of the Foramen magnum (see arrow) of individual KG-057-0415 (Burial 23). The other side could not be determined

Burial 24 (KG-057-0414)

Individual KG-057-0414 was only partly preserved (Fig. 203) with strong taphonomic damages to the bone surface. Sex determination was not possible since diagnostic parts of the skeleton were not preserved. The mandible indicated a probably male individual. However, without any further sex-specific criteria, the individual's sex remains unknown. The examination of the Facies symphysialis of the right pelvis (left nd) revealed an age at death of about 50 to 70 years.

The left tibia showed a strong periostitis in combination with an osteomyelitis at the anterio-lateral side of

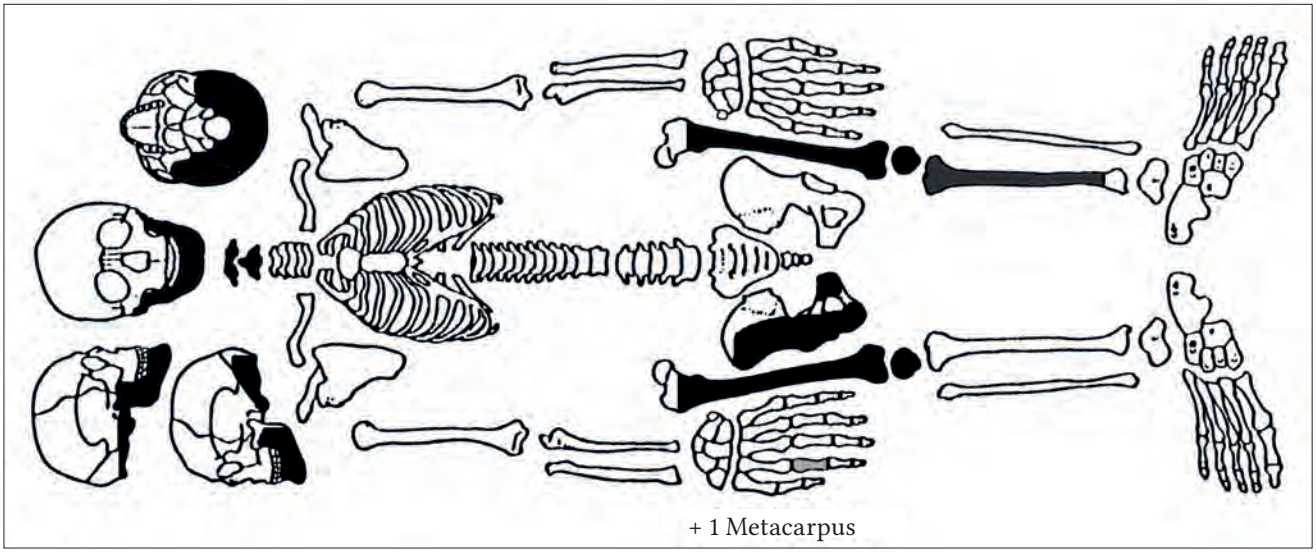

Fig. 203. Skeletal scheme of KG-057-0414 (Burial 24). Bones of indeterminable siding and/or position are shown in grey

Fig. 204. Osteomyelitis (see arrows) at the anterior-lateral side of the left tibia of individual KG-057-0414 (Burial 24)

Fig. 205. Periostitis on the anterior side of the left tibia of individual KG-053-0208 (Burial 25)

the proximal part of the bone (Fig. 204). The osteomyelitis might have been caused by an injury of the tibia. It is not clear if the hole visible close to the proximal end of the bone was caused by a trauma or if it was the typical cloaca associated with osteomyelitis (compare Fig. 216) due to postmortal damage (see ch. V.4.5).

Postcranial indices revealed an eurycnemic (76.3) left tibia (right nd), an eurymeric (88.9) right, and a platymeric (77.1) left femur (see ch. V.4.3.2).

Burial 25 (KG-053-0208)

Skeleton KG-053-0208 was well preserved and almost complete (Fig. 206). According to relevant criteria on the pelvic bone, the mandible and the cranium the individual was determined as male. In addition, the skeleton was very robust (compared to the other skeletons from the site), which also points to a probably male individual. According to the examination of the Facies symphysialis the individual's age at death was estimated at about 40 to 70 years (state 3–4). Cranial sutures were not valid for age determination due to the presence of ossicles at the lambdoid sutura (Fig. 207).

The twelfth thoracic vertebra and three lumbar vertebrae (L1, L3, and L4) showed small osteophytes (< 3 mm) on the anterior (L1, L3, L4) or posterior (T10, L3) side of the vertebral body. These small changes are in line with the mature to senile age at death.

The left tibia showed a slight periostitis with longitudinal stripes on the distal part of the diaphysis (Fig. 205; see ch. V.4.5).

As already mentioned the individual showed lambdoid ossicles at the lambdoid suture (Fig. 207). Furthermore, bilateral Foramina transversa bipartita were present on the cervical vertebrae C4 and C5, while the other cervical vertebrae did not show this variant (see ch. V.4.6).

Craniometry revealed a mesocephalic (75.5), orthocranic (70.7), metriocranic (93.5), euryprosopic (84.4),

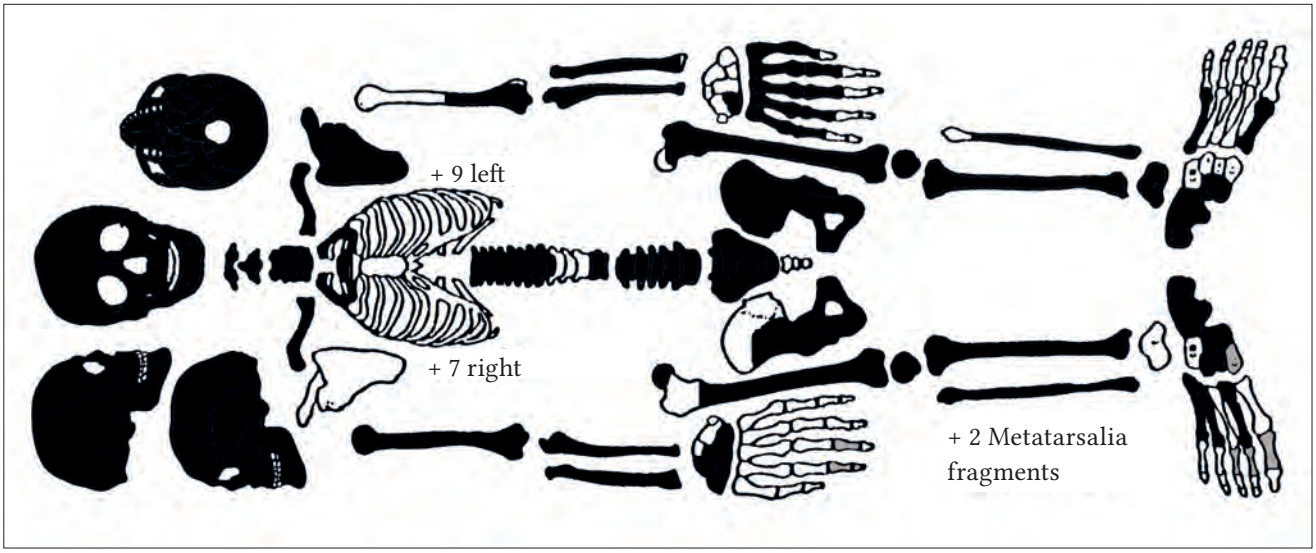

Fig. 206. Skeletal scheme of KG-053-0208 (Burial 25). Bones of indeterminable siding and/or position are shown in grey

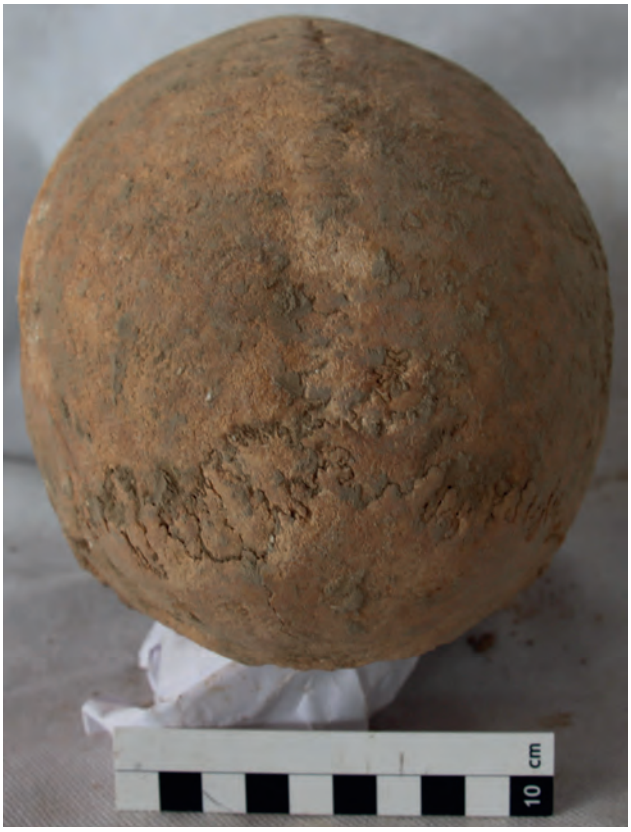

Fig. 207. Lambdoid ossicles at the Sutura lambdoidea of individual KG-053-0208 (Burial 25)

Fig. 208. Norma frontalis of the skull of individual KG-053-0208 (Burial 25)

euryene (47.4), mesoconch (77.5), and mesorrhine (47.9) skull. Consequently, the individual was medium-headed with a medium-sized braincase, a short facial skull, a broad upper head, with medium high orbits, and a medium nose width (Fig. 208 and Fig. 209; see also Table 17 and ch. V.4.3.1). The individual showed a platymeric (81.6) right femur. The left femur could not be assessed. In case of the tibiae, the right one was mesocnemic (68.6), while the left one was platycnemic (59.5). The robustness index of the right humerus and right radius was determined as 21.8 (left nd) and 19.4 (left nd), respectively. Furthermore, the robustness index of both ulnae revealed

Fig. 209. Norma lateralis of the skull of individual KG-053-0208 (Burial 25)

a higher index for the left (18.3) compared to the right (17.1) bone. According to long bone measures the body height of the individual was estimated at about 167 cm to 172 cm after the equations of Trotter and Gleser (1958) (see ch. V.4.3.2).

Burial 26 (KG-066-0392)

The skeleton of individual KG-066-0392 was only partially preserved (Fig. 211) and highly fragmented with slight taphonomic damages. The sex was determined as probably female due to the partly preserved right pelvic bone. A morphological determination of the age at death was not possible. The individual's biologial age at death was histomorphometrically estimated at 64 years (± 10 years) according to Ericksen (1991).

The grave also contained one bone of a fetal or neonatal non-human mammal, which could not be specified more closely.

The diaphysis of the left ulna showed a healed fracture of the proximal half of the diaphysis (Fig. 210). The left radius was not preserved. Thus, it might be both a parry fracture of the ulna caused by a blow and a forearm fracture of ulna and radius caused by a forced pronation (Lovell/Grauer 2019). The fracture was healed slightly displayed, leading to a shortening of the bone (see ch. V.4.5).

Fig. 210. Healed fracture (see arrows) of the posterior part of the left ulna of individual KG-066-0392 (Burial 26)

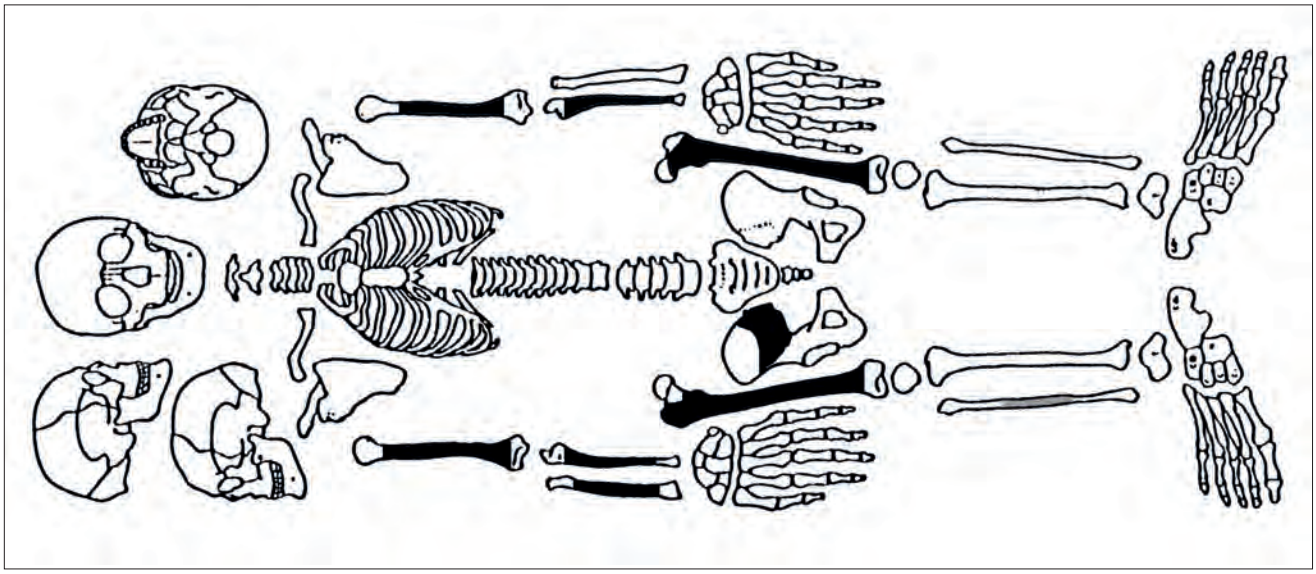

Fig. 211. Skeletal scheme of KG-066-0392 (Burial 26). Bones of indeterminable siding and/or position are shown in grey

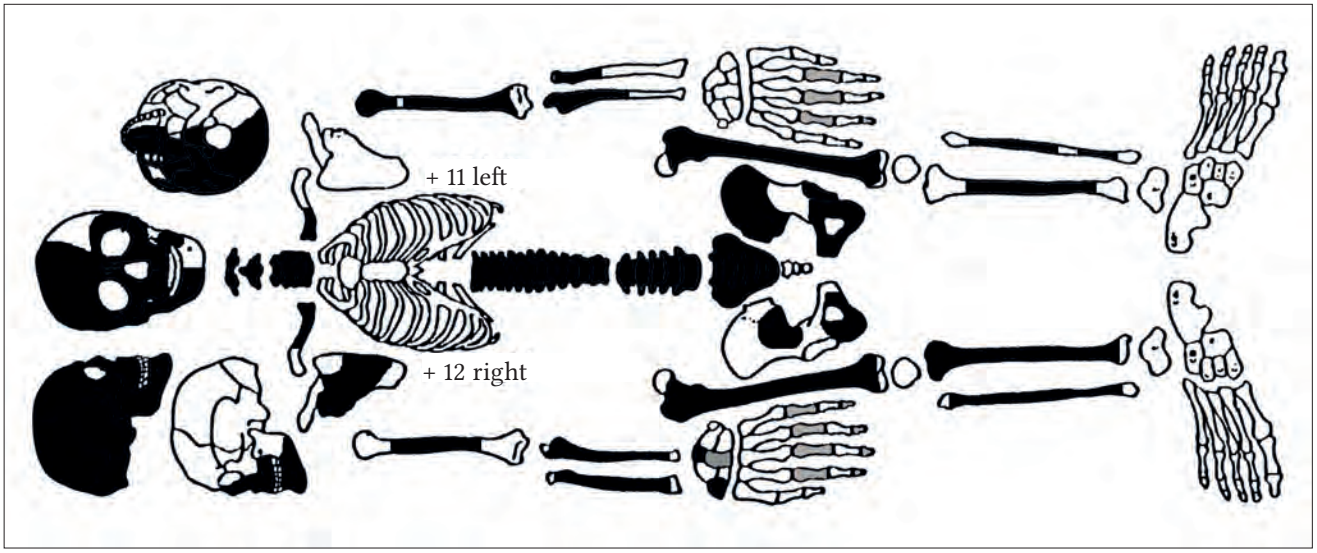

Fig. 212. Skeletal scheme of KG-097-0455 (Burial 27). Bones of indeterminable siding and/or position are shown in grey

Burial 27 (KG-097-0455)

The skeleton of individual KG-097-0455 was well preserved (Fig. 212) with only slight damage to the bone surfaces. Sex determination revealed a probably male individual on the basis of sex-specific features of the pelvis and the skull. The age at death was determined as about 40 to 46 years according to epiphyseal fusion and cranial sutures. Epi- or apophyses of the clavicle, acromion of the scapula, humerus, fingers, and iliac crest were already fused (> 25 years). The cranial sutures, indicating an at least adult age, are not valid due to the presence of an ossicle at the lambda (Fig. 214). The abrasion of teeth was relatively high, which might indicate higher age at death but as well have been caused by diet. TCA revealed a chronological age around 43 years (± 3 years)

Fig. 213. Foramen transversum bipartitum (see upper arrow) as well as Processus spinosus bipartitus (see lower arrow) on the sixth cervical vertebra of individual KG-097-0455 (Burial 27)

Fig. 214. Norma occipitalis of the skull of individual KG-097-0455 (Burial 27) with an ossicle at the lambda (see arrows)

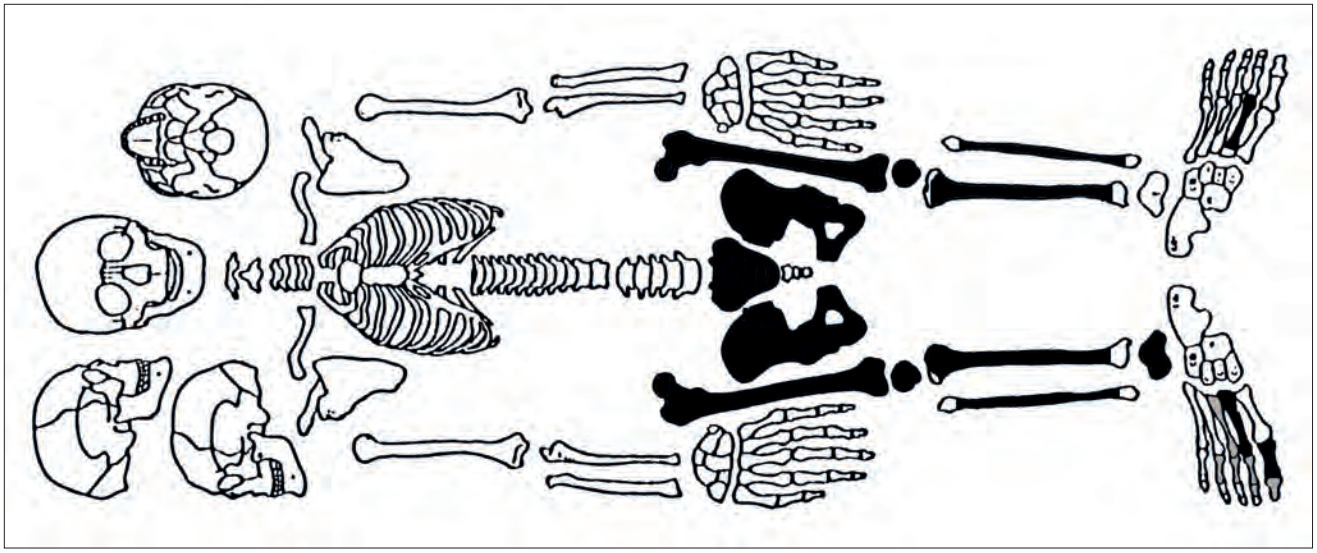

Fig. 215. Skeletal scheme of KG-027-0106 (Burial 28). Bones of indeterminable siding and/or position are shown in grey

for a tooth sample (Kagerer/Grupe 2001). Accordingly, the individual probably died at an age between 40 and 46 years.

Hand joints of both hands showed small osteophytes (< 3 mm). This is fully in agreement with the estimated age at death. Two cervical vertebrae (C5, C6) showed Schmorl's nodules on the anterior side of the vertebral body. The posterior sides were not affected. The individual also showed a slight enthesiopathy at the medial inferior part of both clavicles (see ch. V.4.4).

The sixth cervical vertebra showed two anatomical variants, namely Foramen transversum bipartitum on the right side (left nd) as well as Processus spinosus bipartitus (Fig. 213; see ch. V.4.6).

V.3.3 Medieval Burials

Burial 28 (KG-027-0106)

Only some bones of the lower body of skeleton KG-027-0106 were preserved (Fig. 215). The pelvic girdle was poorly preserved. However, based on the right pelvic bone this individual could be determined as a male individual. The suture at the anterior superior iliac spine of the right pelvic bone was still visible, which points to an age at death of 17 to 22 years. Furthermore, the proximal end of the femoral bone was not completely fused (~ 16–19 years). In addition, X-ray analysis (see below; Fig. 218) shows the partial fusion of the proximal epiphysis of the right tibia. This is indicative of an age between 14 and 19 years (Ebeye et al. 2016; Patond et al. 2015). Con-

Fig. 216. Anterior-lateral view on the right tibia of individual KG-027-0106 (Burial 28) with an osteomyelitis at the proximal part of the bone shaft including a central sisus (cloaca) for pus drainage. The central sisus (cloaca) and the coarsely woven bone at the cortex are clearly visible

Fig. 217. Lateral view on the right tibia of individual KG-027-0106 (Burial 28) with an osteomyelitis at the proximal part of the bone shaft. The coarsely woven bone at the cortex and consequent thickening of the bone are clearly visible

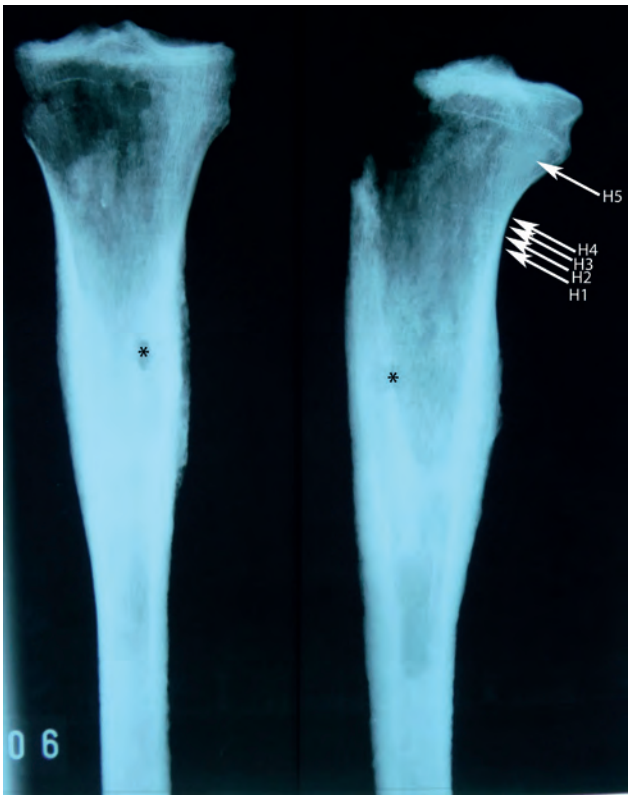

Fig. 218. X-ray Image (10 mAs, 52 kVp) of the proximal part of the right tibia of individual KG-027-0106 (Burial 28) from anterior (left) and lateral (right). Harris lines (H1–H5) are indicated by arrows. For better comparability with Fig. 216 and Fig. 217 the central sinus (cloaca) is marked with an asterisk. The numbers on the X-ray image, which have a height of 1 cm, serve as a scale

sequently, the individual most probably died at an age of about 16–19 years.

The individual showed a rather light periostitis in the upper part of the right femoral bone, while the right tibia showed an osteomyelitis at the proximal half of the bone (Fig. 216 and Fig. 217, see ch. V.4.5). X-ray analysis revealed the involvement of the medullary cavity (Fig. 218). Furthermore, on the proximal part of the bone (at least) five Harris lines are visible in Fig. 218 (see ch. V.4.5). Since the distal part of the bone was not preserved, it was not possible to measure the total length of the tibia. This measure was, however, estimated at about 36 to 37 cm. Using the formula of Byers (1991) for proximal Harris lines on the tibia the lines developed at an age of about 11/12 years, 12/13 years, 13/14 years, and 16/17 years. The last Harris line is of special importance as it occurred quite late in the individual's life. The individual probably died relatively soon after the last period of stress had been overcome. However, the age at formation of the Harris lines has to be understood as a rough approximation due to the estimated total length.

Postcranial indices showed eurycnemic right (111.1) and left (128.0) tibiae and an eurymeric (85.3) right as well as a hyperplatymeric (73.7) left femur. The robustness index of the femoral bones was calculated as 12.8 and 11.4 for right and left femur, respectively. According to Trotter and Gleser (1958) the body height calculated from the femur was about 167–169 cm (see ch. V.4.3.2).

Burial 29 (KG-031-0120)

The skeleton of individual KG-031-0120 was almost completely preserved (Fig. 221). According to sex-specific features of the pelvic bones, the cranium, and the femoral bones the individual was determined as male. According to epiphyses and apophyses as well as cranial sutures death occurred at an age of 20 to 25 years.

The joints of the right hand showed minor changes, probably due to bearing heavy weights or extensive usage. All other joints were inconspicuous. The right elbow

Fig. 219. Cribra orbitalia (see arrows) in the right and left orbit of individual KG-031-0120 (Burial 29)

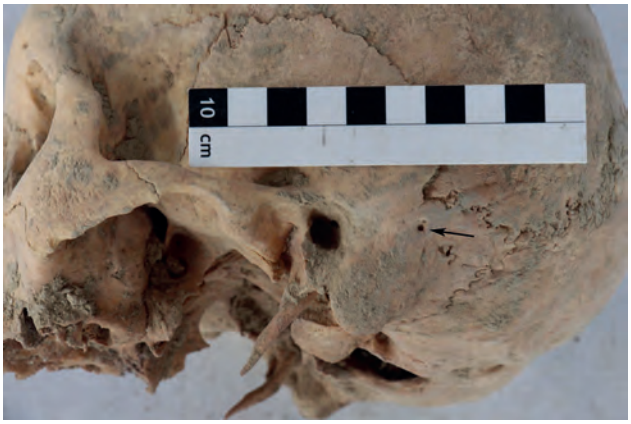

Fig. 220. Exsutural Foramen mastoideum (see arrow) on the left side of the skull of individual KG-031-0120 (Burial 29)

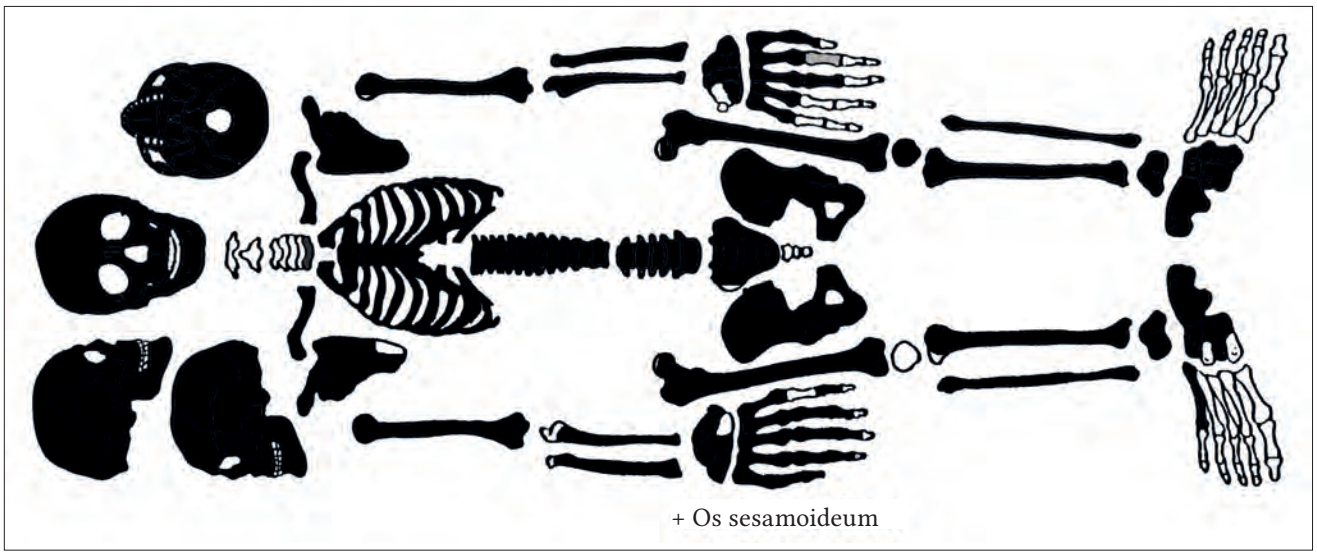

Fig. 221. Skeletal scheme of KG-031-0120 (Burial 29). Bones of indeterminable siding and/or position are shown in grey

Fig. 222. Processi spinosi bipartiti (see arrows) on cervical vertebrae C3–C6 of individual KG-031-0120 (Burial 29)

Fig. 223. Foramen transversum bipartitum (see arrrow) on the right side of cervical vertebra C7 of individual KG-031-0120 (Burial 29). The left side could not be determined

as well as both hip joints could, however, not be examined. Three teeth (II 6, II 7, IV 7) were severely affected by caries of state 4 (II 6, IV 7) to 5 (II 7). In addition, intra-vital tooth loss had occurred (tooth III 1 and IV 6). A rather slight abrasion was visible on several teeth (see ch. V.4.5). Both orbits showed a slight form of cribra orbitalia (Fig. 219; see ch. V.4.5).

The skeleton showed a number of epigenetic skeletal variants (see ch. V.4.6): An exsutural mastoid foramen (Fig. 220) was present on both sides of the skull. Furthermore, the third to sixth cervical vertebrae showed Processi spinosi bipartiti (Fig. 222). At the seventh cervical vertebra a Foramen transversum bipartitum was detected on the right side (Fig. 223). The left side could not be appraised.

The cranium was determined as brachycephalic (86.5), hypsicranic (76.7), tapeinocranic (88.5), euryprosopic (80.3), hypereuryene (44.5), hypsiconch (91.9), and leptorrhine (46.2). Consequently, this individual was short-headed with a high, broad braincase, a short craniofacial part, a very broad upper face, high orbits, and a narrow nose (Fig. 224 and Fig. 225; see ch. V.4.3.1).

The individual showed an eurymeric index platymericus on the right (93.5) as well as on the left (96.8) femo-

Fig. 224. Norma frontalis of the skull of individual KG-031-0120 (Burial 29)

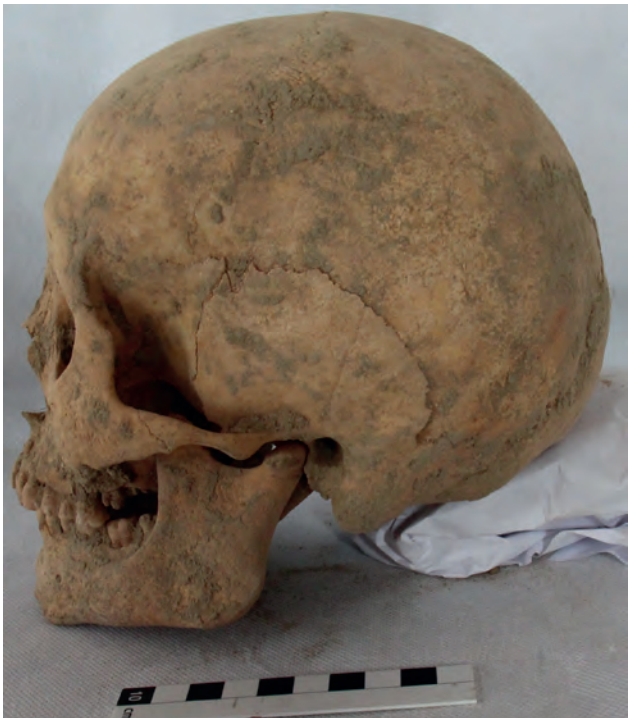

Fig. 225. Norma lateralis of the skull of individual KG-031-0120 (Burial 29)

Several teeth (I 1, I 2, I 3, II 2, III 3, IV 3) showed linear enamel hypoplasia (LEH; see ch. V.4.5). According to the chart after Massler et al. (1941) the LEH formed when

ral bone and a mesocnemic index cnemicus for both the right and the left tibia (66.7). The robustness indices of humerus, radius, ulna, and tibia could only be assessed for the left bones with values of 20.1, 17.4, 16.7, and 20.9, respectively. According to the measurements of the left humerus, the left radius and the right tibia the body height is estimated at 165–171 cm following Trotter and Gleser (1958) (see ch. V.4.3.2).

Burial 30 (KG-036-0134)

The skeleton of individual KG-036-0134 was partially preserved (Fig. 227). The skull and the pelvic girdle allowed both age and sex determination. According to sex-specific criteria on the pelvis, mandible, cranium, and Caput femoris the individual was determined as female. The age at death was determined as about 40 to 50 years based on the cranial sutures. This is also in accordance with the abrasion of the teeth and intra-vital tooth loss (IV 5, IV 6).

Fig. 226. Doubled Foramen zygomaticofaciale (see arrows) on the left Os zygomaticum of individual KG-036-0134 (Burial 30)

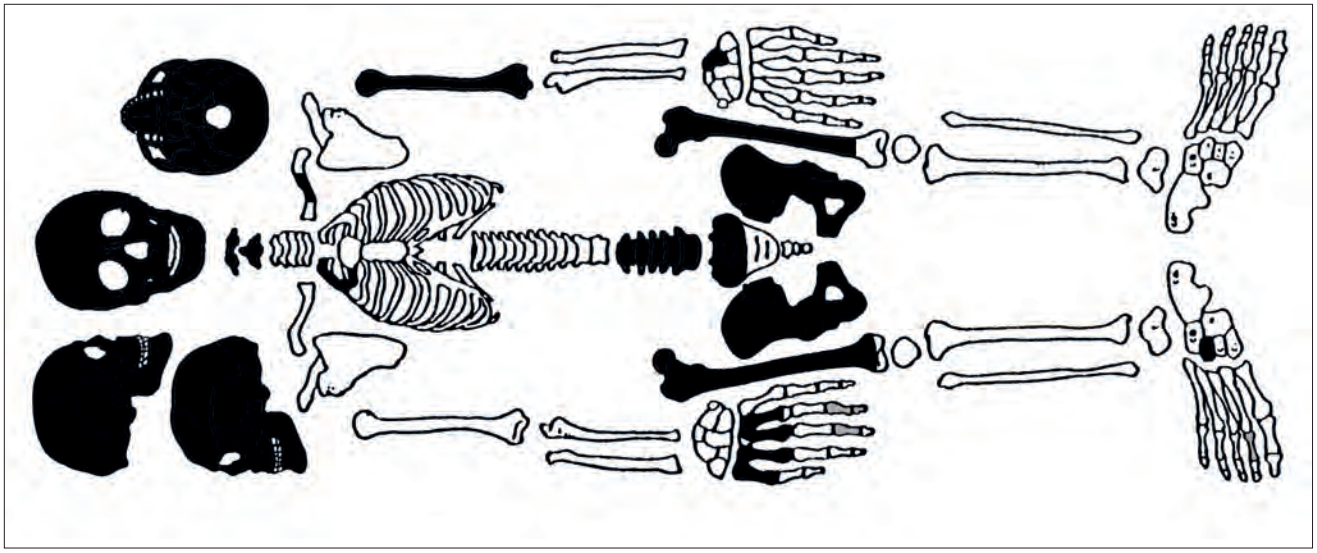

Fig. 227. Skeletal scheme of KG-036-0134 (Burial 30). Bones of indeterminable siding and/or position are shown in grey

Fig. 228. Norma frontalis of the skull of individual KG-036-0134 (Burial 30)

the individual was about three years old, pointing to a period of severe deficiency at this age.

Fig. 229. Norma lateralis of the skull of individual KG-036-0134 (Burial 30)

The left zygomatic bone showed an epigenetically doubled Foramen zygomaticofaciale (Fig. 226), while the right side showed only one foramen (see ch. V.4.6).

According to cranial measurements the skull was determined as brachycephalic (84.8), hypsicranic (76.4), tapeinocranic (90.0), hyperleptoprosopic (111.0), hyperleptene (60.6), hypsiconch (89.2), and leptorrhine (42.3). Thus, the individual had a short head with a high and broad braincase, a long craniofacial part, a very narrow upper face, high orbits, and a narrow nose (Fig. 228 and Fig. 229; see also Table 17 and ch. V.4.3.1).

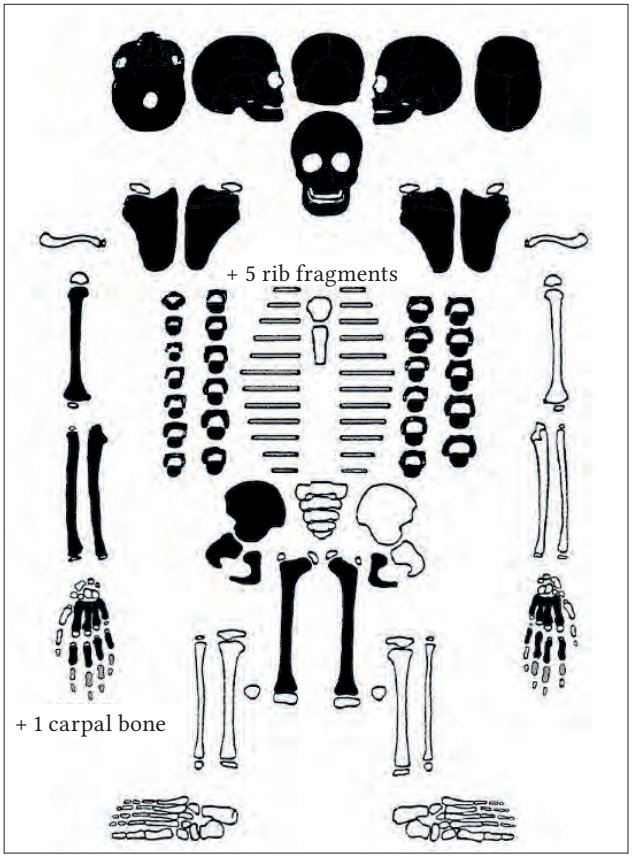

Fig. 230. Skeletal scheme of KG-042-0173 (Burial 31). Bones of indeterminable siding and/or position are shown in grey

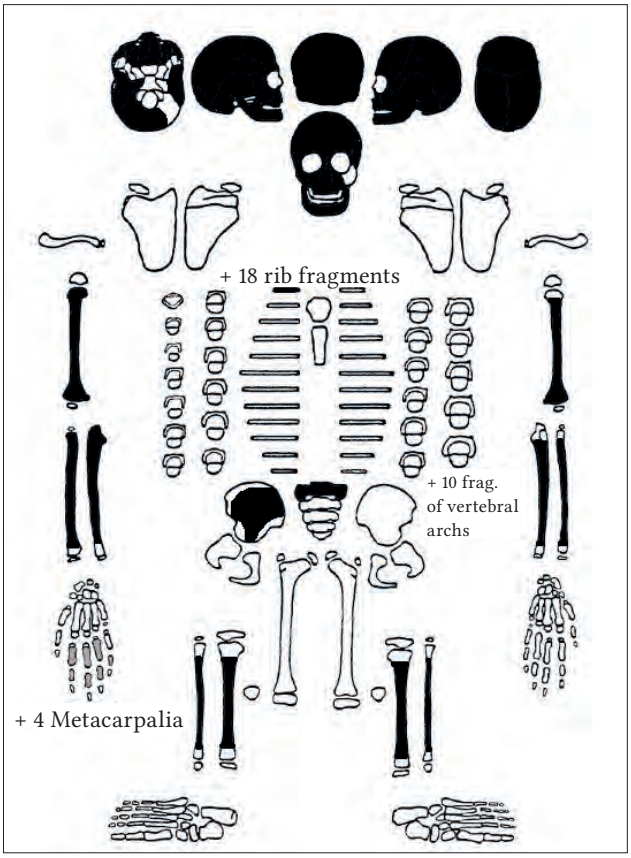

Fig. 231. Skeletal scheme of KG-045-0193 (Burial 32). Bones of indeterminable siding and/or position are shown in grey

A few animal bones, which remained unspecified, were detected.

Burial 31 (KG-042-0173)

The skeleton of the child KG-042-0173 was quite well preserved, but not complete, with the lower legs and the left arm bones missing (Fig. 230). According to sex-specific features of the pelvis and the mandible, the individual was determined as probably female. The age at death was determined as about 5–7 years. Due to the ossification of the Partes laterales ossis occipitalis and Pars basilaris at the Os occipitale the age at death had to be above 5 to 7 years. However, the Ramus inferior ossis pubis and the Ramus superior ossis ischii were not fused indicating an age below six to eight years. Following the dental chart, the individual died at an age of about seven years (± 24 months). In addition, the length of the right ulna of around 148 mm was in the range of individuals of six to eight years of age (see Stloukal/Hanakova 1978). All considered, the age at death was determined as about 5 to 7 years.

Burial 32 (KG-045-0193)

The skeleton of child KG-045-0193 was only partially preserved (Fig. 231), but unfragmented. The surface of the bones was highly eroded. Although the mandible showed characteristics of a probably male individual, due to poor preservation of the pelvis no sex determination was possible. The individual's age at death was estimated at 4 to 6 years. This estimation was based on the tooth development (6 ± 2 years), the completed fusion of the Partes laterales ossis occipitalis and the Squama occipitalis (> 3 years), as well as the completed fusion of vertebral arches and vertebral bodies (> 3 years), while Partes laterales ossis occipitalis and Pars basilaris were not fused (< 5–7 years).

Burial 33 (KG-046-0192)

The skeleton of individual KG-046-0192 was nearly complete (Fig. 232) and unfragmented with only slight taphonomic damages. According to the sex-specific features of

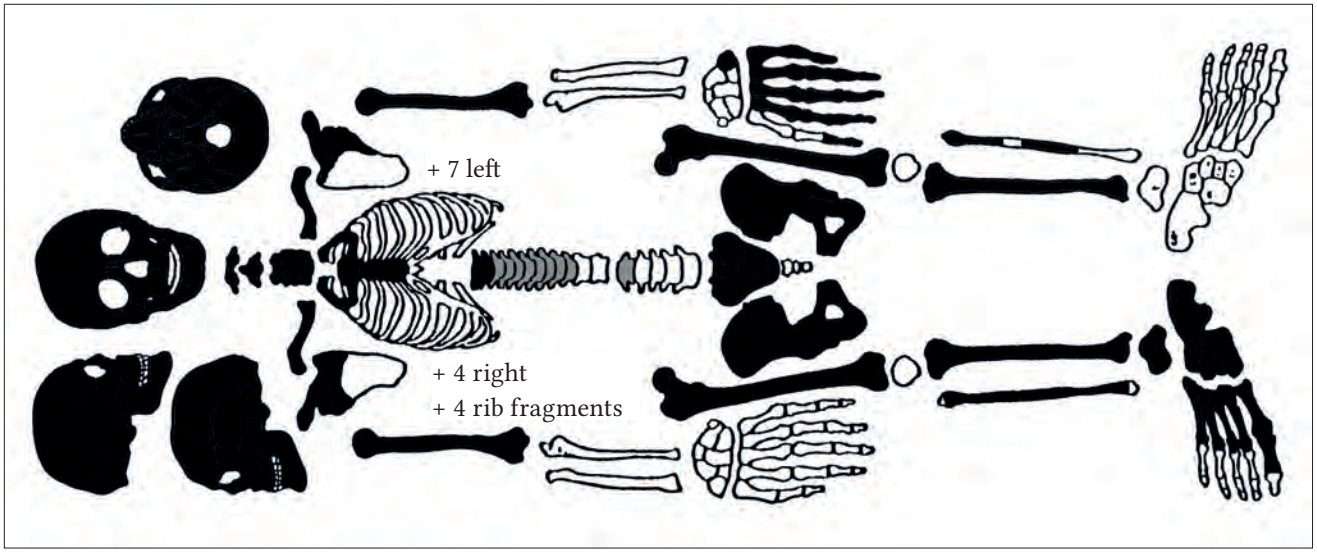

Fig. 232. Skeletal scheme of KG-046-0192 (Burial 33). Bones of indeterminable siding and/or position are shown in grey

Fig. 233. Norma frontalis of the skull of individual KG-046-0192 (Burial 33)

Fig. 234. Norma lateralis of the skull of individual KG-046-0192 (Burial 33)

the pelvic girdle, mandible, cranium, and Caput femoris the individual was determined as male. Epiphyseal and apophyseal closure allowed a determination of the age at death of about 21 to 24 years. This determination was based on the incomplete fusion of the epiphysis of the clavicula c. 22–24 years) and the still visible suture at the left ischium (c. 21–24 years), while the epiphyses at the proximal and distal humerus, femur, and tibia were completely fused.

Cranial measurements revealed a brachycephalic (82.9), hyperhypsicranic (90.3), hyperacrocranic (109.3),

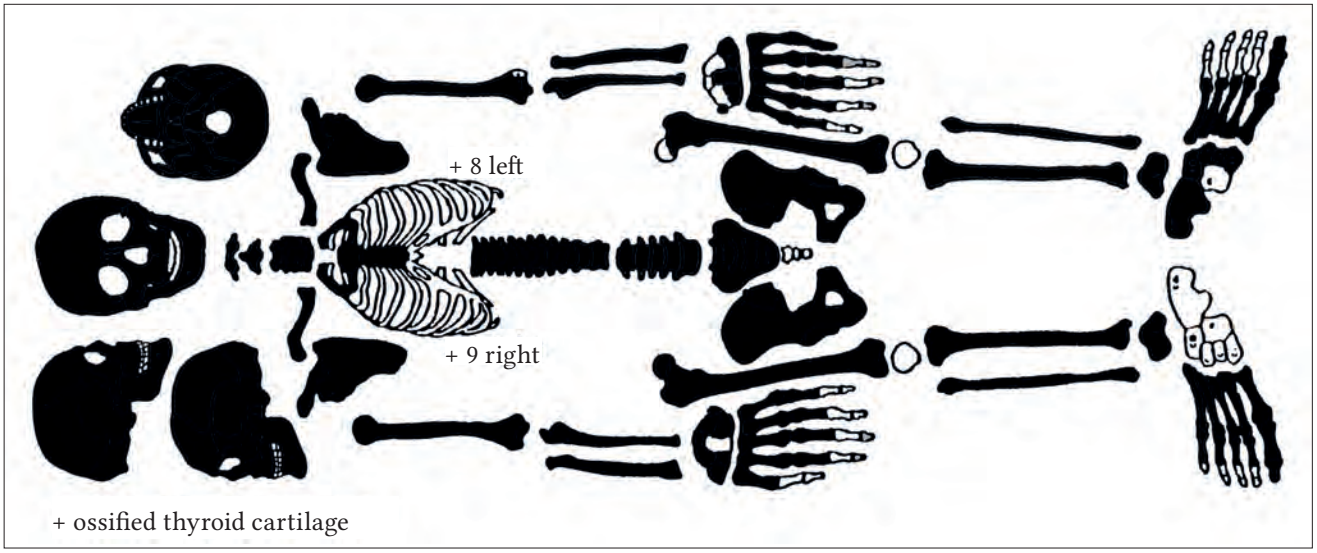

Fig. 235. Skeletal scheme of KG-048-0197 (Burial 34)

euryprosopic (80.3), euryene (46.0), mesoconch (80.0), and leptorrhine (41.8) skull. The individual had a short skull, with a very high and narrow braincase, a short facial skull, a broad upper face, medium high orbits, and a narrownose (Fig. 233 and Fig. 234; see also Table 17 and ch. V.4.3.1). Furthermore, the individual showed a hyperplatymeric index platymericus (right: 73.7, left: 73.0) and a hypereurycnemic index cnemicus (right: 86.5, left: nd). The robustness index of humerus, femur, and tibia could only be determined for the right side with 23.6, 13.5, and 22.8, respectively. The body height was estimated at about 170 to 173 cm using the linear equations of Trotter and Gleser (1958) (see ch. V.4.3.2).

Fig. 236. Bony spurs (see arrows) at the Os ischii projecting in the Foramen obturatum of the right pelvis of individual KG-038-0197 (Burial 34)

Burial 34 (KG-048-0197)

The skeleton of individual KG-048-0197 was quite well preserved and almost complete (Fig. 235). According to sex-specific features of the pelvic girdle, mandible, cranium, and Caput femoris the individual was determined as male. The age at death was quite high with more than 60 years. The Facies symphysialis on both the right and the left pelvis showed states 4 to 5 indicating an age of 50 to 80 years. According to the state of the Facies auricularis, which could only be examined on the left pelvis, the age at death was between 53 and 92 years. The preserved ossified thyroid cartilage is also indicative of a high age at death. Histomorphometrical age determination after Ericksen (1991) was in accordance with the morphological age determination with an estimated biological age of 66 years (± 10 years) without specified sex and an age

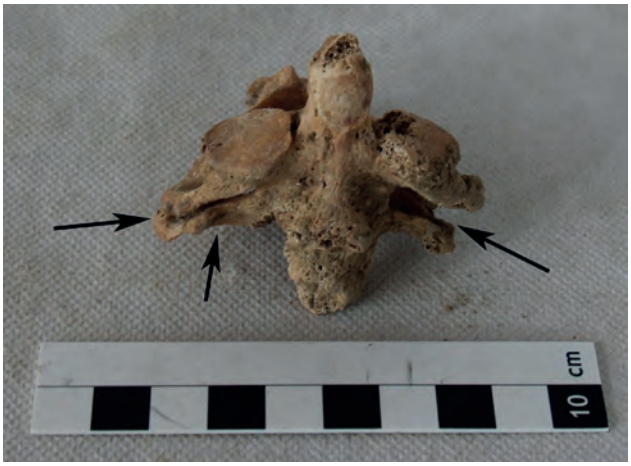

Fig. 237. Fusion of the second and third cervical vertebrae (see arrows) of individual KG-048-0197 (Burial 34)

Fig. 238. Supraorbital notches (see arrows above orbits) and accessory Foramina infraorbitalia (see arrows below orbits) on both sides of the facial skull of individual KG-048-0197 (Burial 34)

Fig. 239. Facies articularis superior atlantis bipartita on the superior side of the atlas of individual KG-048-0197 (Burial 34)

Fig. 240. Norma frontalis of the skull of individual KG-048-0197 (Burial 34)

Fig. 241. Norma lateralis of the skull of individual KG-048-0197 (Burial 34)

around 59 years (± 10 years) for a male individual. Age estimation using TCA (see Kagerer/Grupe 2001) only revealed a chronological age at death of 43 years (± 3 years), which, given all other evidence, is probably underestimating the individual's age. Altogether, the individual probably died at an age between about 49 and 76 years.

The individual showed bony spurs at the Os ischii projecting in the Foramen obturatum of the right pelvis (Fig. 236; see ch. V.4.5). These bony spurs probably indicate an ossification of the Membrana obturatoria, which covers the Foramen obturatum. Two muscles arise from the obturator membrane and the surrounding bony margin, namely M. obturator externus and M. obturator internus,

which are responsible for adduction, external rotation, and extension of the hip joint. A unilateral distribution of the weight as well as an over stretching of the membrane could lead to the formation of bony spurs. Even an injury of either the membrane or one of the muscles would be possible. It can be assumed that the individual did not use the right leg in a normal way after the injury. Indeed, postcranial measurements (index cnemicus, see below) indicate that the right leg was immobilized or non-weight bearing for quite some time.

Furthermore, the second and third cervical vertebrae were fused at the vertebral bodies and the Processi spinosi (Fig. 237; see ch. V.4.5). However, no hint of a traumatic event could be detected.

In addition, the skull of the individual showed two different epigenetic variants, namely supraorbital notches and accessory Foramina infraorbitalia, which were present on both sides of the skull (Fig. 238; see ch. V.4.6).

Moreover, the first cervical vertebra (atlas) showed a bipartite superior articular surface on both the right and the left side (Facies articularis superior atlantis bipartita; Fig. 239). Finally, the second and third cervical vertebrae showed a bipartite Processus spinosus (Processus spinosus bipartitus) (see ch. V.4.6).

Cranial measurements revealed a hyperbrachcephalic (91.1), orthocranic (71.4), hypertapeinocranic (78.4), mesoprosopic (85.1), mesene (53.9), hyperhypsiconch (100.0), and leptorrhine (36.1) skull. According to these measurements the individual's skull was very short, with a medium high, but very broad braincase, a medium facial skull, a medium wide forehead, very high orbits, and a very narrow nose (Fig. 240 and Fig. 241; see also Table 17 and ch. V.4.3.1). Both right and left femora were platymeric with an index platymericus of 81.8 and 80.0, respectively. Furthermore, the index cnemicus revealed an eurycnemic right (73.5), but a mesocnemic left tibia (67.6). This might be related to the injury of the obturator membrane or the obturator muscles of the right pelvic (see above). The robustness index of the humerus showed no side preference with an index of 20.6 the right and 20.8. for the left bone. Radius and ulna also showed only slight side-specific differences with indices of 20.6 (right) and 19.8 (left) in case of the radius and indices of 19.6 (right) and 20.3 (left) in case of the ulna. Long bone metrics allowed for body height reconstruction (Trotter/Gleser 1958), which was calculated as between 166 and 168 cm according to the measurements of the humerus (right), radius (right, left), and tibia (right) (see ch. V.4.3.2).

Burial 35 (KG-047-0217 and KG-098-0467)

The cranial (KG-098-0467) and postcranial part (KG-047-0217) of a skeleton were combined to a single individual (see ch. IV.9). The individual was only partially preserved (Fig. 242). The bone surfaces were highly eroded. Both parts of the skull as well as the lower legs could be examined. Sex determination was only possible on features of the mandible and cranium. According to these features the individual was determined as probably male. Cranial sutures indicated an age below 50. Tooth abrasion was quite strong. However, besides a higher age, this could also be explained by the diet. Histological age determination revealed a biological age at death of 40 years (± 9 years) for a tibia sample (Thompson/Galvin 1983). Accordingly, the age at death was determined as 31 to 49 years.

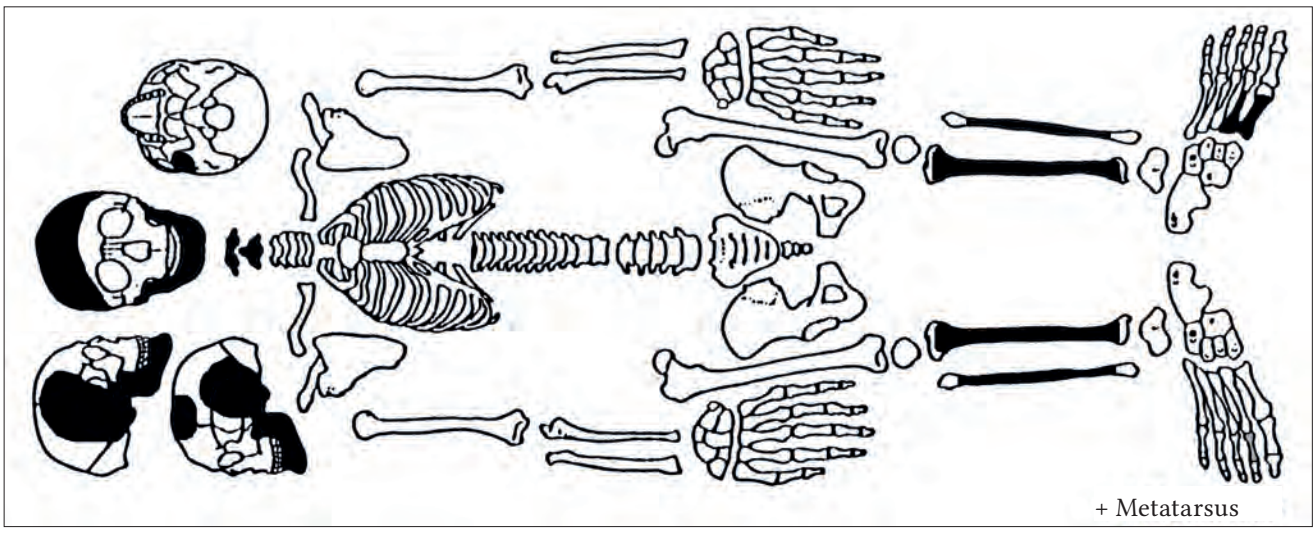

Fig. 242. Skeletal scheme of KG-047-0217 and KG-098-0467 (Burial 35)

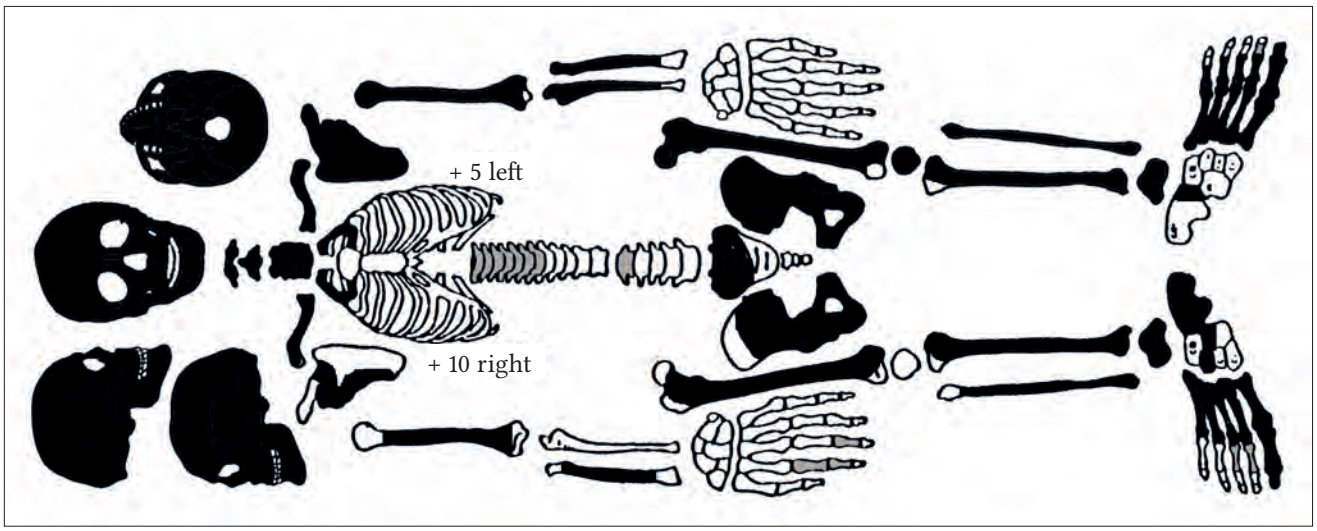

Fig. 243. Skeletal scheme of KG-050-0203 (Burial 36). Bones of indeterminable siding and/or position are shown in grey

Fig. 244. Lambdoid ossicles (see arrows) on the Sutura lambdoidea of individual KG-050-0203 (Burial 36)

Fig. 245. Canalis condylaris on the right side of the Foramen magnum (left arrow) of individual KG-050-0203 (Burial 36), while the canal is not patent on the left side (right arrow)

Burial 36 (KG-050-0203)

Skeleton KG-050-0203 was well preserved and almost complete (Fig. 243). According to sex-specific features of the pelvis, mandible, and cranium the individual was determined as male. All preserved epi- and apophyses were completely fused. Age determination of the Facies symphysialis on the pelvic bone showed state 4 on both sides. This is indicative of an age at death of about 50–70 years. Cranial sutures showed an age between 40 and 60 years. However, due to the presence of lambdoid ossicles on the lambdoid suture (Fig. 244; see below), the cranial sutures are not valid. Altogether, the individual probably died at an age of 50 to 70 years.

The left elbow (right nd), left hip (right nd), both knees, and foot joints showed small osteophytes (< 3 mm), which is, however, fully appropriate for an individual dying at such an advanced age. Furthermore, both cervical and thoracic vertebrae showed a medium state of spondylolysis. The lumbar vertebrae could not be examined. Again, the mature to senile age could explain the spondylolysis.

The individual showed medium abrasion of the teeth. More importantly, several teeth showed a relatively severe form of calculus (II 7, II 8, III 5, III 6, III 7, III 8, IV 6) on the buccal or lingual side of the teeth. In addition,

Fig. 246. Foramen supratrochleare (see arrows) on the distal end of the left Humerus of individual KG-050-0203 (Burial 36)

Fig. 247. Norma frontalis of the skull of individual KG-050-0203 (Burial 36)

tooth II 5 was affected by caries of state 5 in combination with an abscess at the root collar of the respective tooth (see ch. V.4.5).

Besides the above mentioned lambdoid sutural bones, the individual also showed a patent Canalis condylaris on the right side of the Foramen magnum (Fig. 245; see ch. V.4.6). The canal was, however, not patent on the left side. The left humerus showed a Foramen supratrochleare on the distal end of the bone (Fig. 246). The right humerus could not be assessed.

Cranial measurements revealed a hyperbrachycephalic (93.6), hypsicranic (81.5), tapeinocranic (87.1), hy-

Fig. 248. Norma lateralis of the skull of individual KG-050-0203 (Burial 36)

perleptoprosopic (95.6), mesene (52.6), hypsiconch (94.4), and leptorrhine (46.2) skull. In addition, the jugo-frontal and the jugo-mandibular index were identical (66.7). According to these measures the individual had a short and rather angular head, with a high and broad braincase and a medium wide upper face. The individual's face was very long with high orbits and a small nose (Fig. 247 and Fig. 248; see also Table 17 and ch. V.4.3.1). The individual showed mesocnemic right (68.8) and left (67.7) tibiae and hypereurycnemic femoral bones (right: 82.8, left: 83.9). The left tibia (right nd) showed a robustness index of 19.8. Body height estimations (after Trotter/Gleser 1958) revealed a body height of about 161 cm (left humerus) to 165 cm (right tibia) (see ch. V.4.3.2).

Burial 37 (KG-052-0205)

The skeleton of individual KG-052-0205 (Fig. 249) was relatively well preserved and almost complete with only light taphonomic damages. The child was determined as probably male according to sex-specific criteria on both the pelvis and the mandible. Age determination revealed an age at death of 10 to 13 years. This estimation was mainly based on the fact that all epiphyses were still open indicating an age below 14, and on the tooth development indicating an age at death of 12 years (± 30 months). In addition, the vertebrae showed a complete synostosis and the ossification center of the Apex dentis

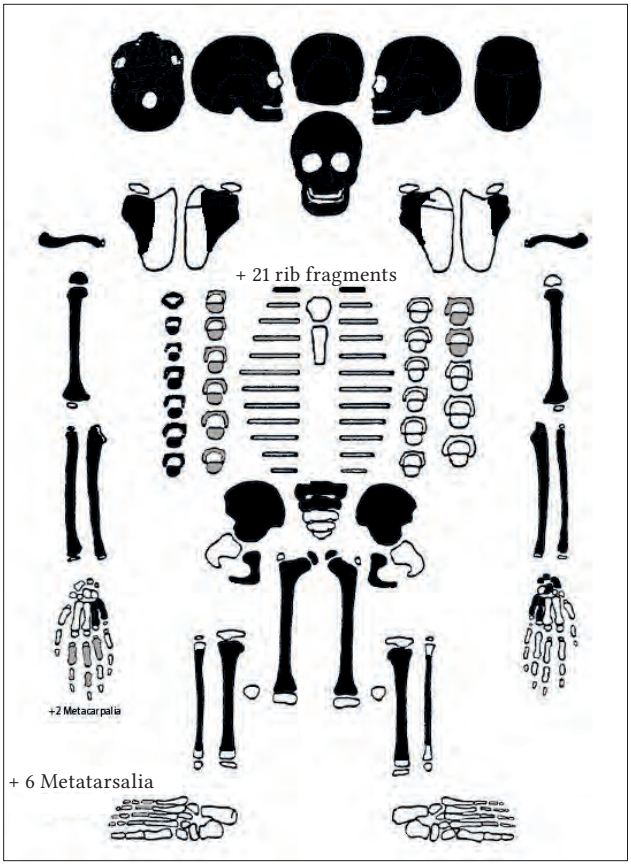

Fig. 249. Skeletal scheme of KG-052-0205 (Burial 37). Bones of indeterminable siding and/or position are shown in grey

Fig. 251. Norma frontalis of the skull of individual KG-073-0508 (Burial 38)

Fig. 250. Foramen transversum bipartitum (see arrows) on two cervical vertebrae (vertebra C4 and C5) of individual KG-052-0205 (Burial 37). The foramina on the fifth vertebra (right) are damaged and only partly visible

Fig. 252. Norma lateralis of the skull of individual KG-073-0508 (Burial 38)

had already fused to the Dens axis. This is indicative of an individual of the age class Infans II.

Two cervical vertebrae (C4 and C5) showed an epigenetic trait, namely Foramina transversa bipartita on both the right and the left side (Fig. 250; see ch. V.4.6).

Two bones, the first right Metacarpus as well as the right Os cuboideum, of an adult individual were mixed in the bones of individual KG-052-0205.

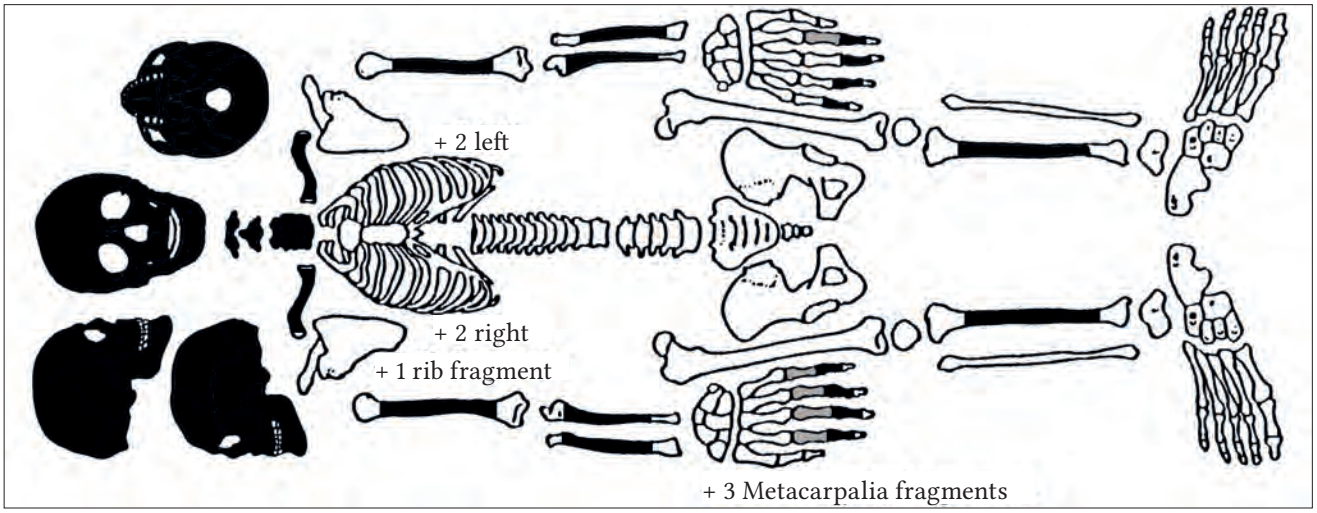

Fig. 253. Skeletal scheme of KG-073-0508 (Burial 38). Bones of indeterminable siding and/or position are shown in grey

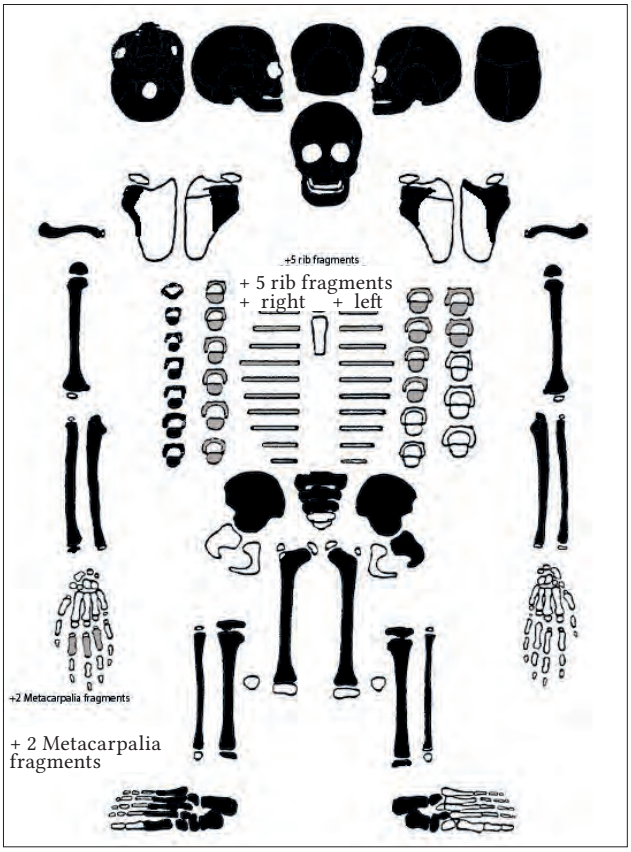

Fig. 254. Skeletal scheme of KG-077-0517 (Burial 39). Bones of indeterminable siding and/or position are shown in grey

Burial 38 (KG-073-0508)

The partially preserved skeleton of individual KG-073-0508 (Fig. 253) showed high taphonomic damages to the bones. The individual was determined as probably female according to the sex-specific features of the skull. The pelvic bones were not preserved. According to the cranial sutures the individual died at an age of 40 to 59 years.

Cranial measurements revealed a hyperbrachycephalic (85.5), orthocranic (73.9), tapeinocranic (86.5), hyperleptoprosopic (97.3), leptene (57.7), hypsiconch (88.2), and leptorrhine (42.9) skull: The individual showed a very short head with a medium sized and broad braincase, a long face, and a narrow forehead, with high orbits and a narrow nose (Fig. 251 and Fig. 252; see also Table 17 and ch. V.4.3.1).

Burial 39 (KG-077-0517)

The skeleton of individual KG-077-0517 was well preserved and almost complete (Fig. 254). Sex and age determination revealed a male child of c. 9 to 12 years. The sex determination was based on sex-specific features of both pelvis and mandible. Ramus inferior ossis pubis and Ramus inferior ossis pubis were fused indicating an age above 6 to 8 years. The apical ossification center of the Dens axis was already fused and the synostosis was complete indicating age class Infans II. Furthermore, long bone measurements of femur, tibia, humerus, radius, and ulna were in agreement with an age at death between 7 and 12 years (see Stloukal/Hanakova 1978). In addition, according to the tooth development an age of about 12 years (± 30 months) was determined (AlQahtani et al. 2010). In sum, the age at death was estimated at about 9 to 12 years.

The individual displayed an epigenetic variant, namely a bifurcated right rib (see ch. V.4.6). The remaining ribs were inconspicuous. Long bone metrics revealed an es-

timated body height between 114 cm and 120 cm according to the regression formulas of Telkkä et al. (1962) (see ch. V.4.3.2).

Burial 40 (KG-089-0387)

The skeleton of child KG-089-0387 was incompletely preserved (Fig. 255) and showed strong taphonomic damages to the bone surface. Sex determination was not possible due to missing pelvic bones. However, age determination revealed an age at death of 10 to 14 years. This estimation was mainly based on the tooth development indicating an age at death of 12 years (± 30 months) according to the scheme of AlQahtani et al. (2010).

Burial 41 (KG-093-0480)

The skeleton of individual KG-093-0480 was well preserved and almost complete (Fig. 257). Sex determination on the pelvis, the skull, and the femoral head showed it to be a male individual. The age at death was determined as about 50 to 60 years. This estimation was based on the Facies symphysialis of the left pelvis (right nd) of state 3 to 4 indicating an age at death between 40 and 70 years. In addition, the Facies auricularis of the left pelvis (right nd) revealed an age at death of 53 to 92 years. According to the cranial sutures, this individual was younger than 60 years. Thus, the age at death most likely was between 50 and 59 years.

The individual suffered from a mild arthrosis of the right and left elbows, the left hand, and the right hip with osteophytes below 3 mm. In addition, thoracic vertebrae showed a mild spondylarthrosis. The lumbar vertebrae showed a strong spondylosis with rather strong osteophytes (Fig. 256). In the case of the lumbar vertebrae the osteophytes are possibly indicative of some sort of physiological stress or false posture. This might be connected to the mild arthrosis of the right hip. Thoracic vertebra T7 to T12 and lumbar vertebra L2 to L4 (L1 nd) showed Schmorl's nodules on either the anterior side, the posterior side or on both (see ch. V.4.4).

Besides the vertebrae the individual showed several other abnormalities, which might also be connected to either physiological stress or a trauma (see ch. V.4.5). The left tibia showed quite large osteophytes on the medial proximal part close to the Tuberositas tibiae (Fig. 258). This is probably caused by a trauma of the Ligamentum collaterale tibiae. Bony spurs were present at the Facies

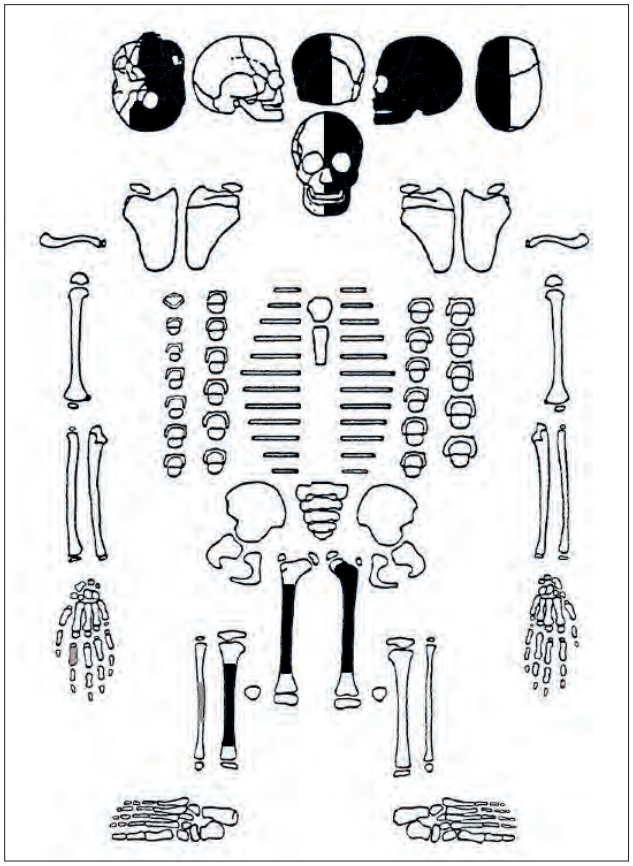

Fig. 255. Skeletal scheme of KG-089-0387 (Burial 40). Bones of indeterminable siding and/or position are shown in grey

auricularis of the left pelvis (Fig. 259) as well as the sacrum with relatively large osteophytes (Fig. 260). In addition, enthesiopathies were detected at the the conoid tubercle of both clavicles (Fig. 261), the tibial tuberosity, and the calcaneal tuberosities of both right and left calcaneus.

Two acquired bone variants were present (see ch. V.4.6): Rhomboid fossae were detected in the area of the impression for the costoclavicular ligament of both right and

Fig. 256. Osteophytes (see arrows) at the anterior side of four lumbar vertebrae of individual KG-093-0480 (Burial 41)

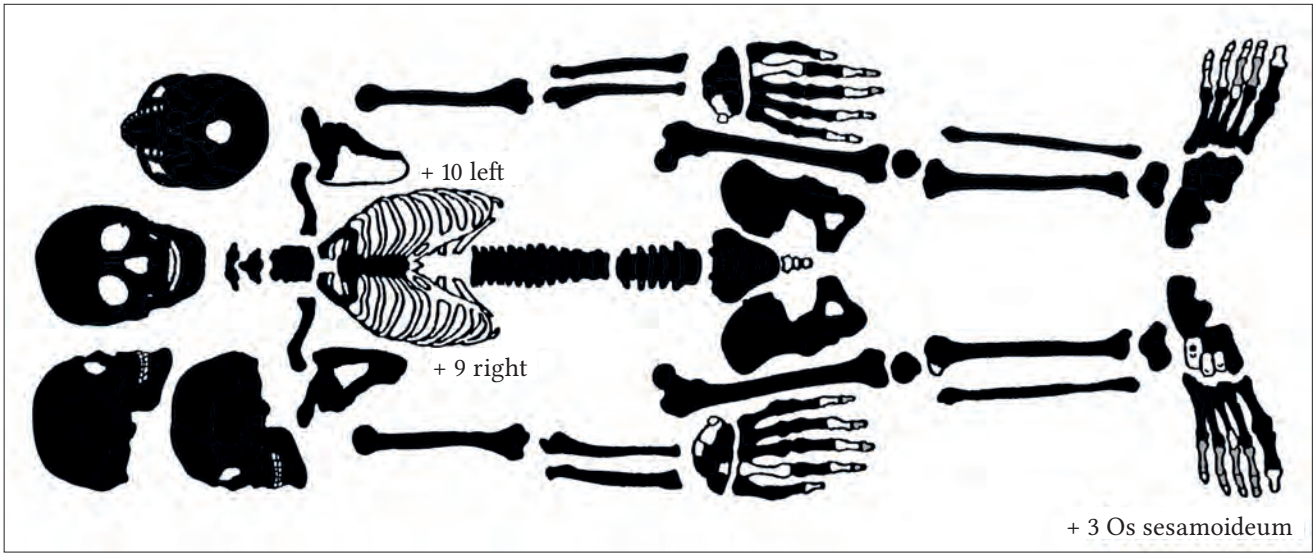

Fig. 257. Skeletal scheme of KG-093-0480 (Burial 41)

Fig. 258. Posterior view on the proximal part of the left tibia of individual KG-093-0480 (Burial 41) with osteophytes (see arrows) at the medial side, probably caused by an injury of the Ligamentum collaterale tibiae

Fig. 259. Osteophytes (see arrows) at the Facies auricularis of the left pelvis of individual KG-093-0480 (Burial 41)

Fig. 260. Damage of the right joint (left nd) of the sacrum of individual KG-093-0480 (Burial 41) with relatively large osteophytes (see arrows). The corresponding Facies auricularis of the right pelvis could not be examined

Fig. 261. Enthesiopathy (lateral) and rhomboid fossae (medial) on both clavicles of individual KG-093-0480 (Burial 41)

left clavicle (Fig. 261). Also the left femur showed a modification of Allen's fossa at the femoral neck (Fig. 262). In contrast to the usual appearance of this variant (see e. g.

Fig. 262. Variant of Allen's fossa (see arrows) at the femoral neck of the left femur of individual KG-093-0480 (Burial 41)

Fig. 263. Processus supracondylaris (see arrow) on the posterior side of the left humerus diaphysis of individual KG-093-0480 (Burial 41)

Fig. 264. Canales condylares (see arrows) present on both sides of the Foramen Magnum of individual KG-093-0480 (Burial 41)

Fig. 265. Foramen supraorbitale with a vertical septum (see arrows) on the left side of the skull of individual KG-093-0480 (Burial 41)

Allen 1884; Finnegan/Faust 1974) the affected area at the femoral neck is not circular but lobulated. The trabeculae are only partly visible, while they are usually clearly visible in the whole area of the fossa.

The individual also showed different epigenetic variants (see ch. V.4.6): At the left humerus a so-called Processus supracondylaris was visible (Fig. 263). Furthermore, a posterior condylar canal (Canalis condylaris) was patent on both sides of the Foramen magnum (Fig. 264). The Foramen supraorbitale on the left side of the skull was complete and showed a vertical septum (Fig. 265). Even a sesamoid bone could be detected.

According to the cranial measurements taken the individual had a hyperbrachycephalic (90.4), hypsicranic (80.1), tapeinocranic (88.7), mesoprosopic (88.4), mesene (51.9), hypsiconch (89.2), and leptorrhine (42.3) skull. In other words, the individual exhibited a very short head with a high and broad braincase, a medium facial skull as well as a medium wide upper face, high orbits, and a narrow nose (see also Table 17 and ch. V.4.3.1).

Postcranial indices revealed an eurymeric (90.9) right and a platymeric (81.1) left femur. Both tibiae were eurycnemic with an index of 77.1 and 71.4 for the right and the left tibia, respectively. The robustness index of the humerus showed a slightly higher value for the right (22.5) compared to the left (21.2) side. The robustness index of the right (23.7) and left (23.5) tibiae was almost identical. In case of the robustness of radius and ulna as well as the femur only one side could be measured. This results in a robustness index of the left radius and ulna of 21.3 and 22.0, respectively. The right femur showed a robustness index of 13.5. According to the regression

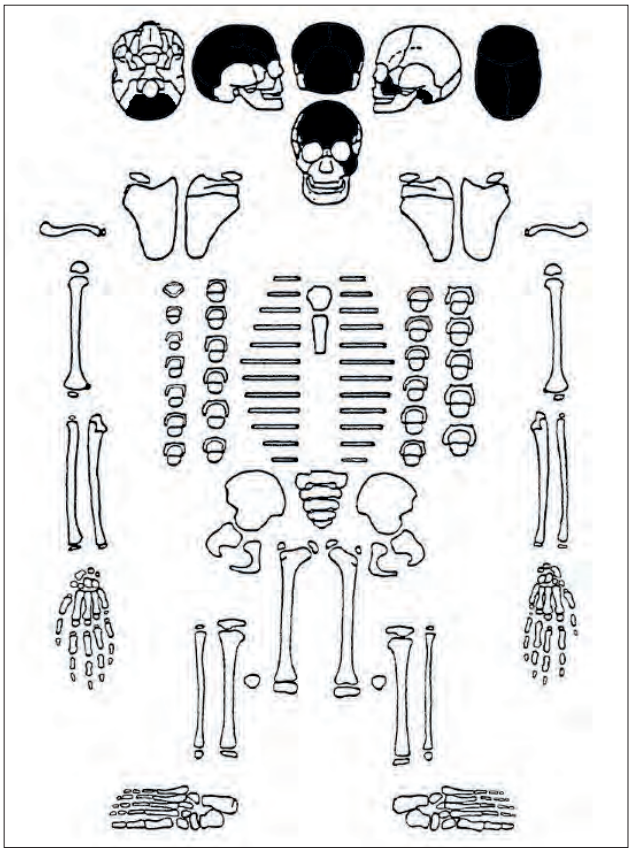

Fig. 266. Skeletal scheme of KG-035-0136 (Burial 42). Bones of indeterminable siding and/or position are shown in grey

Fig. 267. Cribra orbitalia (see arrows) on both orbits of individual KG-035-0136 (Burial 42)

equations of Trotter and Gleser (1958) the body height was estimated at about 161 to 165 cm with the help of the bone lengths of humerus, radius (right nd), femur (left nd), and tibia (see ch. V.4.3.2).

Two animal bones were detected in the grave. One of these could not be determined. The other bone was a tibiotarsus of a wild bird.

V.3.4 Undated burials

Burial 42 (KG-035-0136)

The skeleton of individual KG-035-0136 was only partly preserved. Only parts of the skull and two vertebral arches were recovered from the grave (Fig. 266). Age determination of the skull revealed an age at death of about 3 to 9 months. The posterior fontanel was already closed pointing to an age of more than three months, while the Alae majores ossis sphenoidales were not connected to the sphenoid bone, indicating an age below nine months. The individual's sex could not be determined.

The individual showed a rather strong Cribra orbitalia in both orbits (Fig. 267; see ch. V.4.5).

Burial 43 (KG-076-0515)

The skeleton of individual KG-076-0515 only consisted of a metacarpus, three phalanges and a cervical vertebra, as well as two teeth (III 2, III 3) (Fig. 269). Neither sex nor age at death could be determined.

A cervical vertebra (C6) showed a Foramen transversum bipartitum at the left side (Fig. 268). The right side did not show this bone variant. In addition, a Processus spinosus bipartitus was present (Fig. 268; see ch. V.4.6).

Burial 44 (KG-092-0398)

The skeleton of individual KG-092-0398 was only incompletely preserved (Fig. 270) and highly fragmented. The bone surfaces showed slight taphonomic damage. Sex determination was not possible due to the poor state of

Fig. 268. Foramen transversum bipartitum (see left arrow) as well as Processus spinosus bipartitus (see right arrow) at the sixth cervical vertebra of individual KG-076-0515 (Burial 43)

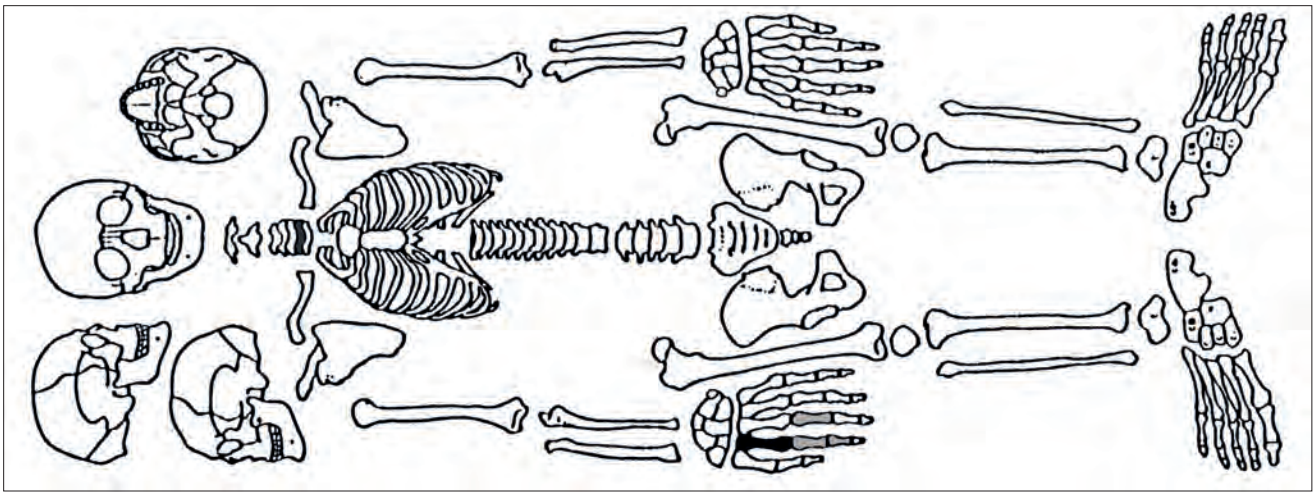

Fig. 269. Skeletal scheme of KG-075-0515 (Burial 43). Bones of indeterminable siding and/or position are shown in grey

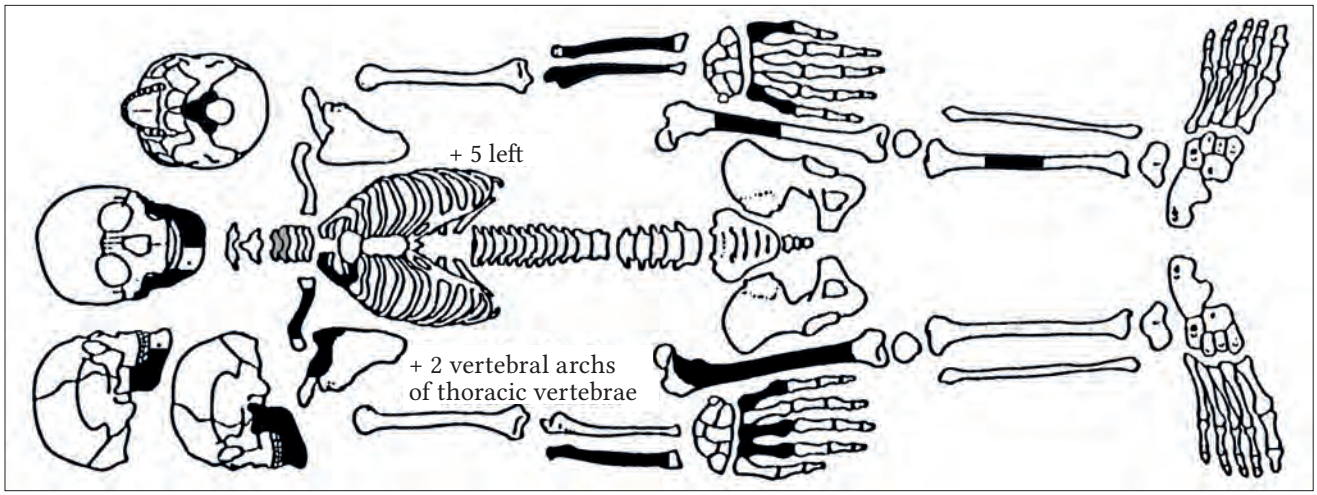

Fig. 270. Skeletal scheme of KG-092-0398 (Burial 44). Bones of indeterminable siding and/or position are shown in grey

preservation. Morphological age at death could only be determined as at least adult. The relative high level of abrasion, even on the third molars, may indicate a quite high age at death. The same probably holds true for a mild arthrosis of the left elbow and a mild spondylosis of the two cervical vertebrae preserved. This is in accordance with the histomorphometrically determined biological age at death, which was calculated as about 66 years (± 10 years) according to the method of Ericksen (1991). TCA revealed a chronological age at death of about 62 years (± 3 years).

Burial 45 (KG-096-0445)

Only some rib fragments and two teeth (IV2, IV3) of individual KG-096-0445 were preserved.

Burial 46 (KG-099-0460)

Only parts of the skeleton of individual KG-099-0460 were preserved (Fig. 272). Bone surfaces showed strong taphonomic damages. Only parts of the left lower arm were preserved, therefore neither sex nor age determination was possible.

Fig. 271. Osteomyelitis (see arrows) on the distal diaphyseal part of the left radius of individual KG-099-0460 (Burial 46)

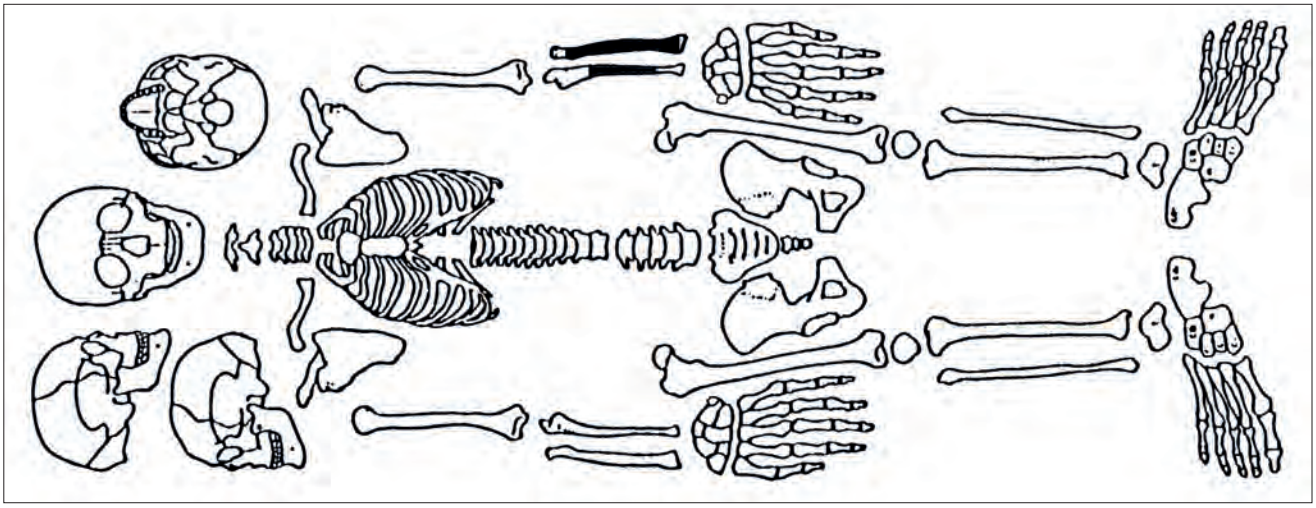

Fig. 272. Skeletal scheme of KG-099-0460 (Burial 46)

The left radius showed an osteomyelitis on the distal part of the bone (Fig. 271; see ch. V.4.5). However, due to the damaged bone surface it could not be determined if the osteomyelitis was still active when the individual died. No external injuries were visible on the bone.

V.4 Morphological results and discussion

V.4.1 State of preservation

Within the dated burials an overall tendency can be observed that skeletons of individuals dated to the Late Bronze Age/Early Iron Age as well as Antiquity are worse preserved than younger burials. This is especially the case for the overall preservation as well as fragmentation of the skeletal elements. Damages to skeletons occur over time, e. g. due to the construction of younger graves which disturb older burials. Consequently, the state of preservation across time periods was as expected.

V.4.2 Age and sex distribution

The low number of individuals from any given time period does not permit the calculation of a valid mortality table, including, for example, the mortality rate and an average life expectancy per age class. For the same reason, neither the ratio of male to female individuals, presented in the form of the so-called masculinity index, nor the population size can be calculated for Tepe 5, Karacamirli.

In total, 38 different individuals were investigated (see Table 16). Eight individuals were identified as male, seven as probably male, another one as female, and three as probably female. The sex of 19 individuals could not be determined (Fig. 273, Table 16). The majority of individuals (n = 22; 58.0 %) was at least adult (≥ 20 years). Several individuals (n = 12, 31.6 %) were classified as mature to senile. Only eight individuals were younger than adult and only five children (13.2 %) were excavated at Tepe 5 (Fig. 274, Table 16). This deficit in infant burials is a typical observation on graveyards and is probably caused by the comparatively bad preservation of the fragile infant bones. A sex-specific higher mortality in a certain age class could not be detected (Fig. 275). However, as already mentioned above, several individuals could be determined neither by sex nor by age and the number of female individuals determined was very low.

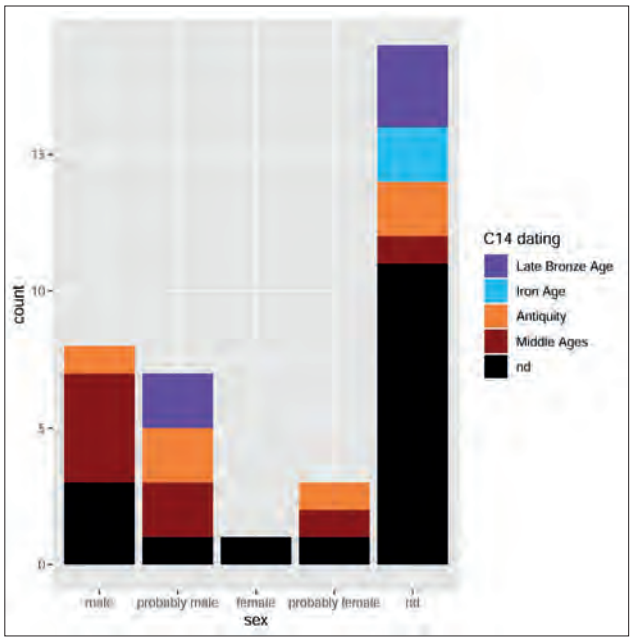

Fig. 273. Sex distribution of the individuals from Karacamirli separated by ^{14}C dating; nd = not determinable

burial	context	number	sex	biological age (morphology)	biological age (histomorphometry of bones)	chronological age (TCA)	age class
1	KG-094	0474	nd	nd			nd
4	KG-039/040	0163/0165	nd	nd	34–52		Adultas–Maturitas
5	KG-038	0146	prob. male	20–30			Adultas
6	KG-095	0468/0497	nd	nd			nd
7	KG-026	0105	prob. male	20–30			Adultas
8	KG-057	0247/0404	nd	40–70			Maturitas–Senilis
9	KG-043	0204	nd	nd			nd
11 (f)	KG-029	0115	nd	nd			nd
13	KG-032	0137/0166	nd	nd	55–75	52–56	Maturitas–Senilis
14	KG-059	0346	nd	nd			nd
15	KG-058	0243	nd	nd	53–73		Maturitas–Senilis
20	KG-030/102	0113/0491	nd	nd	53–73		Maturitas–Senilis
21	KG-074	0507	prob. male	> adult	55–75/48–68		Maturitas–Senilis
22	KG-095	0496	nd	nd (Inf I–II)	(Inf I)		Infans I–Infans II
23	KG-057	0415	prob. male	nd	53–73/49–69	49–55	Maturitas-Senilis
24	KG-057	0414	nd	50–70			Maturitas–Senilis
25	KG-053	0208	male	40–70			Maturitas–Senilis
26	KG-066	0392	prob. female	nd	54–74		Maturitas–Senilis
27	KG-097	0455	prob. male	> 25		40–46	Maturitas
28	KG-027	0106	male	16–19			Juvenis
29	KG-031	0120	male	20–25			Adultas
30	KG-036	0134	female	40–50			Maturitas
31	KG-042	0173	prob. female	5–7			Infans I–Infans II
32	KG-045	0193	nd	4–6			Infans I
33	KG-046	0192	male	21–24			Adultas
34	KG-048	0197	male	> 60	56–76/49–69	40–46	Senilis
35	KG-047/098	0217/0467	prob. male	> adult	31–49		Adultas–Maturitas
36	KG-050	0203	male	50–70			Maturitas–Senilis
37	KG-052	0205	prob. male	10–13			Infans II–Juvenis
38	KG-073	0508	prob. female	40–59			Maturitas
39	KG-077	0517	male	9–12			Infans II
40	KG-089	0387	nd	10–14			Infans II–Juvenis
41	KG-093	0480	male	50–59			Maturitas
42	KG-035	0136	nd	3–9 months			Infans I
43	KG-076	0515	nd	nd			nd
44	KG-090	0398	nd	> adult	56–76	59–64	Maturitas–Senilis
45	KG-096	0445	nd	nd			nd
46	KG-099	0460	nd	nd			nd

Table 16. Summary of determined sex and age of the individuals from Karacamirli sorted by context. nd = not determinable

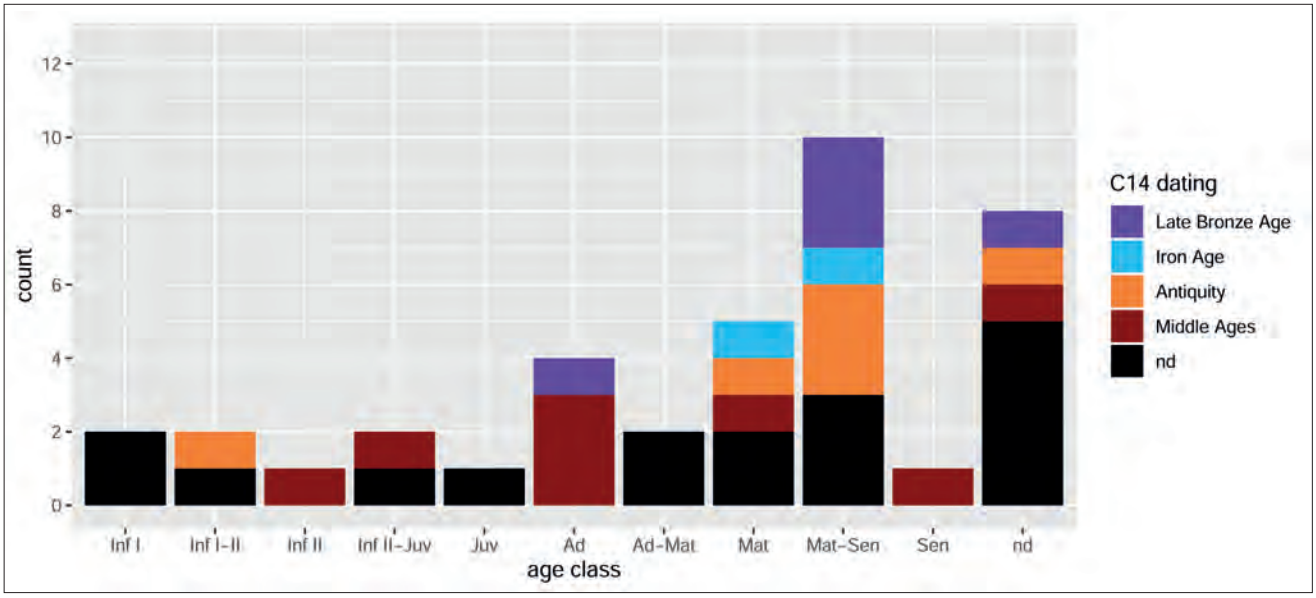

Fig. 274. Distribution of age classes of the individuals from Karacamirli separated by ^{14}C dating. Inf I = Infans I, Inf I–II = Infans I–Infans II, Inf II = Infans II, Inf II–Juv = Infans II–Juvenis, Juv = Juvenis, Ad = Adultas, Ad–Mat = Adultas–Maturitas, Mat = Maturitas, Mat–Sen = Maturitas–Senilis, Sen = Senilis, nd = not determinable

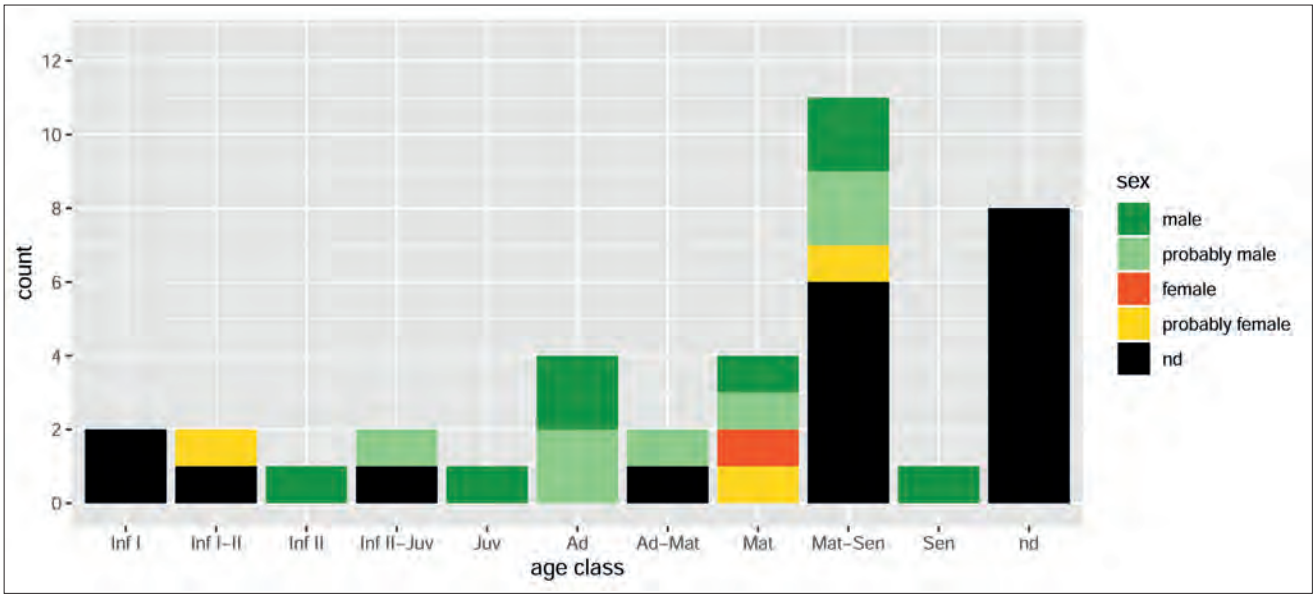

Fig. 275. Distribution of sex per age class of the individuals from Karacamirli. Inf I = Infans I, Inf I–II = Infans I–Infans II, Inf II = Infans II, Inf II–Juv = Infans II–Juvenis, Juv = Juvenis, Ad = Adultas, Ad–Mat = Adultas–Maturitas, Mat = Maturitas, Mat–Sen = Maturitas–Senilis, Sen = Senilis, nd = not determinable

V.4.3 Osteometry

V.4.3.1 Cranial measurements

In the case of nine individuals (Burials 7, 25, 29, 30, 33, 34, 36, 38, 41) measurements of the skull were possible (see Table 17). Of these individuals one was dated to Late Bronze Age/Early Iron Age (Burial 7), one to the Late Antique period (Burial 25), and seven were dated to the Medieval period (Burials 29, 30, 33, 34, 36, 38, 41) (see ch. IV for more details on the dating).

The individual in Burial 25 (ANT) is the only mesocephalic (medium-headed) individual in the group, while all other individuals were brachycephalic (short-headed; Fig. 276). Three individuals, namely those in Burials 25, 34 (MA), and 38 (MA), were orthocranic (medium high braincase), the others were hypsicranic (high braincase) (Fig. 276, Table 17).

Cranial Indices	Burial 7	Burial 25	Burial 29	Burial 30	Burial 33	Burial 34	Burial 36	Burial 38	Burial 41
Cranial Index	82.6	75.5	86.5	84.8	82.9	91.1	93.6	85.5	90.4
Basio-Bregmatic Longitudinal Index	80.2	70.7	76.6	76.4	90.3	71.4	81.5	73.9	80.1
Basio-Bregmatic Transversal Index	97.1	93.5	88.5	90.0	109.0	78.4	87.1	86.5	88.7
Porio-Bregmatic Longitudinal Index	81.4	64.7	74.9	75.8	71.4	73.2	79.6	75.2	76.5
Transverse Frontal index	86.0	75.0	77.2	89.5	81.8	81.5	74.4	89.1	77.9
Transverse Fronto-Parietal Index	66.7	64.7	66.2	67.1	62.1	57.5	61.2	63.8	63.3
Sagittal Frontal-Parietal Index	89.7	103.2	86.7	nd	114.4	92.2	88.1	94.3	100.0
Sagittal Frontal Index	86.0	88.9	87.5	87.6	89.0	85.2	86.7	87.0	89.1
Jugo-Frontal Index	68.1	66.7	71.5	86.2	65.7	62.4	66.7	81.1	73.6
Jugo-Mandibular Index	nd	nd	68.6	77.1	80.3	59.6	66.7	73.9	76.7
Transverse Cranio-Facial Index	97.8	97.1	92.6	77.9	94.5	92.2	91.8	78.7	86.0
Total Facial Index	nd	84.4	80.3	111.0	80.3	85.1	95.6	97.3	88.4
Superior Facial Index	43.7	47.4	44.5	60.6	46.0	53.9	52.6	57.7	51.9
Orbital Index	86.8	77.5	91.9	89.2	80.0	100.0	94.4	88.2	89.2
Nasal Index	54.3	47.9	46.2	42.3	41.8	36.1	46.2	42.9	42.3

Table 17. Results of the cranial indices for nine individuals from Karacamirli, where cranial measurements were possible. nd = not determinable

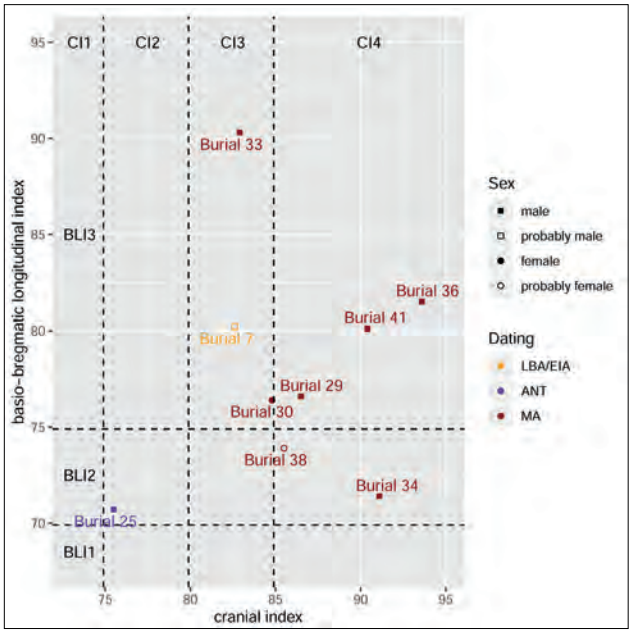

Fig. 276. Cranial index and basio-bregmatic longitudinal index of nine individuals from Karacamirli. Cranial index CI1: dolichocephalic (70.0–74.9), CI2: mesocephalic (75.0–79.9), CI3: brachycephalic (80.0–84.9), CI4: hyperbrachycephalic (≥ 85.0); basio-bregmatic longitudinal index BLI1: chamaecranic (≤ 69.9), BLI2: orthocranic (70.0–74.9), BLI3: hypsicranic (≥ 75.0)

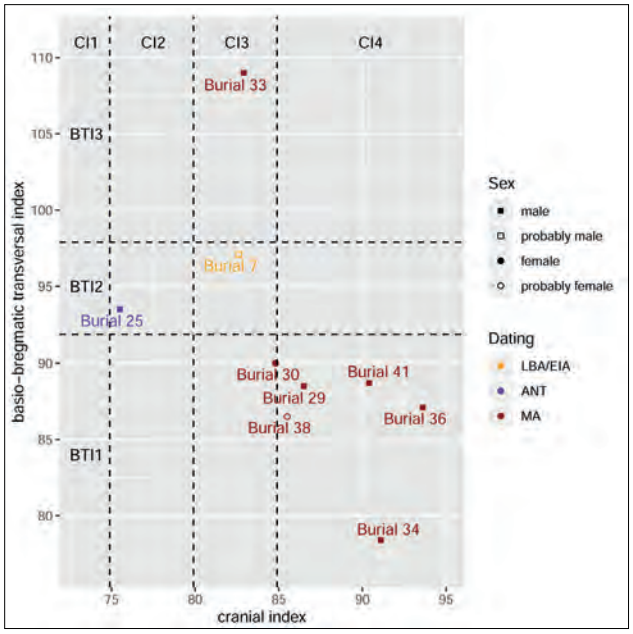

Fig. 277. Cranial index and basio-bregmatic transversal index of nine individuals from Karacamirli. Cranial index CI1: dolichocephalic (70.0–74.9), CI2: mesocephalic (75.0–79.9), CI3: brachycephalic (80.0–84.9), CI4: hyperbrachycephalic (≥ 85.0); basio-bregmatic transversal index BTI1: tapeinocranic (≤ 91.9), BTI2: metriocranic (92.0–97.9), BTI3: acrocranic (≥ 98.0)

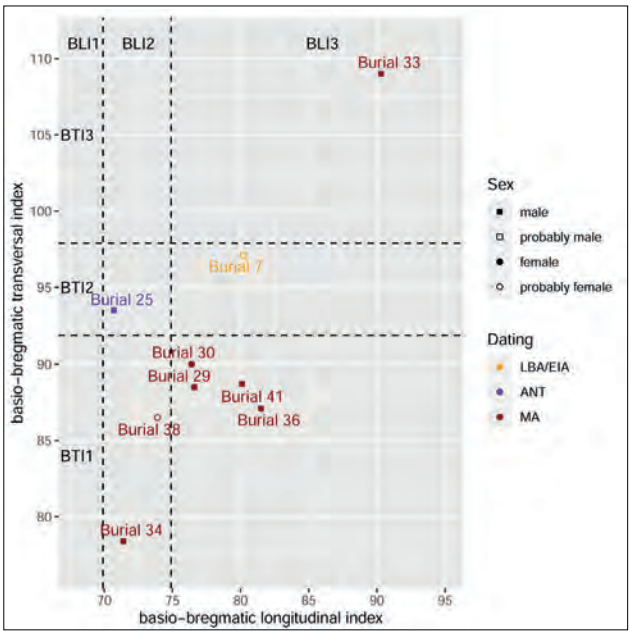

Fig. 278. Basio-bregmatic longitudinal index and basio-bregmatic transversal index of nine individuals from Karacamirli. Basio-bregmatic longitudinal index BLI1: chamaecranic (≤ 69.9), BLI2: orthocranic (70.0–74.9), BLI3: hypsicranic (≥ 75.0); basio-bregmatic transversal index BTI1: tapeinocranic (≤ 91.9), BTI2: metriocranic (92.0–97.9), BTI3: acrocranic (≥ 98.0)

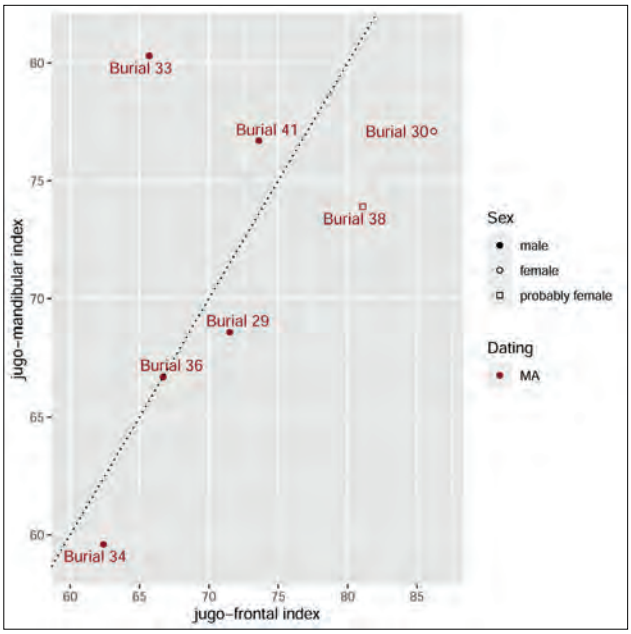

Fig. 279. Jugo-frontal index and jugo-mandibular index of seven individuals from Karacamirli. Diagonal: jugo-frontal index = jugo-mandibular index

With respect to both the basio-bregmatic longitudinal and basio-bregmatic transversal index the individual in Burial 33 (MA) was conspicuous due to a hyperhypsicranic (very high braincase) and hyperacrocranic (very narrow braincase) skull (Fig. 277 and Fig. 278, Table

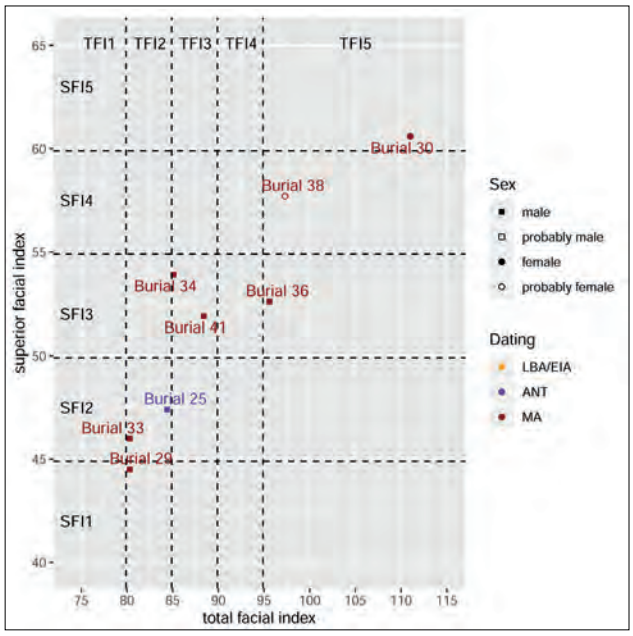

Fig. 280. Total facial index and superior facial index of eight individuals from Karacamirli. Total facial index TFI: hypereuryprosopic (≤ 79.9), TFI2: euryprosopic (80.0–84.9), TFI3: mesoprosopic (85.0–89.9), TFI4: leptoprosopic (90.0–94.9), TFI5: hyperleptoprosopic (≥ 95.0); Superior facial index SFI1: hypereuryene (≤ 44.9), SFI2: euryene (45.0–49.9), SFI3: mesene (50.0–54.9), SFI4: leptene (55.0–59.9), SFI5: hyperleptene (≥ 60.0)

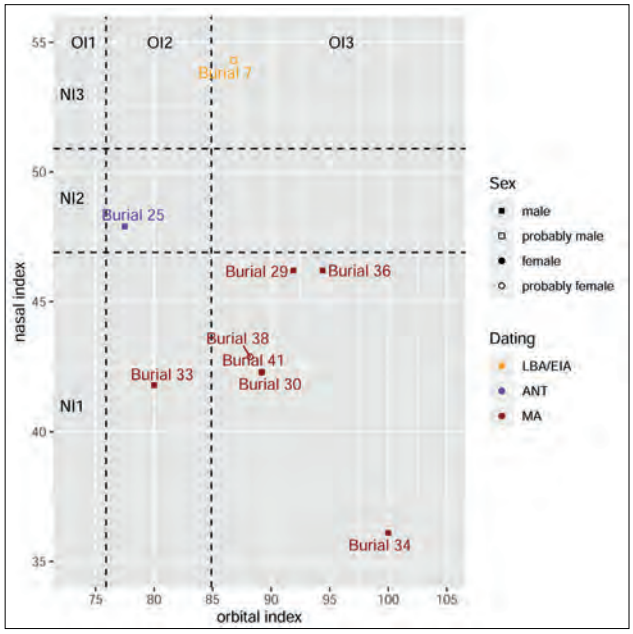

Fig. 281. Orbital index and nasal index of nine individuals from Karacamirli. Orbital index OI1: hypermesoconch (≤ 75.9), OI2: mesoconch (76.0–84.9), OI3: hypsiconch (≥ 85.0); nasal index NI1: leptorrhine (≤ 46.9), NI2: mesorrhine (47.0–50.9), NI3: chamaerrhine (51.0–57.9)

17). On the other hand, the individual in Burial 34 had an orthocranic (medium high braincase) and hyperta-

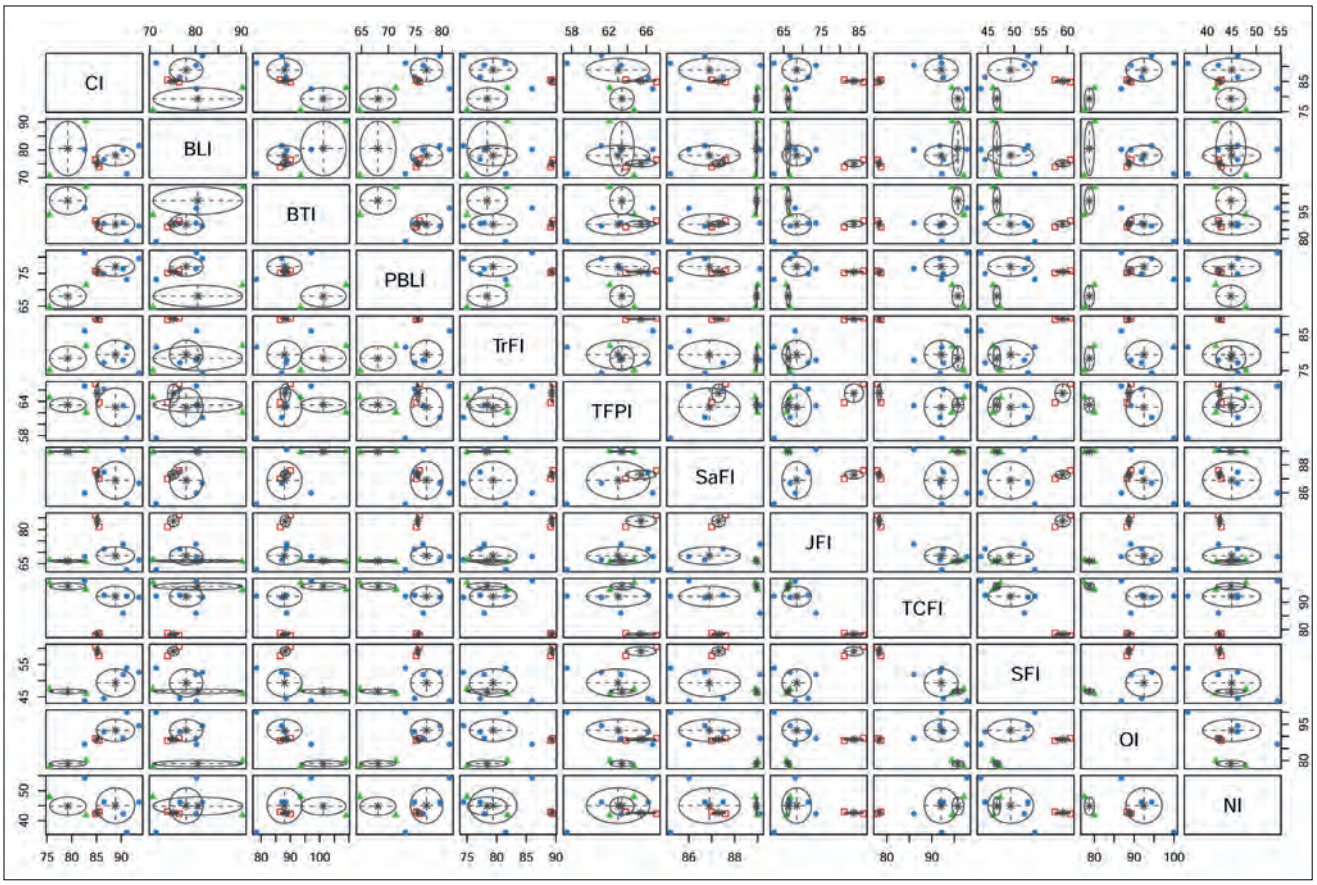

Fig. 282. Pairwise bivariate plot of the resulting three clusters (see Table 19) on the twelve-dimensional craniometry dataset (CI = cranial index, BLI = basio-bregmatic longitudinal index, BTI = basio-bregmatic transversal index, PBLI = porio-bregmatic longitudinal index, TrFI = transvere frontal index, TFPI = transverse fronto-parietal index, SaFI = sagittal frontal index, JFI = jugo-frontal index, TCFI = transverse cranio-facial index, SFI = superior facial index, OI = orbital index, NI = nasal index) of nine humans from Karacamirli; cluster 1: blue (dots), cluster 2: red (squares), cluster 3: green (triangles) (for the methodology see Scrucca et al. 2016)

peinocranic (very broad braincase) skull (Fig. 278, Table 17).

Two Medieval individuals (Burials 30 and 38) show a high jugo-frontal index compared to the other individuals from Karacamirli (Fig. 279, Table 17). This index shows a sex-specific trend with higher values in females compared to males (Martin 1914). Indeed, the individuals of Burials 30 and 38 were the only (probably) female individuals in the craniometry dataset. In addition, the individual in Burial 36 (MA) has to be mentioned here. The jugo-frontal and the jugo-mandibular index were identical (66.7) for this individual (Fig. 279, Table 17). The skull of this individual was thus rather quadratic (see Fig. 247 and Fig. 248).

The individuals can also be separated with respect to their facial skull measures (see Fig. 280 and Fig. 281). Three individuals showed an euryprosopic (Burials 25 (ANT), 29 (MA), 33 (MA)) facial index. In the case of three medieval individuals (Burials 30, 36, 38) a hyperleptoprosopic face was detected. The individuals of Burials 34 (MA) and 41 (MA) had a medium facial index. With respect to the superior facial index four individuals showed a euryene (Burials 25, 33) or hypereuryene (Burials 7 (LBA/EIA), 29) skull, another two had a leptene (Burial 38) or hyperleptene (Burial 30) index. The skulls of the remaining three individuals (Burials 34, 36, 41) were mesene (Fig. 280, Table 17).

The individual of Burial 7 showed a hypsiconch and chamaerrhine skull, consequently the individual had high orbits and a broad nose. Apart from the individual of Burial 25 with a mesorrhine skull, all other individuals of the group had a leptorrhine skull with a narrow nose. Nearly all individuals showed a hypsiconch or even hyperhypsiconch (Burial 34) skull with high (or very high) orbits, only two individuals (Burials 25, 33) had a mesoconch skull with medium high orbits (Fig. 281, Table 17).

The only Late Antique individual of Burial 25 (♂, 40–70 years) is conspicuous with respect to a variety of indices (cranial index, basio-bregmatic longitudinal index, basio-bregmatic transversal index, porio-bregmatic longitudinal index, sagittal frontal-parietal index, ju-

	μ			sd		
	cluster 1	cluster 2	cluster 3	cluster 1	cluster 2	cluster 3
CI	88.8	85.2	79.2	3.9	0.4	3.7
BLI	78.0	75.2	80.5	3.7	1.3	9.8
BTI	88.0	88.3	101.3	5.9	1.8	7.8
PBLI	77.1	75.5	68.1	3.0	0.3	3.4
TrFI	79.4	89.3	78.4	4.0	0.2	3.4
TFPI	63.0	65.5	63.4	3.4	1.7	1.3
SaFI	86.9	87.3	89.0	1.3	0.3	0.1
JFI	68.5	83.7	66.2	3.9	2.6	0.5
TCFI	92.1	78.3	95.8	3.7	0.4	1.3
SFI	49.3	59.2	46.7	4.3	1.5	0.7
OI	92.5	88.7	78.8	4.6	0.5	1.3
NI	45.0	42.6	44.9	5.9	0.3	3.1

Table 18. Mean (μ) and standard deviation (sd) of the twelve-dimensional craniometry dataset (CI = cranial index, BLI = basio-bregmatic logitudinal index, BTI = basio-bregmatic transversal index, PBLI = porio-bregmatic longitudinal index, TrFI = transvere frontal index, TFPI = transverse fronto-parietal index, SaFI = sagittal frontal index, JFI = jugo-frontal index, TCFI = transverse cranio-facial index, SFI = superior facial index, OI = orbital index, NI = nasal index) of nine humans from Karacamirli according to GMM clustering performed with three clusters

go-frontal index, jugo-mandibular index, cranio-facial transversal index, orbital index, nasal index; see Fig. 208 and Fig. 209, Fig. 278–Fig. 280, Table 17). The medieval individual in Burial 34 (♂, > 60 years) showed striking indices, namely basio-bregmatic longitudinal index, basio-bregmatic transversal index, orbital index, and nasal index (see Fig. 240 and Fig. 241, Fig. 278, Fig. 281, Table 17). Cranial measurements of the skull of another medieval individual, Burial 33 (♂, 21–24 years), indicate a conspicuous basio-bregmatic longitudinal index, basio-bregmatic transversal index, sagittal fronto-parietal index, and orbital index (see. Fig. 233 and Fig. 234, Fig. 278, Fig. 281, Table 17).

Another individual should be mentioned here, namely the individual of Burial 30 (♀, 40–50 years). This medieval individual showed a hyperleptoprosopic and hyperleptene face and forehead, respectively. In addition, the jugo-frontal index is comparatively high. Other cranial indices are inconspicuous (see Fig. 228 and Fig. 229, Fig. 279, Fig. 280, Table 17). A sex-specific difference is possible here because with the exception of one individual (Burial 38) all other individuals, which could be craniometrically examined, were males. Actually, the individuals of both Burials 30 and 38 were also different from all other individuals with respect to the jugo-frontal index, which is usually higher in females (Martin 1914). The medieval individual in Burial 38 was also conspicuous with respect to another two indices. The individual showed a leptene superior facial index and a hyperleptoprosopic total facial index (see Fig. 280, Table 17).

Finally, the individual in Burial 7 (probably ♂, 20–30 years), dated into Late Bronze Age or Early Iron Age, showed a metriocranic basio-bregmatic transversal index, a hypereuryene superior facial index, and a chamaehine nasal index (see Fig. 188, Fig. 189, Fig. 280, Table 17).

Even mathematically some individuals with conspicuous cranial measures can be detected. GMM cluster analysis was performed on 12 cranial measures (cranial index, basio-bregmatic longitudinal index, basio-breg-

cluster 1	cluster 2	cluster 3
Burial 7	Burial 30	Burial 25
Burial 29	Burial 38	Burial 33
Burial 34		
Burial 36		
Burial 41		

Table 19. Results of GMM cluster analyses on the twelve-dimensional craniometry dataset

matic transversal index, porio-bregmatic longitudinal index, transverse frontal index, transverse fronto-parietal index, sagittal frontal index, jugo-frontal index, transverse cranio-facial index, superior facial index, orbital index, nasal index) of nine individuals. This limitation of cranial measures was due to the fact that missing data (see Table 17) cannot be included in GMM cluster analysis. With a given number of three clusters GMM identifies a cluster of individuals (n = 5) which are quite similar to each other with respect to their craniometry (cluster 1) as well as two clusters with two individuals each which exhibit conspicuous craniometric results (see Fig. 282, Table 18).

Individuals grouped into the second cluster (Burials 30, 38) show higher mean values for the transverse frontal index (89.3 ± 0.2), jugo-frontal index (83.7 ± 2.6), and superior facial index (59.2 ± 1.5) compared to all other individuals in the dataset (see Fig. 282, Table 19). Accordingly, the individuals in both Burial 30 (♀, 40–50 years) and Burial 38 (probably ♀, 40–59 years) showed a narrow or even very narrow upper face (leptene or hyperleptene superior facial index), a broad forehead (hypereurymetopic fronto-transversal index), and a very broad face (jugo-frontal index) (see Table 17). Interestingly, this cluster includes the only two medieval (probably) female individuals with craniometric measurements. This is probably caused by the sex-bias of i. e. the jugo-frontal index, which is generally higher in females (Martin 1914) as it is the case here.

Cluster 3 includes the individuals of Burials 25 and 33. Compared to all other individuals in the dataset both individuals show a higher mean value for the basio-bregmatic transversal index (101.3 ± 7.8) and lower mean values for the cranial index (79.2 ± 3.7), porio-bregmatic longitudinal index (68.1 ± 3.4), and orbital index (78.8 ± 1.3) (see Fig. 282, Table 19). The two individuals thus were short- or medium-headed (brachycephalic or mesocephalic cranial index), with a very high and narrow or medium broad braincase (hyperacrocranic or metriocranic basio-bregmatic transversal index), high braincase (hypsicranic porio-bregmatic longitudinal index), and orbits of medium height and breadth (mesoconch orbital index) (see Table 17).

Interestingly, clusters 2 and 3 include only individuals which were conspicuous with respect to at least one craniometric measure as mentioned above. Consequently, GMM validates the differentiation of at least four individuals, namely those of Burial 25, Burial 30, Burial 33, and Burial 38. All these individuals have already been identified as conspicuous with respect to some of their cranial measures without clustering (see above). However, the additional separation of these individuals by GMM cluster analysis can be understood as an additional (mathematical) verification of the conventional method.

Two individuals of cluster 1 (Burials 7, 34) were identified as conspicuous due to several cranial measures. Nevertheless, they do not fall into a separated cluster, what is caused by the fact that the cluster number was manually limited due to the rather small sample size. Cluster 1 shows a high standard deviation with respect to almost all cranial measures (see Fig. 282, Table 19). Therefore, even individuals with some extreme measures are included (see Fig. 282).

It is possible that the above-mentioned individuals, which are conspicuous with respect to their cranial appearance, or their ancestors are of non-local origin. However, this cannot be answered on the basis of craniometry. Similarly, individuals who show inconspicuous cranial measures are not necessarily local. Stable isotopes have to be investigated for the detection of non-local individuals (see ch. VI).

V.4.3.2 Postcranial measurements

Index platymericus and index cnemicus (Table 20) indicate the muscle activity of an individual. Elliptic bone cross-sections, which are caused by high activity of muscles, result in rather low indices. Round femur and tibia

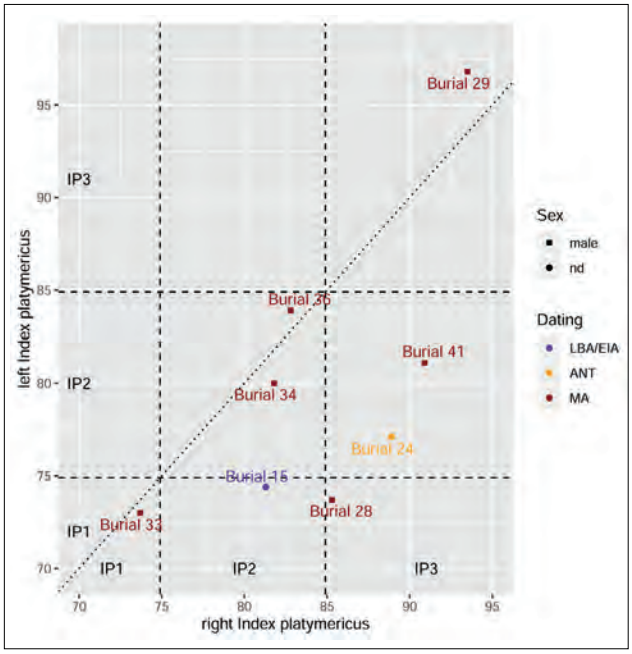

Fig. 283. Index platymericus of eight individuals from Karacamirli. Diagonal: right index = left index. IP1: hyperplatymeric (≤ 74.9), IP2: platymeric (75.0–84.9), IP3: eurymeric (85.0–99.9); nd = not determinable

	Burial 7		Burial 15		Burial 24		Burial 25		Burial 29		Burial 33		Burial 34		Burial 36		Burial 41	
Humerus	right	left	right	left	right	left	right	left	right	left	right	left	right	left	right	left	right	left
Robustness index	nd	nd	nd	nd	nd	nd	21.8	nd	nd	20.1	23.6	nd	20.6	20.8	nd	nd	22.5	21.2
Radius	right	left	right	left	right	left	right	left	right	left	right	left	right	left	right	left	right	left
Robustness index	nd	nd	nd	nd	nd	nd	19.4	nd	nd	17.4	nd	nd	20.6	19.8	nd	nd	nd	21.3
Ulna	right	left	right	left	right	left	right	left	right	left	right	left	right	left	right	left	right	left
Robustness index	nd	nd	nd	nd	nd	nd	17.1	18.3	nd	16.7	nd	nd	19.6	20.3	nd	nd	nd	22.0
Femur	right	left	right	left	right	left	right	left	right	left	right	left	right	left	right	left	right	left
Index platymericus	85.3	73.7	81.3	74.4	88.9	77.1	81.6	nd	93.5	96.8	73.7	73.0	81.8	80.0	82.8	83.9	90.9	81.1
Robustness index	12.8	11.4	nd	nd	nd	nd	nd	nd	nd	nd	13.5	nd	nd	nd	nd	nd	13.5	nd
Tibia	right	left	right	left	right	left	right	left	right	left	right	left	right	left	right	left	right	left
Index cnemicus	111.1	128.0	nd	nd	nd	76.3	68.6	59.5	66.7	66.7	86.5	nd	73.5	67.6	68.8	67.7	77.1	71.4
Robustness index	nd	nd	nd	nd	nd	nd	nd	nd	nd	20.9	22.8	nd	nd	nd	nd	19.8	23.7	23.5

Table 20. Results of the postcranial Indices for nine individuals from Karacamirli, where postcranial measurements were possible

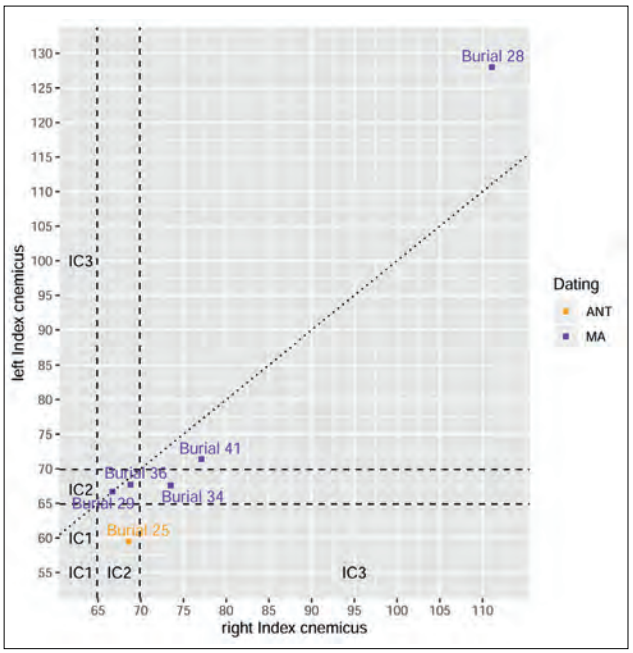

Fig. 284. Index cnemicus of six individuals from Karacamirli. Diagonal: right index = left index. IC1: platycnemic (≤ 64.9), IC2: mesocnemic (65.0–69.9), IC3: eurycnemic (≥ 70.0); nd = not determinable

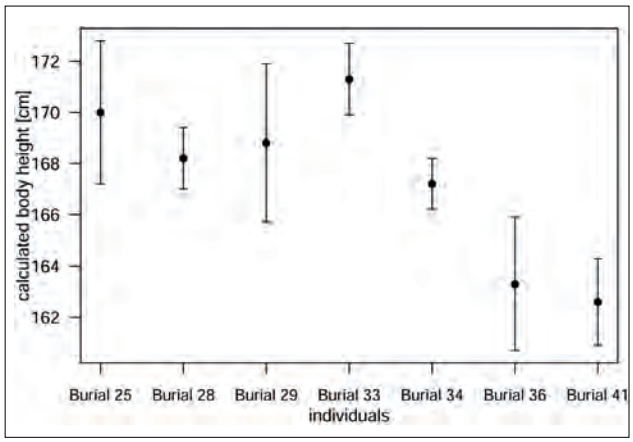

Fig. 285. Mean estimated body height (after Trotter/Gleser 1958) for seven at least juvenile individuals from Karacamirli. Error bars indicate standard deviations

cross-sections with a consequently high index (close to 100) are considered indicative of rather low activity.

Fig. 283 illustrates the right and left index platymericus of eight individuals from Karacamirli. The individual in Burial 33 (MA; ♂, 21–24 years) showed a hyperplatymeric index (right: 73.7, left: 73.0), thus indicating very high mobility. Even the individuals of Burial 15 (LBA/EIA; nd, nd/histological age: 53–73 years), Burial 34 (MA; ♂, > 60 years), and Burial 36 (MA; ♂, 50–70 years) showed platymeric right and left femora with indices below 85 (Fig. 283). In case of the individual of Burial 28 (MA; ♂, 16–19 years) the right femur was eurymeric, while the left femur was hyperplatymeric. This is probably due to a higher load carried by the left leg, caused by the osteomyelitis of the right tibia (see Fig. 216, Fig. 217, Fig. 218). The individual of Burial 29 (MA; ♂, 20–25 years) had an eurymeric right and left femur. This indicates a rather low activity level.

The calculated index cnemicus of six individuals is illustrated in Fig. 284. The individual in Burial 25 (ANT; ♂, 40–70 years) had a platycnemic left and a mesocnemic right tibia (Fig. 284). Thus, both tibiae were quite robust.

The individual in Burial 28 showed a very high index. In the case of the right tibia (index cnemicus: 111.1) this can be explained by the osteomyelitis (see Fig. 216, Fig. 217, Fig. 218) accompanied by a thickening of the bone due to coarsely woven bone. In the case of the left tibia, where no inflammatory process could be detected, an index of 128.0 clearly indicates a low robustness. However, the respective individual was probably inactive due to the severe osteomyelitis, possibly associated with muscular atrophy resulting in a high index cnemicus. Even the individual of Burial 41 (MA; ♂, 50–59 years) had an eurymeric index for both the right and the left tibia (Fig. 284). This individual suffered from an injury to the left tibia (see Fig. 258).

In addition to both index cnemicus and index platymericus the robustness indices of tibia and femur can be calculated. These indices provide information on the muscular activity of the legs. Both right and left robustness indices of the femur could only be calculated for the individual in Burial 28, while only for the individual of Burial 41 both tibiae could be examined with respect to robustness. The individual of Burial 28 showed a higher index for the right femur (12.8) compared to the left (11.4), while the individual in Burial 41 did not show a difference in the robustness of the right (23.7) and the left (23.5) tibiae. Both legs were thus used similarly. With respect to the injury on the left tibia (see Fig. 258) as well as the eurycnemic index cnemicus (see above), this might further indicate a less mobile individual.

The robustness indices of humerus, radius, and ulna can give hints on the handedness of an individual. The arm which is used more frequently or for harder work should show a higher index. Only three individuals (Burials 25, 34, 41) could be examined for handedness, which requires the measurement of both right and left bones. The individual in Burial 34 (MA; ♂, > 60 years) showed no or only slight side differences in humerus (right: 20.6, left: 20.8), radius (right: 20.6, left: 19.8), and ulna (right: 19.6, left: 20.3). The individual of Burial 25 (ANT; ♂, 50–70 years), however, showed a higher index in the left (18.3) compared to the right (17.1) ulna. Accordingly, the left arm was probably used more often or with higher activity than the right arm. Unfortunately, the robustness of the left humerus and left radius could not be determined, so the index cannot be compared for both humerus and radius. In the case of the individual of Burial 41 (MA; ♂, 50–59 years) only the robustness of the humerus could be determined. The index was higher on the right (22.5) compared to the left side (21.2). This indicates a right-handed individual. However, even in this case the robustness of the right radius and the right ulna could not be calculated.

Body height could be calculated for seven at least juvenile individuals (Burial 25 (ANT; ♂, 40-70 years), Burial 28 (MA; ♂, 16–19 years), Burial 29 (MA; ♂, 20–25 years), Burial 33 (MA; ♂, 21–24 years), Burial 34 (MA; ♂, > 60 years), Burial 36 (MA; ♂, 50-70 years), Burial 41 (MA; ♂, 50–60 years) and one child (Burial 39; MA; ♂, 9–12 years). As illustrated in Fig. 285 the body height of the at least juvenile individuals varies between c. 163 cm (Burial 36) and c. 171 cm (Burial 33). No change in body height is observed over the different time periods from Antiquity (Burial 25) to medieval times (Burials 28, 29, 33, 34, 36, 41; see Fig. 285). However, the sample size is very small (n = 7). The child of Burial 39 had a mean estimated body height of about 117.5 cm (± 2.0 cm).

V.4.4 Joint status

The joints of 34 at least juvenile individuals were examined and classified as state 0 to state 3 (see 2.1). A severe state of 4 and 5 (see 2.1) was not observed within

joint	side/position	state			
		0	1	2	3
shoulder	left	23	6		
	right	24	5		
elbow	left	23	3	3	
	right	24	4	1	
hand	left	22	5	2	
	right	21	6	2	
hip	left	25	3	1	
	right	24	4	1	
knee	left	23	5	1	
	right	22	6	1	
foot	left	25	3	1	
	right	24	4	1	
cervical vertebrae	vertebral bodies	18	8	3	
	intervertebral joints	17	12		
thoracic vertebrae	vertebral bodies	23	4	2	
	intervertebral joints	21	6	1	
lumbar vertebrae	vertebral bodies	23	3	1	2
	intervertebral joints	21	7		

Table 21. Overview of the distribution of the joint status (see ch. V.2.1) for different joints and vertebrae of all 34 at least adult individuals from Karacamirli

the sample. The joint status of the majority of examined individuals could not be assessed (state 0; Table 21) due to poor preservation or missing bones. The remaining joints were of state 1 (no changes) and 2 (minor rim, osteophytes < 3 mm). In case of the vertebral bones states 1 to 3 (major changes) were detected (see 2.1). Minor changes of the joints with age is expected. All individuals with state 2 or 3 are at least adult and mainly of age class Maturitas and Senilis except the individual in Burial 43, whose age at death could not be determined (nd). The two individuals with major changes on the lumbar vertebrae (state 3; Table 21) were rather old with ages of 50–59 years (Burial 41) and above 60 years (Burial 34). Again, these changes are likely due to the individuals' age. In total, the joint status indicates only low or medium work load for the majority of individuals which could be assessed and arthrosis is age-related as expected.

Schmorl's nodules were present on the thoracic (T7–T12) and lumbar vertebrae (L2–L4, L1 nd) of the individual in Burial 41 (MA; ♂, 50–59 years) and on two cervical vertebrae (C5, C6) of the individual of Burial 27 (ANT; probably ♂, 25–50 years). These nodules are caused by the collapse of intervetebral discs into the vertebral bodies (Brossmann et al. 2001) in the aging spine.

bone	side	state						
		0	1	2	3	4	5	6
clavicle	left	26	8					
	right	26	8					
humerus	left	29	5					
	right	29	5					
ulna	left	27	7					
	right	28	6					
radius	left	27	6					1
	right	28	6					
femur	left	26	8					
	right	27	7					
tibia	left	26	6	1				1
	right	26	8					
fibula	left	28	6					
	right	28	6					
ribs	left	25	9					
	right	25	9					

Table 22. Overview of the distribution of the status of the bone surfaces (see ch. V.2.1) for different bones of all 34 at least adult individuals from Karacamirli

V.4.5 Pathological alterations of bones and teeth

Four different types of pathological abnormalities on the skeletons from Karacamirli can be distinguished: healed bone fractures, inflammatory processes on the bone (surface), possible manifestations of deficiencies, and changes due to either age or physiological stress. These four types are described in more detail in the following.

Healed fractures were observed in two cases with a fracture of a right rib (Burial 13 (LBA/EIA)) and a left ulna (Burial 26 (ANT)). Only a single rib of the skeleton of the individual of Burial 13 (nd, 52–75 years) was preserved. Consequently, it cannot be evaluated if a single fracture or a serial fracture of several ribs had occurred. As already mentioned the fracture of the ulna of the individual in Burial 26 (probably ♀, 54–74 years) might be classified as a parry fracture if only the ulna was affected. Since the left radius was not preserved, even a forearm fracture of both left ulna and left radius is possible (Lovell/Grauer 2019). A parry fracture is often used as a possible indicator of interpersonal violence (e. g. Grauer/Roberts 1996).

Inflammatory processes, including osteomyelitis and periostitis, were detected on four different individuals, namely those in Burial 24 (ANT), Burial 25 (ANT), Burial 28 (MA), and Burial 46 (UD). Table 22 and Table 23 give an overview on the state of the bone surfaces with respect to periostitis in at least adult (Table 22) and infant/juvenile (Table 23) individuals. For the at least adult individuals, state 0 to state 6 was assessed. Bones which show osteomyelitis are classified as state 6. Osteomyelitis is an inflammatory process, caused by a chronic infection by pyogenic bacteria, which usually enter the bone through a wound (Ortner/Putschar 1981). This was the case for two at least adult individuals (Table 22), namely the individuals in Burial 24 (nd, 50-70 years) and Burial 46 (nd, nd). Another individual (Burial 25; MA; ♂, 40–70 years) showed minor periostitis of state 2 on a tibia (Table 23).

Of eight infant and juvenile burials periostitis and osteomyelitis were observed at only one skeleton (Burial 28; MA; 16–19 years). This individual showed severe osteomyelitis of the right tibia as well as a periostitis of state 3 on the right femur. However, the majority of individuals could not be assessed (Table 22).

Four individuals, namely those of Burial 28 (MA), Burial 29 (MA), Burial 30 (MA), and Burial 42 (UD), showed a possible indication of deficiency:

bone	side	state						
		0	1	2	3	4	5	6
clavicle	left	6	2					
	right	6	2					
humerus	left	6	2					
	right	5	3					
ulna	left	6	2					
	right	5	3					
radius	left	6	2					
	right	6	2					
femur	left	4	4					
	right	5	2		1			
tibia	left	6	2					
	right	6	1					1
fibula	left	6	2					
	right	6	2					
ribs	left	5	3					
	right	5	3					

Table 23. Overview of the distribution of the status of the bone surfaces (see ch. V.2.1) for different bones of all eight infant or juvenile individuals from Karacamirli

X-ray revealed five Harris lines for the individual in Burial 28 (♂, 16–19 years) (see Fig. 218). These lines developed at different time periods between the age of approximately 11 and 17 years (after Byers 1991). Harris lines indicate recovery after periods of malnutrition, diseases, immobilization, and even psychological distress during childhood, which can lead to a growth arrest of the bones. Re-established growth causes an increased cartilaginous proliferation as well as an increased activity of osteoblasts leading to thickened transverse lines (Kulus/Dąbrowski 2019; Sajko et al. 2011). The respective individual died quite soon after the last period of re-established growth. However, the death of this individual is not necessarily related to the factor which caused the Harris lines. The individual of Burial 28 was the only individual from Karacamirli, where X-ray analysis was performed. Thus, it is possible that further X-ray images would have revealed additional cases of Harris lines in other individuals.

The individuals in Burial 29 (♂, 20–25 years) and Burial 42 (nd, 3–9 months) exhibited a slight and a rather severe Cribra orbitalia, respectively (Fig. 267), which can indicate unspecific deficiencies. Cribra orbitalia is visible as small to large holes with a sieve-like appearance in the upper part of the orbits. This might be caused by anemia, a limited diet supply (i. e. lack of vitamins B12 and C), nutrient losses due to diarrhea (i. e. weanling diarrhea) or infectious diseases (e. g. Stuart-Macadam 1985; Walker 1986; Walker et al. 2009; Wapler et al. 2004).

The individual of Burial 30 (♀, 40–50 years) survived a period of deficiency during childhood at an age of about three years, as indicated by enamel hypoplasia (see Massler et al. 1941). Linear enamel hypoplasia (LEH) is visible as grooves encircling the teeth. Similar to the Harris lines, LEH can be understood as hypoplastic defects caused by a lack in dietary supply, fever or infections during childhood (e. g. Grupe et al. 2015; Ogden et al. 2007). The crisis took place at an age when weaning probably stopped. Children are usually very prone to diseases in this phase. However, the individual of Burial 30 survived this period of high mortality.

Possible alterations due to either age or physiological stress were present in five individuals with a fusion of cervical vertebrae (Burial 34 (MA)), bony spurs at the pelvis (Burial 34 (MA)), osteophytes at vertebral bones (Burial 25 (ANT), Burial 41 (MA)), tibia, pelvis and sacrum (Burial 41), and enthesiopathies at the clavicles (Burial 27 (ANT), Burial 41), calcanei, and tibiae (Burial 41). All mentioned individuals were mature to senile, which might explain the osteophytes. In the case of the individual in Burial 41 (♂, 50–59 years), the detected alterations on the skeleton were probably connected. An injured ligament on the left tibia (Fig. 258), probably the tibial collateral ligament, may have caused a malposition or an incorrect loading of the left leg. This is partly visible on the auricular surface of the left pelvis (Fig. 259). It is likely that the individual put more weight on the right compared to the left leg. This could explain the osteophytes at the right auricular surface of the sacrum (Fig. 260) as well as on the right side of some vertebrae. The auricular surface of the right pelvis could not be examined. The individual also showed a strong enthesiopathy on both clavicles at the attachment sites of the Musculus pectoralis major and the Musculus trapezius (Fig. 261). This indicates a high work-load, e. g. carrying heavy loads, and a rather strong individual. With respect to the leg injury (see above), it is also possible that the individual walked with crutches for a rather long time. As previously mentioned, the bony spurs at the Os ischii of the right pelvis of the individual in Burial 34 (♂, 49–76 years) were likely caused by either unilateral weight distribution or an over stretching of the obturator membrane.

A variety of individuals showed oral pathologies. Besides the already discussed LEH (see above) caries and dental calculus were observed. In addition, some indi-

viduals showed a quite distinct abrasion pattern which will be discussed below. For 13 at least juvenile individuals caries could not be determined. Caries of state 2 (Burial 41 (MA)), 3 (Burial 30 (MA)), 4 (Burial 23 (ANT), Burial 29 (MA), Burial 36 (MA)), and 5 (Burial 29) was observed. In all cases only one or two teeth were affected with a fraction of affected teeth of 1/31 (Burial 41), 2/24 (Burial 30), 2/27 and 1/27 (Burial 29; state 4 and 5), 1/28 (Burial 36), and 2/16 (Burial 23), respectively. Various teeth were affected, namely I 3 (Burial 23), I 4 (Burial 23), II 5 (Burial 36), II 6 (Burial 29), II 7 (Burial 29), III 6 (Burial 30), IV 6 (Burial 41), as well as IV 7 (Burial 30, Burial 29). An abscess associated with the caries was detected in the individual of Burial 36. The examined non-adult individuals did not show traces of caries (1 nd). Acidogenic oral plaque bacteria ferment carbohydrates, what leads to the production of organic acids. These acids dissolve the mineral crystals of the enamel, dentine, or cementum of teeth leading to a cavitation known as caries if the process continues (Featherstone 2000; 2004).

Under high pH conditions dental plaque mineralizes causing dental calculus (Hillson 2005). Only two individuals showed a dental calculus of state 2 (Burial 5 (LBA/EIA), Burial 36 (MA)), 3 (Burial 5), and 4 (Burial 36). The fraction of affected teeth was 10/24 and 3/24 for the individual in Burial 5 (state 2 and 3, respectively) as well as 6/28 and 1/28 for the individual in Burial 36. Non-adult individuals did not show dental calculus (1 nd). For 13 individuals dental calculus could not be determined.

Lastly, abrasion of state 2 to 7 was detected in a number of individuals. Some abrasion is normal with increasing age. However, diet can also cause a severe tooth abrasion. Individuals with an abrasion of state 6 (Burial 13 (LBA/EIA), Burial 25 (ANT), Burial 34 (MA)) or 7 (Burial 13, Burial 21 (ANT), Burial 35 (MA)) were at least mature or senile. The teeth of five children showed slight abrasion of state 2 (Burial 31 (MA), Burial 32 (MA), Burial 37 (MA), Burial 39 (MA), Burial 40 (MA)) and 3 (Burial 32, Burial 37), respectively. In the case of the individuals in Burial 37 (probably ♂, 10–13 years) and Burial 39 (♂, 9–12 years) the permanent teeth showed slight abrasion, while in all other individuals the deciduous teeth were affected.

Altogether, the number of pathological diseases or alterations, which could be examined on the skeletons, was rather low. This might indicate that the people from Karacamirli were either quite healthy and had a good health care or that people died from severe diseases after a very short time, which is then usually invisible in a morphological survey. However, as previously mentioned, only a small proportion of diseases is visible on the skeleton, anyway.

V.4.6 Acquired and epigenetic non-metric variants of bones

A number of acquired or epigenetic variants could be detected on the skeletons from Karacamirli. In the following, the two different types of variants are explained in more detail:

Two of these variants are classified as acquired, namely the modification of the so-called Allen's fossa and the rhomboid fossa (Burial 41 (MA)). As mentioned above the modified Allen's fossa described for this individual (Fig. 262) differs from the usual appearance of the variant as described by Allen (1884) (see also Finnegan/Faust 1974). While Allen's fossa should be of a rather circular appearance, the fossa on the left femur of the individual in Burial 41 (♂, 50–59 years) was more lobulated. In addition, Allen's fossa is characterized by the trabeculae, which become visible. This is only partly the case for the individual of Burial 41. The area seems to be rather smooth, which is untypical for Allen's fossa. It is likely that a primary Allen's fossa was modified due to an unusual locomotion resulting from the trauma on the left tibia (see Fig. 258). The most probable explanation for the development of Allen's fossa is a roughening of the respective area on the femoral neck caused by the Zona orbicularis. These circular fibers of the hip joint capsule can be in contact with the femoral neck and thereby cause the fossa (Angel 1964; Odgers 1931). The respective individual probably did not use his left leg in a normal way for an extended period of time due to the trauma on his left tibia (see above). This is also suggested by osteophytes on the pelvis as well as the sacrum. In sum, it is suggested that Allen's fossa became lobulated and smoothed by an unusual way of locomotion.

Similar to the development of Allen's fossa, the rhomboid fossa on the clavicle (Fig. 256) develops by a depression of the costoclavicular ligament (Paraskevas et al. 2009; Rani et al. 2011; Rogers et al. 2000). This activity marker is more common in males than in females. Even a correlation with age seems to exist with a higher frequency in young compared to old individuals (Paraskevas et al. 2009; Rogers et al. 2000). Paraskevas et al. (2009) also found a correlation with handedness. The individual in Burial 41 was determined as a male, who died at an age of about 50 to 59 years. As previously mentioned, this individual suffered from a trauma on the left tibia. It is conceivable that he used some sort of crutches in order to move. This could explain the presence of the rhomboid fossa on both right and left clavicles. However, even a high physical load could explain this variant.

A variety of epigenetic non-metric traits could be observed on the skeletons from Karacamirli. This includes

cranial as well as postcranial variants. The following cranial variants were observed: patent Canalis condylaris (Burial 23 (ANT), Burial 36 (MA), Burial 41 (MA)), accessory Foramen infraorbitale (Burial 34 (MA)), complete Foramen supraorbitale (Burial 41), exsutural Foramen mastoideum (Burial 29 (MA)), doubled Foramen zygomaticofaciale (Burial 30 (MA)), supraorbital notch (Burial 34), ossicle at the lambda (Burial 23, Burial 25 (ANT)), and lambdoid ossicles (Burial 23, Burial 25 (ANT), Burial 27 (ANT), Burial 36).

Three individuals – in Burial 23 (probably ♂, 49–73 years), Burial 36 (♂, 50–70 years), and Burial 41 (♂, 50–59 years) – showed a patent Canalis condylaris (e. g. Fig. 264). This rather common trait is characterized by a patent canal behind the occipital condyle (Berry/Berry 1967; Hanihara/Ishida 2001). A patent Canalis condylaris seems to be more frequent in females as well as in older individuals. However, no significant difference between either males and females or between younger and older individuals was detected (Hanihara/Ishida 2001; Perizonius 1979).

A bilateral accessory Foramen infraorbitale (Fig. 238) was found on the skull of the individual in Burial 34 (♂, 49–76 years). This rather rare variant is manifested by an additional foramen adjacent to the infraorbital foramen (Berry/Berry 1967; Hanihara/Ishida 2001).

The individual of Burial 41 (♂, 50–59 years) showed a unilaterally (left) complete Foramen supraorbitale (Fig. 265), which opens into the orbital cavity (Berry/Berry 1967; Hanihara/Ishida 2001), with a vertical septum. As illustrated by Fallucco et al. (2012) a complete foramen can cause the compression of the supraorbital nerve. The vertical septum divides the supraorbital neurovascular bundles (see Fallucco et al. 2012). While the complete supraorbital foramen is a common feature, the presence of a vertical septum is a rather rare subtype (Fallucco et al. 2012; Hanihara/Ishida 2001). Furthermore, the variant usually shows a slight sex difference with a higher frequency in females (Hanihara/Ishida 2001). In the present case, a male individual was affected.

In the case of the individual of Burial 29 (♂, 20–25 years) an exsutural Foramen mastoideum (Fig. 220) could be observed on both sides of the skull. This cranial variant is rather common (Berry/Berry 1967; Perizonius 1979).

The Foramen zygomaticofaciale was unilaterally (left side) doubled (Fig. 226) in the individual of Burial 30 (♀, 40–50 years), while on the right side only a single foramen was present. In the case of a doubled foramen the zygomaticofacial nerve is divided and exits the zygomatic bone through both foramina (Loukas et al. 2008; Perizonius 1979). The variant is often unilaterally present (Loukas et al. 2008).

The individual in Burial 34 (♂, 49–76 years) showed a bilateral supraorbital notch (Fig. 238), which can be understood as an incomplete Foramen supraorbitale (Berry/Berry 1967). Similar to the Foramen supraorbitale (see above) a supraorbital notch can cause the compression of the supraorbital nerve (Fallucco et al. 2012).

Four individuals (Burial 23 (ANT), Burial 25 (ANT), Burial 27 (ANT), Burial 36 (MA)) either showed an ossicle at the lambda (Burial 27), lambdoid ossicles (Burial 25, Burial 36), or both (Burial 23). An ossicle at the lambda (Fig. 201) is located at the position of the posterior fontanel, while lambdoid ossicles (e. g. Fig. 200) are located at the lambdoid suture (Berry/Berry 1967). These supernumerary cranial bones result from abnormal additional ossification centres along the lamboid suture (Bellary et al. 2013).

Vertebral bones and ribs also showed some variants, namely Facies articularis superior atlantis bipartita (Burial 34 (MA)), Foramen transversum bipartitum (Burial 25 (ANT), Burial 27 (ANT), Burial 29 (MA), Burial 37 (MA), Burial 43 (UD)), Processus spinosus bipartitus (Burial 27, Burial 29, Burial 34, Burial 43) as well as a bifurcated rib (Burial 39 (MA)).

A so-called Facies articularis superior atlantis bipartita (Fig. 239) is characterized by a subdivision of the Facies articularis superior of the first cervical vertebra (atlas) into two parts. The individual in Burial 34 (♂, 49–76 years) showed a bilateral and complete subdivision. Depending on the population this might be a rather rare variant (see Prescher 1997). The subdivision can be explained by the development of the atlas from two different sources. While the dorsal part originates from the proatlas, the anterior part originates from the segment of the first cervical vertebra (Prescher 1997).

Five individuals from Karacamirli, namely the individuals of Burial 25 (♂, 40–70 years; ANT), Burial 27 (probably ♂, 40–46 years; ANT), Burial 29 (♂, 20-–25 years; MA), Burial 37 (probably ♂, 10–13 years; MA), and Burial 43 (nd, nd; UD), showed a Foramen transversum bipartitum (e. g. Fig. 250) on at least one cervical vertebra. This variant on cervical vertebrae C3 to C7 is quite common (Finnegan 1978; Finnegan/Faust 1974). Cervical vertebra C3 was not affected in the individuals of Burials 25, 27, and 37, respectively. This vertebra was, however, missing in the other two individuals (Burial 29, Burial 43). Both cervical vertebrae C4 and C5 showed a bilateral variant in case of the individuals in Burials 25 and 37. These vertebrae were not preserved in the remaining individuals. The individuals of Burial 27 and Burial 43 showed a Foramen transversum bipartitum on the right side of the sixth cervical vertebrae. The respective left side of the vertebra could not be determined

in both individuals. The foramen was not present in the individual of Burial 25, could not be determined in case of the individual of Burial 37, and the respective vertebra was missing in case of the individual of Burial 29. Finally, the right side of cervical vertebra C7 of the individual in Burial 29 showed a foramen, while the left side could not be examined. No foramen was present in the individuals of Burial 25, 27, and 37, respectively. The respective bone was missing in the case of the individual in Burial 43. In total, the fraction of cervical vertebrae with a Foramen transversum bipartitum (see Finnegan/Faust 1974) differed with 1/3 for the individual in Burial 37 (foramen in C4 and C5, C6 nd), 2/7 for the individual of Burial 25 (foramen in C4 and C5), and 1/7 for the individual of Burial 27 (foramen in C6). For the remaining individuals only one cervical vertebra was preserved. The right side of the cervical vertebrae of eight and the left side of seven adult individuals could be assessed. In 50.0 % of the right and 43.9 % of the left sides of the cervical vertebrae of adult individuals from Karacamirli showed the foramen. The frequency in children was one third with only three determinable individuals.

Processi spinosi bipartiti (e. g. Fig. 268) were detected on the vertebrae of four individuals (Burial 27 (ANT), Burial 29 (MA), Burial 34 (MA), Burial 43 (UD)). This variant is characterized by a bifid spinous process. Out of only eight adult skeletons that could be examined with respect to this variant the observed frequency in adults was 50.0 %. The two determinable child skeletons did not show a Processus spinosus bipartitus. Interestingly, all four individuals also showed a Foramen transversum bipartitum (see above).

The individual in Burial 39 (♂, 9–12 years; MA) showed a bifurcated rib. This congenital abnormality usually occurs through the dorsal fusion of two ribs (Brossmann et al. 2001). Further postcranial variants detected on the individuals from Karacamirli are a Foramen supratrochleare (Burial 36 (♂, 50–70 years; MA)) as well as a Processus supracondylaris (Burial 41 (♂, 50–59 years; MA)).

In the case of the variant called Foramen supratrochleare the Fossa olecrani shows a hole of varying diameter (Fig. 246). This is a rather common finding (e. g. Finnegan 1978). However, only one individual from Karacamirli, namely the individual in Burial 36, out of eight determinable adult individuals (12.5 %) showed the respective variant. The respective individual showed a Foramen supratrochleare on the left humerus, while the right humerus could not be determined.

The Processus supracondylaris, as detected on the left humerus of the individual in Burial 41, is visible as a bony spur at the medial supracondylar ridge few centimeters above the medial epicondyle (Fig. 263). This variant is thought to be equivalent to an atavism (Brossmann et al. 2001) and is a rare finding (Finnegan 1978). The frequency of the trait was the same as for the Foramen supratrochleare with 12.5 %. The individual in Burial 41 only showed the variant on the left humerus, while no Processus supracondylaris was present on the right humerus.

V.5 Summary

In total, 38 human skeletons were morphologically examined, including burials from Late Bronze Age/Early Iron Age (n = 12), Antiquity (n = 7), and Middle Ages (n = 14). Morphology revealed mainly male (n = 15, 39.5 %) and only few female individuals (n = 4, 10.5 %). However, sex determination was not possible for the remaining 19 (50.0 %) individuals due to a poor or incomplete preservation of the skeleton. The comparatively low number of female individuals may be an artefact due to the rather high number of indeterminable individuals. In the case of 8 (21.1 %) individuals the age at death could not be determined. The majority of the remaining individuals (n = 16, 84.2 %) reached a mature to senile age. Infant and juvenile individuals were rare (n = 8, 21.1 %), which is, however, in agreement with a general deficit of infant burials on graveyards due to a poor preservation of infant bones.

Craniometry mathematically reveals several individuals with conspicuous measures. This might indicate a non-local origin of the respective individuals or their ancestors. However, the question of provenance cannot be answered solely based on morphology but also requires stable isotope analyses (see ch. VI).

Postcranial indices suggest different levels of activity as well as robustness. The majority of individuals showed a quite high activity as well as high robustness. In some cases, low activity or low robustness were related to pathological skeletal conditions. In addition, a variety of (non-pathological) variants, both acquired and epigenetic, could be observed at the cranial and postcranial skeleton.

The living conditions of the individuals from Karacamirli were obviously quite good. Evidence for deficiencies is rare. The majority of individuals did not show signs of pathologies on their skeleton. It is important to mention that bones and teeth only reflect a small range of pathologies. Furthermore, some diseases only leave their mark on the bone after some time of illness. Thus, if an individual died quite early due to a disease, this would not necessarily be visible in the skeleton. Nevertheless, the low number of pathologies might indicate a majority of quite healthy individuals. This is also in agreement with the rather high number of mature and senile individuals.

VI. Multi-isotope fingerprint of humans, animals, and environmental samples from Karacamirli

Andrea Göhring / Stefan Hölzl / Michael Joachimski / Christoph Mayr / Gisela Grupe

VI.1 Introduction

Stable isotope analyses have been used in anthropological as well as archaeological studies for decades in order to inform on the dietary behavior and migratory events of past humans as well as on ancient environments. The stable isotope ratio of a light element »Y« is expressed by the δ-notation according to Eq. 1, where »R« describes the abundance of the heavy isotope (^{X}Y) relative to the light isotope in the analysed sample and standard, respectively (Coplen 2011):

$$\delta^{X}Y = \frac{R_{sample}}{R_{standard}} - 1\ [‰] \qquad \text{(Eq. 1)}$$

The δ-values (e. g. $\delta^{13}C$) are given in per mil. In the case of heavy elements (atomic weight > 50 u) no δ-notation but the absolute ratio of heavy to light isotope (e. g. $^{87}Sr/^{86}Sr$) is used. In contrast to radionuclides (e. g. ^{14}C) stable isotopes (e. g. ^{13}C) have an indefinite lifetime.

Stable isotope values in skeletal tissue, such as bones or teeth, are dependent on the remodeling rate of the analysed material. Enamel preserves the isotopic signal of the period of its formation during childhood or juvenile age and does not change afterwards. Thus, it can be understood as an archive of an individual's childhood (Grupe 1998). Bone tissue, on the other hand, is remodeled with a certain rate depending on the bone type. Thus, stable isotope values of a bone sample reflect the isotopic signature of the last ~20 years (Martin et al. 2015) before the individual died.

The major bone component (c. 70 %) is made up of bioapatite, while the organic fraction contributes about 22 % (Hillson/Antoine 2003). More than 90 % of the organic fraction is collagen of type I (Gelse et al. 2003; Knott/Bailey 1998). The mineral bioapatite (carbonate-hydro-apatite; see Greiner et al. 2019) can be approximated as (Ca, Mg, Na, vacancy)$_5$(PO_4, HPO_4, CO_3)$_3$ (CO_3, H_2O, OH, F, Cl etc.) (Elliott 2002; Greiner et al. 2019; LeGeros/LeGeros 1984; LeGeros et al. 1969; Schmahl et al. 2017; 2016). Substitutions can occur at all crystal positions of the bioapatite. For example, Na^+, Mg^{2+}, Sr^{2+}, and Pb^{2+} can occupy the Ca^{2+} sites. The phosphate group (PO_4^{3-}) can be substituted by CO_3^{2-} (type A substitution), HPO_4^-, and $P_2O_7^{4-}$. Furthermore, the hydroxyl group (OH^-) can be substituted by CO_3^{2-} (type B substitution), Cl^-, F^-, and H_2O (Greiner et al. 2019; Schmahl et al. 2017; 2016).

The composition of tooth dentine is very similar to that of bone. In contrast, enamel consists of more than 96 % bioapatite (Hillson/Antoine 2003) and is free of collagen.

Several different isotopic systems can be analysed in bones and teeth. In the present study, $\delta^{13}C_{collagen}$ and $\delta^{15}N_{collagen}$ of bone collagen as well as $\delta^{13}C_{carbonate}$, $\delta^{18}O_{carbonate}$, and $\delta^{18}O_{phosphate}$ of bone apatite were measured. Furthermore, the $^{87}Sr/^{86}Sr$ ratio of both bone and enamel was analysed. In the following the different isotopic systems are explained in more detail.

Stable carbon and nitrogen isotope values of bone collagen are mainly related to the protein of the consumed diet (Ambrose et al. 1997; Bonsall et al. 2000; Jim et al. 2004; Johansen et al. 1986; Krueger/Sullivan 1984; McCutchan et al. 2003; Schoeninger/DeNiro 1984; Tieszen/Fagre 1993). Carbon fixated by plants as CO_2 is used for amino acid synthesis. It is possible to distinguish so-called C_3 and C_4 plants, which show a different pathway for CO_2 fixation due to a different frequency of the main enzymes ribulose-1,5-bisphosphate carboxylase/oxygenase (RuBisCO) and phosphoenolpyruvate carboxylase (PEPC). While C_3 plants show an excess in RuBisCO compared to PEPC, C_4 plants mainly use PEPC for CO_2 fixation (Melzer/O'Leary 1987). The different photosynthetic pathways lead to different $\delta^{13}C$ values

in C_3 compared to C_4 plants with mean values of about -28 ‰ and -13 ‰, respectively (Ehleringer/Osmond 1989; Kohn/Cerling 2002; O'Leary 1988; Schmidt 2003). Consequently, the $\delta^{13}C_{collagen}$ values of herbivores consuming a diet mainly based on C_3 or C_4 plants differ accordingly. An isotopic fractionation occurs during the digestion and incorporation of the plant food. As a consequence, bone collagen is isotopically enriched by 5 to 6 ‰ compared to the consumed plants (Krueger/Sullivan 1984; Sullivan/Krueger 1981; Vogel 1978). Accordingly, an herbivorous animal which mainly feeds on C_3 plants exhibits a $\delta^{13}C_{collagen}$ value of about -23 ‰, while an herbivore feeding on a C4-based diet should show an isotope value of about -7 ‰.

The $\delta^{15}N_{collagen}$ value of a consumer is by about 3 ‰ enriched compared to a consumer's diet according to the rule »You are what you eat (plus a few ‰)« (DeNiro/Epstein 1976; Minagawa/Wada 1984; Post 2002). Consequently, nitrogen isotope values increase with each trophic level by about 3.4 ‰. This trophic level effect allows to differentiate animals according to their primary food source. As a consequence, it is possible to distinguish herbivores from carnivores and omnivores. Likewise, breast feeding causes an enrichment in ^{15}N in the infant compared to the mother, because milk proteins (i. e. casein) are enriched with ^{15}N compared to the isotopic signal of the mother's tissue protein (Knobbe et al. 2006; Kornexl et al. 1997; Steele/Daniel 1978). In addition, starvation will lead to more positive $\delta^{15}N$ values in the body. Digestion of endogenous proteins, e. g. by degradation of skeletal muscles, further contributes to this trophic level effect (Mekota et al. 2006).

For the reconstruction of the palaeodiet, the calculation of so-called isotope mixing models is helpful (see e. g. Grupe 2014; Phillips 2012; 2001; Phillips et al. 2014). Since the carbon and nitrogen concentrations are not identical in different food sources, especially when combining e. g. meat and plants, a concentration-dependent mixing model should be applied (Phillips/Koch 2002). In the present study the program »SISUS« (Erhardt 2014; Erhardt et al. 2014) was used for the calculation of such mixing models (see ch. VI.2.3). Isotope mixing models use approximated dietary $\delta^{13}C$ and $\delta^{15}N$ values, which can be calculated from the $\delta^{13}C_{collagen}$ and $\delta^{15}N_{collagen}$ values according to the following equations (e. g. Grupe 2014; Krueger/Sullivan 1984; Newsome et al. 2004; Sullivan/Krueger 1981):

$$\delta^{13}C_{diet\ (human)} = \delta^{13}C_{collagen\ (human)} - 5\ ‰ \quad \text{(Eq. 2)}$$

$$\delta^{15}N_{diet\ (human)} = \delta^{15}N_{collagen\ (human)} - 3\ ‰ \quad \text{(Eq. 3)}$$

Food sources can also be approximated using the collagen isotope values of animal remains with known feeding habits according to Eqs. 4 to 9 (e. g. Grupe 2014; Krueger/Sullivan 1984).

$$\delta^{13}C_{meat} = \delta^{13}C_{collagen} - 4\ ‰ \quad \text{(Eq. 4)}$$

$$\delta^{15}N_{meat} = \delta^{15}N_{collagen} \quad \text{(Eq. 5)}$$

$$\delta^{13}C_{milk/cheese} = \delta^{13}C_{collagen\ (cattle,\ sheep,\ goat)} - 3\ ‰ \quad \text{(Eq. 6)}$$

$$\delta^{15}N_{milk/cheese} = \delta^{15}N_{collagen\ (cattle,\ sheep,\ goat)} + 3\ ‰ \quad \text{(Eq. 7)}$$

$$\delta^{13}C_{plant} = \delta^{13}C_{collagen\ (herbivore)} - 5\ ‰ \quad \text{(Eq. 8)}$$

$$\delta^{15}N_{plant} = \delta^{15}N_{collagen\ (herbivore)} - 3\ ‰ \quad \text{(Eq. 9)}$$

Because of the concentration dependency the carbon (%C) and nitrogen (%N) concentration needs to be known. While measured %C and %N values may be used, calculated carbon and nitrogen concentrations are thought to be more realistic in mixing models (see e. g. Robbins et al. 2002). The concentrations can be calculated by using the percentage (dry weight) of protein, fat, and carbohydrates in the food sources (according to USDA Food Composition Databases; www.ndb.nal.usda.gov/ndb/). According to Haurowitz (1955) carbohydrates, fat/lipids, and proteins contain 44 %, 75 %, and 54 % dry weight carbon, respectively. Furthermore, proteins contain 16 % nitrogen (Haurowitz 1955). The digestibility of protein in meat or fish is about 100 %, while only c. 90 % of plant protein can be digested by humans (Newsome et al. 2004; Pritchard/Robbins 1990). Accordingly, %C and %N of animal and plant diet for human consumers can be calculated as follows:

$$\%C_{animal\ diet} = 54 * protein_{wt\%} + 75 * fat_{wt\%} \quad \text{(Eq. 10)}$$

$$\%N_{animal\ diet} = 54 * protein_{wt\%} \quad \text{(Eq. 11)}$$

$$\%C_{plant\ diet} = 54 * 0.90 * protein_{wt\%} + 75 * fat_{wt\%} + 45 * carbohydrate_{wt\%} \quad \text{(Eq. 12)}$$

$$\%N_{plant\ diet} = 16 * 0.90 * protein_{wt\%} \quad \text{(Eq. 13)}$$

For dairy products (e. g. milk, cheese) a carbon and nitrogen concentration of 6.5 and 0.5 % were chosen according to Hagl et al. (2013).

Carbon of bone carbonate originates from CO_2 dissolved in the blood serum as well as blood bicarbonate (Ambrose et al. 1997; Poyart et al. 1975; Sullivan/Krueger 1981). $\delta^{13}C_{carbonate}$ also shows a diet-related trophic shift.

While the isotopic fractionation between herbivorous consumer and plant is about 12–13 ‰, on higher trophic levels, the consumer is only enriched by about 3–4 ‰ compared to the prey (Krueger/Sullivan 1984; Sullivan/Krueger 1981). In contrast to $\delta^{13}C_{collagen}$, $\delta^{13}C_{carbonate}$ is not only related to the dietary protein but rather to the whole diet (protein, carbohydrate, fat; Ambrose/Norr 1993; Howland et al. 2003; Jim et al. 2004). The $\delta^{13}C_{carbonate}$ value is strongly correlated with both carbohydrates and fat concentration (Jim et al. 2004). Fat is depleted in ^{13}C compared to other food components, resulting in more negative $\delta^{13}C_{carbonate}$ values in carnivores (Clementz et al. 2009; Howland et al. 2003; Jim et al. 2004; Krueger/Sullivan 1984). Carnivores show more negative $\delta^{13}C$ isotope values than herbivores, because of a diet based on animal protein and fat, while the latter mainly consume proteins of plant origin as well as carbohydrates. Thus, it is possible to use $\delta^{13}C_{carbonate}$ to distinguish between herbivorous and carnivorous animals.

$\Delta\delta^{13}C_{carbonate\text{-}collagen}$ (= $\delta^{13}C_{carbonate}$ - $\delta^{13}C_{collagen}$) can be used to highlight the lipid content of the diet. A diet rich in fat results in lower $\Delta\delta^{13}C_{carbonate\text{-}collagen}$ values and vice versa. Thus, carnivores exhibit $\Delta\delta^{13}C_{carbonate\text{-}collagen}$ values which are significantly lower than those of herbivores (Lee-Thorp et al. 1989). Herbivorous animals exhibit a larger difference between $\delta^{13}C_{carbonate}$ (whole diet) and $\delta^{13}C_{collagen}$ (protein part of the diet) than carnivores (Krueger/Sullivan 1984).

Similar to carbon, oxygen in bone carbonate originates from blood bicarbonate (Ambrose et al. 1997; Gannes et al. 1998; Sullivan/Krueger 1981). Due to the constant body temperature in mammals (c. 37°C), $\delta^{18}O_{carbonate}$ is influenced by the oxygen isotopic composition of the body water and mainly reflects the isotope value of metabolic water (from food) as well as atmospheric oxygen (Bryant/Froelich 1995; Kirsanow/Tuross 2011; Kohn 1996). Metabolic oxygen is produced by catabolism of dietary carbohydrates, fats, and proteins. The oxygen of the emerged CO_2 and H_2O quickly exchanges with blood oxygen (Bryant/Froelich 1995; Green et al. 2018).

Due to the constant body temperature in mammals, $\delta^{18}O_{phosphate}$ values reflect the isotopic composition of body water (Longinelli 1984; Luz/Kolodny 1985; Luz et al. 1984). Oxygen isotope exchange occurs between phosphate and body water (Bryant et al. 1996). The oxygen isotopic composition of body water is mainly influenced by the $\delta^{18}O$ value of drinking water (Podlesak et al. 2008). Thus, $\delta^{18}O_{phosphate}$ values are mainly related to the local drinking water (Kirsanow/Tuross 2011; Longinelli/Peretti Padalino 1980; Longinelli/Selmo 2011; Luz et al. 1990; Luz/Kolodny 1985). Accordingly, while $\delta^{18}O_{carbonate}$ mainly reflects the isotopic composition of the ingested food, $\delta^{18}O_{phosphate}$ mirrors the isotopic composition of the (meteoric) drinking water (Kirsanow/Tuross 2011).

Herbivores exhibit more positive $\delta^{18}O_{carbonate}$ values than carnivores at the same location (Sponheimer/Lee-Thorp 2001; 1999). This can be explained by the fact that carbohydrates, which constitute the major part of the herbivorous diet, are depleted in ^{18}O compared to proteins, which dominate the diet of carnivores (Sponheimer/Lee-Thorp 2001). However, with respect to $\delta^{18}O_{phosphate}$, carnivorous mammals exhibit more positive values than herbivores (White et al. 2004). Carnivores usually drink their prey's blood (Longinelli/Peretti Padalino 1980) rather than meteoric water. Even physiological differences (e. g. panting vs. sweating, grazer vs. browser, drinking behavior) have an effect on the $\delta^{18}O$ value of an individual (Bocherens et al. 1996; Kohn 1996; Kohn et al. 1996; Sponheimer/Lee-Thorp 2001; 1999).

Environmental factors affect both $\delta^{18}O_{carbonate}$ and $\delta^{18}O_{phosphate}$, albeit with a different magnitude. Humidity, precipitation, and temperature mainly have an effect on the meteoric drinking water, thus on $\delta^{18}O_{phosphate}$. With increasing precipitation (and thus increasing humidity) the $\delta^{18}O$ value of the meteoric water decreases due to a decreased evaporation. On the other hand, with increasing temperature the $\delta^{18}O$ value of precipitation as well as meteoric waters will increase (Marshall et al. 2007). Geographical factors (e. g. latitude, altitude) also have an impact on the oxygen isotope ratios. With increasing latitude and likewise decreasing temperature, $\delta^{18}O$ values of precipitation decrease. Similarly, the oxygen isotope ratio decreases with increasing altitude as well as distance from the coast (Marshall et al. 2007).

Oxygen isotope spacing $\Delta\delta^{18}O$ (= $\delta^{18}O_{carbonate}$ - $\delta^{18}O_{phosphate}$, with both values given relative to the V-SMOW standard; see Coplen 1988) as well as the linear regression between $\delta^{18}O_{carbonate}$ and $\delta^{18}O_{phosphate}$ has been frequently used to validate the preservation state of the bones or to calculate the $\delta^{18}O_{phosphate}$ value from the respective measured $\delta^{18}O_{carbonate}$ value (e. g. Bryant et al. 1996; Iacumin et al. 1996; Martin et al. 2008; Pellegrini et al. 2011). However, it has been shown recently that factors such as species, diet, physiology, habitat, and climate have a major impact on both $\Delta\delta^{18}O$ as well as the regression model (Göhring et al. 2019b; 2019a). Therefore, it is not advisable to use both a fixed value for $\Delta\delta^{18}O$ and a general regression model independent from factors such as diet.

Strontium is a heavy element. Isotopic changes caused by fractionation processes are lower than the measurement errors. For that reason, fractionation processes are negligible (Flockhart et al. 2015). $^{87}Sr/^{86}Sr$ can be used to identify primarily non-local individuals based on the

strontium isotopic fingerprint of a given site. Erosion of underlying bedrock leads to soil formation. By weathering of the bioavailable components in the soil, strontium can enter the biosphere (Bataille/Bowen 2012). Bioavailable strontium is incorporated into local plants and animals. Strontium is always associated with calcium, as both are alkaline earth metals and react in a similar way. However, since strontium is not essential, a discrimination in favor of calcium occurs in the intestinal tract (Wasserman et al. 1958). The phenomenon of biopurification is of special importance when analysing strontium isotope ratios. The term biopurification describes the preferential assimilation of calcium in preference to both barium and strontium. This leads to reduced Ba/Ca as well as Sr/Ca ratios compared to the diet (Burton et al. 1999). As a consequence, the variance in the Sr/Ca ratio as well as in the strontium isotope ratio decreases with increasing trophic level (Bentley 2006; Price et al. 2012). Consequently, geological materials show a variance which is by some magnitudes higher than the variance in biological tissues such as bones and teeth. Local animal and human strontium isotope ratios in enamel only differ by less than 0.00015 to 0.0003 (Burton/Hahn 2016; Burton/Price 2013). Bones and teeth average the bioavailable strontium isotope signal, which is mainly influenced by food, drinking water, and atmospheric strontium (Bentley 2006; Capo et al. 1998; Lengfelder et al. 2019; Price et al. 2002; Söllner et al. 2016). Biologically available strontium isotope ratios (e. g. faunal and environmental samples) have to be measured in order to define local $^{87}Sr/^{86}Sr$ values more closely (Price et al. 2012) as well as detect possible small-scale variations at a site or in a region. The $^{87}Sr/^{86}Sr$ ratio is a valid tool to track migratory events as well as diet of animals and humans (Capo et al. 1998). Moreover, the strontium isotopic signature of animals and humans allows to define their local home range reflected by their tissues. According to Price et al. (2002) the local strontium isotope range can be grossly approximated as follows with mean μ and standard deviation sd:

$$\text{local range} = \mu\,(\text{animals}) \pm 2 * \text{sd}\,(\text{animals}) \qquad \text{(Eq. 14)}$$

The local strontium isotope signature can be used for the reconstruction of the place of origin, migratory events, as well as trade. If an individual falls outside this range, it was probably primarily non-local to the site or region. However, a strontium isotope ratio which fits into the range does not necessarily imply a local origin of the individual tested. Migratory events during life time can be visualized by the parallel analysis of bone and enamel samples. The $^{87}Sr/^{86}Sr$ ratio of childhood is preserved in enamel. Bone, on the other hand, reflects the last years before an individual died (see above). A change in $^{87}Sr/^{86}Sr$ from enamel to bone is indicative of at least one migratory event or a possible dietary change (see e. g. Burton/Price 1999; Price et al. 2002) after childhood. However, even the locality of the mother is implemented in the child's strontium isotope signal due to weaning. Consequently, a primarily non-local mother transfers a mixed isotope signal to the child. The child is thus seemingly non-local, although it was born at the site. Individuals who migrated late in their life show a mixed isotopic signal in their bones. A non-local strontium isotope ratio in the enamel implies immigration. Accordingly, it is necessary to determine the (expected) local strontium isotope ratios.

VI.2 Material and Methods

VI.2.1 Material

Isotope analysis was conducted on thirteen archaeological human remains, seven (archaeological) animals, as well as four (modern) environmental samples (straw, soil, well water) from Tepe 5 at Karacamirli (see Table 24). The respective humans were chosen for isotope analysis because of their preservation and burial context (see ch. IV). Modern straw was collected on a field next to Tepe 5. Soil sample T5-7 was collected at the northern profile of Tepe 5 at a depth of about 1.6 m. The second soil sample, KS17-14, was collected in the course of an old river (Eastern river) at a depth of about 0.5 m. The well water was sampled from a modern well close to the site of excavation.

VI.2.2 Extraction of collagen and apatite and mass spectrometry

VI.2.2.1 Extraction and measurement of $\delta^{13}C_{collagen}$ and $\delta^{15}N_{collagen}$ of bone collagen

For the determination of carbon ($\delta^{13}C_{collagen}$) and nitrogen ($\delta^{15}N_{collagen}$) stable isotope ratios in bone collagen, collagen was extracted as gelatine. Bones were washed with deionized water in an ultrasonic bath and air dried for several days. Afterwards, the samples were homogenized using a ball mill. 8 ml of 1 M HCl were added to 500 mg of bone powder filled into Teflon tubes. This demineralization step lasted 20 minutes. Afterwards, the samples were washed with deionized water until

burial	context	individual	sample type	sampled material
5	KG-038	0146	human	femur; tooth II6
7	KG-026	0105	human	tooth I6
8	KG-057	0247/0404	human	tibia
9	KG-043	0204	human	tooth crown
21	KG-074	0507	human	femur; tooth IV6
25	KG-053	0208	human	femur; tooth III6
26	KG-066	0392	human	femur
27	KG-097	0455	human	femur
28	KG-027	0106	human	metacarpus
29	KG-031/050	0120	human	femur; tooth II6
34	KG-048	0197	human	femur; tooth III6
35	KG-047/098	0217/0467	human	tooth III6
37	KG-052	0205	human	femur; tooth IV6
38	KG-073	0508	human	tibia; tooth III6
39	KG-077	0517	human	femur; tooth III6
-	KG-032	0553	sheep/goat	humerus
-	KG-025	0554	dog/fox puppy	humerus
-	KG-057	0552	sheep	tibia
-	KG-023	0421	sheep/goat	talus
-	KG-074	0551	sheep/goat	humerus
-	KG-094	0451a	piglet	mandible
-	KG-094	0451b	mouse	tooth
-	KG-094	0451c	sheep/goat	phalanx
-	-	straw	straw	straw (modern)
-	-	T5-7	soil	soil
-	-	KS17-14	soil	soil
-	-	water	well water	well water (modern)

Table 24. Overview of the archaeological and modern samples from Karacamirli used for stable isotope analysis (see Table 16 in ch. V for more details on the humans). Sampled teeth are labelled according to the dental quadrant (I to IV) counting from the right upper quadrant (I) to the right lower quadrant (IV). First molars (tooth number 6) were sampled

neutrality (pH ≈ 5–6). This step was followed by incubation in 8 ml of 0.125 M NaOH for 20 hours. As a result of this treatment, humic substances are removed from the samples. After 20 h the samples were again washed until neutrality. For gelatinization, the samples were incubated for 10 h to 17 h with 8 ml of 1 M HCl (pH = 3) at 90℃ (water bath). Afterwards, the samples were filtered (pore size 4–5 µm) and lyophilized. About 0.5 mg of the lyophilized gelatine was weighed into tin capsules for the mass spectrometry. Isotope ratios were measured with a Flash EA 2000 elemental analyser connected to an isotope-ratio mass spectrometer (Thermo Finnigan Delta V Plus; GeoZentrum Nordbayern, Friedrich-Alexander University Erlangen-Nuremberg, Germany). Stable carbon and nitrogen isotope ratios are expressed relative to the V-PDB (Vienna Pee Dee Belemnite; Section of Isotope Hydrology of the International Atomic Energy Agency, IAEA) and the AIR (atmospheric nitrogen; IAEA)

standards, respectively. Two laboratory standards, a casein standard ($\delta^{13}C$ = -27.32 ‰ ± 0.11 ‰, $\delta^{15}N$ = 5.94 ‰ ± 0.06 ‰; n = 5) as well as a cyclohexane standard ($\delta^{13}C$ = -29.43 ‰ ± 0.04 ‰, $\delta^{15}N$ = -4.99 ‰ ± 0.03 ‰; n = 2), calibrated to the international glutamic acid standards USGS 40 and USGS 41 (IAEA) were used to test for reproducibility as well as the accuracy of carbon and nitrogen isotope analyses. For quality control of the extracted gelatine, the C/N molar ratio was calculated according to

$$\frac{\%C/\%N}{12/14} \qquad \text{(Eq. 15)}$$

based on wt% carbon and nitrogen. Intact collagen exhibits a C/N molar ratio of 3.2. However, as shown by DeNiro (1985) slightly degraded collagen with a C/N molar ratio between 2.9 and 3.6 also results in valid isotope values.

VI.2.2.2 Extraction and measurement of $\delta^{13}C_{carbonate}$ and $\delta^{18}O_{carbonate}$ of bone apatite

The extraction protocol of structural bone carbonate was modified after Lee-Thorp et al. (1989). Bones were washed with deionized water in an ultrasonic bath and afterwards air dried for several days. The samples were homogenized with a ball mill (Retsch). About 100 mg of bone powder were weighed into Teflon tubes. 5 ml of NaOCl (4 %) were added in order to remove organic bone constituents. After two days, NaOCl was removed and replaced by a fresh solution. The samples remained in the new solution for another two days. Then, the samples were washed to neutrality (ph ≈ 5–6) with deionized water and incubated in 5 ml of 1 M acetic acid calcium acetate buffer (pH ≈ 5) for 12 h. Finally, samples were rinsed with deionized water and lyophilized. The lyophilized samples were weighed into septum vials. These vials were automatically flushed with helium. Phosphoric acid (100 %) was added in a Gasbench II. After reaction at 70°C for at least three hours the evolved carbon dioxide was measured with an isotope-ratio mass spectrometer (Thermo Finnigan Delta V Plus; GeoZentrum Nordbayern, Friedrich-Alexander University of Erlangen-Nuremberg, Germany).

For monitoring of both reproducibility and accuracy of the measurements, two laboratory calcium carbonate standards (calibrated to the international NBS 19 (TS-limestone; $\delta^{13}C$ = 1.95 ‰, $\delta^{18}O$ = -2.20 ‰; IAEA) and IAEA-CO-9 standards (barium carbonate standard; $\delta^{13}C$ = -47.3 ‰, $\delta^{18}O$ = -23.2 ‰; IAEA)) were measured together with the samples. Analytical precision was about ± 0.1 ‰ (standard deviation) for both oxygen and carbon isotope analysis.

VI.2.2.3 Extraction and measurement of $\delta^{18}O_{phosphate}$ of bone apatite

Extracted bone apatite (see ch. VI.2.2.2) was further processed for phosphate extraction (after Mayr et al. 2016). About 3 mg of bone apatite were weighed into 2 ml Eppendorf tubes and dissolved in 115 µl HF (2 M) for 6 hours in order to remove calcium. The samples were then neutralized with 115 µl KOH (2 M). After centrifugation for 15 min (3000 rpm) the supernatant was transferred into a fresh 2 ml Eppendorf tube of known weight. Silver phosphate was precipitated by adding 1.5 ml $AgNO_3$ solution (pH = 10–11). For 20 samples 0.34 g $AgNO_3$, 0.28 g NH_4NO_3, and 1 ml NH_3 (25 %) were diluted with water to 30 ml. The Eppendorf tubes were put into a water bath (60°C) for 12 h. Afterwards, the remaining $AgNO_3$ solution was removed and the precipitated $AgPO_4$ crystals were washed with deionized water in an ultrasonic bath. The samples were dried in an oven (60°C) for several hours. Finally, the crystals were pounded in the Eppendorf tubes and 0.92 to 0.94 mg of the powder were weighed into silver capsules.

Before analyses, the samples were dried in a vacuum drying cabinet (60°C) for 48 h and afterwards immediately transferred into a helium-flushed auto sampler. After quantitative pyrolysis at 1490°C in the presence of glassy and granulated carbon in the SiC reaction tube of a high-temperature pyrolysis oven (HEKAtech), the resulting CO gas was transferred to the isotope-ratio mass spectrometer (Delta V Advantage, Thermo Fisher Scientific; Institute of Geography, Friedrich-Alexander University Erlangen-Nuremberg, Germany) in a continuous helium flow with a measurement precision of ± 0.2 ‰. The phosphate extraction procedure was validated using the phosphate rock standard NBS 120c (21.97 ‰, n = 1; National Institute of Standards and Technology NIST, Florida, USA).

For quality control and calibration the international benzoic acid standards IAEA 601 (23.22 ‰ ± 0.22 ‰, n = 3) and IAEA 602 (71.38 ‰ ± 0.02 ‰, n = 3), and the laboratory standards α-cellulose (32.04 ‰ ± 0.32 ‰, n = 30), sucrose (30.28 ‰ ± 0.17 ‰, n = 3), and stearic acid (4.10 ‰ ± 0.76 ‰, n = 3) were measured. The purity of the extracted samples was controlled by checking the oxygen content (%O) obtained from the peak area relative to sample weight. Samples which show a low peak area out of the linearity range have to be excluded from further evaluations.

VI.2.2.4 Extraction and measurement of $^{87}Sr/^{86}Sr$ of bones, teeth, and environmental samples

The extraction procedure of $^{87}Sr/^{86}Sr$ in bones and teeth is based on a protocol modified after Pin et al. (2003). Extraction of strontium isotope ratios from soil, water, and plant samples was performed according to Lengfelder et al. (2019; see also Toncala et al. 2017).

After cleaning the samples in an ultrasonic bath, dried tooth samples were heated at 300℃ in a muffle furnace (Heraeus) for 2 h. Enamel and dentine were separated mechanically using a mortar. Both bone and enamel samples were twice treated with concentrated HCOOH (98 %) for five minutes in an ultrasonic bath and subsequently washed with deionized water until neutrality (pH ≈ 5–6). This step is important to remove contaminations by carbonates as well as diagenetically altered material (see e. g. Price et al. 1992). Afterwards, the bone and enamel samples were ashed in a furnace for 12 h at 800℃ (bone sample) and 500℃ (enamel sample), respectively. About 20 mg of ash were weighed into Teflon cubes. Samples were dissolved in 1 ml of 69 % HNO_3** in the closed cubes for 24 h on a hotplate at 120℃. The liquid was evaporated at 120℃ for about three to five hours. For column separation the samples were solubilized in 1 ml 8 N HNO_3*** for at least 20 min (120℃).

The water sample was filtered (MN 615 filter) to remove suspended matter. 15 ml of the water sample was filled into a Teflon cube and subsequently evaporated for about nine hours (120℃). Afterwards, the sample was dissolved in 1 ml of 69 % HNO_3** for 24 h (120℃). After evaporation the sample was solubilized in 1 ml HNO_3*** (8 N) at 120℃ for at least 24 h. The sample was solubilized for at least 20 min (120℃) by adding 1 ml of 8 N HNO_3***.

The soil samples were sieved through a 0.5 mm mesh. About 300 mg were weighed into Teflon cubes. After dissolving the samples in 2 ml of 35 % HCl** for 24 h (120℃), samples were evaporated and subsequently dissolved in 1 ml of 65 % HNO_3** for another 24 h (120℃). The remaining undissolved matter was removed by centrifuging (11000 rpm, 10 min). The liquid was transferred into a new Teflon cube and evaporated. The samples were dissolved in 1 ml 65 % HNO_3** (24 h, 120℃) followed by an evaporation step. Finally, 1 ml of 8 N HNO_3*** was added to solubilize the samples for at least 20 min (120℃).

The straw sample was ashed in the furnace for 12 h (800℃). About 40 mg of the ash was weighed into a Teflon cube and subsequently dissolved in 1 ml HNO_3** (69 %) for 24 h (120℃). The sample was evaporated for three to five hours. Finally, the sample was solubilized using 1 ml 8 N HNO_3*** for at least 20 min (120℃).

For column separation the columns have to be conditioned first. About 75 µl Sr-spec resin and 1 ml H_2O** were loaded. Bivalent ions and lead were removed by adding 1 ml 8 N HNO_3*** and 1 ml 6.5 N HCl***, respectively. The columns were subsequently washed with 1 ml H_2O**. Finally, the columns were conditioned with 100 µl 8 N HNO_3***. For bone, enamel, soil, and straw 300 µl of the dissolved sample were then pipetted into the column. In the case of the water sample 1 ml was added. The columns were flushed with 100 µl 8 N HNO_3***, followed by another 200 µl, 600 µl, and 200 µl of 8 N HNO_3***. These steps elute Rb, while Sr binds to the resin. Finally, strontium was eluted by adding 1 ml 0.05 N HNO_3*** and collected in Teflon cubes. The remaining liquid was evaporated.

The strontium isotope ratios were measured with a thermal ionization mass spectrometer (Finnigan MAT 261.5; *Rieskrater Museum Nördlingen*, Germany) with a precision of better than 0.00002 and an analytical accuracy of better than ± 0.00004. The extracted samples were loaded in a mixture of $TaCl_5$, HF, HNO_3, H_3PO_4, and H_2O on single-band tungsten filaments. Each sample was measured 19 times in three subsequent blocks resulting in 57 measurements per sample. For measurement control the international strontium carbonate standard SRM 987 (NIST) was carried along. The extraction procedure was validated using the international bone ash standard SRM 1400 (NIST; $^{87}Sr/^{86}Sr = 0.713045 \pm 0.000037$; n = 2). Samples with a double standard error (2SE[%]) smaller than 0.0055 were accepted as valid.

VI.2.3 Data analysis

Plots were created with the statistical software »R« (R Core Team 2018) using the packages »graphics« (R Core Team 2018), »ggplot2« (Wickham 2016), and »ggrepel« (Slowikowski 2018).

For the calculation of the concentration-dependent isotope mixing model, the probabilistic program »SISUS« (Stable Isotope Sourcing using Sampling) was used as an »R« package (»sisus« version 3.9-14; Erhardt 2014; Erhardt et al. 2014). For the installation of this package the file named sisus_3.9-14.tar.gz has to be downloaded from https://statacumen.com/sisus. Prior to installation of the sisus package Perl and the R packages »RColorBrewer« (Neuwirth 2014), »coda« (Plummer et al. 2006), »gdata« (Warnes et al. 2017), »gtools« (Warnes et al. 2018), »moments« (Komsta/Novomestky 2015), »polyapost« (Meeden et al. 2017), and »rcdd« (Geyer/Meeden 2017) have to be installed. Only then, the »sisus« package

burial	context	individual	sample type	$\delta^{13}C_{collagen}$ (VPDB)	%C	$\delta^{15}N_{collagen}$ (AIR)	%N	C/N molar	$\delta^{13}C_{carbonate}$ (VPDB)	$\Delta\delta^{13}C_{carbonate-collagen}$	$\delta^{18}O_{carbonate}$ (VPDB)	$\delta^{18}O_{phosphate}$ (VSMOW)	$\delta^{18}O_{carbonate}$ (VSMOW)	$\Delta\delta^{18}O_{carbonate-phosphate}$	%O	$^{87}Sr/^{86}Sr$ bone	2 SE (M) [%] bone	$^{87}Sr/^{86}Sr$ enamel	2 SE (M) [%] enamel	$^{87}Sr/^{86}Sr$ environment	2 SE (M) [%] environment
5	KG-038	0146	human	-19.88	37.0	12.15	13.7	3.15	-13.16	6.73	-9.08	14.63	21.55	6.92	13.07	0.707256	0.0020	0.707301	0.0027		
7	KG-026	0105	human															0.707248	0.0023		
8	KG-057	0247	human	-19.20	39.2	10.11	14.4	3.19	-12.51	6.69	-8.24	16.01	22.42	6.41	14.40						
9	KG-043	0204	human															0.707193	0.0021		
21	KG-074	0507	human	-19.01	42.5	11.10	15.5	3.19	-13.04	5.97	-8.91	16.39	21.73	5.33	14.44	0.707397	0.0015	0.707375	0.0016		
25	KG-053	0208	human	-18.98	40.7	11.71	15.1	3.15	-13.27	5.71	-9.00	16.00	21.64	5.63	14.66	0.707351	0.0028	0.707313	0.0026		
26	KG-066	0392	human	-19.18	43.5	9.87	15.9	3.19	-12.58	6.60	-10.06	15.43	20.54	5.11	14.51						
27	KG-097	0455	human	-19.22	39.5	11.77	14.5	3.18	-12.50	6.71	-8.21	17.08	22.44	5.36	15.03	0.707326	0.0017				
28	KG-027	0106	human	-19.32	42.7	10.50	15.8	3.15	-13.37	5.95	-8.81	15.41	21.82	6.41	14.44	0.707351	0.0032				
29	KG-031/050	0120	human	-19.65	42.8	9.84	15.7	3.18	-14.52	5.13	-9.75	14.45	20.86	6.41	12.74	0.707468	0.0019	0.707636	0.0026		
34	KG-048	0197	human	-19.39	40.8	10.73	15.0	3.18	-14.89	4.50	-9.91	15.17	20.70	5.52	13.85	0.707343	0.0017	0.707269	0.0016		
35	KG-047/098	0217/0467	human															0.707490	0.0014		
37	KG-052	0205	human	-19.22	39.8	10.40	14.8	3.15	-13.65	5.57	-10.44	14.97	20.15	5.18	14.56	0.707343	0.0023	0.707319	0.0019		
38	KG-073	0508	human	-19.95	41.7	10.73	15.3	3.18	-13.77	6.18	-9.53	15.76	21.09	5.33	10.82	0.707296	0.0022	0.707256	0.0019		
39	KG-077	0517	human	-19.39	43.2	10.19	15.8	3.18	-13.23	6.16	-9.05	15.46	21.58	6.13	16.08	0.707350	0.0017	0.707380	0.0017		
	KG-023	0421	sheep/goat	-19.78	41.2	9.98	15.1	3.18													
	KG-023	0554	dog/fox puppy													0.707279	0.0014				
	KG-032	0553	sheep/goat	-20.32	43.4	9.55	15.7	3.24													
	KG-057	0552	sheep	-19.55	44.0	9.58	16.0	3.21													
	KG-074	0551	sheep/goat	-18.49	41.3	10.16	15.2	3.16													
	KG-094	0451a	piglet													0.707324	0.0027				
	KG-094	0451b	mouse															0.707298	0.0016		
	KG-094	0451c	sheep/goat	-20.84	42.2	6.12	15.5	3.17													
		straw	straw (modern)																	0.707433	0.0019
		soil T5-7	soil																	0.707372	0.0019
		soil KS17-14	soil																	0.706988	0.0021
		water	well water																	0.706620	0.0021

Table 25. Results of isotope analyses of collagen and apatite for humans, animals and environmental samples from Karacamirli

can be installed (install.packages(»/Users/.../sisus_3.9-14.tar.gz«); Erhardt 2014; Erhardt et al. 2014).

A Gaussian Mixture Model (GMM) clustering approach was chosen for cluster analysis using the »R« package »mclust« (version 5.4.1; Scrucca et al. 2016). For more details see ch. V.2.4.

VI.3 Results

The results of all isotope analyses of the samples from Karacamirli are given in Table 25. Quality criteria (see ch. VI.2.2) were met by all samples. The overall variation within the different isotopic systems is rather low (see Table 26). This might indicate that several individuals under study were local and only some of the examined individuals were primarily non-local to the site. Four individuals exhibit minimum and/or maximum values in several isotopic systems: Burial 5 (KG-038-0146; $\delta^{15}N_{collagen}$, $^{87}Sr/^{86}Sr_{bone}$, $\Delta\delta^{13}C_{carbonate\text{-}collagen}$, $\Delta\delta^{18}O_{carbonate\text{-}phosphate}$), Burial 27 (KG-097-0455; $\delta^{13}C_{carbonate}$, $\delta_{18}O_{carbonate}$, $\delta^{18}O_{phosphate}$), Burial 29 (KG-031-0120; $\delta^{15}N_{collagen}$, $\delta^{18}O_{phosphate}$, $^{87}Sr/^{86}Sr_{bone}$, $^{87}Sr/^{86}Sr_{enamel}$), and Burial 34 (KG-048-0197; $\delta^{13}C_{carbonate}$, $\Delta\delta^{13}C_{carbonate\text{-}collagen}$) (see Table 25 and Table 26). The respective individuals were thus potentially not local to Karacamirli, which will be discussed in more detail in the following analysis (see ch. VI.3.1 and ch. VI.3.2).

	minimum	μ ± sd	maximum
$\delta^{13}C_{collagen}$	-20.0	-19.4 ± 0.3	-19.0
$\delta^{15}N_{collagen}$	9.8	10.8 ± 0.8	12.2
$\delta^{13}C_{carbonate}$	-14.9	-13.4 ± 0.7	-12.5
$\delta^{18}O_{carbonate}$	-10.4	-9.3 ± 0.7	-8.2
$\delta^{18}O_{phosphate}$	14.5	15.6 ± 0.7	17.1
$^{87}Sr/^{86}Sr_{bone}$	0.707256	0.707348 ± 0.000056	0.707468
$^{87}Sr/^{86}Sr_{enamel}$	0.707193	0.707344 ± 0.000126	0.707636
$\Delta\delta^{13}C_{carbonate\text{-}collagen}$	4.5	6.0 ± 0.7	6.7
$\Delta\delta^{18}O_{carbonate\text{-}phosphate}$	5.1	5.8 ± 0.6	6.9

Table 26. Overview of minimum, mean (μ), standard deviation (sd), and maximum isotope value of the analysed isotopic systems for the humans from Karacamirli (see Table 25)

VI.3.1 Diet reconstruction

Fig. 286 shows the $\delta^{13}C_{collagen}$ and $\delta^{15}N_{collagen}$ values of twelve human individuals from Karacamirli (see Table 25). $\delta^{13}C_{collagen}$ values of about -19 to -20 ‰ are indicative

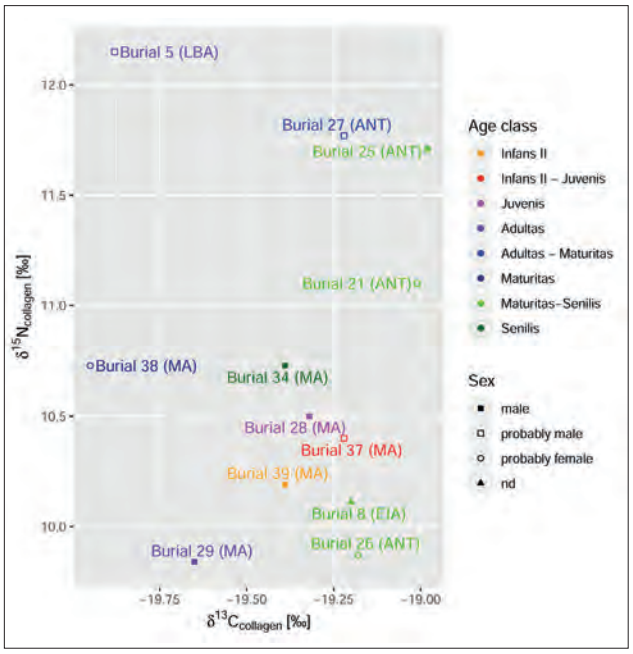

Fig. 286. $\delta^{13}C_{collagen}$ and $\delta^{15}N_{collagen}$ values of twelve individuals from Karacamirli differentiated by age, sex, and ^{14}C dating (LBA = Late Bronze Age, ANT = Antiquity, MA = Middle Ages)

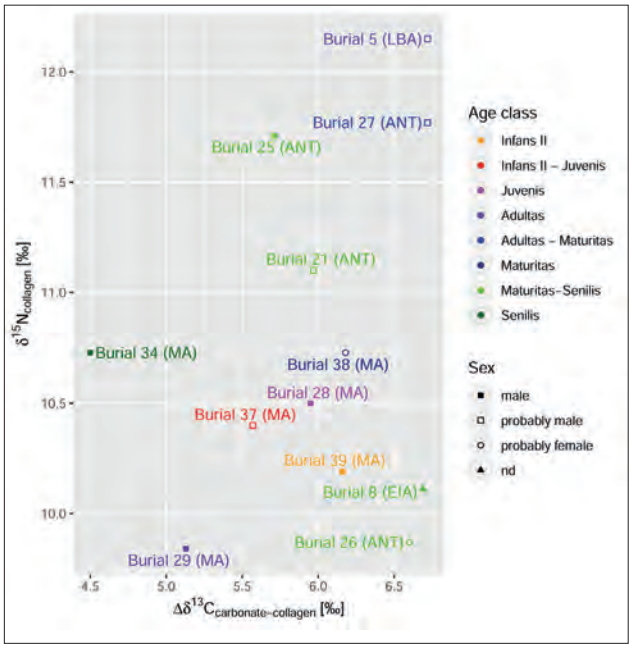

Fig. 287. $\Delta\delta^{13}C_{carbonate\text{-}collagen}$ and $\delta^{15}N_{collagen}$ values of twelve individuals from Karacamirli differentiated by age and sex, and ^{14}C dating (LBA = Late Bronze Age, ANT = Antiquity, MA = Middle Ages)

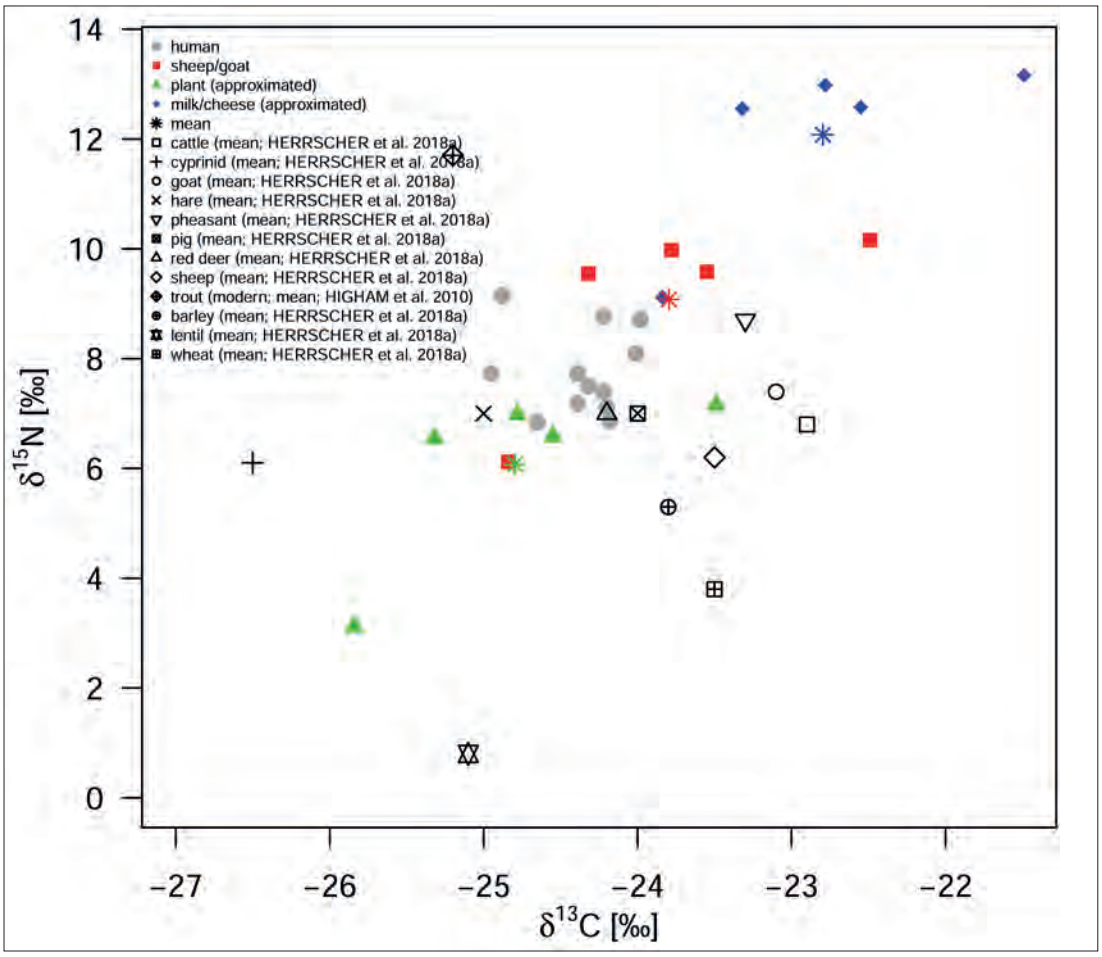

Fig. 288. Diet-adjusted $\delta^{13}C$ and $\delta^{15}N$ (see Table 27 and Table 28) of possible food sources and humans from Karacamirli including source data from Herrscher et al. (2018a) and Higham et al. (2010). For details see Table 28

of a diet which was mainly based on terrestrial or freshwater food sources. The same holds for the range of the $\delta^{15}N_{collagen}$ values (Bonsall et al. 2000; Johansen et al. 1986; Richards et al. 2006). A C_4 plant signal (see ch. VI.1) cannot be observed.

Three individuals are more enriched in ^{15}N compared to the remaining individuals with $\delta^{15}N_{collagen}$ values between 11.7 ‰ and 12.2 ‰, namely Burial 5 (KG-038-0146; probably ♂, 20–30 years; LBA/EIA), Burial 25 (KG-053-0208; ♂, 40–70 years; ANT), and Burial 27 (KG-097-0455; rather ♂, 25–50 years; ANT). This could be explained by a diet with a higher protein content, e. g. meat of terrestrial animals or freshwater food sources, i. e. fish and aquatic birds (Bonsall et al. 2000; Hobson et al. 1999). The individual in Burial 38 (KG-073-0508; probably ♀, 40–59 years; MA) shows a rather negative $\delta^{13}C_{collagen}$ value of -20.0 ‰ (see Fig. 286, Table 25) indicative of a diet based, for example, on meat of terrestrial herbivores or freshwater fish (Bonsall et al. 2000).

While $\delta^{15}N_{collagen}$ values in both the Late Bronze Age and Late Antiquity were quite variable, individuals dated to the Medieval period were relatively depleted in ^{15}N (Fig. 286) indicative of a comparably low dietary protein content or a rather terrestrial based diet instead of freshwater food sources (Bonsall et al. 2000).

Fig. 287 indicates the fat ($\Delta\delta^{13}C_{carbonate\text{-}collagen}$) and protein ($\delta^{15}N_{collagen}$) content of the diet consumed by the examined individuals from Karacamirli (see Table 25). Accordingly, the individuals in Burial 5 (KG-038-0146; probably ♂, 20–30 years; LBA/EIA), Burial 25 (KG-053-0208; ♂, 40–70 years; ANT), and Burial 27 (KG-097-0455; probably ♂, 25–50 years; ANT), who exhibit both high $\Delta\delta^{13}C_{carbonate\text{-}collagen}$ and $\delta^{15}N_{collagen}$ values (see Fig. 287 and Table 25), consumed a high-protein but low-fat diet. Moreover, three individuals (Burial 8; KG-057-0247; nd, 40–70 years; LBA/EIA), Burial 26 (KG-066-0392; probably ♀, 54–74 years; ANT), Burial 39 (KG-077-0517; ♂, 9–12 years; MA)) show high $\Delta\delta^{13}C_{carbonate\text{-}collagen}$ values combined with low $\delta^{15}N_{collagen}$ values, which can be explained by a low-protein and

burial	context	number	$\delta^{13}C_{collagen}$	$\delta^{13}C_{diet}$	$\delta^{15}N_{collagen}$	$\delta^{15}N_{diet}$
5	KG-038	0146	-19.88	-24.88	12.15	9.15
8	KG-057	0247	-19.20	-24.20	10.11	7.11
21	KG-074	0507	-19.01	-24.01	11.10	8.10
25	KG-053	0208	-18.98	-23.98	11.71	8.71
26	KG-066	0392	-19.18	-24.18	9.87	6.87
27	KG-097	0455	-19.22	-24.22	11.77	8.77
28	KG-027	0106	-19.32	-24.32	10.50	7.50
29	KG-031/050	0120	-19.65	-24.65	9.84	6.84
34	KG-048	0197	-19.39	-24.39	10.73	7.73
37	KG-052	0205	-19.22	-24.22	10.40	7.40
38	KG-073	0508	-19.95	-24.95	10.73	7.73
39	KG-077	0517	-19.39	-24.39	10.19	7.19

Table 27. Diet-adjusted $\delta^{13}C$ and $\delta^{15}N$ values (see Eqs. 2 and 3) for the human consumers from Karacamirli

food source	$\delta^{13}C_{food}$ μ	$\delta^{13}C_{food}$ sd	$\delta^{15}N_{food}$ μ	$\delta^{15}N_{food}$ sd	%C	%N
domesticated mammals	-23.4	0.7	7.3	1.4	52.8	12.0
wild mammals	-24.6	0.6	7.0	0.0	50.2	13.1
cyprinids	-26.5	0.2	6.1	0.1	54.3	12.0
trout (modern)	-25.2	0.0	11.7	0.0	52.7	11.6
pheasant	-23.3	0.0	8.7	0.0	54.2	11.3
milk/cheese	-22.3	0.7	10.3	1.5	6.5	0.5
barley/wheat	-23.7	1.3	4.6	1.6	44.6	1.9
lentil	-25.1	1.4	0.8	0.6	44.5	3.7

Table 28. Isotope values (mean μ, standard deviation sd) of the food sources (input data) from Karacamirli, Herrscher et al. (2018a), and Higham et al. (2010) were used for the calculation of the concentrated-weighted mixing model. Domesticated mammals include data of cattle, goat, sheep, and pig. Wild mammals include data of hare and red deer. Carbon (%C) and nitrogen (%N) concentrations of meat, fish, and plant sources were calculated according to Eqs. 10–13. Carbon and nitrogen concentrations of milk/cheese were chosen after Hagl et al. (2013). The modern trout sample (Higham et al. 2010) was corrected against the fossil fuel effect (+ 1.5 ‰; Freyer 1986)

low-fat diet (see Fig. 287 and Table 25). The individual in Burial 34 (KG-048-0197; ♂, > 60 years; MA) exhibits a quite low $\Delta\delta^{13}C_{carbonate\text{-}collagen}$ value of 4.5 ‰ (see Fig. AG2 and Table 25). Thus, this individual consumed a high-fat diet. Finally, the individual of Burial 29 (KG-031-0120; ♂, 20–25 years; MA) exhibits low $\Delta\delta^{13}C_{carbonate\text{-}collagen}$ and $\delta^{15}N_{collagen}$ values indicative of a diet with low protein but high fat content (Fig. 287 and Table 25).

Accordingly, the majority of the examined individuals consumed a rather low-fat diet. This also includes the two investigated probably female individuals in Burial 26 (KG-066-0392) and Burial 38 (KG-073-0508). The protein content was also rather low in most of the individuals with only three exceptions in Burial 5 (KG-038-0146), Burial 25 (KG-053-0208), and Burial 27 (KG-097-0455). These three individuals were adult to senile males. Another senile male individual in Burial 34 (KG-048-0197) exhibited a rather high-fat diet, while the protein content was similar to the overall average of the examined group. The two children under study, namely in Burial 37 (KG-052-0205; probably ♂, 10–13 years; MA) and in Burial 39 (KG-077-0517; ♂, 9–12 years; MA),

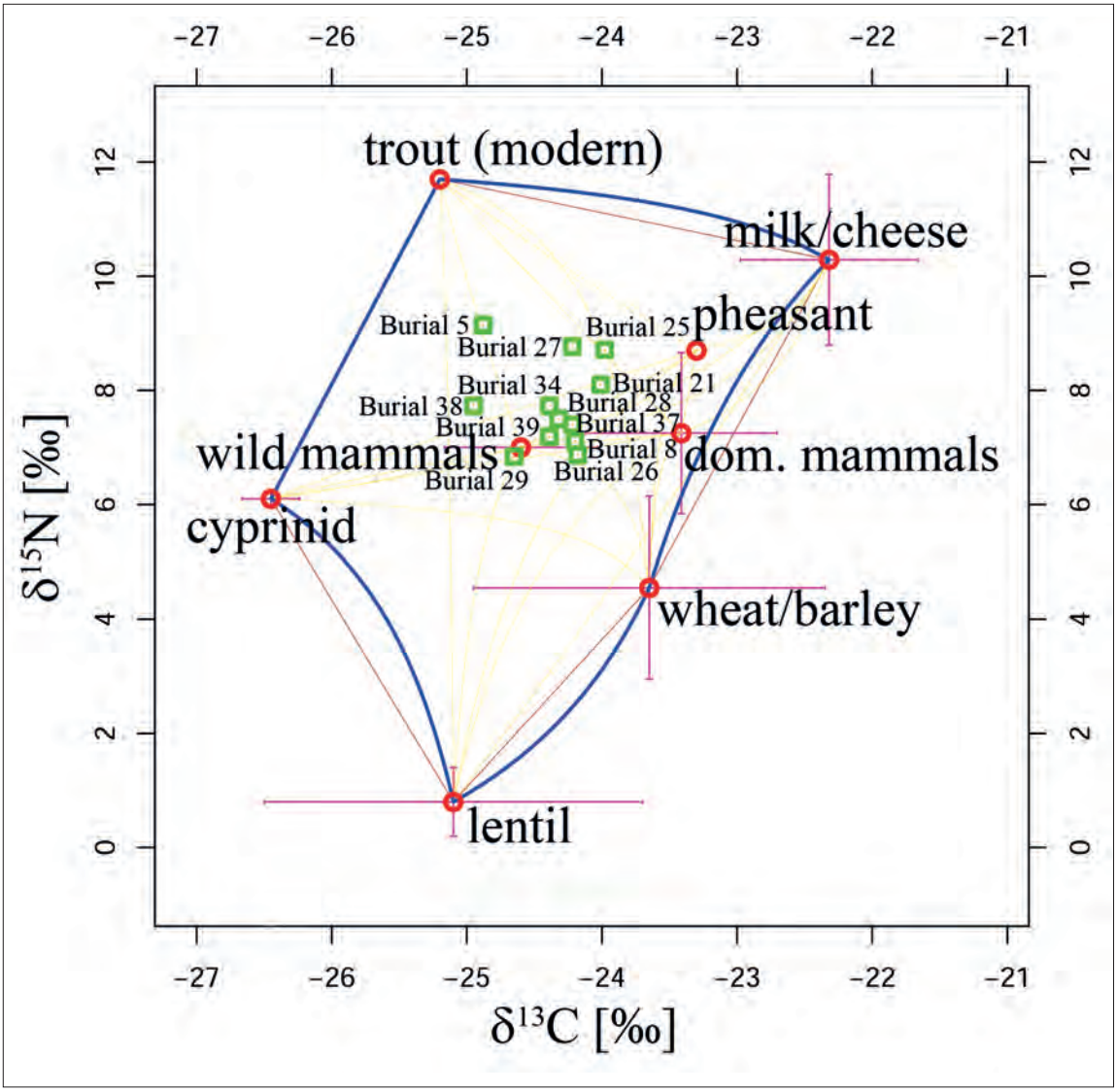

Fig. 289. Concentration-weighted mixing model for the humans (green squares) from Karacamirli calculated with SISUS (Erhardt et al. 2014) using eight different food sources (red circles). For details see Table 27–Table 29

exhibited rather low $\delta^{15}N_{collagen}$ values but rather high $\Delta\delta^{13}C_{carbonate\text{-}collagen}$ values (see Fig. 287 and Table 25) both indicating a low-protein and low-fat diet. However, they still plot within the mean isotopic range for both $\delta^{15}N_{collagen}$ (10.8 ‰ ± 0.8 ‰) and $\Delta\delta^{13}C_{carbonate\text{-}collagen}$ (6.0 ‰ ± 0.7 ‰; see Table 25).

While individuals dated to the Middle Ages are quite variable with respect to their $\Delta\delta^{13}C_{carbonate\text{-}collagen}$ values, individuals of both Late Bronze Age/Early Iron Age and Late Antiquity show a diet with rather low fat content (see Fig. 287). However, it has to be emphasized that more medieval individuals than individuals from both Late Bronze Age/Early Iron Age and Late Antiquity were analysed. Thus, the higher variability in the Medieval period relative to older individuals may be a bias of unequal sample sizes.

$\delta^{13}C_{collagen}$ and $\delta^{15}N_{collagen}$ values of human and animal samples are adjusted to dietary $\delta^{13}C$ and $\delta^{15}N$ values, respectively, according to Eqs. 2–9 (see Table 27 and Table 28). Fig. 288 illustrates possible (calculated) food sources for the individuals from Karacamirli. Accordingly, for the reconstruction of the palaeodiet, eight different food sources were chosen, namely domesticated mammals, wild mammals, fish (cyprinids, trouts), birds (pheasants), milk/cheese, barley/wheat, and lentil (see Table 28). Modern trout data was additionally corrected for the fossil fuel effect (Freyer 1986). Carbon and nitrogen concentrations were calculated based on the content of proteins, fats, and carbohydrates in modern food sources (see Eqs. 10–13). Carbon and nitrogen concentrations in milk/cheese were chosen after Hagl et al. (2013) (Table 28).

burial	context	number	dom. mammals			wild mammals			cyprinids			trout			pheasant			milk/cheese			barley/wheat			lentil		
			min	mean	max	min	mean	max	min	mean	max	min	mean	max	min	mean	max	min	mean	max	min	mean	max	min	mean	max
5	KG-038	0146	0	0.05	0.32	0	0.09	0.50	0	0.11	0.26	0.13	0.39	0.49	0	0.06	0.34	0	0.13	0.75	0	0.07	0.43	0	0.10	0.41
8	KG-057	0247	0	0.17	0.73	0	0.14	0.68	0	0.07	0.26	0	0.04	0.15	0	0.11	0.51	0	0.17	0.90	0	0.18	0.79	0	0.13	0.50
21	KG-074	0507	0	0.15	0.72	0	0.08	0.46	0	0.04	0.22	0	0.11	0.23	0	0.23	0.76	0	0.19	0.92	0	0.15	0.82	0	0.06	0.32
25	KG-053	0208	0	0.11	0.64	0	0.05	0.27	0	0.02	0.14	0.03	0.17	0.32	0	0.27	0.73	0	0.22	0.91	0	0.13	0.81	0	0.04	0.21
26	KG-066	0392	0	0.16	0.72	0	0.12	0.57	0	0.06	0.23	0	0.03	0.14	0	0.09	0.48	0	0.17	0.89	0	0.21	0.80	0	0.16	0.52
27	KG-097	0455	0	0.12	0.59	0	0.07	0.35	0	0.04	0.18	0.05	0.23	0.37	0	0.17	0.63	0	0.19	0.88	0	0.14	0.72	0	0.05	0.27
28	KG-027	0106	0	0.13	0.66	0	0.15	0.75	0	0.09	0.31	0	0.08	0.20	0	0.14	0.57	0	0.16	0.89	0	0.14	0.73	0	0.11	0.48
29	KG-031/050	0120	0	0.11	0.59	0	0.16	0.91	0	0.16	0.40	0	0.05	0.21	0	0.08	0.41	0	0.15	0.86	0	0.12	0.64	0	0.18	0.62
34	KG-048	0197	0	0.12	0.61	0	0.14	0.71	0	0.09	0.34	0	0.12	0.24	0	0.13	0.62	0	0.16	0.88	0	0.13	0.70	0	0.10	0.47
37	KG-052	0205	0	0.15	0.70	0	0.14	0.72	0	0.08	0.27	0	0.06	0.18	0	0.14	0.56	0	0.17	0.91	0	0.16	0.77	0	0.11	0.47
38	KG-073	0508	0	0.07	0.41	0	0.11	0.69	0	0.22	0.48	0.05	0.18	0.33	0	0.08	0.44	0	0.13	0.79	0	0.08	0.49	0	0.12	0.60
39	KG-077	0517	0	0,13	0,66	0	0,17	0,84	0	0,10	0,32	0	0,06	0,18	0	0,11	0,50	0	0,16	0,89	0	0,14	0,72	0	0,13	0,53

Table 29. Source contributions (minimum, mean, maximum) for the individuals from Karacamirli calculated with SISUS (Erhardt et al., 2014) using eight food sources (see Table 27 and Table 28)

The concentration-weighted mixing model calculated with SISUS is shown in Fig. 289. The calculated mixing model (see Fig. 289 and Table 29) is the optimal model with the available end members. Diet reconstruction with the eight food sources mentioned above (see also Table 28) is possible for all examined individuals (Fig. 289 and Table 29). It must be emphasized that the calculated dietary proportions should not be understood as exact values although they are mathematically calculated as such. The proportions of the different dietary sources should be compared to each other instead in order to find dietary preferences.

Freshwater fish (cyprinid, trout), meat from both domesticated and wild mammals, and plants (barley/wheat, lentil) were important for the majority of the examined individuals (Table 29). For some individuals even a minimum dietary proportion of trout can be observed (Burials 5, 25, 27, 38; Table 29). Milk/cheese were of some importance for all individuals (13–22 %; Table 29). In addition, dairy products were of higher importance than the meat of domesticated mammals (Table 29), which seems plausible.

Three individuals show a distinct proportion of freshwater fish (c. 30–50 %), namely Burial 5 (KG-038-0146; probably ♂, 20–30 years; LBA), Burial 27 (KG-097-0455; probably ♂, 25–50 years; ANT), and Burial 38 (KG-073-0508; probably ♀, 40–59 years; MA). The individuals in Burials 5 and 27 are relatively enriched in ^{15}N (see Fig. 286, Table 25) indicative of a protein-rich diet. The individual in Burial 38, on the other hand, is depleted in ^{13}C (see Fig. 286, Table 25) consistent with a diet based on freshwater fish.

Two individuals, Burial 21 (KG-074-0507; probably ♂, 48–75 years; ANT) and Burial 25 (KG-053-0208; ♂, 40–70 years; ANT), show a quite high average proportion of pheasant of 27 % and 23 %, respectively (Table 29). Additionally, the individual in Burial 25 consumed much dairy products (22 %; Table 29). Both individuals were enriched with ^{13}C and ^{15}N in the bone collagen. The individual in Burial 25 also exhibited a high $\Delta\delta^{13}C_{carbonate\text{-}collagen}$ value. Consequently, a diet low in fat but high in protein is expected. Actually, the high dietary proportion of pheasant and milk/cheese of this individual is in good agreement with this expectation.

In the case of the individuals of Burial 8 (KG-057-0247; nd, 40–70 years; EIA), Burial 26 (KG-066-0392; probably ♀, 54–74 years; ANT), Burial 29 (KG-031-0120; ♂, 20–25 years; MA), and Burial 37 (KG-052-0205; probably ♂, 10–13 years; MA), plant protein is especially important amounting to about one third of the diet (31 %, 37 %, 30 %, and 27 %, respectively; see Table 29). This is in accordance with the depletion in ^{15}N in all three individuals as well as the high $\Delta\delta^{13}C_{carbonate\text{-}collagen}$ values of the individual in Burial 8 and Burial 26 (Fig. 286 and Fig. 287). However, the $\Delta\delta^{13}C_{carbonate\text{-}collagen}$ value of the individual of Burial 29 (5.1 ‰) implies a high-fat diet (see above; Fig. 287), which contradicts the calculated mixing model (Table 29). A non-local origin is possible, but that requires a closer look at other isotopic systems (see ch. VI.3.2).

The individual in Burial 34 (KG-048-0197; ♂, > 60 years; MA) showed a low $\Delta\delta^{13}C_{carbonate\text{-}collagen}$ value and therefore might have fed on a high-fat diet (see above; Fig. 287). However, this also does not fit the calculated dietary proportions, which are relatively balanced with respect to all examined food sources. The overall isotopic fingerprint must be evaluated in order to decide if a non-local origin might have caused the isotopic signature of the individual in Burial 34 (see ch. VI.3.2).

Altogether, the diet of the individuals from Karacamirli was mainly based on freshwater fish, plants, and meat of domesticated and wild mammals. The meat of wild birds (here: pheasant) was of minor importance. Milk and cheese, however, were more important than the meat of domesticated mammals for all individuals.

With respect to the different time periods, no overall differences in the mixing models were observed. There is a tendency of individuals of the Late Antiquity (n = 3) to show only a minor proportion of lentils in the diet (4–6 %; Table 29). However, this is not the case for the Late Antique individual in Burial 26, who consumed 16 % of lentils on average (Table 29). The rather low number of individuals does not allow a more detailed look at time-specific differences. Furthermore, pheasant seems to be important only for three Late Antique individuals (Burials 21, 25, 27). Pheasants were indigenous in the Caucasus region. The only other Late Antique individual in the sample, Burial 26, was a mature to senile female that showed a low proportion of pheasant in her diet (see Table 29). Thus, a social factor might play a role here.

VI.3.2 Assessment of the places of origin

The individual in Burial 27 (KG-097-0455; probably ♂, 25–50 years; ANT) was enriched in ^{18}O in both carbonate ($\delta^{18}O_{carbonate}$ = -8.2 ‰) and phosphate ($\delta^{18}O_{phosphate}$ = 17.1 ‰) compared to the majority of other individuals (Fig. 290). This indicates a different source of both food ($\delta^{18}O_{carbonate}$) and drinking water ($\delta^{18}O_{phosphate}$) (see Kirsanow/Tuross 2011). Accordingly, it is probable that the individual in Burial 27 was primarily not local to the site. Furthermore, compared to the majority of individuals from Karacamirli two individuals, Burial 29 (KG-031-0120, ♂, 20–25 years; MA) and Burial 5 (KG-038-0146; probably ♂, 20–30

years; LBA), were relatively depleted in $^{18}O_{phosphate}$ (see Fig. 290) with a $\delta^{18}O_{phosphate}$ value of 14.5 ‰ and 14.6 ‰, respectively. Again, this is indicative of a different source of

$$\delta^{18}O_{phosphate} = 0.6758 * \delta^{18}O_{carbonate} + 1.1180 \quad \text{(Eq. 16)}$$

drinking water, what might indicate a non-local origin of both individuals.

Due to the limited number of isotope measurements, regression analysis between $\delta^{18}O_{carbonate}$ and $\delta^{18}O_{phosphate}$ as

$$\delta^{18}O_{phosphate} = 0.98 * \delta^{18}O_{carbonate} - 8.5 \quad \text{(Eq. 17)}$$

shown in Eq. 16 can only be understood as a tendency:

Neither the regression model (Eq. 16) nor the calculated $\Delta\delta^{18}O_{carbonate\text{-}phosphate}$ values (5.8 ‰ ± 0.6 ‰; see Table 25) fit to the commonly accepted regression model after Iacumin et al. (1996) with

and the fixed $\Delta\delta^{18}O_{carbonate\text{-}phosphate}$ value of about 9 ‰ (e. g. Chenery et al. 2012; Iacumin et al. 1996; Pellegrini et al. 2011). This is not surprising as a variety of factors (e. g. physiology, diet, habitat, and climate) render it impossible to establish a general regression model or an overall $\Delta\delta^{18}O_{carbonate\text{-}phosphate}$ value (Göhring et al. 2019a).

Individuals of different time periods can be separated with respect to both their $\delta^{18}O_{carbonate}$ and $\delta^{18}O_{phosphate}$ values (see Fig. 290). The correlation between the two oxygen isotopic systems seems to vary dependent on the dating. However, the number of individuals is too small to verify this statistically. Variability in medieval individuals is again quite high (see Fig. 290) as is the case for other isotopic systems (see ch. VI.3.1).

Animal $^{87}Sr/^{86}Sr$ isotope values can be used for the estimation of the local range. The strontium isotope ratios of three animals, a dog/fox puppy (KG-023-0554), a piglet (KG-094-0451a), and a mouse (KG-094-0451b) were measured. All three bones were remains of animal burrowing and not part of the burials. These individuals showed a $^{87}Sr/^{86}Sr$ range between 0.707279 and 0.707324 (see Table 25). The local strontium isotope range (see Eq. 14) for Karacamirli was approximated as 0.707255 – 0.707346. The modern straw sample shows a $^{87}Sr/^{86}Sr$ value of 0.707433. Accordingly, a $^{87}Sr/^{86}Sr$ of 0.707255 up to 0.707433 should characterize the local bioavailable ratios. Soil sample T5-7 (0.707372) also fits into this local range (Fig. 291). However, soil sample KS17-14 (0.706988) is markedly lower (Fig. 291). This sample originates from the sediment of the Eastern River which is located about 1 km east of Tepe 5 (see ch. VII). As demonstrated by Garçon et al. (2014) strontium isotope ratios of river sediments can

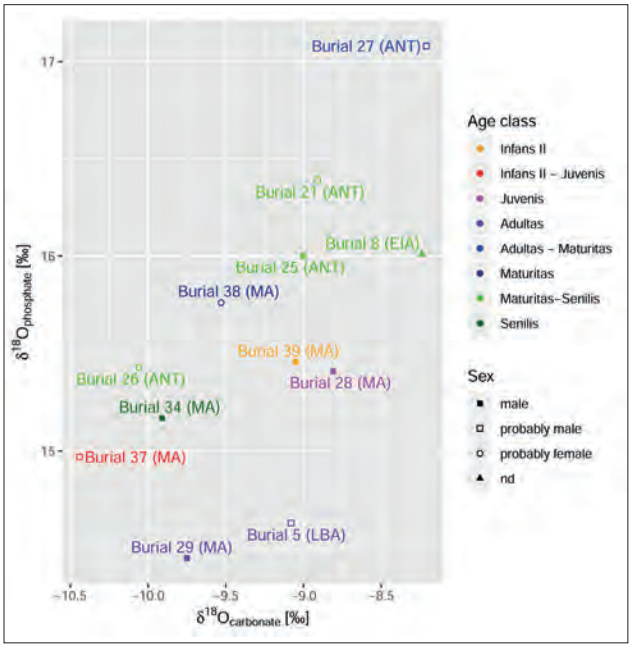

Fig. 290. $\delta^{18}O_{carbonate}$ and $\delta^{18}O_{phosphate}$ values of twelve individuals from Karacamirli differentiated by age, sex, and ^{14}C dating (LBA = Late Bronze Age, ANT = Antiquity, MA = Middle Ages)

be strongly biased by mineral sorting processes during the fluvial transport. Thus, the $^{87}Sr/^{86}Sr$ ratio measured for KS17-14 cannot be seen as a reliable proxy for provenance analysis. The well water sample (0.706620) gives a markedly less radiogenic value than all other samples of the site (Fig. 291). However, the strontium concentration in rainwater is generally rather low (see e. g. Lengfelder et al. 2019). As a consequence, no major influence of the (meteoric) drinking water is expected anyway. Nevertheless, a different water source than the sampled well water is also possible here.

Two individuals show a distinct difference of about 0.0001 to 0.0002 between the $^{87}Sr/^{86}Sr$ value of enamel and that of bone: This holds for the individuals in Burial 29 (KG-031-0120; ♂, 20–25 years; MA) and Burial 34 (KG-048-0197; ♂, > 60 years; MA) (see Fig. 291). The strontium isotope ratio of enamel reflects the signal during early childhood, while the $^{87}Sr/^{86}Sr$ value of bone integrates over the last about 20 years before death (Martin et al. 2015). Consequently, a shift between enamel and bone strontium isotope ratio can be interpreted by a migratory event during life time (see ch. VI.1). However, even a dietary shift could explain the difference between enamel and bone sample (see e. g. Burton/Price 2013).

The individual in Burial 29 (KG-031-0120) shows quite high strontium isotope values in both enamel and bone sample. This individual was probably primarily non-local to the site but came from a region with higher $^{87}Sr/^{86}Sr$ values. However, the bone sample indicates a mixed sig-

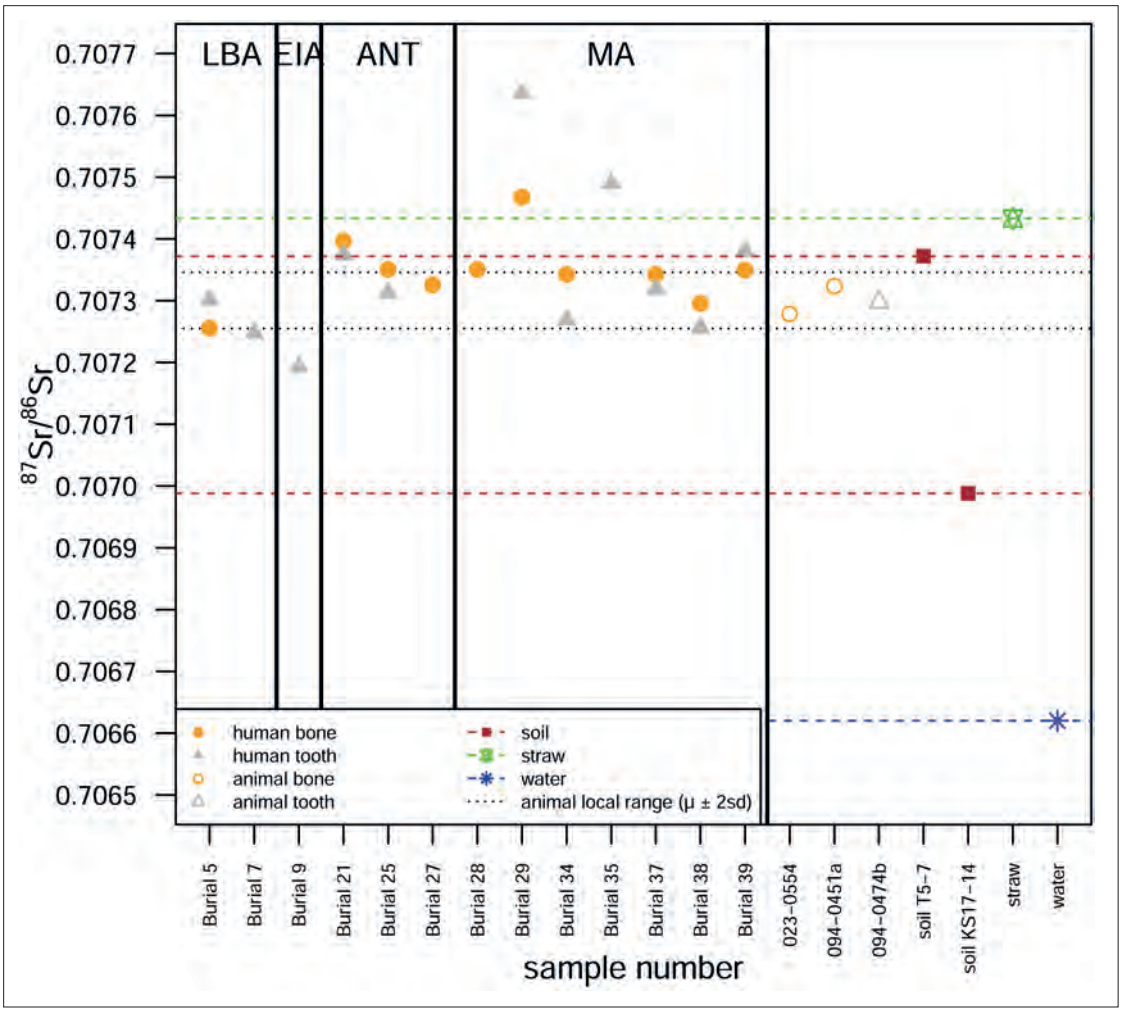

Fig. 291. $^{87}Sr/^{86}Sr$ values of human bones and teeth (enamel), animal bones and teeth (enamel), as well as modern environmental samples from Karacamirli. Human samples are sorted according to ^{14}C/archaeological dating (LBA = Late Bronze Age, ANT = Antiquity, MA = Middle Ages)

nal between the enamel sample and the local strontium isotope signal. Due to the quite young age of this individual (20–25 years), the bone sample still contains a certain childhood signal.

The individual in Burial 34 shows local strontium isotope values in both enamel and bone samples, however, the difference between tooth (0.707269) and bone (0.707343) indicates the non-local origin of the individual's mother, who probably originated from an area of lower $^{87}Sr/^{86}Sr$ ratios and migrated to Karacamirli before giving birth to the individual in Burial 34. The latter thus shows a mixed signal in the enamel sample (Fig. 291).

The individual in Burial 35 (KG-047-0217/KG-098-0467) exhibits a high strontium isotope value in the enamel sample (0.707490). Thus, the individual was probably primarily non-local to Karacamirli but originated from an area with higher local isotope values. The $^{87}Sr/^{86}Sr$ ratio of bone is not available here.

The enamel value of the individual in Burial 7 matches the lowest local ratio (0.707248). Similar to Burial 34, it is likely that the mother of the respective individual was primarily not local to the site but originated from a site with lower local $^{87}Sr/^{86}Sr$ values (Fig. 291). She would have migrated to Karacamirli and transferred a mixed signal to her child, observable in the enamel value. However, the $^{87}Sr/^{86}Sr_{bone}$ ratio of the individual is not available here.

Only teeth of the individual in Burial 9 (KG-043-0204; nd, nd) were preserved, so only the strontium isotope signal of the teeth could be measured. According to the enamel strontium isotope signal (0.707193), the individual can be classified as primarily non-local. The individual originated from a region with lower $^{87}Sr/^{86}Sr$ values.

The individuals in Burial 21 (KG-074-0507; probably ♂, 48–75 years; ANT) and in Burial 39 (KG-077-0517; ♂, 9–12 years; MA) exhibit rather high strontium isotope values. However, they still fit into the expected local range when

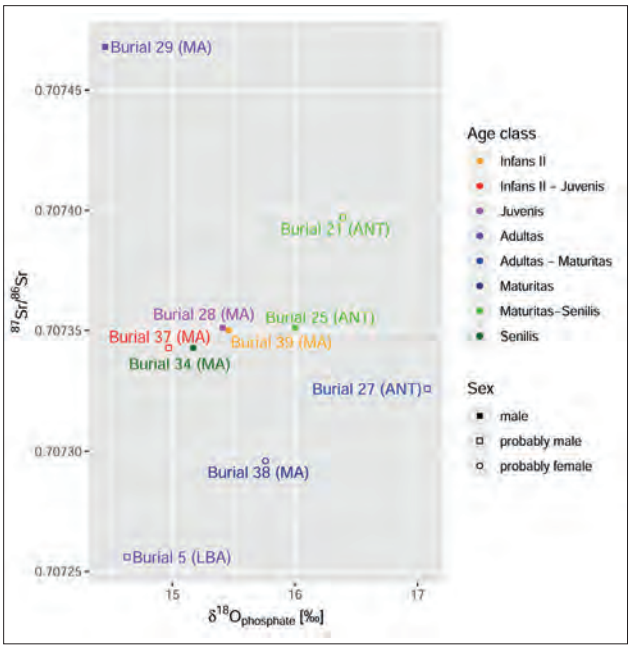

Fig. 292. $\delta^{18}O_{phosphate}$ and $^{87}Sr/^{86}Sr$ values of ten individuals from Karacamirli differentiated by age, sex, and ^{14}C dating (LBA = Late Bronze Age, ANT = Antiquity, MA = Middle Ages)

considering the modern straw sample. Furthermore, the difference between enamel and bone is below 0.0003, which is the normal variation in local humans (Burton/Hahn 2016).

Probably non-local individuals can be observed within the time period of both Late Antiquity and the Medieval period (Fig. 291). The individual in Burial 9 could not be ^{14}C-dated, however was archaeologically dated to Late Bronze Age/Early Iron Age.

A parallel view on both $\delta^{18}O_{phosphate}$ and $^{87}Sr/^{86}Sr$ values of bone samples is illustrated in Fig. 292. Three individuals should be mentioned here, namely the individuals in Burial 29 (KG-031-0120; ♂, 20–25 years; MA), Burial 5 (KG-038-0146; probably ♂, 20–30 years; LBA), and Burial 27 (KG-097-0455; probably ♂, 25–50 years; ANT). The individual of Burial 29 exhibits a rather high strontium isotope value of 0.707468 (Table 25). As already mentioned before, this individual is probably primarily not local to the site. Due to the young age of the individual the strontium isotope ratio in the bone should still reflect a mixture of the expected local value and the strontium isotope value during childhood (see enamel value). Likewise, even the $\delta^{18}O_{phosphate}$ value has to be interpreted as a mixed isotope signal of the examined site of Karacamirli and the site where the individual lived during early childhood or at least a nursing signal introduced by the mother. The bone sample of this individual is relatively depleted in ^{18}O of the phosphate fraction (14.5 ‰; Fig. 292, Table 25). This indicates an origin from a site where the meteoric drinking water is relatively depleted in ^{18}O. In combination with the non-local strontium isotope signature (see above) the conspicuous $\delta^{18}O_{phosphate}$ value is a further indicator of a primarily non-local origin of the individual in Burial 29.

The individual in Burial 5 also exhibited a rather low $\delta^{18}O_{phosphate}$ value (14.6 ‰; Fig. 292, Table 25). With respect to the strontium isotope ratios the individual is still within the local strontium isotope range (Fig. 294, Table 25). Nevertheless, the relatively low oxygen isotope value might indicate a different water source, thus a probably different origin of the respective individual.

The individual of Burial 27 is relatively enriched in ^{18}O ($\delta^{18}O_{phosphate}$ = 17.1 ‰; Fig. 292, Table 25). The $^{87}Sr/^{86}Sr_{bone}$ ratio (0.707326) is within the local range (Fig. 292, Table 25). However, the enrichment in ^{18}O can be explained by a different water source, thus a probably non-local origin of the individual.

VI.3.3 Cluster analysis

Cluster analysis was performed on the Karacamirli multi-isotope dataset with a given cluster number of two in order to identify a group of possibly non-local indi-

burial	context	individual	GMM with 5 dimensions	GMM with 6 dimensions ($^{87}Sr/^{86}Sr_{bone}$)	GMM with 6 dimensions ($^{87}Sr/^{86}Sr_{enamel}$)
5	038	0146	1	2	1
8	057	0247	2	-	-
21	074	0507	2	2	2
25	053	0208	2	2	2
26	066	0392	1	-	-
27	097	0455	2	2	-
28	027	0106	2	1	-
29	031/050	0120	1	1	1
34	048	0197	1	1	1
37	052	0205	1	1	1
38	073	0508	2	1	1
39	077	0517	2	1	1

Table 30. Results of GMM cluster analyses with five ($\delta^{13}C_{collagen}$, $\delta^{15}N_{collagen}$, $\delta^{13}C_{carbonate}$, $\delta^{18}O_{carbonate}$, $\delta^{18}O_{phosphate}$) and six isotopic dimensions ($\delta^{13}C_{collagen}$, $\delta^{15}N_{collagen}$, $\delta^{13}C_{carbonate}$, $\delta^{18}O_{carbonate}$, $\delta^{18}O_{phosphate}$, and $^{87}Sr/^{86}Sr_{bone}$ or $^{87}Sr/^{87}Sr_{enamel}$)

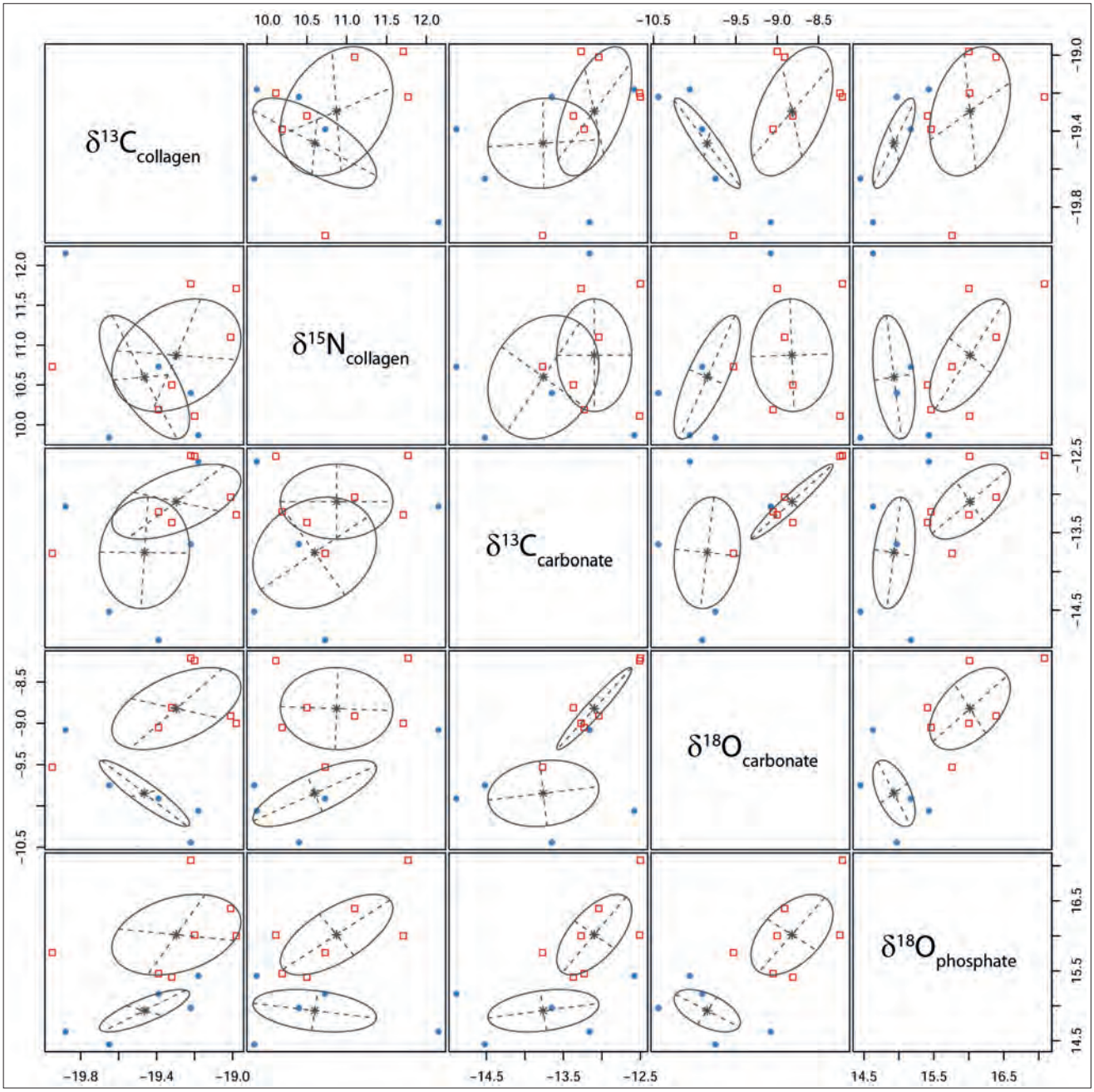

Fig. 293. Pairwise bivariate plot of the resulting two clusters (see Table 30) on the five-dimensional isotopic dataset ($\delta^{13}C_{collagen}$, $\delta^{15}N_{collagen}$, $\delta^{13}C_{carbonate}$, $\delta^{18}O_{carbonate}$, $\delta^{18}O_{phosphate}$) of the humans from Karacamirli; cluster 1: blue (dots), cluster 2: red (squares) (for the methodology see Scrucca et al. 2016)

viduals. In the case of the five-dimensional data set (excluding $^{87}Sr/^{86}Sr$), five individuals were grouped into the first cluster, while seven individuals were grouped into the second cluster (Fig. 293 and Table 30). Individuals of cluster 2 are enriched in both $^{18}O_{carbonate}$ (-8.8 ‰ ± 0.5 ‰) and $^{18}O_{phosphate}$ (16.0 ‰ ± 0.6 ‰) compared to individuals of cluster 1 with mean $\delta^{18}O_{carbonate}$ and $\delta^{18}O_{phosphate}$ values of -9.9 ‰ (± 0.4 ‰) and 14.9 ‰ (± 0.3 ‰), respectively (Fig. 290 and Table 31). As illustrated in Fig. 293 the clustering structure is mainly caused by the oxygen isotopic ratios. $\delta^{13}C_{carbonate}$ is of minor importance for cluster separation with only slightly more positive values for individuals of cluster 2 (-13.1 ‰ ± 0.5 ‰) compared to cluster 1 (-13.8 ‰ ± 0.7 ‰) (Fig. 293 and Table 31). Clusters do not differ from each other with respect to either $\delta^{13}C_{collagen}$ or $\delta^{15}N_{collagen}$ values (Fig. 293 and Table 31).

Cluster analyses using either bone or enamel $^{87}Sr/^{86}Sr$ ratios produce identical cluster labels for seven individu-

μ	cluster 1	cluster 2
$\delta^{13}C_{collagen}$	-19.46	-19.30
$\delta^{15}N_{collagen}$	10.60	10.87
$\delta^{13}C_{carbonate}$	-13.76	-13.10
$\delta^{18}O_{carbonate}$	-9.85	-8.82
$\delta^{18}O_{phosphate}$	14.93	16.02
sd	cluster 1	cluster 2
$\delta^{13}C_{collagen}$	0.24	0.34
$\delta^{15}N_{collagen}$	0.78	0.71
$\delta^{13}C_{carbonate}$	0.72	0.49
$\delta^{18}O_{carbonate}$	0.40	0.50
$\delta^{18}O_{phosphate}$	0.30	0.58

Table 31. Mean (μ) and standard deviation (sd) of the five-dimensional isotopic dataset ($\delta^{13}C_{collagen}$, $\delta^{15}N_{collagen}$, $\delta^{13}C_{carbonate}$, $\delta^{18}O_{carbonate}$, $\delta^{18}O_{phosphate}$) of the humans from Karacamirli according to GMM clustering performed with two clusters

μ	cluster 1	cluster 2
$\delta^{13}C_{collagen}$	-19.49	-19.27
$\delta^{15}N_{collagen}$	10.40	11.68
$\delta^{13}C_{carbonate}$	-13.91	-13.00
$\delta^{18}O_{carbonate}$	-9.58	-8.80
$\delta^{18}O_{phosphate}$	15.20	16.03
$^{87}Sr/^{86}Sr_{bone}$	0.707360	0.707330
sd	cluster 1	cluster 2
$\delta^{13}C_{collagen}$	0.30	0.30
$\delta^{15}N_{collagen}$	0.34	0.34
$\delta^{13}C_{carbonate}$	0.50	0.50
$\delta^{18}O_{carbonate}$	0.47	0.47
$\delta^{18}O_{phosphate}$	0.65	0.65
$^{87}Sr/^{86}Sr_{bone}$	0.000052	0.000052

Table 32. Mean (μ) and standard deviation (sd) of the six-dimensional isotopic dataset ($\delta^{13}C_{collagen}$, $\delta^{15}N_{collagen}$, $\delta^{13}C_{carbonate}$, $\delta^{18}O_{carbonate}$, $\delta^{18}O_{phosphate}$, $^{87}Sr/^{86}Sr_{bone}$) of the humans from Karacamirli according to GMM clustering performed with two clusters

μ	cluster 1	cluster 2
$\delta^{13}C_{collagen}$	-19.58	-19.00
$\delta^{15}N_{collagen}$	10.67	11.41
$\delta^{13}C_{carbonate}$	-13.87	-13.16
$\delta^{18}O_{carbonate}$	-9.63	-8.96
$\delta^{18}O_{phosphate}$	15.07	16.20
$^{87}Sr/^{86}Sr_{enamel}$	0.707360	0.707340
sd	cluster 1	cluster 2
$\delta^{13}C_{collagen}$	0.23	0.23
$\delta^{15}N_{collagen}$	0.65	0.65
$\delta^{13}C_{carbonate}$	0.55	0.55
$\delta^{18}O_{carbonate}$	0.87	0.87
$\delta^{18}O_{phosphate}$	0.40	0.40
$^{87}Sr/^{86}Sr_{enamel}$	0.000113	0.000113

Table 33. Mean (μ) and standard deviation (sd) of the six-dimensional isotopic dataset ($\delta^{13}C_{collagen}$, $\delta^{15}N_{collagen}$, $\delta^{13}C_{carbonate}$, $\delta^{18}O_{carbonate}$, $\delta^{18}O_{phosphate}$, $^{87}Sr/^{86}Sr_{enamel}$) of the humans from Karacamirli according to GMM clustering performed with two clusters

als (Burials 21, 25, 29, 34, 37, 38, 39) (Fig. 294 and Fig. 295, Table 30). The individual in Burial 5 was grouped into the second cluster using the bone $^{87}Sr/^{86}Sr$ ratio, however into the first cluster while using enamel $^{87}Sr/^{86}Sr$. For two individuals (Burials 27 and 28) only bone was available (see Table 30).

In the six-dimensional dataset using the $^{87}Sr/^{86}Sr$ ratio of bone six individuals were grouped within cluster 1, while the remaining four individuals were grouped into a second cluster (Fig. 294, Table 30). Cluster analysis using enamel strontium isotope ratios results in the separation of two individuals (Burials 21 and 25) in the second cluster (Fig. 294, Table 30). These individuals are relatively enriched in $^{13}C_{collagen}$, $^{18}O_{carbonate}$, and $^{18}O_{phosphate}$ (Fig. 294, Table 30).

In both cases the clusters are still mainly influenced by $\delta^{18}O_{carbonate}$ and $\delta^{18}O_{phosphate}$ (Fig. 294 and Fig. 295, Table 30), but even $\delta^{15}N_{collagen}$ and $\delta^{13}C_{carbonate}$ values have an impact with enriched values in cluster 2 compared to cluster 1 (Fig. 294 and Fig. 295, Table 32 and Table 33). Individuals of the second cluster are generally enriched in the heavy isotope for all isotopic systems, although the difference between the two clusters is rather small for $\delta^{13}C_{collagen}$ and $^{87}Sr/^{86}Sr$ (Fig. 294 and Fig. 295, Table 32 and Table 33). This is probably a mathematical artefact, at least in case of the strontium isotope ratios, due to the smaller absolute variance within this isotopic system compared to the isotopic systems of the light elements. Thus, the small inter-cluster difference for $^{87}Sr/^{86}Sr$ prob-

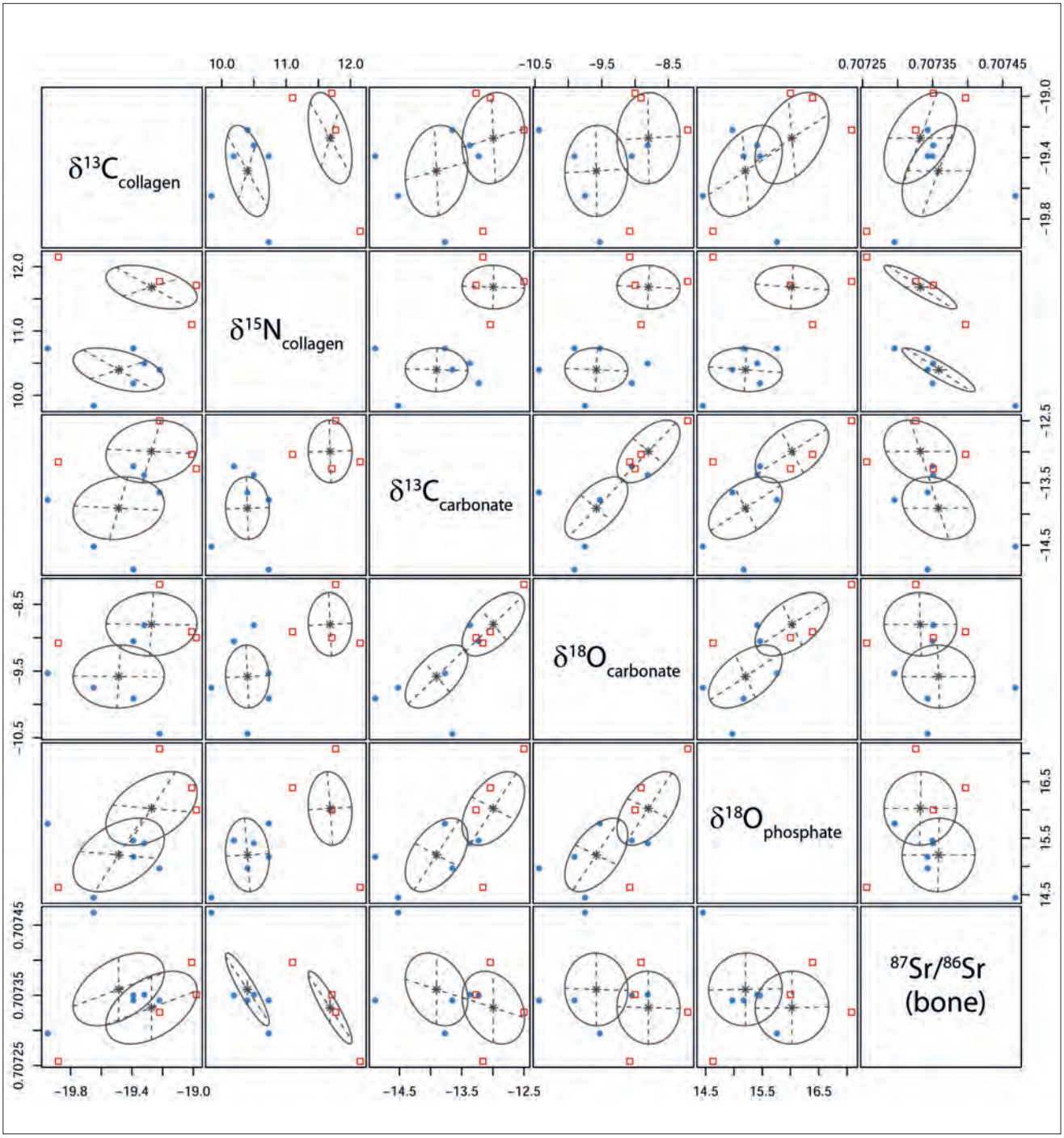

Fig. 294. Pairwise bivariate plot of the resulting two clusters (see Table 30) on the six-dimensional isotopic dataset ($\delta^{13}C_{collagen}$, $\delta^{15}N_{collagen}$, $\delta^{13}C_{carbonate}$, $\delta^{18}O_{carbonate}$, $\delta^{18}O_{phosphate}$, $^{87}Sr/^{86}Sr_{bone}$) of the humans from Karacamirli; cluster 1: blue (dots), cluster 2: red (squares) (for the methodology see Scrucca et al. 2016)

ably does not have a physiological but a mathematical cause.

With respect to chronology, in the case of the cluster analysis using bone $^{87}Sr/^{86}Sr$ ratios cluster 1 includes all Medieval individuals, while both Late Bronze Age/Early Iron Age and Late Antique individuals (n = 4) are grouped in the second cluster (Table 30). This again illustrates the isotopic difference of Medieval individuals from individuals of earlier periods (see above). When using enamel instead of bone $^{87}Sr/^{86}Sr$ ratios, the two remaining Late Antique individuals of Burial 21 and Burial 25, grouped into the second cluster, are separated from the Late Bronze Age/Early Iron Age and Medieval individuals (Table 30).

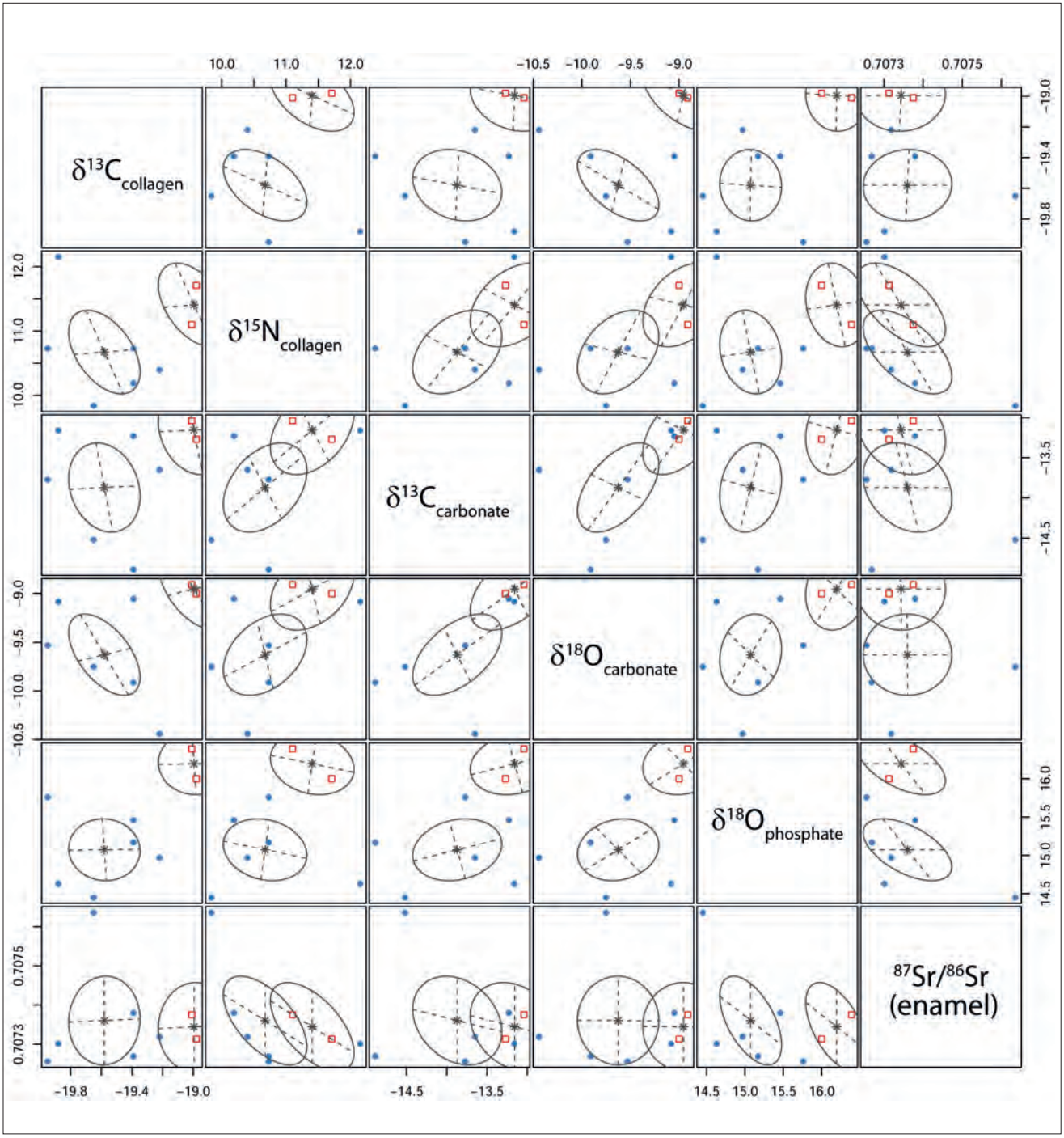

Fig. 295. Pairwise bivariate plot of the resulting two clusters (see Table 30) on the six-dimensional isotopic dataset ($\delta^{13}C_{collagen}$, $\delta^{15}N_{collagen}$, $\delta^{13}C_{carbonate}$, $\delta^{18}O_{carbonate}$, $\delta^{18}O_{phosphate}$, $^{87}Sr/^{86}Sr_{enamel}$) of the humans from Karacamirli; cluster 1: blue (dots), cluster 2: red (squares) (for the methodology see Scrucca et al. 2016)

VI.4 Discussion

Stable isotope analysis reveals insights into the diet as well as the mobility patterns of ancient humans. Diet reconstruction revealed a diet with a rather high proportion of freshwater fish (up to ~50 % on average; Table 29). In addition, meat of domesticated and wild mammals (up to ~30 % on average; see Table 29) as well as plants (barley, lentil; up to ~40 % on average; see Table 29) were a regular part of the diet. However, dairy goods (up to ~22 % on average; see Table 29) were of higher importance than meat of domesticated mammals (up to ~17 % on average; see Table 29). Pheasants were of rather minor importance for most individuals from Karacamirli (Table 29).

In the following, the different food sources will be discussed in detail sorted by their overall relevance for the diet of individuals from Karacamirli:

A fish-based diet is expected given the proximity of the Kura river. Individuals from all time periods (LBA/EIA, ANT, MA) showed some proportion of fish in their diet (see Table 29). This is especially the case for the individual of Burial 5 (KG-038-0146; ~50 % fish; probably ♂, 20–30 years, LBA), Burial 27 (KG-097-0455; ~30 % fish; probably ♂, 25–50 years, ANT), and Burial 38 (KG-073-0508; ~40 % fish; probably ♀, 40–59 years, MA). Thus, fishing represented an appropriate way of animal protein supply for all individuals. The high proportion of freshwater fish and plants is in agreement with the trend reported by Herrscher et al. (2018a) who based their results exclusively on $\delta^{13}C_{collagen}$ and $\delta^{15}N_{collagen}$ without applying mixing models, as would have been advisable. However, the authors showed that this finding holds true mainly for Neolithic individuals, while individuals of later periods (until the Late Bronze Age) showed a higher proportion of protein of domesticated animals in the diet.

Dairy products (e. g. milk, cheese) represent a quite important part of the diet for all individuals (13–22 %; see Table 29). Secondary products such as milk or cheese are rich in protein, calcium, and carbohydrates. People obviously used these secondary products rather than slaughtering their domesticated animals. The latter, to be sure, were consumed on a regular basis, but the dietary proportion of dairy products exceeded the proportion of domesticated mammals' meat in all individuals under study. This holds true for individuals of all time periods (LBA, ANT, MA).

As already mentioned, meat of both domesticated and wild mammals was a regular part of everyone's diet throughout all time periods (14–31 %; see Table 29). Two individuals, however, showed a comparatively low proportion of meat in their diet: Burial 5 (KG-038-0146; probably ♂, 20–30 years, LBA) and Burial 25 (KG-053-0208; ♂, 40–70 years; ANT). The individual in Burial 5 instead consumed a very high proportion of freshwater fish (~50 %; see Table 29). Thus, this individual received necessary animal protein mainly via fish consumption. The individual of Burial 25, on the other hand, showed a high proportion of pheasant meat (~30 %; see Table 29) as well as dairy products (~22 %; see Table 29) in his diet, again receiving enough animal protein without consuming too much meat of either domesticated or wild mammals.

Consumption of plants or plant products was also important for all individuals from Karacamirli, although meat (of domesticated and wild mammals) and dairy products were of higher importance for the majority of analysed humans. No difference with respect to particular periods is visible. Four individuals showed a plant dietary proportion of about one third or even higher. This is the case for the individual in Burial 8 (KG-057-0247; nd, 40–70 years; EIA), Burial 26 (KG-066-0392; probably ♀, 54–74 years; ANT), Burial 29 (KG-031-0120; ♂, 20–25 years; MA), and Burial 37 (KG-052-0205; probably ♂, 10–13 years; MA). This high proportion of plant food (here: barley/wheat, lentil) is remarkable. The meat and fish supply was also quite high for all these individuals. Besides a slight case of Cribra orbitalia in the individual in Burial 29 (see ch. V.4.4 and Fig. 219) none of these individuals showed any sign of deficiencies. Cribra orbitalia, however, can have several causes such as infectious diseases or diarrhea and is not necessarily caused by a limited diet supply (i. e. vitamin B12 and C deficit) as explained in ch. V.4.4 (e. g. Stuart-Macadam 1985; Walker 1986; Walker et al. 2009; Wapler et al. 2004). Lentils are rich in protein. Accordingly, even individuals consuming about one third of plant products obviously were healthy and well-nourished. For individuals from Karacamirli no consumption of C_4 plants (e. g. millet) can be observed. This is in accordance with the results of e. g. Messager et al. (2015) who could not find any evidence of millet consumption at the Early Bronze Age site Chobareti in Georgia. Another study at Chobareti showed botanical evidence for millet, however the consumption could not be validated by isotope analyses. Hence, millet consumption was of minor importance here (Kakhiani et al. 2013). However, millet was consumed in other sites close to the Caucasus, e. g. Mentesh Tepe (Western Azerbaijan; Neolithic; Herrscher et al. 2018a), Treli and Treligorebi (Central Georgia; Late Bronze Age; Herrscher et al. 2014), and Koban (Southern Russia, Early Iron Age; Herrscher et al. 2018b). Data suggest significant millet consumption since Early or Middle Bronze Age with high regional differences (Herrscher et al. 2014; 2018b). Neither environmental nor climatic factors can explain this. However, this might have been a regional particularism (Herrscher et al. 2018b).

Consumption of birds (here: pheasant) is of lower importance for the majority of individuals under study. Nevertheless, three Late Antique individuals from Karacamirli (Burial 21 (KG-074-0507; probably ♂, 48–75 years), Burial 25 (KG-053-0208; ♂, 40–70 years), and Burial 27 (KG-097-0455; probably ♂, 25–50 years)) showed a comparatively high proportion of pheasant meat in their diet with 27 %, 23 %, and 17 %, respectively (see Table 29). This is, however, not an exclusively chronological pattern since another individual of this time period, Burial 26 (KG-066-0392; probably ♀, 54–74 years) shows a rather low proportion of pheasant in her diet (9 %; see Table 29). This can indicate a sex-specific or even social differ-

ence within the antique individuals. However, whether sex-specific or social factors played a role is impossible to differentiate on the basis of such a small sample.

A detailed analysis of the archaeozoological remains must be carried out in order to validate the calculated dietary proportions using isotope mixing models. However, the resulting major food sources (freshwater fish, dairy products, plant products) are plausible with respect to the locality (Kura valley) as well as the time periods from the Late Bronze Age to the Middle Ages. For two medieval individuals, in Burial 29 (KG-031-0120) and Burial 34 (KG-048-0197), the calculated mixing models did not fit their $\Delta\delta^{13}C_{carbonate\text{-}collagen}$ values. Both individuals were probably primarily not local to the site (see below). The rather low number of analysed humans does not permit a detailed look at sex- or age-specific patterns in the diet.

Some individuals excavated in Karacamirli were probably primarily not local according to their isotopic fingerprints. The individuals in Burial 5 (KG-038-0146; probably ♂, 20–30 years; LBA), Burial 27 (KG-097-0455; probably ♂, 25–50 years; ANT), Burial 29 (KG-031-0120; ♂, 20–25 years; MA), and Burial 34 (KG-048-0197; ♂, > 60 years; MA) exhibit an isotopic fingerprint which is quite different from that of the majority of humans from Karacamirli with respect to several isotopic systems.

The individual in Burial 29 exhibits relatively low $\Delta\delta^{13}C_{carbonate\text{-}collagen}$, $\delta^{15}N_{collagen}$, $\delta^{13}C_{carbonate}$, and $\delta^{18}O_{phosphate}$ values. The individual's isotopic fingerprint contradicts the calculated mixing model (see ch. VI.3.1). In addition, the $^{87}Sr/^{86}Sr$ ratio of both bone (0.707468) and enamel (0.707636) exceeds the calculated local range (0.707255 – 0.707433). As mentioned before (see ch. VI.3.2) this individual probably originated from a site with a higher local strontium isotope ratio. The bone integrates a mixed isotope signal from both the primary site and from Karacamirli. Given the young age of this individual (20–25 years) the migratory event probably occurred very early

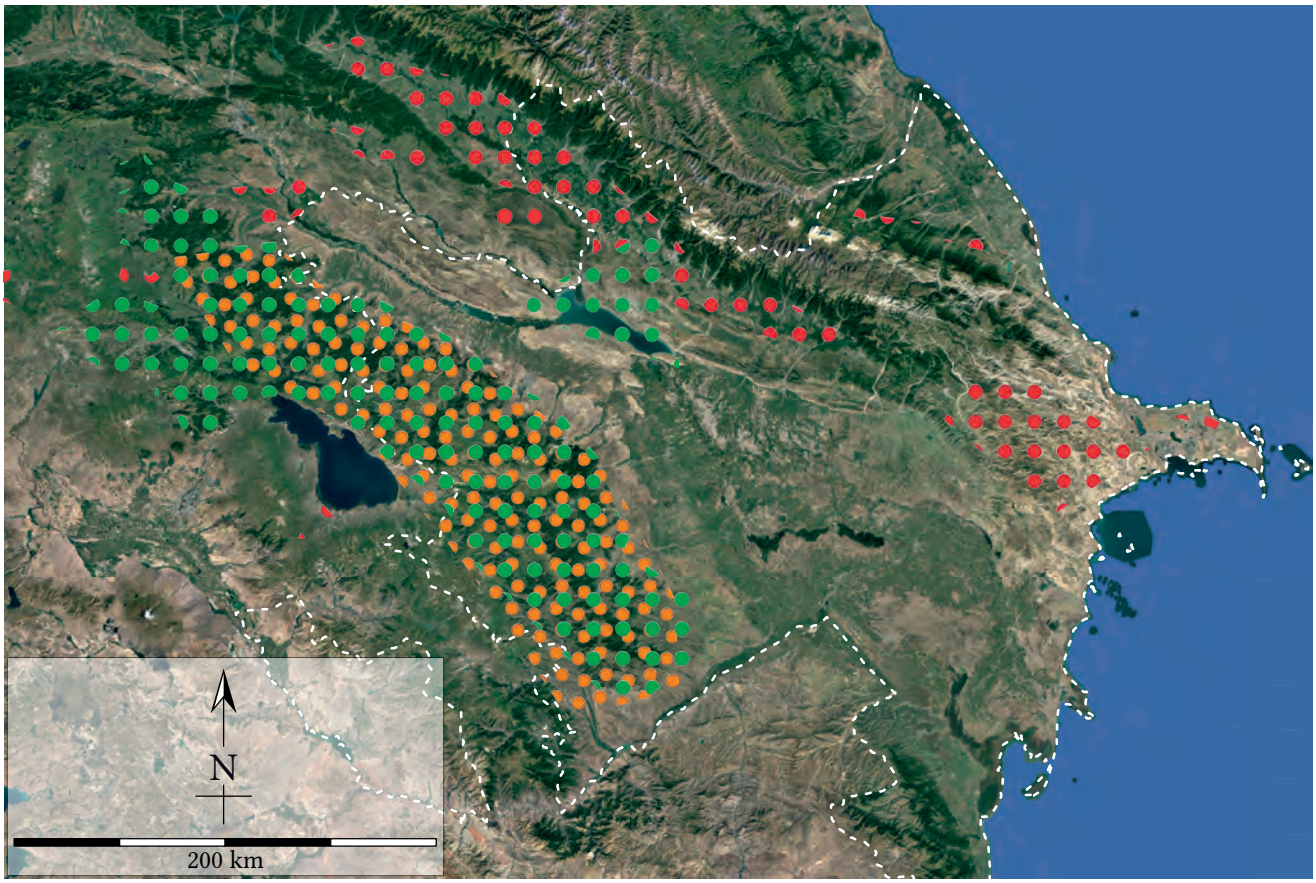

Fig. 296. Map approximatively indicating the (most probable) regions of origins for the primarily non-local individuals from Karacamirli (see text). Three different regions of origin (green, orange, red) can be established. Green: North-western Azerbaijan, mountainous regions along the borders between Azerbaijan, Armenia, and Georgia (Carbon). Orange: Southern/south-western Azerbaijan, northern/north-eastern Armenia (Jurassic, Cretaceous). Red: Eastern/north-eastern Azerbaijan, northern/eastern Armenia, eastern Georgia (Neogene, Quarternary). The map is based on the geological maps of Bairamov et al. (2008) for Azerbaijan, Kharazyan (2005) for Armenia, and Asanidze et al. (2019) for Georgia as well as on the strontium isotope values of the studies by Chazin et al. (2019) and Shishlina et al. (2016)

in life. The $^{87}Sr/^{86}Sr_{enamel}$ value is close to values of snail samples from the north-western part of Azerbaijan (0.70727–0.70766; Shishlina et al. 2016). In another study in northern Armenia a local strontium isotope range of 0.7067–0.7084 was recorded based on animal samples (Chazin et al. 2019). With respect to the strontium isotope data an origin from either north-western Azerbaijan or northern Armenia is conceivable (see Fig. 296). The ^{18}O depletion in bone phosphate (14.5 ‰; see Fig. 290) could also be explained by an origin close to the Greater Caucasus. With increasing latitude the $\delta^{18}O$ value of precipitation decreases (Marshall et al. 2007), which has an impact on the meteoric drinking water and thus the $\delta^{18}O_{phosphate}$ values (see ch. VI.1). In addition, a higher altitude also results in lower $\delta^{18}O$ values (Marshall et al. 2007). Thus, a higher altitude of the place of origin is plausible in the case of the individual of Burial 29. The individual in Burial 5 also showed a depletion in ^{18}O in the phosphate fraction. While this individual is not remarkable with respect to the strontium isotope ratios of both bone and enamel, the rather low $\delta^{18}O_{phosphate}$ value (14.6 ‰; see Fig. 290) could also be indicative of an origin at a higher latitude and/or altitude (see Fig. 296).

Even the individual in Burial 35 ($^{87}Sr/^{86}Sr_{enamel}$ = 0.707490) probably originated from a region with a higher local strontium isotope ratio, however far more to the south than the place of origin of the individual of Burial 29 (see Fig. 291). Broadly speaking, older rock types show higher $^{87}Sr/^{86}Sr$ ratios compared to younger ones (see e. g. Bentley 2006). In addition, different types of rock (e. g. carbonates, basalt, crustal rock) are different in terms of their strontium isotope ratios. Slightly younger rock types (Jurassic, Cretaceous) compared to the High Caucasus region (see above) are present in the southern and south-western parts of Azerbaijan, the Small Caucasus (Bairamov et al. 2008) as well as in the northern and north-eastern parts of Armenia (Kharazyan/Sargsyan 2005) (see Fig. 296). Thus, the individual of Burial 35 might originate from a more southern region.

An origin from a more southern region could also explain the ^{18}O enrichment in both oxygen isotopic systems ($\delta^{18}O_{carbonate}$ = -8.2 ‰, $\delta^{18}O_{phosphate}$ = 17.1 ‰) in the case of the individual of Burial 27, since a lower latitude should result in higher $\delta^{18}O$ values (Marshall et al. 2007).

The strontium isotope ratios of both bone (0.707343) and enamel (0.707269) of the individual in Burial 34 lie within the expected local range (0.707255–0.707433). However, as mentioned above (see ch. VI.3.2), the rather big difference between $^{87}Sr/^{86}Sr_{enamel}$ and $^{87}Sr/^{86}Sr_{bone}$ is likely caused by the migration of the individual's mother, who might have originated from a region characterized by lower strontium isotope ratios. An origin from an area with even younger rock types than in case of the individual in Burial 35 seems likely. Young rock types (Neogene, Quaternary) are present in the north-eastern and the eastern part of Azerbaijan (Bairamov et al. 2008), in parts of northern and eastern Armenia (Kharazyan/Sargsyan 2005), as well as in eastern Georgia (Asanidze et al. 2019) (see Fig. 296). Consequently, there might have been a migratory event within the life time of the individuals' mothers. Moreover, as in the case of the individual in Burial 29 (see above), the isotopic signature of this individual does not fit the calculated dietary proportions (see ch. VI.3.1). A non-local origin of this individual or a different cultural background would be plausible here.

The individual in Burial 9 (KG-043-0204; nd, nd) exhibits a $^{87}Sr/^{86}Sr_{enamel}$ value of 0.707193, which is below the assumed local $^{87}Sr/^{86}Sr$ range (see Fig. 291). Only teeth were preserved, so no comparison between the childhood and the adulthood signal is possible. Nevertheless, according to the low strontium isotope ratio this individual was probably primarily not local to the site but originated from a region with young rock types (see above; Fig. 296).

According to the stable isotope ratios, we can suggest three different regions of origin for six potentially non-local individuals. An origin from north-western Azerbaijan or northern Armenia (close to the mountains) is likely for the individual of Burial 29 (MA). The individual of Burial 5 (LBA) also originated from a mountainous region, e. g. the mountains between Azerbaijan and Armenia or Georgia (see Fig. 296). The individual in Burial 35 (MA) probably originated from the southern or south-western parts of Azerbaijan or northern/north-eastern Armenia (see Fig. 296). This might also be true for the individual in Burial 7 (LBA). Finally, the eastern and north-eastern parts of Azerbaijan, northern/eastern Armenia, and eastern Georgia are possible regions of the origin for the individuals in Burial 9 (LBA/EIA) and Burial 34 (MA) (see Fig. 296). From the archaeological point of view, burials dated to the Late Bronze/Early Iron Age show connections with Armenia or eastern Georgia (see ch. IV.2.2). The individual of Burial 9 is archaeologically dated to Late Bronze Age/Early Iron Age. An origin from either eastern/northern Armenia or eastern Georgia is in accordance with the expected possible regions of origin (see Fig. 296). The individual in Burial 5 (LBA) is isotopically connected with mountainous regions, which could, however, also include mountains in northern Armenia and eastern Georgia. Thus, the isotopically determined region of origin is again in agreement with the archaeological expectations. Late Antique burials cannot be linked to a specific region archaeologically. According to the isotopic fingerprints, Medieval individuals came from two main regions, north-western

Azerbaijan or northern Armenia on the one hand (Burial 29) and eastern/north-eastern Azerbaijan, northern/eastern Armenia, or eastern Georgia on the other hand (Burial 34). Although an even more distant origin would be possible, according to the principle of Occam's razor the most likely regions of origin should be close to Karacamirli.

With the exception of the individual of Burial 9 with unknown sex, all probably non-local individuals were males. In one case (Burials 34), however, it is likely that the individual's mother had migrated to the site. This burial is dated to the Middle Ages. While another Medieval individual (Burial 29) probably migrated to the site on his own, the latter individual was eventually local but had a non-local mother who transferred the non-local signal to her unborn child (see ch. VI.1). Patrilocality might have been common practice during the Middle Ages in contrast to the other time periods. However, the numerical superiority of males in the isotope dataset (see Table 25), as well as on the overall burial site (see Table 16), might, however, be misleading here. Only for one probably female individual (Burial 38) strontium isotope analysis was performed. Consequently, no overall pattern on matri- or patrilocality is apparent here.

One of the above-mentioned Medieval individuals (Burial 34) showed several conspicuous craniometric measures (see ch. V.4.3.1). A non-local origin of this individual, as assumed with respect to its morphological appearance, is validated by the isotopic fingerprints. However, the isotopic signatures of the individuals in Burial 25 and Burial 38, who also showed a striking craniometry (see ch. V.4.3.1), do not in themselves suggest a non-local origin, although they do not fully exclude it either (see ch. VI.1). In the case of Burial 7, which is another case of conspicuous craniometry (see ch. V.4.3.1), only the $^{87}Sr/^{86}Sr$ ratio of enamel was available. While this value is very close to the calculated local strontium isotope range, a non-local origin of this individual cannot be validated based on the isotopic data.

GMM clustering of the five-dimensional stable isotope data results in two clusters separated by the individuals' $\delta^{18}O_{carbonate}$ and $\delta^{18}O_{phosphate}$ values. Individuals of cluster 2 are enriched in ^{18}O compared to humans grouped within the first cluster (Table 31). If the strontium isotope ratios of either bone or enamel are added to the clustering dataset the clusters change markedly (Table 32 and Table 33). The overall clustering pattern is influenced by the strontium isotope signal although individuals do not group according to their $^{87}Sr/^{86}Sr$ values (see Fig. 294 and Fig. 295). The clustering results slightly change if strontium isotope values of enamel instead of bone are used (see Table 30). The cluster results suggest that origin (i. e. $^{87}Sr/^{86}Sr$) is more important for the cluster pattern than diet.

The changed clustering structure in the six-dimensional compared to the five-dimensional dataset requires closer investigation. Two individuals (Burials 8 and 26) had to be removed from the dataset due to missing strontium isotope values (see Table 25). Both individuals exhibited relatively high $\delta^{13}C_{carbonate}$ values of -12.5 ‰ and -12.6 ‰. The individual in Burial 8 also shows ^{18}O enrichment in the carbonate fraction (-8.2 ‰; see Table 25). For the six-dimensional dataset using enamel $^{87}Sr/^{86}Sr$ another two individuals (Burials 27 and 28) had to be removed. The individual in Burial 27 was especially remarkable with respect to his $\delta^{13}C_{carbonate}$, $\delta^{18}O_{carbonate}$, and $\delta^{18}O_{phosphate}$ values. The exclusion of these four individuals from the six-dimensional cases might have caused changes to the clustering structure, especially due to the low number of data points (five-dimensional case: n = 12, six-dimensional case using $^{87}Sr/^{86}Sr$ ratios of bone: n = 10, six-dimensional case using $^{87}Sr/^{86}Sr$ ratios of enamel: n = 8).

In the five-dimensional case three individuals (Burials 5, 29, and 34) who are conspicuous with respect to their isotopic fingerprint are grouped into the first cluster. The clustering of the examined individuals is probably based on the isotope values of the light elements, mainly $\delta^{18}O_{carbonate}$ and $\delta^{18}O_{phosphate}$, which among others indicate diet and drinking water, respectively (see Kirsanow/Tuross 2011). A higher number of individuals would be required to get a more detailed image of the local isotope fingerprint. Then, non-local individuals could eventually be detected more easily by GMM clustering.

With inclusion of either $^{87}Sr/^{86}Sr_{bone}$ or $^{87}Sr/^{86}Sr_{enamel}$ values clusters are still mainly separated by the oxygen isotope ratios. However, even $\delta^{15}N_{collagen}$ and $\delta^{13}C_{carbonate}$ differ between the two clusters. In the six-dimensional case using $^{87}Sr/^{86}Sr_{bone}$, two individuals with notable isotope fingerprints (Burials 5 and 27) are grouped into cluster 2, while another individual (Burial 29) with conspicuous isotopic data is clustered into the first group (see Table 30). Consequently, both clusters may include primarily non-local individuals. This clustering clearly separates medieval individuals from individuals of older periods (LBA, ANT). All Medieval individuals of the dataset are grouped into the first cluster. Individuals dated to the Late Bronze Age or Late Antiquity show relatively high $\Delta\delta^{13}C_{carbonate\text{-}collagen}$ values indicative of a high-fat diet. Their $\delta^{15}N_{collagen}$ values were quite variable. Medieval individuals are characterized by rather low $\delta^{15}N_{collagen}$ values, while all other isotopic systems are more variable. A diet with a low protein content (compared to other individuals from Karacamirli) would explain this. However, it has to be mentioned that besides the individual in

Burial 29 showing a slight form of Cribra orbitalia (see AG3 and AG4.4) none of the Medieval individuals (Burials 28, 34, 37, 38, 39) showed signs of deficiencies on their skeletons (see AG3). Actually, starving would lead to an increase in ^{15}N as described before (see ch. VI.1), while all medieval individuals show low $\delta^{15}N_{collagen}$ values. Accordingly, these individuals probably did not die of hunger, at least not of persistent starvation. Although this can only be understood as tendency due to the low sample size, there might have been a shift in diet, at least from Late Bronze Age/Antiquity to the Middle Ages. The distinction of Medieval individuals from older ones is even mathematically validated by the GMM cluster analysis. The reasons for such a dietary shift can be political, climatic, or genetic. To understand them will require a much bigger and chronologically more balanced dataset.

The six-dimensional data set using the strontium isotope ratio of enamel separates two individuals (Burials 21 and 25). These two Late Antique individuals are remarkable with respect to their diet, consuming a comparably high proportion of pheasant (27 % and 23 %). The individual in Burial 25 also consumed a quite high proportion of dairy products (22 %). As already mentioned, the latter individual also showed a striking craniometry. Accordingly, with respect to GMM cluster analysis using $^{87}Sr/^{86}Sr_{enamel}$ these two individuals are separated from the remaining individuals grouped into cluster 1, which also included some probably non-local individuals (see above). Interestingly, Burials 21 and 25 were the only Late Antique burials in the enamel dataset and were separated from the Late Bronze Age (Burial 5) and Medieval individuals (Burials 29, 34, 37, 38, 39). GMM cluster analysis including $^{87}Sr/^{86}Sr_{enamel}$ values suggests an exceptional position of Late Antique individuals with respect to their diet. While a different culture is conceivable here, this could also be explained by a primarily non-local origin of the individuals in Burials 21 and 25. However, even in this case, this tendency has to be confirmed on a bigger dataset, also including more Late Antique individuals.

VI.5 Conclusion

Stable isotope analyses are an important source of information on the daily life of ancient humans. The multi-isotope approach used in this study allowed identifying several individuals which were probably primarily not local to the site of Karacamirli. These individuals might have originated from today's north-western Azerbaijan or northern Armenia close to the mountains (Burials 5 and 29), from eastern/north-eastern Azerbaijan or northern/eastern Armenia, and eastern Georgia (Burials 9 and 34) and from the southern/south-western part of Azerbaijan or the northern/north-eastern part of Armenia (Burial 35). An origin from Armenia or eastern Georgia would comply with the archaeological links for Late Bronze Age/Early Iron Age individuals (see ch. IV). Isotopically, both Burial 5 and Burial 9, dated to the Late Bronze Age/Early Iron Age, can be connected with these regions. Medieval individuals did not have grave goods, thus cannot be connected with specific regions archaeologically (see ch. IV). For the Late Antique individual in Burial 27 an origin from a more southern region is plausible with respect to the oxygen isotope values. However, the strontium isotope ratio is within the calculated local range, what, however, does not necessarily confirm a local origin. The Medieval individual in Burial 35 isotopically rather points to regions in southern/south-western Azerbaijan as well as northern/north-eastern Armenia. Nevertheless, an origin from eastern Azerbaijan cannot be excluded. According to their stable isotope fingerprints the Medieval individual in Burial 29 probably originated from north-western Azerbaijan or northern Armenia, while another Medieval individual (Burial 34) probably came from eastern/north-eastern Azerbaijan, northern/eastern Armenia, and eastern Georgia, respectively. According to the principle of Occam's razor the easiest explanation should always be preferred. Thus, an origin from close to the examined site is more plausible than an origin from far away although the latter cannot be excluded.

The approximated diet using SISUS indicates a diet with a marked proportion of freshwater fish for most individuals. In addition, plants (barley/wheat, lentil) and meat of domesticated as well as wild mammals were consumed. Dairy products were, however, of higher importance than the meat of the respective domesticated mammals. Individuals dated to the Late Bronze Age/Early Iron Age as well as Late Antiquity fed on a high-fat diet according to their $\Delta\delta^{13}C_{carbonate\text{-}collagen}$ values, while the protein content of their diet was quite variable ($\delta^{15}N_{collagen}$). Medieval individuals, by contrast, fed on a low-protein diet of varying fat content. The dietary shift towards a low-protein diet can only be understood as a trend due to the small sample size. Nevertheless, this shift might be characteristic for Medieval times, a politically turbulent period (see ch. IV.4.1). The Medieval individuals did not show signs of starvation either on their skeletons or with respect to their isotopic signals. Different factors, such as the political situation, climate, as well as a genetic components are conceivable here. This can, however, not be resolved without additional anthropological, archaeometric, and archaeological data.

Our study gives insights into the isotopic signatures of archaeological individuals from Azerbaijan and illustrates the advantage of multi-isotope studies in archaeological contexts. Many more isotope studies on archaeological human as well as animal remains excavated in the region will be needed to gain a better understanding of the isotopic fingerprints of this region.

VII. Portable X-ray Analysis

Michaela Schauer
(with a contribution by M. Gruber and K. Kaniuth)

X-ray analysis is a common technique in archaeometry and geological research through which the elemental composition or fingerprint of a given sample can be characterized qualitatively and quantitatively (Speakman et al. 2011: 3485): X-ray fluorescence is a process whereby electrons are displaced from their atomic orbital positions, releasing energy that is characteristic of a specific element. This release of energy is then registered by the detector in the XRF instrument, which in turn categorizes the energies by element with the help of an algorithm (Shackley 2012a: 16). The characteristic energy of light elements can only be detected in some microns distance, heavier elements in several hundred microns distance (Pollard et al. 2007: 102). Therefore the texture of the samples' surface is of great importance (Mecking et al. 2013: 54; see more below). The main elemental values are given in weight percent, trace element values in parts per million (Shackley 2012a: 19). Cluster analyses, the Principal Component Analysis (PCA) – which stresses the similarities between samples of a given dataset (Drennan 2010: 300–305) and Discriminant Analysis (LDA), which emphasizes the similarities in defined groups and differences between groups (Mecking 2010: 119–120), are then used to explore the data. The data interpretation itself is mostly based on identifying patterns in the scatterplots or in ternary plots (Pillay et al. 2000: 55).

P-XRF-devices have become relatively cheap and are a widely available tool for archaeological field research. Other than laboratory analyses, p-XRF is often used as a 'point and shoot method', but many factors have to be taken into account to use the method properly: The Bruker Tracer 5i and the Niton XL3t used here were equipped with proprietary fundamental parameter algorithms (FP) which deal with factors such as emission effects, scattering, efficiency, secondary and tertiary absorption and other parameters. This is necessary to convert fluorescent peaks into concentration values. These algorithms are developed in relation to a specific matrix type (metals, aluminosilicates, etc.) but are often not sufficient for the analyses of archaeological material. A fine-tuned calibration must therefore be developed. For each matrix type and each device this has to be done on reference standards (Glascock/Ferguson 2012: 87–88). On a fresh brake of pre-modern pottery for example, the samples' surface structure differs from that of the powder samples used to create the FP (Helfert 2013: 22–26). The standards should be quantified by different laboratory methods so that the given values – the values identified by the laboratory methods – and the values measured by the device can be used to develop corrective factors for each device and matrix (Golitko 2019: 87–88). This then produces the transparent data guaranteeing at least a degree of comparability between studies and which has the potential to be used in other studies (Shackley 2012b: 3).

For the pottery and obsidian studied here, data generated with a Niton XL3t is used. The calibration for pottery was developed for the TestAllGeo-mode on standards of Roman pottery from the Frankfurt laboratory (Helfert 2013b: 25), the calibration for the TestAllGeo-mode for obsidian is based on the calibration set of the Archaeometry Laboratory at MURR (Glascock/Ferguson 2012). Each sample has been measured three times on different parts of the fresh brake (pottery) or the object (obsidian) for 300 seconds per measurement to compensate for possible effects of inhomogeneity. After eliminating all analyses with exceedingly high variability, the average of three measurements was used for statistics and data interpretation.

The Bruker Tracer 5i data is used for metal objects. These were measured three times per sample on the surface for 120 seconds in Ancient Copper mode. The calibration for metals is based on metal standards from the German Archaeological Institute (DAI) Berlin and the *Bayerisches Landesamt für Denkmalpflege* (BLfD) Munich. For the Graphics, R (Version 3.5.0) was used.

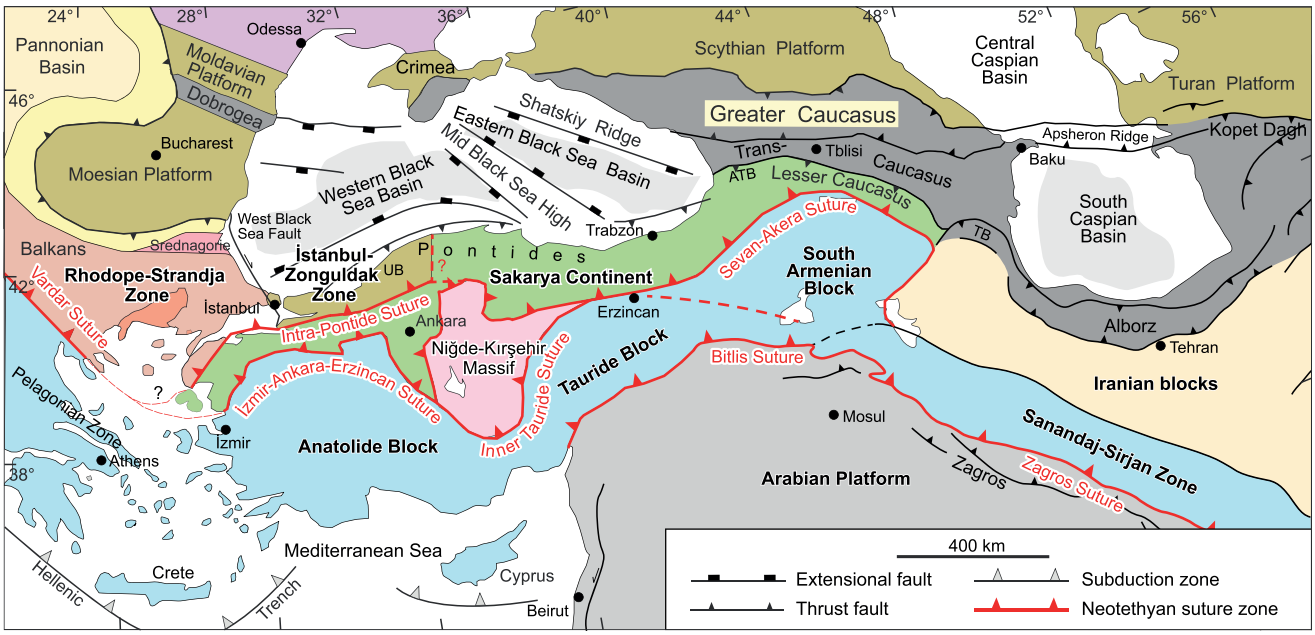

Fig. 297. Tectonic map of the Caucasus (after Vincent et al. 2016: Fig. 1)

VII.1 Geological background

VII.1.1 Geology of the Caucasus and Azerbaijan

Azerbaijan is part of the Black Sea/Caspian Sea region where the Eurasian and the African-Arabian lithospheric plates meet (Fig. 297). In the Late Proterozoic, Palaeozoic, Mesozoic and Early Cenozoic it formed part of the Tethys Sea and the shores of Gondwana. From the Oligocene up to the Quaternary the evolution of the region was defined by syncollisional and postcollisional stages of the Late Alpine tectonic cycle (Adamia et al. 2011: 490). Through the collision of the Eurasian and African-Arabian plates fold-thrust belts – the Greater and Lesser Caucasus – and the Transcaucasian intermontane depression were formed (Vincent et al. 2016: 2958). The open marine basins of the Neothetys were replaced by euxinic, semi-closed basins of the Paratethys which in the Late Miocene transformed into continental basins with subaerial conditions for sedimentation (Adamia et al. 2011: 490). During this epoch, the Lesser Caucasian ophiolite suture zones Izmir-Ankara-Erzincan and Amasia-Sevan-Akera (Hässig et al. 2016: 36) divide the landscape into two main geological provinces: Southern Tethyan and northern Tethyan. Those ophiolite suture zones consist of garnet-amphibolites, amphibolites, micaschists and continental metamorphic rocks like marbles, limestones, skarns and greenschists. They also include breccia-conglomerates, clasts like gabbros, diabases, altered basalts and other basic rocks (Adamia et al. 2011: 490. 491. 493).

As part of Gondwana, in the Palaeozoic the southern Tethyan mainly consisted of shallow marine platform sediments, while the northern Tethyan was characterized by volcanism, deep regional metamorphism, granite formation, orogenesis and deformation. Basement rocks of this time consist of metamorphosed sedimentary, plutonic and volcanic rocks. Basic magmatic rocks formed in the ocean basins of the Proto- and Palaeotethys and can be found today in all main tectonic zones of the Caucasus. Other important rocks of the pre-Mesozoic ocean basins are granite-gneiss-rock complexes which are common in the continental and oceanic-continental crust. The volcanic highland chain of the Lesser Caucasus runs from East Anatolia, via Armenia and Georgia to Azerbaijan. A magmatic formation is also found in the central segment of the Greater Caucasus (Adamia et al. 2011: 491–493. 531).

In the Late Sarmatian nearly the entire Caucasus fell dry. Clastic source areas consisting of sandstones and clays, but dominated by coarse molasses, were lifted (Adamia et al. 2011: 525). The Greater Caucasus formations of this time with its cretaceous-paleogene flysch and the Lesser Causcasus with Mesozoic-Cenozoic volcanic rocks (Abdullayev/Leroy 2016: 519) can be divided by their composition of clastic material. In the Greater Caucasus, molasses formations are exposed on the eastern and western fringes matching those which are found in the Transcaucasus foreland and pre-Caucasus foredeeps. Upper Sarmatian shallow marine sediments

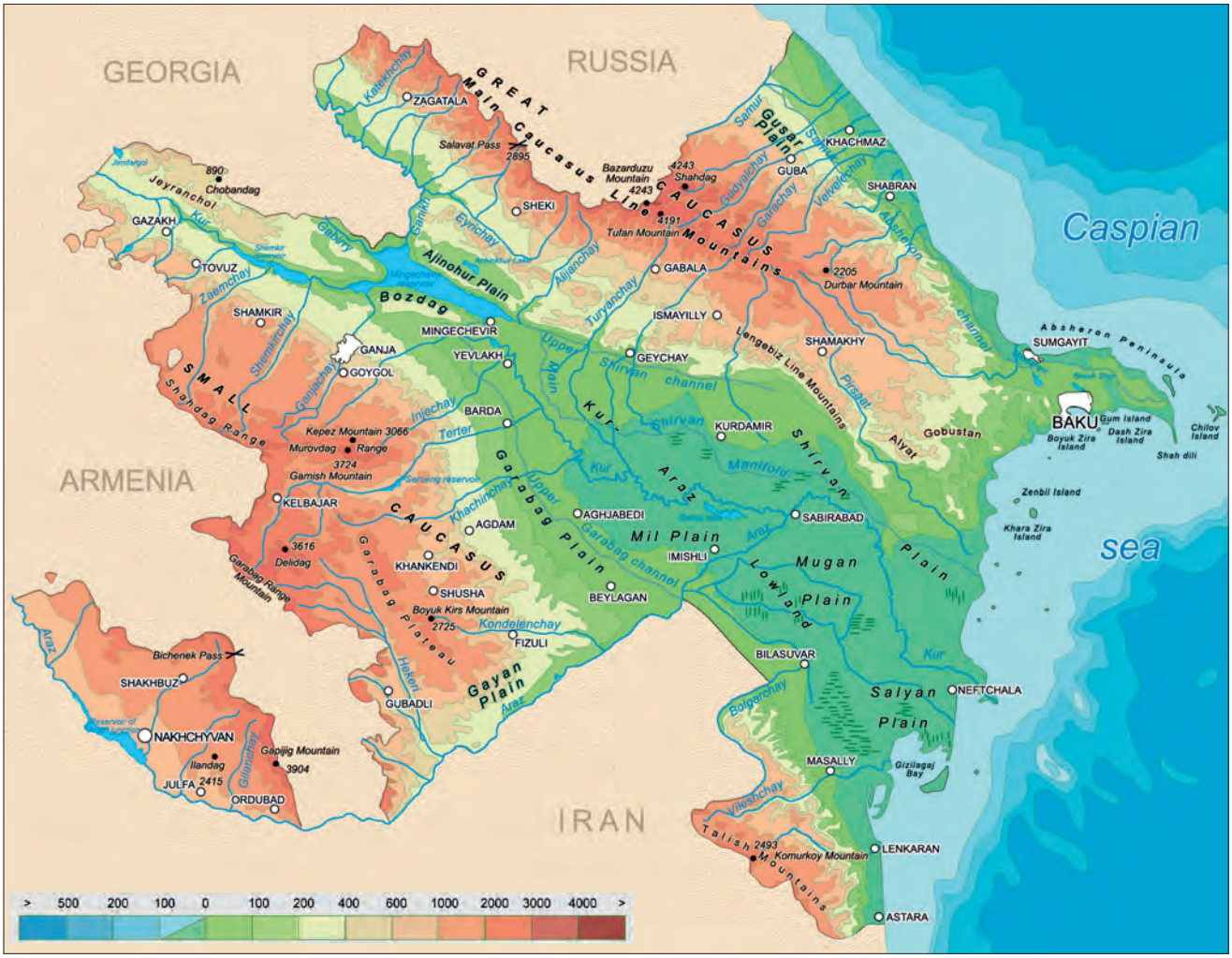

Fig. 298. Physical map of Azerbaijan

are found in the Shakhdag Mountains and above 3550 m height (Adamia et al. 2011: 528–530).

The Transcaucasian Massif (Artvin-Bolnisi formation) of Georgia and Azerbaijan is part of the Late Mesozoic-Eocene island-arc-type magmatic belt which is associated with the subduction of the Neothethyan crust (Adamia et al. 2018: 10). It mainly consists of granites, volcanic rocks (calc-alkaline basalt, andesite, dacite and rhyolite), alluvial sedimentary rocks (Popkhadze et al. 2014: 309. 311) and shallow-water lacustrine coal-rich, salty deposits. In Azerbaijan deep-sea terrigenous turbidites, lavas of andesite-basaltic and dacite-rhyolitic composition and coarse volcaniclastics are present (Adamia et al. 2011: 514). The Azerbaijan Massifs' Low- and Mid-Jurassic layer starts with terrigene clastics followed by dacites/rhyolites which are covered by an island-arc which was formed by plate-type volcanism. The Upper Jurassic formation consists of dacites/rhyolites, limestones, argillites and gritstones followed by Lower Cretaceous grit- and limestones. Upper Cretaceous dacites/rhyolites, an island-arc formed by plate-type volcanism and limestones follow. Paleocene and Eocene layers of terrigene clastics form the upper levels of the Azerbaijani Transcaucasian Massif (after Adamia et al. 2011: 516).

The Transcaucasian Basin is divided by the Dzirula massif – consisting mainly of Gondwana-derived gneiss-magmatite and ensialic island arc (Okrostsvaridze/Tormey 2013: 37) – into the Kura basin in the east and the Rioni basin in the west. Both are dominated by gypsiferous clays, sands and sandstones of the Oligocene and Lower Miocene. These sediments of the Maikop series can reach a thickness of up to 3 km (Adamia et al. 2011: 525). Interestingly, Maikop sediments include a great amount of Black shale which is formed under anoxic, reducing conditions following the restriction of water circulation between the Paratethys and the open ocean (van der Boon et al. 2017: 145). In the Middle and Late Miocene sandstones with marls and deep marine

carbonate clays were deposited. On the shallow marine fringes, terrigenous-carbonate rocks were accumulated. Variegated clays, gritstones with pebbles of metamorphic and crystalline rocks of the Lesser Caucasus and cross-bedded sandstone of the Upper Sarmatian are part of the central and southern regions of the Kura Depression. These rocks are highly gypsiferous with no traces of marine fauna. In the Middle Pliocene on the eastern on- and offshore zones of the Kura basin oil and gas accumulated in fluvial-deltaic and lacustrine sediments (Adamia et al. 2018: 525. 528).

The Kura foreland lithology of the Oligocene starts with a foundation of gritstones followed by carbonaceous clays mixed with lignites and/or coal in the lower Miocene. In the Middle Miocene sandy argillites are followed by marls and gritstones between two layers of lignites and/or coal. The Upper Miocene layer consists of gritstones, siderite concretions, limestones, sandy argillites, lignites and/or coal. The Pliocene starts with conglomerates, gritstones, claystones, argillites and siltstones followed by sandy argillites. The second half of the Pliocene formation starts with conglomerates, gritstones, sandstones, claystones, argillites and siltstones, river terrace deposits and ends as it started, supplemented with sandy argillites. The Pleistocene formation is built of limestone, andesitic volcanic rocks, sandy argillites, gritstone and siderite concretions. The Holocene layer consists of river terrace deposits (after Adamia et al. 2011: 526).

Another important morphostructural unit that should be mentioned is the monocline plateau of the Gusar sloping plane with its eroded, step-like structure that is crossed by many rivers while the Samur-Devechi lowland forms the most recent alluvial-proluvial deposit. It mainly consists of clay loams above the boulder and gravel deposits of the crossing rivers. The Greater Caucasus occupies the northern part of Azerbaijan, bordering the Kur intermontane depression. The depression is composed of quaternary deposits in the river valleys but mainly by sedimentary rocks of the Mesozoic, Paleocene and Neocene ages. The Shahdagh basin and the Murovdagh Ridge as part of the Lesser Caucasus consist of Upper Cretaceous, Eocene carbonate and volcanogenic rocks. The Karabakh highland was created by Late Pliocene and Quaternary andesite basaltic lava outflows with Upper Pliocene volcanoes and Quaternary cinder cones on top. Between Greater and Lesser Caucasus, the Kura-Araxes lowland, which is mainly filled by Neogene and Quaternary argillo-arenaceous rocks, is quite diverse in its geological and topographical structure. The alluvial lowland of Ganja is situated south of the Kura Valley between the Khrami and Ganjachay River valleys (Alizadeh et al. 2016: 11. 14–15. 17. 22).

VII.1.2 Geology of the Ganja-Qazakh region

The territory of modern Shamkir is situated in the Ganja-Qazakh region of Western Azerbaijan, bordered by Armenia in the south-west and Georgia to the north-west. The area has a great diversity of landscapes: alpine zones, intermediate highlands, foothills and plains, each possessing a different climate (IHPA NGO 2013: 13). Two of the main orographic units of Azerbaijan – the Lesser Caucasus and the Kura Depression – define the Ganja-Qazakh region. The Lesser Caucasus area mainly consists of volcanic tuff and chalky rocks – sandstone, argillaceous slates, limestone derived from chalky clay, sandstone and limestone. Tuff conglomerates, sands and porphyrities and their tuff derive from the Jurassic period. In the foothills, volcanic rocks (basalts), continental-sedimentary rocks (boulders, pebbles, sands, gravel, clays, sandy loams, etc.) and tertiary deposits are found (Fig. 299). In the Kura Depression the Ganja-Qazakh flatland, consisting of alluvial-proluvial elements, is one of the biggest orographic units. It is bordered by the Khrami river to the north-west, the middle Kura river valley to the north, the Karabakh sloping plain to the south and the foot of the Bozdag to the east. The most common soil types are wet grassland/forest, wetland-grassland, grey, dark grey-brown and light grey-brown soils. Their distribution is linked to height above sea level, therefore soil types expand from the banks of the Kura River plains to the medium and low highlands (IHPA NGO 2013: 18–19).

The dominant river of the area, the Kura, originates near Lake Kartsakhi (Aktash) in Turkey. After traversing Georgia it enters Azerbaijan and finally discharges into the Caspian Sea. Between Agstafa and Shamkir it runs between cliffs of Miocene marly limestone gypsum and Pliocene marls with alluvial pebbles on the left bank and the Lesser Caucasus with volcanic, sedimentary and metamorphic rocks and pebbles, but also aeolian and silty or sandy alluvial deposits, on the right. The profiles of the riverbanks are dominated rather by the tributary fans than by accumulations of material brought by the Kura itself (Ollivier et al. 2015: 110. 113). The tributary rivers of the Kura in the Ganja-Qazakh region run from the lesser Caucasus directly into the reservoirs of the Kura or into the Kura river (Fig. 299). They were and are the only source of freshwater in the area (IHPA NGO 2013: 6). For the Shamkir region the most important rivers are the Shamkirchay in the east and the Zayamchay to the west, both of which nowadays flow into the Shamkir Reservoir (IHPA NGO 2013: 5; see Fig. 300). The Shamkirchay springs up as Aghdashsu river in the Shahdagh massif and as Sarisu river in the Hinaldagh. On its way many other tributaries join the Shamkirchay

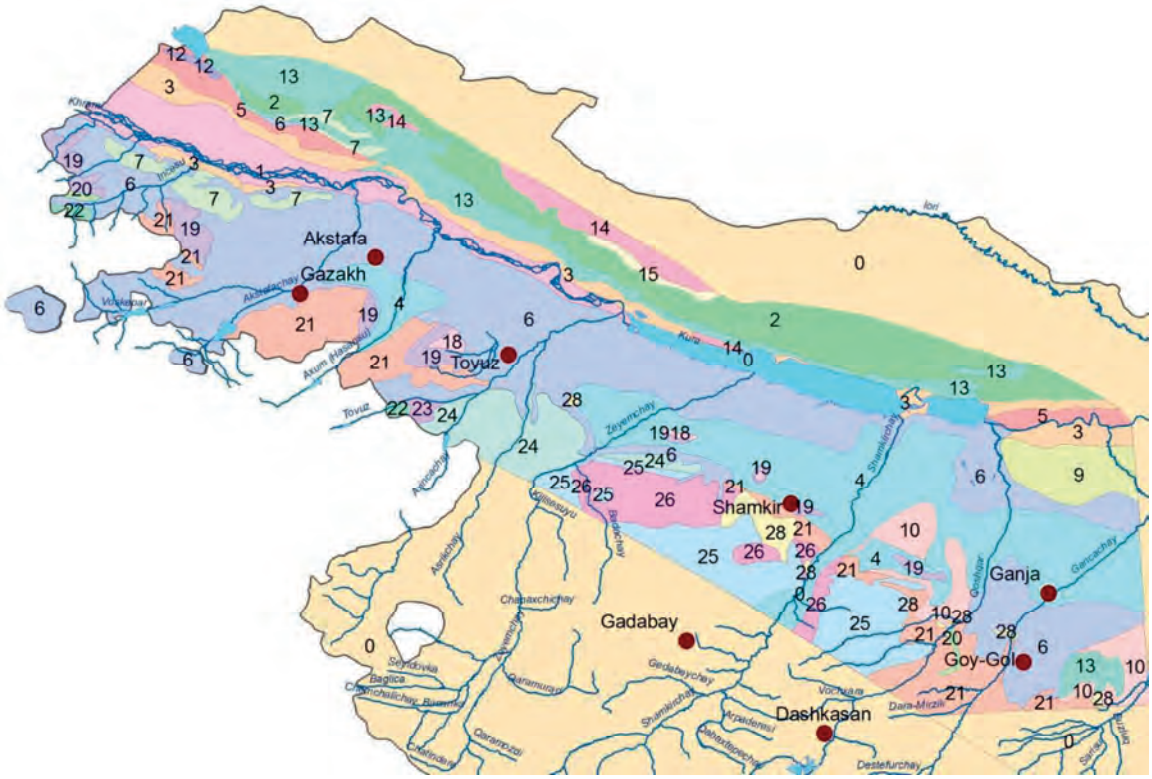

1	Modern	alluvium
2	Upper Quaternary	diluvium, proluvium
3	Khvalyn	Terrace of Kura
4	Khvalyn, Khazar stage	diluvium-proluvium-alluvium
5	Khazar stage	Terrace of Kura
6	Gorgan Horizon	diluvium, proluvium, alluvium
7	Gorgan Horizon	lacustrine sediments
8	Gorgan Horizon	dislocated continental-marine sediments
9	Gorgan Horizon	Terrace of Kura
10	Baku stage	diluvium, proluvium, alluvium
11	Baku stage	dislocated continental-marine sediments
12	Baku stage	Terrace of Kura
13	Absheron stage	continental-marine sediments
14	Agchagil stage	marine sediments
15	Miocene without subdivisions	marine sediments
16	Oligocene, lower parts of middle Miocene	Maykop Suite, clay and sandstone
17	Eocene	foraminiferal layers, clays, marls, sandstones
18	Upper Cretaceous, Maastrichtian	limestones
19	Upper Cretaceous	limestones, marls
20	Upper Cretaceous, Upper Turonian	turf-sandstones, sandstones, clays
21	Upper Cretaceous, Lower Turonian	volcanogenic series
22	Upper Cretaceous, Cenomanian	sandstones, clays, limestones
23	Upper and Lower Cretaceous, Cenomanian	Albuquerque volcanogenic-sedimentary series
24	Middle Jurassic, Bathonian	volcanogenic series
25	Middle Jurassic, Bajocian	quartz porphyries and tuffs
26	Middle Jurassic, Middle and Lower Bajocian	volcanogenic series
27	Mesozoic	without dismemberment
28	Cambrian, Precambrian	grantes, granodiorites, diorites

Fig. 299. Geological map of the Ganja-Qazakh region (IHPA NGO 2013: 28 Fig. 1.6)

which originally ran into the Kura river near today's town of Kür. The Göygöl stream additionally feeds the Shamkirchay during the rainy season (IHPA NGO 2013: 12–13). The Zayamchay has its sources – Inakboganchay

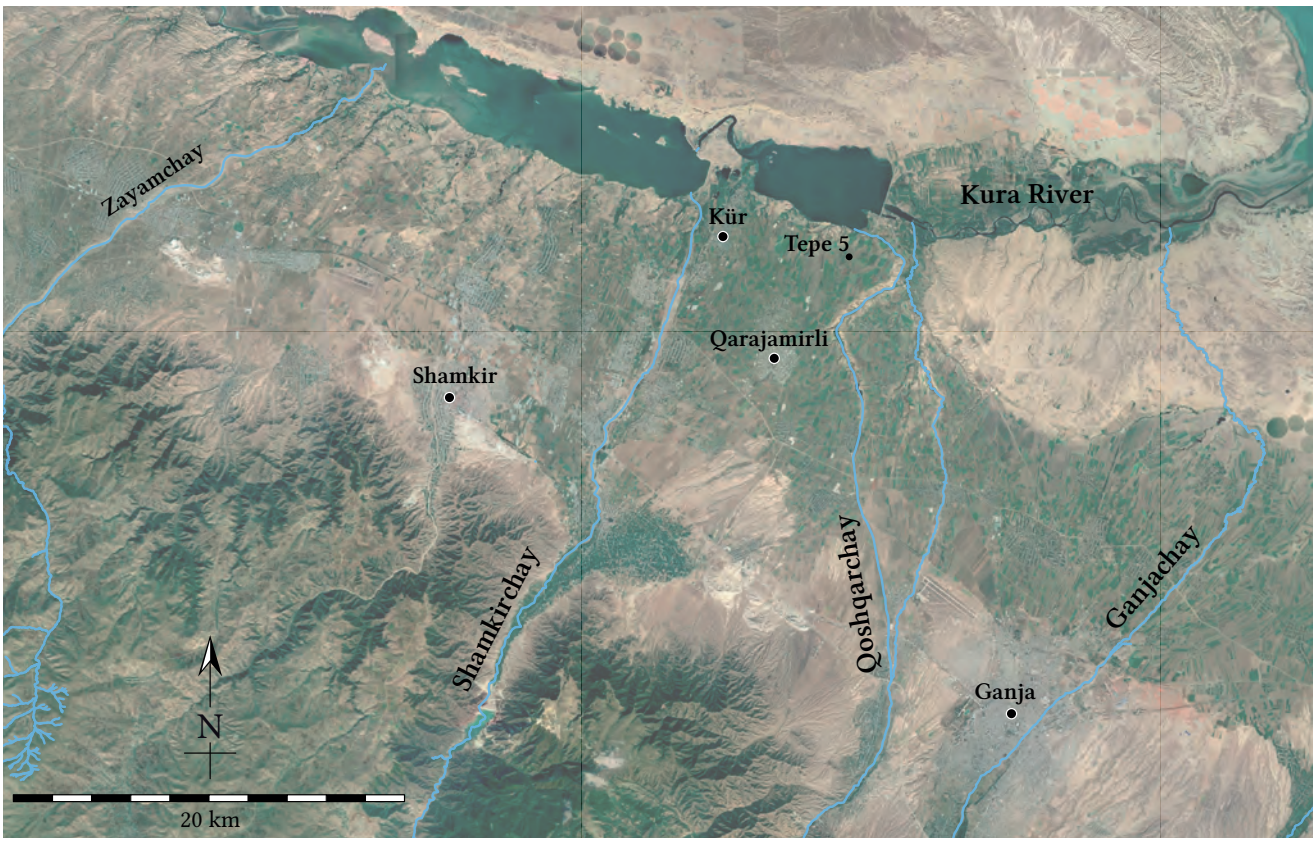

Fig. 300. The location of Tepe 5

and Qaramuradchay – in the lesser Caucasus near the Hacaqaya mountain. It joins the Kura close to the village of Bayramli.

The geological formations along the river Zayamchay are well investigated. On its banks, five terrace levels are documented. The Pleistocene-Late Glacial terrace, dating to from 32.234 to 14.130 calBP, is dominated by silts, sands and pebbles separated by paleosols. Geologic variations dating to 3.409 calBP characterize the first Holocene period terrace, pebbles and sand the first layer of the second Holocene period terrace which dates to 1.696 calBP. The second layer of the second terrace, dating to 393 calBP, is richer in hydromorphic soils and silts with small gravels, pebbles and sandy lenses. The later three levels are well documented in the thalweg. Upstream of the tributaries the soils are more silty while downstream, towards the Kura, pebbles and sands become more frequent. From the Neolithic to the Bronze Age, settlements are mostly found on the areas with silty deposits. Short term flow conversion which results in silty fans over the upper terraces is often documented for this period (Ollivier et al. 2015: 114; 2016: 84. 86).

In the Ganja-Qazakh region the most important underground resources are stone marble, gypsum, zeolite, crude cement, bentonite, cobalt, barite, alunite, sulphuric pyrites, gold, iron ore, copper and limestone. Both rayons south of the Shamkir Rayon are regions rich in metals and other mining resources (iron ore, alunite, marble, limestone, cobalt): In Dashkesan near the Qoshqarchay River, at least four modern iron ore fields are known. In the Gadabay region, gold, copper, non-ferrous metal ores and uranium are mined (IHPA NGO 2013: 41). The Gadabay-Bittibulag-Gadir deposit in the east of Yogundag mountain is characterized as Pb-Zn-Cu-Ag-Au vein type which is characteristic of low-sulfidation epithermal deposits but also for enrichment in Te, Se, Hg, Sb and As. The main minerals are sulfides which mainly consist of sphalerite, galena, pyrite and trace amounts of chalcopyrite. Bittibulag is a cooper-arsenic deposit (Veliyev et al. 2018: 78. 94).

Today, in the plains the climate is dry and warm. Temperate warm and dry steppic winters dominate in the lowlands, and a cold and humid climate in the mountain areas. The temperatures today can reach 40°C in the summer and drop to about 0°C in winter. It is worth mentioning that over the last 20 years temperatures have increased, and precipitation decreased. Rainfall today ranges from 250 to 500 mm. Due to intensified exploitation soils suffer from salinity and the amount of humus in grey(-brown) soils can reach up to 3 %. Sediment flow,

landslides, floods and mudflows are common natural calamities in the region (IHPA NGO 2013: 13. 19. 20).

VII.1.3 The Location of Tepe 5

Tepe 5 is located only 1.2 kilometres south of the Yenikand reservoir. Together with the neighbouring sites of Gurban Tepe, Ilyas Tepe, Ideal Tepe, Rizvan Tepe, Northern Complex and Dara Yatax the Tepe 5 belongs to the archaeological site of Karacamirli, named after a modern village one further kilometre to the south (Fig. 3). The distance from Tepe 5 to the ancient Kura bed was roughly 2 km. Several rivers are flowing by in a south-north direction, dividing the plain into discrete sections, eventually discharging into the Kura/Shamkir reservoir: The Shamkirchay and the Zayamchay flow to the west, the Qoshqarchay and Ganjachay to the east of the site of Karacamirli. As a consequence, the southern Kura plain is mainly defined by sedimentary deposits (Chambrade/Metz 2017: 1).

During a short field trip in July and August 2017, M.-L. Chambrade and S. Metz explored the banks of the Shamkirchay near Kür. Based on earlier research (Ollivier et al. 2016), they confirmed previous observations on the sedimentary composition at the Shamkirchay. Regarding Tepe 5, their research suggests that it is probably situated on the top of a silty river fan. During the Achaemenid period, when the locations of Gurban Tepe and Dara Yatax where occupied, the riverbed of the Shamkirchay was about 10 m higher than today (Chambrade/Metz 2017: 3).

VII.1.4 Soil samples

To identify the clay source for a given pottery, one has to accept the assumption that the characteristic elemental fingerprint of the source rock is reflected in the clay source (Pillay et al. 2000: 54). Therefore, all pottery with the same chemical fingerprint should be considered as product of the same clay source – provided the same processing method was used (Mommsen 2007: 182).

From a geological point of view, pottery can be characterized as sedimentary rock. Therefore it is necessary to understand the principal geochemistry of possible clay sources (Rice 1987: 33–34) – a task beyond traditional archaeological methodology. Geochemical analysis of sediments reconstructs the source rock of the analysed sediments by its main and trace elements (Mommsen 2007: 179) and/or isotopes. For example, the ratio of alumina (Al_2O_3) to bases is an indicator to identify the weathering history of the source rock for a given clay (Nesbitt/Young 1982: 715) – which itself is a weathering product of the source rock (Rice 1987: 40). Heavier elements like Rb or Ba are more resistant to the weathering process than

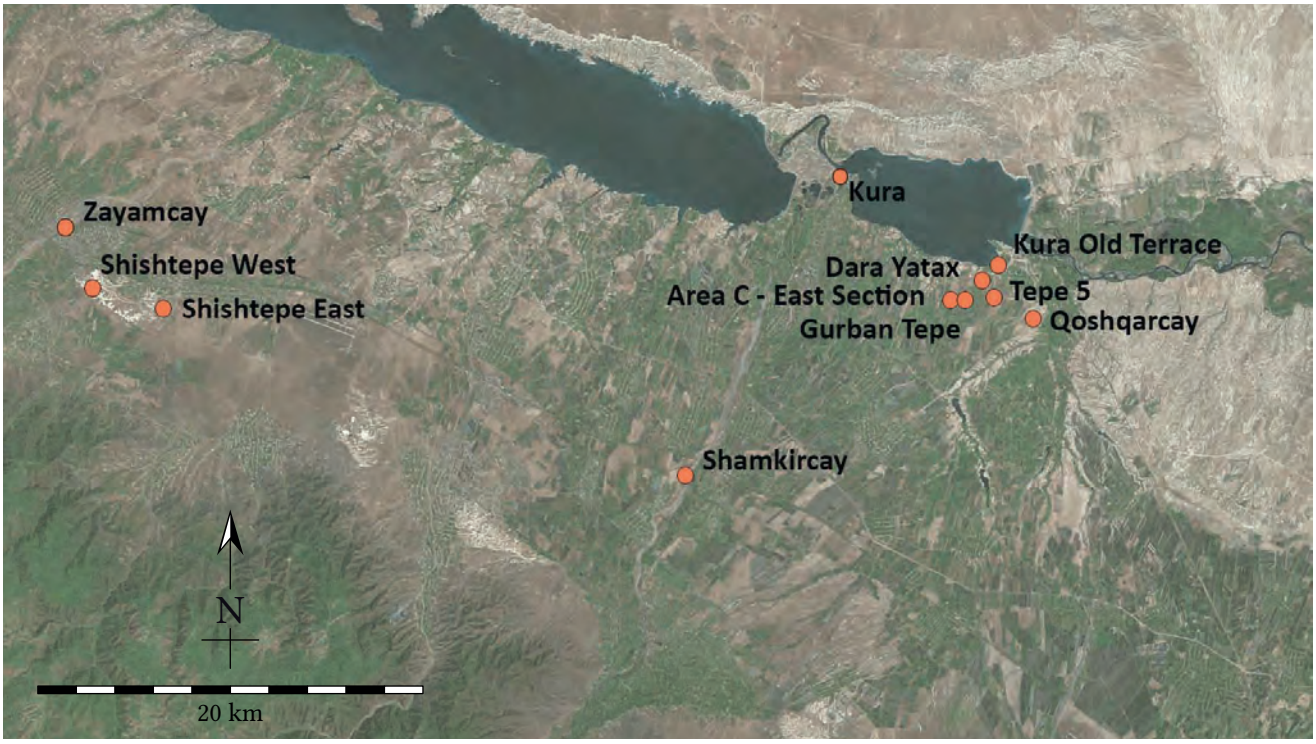

Fig. 301. The location of clay samples used in this study

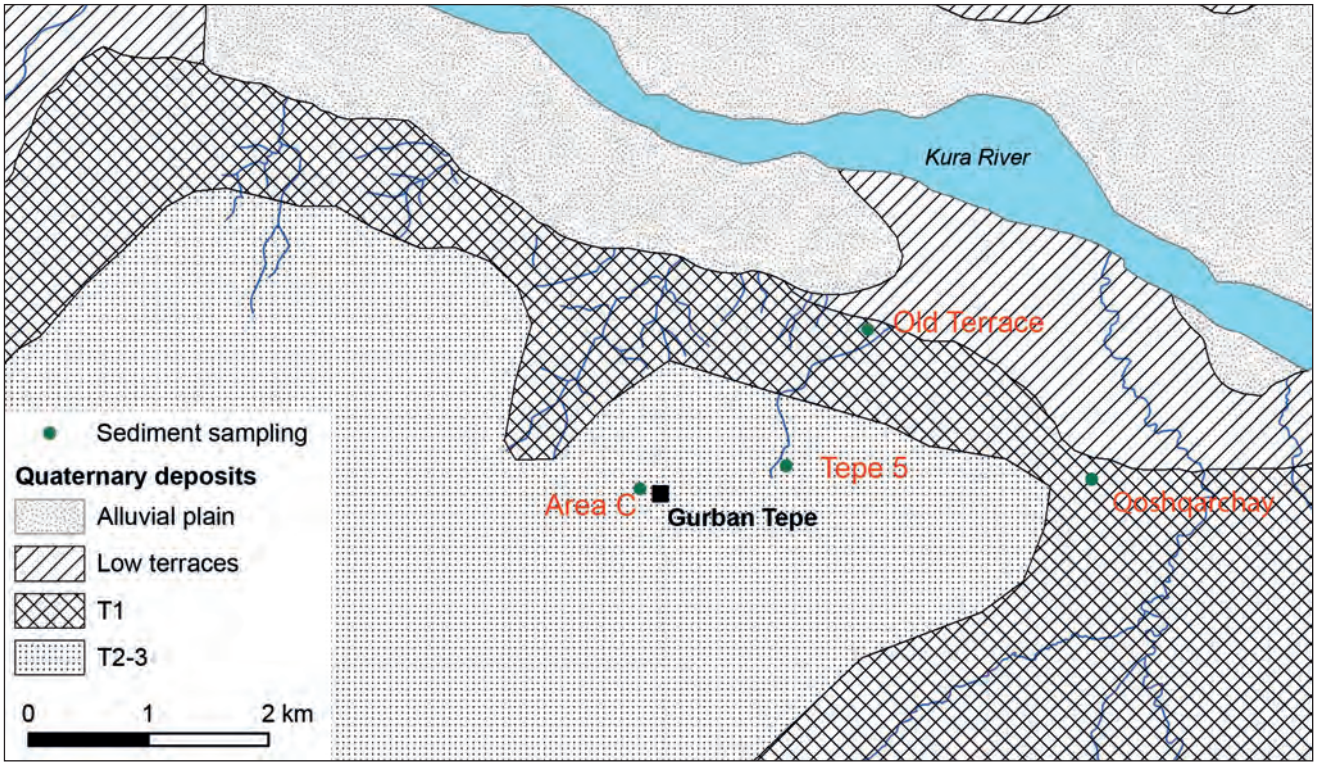

Fig. 302. The location of clay samples from the vicinity of Tepe 5

lighter elements such as Na, Ca and K (Sawyer 1986: 87–89). The higher the relation of Rb to Sr or the amount of Al_2O_3 in sediments, the higher the grade of weathering (Nesbitt et al. 1980: 1665). High values of Al_2O_3 should therefore correspond to clays identified as kaolinites or gypsum (Kibaroğlu 2008: 24). High Al_2O_3 and relatively low SiO_2 concentrations nearing a ratio of 1:2 are characteristic for those clays. Sediments with high SiO_2 but low Al_2O_3 concentrations in a ratio of about 4:1 and often increased K_2O-, MgO- and Fe_2O_3-values are instead suggestive of smectites. Illites are characterized by an Al_2O_3/SiO_2 ratio of 1:6 with higher K_2O- as MgO- (Rice 1987: 45. 47–48) and often also B-values (Heling 1988: 218). Kaolinites often derive from alkaline felsic rocks like granites (Rice 1987: 45), smectites from basic volcanic rocks like basalts (Robert/Bousquet 2018: 126), while illites form in deep water or through the process of diagenesis (Heling 1988: 218).

Rare earth elements and trace elements are stable even under wet conditions, which makes them very important for the identification of clay sources (McLennan et al. 1990: 2020–2022) and their matching to locally produced pottery. Experiments have shown that fine-grained clay sediments are best suited to identify the source rock (Nesbitt et al. 1990: 121). Elemental proportions are often used to identify the lithology of the source rocks (Wronkiewicz/Condie 1987: 2413). La, high Th and Rb values are mostly common in felsic rocks, low Cr/Th and Co/Th values can be attributed to granitic rocks, high Cr/Th values to mafic or ultra-mafic source rocks. For the latter higher Sc, Co, Cr and Ni, low Th/Sc, La/Sc, V/Ni and high Ni/Co or Cr/V values are characteristic, too (McLennan 2001: 2–7. 11–21).

As clays are ubiquitous raw materials used for mudbricks and pottery, the raw material is mostly procured from local clay sources around settlements. Choosing the raw material is linked to environmental parameters but limited by cultural, technological and social factors (Ollivier et al. 2016: 92). Clay minerals are mostly found in young fine-grained sediments of Tertiary and Quaternary deposits (Kibaroğlu 2008: 19). These minerals have a lamellar structure and care called aluminosilicates (Rice 1987: 40–50) as they are a product of weathering processes of silicate rocks like feldspar, amphibole, mica, olivine or pyroxene (Albarède 2003: 19). Clays, which consist of clay minerals, are formed under different conditions. Following their areas of deposition, they can be grouped into lake, fluvial, marine, and shallow marine clays. The most important property of clays – their plasticity – depends on the grain size of the clay. Therefore, clays with finer particles such as smectite have a higher plasticity than coarser grained clays like kaolinite. By adding temper some properties like form stability, fire resistance, etc. can be enhanced (Rice 1987: 58–60. 72. 74).

soil sample	no.	SiO_2	Al_2O_3	Fe_2O_3	MgO	CaO	K_2O	Cr/Th	La/Sc	V/Ni	Th/Sc
C Section East Level 01	1	63.0	12.7	9.8	3.3	7.3	2.6	13.4	7.0	1.2	0.2
Dara Yatax 02	2	52.5	13.1	6.8	3.3	21.5	2.0	4.4	7.1	1.4	0.4
Dara Yatax 03	3	62.8	15.6	7.1	4.3	6.8	2.2	11.0	9.7	1.8	0.6
Dara Yatax 04	4	61.4	14.7	7.2	4.4	9.0	2.2	7.3	10.6	1.5	0.6
Dara Yatax 05	5	61.1	15.2	7.0	5.7	7.7	2.2	9.4	11.7	1.3	0.6
Gurban BP001	6	56.0	18.5	6.5	9.0	7.3	1.8	—	12.4	0.8	—
Gurban P01	7	54.4	17.4	6.4	9.0	8.3	3.3	42.5	6.6	0.8	0.1
Gurban P02	8	49.9	15.5	5.1	15.8	7.3	5.5	—	—	1.7	—
Gurban P03	9	54.1	16.8	6.9	10.4	8.0	2.9	44.5	5.4	0.8	0.1
Gurban P04	10	56.8	15.8	6.3	7.5	9.6	2.9	41.0	9.6	0.8	0.1
Gurban P05	11	55.9	17.3	6.5	8.0	9.1	2.2	42.0	7.7	0.9	0.1
Gurban P06	12	56.5	18.0	6.7	7.4	8.5	1.9	36.0	2.7	1.0	0.1
Gurban side hall 01	13	58.5	15.9	6.8	5.9	9.8	2.2	59.0	10.5	0.7	0.1
Gurban side hall 02	14	60.6	12.5	8.1	5.0	10.1	2.5	—	1.8	1.0	0.0
Kura 01	15	60.7	16.0	6.0	4.4	9.7	2.4	4.6	8.5	1.6	0.5
Kura 02	16	62.5	18.0	6.5	4.9	4.8	2.3	6.2	12.2	2.3	0.7
Kura 03	17	64.2	16.5	7.0	4.7	4.8	1.8	9.5	14.3	1.8	0.5
Kura 05	18	62.9	15.9	7.5	4.0	7.5	1.3	12.8	10.0	1.9	0.5
Kura Old Terrace Level 01	19	61.0	13.7	9.0	3.7	9.6	1.9	11.3	2.4	1.6	0.2
Qoshqarchay Terrace Level 07	20	61.7	12.4	8.6	3.4	10.2	2.5	16.6	3.7	1.3	0.2
Shamkirchay 03	21	61.3	18.2	7.3	5.4	5.2	1.4	21.6	2.1	2.4	0.5
Shishtepe East 01	22	58.1	15.9	6.9	3.9	12.5	1.8	3.4	5.9	1.4	0.3
Shishtepe West 01	23	60.5	15.2	7.2	3.7	10.4	2.2	4.4	9.8	1.9	0.7
Shishtepe West 02	24	61.5	17.8	5.6	4.5	7.6	2.0	9.2	3.9	3.3	0.6
Tepe 5 04	25	53.4	15.4	5.6	6.4	16.3	2.0	3.1	1.1	2.4	0.3
Tepe 5 06	26	59.2	16.6	6.8	5.2	8.9	2.3	5.4	14.4	1.7	0.7
Tepe 5 10	27	61.1	13.5	8.2	4.2	9.4	2.7	11.7	5.3	1.3	0.3
Tepe 5 11	28	53.5	10.5	7.6	3.2	21.9	2.5	12.2	2.0	1.4	0.1
Zayamchay 08	29	61.1	16.0	7.6	2.6	10.0	1.7	3.2	—	2.8	—
Zayamchay 09	30	60.1	20.0	9.1	4.5	3.2	1.8	13.8	10.1	3.9	0.5

Table 34. List of chemical values of the clay samples discussed in this study

VII.1.4.1 Dataset

To understand the geological situation of Tepe 5, 74 samples of soils, rocks and sands were collected in the Shamkir region in the years 2017 and 2018. These samples can be used to identify the chemical composition of the local soils and pebbles but also recent changes in the soil due to human activities like ploughing and fertilization. Here, 30 clay samples are discussed as they represent the potential clay sources for the pottery of Tepe 5 (Table 34). The soil samples were collected during geological surveys with wooden tools and stored in plastic zipper bags. After at least a week of open-air drying, the analyses with p-XRF were performed by placing representative samples of at least one centimetre thickness of each sample on a Mylar foil directly above the measurement window.

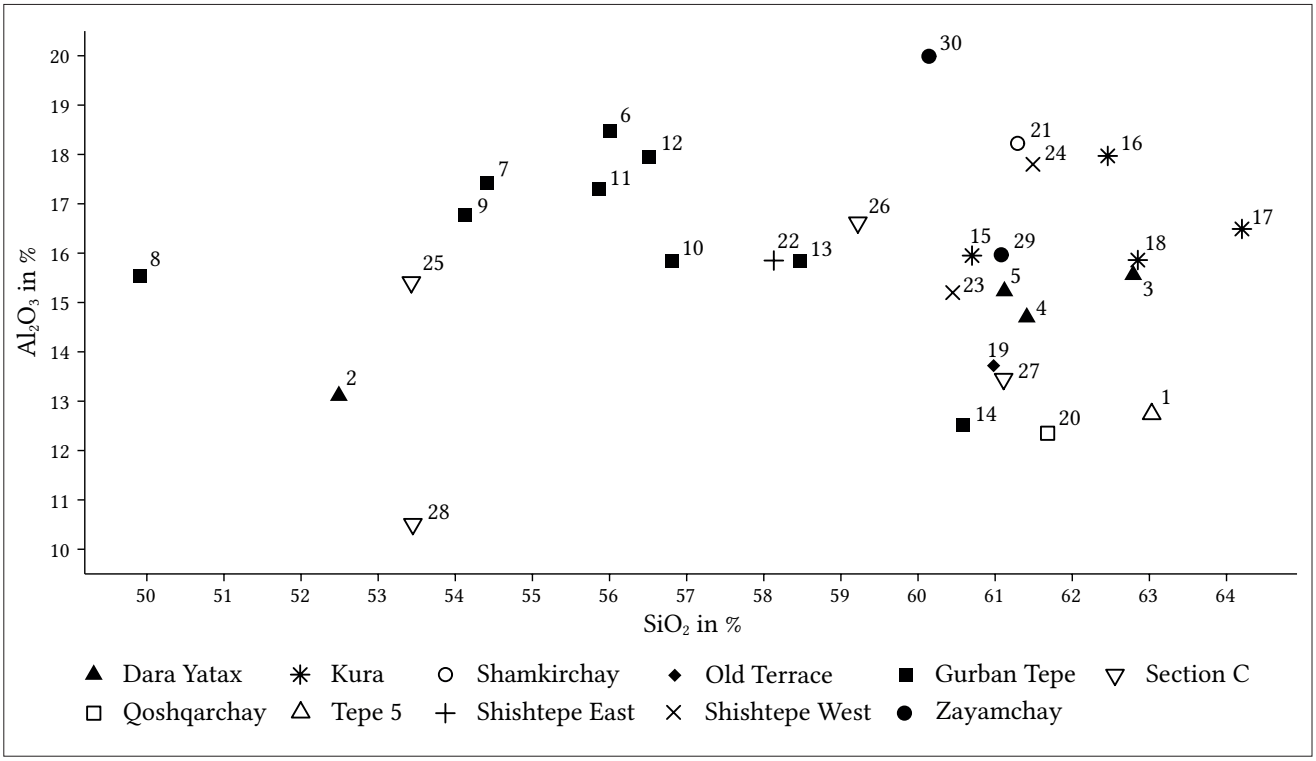

Fig. 303. Tepe 5. Scatterplot of clay samples (n=30) showing SiO_2-Al_2O_3-ratio. The SiO_2-Al_2O_3-values of our clay samples place them in the Smectite group (for the sample numbers see Table 34)

In 2017, four locations in the vicinity of Karacamirli were sampled (Fig. 302). The »Kura Old Terrace«, situated about 2 km northeast of Tepe 5, which potentially dates to the Lower Pleistocene, is characterized by powdery white soils which can be found on the northern bank of the Kura River as well. Eight different layers (Kura Old Terrace Levels 01-08) were documented and sampled. The »Qoshqarchay« sampling location lies about 1 km east of Tepe 5 at the Kura tributary of the same name (Fig. 302). Its eight layers (Qoshqarchay 01-07, 07b) of grey and black sands reflect the typical Kura River activity. Four soil samples (C Section East Levels 01–04) were taken at the western gate of the Achaemenid palace complex in Area C. The upper three sedimentary layers were radiocarbon-dated to the modern period. Therefore, the clay layer of the uppermost Level 1 (Levels 2–4 are non-clay-layers) was excluded as a possible source for all pottery from Tepe 5 (Chambrade/Metz 2017: 4–6). Two samples were taken from the refill of KG-057 and KG-090, which were subsequently relabelled Tepe 5 10 (KG-057) and Tepe 5 11 (KG-090). Two additional soil samples come from the upper two levels of Gurban Tepe »Seitensaal« (Gurban side hall 01–02). These were excluded for all analyses except the Late Antique period as they derive from levels which formed after the Achaemenid period.

In 2018 additional samples were taken from the excavation areas of Karacamirli. Seven more soil samples were taken from a profile at Tepe 5 (Tepe 5 01–07) close to the middle of the hillock, starting from an altitude of 173.90 m and extending to a depth of about 172.50 m. Samples were collected at intervals of 10 to 20 cm. From Gurban Tepe clay sediments (Gurban BP001) and six soil samples – four from the »Audienzsaal« (Audience chamber, R.IX) and two of room R.XXI – were taken. In room R.IX the upper three (Gurban P01–03) and the lowest level (P04), in R.XXI the first (P05) and the last stratum (P06) were sampled. These samples, as the ones from 2017, were only used for the analysis of the post-Achaemenid pottery as these sediments postdate all other periods discussed in this paper. During the excavations at Dara Yatax, two soils samples were taken from context KG-106 (Dara Yatax 01–02), one from natural soil (Dara Yatax 03), one from context KG-158 (Dara Yatax 04) and one from context KG-133 (Dara Yatax 05). Dara Yatax 02 and 03 are included in this study as they are samples of the natural surrounding clay. Samples Dara Yatax 04 and 05 represent quick refillings with natural soil and are therefore included, too.

During a second geological survey in the environs of Karacamirli (Fig. 301), soil samples were collected about 25 km south-west of Tepe 5, at Shishtepe West (Shishtepe

West 01–02). In the riverbed of the Shamkirchay about 8 km west of Tepe 5, five samples of pebbles and soils were taken (Shamkirchay 01–05). About 35 km west of Tepe 5 in the riverbed of the Zayamchay nine more samples were taken, of which only two are relevant for this paper – the Holocene silty fan sediments (Zayamchay 09) and the Pleistocene-Late Glacial sediments (Zayamchay 08). On the southern banks of the Kura, about 7.5 km north-west of Tepe 5, six soil samples were taken (Kura 01–06).

As mentioned previously, to identify the possible clay sources for the pottery of Tepe 5, only clay sediments were included in the analysis for all archaeological periods (Table 34). All discussions about possible sources are therefore limited to these samples and it cannot be ruled out, that other sources which are not included in this dataset could provide a better match.

VII.1.4.2 Comments on the chemistry

All clay samples used in this article show SiO_2-Al_2O_3/MgO ratios of about 4:1 which places them in the Smectite-group (Fig. 303). Quite high Fe_2O_3-, CaO- and MgO-values (Fig. 304) are indicative of mafic or ultra-mafic source rocks (see for example, Drief/Nieto 2000: 673–675), which fits well with an interpretation of those clays being part of the Smectite-group.

The assumption of mafic or ultra-mafic bedrocks is supported by quite high Cr/Th- (up to 59) but low La/Sc- (0–14.4), V/Ni- (0–4.4) and Th/Sc-values (0–0.7) of the samples. Interestingly, the more recently formed soils of Gurban Tepe show the highest Cr/Th-values and the lowest Th/Sc- and V/Ni-values (Table 34). The Holocene silty fan sediments of Zayamchay 9 seem to correspond with the silty sediments of Kura 02 and 03 as with Shamkirchay

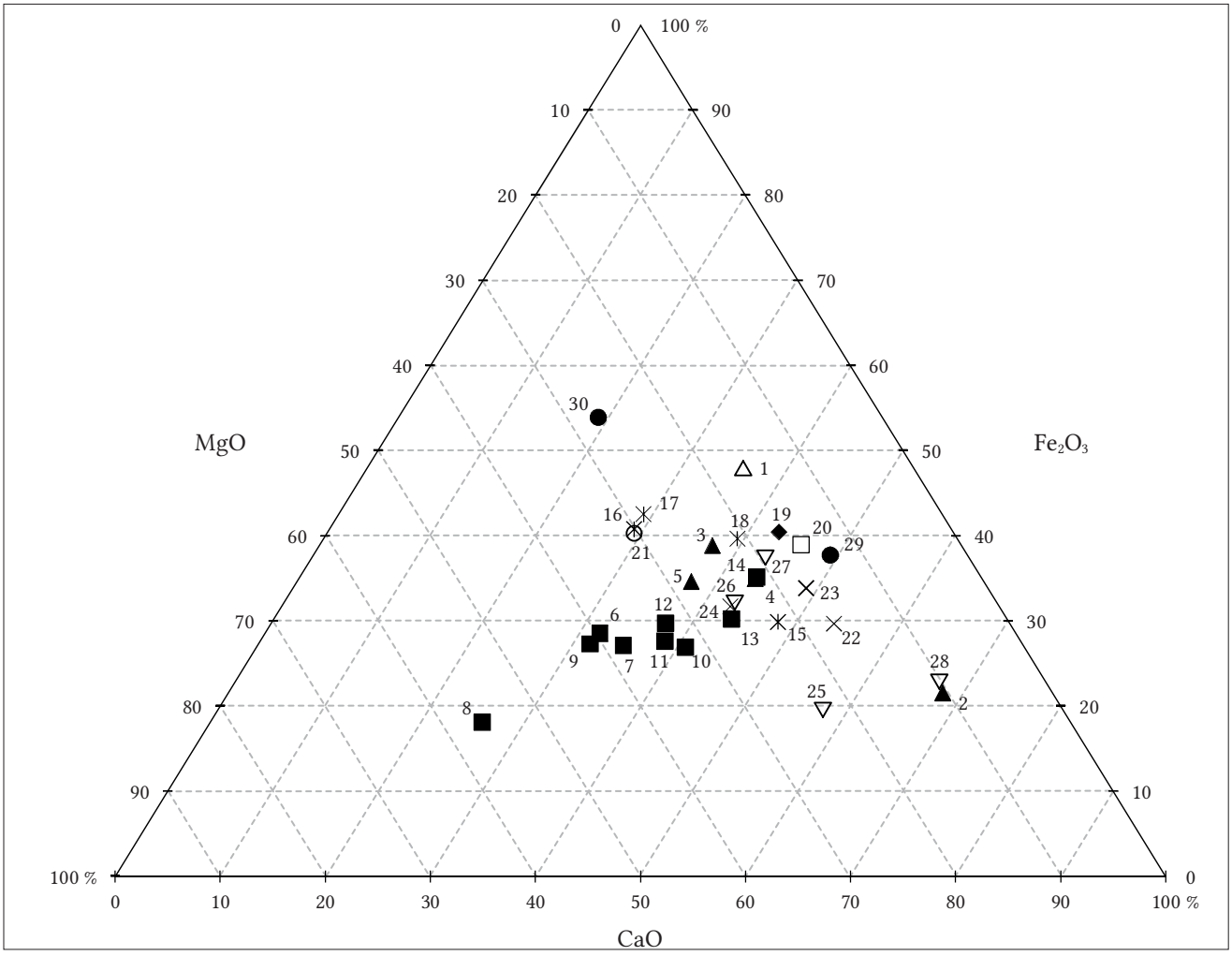

Fig. 304. Tepe 5. Ternary plot of soil samples (n=30) showing Fe_2O_3-, CaO-, and MgO-ratio. The high values are indicative of mafic or ultra mafic source rocks and therefore support the interpretation as clays of the Smectite group

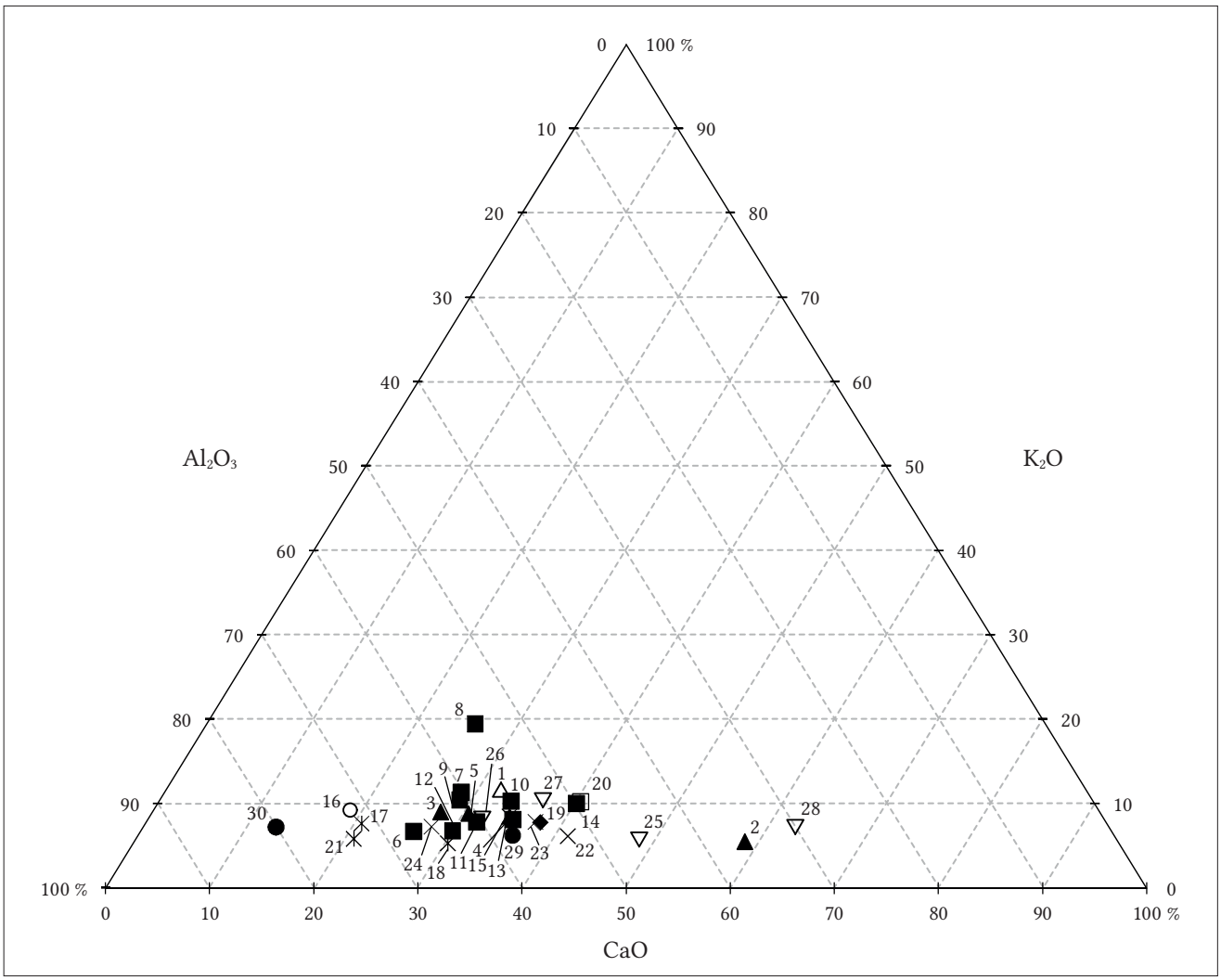

Fig. 305. Tepe 5. Ternary plot of pottery samples (n=30) showing Al_2O_3-, K_2O-, and CaO-ratio. The sediments of the Holocene silty fan belonging to Zayamchay (no. 30), Kura (no. 16, 17), and Shamkirchay (no. 21) seem to be subject to the same formation process

03 in their Al_2O_3-K_2O-CaO-values and might have been subject to the same formation process (Fig. 305).

VII.2 Pottery

Pottery is the most abundant category of material remains archaeologists can use to develop chronologically or regionally meaningful groupings of the archaeological record. Pottery is very resistant to change and modification in form and style while being in the ground. The characteristic features of pottery – style, form, ornaments, fabric, etc. (Pillay et al. 2000: 53) – are used to interpret production and exchange systems but also the social structure of ancient societies. In recent years these classic archaeological methods are supplemented with archaeometric methods such as XRF-analysis (Helfert 2013: 15–16).

The life-cycle of pottery can be divided into four stages: clay mining, production, usage, deposition (Jordan/Zvelebil 2011: 62–68). With archaeometric methods information about all these stages can be gathered. Chemical analysis can be used to identify the potters' paste, processes of production but also the clay source (Behrendt et al. 2012: 107). The chemical fingerprint, i. e. the chemical composition of pottery, enables us to build groups with comparable chemistry. It is important to keep in mind that elemental concentrations can vary in one and the same clay source and that they can be altered by levigation, the addition of temper or the mixing of clays. By levigation, remains weathering can be removed which results in different amounts of Ca, P, Rb or K when comparing the clay source and the pottery produced from it (Mommsen 2007: 183. 186. 188). High amounts of quartz sand or calcite sand temper can also influence the percentages of the main elements (Helfert

2010: 152). In many studies the presence or absence of CaO is the main criterion to divide fabric types and clay sources but pottery with high or low CaO values often occurs in the same period and in the same fabric types (Noll 1991: 23). Nonetheless, main elements are used to inform about the production (Ramminger et al. 2010: 60); less mobile elements (trace elements) are better suited to discuss clay sources (Mommsen 2007: 179). Some element concentrations such as Cs, Ca, Rb, K and Na are strongly affected by the conditions in the soil they are deposited in and by high humidity (Trąbska/Trybalska 2010: 45). To reduce the possibility of misidentification multiple measurements of the same sample are advisable (Mecking et al. 2013: 61).

VII.2.1 The Pottery of Tepe 5

Interments were made at Karacamirli Tepe 5 during three episodes: the Late Bronze/Early Iron Age, in Late Antiquity and the Middle Ages (see ch. IV). Prior to its use as a burial ground, the place had been used by a Chalcolithic population. Of this time, however, only few pits remained (see ch. III). The chemical specifics of the Tepe 5 pottery will be discussed in the following in chronological order. A table summarizing all pottery analyses is appended to this chapter (Table 35).

VII.2.1.1 Results of p-XRF analyses

Early Chalcolithic pottery (5th mill. BC)

The 21 analysed Early Chalcolithic pottery sherds from Tepe 5 date to Mentesh Tepe Periods II (first half of the 5th mill. BC) and III (second half of the 5th mill. BC) (see ch. III). They show a reddish-brown fabric with medium to coarse temper. Based on their Rb/Sr-values (Fig. 306) four chemical groups and two single sherds (Groups 6 and 6) can be identified for this period. The potteries' chemical distinctions are linked to different geological and/or technological features: 1) naturally mica- and pyrite-rich deltaic clay source, 2) mixture of local at least partly mica-rich clay sources with calcite temper 3) naturally lime-rich local clay source with a high amount of plant temper 4) a mixture of local clay sources with quartz-sand temper.

All groups were vegetable-tempered with the highest amount visible in Group 3. This kind of temper has no direct influence on our results as it mainly consists of elements like carbon and oxygen which are not detectable with the pXRF-method. Indirectly, the so called »balance« calculated by the Niton XL3t software gives an impression how much uncounted information – such as undetectable elements, mainly oxygen – is calculated by the device's algorithm for the measurement. The higher

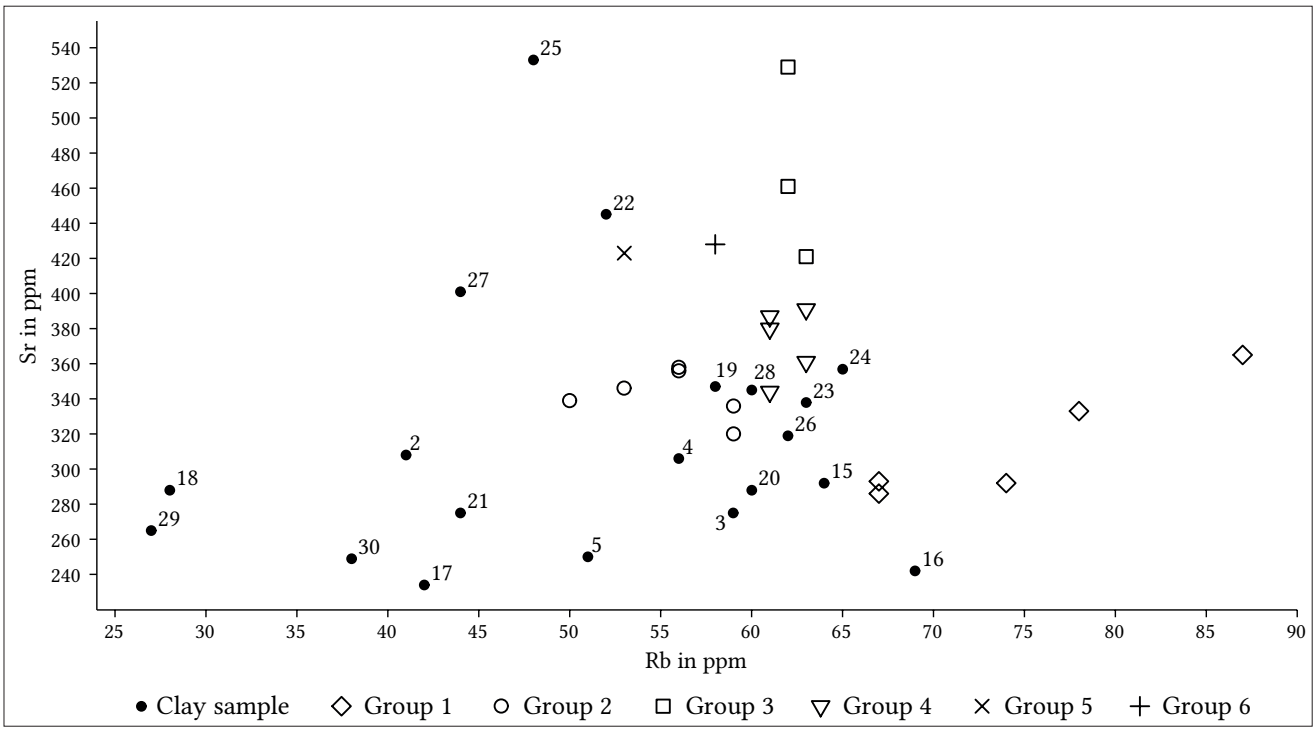

Fig. 306. Tepe 5. Scatterplot of Early Chalcolithic pottery samples (n=21) and clay samples (n=20) showing Rb/Sr-ratio. Based on their Rb- and Sr-values, four Groups (Group 1 to 4) and two single sherds (Groups 5 and 6) can be identified for the Early Chalcolithic pottery

Sample	Period	Fabric	Context		Chem. Group	SiO_2	TiO_2	Al_2O_3	Fe_2O_3	MnO	MgO	CaO	K_2O	P_2O_5	S	Cl	Sc	V
0393-01	Ant	233	KG-066	B. 26	ANT	58.80	0.69	13.81	9.43	0.27	3.22	9.87	3.71	0.21	16036	30646	72	96
0419-01	Ant	242	KG-057	B. 23	ANT	56.85	0.62	11.59	8.77	0.23	4.41	14.01	3.28	0.25	39492	34267	72	83
0472-01	Ant	232	KG-097	B. 27	ANT	57.41	0.85	11.62	9.31	0.19	4.44	11.89	3.97	0.33	42176	16150	72	95
0045-01	EC	213	KG-016	pit fill	EC 3	61.24	0.62	11.04	8.46	0.36	2.61	12.39	3.03	0.25	3428	2502	76	87
0045-05	EC	514	KG-016	pit fill	EC 3	63.39	0.58	10.28	8.39	0.15	1.66	12.64	2.74	0.16	20259	3417	39	88
0049-03	EC	224	KG-018	pit fill	EC 1	59.73	0.60	13.26	7.89	0.18	3.63	11.02	2.08	1.61	4332	4140	54	95
0049-04	EC	223	KG-018	pit fill	EC 1	61.77	0.57	12.27	8.55	0.17	2.46	11.15	2.77	0.30	26638	3798	32	93
0049-05	EC	523	KG-018	pit fill	EC 4	60.53	0.69	13.87	7.04	0.17	4.27	10.25	2.97	0.20	34635	2885	67	103
0049-08	EC	223	KG-018	pit fill	EC 1	63.65	0.56	13.76	9.65	0.19	2.92	5.90	3.08	0.30	9809	5760	43	96
0049-09	EC	224	KG-018	pit fill	EC 1	61.70	0.62	14.56	9.38	0.19	3.67	6.81	2.79	0.27	7564	4992	56	100
0127-01	EC	223	KG-033	subsoil	EC 4	63.91	0.44	13.16	8.21	0.22	2.20	8.75	2.89	0.23	7152	4616	44	76
0127-02	EC	223	KG-033	subsoil	EC 3	63.21	0.73	13.86	7.64	0.31	4.31	6.52	3.15	0.27	19391	3201	49	101
0127-05	EC	221	KG-033	subsoil	EC 5	64.80	0.61	11.70	7.66	0.14	2.64	9.67	2.45	0.33	4955	2193	61	92
0127-06	EC	223	KG-033	subsoil	EC 1	62.24	0.52	14.00	7.85	0.18	3.78	8.81	2.43	0.19	3769	8969	44	92
0196-01	EC	223	KG-049	pit fill	EC 2	59.68	0.61	15.61	9.08	0.17	4.59	7.37	2.56	0.33	8838	9881	66	109
0196-02	EC	524	KG-049	pit fill	EC 2	62.38	0.63	14.41	9.04	0.17	3.24	6.69	3.17	0.27	20538	5285	37	102
0196-04	EC	523	KG-049	pit fill	EC 2	62.53	0.65	12.37	8.67	0.20	2.91	9.85	2.53	0.31	1130	1715	49	96
0196-05	EC	523	KG-049	pit fill	EC 2	58.43	0.78	13.81	8.89	0.19	3.57	11.77	2.24	0.33	31033	4175	69	114
0220-07	EC	214	KG-054	topsoil	EC 2	63.23	0.53	14.35	7.73	0.16	4.07	6.97	2.70	0.26	10057	8998	23	84
0229-01	EC	214	KG-056	pit fill	EC 2	61.78	0.68	12.95	9.19	0.18	4.05	7.90	3.01	0.26	1183	1480	35	97
0229-04	EC	213	KG-056	pit fill	EC 6	66.30	0.64	12.50	7.88	0.14	2.94	6.65	2.68	0.28	1303	2447	53	97
0229-05	EC	533	KG-056	pit fill	EC 4	62.63	0.53	13.97	9.33	0.28	2.48	7.62	2.95	0.21	1890	1597	50	85
0229-06	EC	533	KG-056	pit fill	EC 4	63.14	0.71	13.46	7.94	0.14	3.31	8.83	2.24	0.23	1779	2792	38	103
0229-07	EC	533	KG-056	pit fill	EC 4	64.38	0.66	13.17	7.50	0.13	2.89	8.64	2.33	0.30	8950	2451	48	99
0036-02	EIA	633	KG-015	subsoil	EIA 4	65.36	0.78	15.06	7.53	0.11	28.0	5.08	3.05	0.22	1106	1975	0	113
0144-02	EIA	434	KG-032	B. 13	EIA 2	62.70	0.77	14.92	8.58	0.18	3.93	5.99	2.74	2.00	3925	2284	59	111
0144-04	EIA	434	KG-032	B. 13	EIA 2	67.25	0.65	12.29	9.97	0.16	1.59	4.77	3.08	0.24	8297	19542	22	84
0144-06	EIA	622	KG-032	B. 13	EIA 1	68.42	0.86	15.06	7.11	0.06	2.43	3.31	26.0	0.15	10692	1485	25	116
0144-07	EIA	633	KG-032	B. 13	EIA 3	64.29	0.72	13.39	9.06	0.14	3.08	6.29	2.79	0.25	14486	1995	27	103
0221-01	EIA	133	KG-077	B. 16	EIA 2	63.84	0.67	15.58	7.99	0.13	2.98	5.83	2.69	3.00	700	1810	43	105
0221-02	EIA	422	KG-077	B. 16	EIA 4	69.32	0.79	12.64	8.81	0.09	28.0	2.65	2.58	0.33	1835	1599	16	114
0241-01	EIA	123	KG-058	B. 15	EIA 4	63.58	7.00	13.38	9.38	0.24	2.93	6.47	3.00	0.33	2811	1776	34	101
0241-02	EIA	623	KG-058	B. 8	EIA 4	67.84	0.87	14.21	8.46	0.09	3.64	2.33	24.0	0.15	883	2185	16	119
0241-03	EIA	623	KG-058	B. 15	EIA 1	70.28	0.64	12.31	9.62	0.15	1.46	2.28	2.99	0.27	5165	768	14	93
0241-04	EIA	623	KG-058	B. 15	EIA 3	62.68	0.64	14.53	8.06	0.19	3.99	7.21	2.49	0.22	2562	2088	50	106
0241-05	EIA	623	KG-058	B. 15	EIA 1	63.54	0.66	14.60	7.62	0.13	3.73	7.02	2.46	0.24	7714	1854	35	108
0241-06	EIA	623	KG-058	B. 15	EIA 1	62.76	0.75	13.27	88.0	0.16	31.0	7.98	2.89	0.28	16132	1710	41	103
0241-07	EIA	634	KG-058	B. 15	EIA 3	66.56	0.54	15.40	9.23	0.12	2.25	1.95	3.63	0.32	11022	2685	0	95
0252-01	EIA	132	KG-059	B. 14	EIA 5	65.28	0.66	12.42	11.59	0.15	2.55	3.98	3.13	0.25	20525	10213	10	97
0252-02	EIA	423	KG-059	B. 14	EIA 4	65.79	7.00	10.97	9.85	0.22	2.00	7.11	3.03	0.32	669	835	56	95
0416-01	EIA	632	KG-057	B. 8 (?)	EIA 3	60.09	0.52	13.05	7.86	0.15	2.91	12.32	2.29	0.82	11557	3638	29	93
0417-01	EIA	133	KG-057	B. 8	EIA 3	68.67	7.00	14.70	7.64	0.07	3.01	2.44	2.53	0.24	1801	2482	26	117
0100-01	LBA	123	KG-026	B. 7	LBA 2	64.90	0.65	11.32	9.07	0.14	2.74	8.19	2.78	0.21	19566	1256	23	88
0425-01	LBA	424	KG-094	B. 1	LBA 1	65.50	0.64	16.78	7.67	0.08	4.26	2.59	2.33	0.16	6469	1512	4	115
0425-02	LBA	422	KG-094	B. 1	LBA 1	65.71	0.64	16.53	7.84	0.09	4.19	2.55	2.30	0.15	3249	1447	5	112
0498-01	LBA	122	KG-095	B. 6	LBA 1	66.45	0.74	16.19	7.35	0.18	3.47	3.01	2.44	0.16	22901	1514	0	129
0498-02	LBA	423	KG-095	B. 6	LBA 2	63.11	0.58	16.81	7.15	0.13	4.33	5.52	2.18	0.18	4894	3204	15	107
0498-03	LBA	124	KG-095	B. 6	LBA 1	64.88	0.64	17.51	7.13	0.06	4.48	2.69	2.44	0.16	16126	1706	0	122
0498-06	LBA	122	KG-095	B. 6	LBA 1	65.29	0.54	18.77	6.66	0.06	4.68	1.56	2.29	0.15	2648	2391	6	113

Table 35. List of discussed chemical values of the sampled ceramics in this study

Cr	Co	Ni	Cu	Zn	As	Rb	Sr	Y	Zr	Nb	Pd	Ag	Cd	Sn	Sb	Te	Cs	Ba	La	Ce	Hg	Pb	Th	U	Bal
116	98	75	27	101	4	141	405	27	185	13	3	18	57	24	41	203	23	566	180	57	60	24	4	13	605326
47	0	60	25	76	6	105	466	26	170	12	0	11	46	14	30	131	16	426	129	56	39	23	3	13	642981
82	161	58	27	103	1	124	297	27	173	14	2	3	16	7	12	72	10	347	100	56	25	22	3	12	657330
155	0	64	26	71	6	50	339	23	136	8	0	13	29	10	30	150	18	404	196	57	30	14	3	11	675122
180	0	74	23	69	5	56	358	23	130	7	0	12	39	17	32	150	20	427	216	57	22	15	3	10	709305
107	142	72	28	74	8	62	529	28	171	11	0	9	25	15	26	120	17	438	241	57	62	10	4	11	564083
201	0	60	24	78	6	63	421	25	170	10	0	10	40	14	28	116	16	369	165	56	26	15	0	11	606925
95	0	61	23	73	6	56	356	22	132	8	0	7	19	0	0	52	5	203	0	56	21	13	2	10	537719
210	0	64	26	97	10	74	292	25	152	9	3	10	30	13	21	114	13	338	97	56	33	19	0	11	593421
180	61	75	28	97	12	78	333	27	161	9	5	9	30	14	26	129	15	400	140	56	35	21	2	11	566660
132	43	75	31	76	12	53	346	24	113	2	7	14	62	23	42	200	22	466	146	56	13	17	1	10	689659
89	0	81	25	73	6	59	336	23	148	8	0	0	0	6	11	82	10	318	115	56	26	17	2	11	577875
154	0	60	23	69	8	61	387	24	146	10	0	6	13	7	20	97	14	339	153	57	20	13	3	11	617916
185	0	118	26	74	9	63	391	25	159	8	12	11	60	27	51	237	28	613	252	58	36	13	4	12	578053
233	0	60	27	96	12	87	365	28	165	10	8	8	21	10	10	48	6	244	0	56	43	17	0	10	464301
214	0	56	24	87	9	67	286	26	142	10	0	5	7	6	11	51	6	233	38	56	36	19	2	10	581136
151	0	73	27	73	7	61	344	26	174	10	0	5	13	9	18	98	15	382	175	57	15	19	3	11	619904
195	0	68	26	82	7	62	461	27	179	12	0	6	0	6	12	73	10	343	120	56	32	12	3	12	563081
95	0	85	25	64	0	53	423	24	157	6	5	11	43	20	39	184	20	477	143	56	15	13	2	9	615920
207	0	55	26	85	7	67	293	23	160	7	0	13	51	12	31	158	17	432	160	56	19	16	3	11	636304
149	0	70	28	77	5	63	361	25	157	9	0	9	28	11	24	111	16	389	205	57	26	17	1	11	617214
159	0	83	31	99	13	59	320	25	123	7	9	14	58	23	42	221	26	531	225	58	9	17	0	11	650423
204	0	77	25	67	5	58	428	25	162	8	0	8	21	9	20	96	11	345	87	56	19	16	3	11	558503
170	0	66	25	68	5	61	380	24	152	9	2	6	18	6	18	111	13	355	115	56	16	17	2	11	589877
90	0	76	24	89	6	92	237	24	158	12	7	0	21	10	17	93	12	355	139	56	23	22	3	12	525709
222	0	88	27	83	7	53	289	24	135	9	2	7	23	9	18	111	13	325	123	56	15	16	1	10	550584
55	0	66	22	69	0	77	347	24	148	11	0	6	12	6	11	58	7	418	51	56	35	18	2	11	746930
148	0	62	24	82	2	81	290	23	185	11	0	2	0	0	0	13	3	208	26	56	13	17	1	11	538934
82	0	63	28	87	2	70	322	26	164	10	0	14	48	16	32	168	20	460	169	57	30	20	4	11	612952
190	0	64	26	105	6	58	293	25	119	8	0	6	11	6	12	75	10	271	90	56	21	21	3	10	546913
218	0	66	26	71	3	57	235	23	157	10	0	8	37	13	25	133	16	347	146	56	28	16	0	10	616425
181	0	97	26	90	6	59	251	26	146	8	4	16	55	21	40	206	25	476	228	58	19	15	1	10	621055
247	0	59	24	75	2	57	288	22	183	10	0	5	15	6	9	50	6	228	51	56	10	17	0	10	556938
111	0	70	28	79	6	56	201	27	151	9	0	15	47	22	41	195	23	486	202	57	10	15	1	10	681876
112	0	110	24	81	7	70	318	27	172	11	0	13	43	14	26	151	18	462	164	57	22	18	2	10	50042
82	0	70	24	86	3	65	298	25	149	9	7	5	22	8	14	86	11	336	128	56	16	15	3	10	537284
108	0	78	27	95	6	66	275	24	137	8	3	9	40	15	29	157	20	427	212	57	17	18	3	11	624446
81	0	71	24	99	0	114	201	25	153	10	0	12	37	15	28	135	17	416	151	56	28	22	1	12	602953
109	59	84	27	107	0	89	296	25	195	11	10	13	52	20	40	202	24	488	210	57	33	23	1	11	669126
157	0	56	35	80	7	52	304	26	123	9	0	8	37	16	29	162	18	377	136	56	29	16	0	10	700285
78	0	78	28	66	3	64	331	30	185	10	3	8	27	9	17	100	13	327	141	57	16	17	1	10	585230
259	0	56	22	75	3	69	292	22	177	13	0	3	0	4	13	35	5	235	30	56	16	20	2	11	504699
98	0	74	26	71	0	50	253	22	133	6	0	9	27	17	28	173	23	441	291	58	13	15	0	10	705587
132	45	69	29	87	6	65	246	27	156	10	3	4	12	5	19	81	12	354	188	57	23	19	2	14	488161
108	30	70	28	87	6	64	251	26	155	10	4	5	16	6	25	108	15	393	189	57	23	19	2	13	496954
118	151	58	25	82	5	61	214	25	138	10	0	53	13	6	23	111	15	386	173	52	26	21	3	18	521811
78	0	54	29	87	7	57	307	26	132	10	0	0	5	1	5	19	3	269	117	52	36	15	2	12	463521
205	91	63	33	89	7	68	232	27	158	12	0	0	0	0	0	0	3	239	184	54	22	19	3	17	461780
96	0	71	24	85	4	67	221	25	161	11	0	0	9	4	14	66	9	293	120	52	27	21	2	8492	429690

Continued from previous page

the balance, the higher the amount of those elements. Even though all negative evidence must be handled with extreme caution, our results appear to reflect the macroscopically observed use of organic temper particularly for Group 3, which showed high balance values. Group 1 is characterized by higher Rb, Zn and Cr-values which correlate with higher Fe_2O_3 and S-values (Fig. 306, Fig. 307 and Fig. 308). This may be an indicator for the pres-

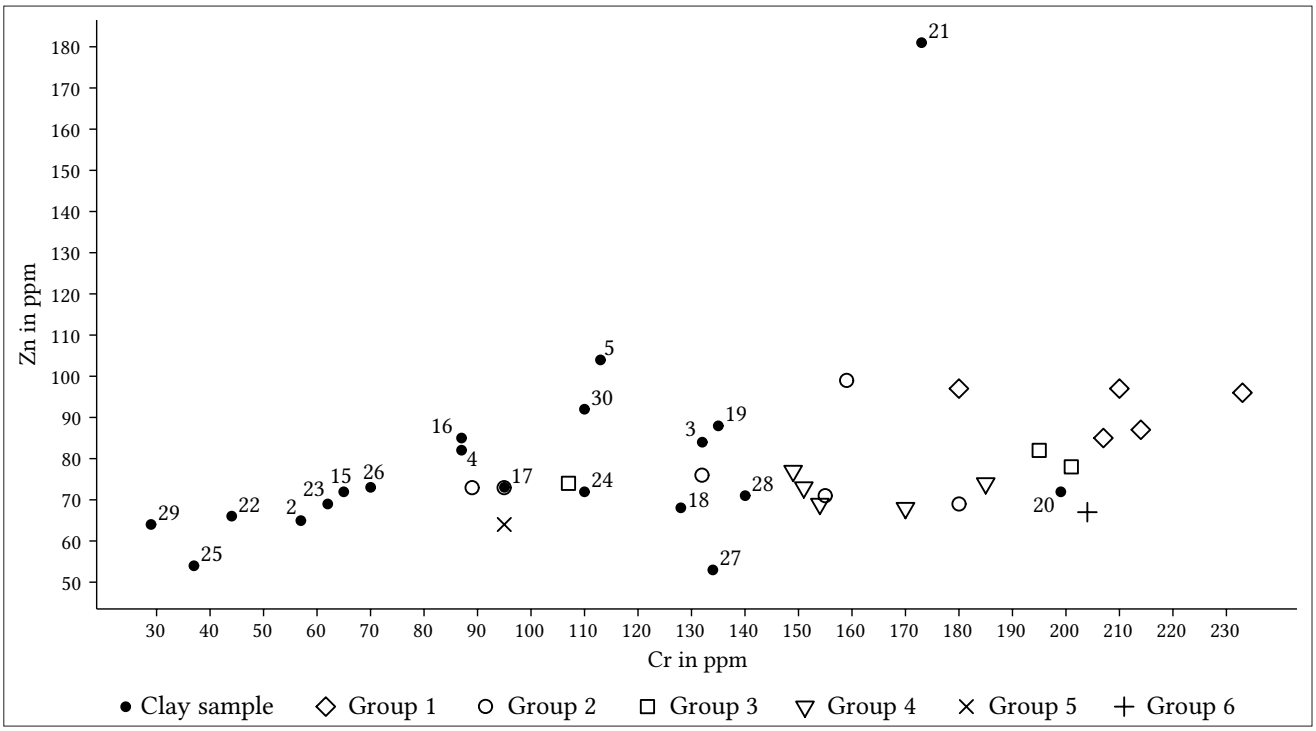

Fig. 307. Tepe 5. Scatterplot of Early Chalcolithic pottery samples (n=21) and clay samples (n=20) showing Cr-/Zn-ratio. Group 1 shows remarkably high Cr- and Zn-values

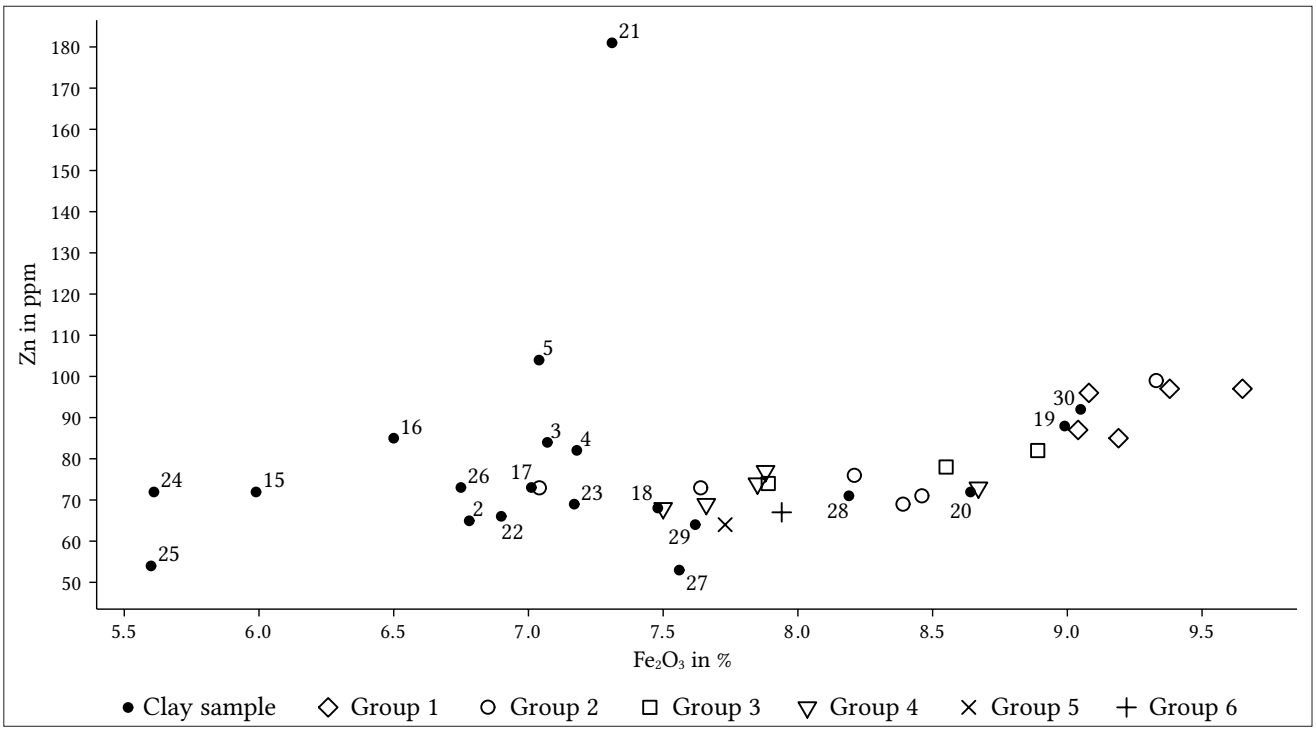

Fig. 308. Tepe 5. Scatterplot of Early Chalcolithic pottery samples (n=21) and clay samples (n=20) showing Fe_2O_3/Zn-ratio

ence of a significant amount of pyrite in the raw clay. Pyrite minerals transform into hematite minerals at a temperature of 350–500°C. Also, a high amount of pyrite minerals affecting the rate of oxidation during the firing process may have caused the ›black core effect‹ observed in all sherds of Group 1 (Bonamartini Corradi et al. 1996: 102. 105–106). Therefore, the macroscopically identified hematite in the sherds of Group 1 should be a natural inclusion, not a temper. Of the soil samples, mainly Kura 01 shows strong correspondence with Group 1, but Qoshqarchay Terrace Level 07 and Dara Yatax 03 must also be taken into account (Fig. 306). The river clays of Zayamchay could also contain a higher amount of pyrite as the river's source lies in the mountains of the Lesser Caucasus, in an area with known pyrite sources (see above), and could have carried the mineral into the clays of the Kura downstream of the Zayamchay confluence.

The use of deltaic clays – as they can be found at the confluence of Zayamchay and Kura River – is suggested by another striking feature: the laminar structure of the clay. Those laminae are normally produced by short-lived fluctuations in depositional conditions which cause variations in the content of the clay, the grain size, the amount of organic material, etc. This typically happens in deltas when huge amounts of fine sediments are periodically supplied by tributaries and rapidly deposited (Boggs 2009: 203). Therefore, it makes sense that the clay samples which resemble the low Sr-values of these sherds are mainly from rivers. Also, the Fe_2O_3- and Zn-values of the pottery which match Zayamchay 09 and Kura Old Terrace Level 01, support this interpretation (Fig. 308).

The high values of K_2O in the sherds of Groups 1 and 2 correspond with a significant amount of mica, which, according to its grain size, seems to be a natural inclusion. (Fig. 309).

With respect to their morphology, all samples in this group (0049-03, 0049-04, 0049-08, 0049-09, 0127-06) were identified as thin walled mangals (Fig. 16, 3. 8). Therefore Group 1 suggests a chronological proximity to Mentesh Tepe Period II (see ch. III) All finds derive from pit filling KG-018 or subsoil layer KG-033.

Group 2 exhibits low Zr- and Rb-values which fall mainly in the range of Dara Yatax 03, 04 and 05, Tepe 5 11, Kura 01 and Shishtepe East 01 (Fig. 310). CaO-values are relatively high in these sherds and would resemble Kura 01, Shishtepe East 01 or Dara Yatax 05 (Fig. 311) unless one would consider that Calcite temper in the sherds explained the CaO-amount. According to the relatively low Sr-values (Fig. 306), Dara Yatax 04, Tepe 5 06 and 11, Kura Old Terrace Level 01 and Qoshqarchay Terrace Level 07 offer the best matches. As samples from Dara Yatax are always chemically closely related to the sherds of Group 2 it seems likely that the clay source for Group 2 can be found locally. Probably different clays from the

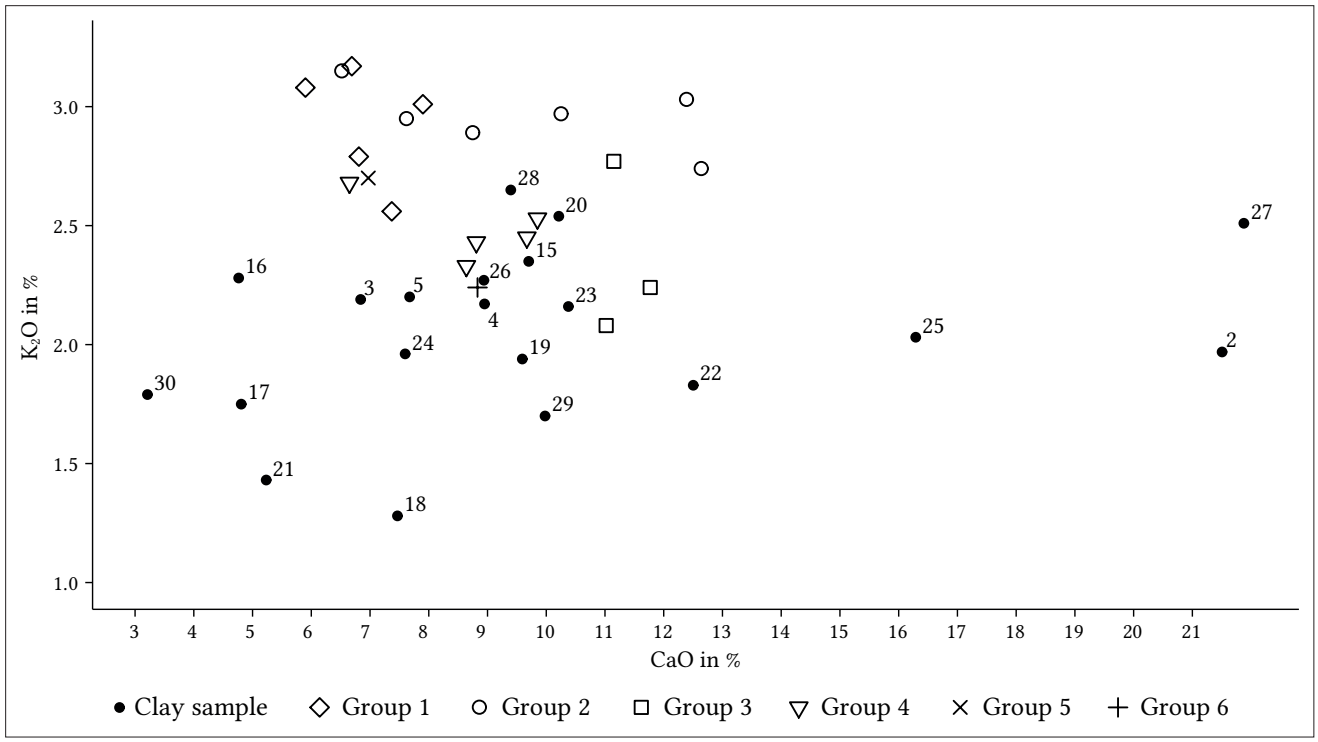

Fig. 309. Tepe 5. Scatterplot of Early Chalcolithic pottery samples (n=21) and clay samples (n=20) showing K_2O/CaO-ratio. The high K_2O-values of Group 1 and 2 correspond with the use a mica-rich clay sources

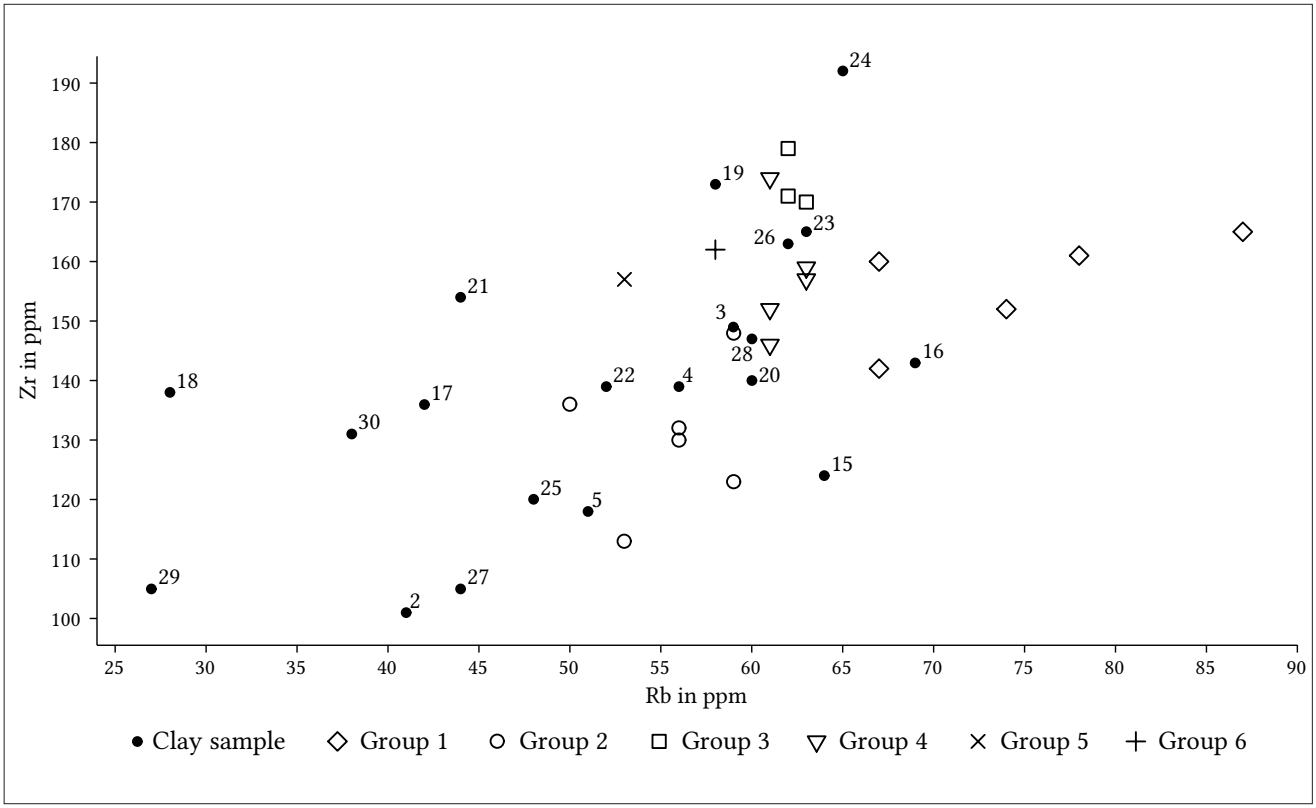

Fig. 310. Tepe 5. Scatterplot of Early Chalcolithic pottery samples (n=21) and clay samples (n=20) showing Zr/Rb-ratio. The Zr- and Rb-values of Group 2 are comparably low

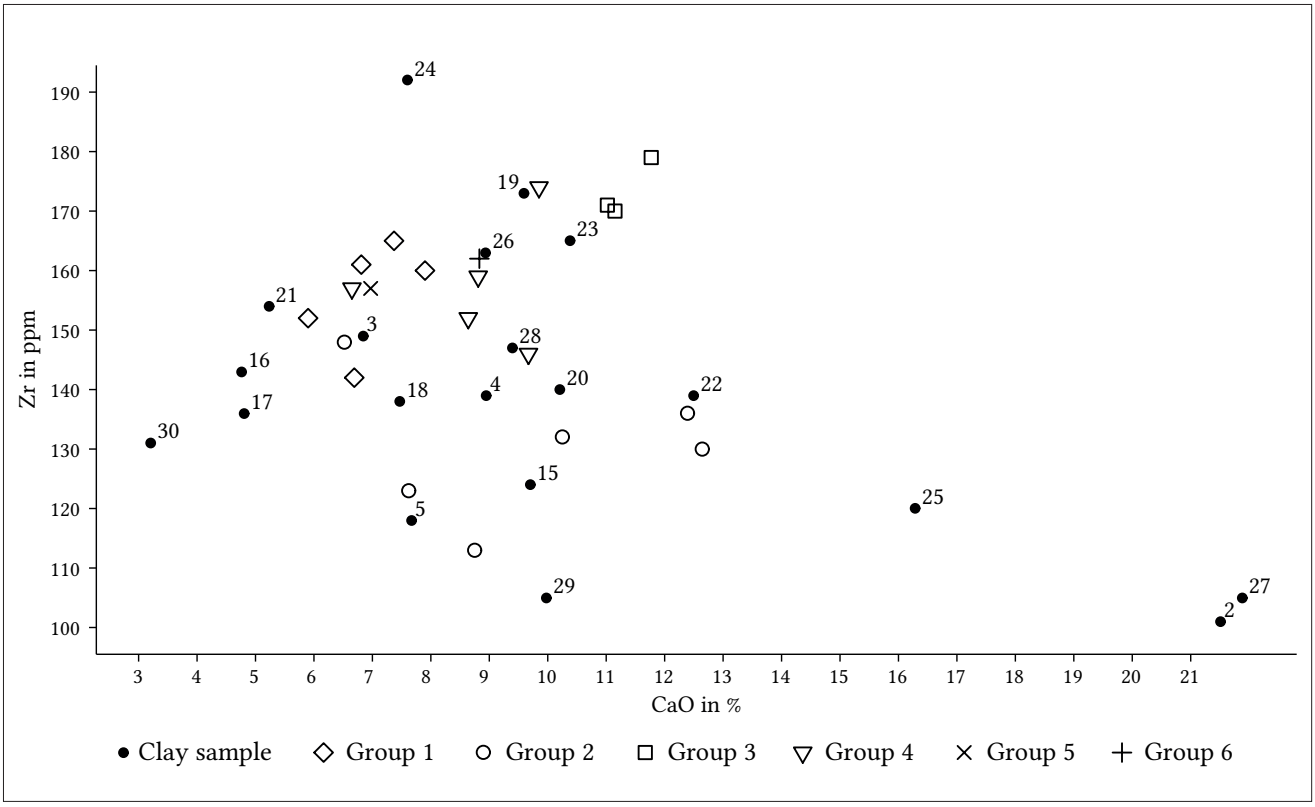

Fig. 311. Tepe 5. Scatterplot of Early Chalcolithic pottery samples (n=21) and clay samples (n=20) showing CaO/Zr-ratio. The CaO-values of Group 2 are comparably high, for Group 3 Zr-values are also increased

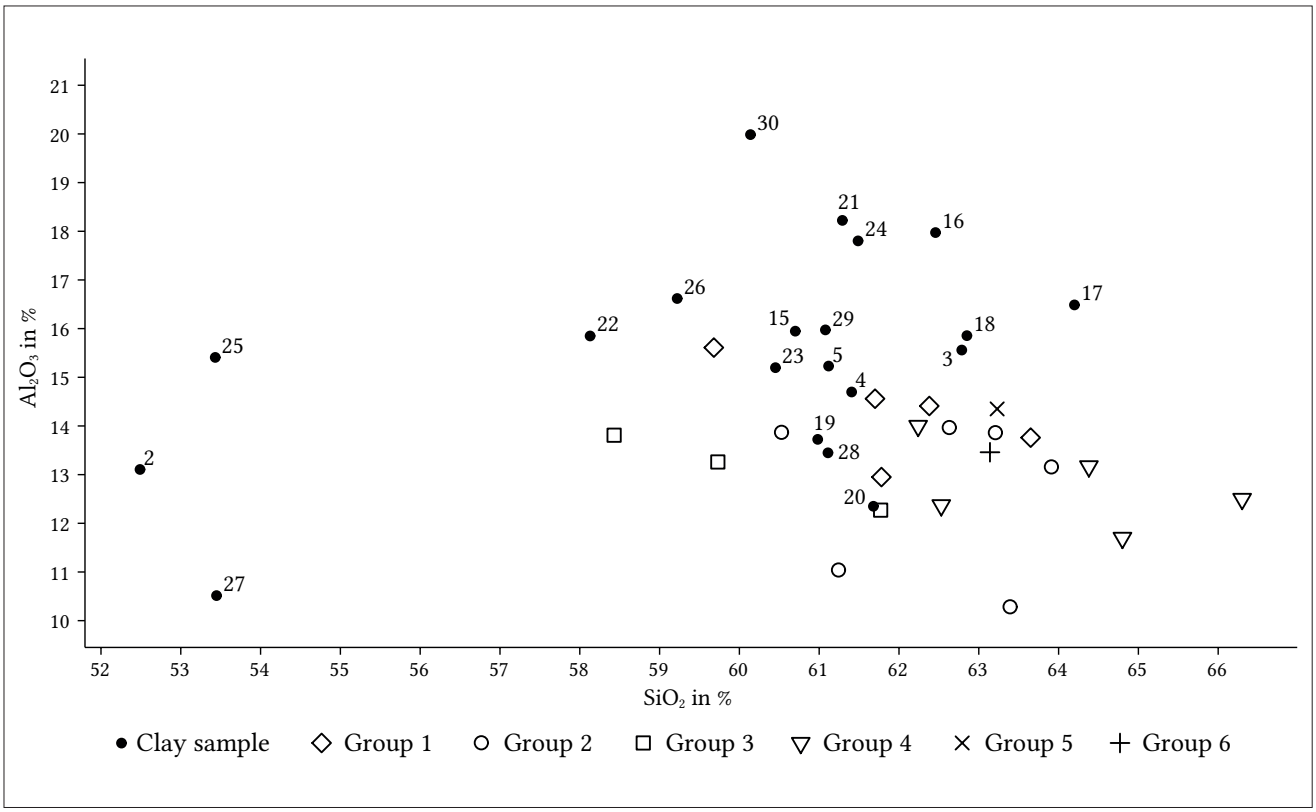

Fig. 312. Tepe 5. Scatterplot of Early Chalcolithic pottery samples (n=21) and clay samples (n=20) showing SiO_2/Al_2O_3-ratio. The Al_2O_3/SiO_2-values of Group 3 are comparably low

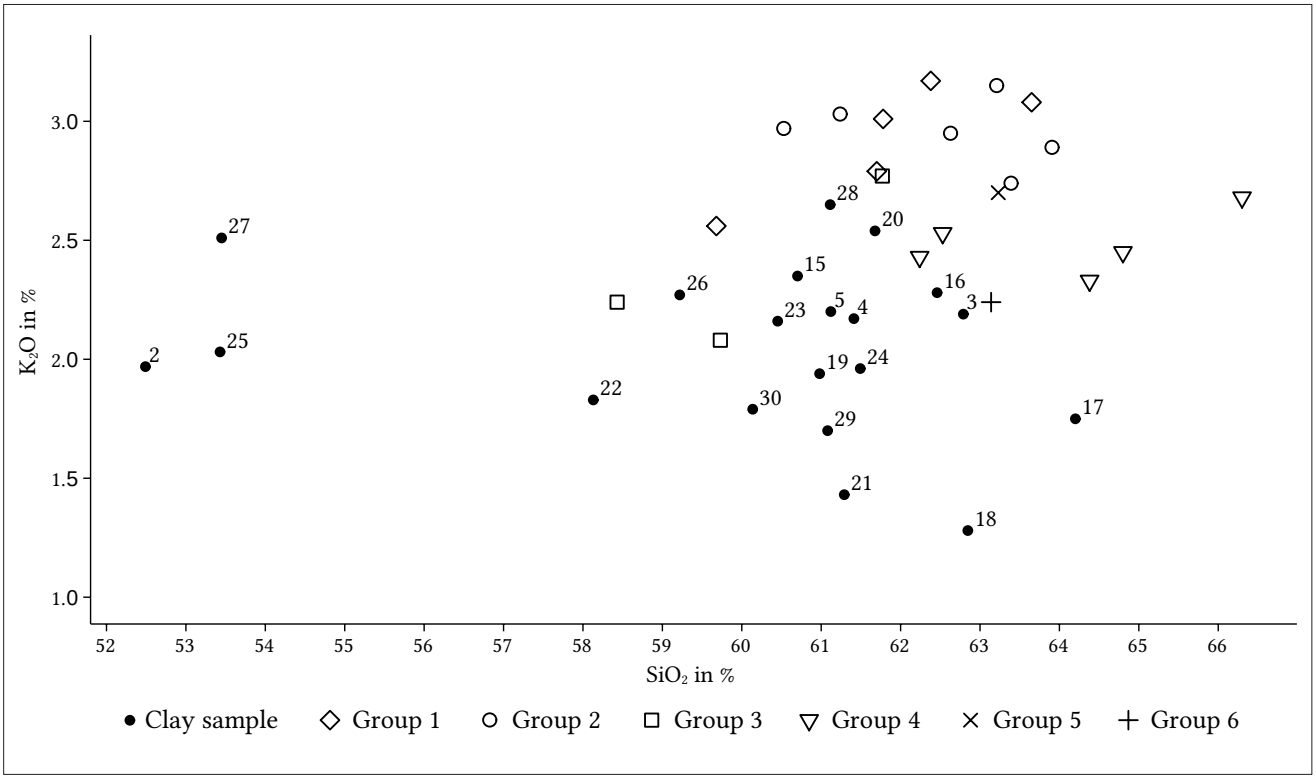

Fig. 313. Tepe 5. Scatterplot of Early Chalcolithic pottery samples (n=21) and clay samples (n=20) showing SiO_2/K_2O-ratio. Compared to the clay sources of Kura 02 (no. 16) or Dara Yatax 03 (no. 3), the SiO_2-values are increased for sherds of Group 4, probably due to the use of quartz sand temper

area of Dara Yatax were mixed to produce this pottery. Morphologically, most samples of Group 2 (0196-02, 0196-04, 0196-05, 0220-07, 0229-01) can be described as mangals with a well-smoothed surface (see for example Fig. 16, 4). An exception is the spouted vessel 0196-01 from pit KG-049 (Fig. 16, 13). All samples derive from either the rubbish pit KG-049, the topsoil layer KG-054 or context KG-056.

Group 3 displays high Zr- and CaO-values corresponding to the soil samples of Shishtepe West 01, Kura Old Terrace Level 01 but also Tepe 5 06 (Fig. 311). In all sherds and in the soil sample Tepe 5 06, very fragile powdery and strongly weathered particles of lime were present which must be natural inclusions. The higher values of CaO correspond well with the higher amount of Sr for these sherds. The Sr-values of the sherds are matched by Tepe 5 04 and Shishtepe East 01 but their Rb-values are not (Fig. 306). The Al_2O_3/SiO_2-values of the sherds are relatively low, as in Qoshqarchay Terrace Level 07. The values could also be achieved by adding mineral temper, like quartz sand, to Tepe 5 04 clay (Fig. 312). This finds no clear support in the macroscopical evidence, though. As mentioned above, Group 3 is also characterised by a high amount of plant temper. In sum, a production using material from the immediate surroundings of Tepe 5 seems very likely. The vessels to which these samples belonged (0045-01, 0045-02, 0127-02) were jars (see for example Fig. 15, 1 and Fig. 17, 1). They were found in the pit KG-016 or in the subsoil layer KG-033.

Group 4 sherds cover a narrow middle range of Sr- and Rb-values that resembles best the soil samples of Shishtepe West 01, Shishtepe West 02, Tepe 5 06 and Tepe 5 11 (Fig. 306). Beyond that, low Fe_2O_3-values are characteristic which mainly match Tepe 5 11, Zayamchay 08 and Kura 05 (Fig. 308). High SiO_2-values reflect the higher amount of quartz sand in these sherds (Fig. 313). Following the K_2O and SiO_2-values, Kura 02 or Dara Yatax 03 could be the source of the clay raw material to which the temper was added. Having these different references, it seems likely that different clays, most possibly from sources close to Tepe 5, were mixed to produce the vessels of Group 4.

Due to their morphology these pieces (0049-05, 0127-01, 0229-05 to -07) are classified as small vessels. They were found in the pit KG-018, the subsoil layer KG-033 and context KG-056.

Two sherds, 0127-05 (Group 5) and 0229-01 (Group 6), could not be attributed to one of the groups mentioned above. Their Sr-values place them with Group 3, their Rb-values resemble those of Group 2 (Fig. 306). The K_2O

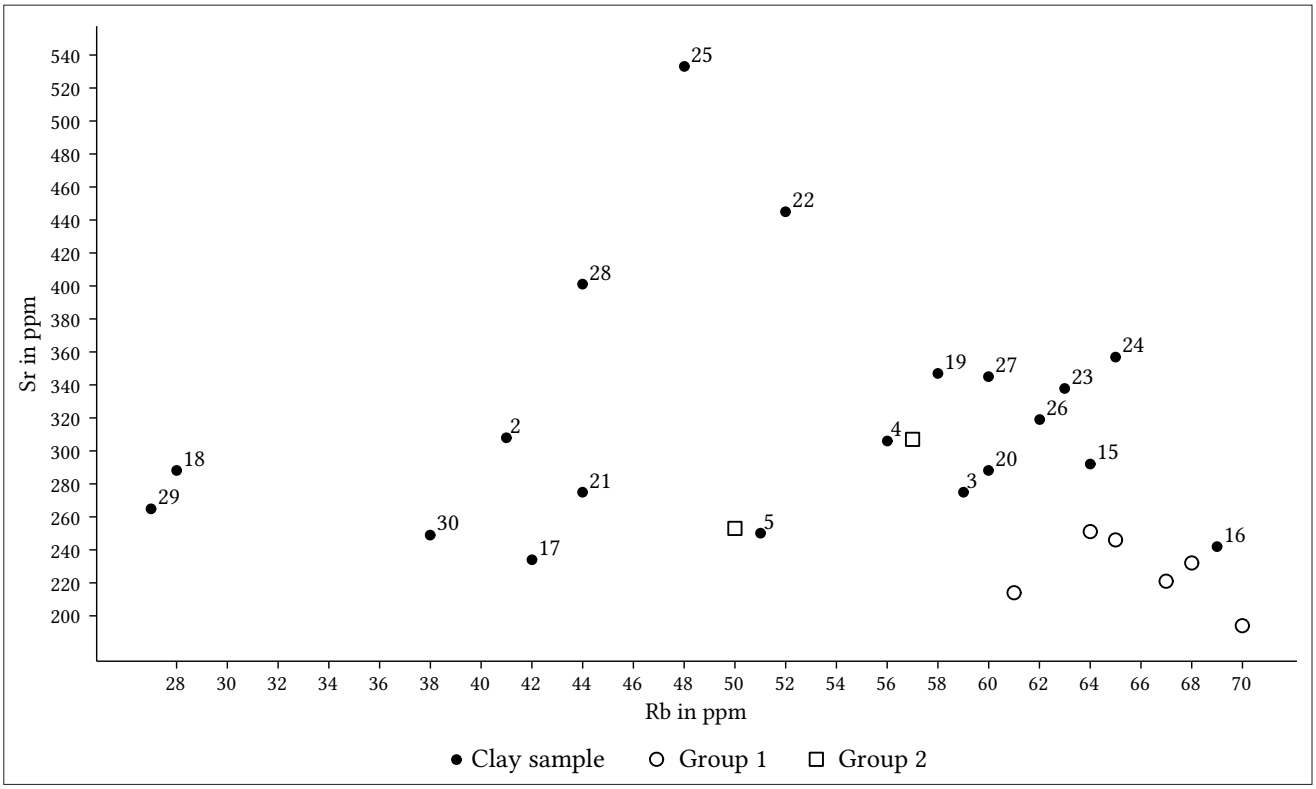

Fig. 314. Tepe 5. Scatterplot of Late Bronze Age pottery samples (n=8) and clay samples (n=20) showing Sr/Rb-ratio. Group 1 shows very low Sr-, but high Rb-values while sherds of Group 2 show medium values

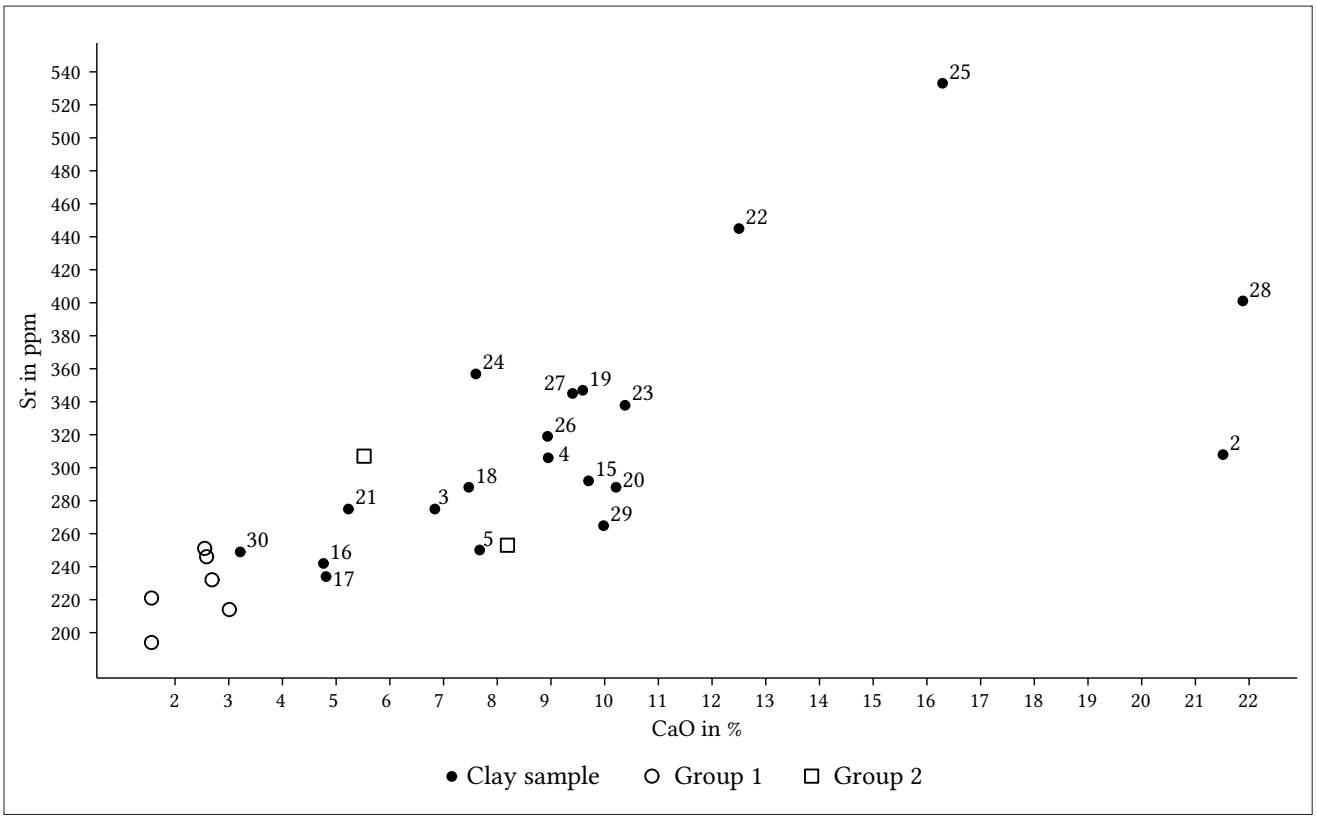

Fig. 315. Tepe 5. Scatterplot of Late Bronze Age pottery samples (n=8) and clay samples (n=20) showing CaO/Sr-ratio. Group 1 shows very low Sr and CaO-values while values for Group 2 are slightly higher

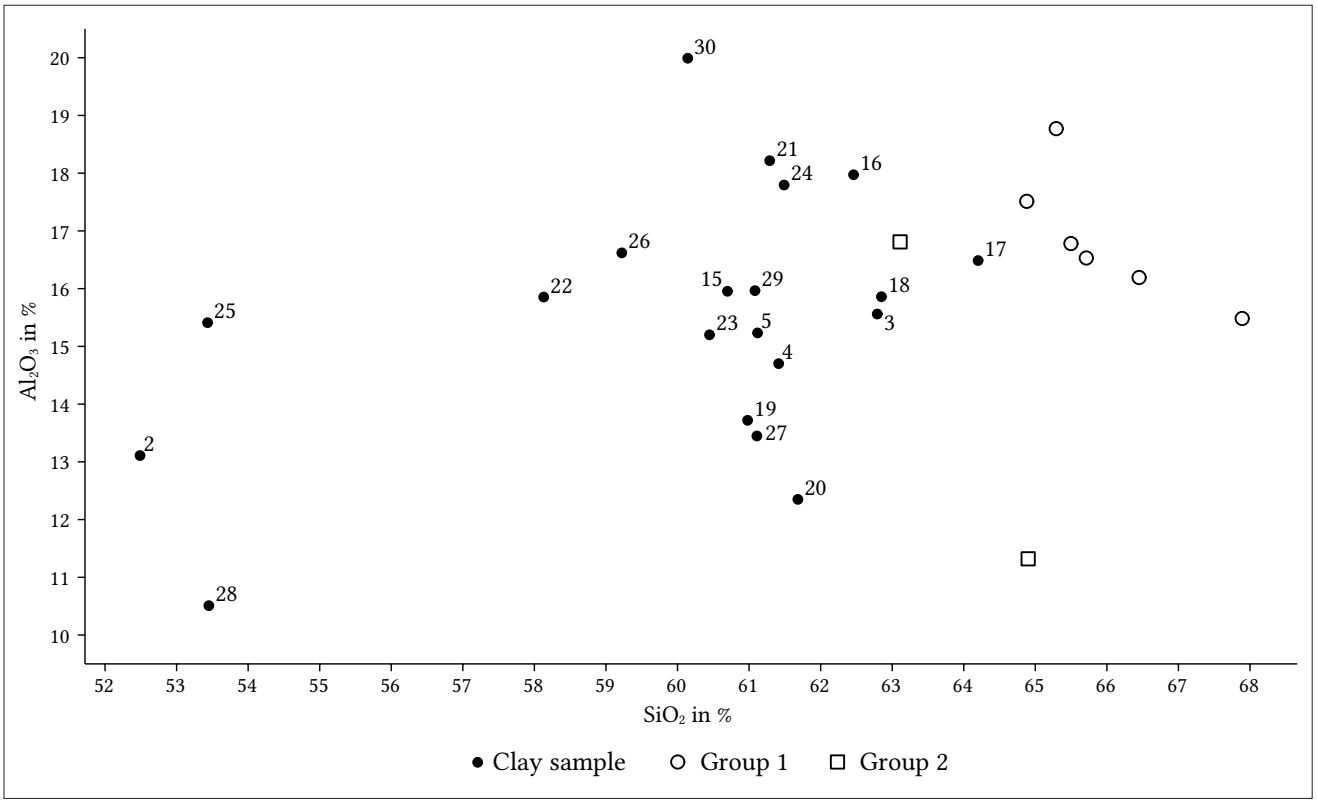

Fig. 316. Tepe 5. Scatterplot of Late Bronze Age pottery samples (n=8) and clay samples (n=20) showing SiO_2/Al_2O_3-ratio. Both values are comparably high for Group 1 while SiO_2-values for Group 2 are slightly increased. Sample 0100-01 shows very low Al_2O_3-values

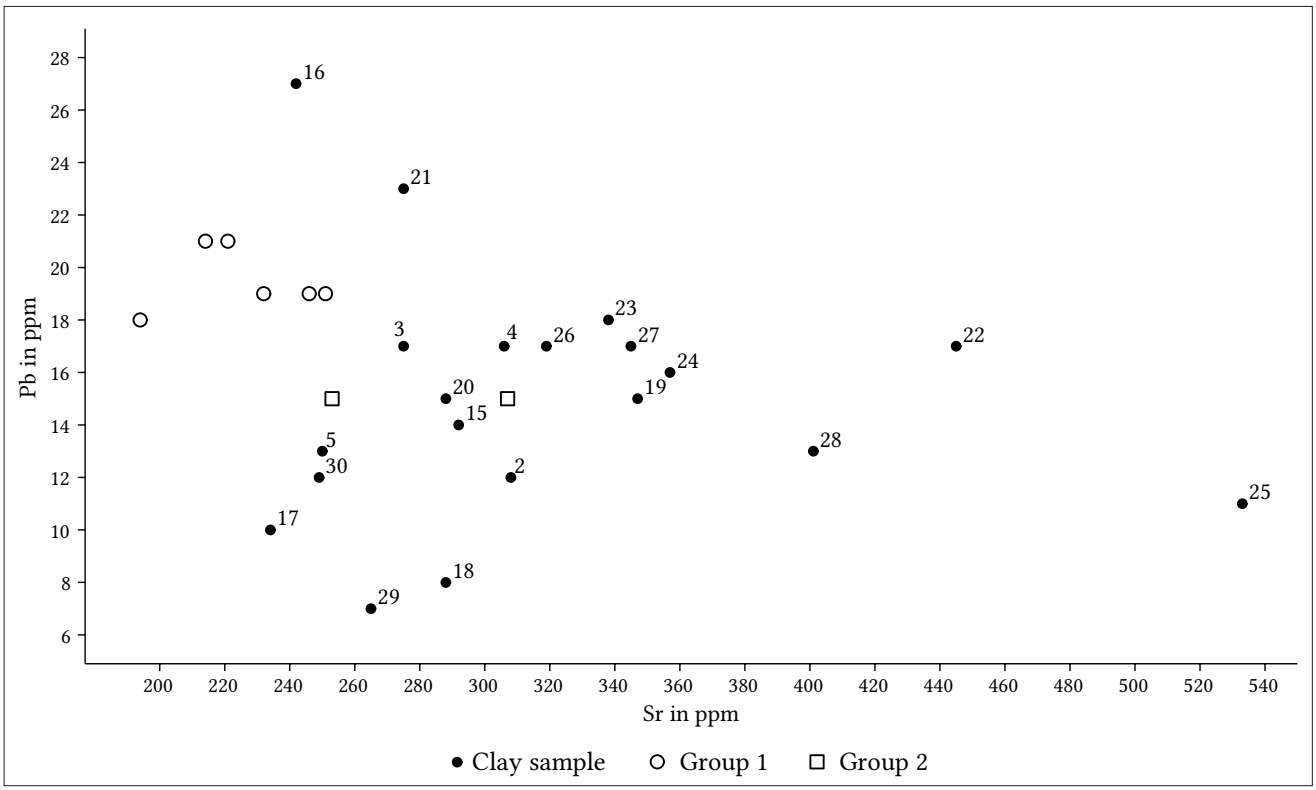

Fig. 317. Tepe 5. Scatterplot of Late Bronze Age pottery samples (n=8) and clay samples (n=20) showing Sr/Pb-ratio. Group 1 yields comparably high Pb-values while Group 2 shows medium Pb-values

and SiO_2-values for 0127-05 (KG-033) resemble Groups 3 and 1, those for 0229-04 (KG-056) Group 4 (Fig. 313). CaO- and Zr-values for 0127-05 match Group 1, those of 0229-04 Group 4 (Fig. 311). Therefore, the overall impression is, that these sherds were also produced primarily of local clays but with a different paste, maybe made by mixing material from several sources.

Late Bronze Age pottery (late 16th to 13th cent. BC)

From an archaeological perspective the differentiation between Late Bronze Age and Early Iron Age pottery is challenging (see ch. IV.2). Interestingly, the chemical fingerprint of the Tepe 5 samples from these two epochs show distinct patterns. Therefore, from a chemical point of view, their separate discussion seems appropriate.

The characteristic grey to black (polished) Late Bronze Age pottery from Tepe 5 is defined by reduced firing conditions but also shows traces of changing firing conditions, e. g. in Burial 6 (0498-01, Fig. 70 and Fig. 72, 6). The eight analysed sherds (Table 35) are medium hard with fine to coarse temper consisting of quartz and black river sand. Chronologically, this group spans the whole Late Bronze Age phase of Tepe 5: Pottery from Burial 1 shows strong connections to the final Middle Bronze Age which speaks for a date on the transition between those two periods (end of 16th cent. BC to the beginning of the 15th cent. BC). Burial 3 chronologically succeeds Burial 1, having stronger relations with the Late Bronze Age proper. The pottery of Burial 6 belonging to Group 1 can be attributed to the mature Late Bronze Age.

Based on their chemical fingerprints, the Late Bronze Age pottery can itself be divided into two groups: 1) deltaic clay sources and 2) local clay sources probably mixed with deltaic clay. Visually, the distinct laminar structure of the deltaic clay used for most of the sherds (0201-01, 0425-01, 0425-02, 0498-01, 0498-03, 0498-06) is striking (see also the Early Chalcolithic Group 1). Those of our clay samples which resemble the low Sr-values of these sherds of Late Bronze Age Group 1 are mainly from rivers – Zayamchay 08, Shamkirchay 03, Kura 02 and 03, with the best fit being Kura 02 and 03 (Fig. 314). The CaO-value of these sherds is relatively low and resembles best Zayamchay 09, Kura 02 and Kura 03 (Fig. 315). Their relatively high Al_2O_3 and SiO_2-values can be explained by the use of very coarse, unevenly distributed quartz sand as temper (Fig. 316). The Pb-values of the pottery are slightly increased and fall within the range of Shamkirchay 03, Kura 02, but also of Dara Yatax 03

(Fig. 317). Probably, clay sources from the Kura tempered with quartz sand and black sand were used for this pottery as the Kura is close and therefore a more readily accessible source than the Zayamchay.

Typologically, Group 1 includes mainly pots of different sizes (Burial 1, 0425-01, 0425-02, Fig. 49 and Fig. 51, 1. 2; Burial 3, 0201-01, Fig. 62, 2; Burial 6, 0498-03, 0498-06, Fig. 72, 1. 4, Fig. 73 and Fig. 74) but also a bowl (Burial 6, 0498-01, Fig. 70 and Fig. 72, 6). Chronologically this group spans the whole Late Bronze Age occupation of Tepe 5: Pottery from Burial 1 shows strong connections to the final Middle Bronze Age which suggests a date on the transition between those two periods (end of 16th cent. BC to the beginning of the 15th cent. BC, see ch. IV). Burial 3 chronologically succeeds Burial 1, having stronger relations with an early stage of the Late Bronze Age. The well-dated pottery of Burial 6 belonging to Group 1 can be attributed to the 15th/14th cent. BC and therefore to the incipient Late Bronze Age stage.

Unsurprisingly, the sherds of Group 2 which do not show a laminar structure (0100-01, 0498-02) can be better attributed to the non-deltaic soil samples of Dara Yatax 03 to 05 (Fig. 314). Compared to Group 1, the CaO-value is slightly higher still, matching best Dara Yatax 03, Dara Yatx 05 but also Kura 05 (Fig. 315). With regard to their Al_2O_3 and SiO_2-values both sherds differ greatly, most possibly to different amounts of medium sized quartz sand and the more intensive use of black sand for 0100-01. For 0498-02 the clay sources of Kura 03 and Kura 05 as Dara Yatax 03 seem a possible source while 0100-01 could have been produced from either Kura 05 or Dara Yatax 03 by adding quartz sand temper (Fig. 316). Following Pb-values both sherds, again, differ but nevertheless match the sources of Dara Yatax 02 to 05, Kura 01 or Qoshqarchay Terrace Level 07 (Fig. 317). Therefore, it seems most likely that sherds of Group 2 were produced from local non-deltaic clay of Dara Yatax mixed with deltaic clay from the Kura.

According to their morphology, sherds of Group 2 are big pots (Burial 7, 0100-01, Fig. 76, 2; Burial 6, 0498-02, Fig. 71 and Fig. 72, 2). With regard to their chronology, Burial 7, but also sherd 0498-02 of Burial 6 show strong parallels to Burial 1. Therefore, Burials 1 and 7 can be grouped with the earliest burials of Tepe 5.

Iron Age pottery (12th to 7th cent. BC)

The Early Iron Age pottery of Tepe 5 is characterized by shifting firing conditions producing a (dark) grey surface and brownish core. The sherds are medium hard to hard, with a dominance of medium to coarse mineral temper. 18 sherds (from as many vessels) were analysed (Table 35).

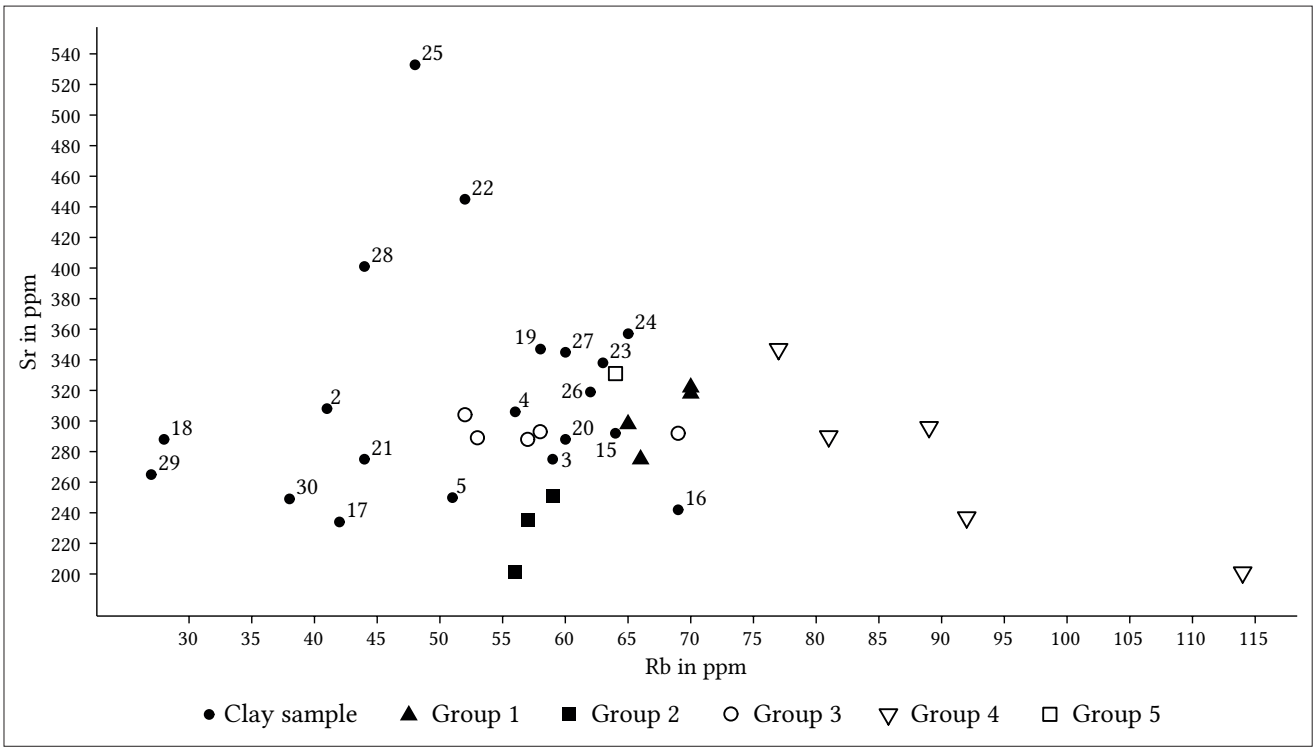

Fig. 318. Tepe 5. Scatterplot of Early Iron Age pottery samples (n=18) and clay samples (n=20) showing Rb/Sr-ratio

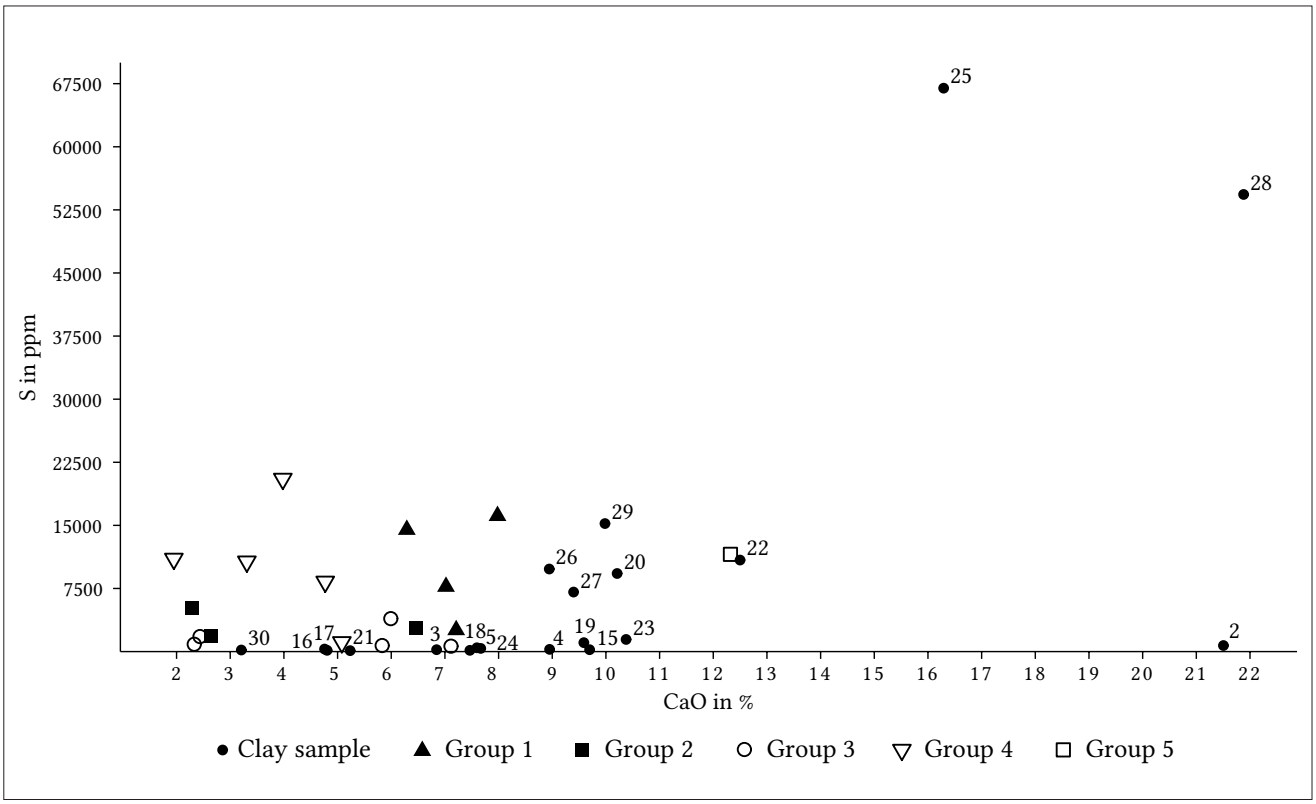

Fig. 319. Tepe 5. Scatterplot of Early Iron Age pottery samples (n=18) and clay samples (n=20) showing CaO/S-ratio. The S-values are high for Groups 1 and 4, while CaO-values are high for Group 1 but low for Group 4. Group 5 shows the highest CaO-value

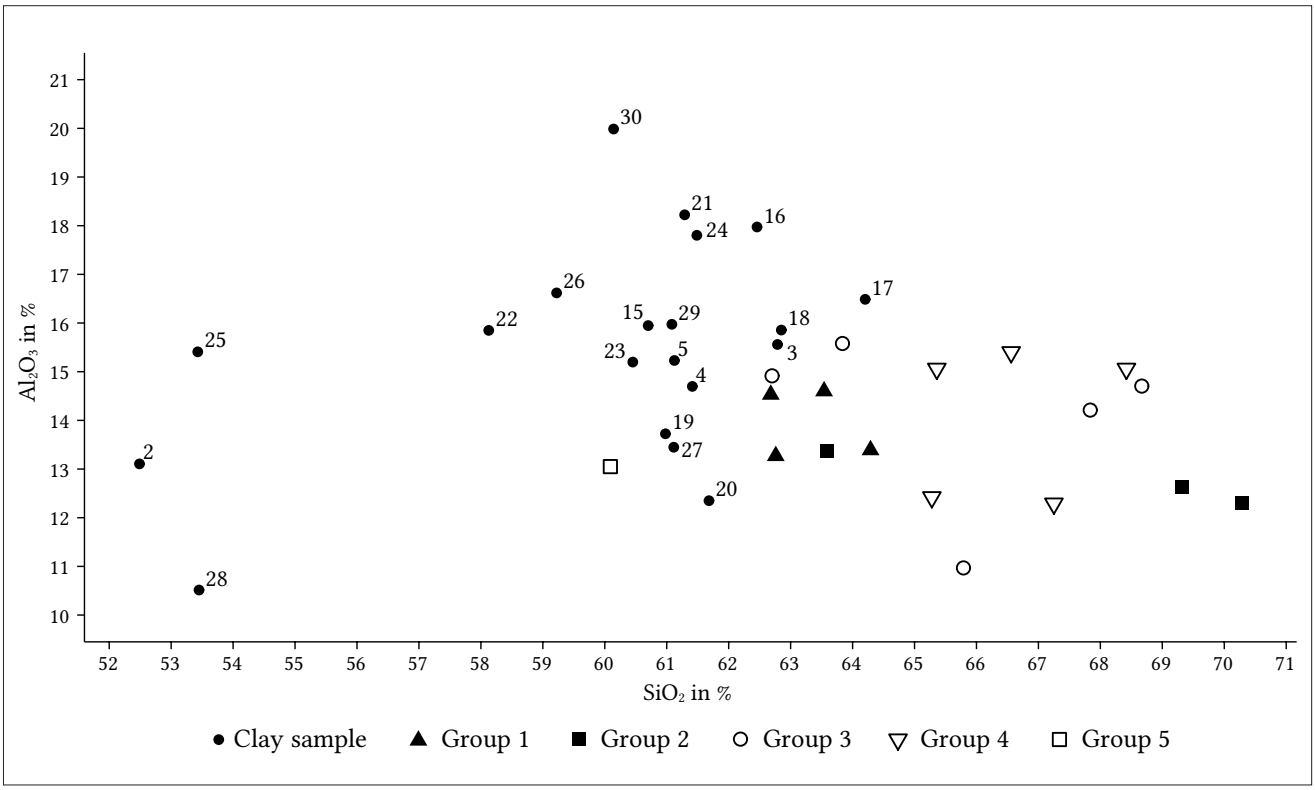

Fig. 320. Tepe 5. Scatterplot of Early Iron Age pottery samples (n=18) and clay samples (n=20) showing SiO_2/Al_2O_3-ratio. Sherds of Group 2 and 3 show very high SiO_2-values while Group 4 is characterized by comparably high SiO_2-values. Very low SiO_2- and Al_2O_3-values characterize Group 5

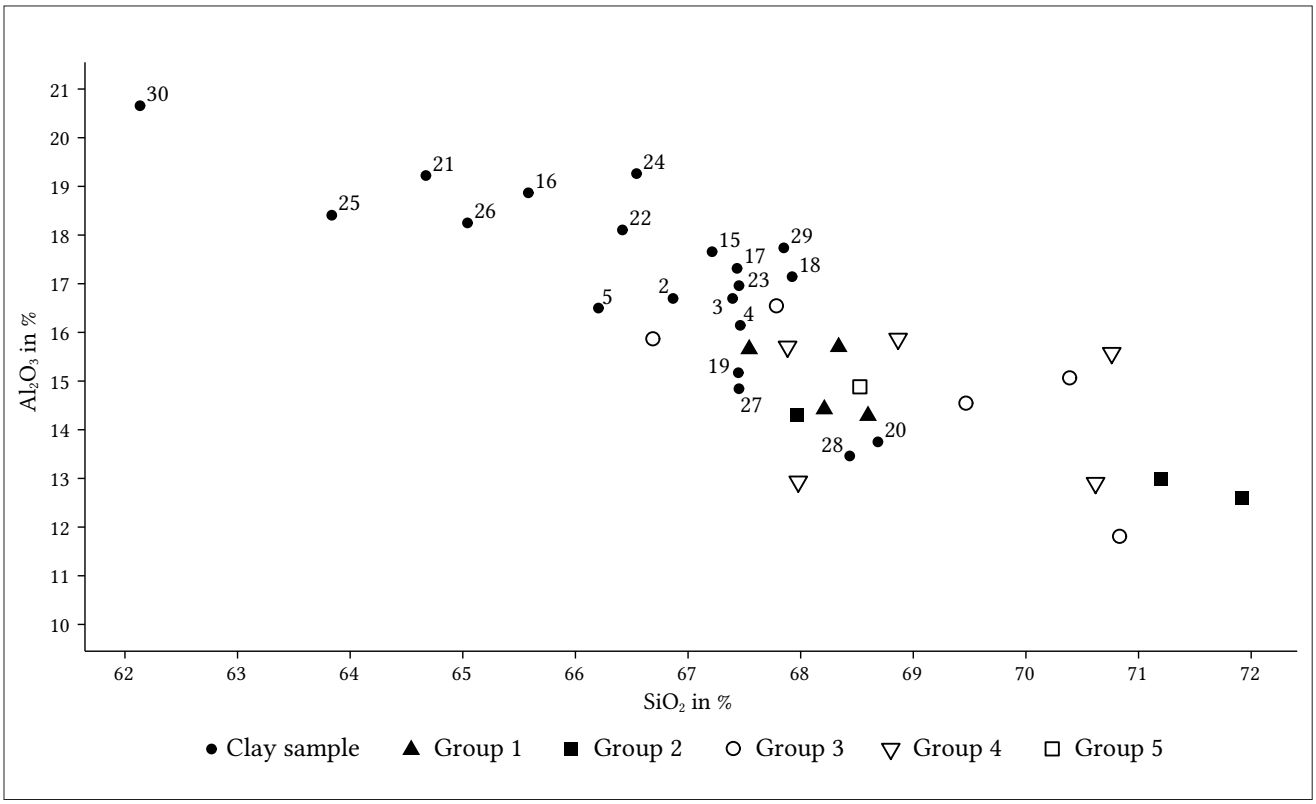

Fig. 321. Tepe 5. Scatterplot of Early Iron Age pottery samples (n=18) and clay samples (n=20) showing SiO_2/Al_2O_3-ratio after removing CaO from the calculation. The most likely clay sources for Group 1 remain the same

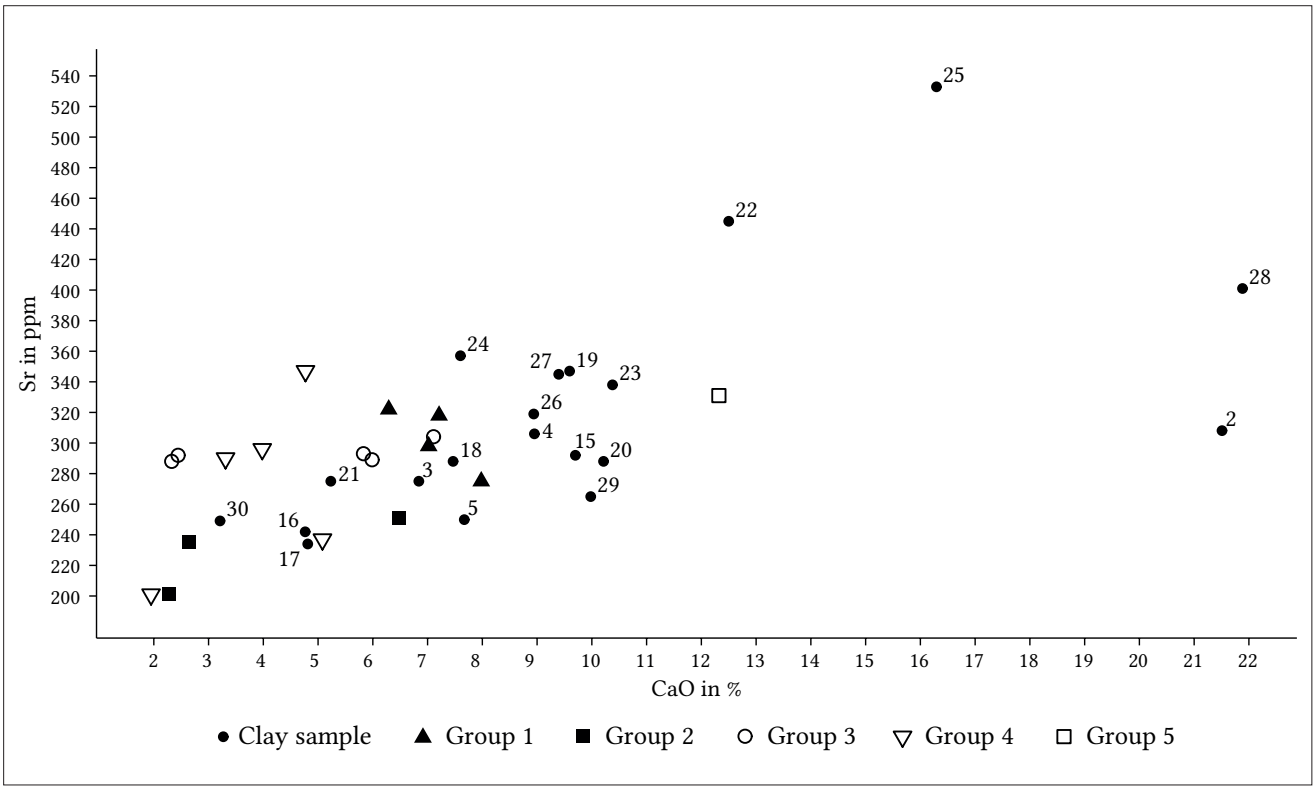

Fig. 322. Tepe 5. Scatterplot of Early Iron Age pottery samples (n=18) and clay samples (n=20) showing CaO/Sr-ratio. Sr-values of Group 1 are unaffected by the use of limestone temper. Group 2 shows noticeably low CaO- and Sr-values comparable to Late Bronze Age Group 1

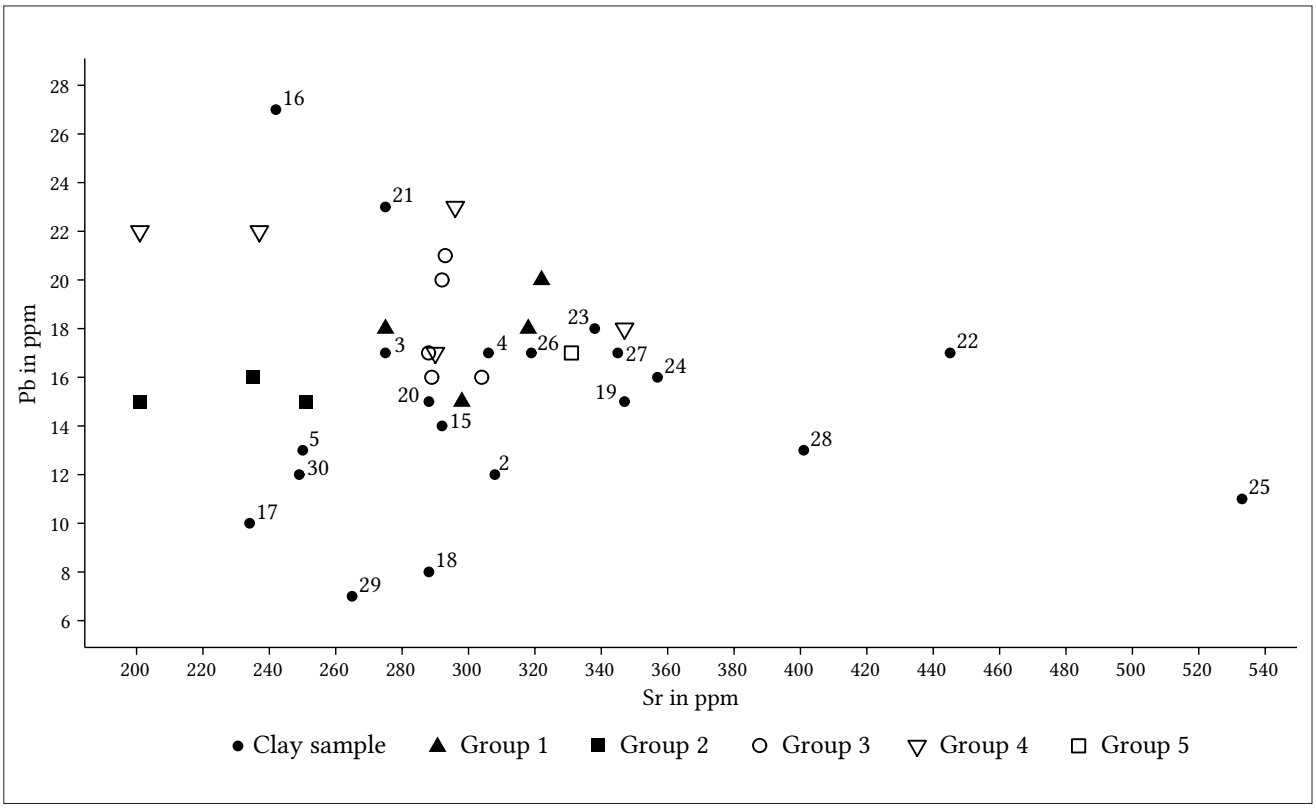

Fig. 323. Tepe 5. Scatterplot of Early Iron Age pottery samples (n=18) and clay samples (n=20) showing Sr/Pb-ratio. Group 2 shows low Pb-values

The pottery can be split into four main groups and one single sherd (Group 5) based on their Rb/Sr-values (Fig. 318): 1) local clay sources with limestone temper 2) deltaic clay sources 3) mixed local clay sources and river clay sources, 4) very high Sr-values without attribution to a clay source included in this dataset. All sherds are tempered with different amounts of mineral temper, often black sand. It is worth mentioning that grog temper is visible in sherds of Groups 1 and 3. As p-XRF does bulk analysis, the signatures of temper and sherds cannot be distinguished. The groups correspond to certain vessel types.

Group 1 is mainly characterized by high CaO and S (Fig. 319) values due to the use of crushed limestone as temper. As limestone sources were included in the geological survey 2018 (also see above), their values can approximatively be compared to those of the limestones in the sherds. This does of course not rule out, that other, unsampled locations could be the source of the limestone used here. From a chemical point of view, the following discussion must therefore be viewed with caution: p-XRF chemical bulk analysis (see above) will always give a signature for a sherds' measurement consisting of the chemical fingerprint of clay and limestone temper. The limestone cannot be tested individually. Therefore only some elements and a qualitative comparison are valid to identify a possible source among the samples included in our dataset: As the value of S differs between limestones (Hansen et al. 1993: 1325), the best matches for the values in the pottery are found in limestone from the Shishtepe outcrops and from Zayam Karrier II.

Clay sample Shishtepe East 01 shows higher CaO- and S-values, too, which may be due to the weathering process of the limestones and the deposition of these elements in the clay. To eliminate the influence which may derive from limestone temper on the main element concentrations, this element was taken out of our examination. Chemically CaO can be considered as a diluting agent – therefore all other main elements concentrations are reduced in their content (Mommsen 2007: 186): According to the SiO_2- and Al_2O_3-values of these sherds with CaO in the calculations, it seems likely that clay from a deposit similar to Shishtepe West 01, Shishtepe East 01 or Dara Yatax 04 and/or 05 was used (Fig. 320). If CaO is not considered and the remaining main elements are recalculated to 100 %, Dara Yatax 04 and 05 remain likely clay sources, but Dara Yatax 02, Tepe 5 04 or 06 cannot be ruled out (Fig. 321). The higher SiO_2-values of the sherds compared to the clay samples can be explained by the use of black sand as temper. As the Sr-values do not

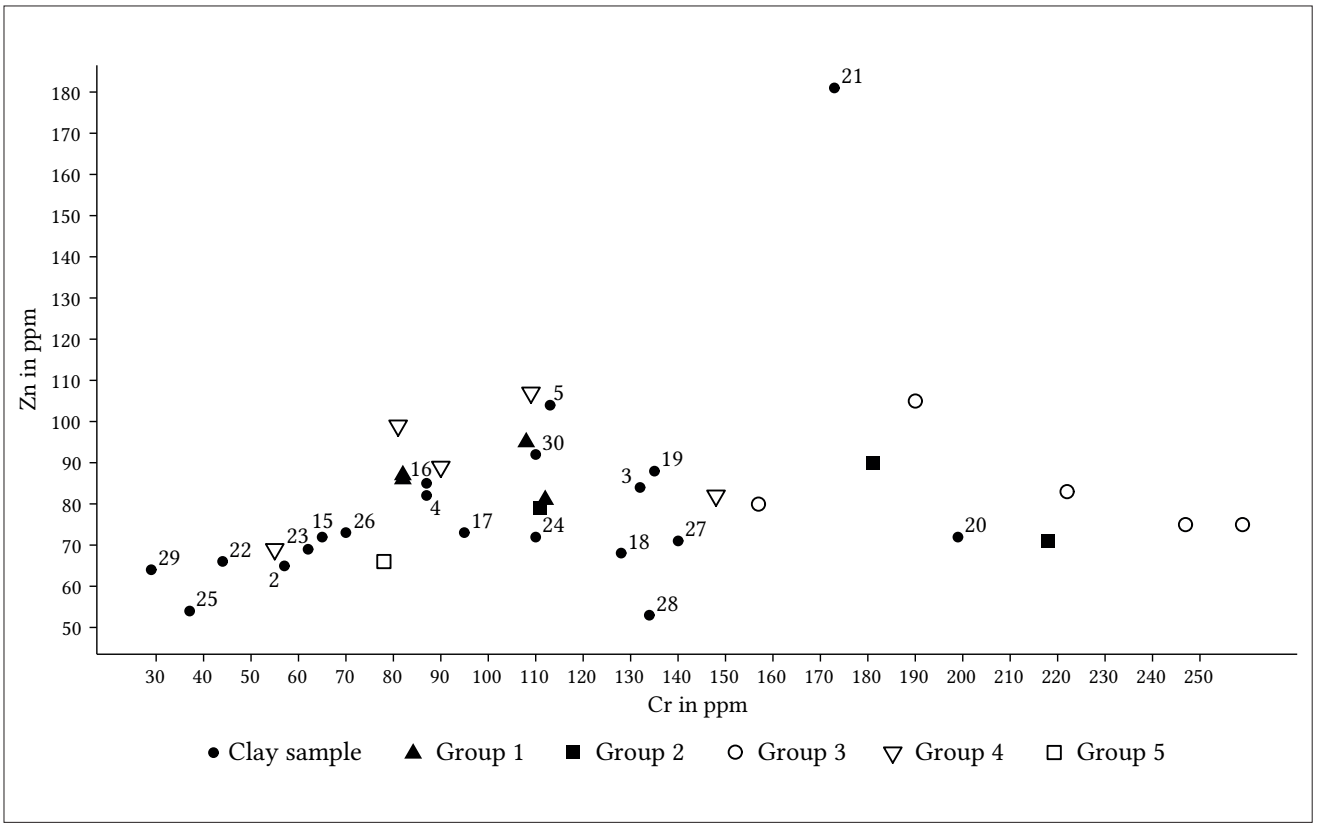

Fig. 324. Tepe 5. Scatterplot of Early Iron Age pottery samples (n=18) and clay samples (n=20) showing Cr/Zn-ratio. Group 3 contains comparatively high amounts of Cr and Zn

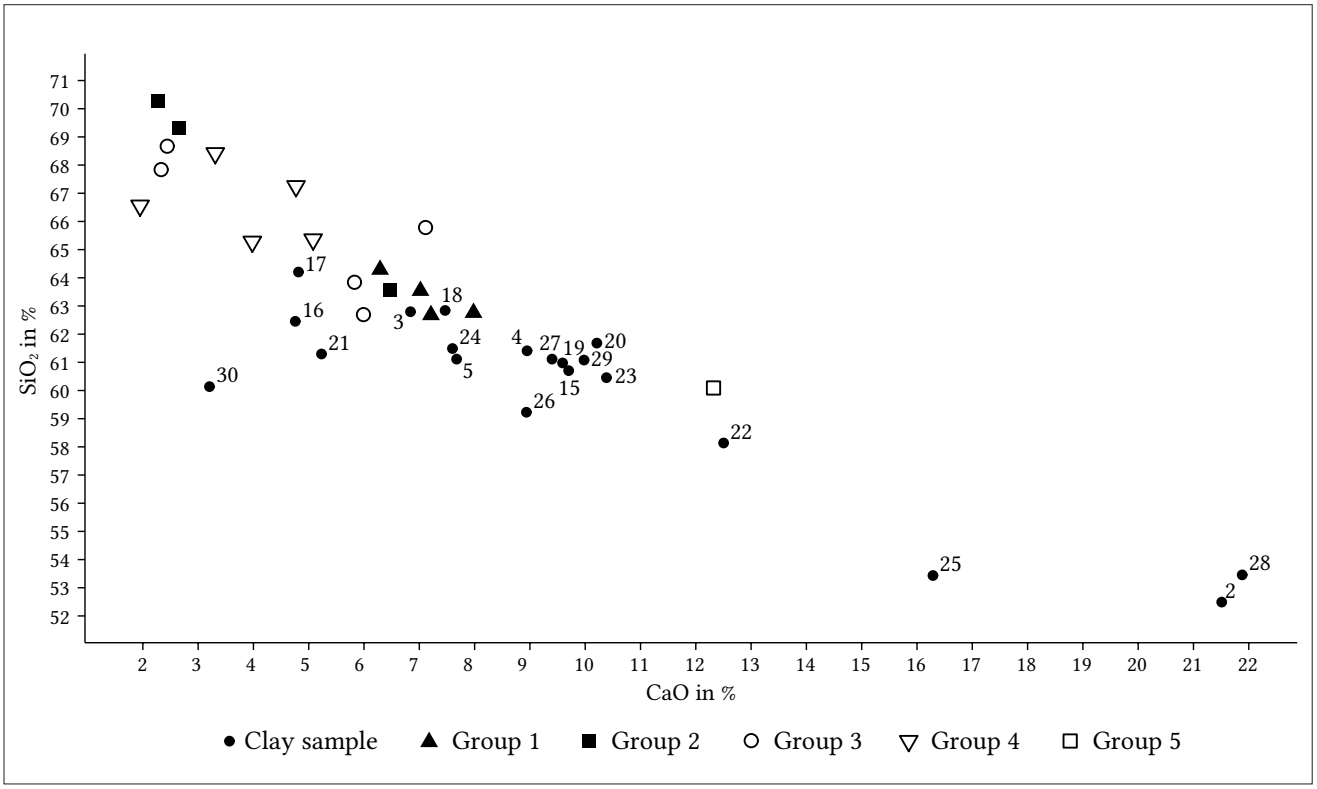

Fig. 325. Tepe 5. Scatterplot of Early Iron Age pottery samples (n=18) and clay samples (n=20) showing CaO/SiO_2-ratio. According to the CaO- and SiO_2-values nearly all clay sources could have been used for the production of Group 3 ceramics

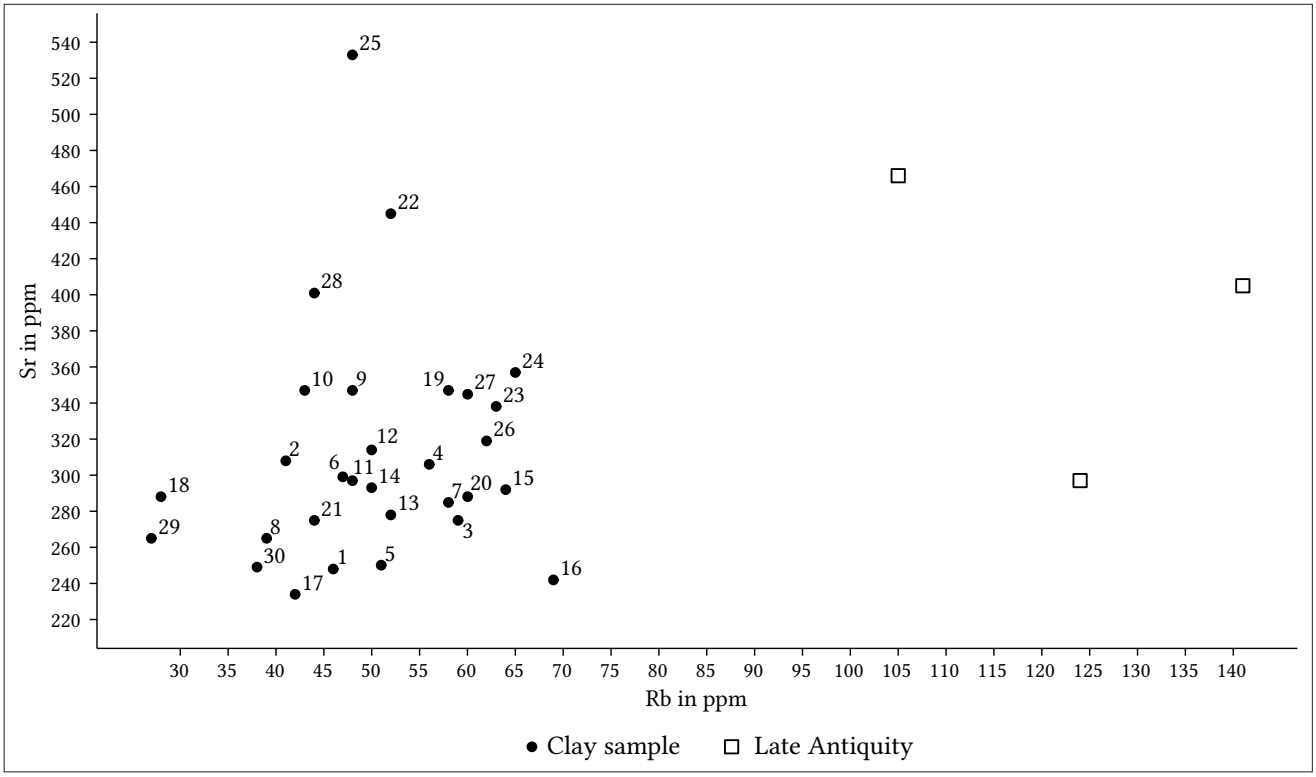

Fig. 326. Tepe 5. Scatterplot of Late Antique pottery samples (n=3) and clay samples (n=30) showing Sr/Rb-ratio. All Late Antique ceramic samples differ greatly from the clay samples

appear to be strongly influenced by the limestone temper (Fig. 319), the Rb and Sr values of the sherds indicate a connection with Kura 01, Tepe 5 06, but also Shishtepe West 01 or 02 (Fig. 318).[8] To conclude, for the sherds of Group 1, clay from the area around Tepe 5 (Dara Yatax or Tepe 5) tempered with black sand and limestone (from Shishtepe or a chemically similar source) was most likely used.

Typologically, vessels within this group are identified as (carinated) bowls. Based on the archaeological evidence Burial 15 (0241-01, 0241-03, 0241-04, Fig. 119, 1–3) dates to the 8th–7th cent. BC (see ch. IV). The sherd 0144-06) was found loose in the fill of Burial 13.

The clay of Group 2 shows, as for the Early Chalcolithic (Group 1) and Late Bronze Age sherds, well visible laminae of about 1 mm thickness which are characteristic for deltaic clays (see above). It makes sense, therefore, that the clay samples which resemble the low Sr-and CaO-values of these sherds are the same as for the Late Bronze Age samples (Fig. 322). The low level of Pb in these sherds exhibits the strongest correspondence with Zayamchay 09, Dara Yatax 05 and Kura 03 (Fig. 323). Quite high amounts of coarse quartz sand and black sand explain their relatively high SiO_2-values. As for Late Bronze Age pottery, clay sources from the Kura (Kura 03 and Kura 05) appear to provide the best fit (Fig. 320).[9] A production using clays from similar sources in the Kura as in the Late Bronze Age, with the addition of black sand and quartz sand as tempers, is highly probable.

Morphologically, the samples of Group 2 belong to pots of different sizes including a tall jar (0144-02, Fig. 105, 2 and Fig. 106), a large pot (Burial 13, 0144-04, Fig. 105, 3 and Fig. 107) and a spherical bowl (Burial 15, 0241-07, Fig. 119, 5 and Fig. 121). Burial 13 was dated by radiocarbon (and ceramic typology) to the 9th cent. BC while Burial 15 dates – based on the archaeological evidence – to the 8th–7th cent. BC (see ch. IV).

Group 3's medium Rb- and Sr-values correspond well with Dara Yatax 03 and 04 or the Qoshqarchay Terrace Level 07 (Fig. 318). These sherds also display relatively high amounts of Cr and Zn, again matching Qoshqarchay Terrace Level 07 (Fig. 324). The presence of these elements results in a more brownish colour, best visible in a fresh break, if the pottery is fired at about 900°C to

8 Interestingly 0241-05 (Group 3) can be found in the group 1 cluster in this scatter plot, but not in any other diagram.

9 The coarse temper explains the quite high variation in some elements of these three sherds.

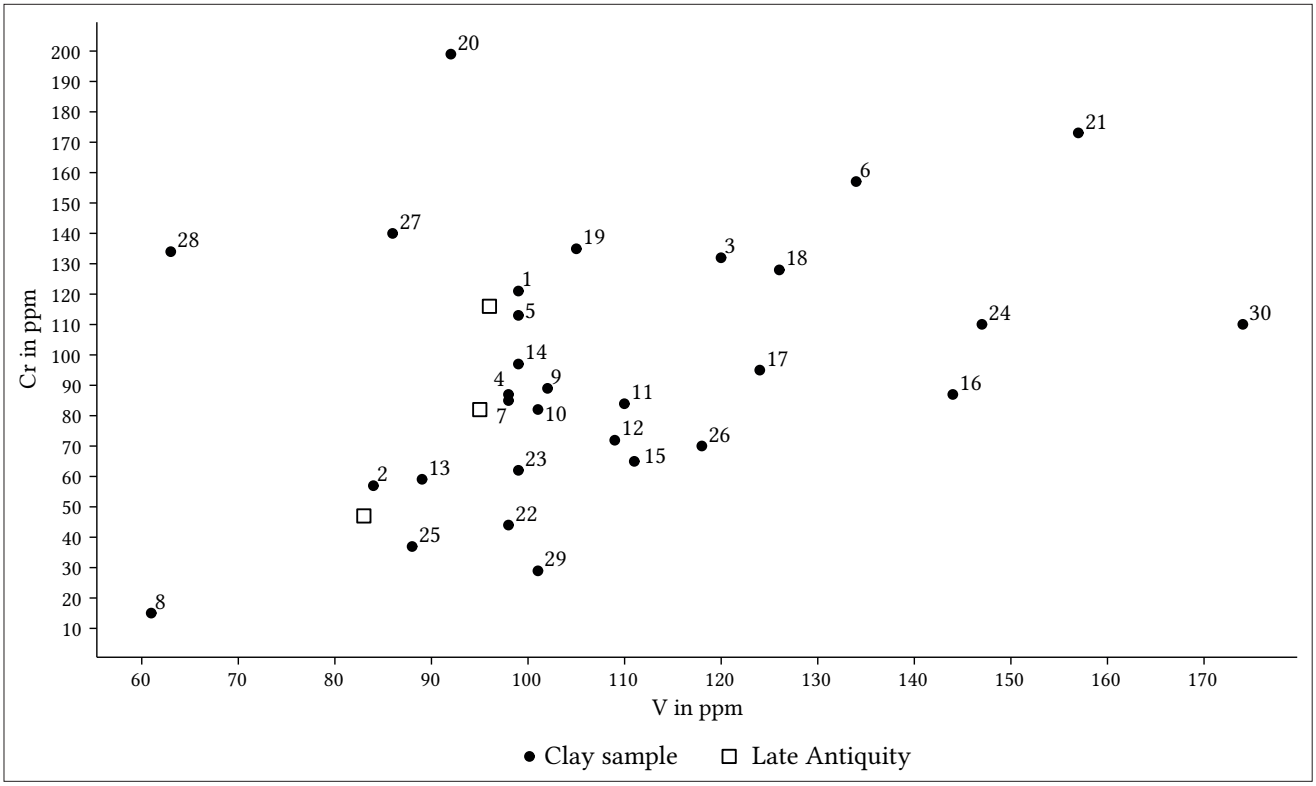

Fig. 327. Tepe 5. Scatterplot of Late Antique pottery samples (n=3) and clay samples (n=30) showing V/Cr-ratio. Late Antique samples show values for V and Cr comparable to those of the clay samples

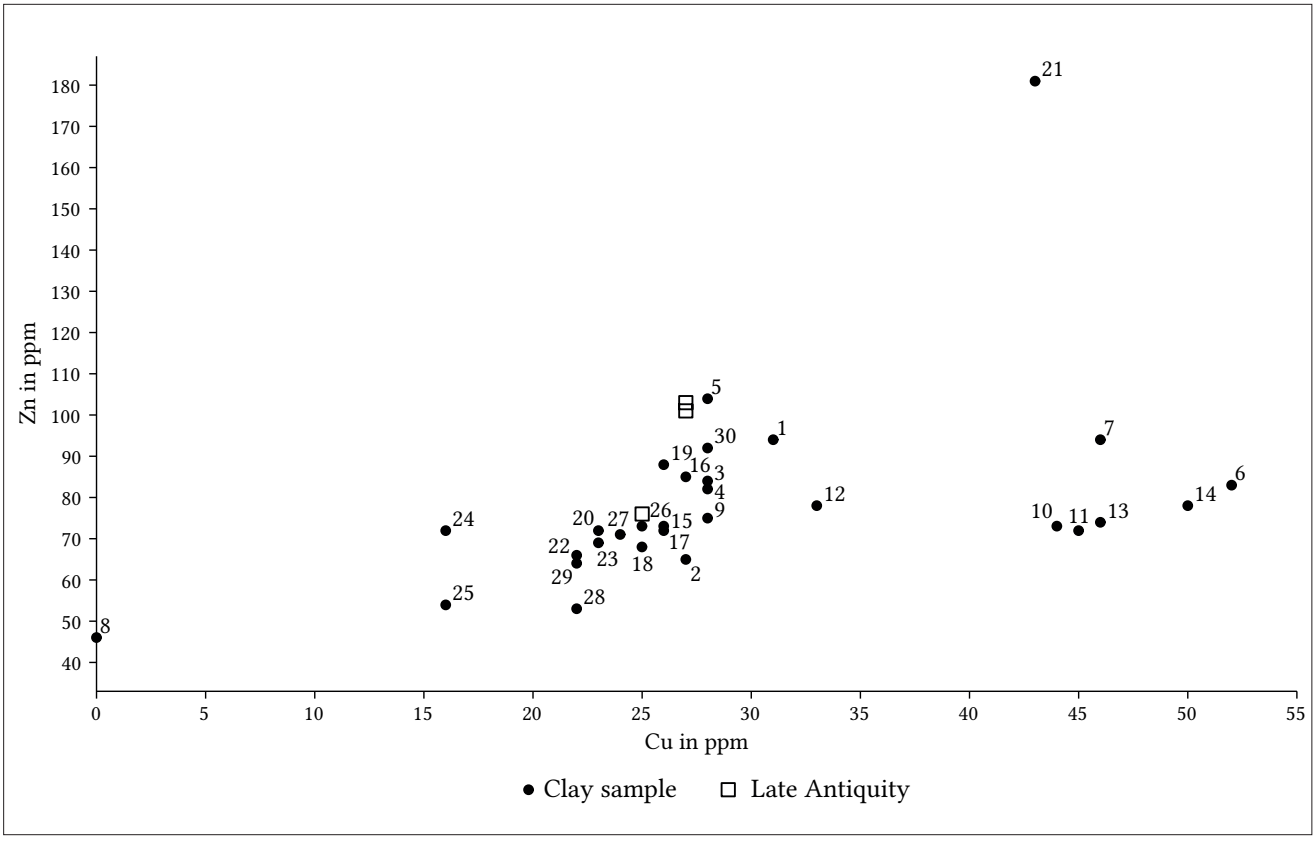

Fig. 328. Tepe 5. Scatterplot of Late Antique pottery samples (n=3) and clay samples (n=30) showing Cu/Zn-ratio. One Late Antique sample matches different sources then the other two

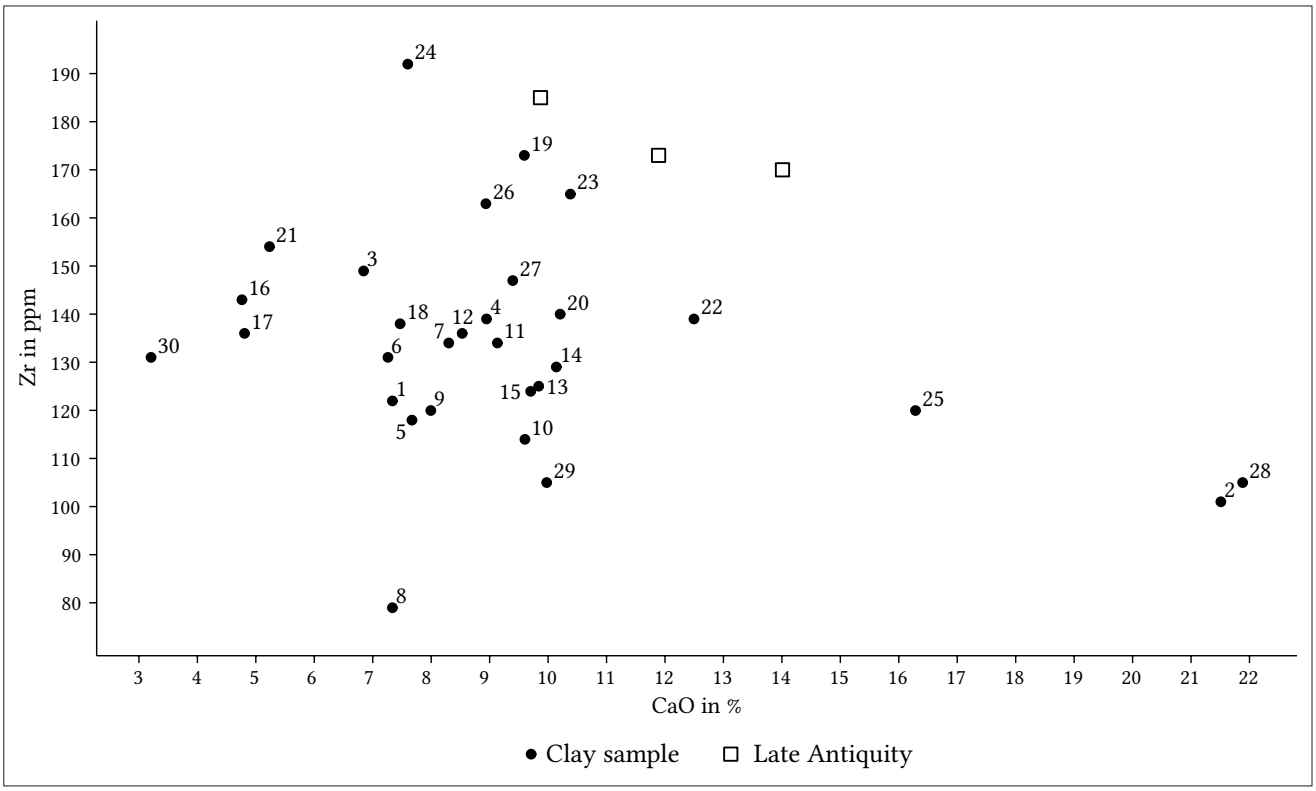

Fig. 329. Tepe 5. Scatterplot of Late Antique pottery samples (n=3) and clay samples (n=30) showing CaO/Zr-ratio. Zr- and CaO-values are comparably high but in the range of some of the clay samples

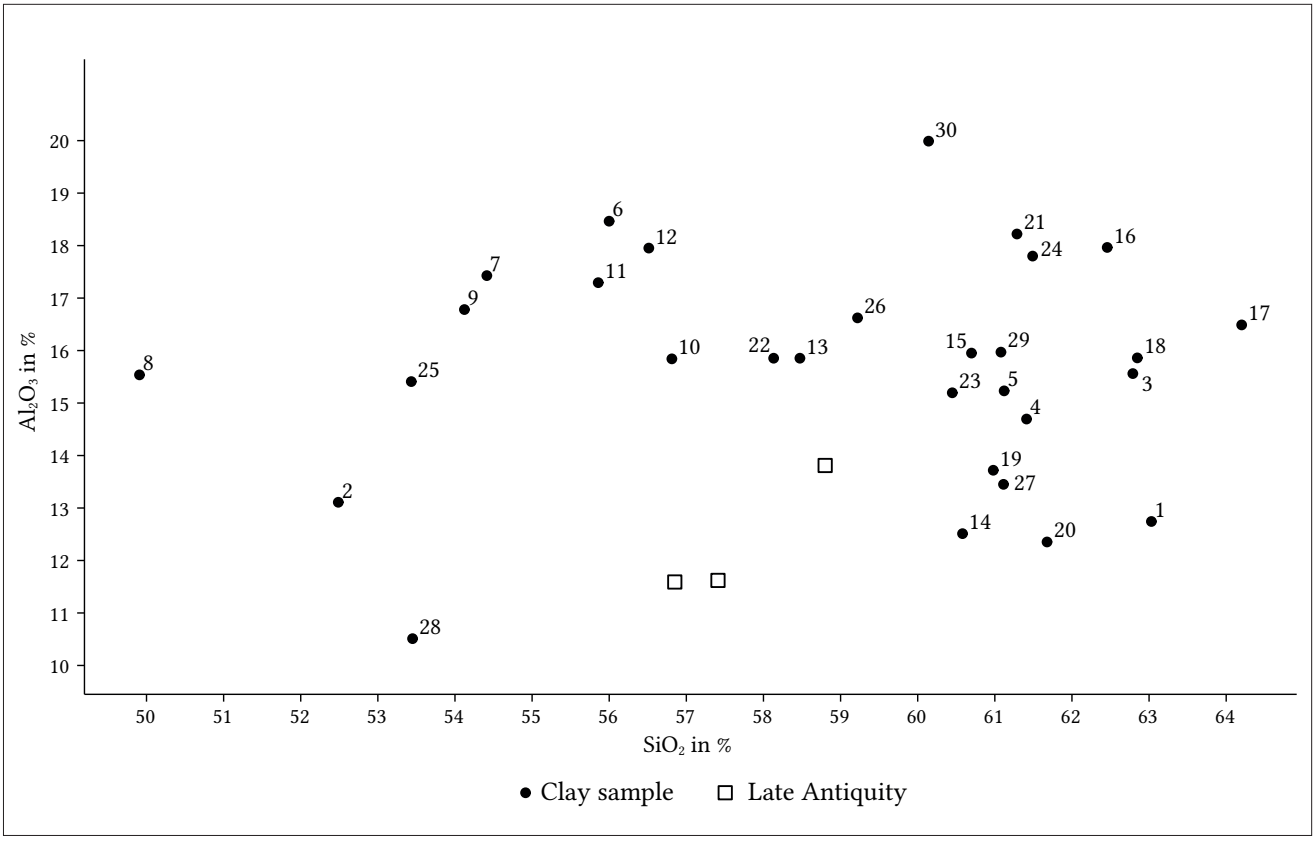

Fig. 330. Tepe 5. Scatterplot of Late Antique pottery samples (n=3) and clay samples (n=30) showing SiO_2/Al_2O_3-ratio. Both values of the Late Antique sherds correspond well with the small amount of mineral temper

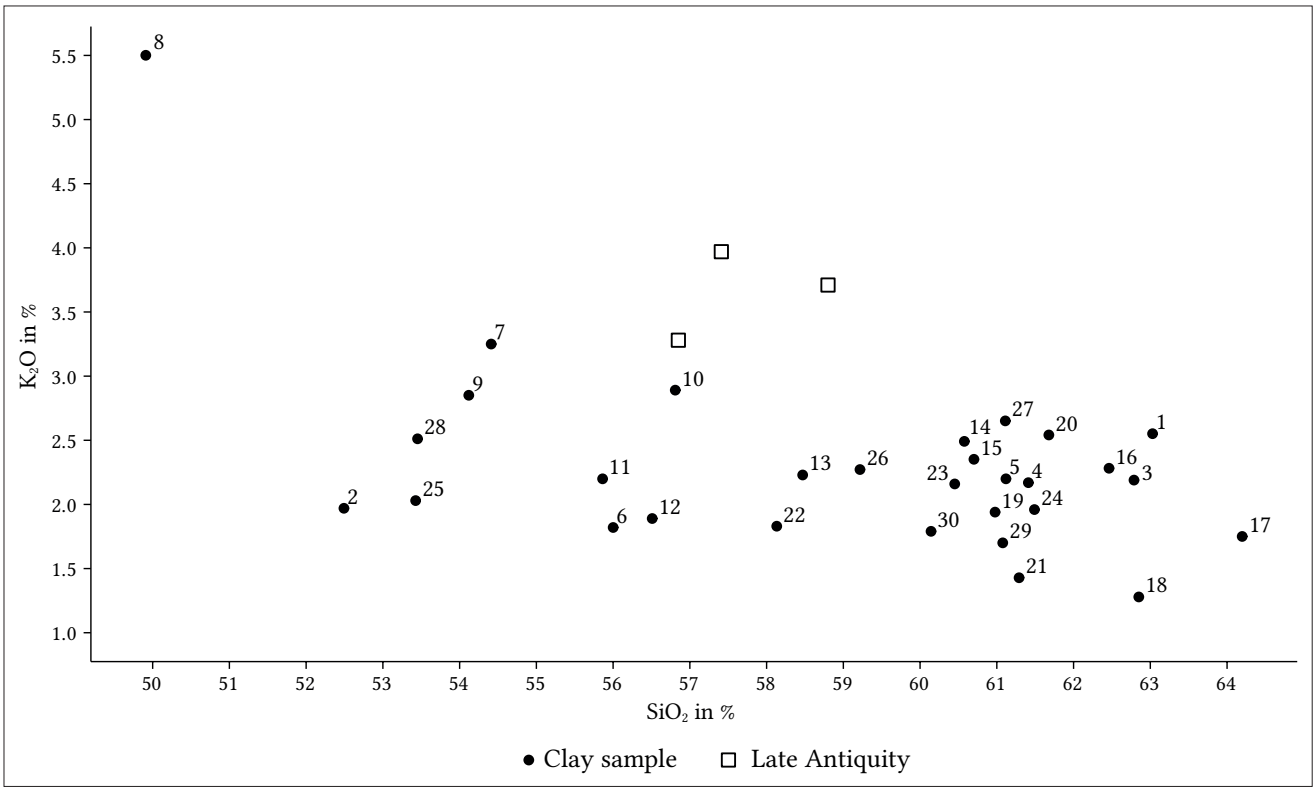

Fig. 331. Tepe 5. Scatterplot of Late Antique pottery samples (n=3) and clay samples (n=30) showing SiO_2/K_2O-ratio. High K_2O-values support the use of feldspar as a temper

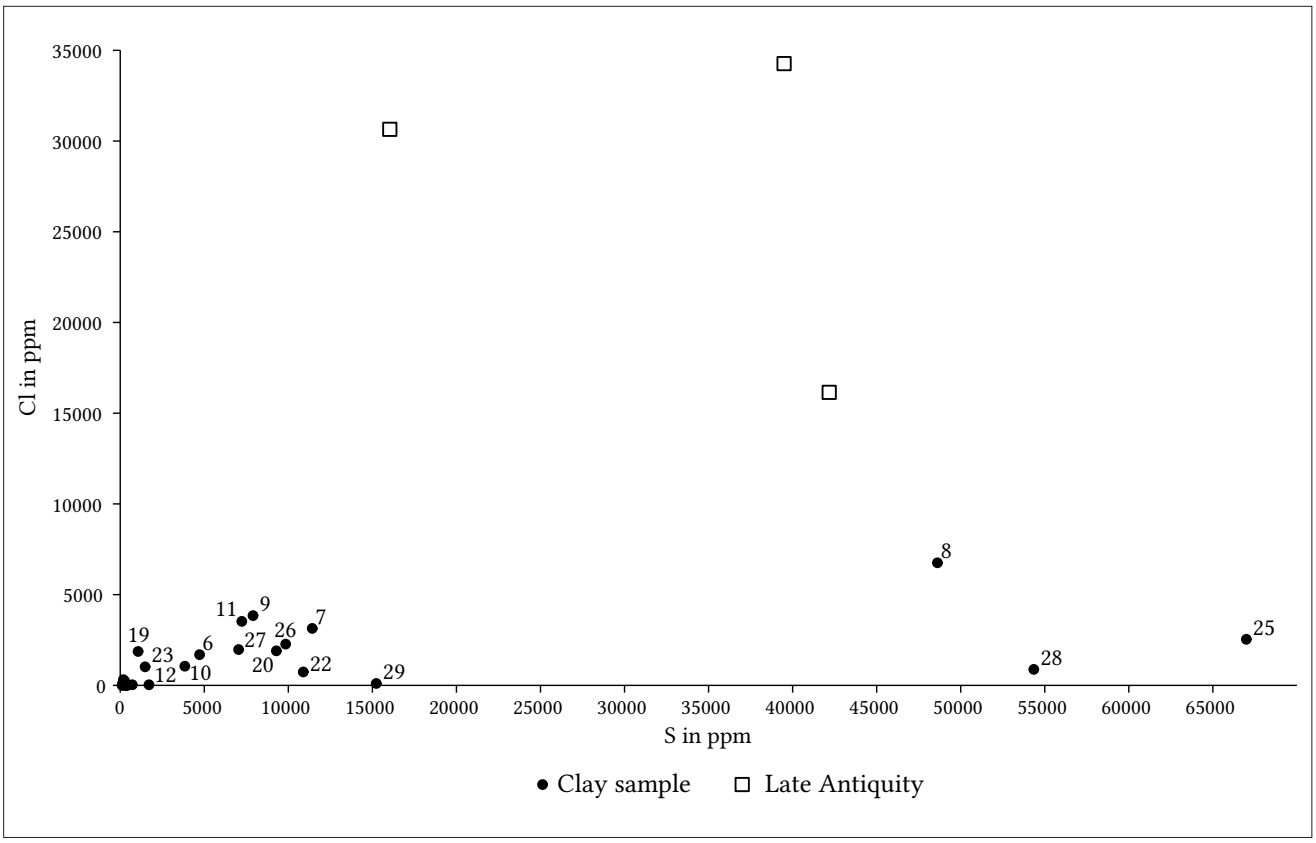

Fig. 332. Tepe 5. Scatterplot of Late Antique pottery samples (n=3) and clay samples (n=30) showing Cl/S-ratio. Late Antique sherds show increased S- and Cl-values

950°C (Hamer/Hamer 2004: 59). When considering the CaO- and SiO_2-values, nearly all clay samples could have been used for the production of these sherds, including Dara Yatax 03 and 04 but excluding Qoshqarchay Terrace Level 07 (Fig. 325). The higher SiO_2 content was caused by coarse quartz sand and black sand temper; two sherds additionally show signs of very fragile, powdery and strongly weathered particles of lime which can be considered as natural inclusions. Tepe 5 04 is the only sample in this analysis matching those. Therefore, for Group 3 a local clay from around Tepe 5 (Tepe 5 and Dara Yatax) was probably used, possibly mixed with clay from the Qoshqarchay and tempered with quartz sand and black sand.

Morphologically these samples are small bowls, pots and a bottle. It is worth mentioning that one half of the carinated bowl 0241-02 was found dislocated in Burial 15, while the other half (0418-01) was discovered in Burial 8 (Fig. 85 and Fig. 86, 2) together with another pot (Fig. 86, 1). Burial 8 dates to the very beginning of the Early Iron Age (the 12th and 11th cent. BC). Burial 15 (0241-05, 0241-06, Fig. 119, 4. 6) is dated archaeologically to the 8th–7th cent. BC, sherd 0144-07 was found in the fill of Burial 13 (see ch. IV).

Group 4 is characterized by its very high Rb-values which find no comparison in the clay samples included in this data set (Fig. 318). Also, their CaO-values are comparably low while the S-values are relatively high (Fig. 319). Bigger vessels (0221-01, 0252-01) of this group show a much higher SiO_2-value due to their more extensive use of river sand as temper (Fig. 320). Therefore, it is possible that the objects of Group 4 were not locally produced.

This group includes jars, jugs and pots. Chronologically speaking, Burial 16 (0221-01, 0221-02, Fig. 124, 1. 2 and Fig. 125) and Burial 14 (0252-01, Fig. 109, 1 and Fig. 111) date to the beginning of the first half of the 1st millennium BC. Two more sherds of this group derive from the fill of Pit-Complex B (0416-01) and the subsoil layer KG-015 (0036-02, not mentioned in ch. IV, as it was not found in a burial context).

Only one pot from Burial 14 (0252-02, Fig. 109, 2), could not be attributed to any of the aforementioned groups. According to its Sr- and Rb-values it could belong to Group 1, but no limestone temper was detected. The best match for a clay source can be found in Shishtepe West 01 and 02, Shishtepe East 01 and Tepe 5 06 (Fig. 318). Also, SiO_2-, Al_2O_3- (Fig. 320), CaO and S-values support the connection with Shishtepe East 01 (Fig. 319). Even if it cannot be ruled out that there is another clay source closer to Tepe 5 which could show the same chemical fingerprint as Shishtepe East 01, it seems possible that 0252-02 is an import.

Late Antique pottery (3rd/4th cent. AD)

Three samples of reddish, hard fired, fine- to medium-tempered vessels from Tepe 5 date to the Late Antiquity: the large pot 0419-01 in Burial 23 (Fig. 137 and Fig. 139, 1), one trefoil jug from Burial 26 (0393-01, Fig. 148) and another trefoil jug from Burial 27 (0472-01, Fig. 149). Their Rb-values are very high and clearly distinct from all other samples discussed here (Fig. 326). The three vessels cover quite distinctive ranges. Their Cr-values are in the range of the soil samples (Fig. 327) of Dara Yatax, the Kura or the Zayamchay. The Zn-values of two samples (0472-01, 0393-01) are slightly above those of the clay samples, except for Dara Yatax 05 (Fig. 328). Zr- and CaO-values are comparably high and in the range of Shishtepe West 01 and 02 as Old Kura Terrace Level 01 (Fig. 329). The Late Antique samples show a high SiO_2-/Al_2O_3-ratio which corresponds to the small amount of mineral temper, probably feldspar, and quartz sand (Fig. 330). The former is supported by high K_2O values (Fig. 331), which hint at the presence of feldspar as temper. The Cl- and S-values are also increased (Fig. 332). Only some samples from Gurban Tepe and Tepe 5 show higher S-values. Therefore, these sherds were probably not produced from local clays.

VII.2.1.2 Chemical groups and related fabric types

M. Gruber and K. Kaniuth

For the Karacamirli project, a descriptive terminology for the macroscopic classification of the fabric of the pottery was used consisting of three digits (Babaev et al. in print). The first digit describes the firing atmosphere, the second the sherd's hardness, the third the grain size of the temper (Table 36). In order to capture different firing intensities, the first category also differentiates between sherds that were fully or only partially oxidized in the kiln. In the following, only sherds analysed with p-XRF are included. The small number of samples reduces the statistical significance, which is why the percentages mentioned may not be regarded as representative of the entire pottery assemblage of each period, but rather as an approximation.

Early Chalcolithic pottery

The Early Chalcolithic sherds (n = 21) are all fired under oxidizing conditions, they can be either oxidized throughout (code no. 2xx, 62 %) or only partially oxi-

Firing conditions	
1xx	Completely reducing atmosphere
2xx	Completely oxidizing atmosphere
3xx	Externally oxidizing atmosphere, internally reducing atmosphere
4xx	Internally reducing atmosphere, externally oxidizing atmosphere
5xx	Oxidizing atmosphere, not fully oxidized core
6xx	Reducing atmosphere, not fully reduced core
7xx	Irregular firing atmosphere
Paste	
x1x	Very fine
x2x	Fine
x3x	Medium fine
x4x	Coarse
Hardness	
xx1	Soft
xx2	Medium hard
xx3	Hard
xx4	Very hard

Table 36. System of ceramic ware codes

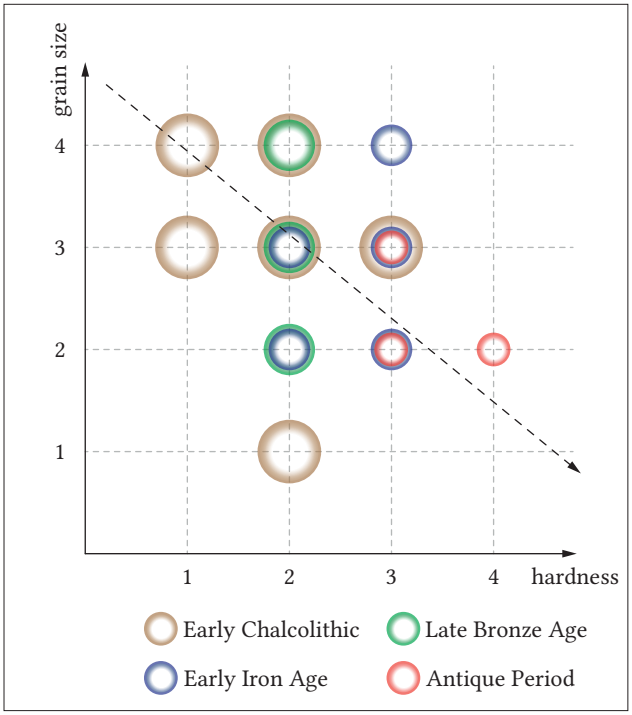

Fig. 333. Ratio of hardness and grain size of the analysed samples according to their dating

dized (code no. 5xx, 38 %), recognizable by a grey or grey-brown core. This »black core effect«, caused by a high amount of pyrite minerals, is particularly noticeable for sherds of Group 1 (see Table 35). A short firing time combined with a high amount of naturally included or added organic material most possibly caused the incompletely oxidized state of some sherds of Group 2 (0196-02, 0196-04, 0196-05), Group 3 (0045-05) and most sherds of Group 4 (0049-05, 0229-05, 0229-06, 0229-07). Their hardness ranges from soft (code no. x1x) through medium hard (code no. x2x) to hard (code no. x3x). With one exception, the grain size of the temper is either medium (code no. xx3) or coarse (code no. xx4). Oxidized burning conditions, medium hardness, and medium grain size (code no. 223) are therefore characteristic for almost 29 % of the Chalcolithic sherds from Tepe 5 analysed by p-XRF (Table 35 and Fig. 333). Partly oxidized sherds with medium hardness and grain size (code no. 523) as hard, partly oxidized sherds with medium grain size (code no. 533) each account for almost 15 %. The chemical Groups 1 and 2 include mainly medium hard sherds with medium to coarse temper (x23, x24), Group 2 additionally has some very soft examples. For Group 3, soft sherds and medium grain size dominate while Group 4 also includes some hard sherds and mainly middle grain-sized temper. Sherd 0127-05 is the only outlier with a very fine temper (221).

Late Bronze Age pottery

The Late Bronze Age pottery (n = 8) is characterized by reducing firing conditions resulting in a black vessel surface and core (code no. 1xx), but also includes sherds with simply a reduced exterior surface, while the core reveals a preceding oxidizing firing atmosphere (code no. 4xx). In tendency, completely reduced conditions dominate in Late Bronze Age Group 1, while both firing types are equally present in Group 2 (Table 35). Late Bronze Age sherds analysed with p-XRF are in general of medium hardness (code no. x2x) with fine (code no. xx2) or coarse (code no. xx4) grain sized temper in the case of Group 1, and medium-sized temper (code no. xx3) in Group 2 (Table 35 and Fig. 333).

Early Iron Age pottery

The analysed Early Iron Age pottery (n = 18) is often produced under shifting firing conditions where the final reducing process did not reach the core of the fabric

(code no. 6xx). For four sherds (0144-02, 0144-04, 0221-02, 0252-02) of Group 2 the reducing process just reached the exterior surface (code no. 4xx). Only one sherd (0241-01) of Group 1 and one of Group 3 (0417-01) are completely reduced, while Group 4 includes two completely reduced sherds (0221-01, 0252-01). Group 1 is dominated by shifting firing conditions (code no. 6xx) but also includes one completely reduced sherd (code no. 1xx). All of them are medium hard (code no. x2x) with fine (code no. xx2) to medium (code no. xx3) grain-sized temper (Table 35 and Fig. 333). Most of the sherds of Group 2 just show a reduced exterior surface (code no. 4xx), several only an oxidised core (code no. 6xx). This group is very narrowly defined by hard sherds (code no. x3x) with coarse temper (code no. xx4). Group 3 shows the same firing conditions as Group 1 but is dominated by hard sherds (code no. x3x) with medium grain-sized temper (code no. xx3). Group 4 is very diverse including different grades of reduced sherds (code no. 4xx and 6xx) but also, to a lesser extent, completely reduced ones (code no. 1xx). Sherds of this group are mostly hard (code no. x3x) with fine (code no. xx2) to medium (code no. xx3) grain sized temper.

Overall, the dominant fabric types are characterized by shifting firing conditions, with a final reducing phase which penetrated the sherd only on the outer (4xx) or outer and inner surfaces (6xx). Medium to hard sherds (x3x) and medium to coarse grain size (xx3, xx4) occur in varying combinations.

Late Antique pottery

The Late Antique pottery (n = 3) is characterized by oxidizing firing conditions (code no. 2xx). The sherds are hard (code no. x3x) to very hard (code no. x4x) with fine (code no. xx2) to medium (code no. xx3) grain sized temper (Table 35 and Fig. 333).

VII.2.1.3 The pottery of Tepe 5 through time

The Early Chalcolithic sherds (5th mill. BC) of Tepe 5 can be grouped into four chemical groups based on different geological and/or anthropologically induced features (Table 35). The Chalcolithic Group 1 is characterized by the use of a naturally mica- and pyrite-rich deltaic clay source which was possibly located close to Zayamchay or the Kura. In regard to their morphology, sherds of Group 1 are identified as thin walled mangals (ch. III). For Groups 2 to 4 and the two outliers, the use of local clay sources in the periphery of Tepe 5 (Dara Yatax or Tepe 5) seems most likely, even if other places with similar chemical signature which were not included in this study, are possible. Group 2 is defined by the mixture of local at least partly mica-rich clay sources and the use of calcite temper. Chemically the signature of those sherds matches best the chemical fingerprint of Dara Yatax soils. This group subsumes the spouted vessel (Fig. 16, 13), bases, mangals, and sherds with circular impressions at the inside below the rim (ch. III). Group 3 demonstrates the use of a naturally lime-rich local clay source, most probably from Tepe 5, and is characterised by the intensive use of high amounts of plant temper. Morphologically these samples include handled jars. Group 4 is characterized by the mixture of local clay sources and the intensive use of quartz-sand temper. The clays derive most probably from the Kura, Dara Yatax and/or Tepe 5. Due to their morphology theses samples are classified as (handled) jars. Although all different chemical groups are found with both earlier and later Chalcolithic material, the association of Group 1 chemism with horizontally lugged mangals appearing in Mentesh II may be indicative of a chronological precedence of this group.

The fabric types of all the Early Chalcolithic sherds included in this study are defined by oxidized burning condition, mainly soft to medium hardness with a dominance of medium to coarse temper. Often the core is not fully oxidized. As Chalcolithic pottery was identified in different areas of the Karacamirli survey (Babaev et al in print), most likely this pottery was locally produced.

Two different groups were defined for the Late Bronze Age (end of 16th to 13th cent. BC) pottery of Tepe 5. The Late Bronze Age Group 1 forms a narrow, chemically well-defined cluster, although typologically it includes pots of different sorts and a bowl (Table 35). All sherds of Group 1 are characterized by a laminar structure of the clay which hints to a river system, especially river deltas, as source, most possibly the Kura. Interestingly, the use of deltaic clay sources can also be found in Early Iron Age Group 2. The Late Bronze Age Group 2 includes two chemical distinct samples of big pots which are united by the use of local clay, most possibly from Dara Yatax, probably mixed with clays from the Kura. Regarding their chronology, those samples seem to mark the beginning of the Late Bronze Age of Tepe 5 (see above). Therefore, Group 2 would precede Group 1.

Coarse to fine quartz sand temper was used for all Late Bronze Age sherds with medium sized temper only occurring in Group 2. Most Late Bronze Age samples are completely reduced, but some solely show a black exterior surface. Pottery production with shifting firing condition and the use of quartz sand is also attested for the Early Iron Age. It's worth mentioning that archaeo-

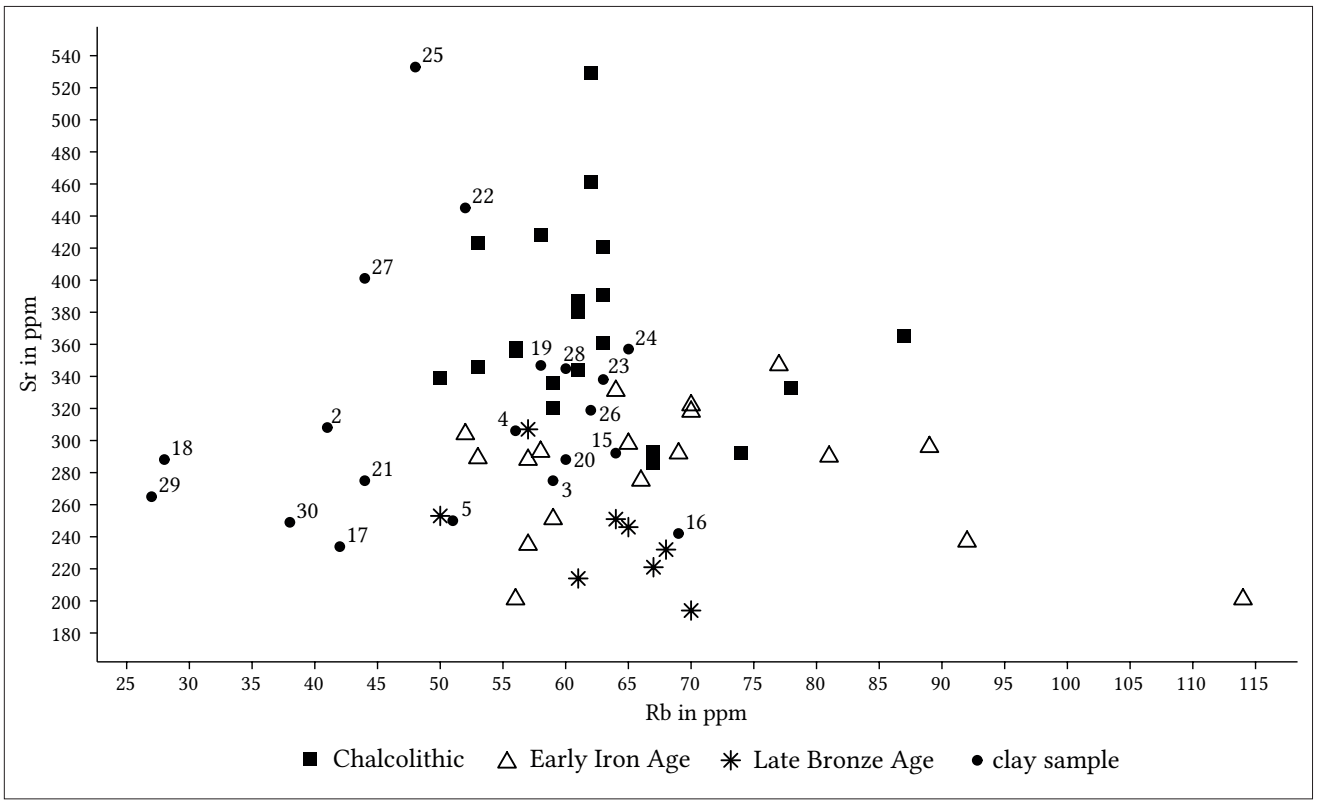

Fig. 334. Tepe 5. Scatterplot of Early Chalcolithic (n=21), Late Bronze Age (n=8), Early Iron Age pottery samples (n=18) and clay samples (n=20) showing Rb/Sr-ratio

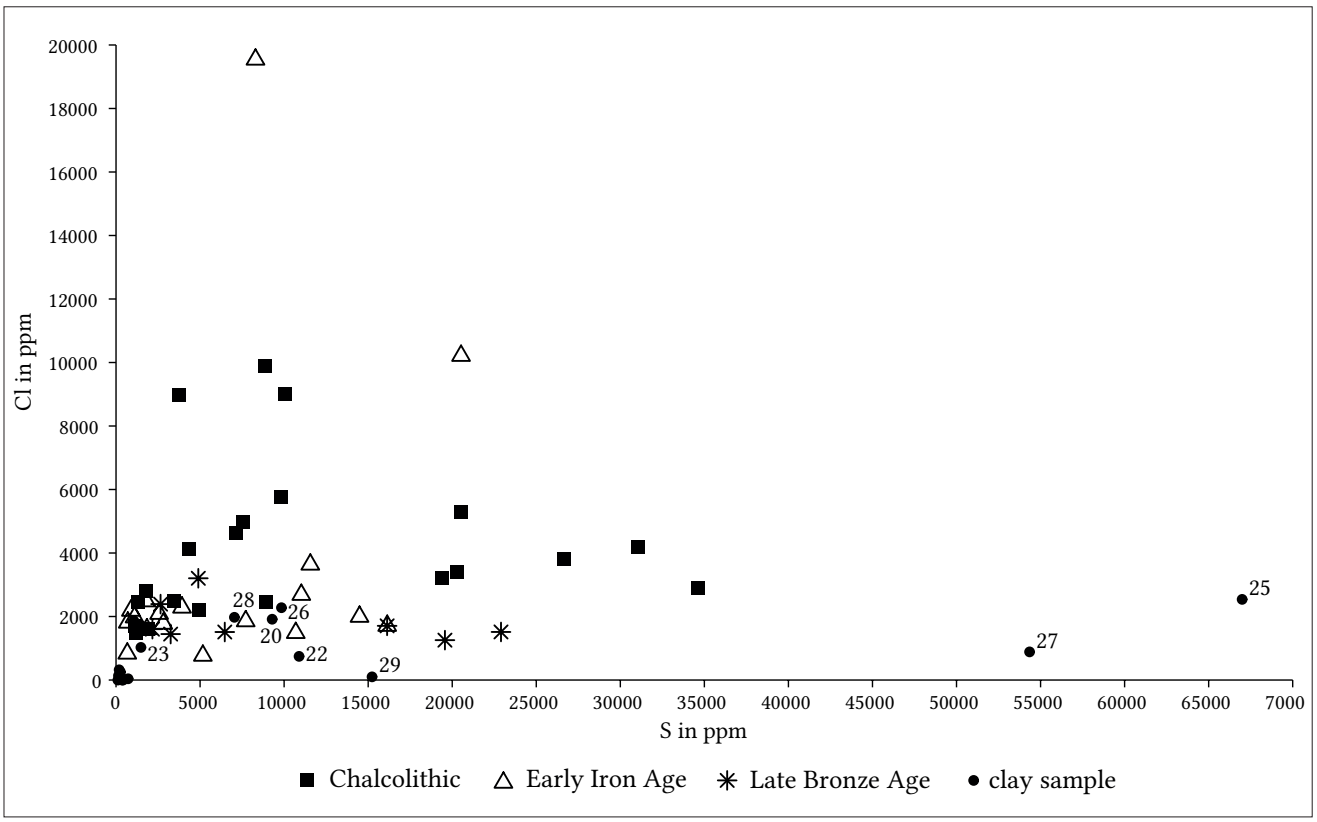

Fig. 335. Tepe 5. Scatterplot of Early Chalcolithic (n=21), Late Bronze Age (n=8) and Early Iron Age pottery samples (n=18) as well as clay samples (n=20) showing S/Cl-ratio

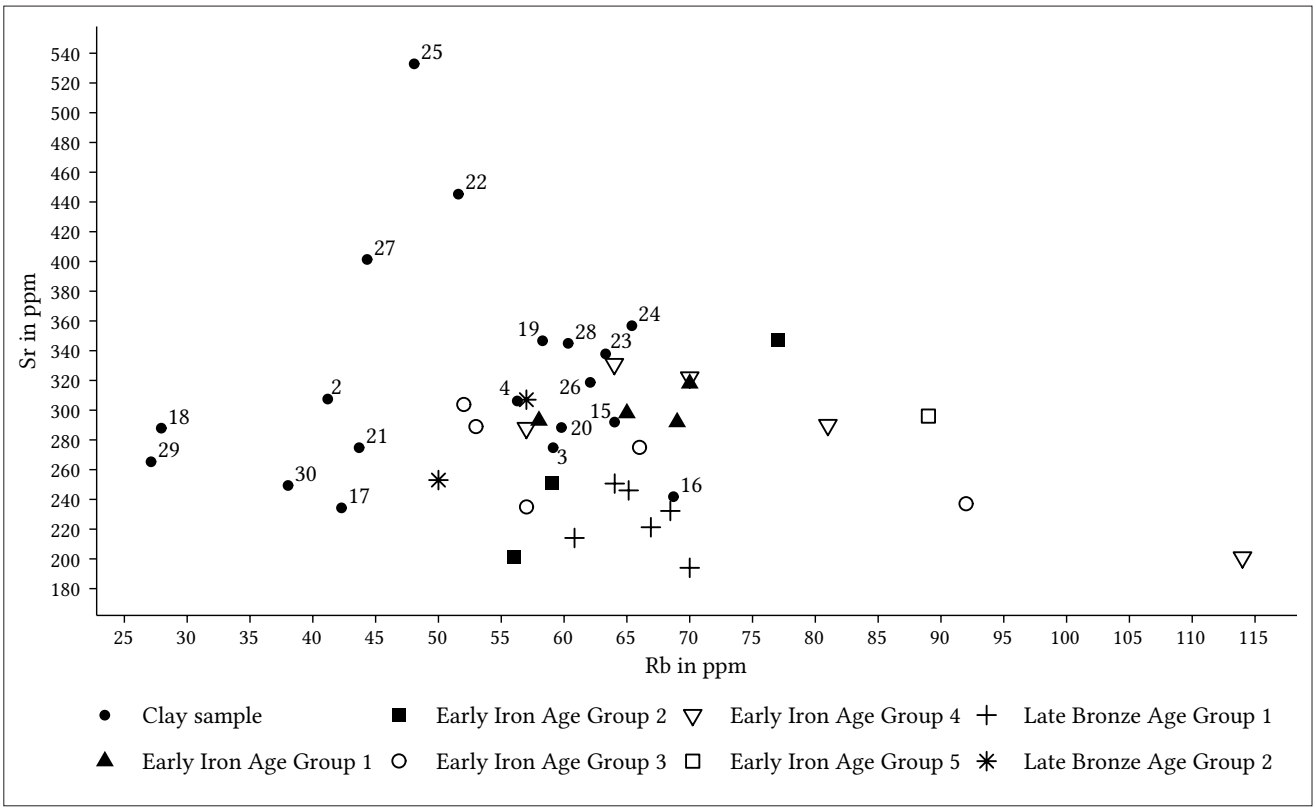

Fig. 336. Tepe 5. Scatterplot of Late Bronze Age (n=8) and Early Iron Age pottery samples (n=18) as well as clay samples (n=20) showing Rb/Sr-ratio

logically speaking sample 0100-01 (Group 2) and 0425-02 (Group 1) belong to the same typological group but differ in their chemical fingerprint, i. e. the used clay sources. With all given caution a local production of all Tepe 5 Late Bronze Age pottery probably done by different potters using distinct pastes within the same cultural framework, seems possible.

The Early Iron Age sherds (12th to 7th cent. BC) of Tepe 5 can be classified into four groups and one single sherd (Group 5) which in chronological terms all span the whole phase. The Early Iron Age Group 1 is mainly characterized by the use of local clay sources from the area of Tepe 5 or Dara Yatax (or chemically similar sources not included in this study) and limestone temper (possibly from the Shishtepe area, 25 km west-southwest of Karacamirli). The samples of Group 1 include a small pot, a carinated bowl and a flask. Group 2 is distinguished from the other groups by the laminar clay structure which suggests a formation process of the clay in a river delta. The clay most possibly derived from the Kura. Both, Group 2 and 3, are tempered with coarse quartz sand and black sand. Group 3, consisting of pots and a carinated bowl, differs in their more brownish colour achieved by mixing local clays with river or deltaic clays. As strongly eroded lime particles are included, the local clay source may have been on or immediately around Tepe 5 (see clay samples Tepe 5 and Dara Yatax). For deltaic clays the best match seems to be Qoshqarchay. Probably, due to the early date of sherds from Burial 8 (12th and 11th cent. BC), this group could be chronologically the oldest. Early Iron Age Group 4 includes sherds with a very high Sr-value which cannot be matched with one of the clay sources included in this study. Morphologically this group consists of carinated bowls, a jug and small pots. As they are also chronologically comparably neatly dated to the 1st millennium BC, i. e. to a late phase of the Early Iron Age, an interpretation as non-local ware seems not unlikely. This argument is additionally supported by the typological connections for some of the vessels of Group 4 (Burials 14 and 16) to Georgian sites (see ch. IV). This includes pot 0252-01 (defined as Group 5) from Burial 14, which is also most possibly non-locally produced, as its best match can be found in the clays of Shishtepe.

Our results support a spatial differentiation of clay sources used throughout the Iron Age. Even though the chronological implications are difficult to assess due to the small sample size, the chemical Groups 3 and 4 are the earliest in our sample (Burial 8), and are only in the later graves found associated with pottery of Groups 1,

2 and 5. Interestingly, even morphologically identical vessels (carinated bowls from Burial 15) can be produced from different clay sources.

The Early Iron Age pottery of Tepe 5 included in this study is predominantly defined by a (dark) grey surface and brownish core and/or interior surface caused by the change from an oxidizing to a reducing firing atmosphere. The samples are mostly medium hard to hard, often with medium to coarsely grained temper. In the Karacamirli survey, very little Early Iron Age pottery was identified (Babaev et al in print). It remains unclear where this pottery was produced, but the chemical fingerprint indicates a production at least for Groups 1 to 3 not too distant from Tepe 5.

The few analysed Late Antique sherds of Tepe 5 form an inhomogeneous group which is easily differentiated from all clay samples of this study. Therefore, it can be assumed that these vessels most probably were not produced locally. They are fired under oxidizing conditions, hard to very hard and with fine to medium temper.

Summing up the above, the pottery of the different periods from Tepe 5 can be chemically distinguished according to their characteristic chemical fingerprint (Fig. 334). Based on the interpretation of the chemical features in regard to their geological origin, further information on pottery production can be given: As one may expect from an archaeological perspective, pottery technology changes considerably from the Early Chalcolithic to the Late Bronze Age, but some parallels can be drawn between those periods. Pottery was produced locally at a household level, levitated, tempered with river sand and mainly fired below 850°C (see Kibaroğlu 2008: 9). The use of deltaic clays, which is already visible in the Early Chalcolithic (Group 1), can be traced through the Late Bronze Age up to the Early Iron Age (Group 2). Sr-, S- and Cl- levels drop significantly from the Early Chalcolithic to the Late Bronze Age, while vessels of the Early Iron Age range in-between those two periods (Fig. 334 and Fig. 335). This might be due to the use of clay layers which were formed under anoxidic conditions where S can accumulate under oxygen-deficient conditions (Rozanov et al. 1998: 91).

For the moment it is unclear, whether the sediments with high amounts of S like Qoshqarchay Terrace Level 07, Zayamchay 08 or Shishtepe East 01 could belong at least in their deeper layers to such geological formations processes. It is worth mentioning that the highest S-values can be identified in the clay samples of Tepe 5 10, Tepe 5 04, but also Tepe 5 06 and 11, and in sherds of the Bronze Age Burial 6 (0498-01, 0498-03) as of Early Iron Age Burial 15 (0241-01, 0241-04). Maybe these values relate to geological process we do not quite understand yet, but as the finds from Tepe 5 all can be attributed to about the same height, this seems less likely. It is also conceivable, the different S-values can be explained by the use of liquids with a comparably high amount of S, like wine, during the burial ritual.

As, in addition to these differences, the Sr-values for the Late Bronze Age pottery are lower than for the Early Chalcolithic sherds (Fig. 334), in general different clay sources or layers of the same sources were used, even if deltaic clays were still exploited. The source for the deltaic clays of the Early Chalcolithic can possibly be located close to Zayamchay or the Kura (Chalcolithic Group 1), while Late Bronze Age Group 1 pottery finds its best match in clays from the Kura, indicating a more exclusive use of clay sources. Due to the large time gap between these two periods, the differences are not surprising and comparisons have to be approached with caution.

With regard to Late Bronze Age and Early Iron Age chemical fingerprint it should not be ignored that a partial overlap of Late Bronze Age Groups 2 sherd 0498-02 and pottery of Early Iron Age Group 3 (sherds 0241-02, 0241-06) occurs (Fig. 336). As the former seems to belong to the earliest Bronze Age contexts of Tepe 5 (end of 16th cent. BC to beginning of the 15th cent. BC; see above) while the later dates to the advanced Early Iron Age of Tepe 5 (8th–7th cent. BC), this overlap might be seen as accidental. But again, Early Iron Age Group 3 could – because of pottery from Burial 8 – date to 12th and 11th cent. BC which would make a relationship between those two groups a distinct possibility. Given these uncertainties, we refrain from further developing this point.

More obvious relations between those two periods are discernible for Late Bronze Age Group 1 and Early Iron Age Group 2. Their connection is visible in many chemical elements (Fig. 336) and in the continuing use of deltaic clays from the Kura. Also, the use of quartz sand as temper continues. Black sand temper, on the contrary, only appears in Early Iron Age Group 2, while the firing conditions seem comparable: Some sherds from both periods show (only) a reduced exterior surface. Completely reduced sherds, which dominate Late Bronze Age Group 1, cannot be found in Early Iron Age Group 2 (see above). As this tendency is visible in all Early Iron Age pottery from Tepe 5 included in this study, a shift to a shorter reducing period seems to define this phase. Considering the time gap of about 500 years and the differences in temper and firing process, the interpretation as an ongoing local tradition from Late Bronze to Early Iron Age has to be treated with caution. Still, it seems possible that the technique (procurement, temper, firing conditions) was already established and kept in use.

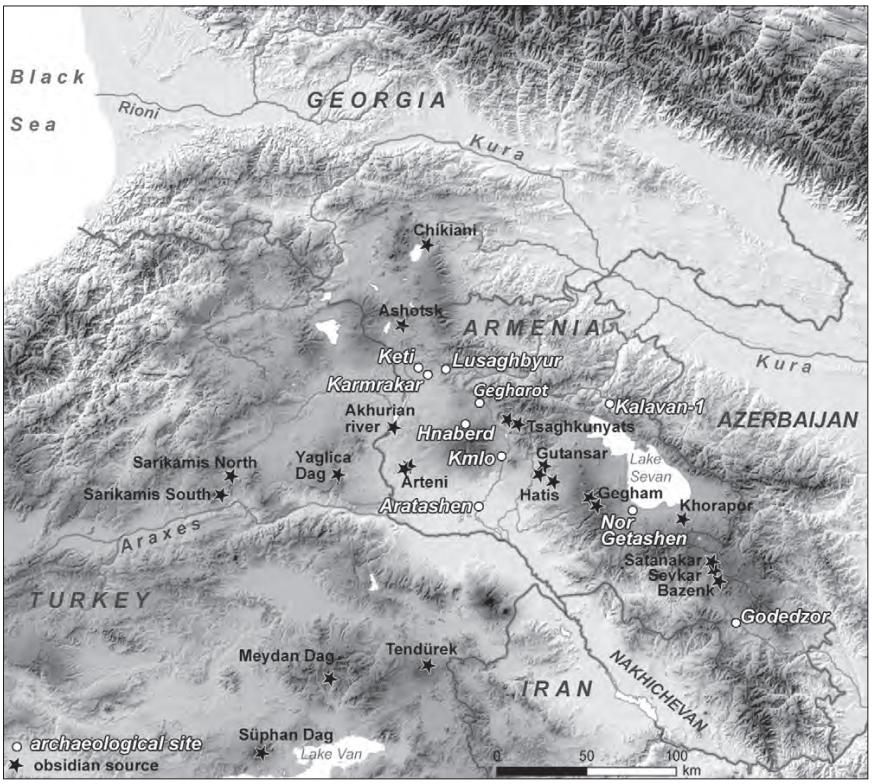

Fig. 337. Map of obsidian sources (after Chataigner/Gratuze 2014: Fig. 1)

The use of quartz sand of different grain sizes and amounts occurs in all periods of Tepe 5, while calcite and organic temper are limited to the Early Chalcolithic. A reconstruction of the firing process showed that pottery containing calcite had to be fired below 700°C, since calcite reacts with clay minerals to form alumosilicates at higher temperatures. Intentional temper with limestone starts not before the Early Iron Age but has already disappeared by the Late Antique period.

An analysis of the fabrics of Tepe 5 shows that in the Early Chalcolithic only oxidized firing conditions are visible. The firing technology became more complex and by the Late Bronze and Early Iron Ages both oxidizing and reducing firing conditions were employed. Lastly, a strong tendency to produce harder pottery with finer grained temper is visible through time (Fig. 333).

VII.3 Obsidian

Obsidian provenance research has its roots in the 1960s. The felsic volcanic glass can be used to link archaeological artefacts with geological sources – given source variability but relative intra-source homogeneity. As obsidian is very resistant to changes in its chemical fingerprint after its formation or during the crafting process of an archaeological artefact, their assignment to resource areas is more straightforward than for other materials (such as metals or pottery). For the past decades, studies of obsidian using p-XRF have steadily increased. Additionally, due to the short sampling times, the number of artefacts included in these studies has multiplied. Visual sourcing, by contrast, is in decline (Golitko 2019: 84–86), also because colour and texture of obsidian can change in the process of dehydration during the eruption of the volcano, making secure identification somewhat hazardous, while the geochemical signature of one glass flow stays the same (Chataigner/Gratuze 2014: 50). The main chemical elements to establish discriminations between obsidian outcrops which are reliably detected by p-XRF are Ba, Rb, Sr, Y, Zr and Nb (Abedi et al. 2018: 408). Unfortunately, the Ba calibration for our instruments is not sufficiently accurate. Therefore, Zr and ratios of this element are used in this study. The availability of samples from possible sources in the area has, on the other hand, compensated for a deficiency often encountered in past studies, which lacked sufficient background data on available sources in the region (Golitko 2019: 89–90).

VII.3.1 Sources

For this study seven obsidian sources close to Tepe 5 were considered: Arteni, Ashotsk, Chikiani, Dzhraber Gutan-

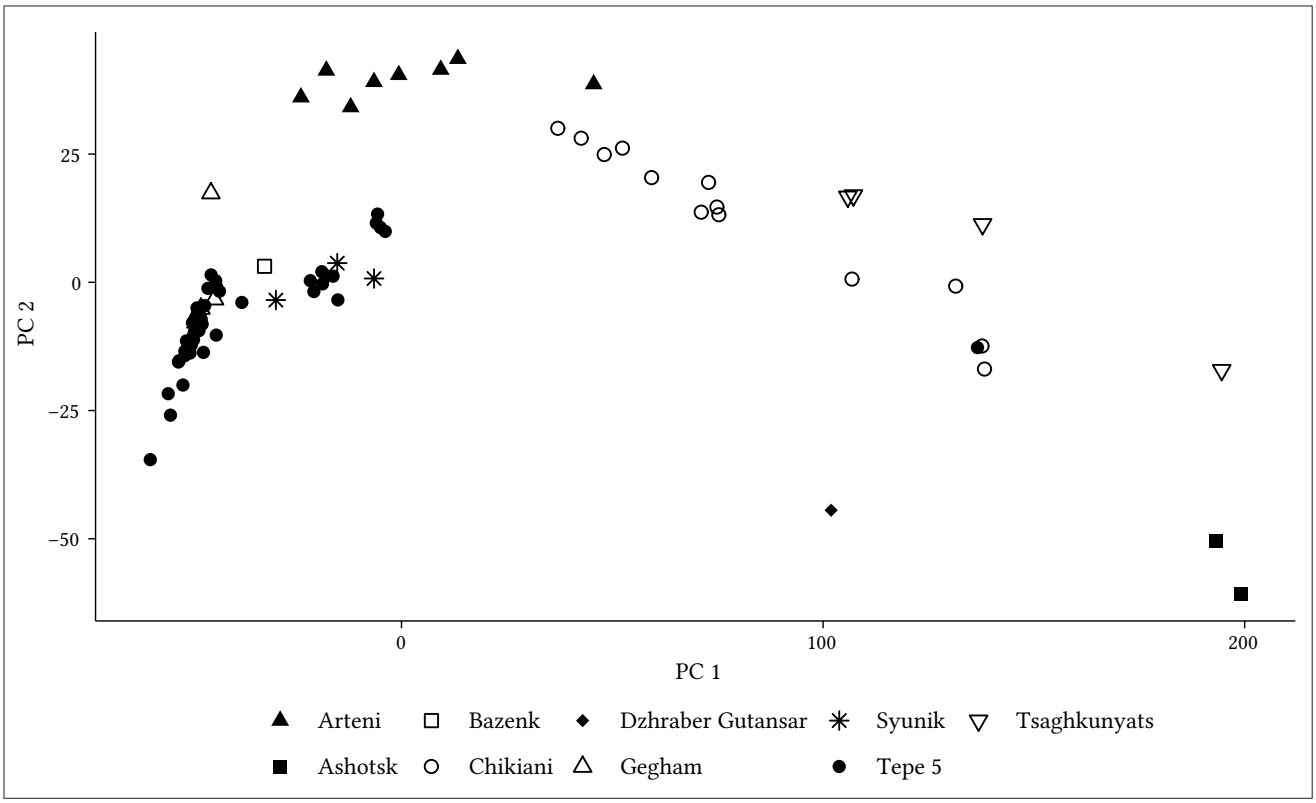

Fig. 338. Tepe 5. PCA of obsidian artefacts (n=48) and source regions (n=37).
Most obsidian found at Tepe 5 stems from the outcrops of Gegham

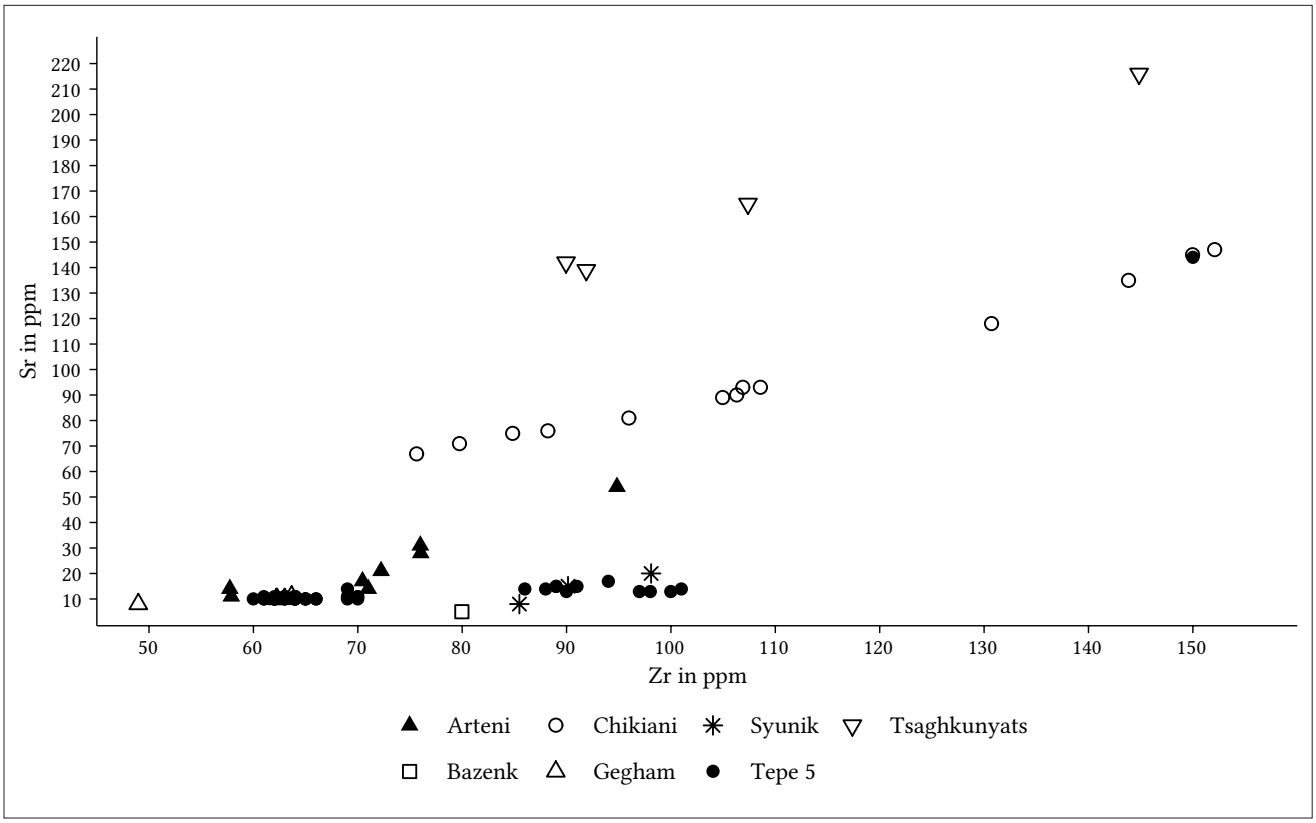

Fig. 339. Tepe 5. Scatterplot of obsidian artefacts (n=48) and sources (n=37) showing Zr/Sr-ratio.
The Zr- and Sr- values of 0489 match the Chikiani 3 outcrop

Sample	Context	Source	Zr	Sr	Rb	Nb	Y
0038	KG-016	Syunik	89	15	164	34	5
0039	KG-016	Gegham Geghasar	64	11	180	48	17
0051	KG-018	Gegham Geghasar	60	10	179	48	17
0052	KG-017	Syunik	86	14	166	33	6
0061	KG-017	Syunik	88	14	162	34	5
0075	KG-022	Gegham Geghasar	64	11	189	51	17
0079	KG-022	Syunik	101	14	143	33	6
0087	KG-024	Gegham Geghasar	63	11	195	51	16
0088	KG-023	Gegham Geghasar	64	10	187	49	18
0092	KG-023	Gegham Geghasar	65	10	195	51	18
0095	KG-023	Gegham Geghasar	61	10	182	47	16
0097	KG-023	Gegham Geghasar	61	10	186	50	17
0126	KG-023	Gegham Geghasar	61	11	180	46	16
0167	KG-032	Syunik	94	17	164	34	5
0383	KG-066	Gegham Geghasar	63	11	190	50	17
0388	KG-066	Gegham Geghasar	62	10	188	50	17
0395	KG-057	Gegham Geghasar	63	10	184	50	18
0397	KG-057	Gegham Geghasar	64	11	188	49	17
0399	KG-057	Gegham Geghasar	69	10	199	53	17
0401	KG-057	Syunik	90	13	166	34	6
0402	KG-057	Gegham Geghasar	66	10	203	54	18
0405	KG-074	Syunik	100	13	143	33	6
0412	KG-057	Gegham Geghasar	69	14	180	43	15
0413	KG-057	Syunik	91	15	161	33	5
0426	KG-074	Gegham Geghasar	66	10	194	50	17
0429	KG-095	Gegham Geghasar	70	11	216	56	19
0431	KG-095	Gegham Geghasar	65	10	193	51	17
0433	KG-095	Gegham Geghasar	64	10	197	51	17
0434	KG-095	Gegham Geghasar	64	10	192	52	17
0446	KG-100	Gegham Geghasar	62	10	187	50	17
0457	KG-094	Gegham Geghasar	64	10	190	50	17
0461	KG-074	Gegham Geghasar	64	11	193	50	18
0463	KG-094	Gegham Geghasar	69	11	206	54	18
0469	KG-095	Gegham Geghasar	70	10	191	50	17
0476	KG-094	Gegham Geghasar	62	10	186	48	17
0482	KG-100	Gegham Geghasar	65	10	191	51	17
0483	KG-095	Syunik	89	15	162	34	6
0485	KG-095	Syunik	98	13	143	34	6
0486	KG-095	Gegham Geghasar	62	10	189	50	18
0487	KG-095	Gegham Geghasar	64	10	197	52	17
0488	KG-102	Gegham Geghasar	70	11	187	48	16
0489	KG-095	Chikiani	150	144	101	15	9
0492	KG-095	Gegham Geghasar	64	10	192	51	17
0493	KG-095	Syunik	97	13	142	32	6
0502	KG-074	Gegham Geghasar	64	11	194	50	18
0513	KG-095	Gegham Geghasar	63	10	193	50	17
0516	KG-077	Gegham Geghasar	62	11	180	48	16
0531	KG-083	Gegham Geghasar	63	11	191	50	17

Table 37. List of sampled obsidian from Tepe 5

sar, Gegham, Tsaghkunyats and Syunik (Chataigner/Gratuze 2014: 49). The four locations matching the chemistry of artefacts from Tepe 5 will be discussed briefly. All sites are part of the Lesser Caucasus, a highly active volcanic zone, which has been intensely exploited for obsidian (Fig. 337).

The Armenian outcrop of Arteni, which is part of the Aragats flow (Chataigner/Gratuze 2014: 65), was intensively exploited by populations of the Chalcolithic Sioni culture of the Arax Basin and also by the Neolithic Shulaveri-Shomutepe culture in the Kura Basin (Chataigner/Gratuze 2014: 61). In Armenia, at sites like Aratashen, a high percentage of Arteni material was used for temper but also tools were made of material from this source (Palumbi et al. 2018: 129–131). Three individual sources can be differentiated by their location at the volcano: Arteni, Mets Arteni and Pokr Arteni (Abedi et al. 2018: 408). The sources are defined by comparably high Y/Zr-ratios and Nb/Zr-ratios. Only the source of Gegham shows higher Nb/Zr-ratios (Chataigner/Gratuze 2014: 53).

The south Georgian source of Chikiani is located some 85 km south-west of Tiblisi near the Kura tributary Khrami (Biagi et al. 2017a: 3. 14–18). It is characterized by low Zr and high Ba contents. At Chikiani we find at least three chemical groups (Biagi/Gratuze 2016: 21–31): Groups 1 and 3 can be further divided into sub-groups with lower (1a, 3a) or higher (1b, 3b) Zr/Ba-ranges (Biagi et al. 2017b: 11–16). Finds from those outcrops were never found in Armenia, but Chikiani was one of the main

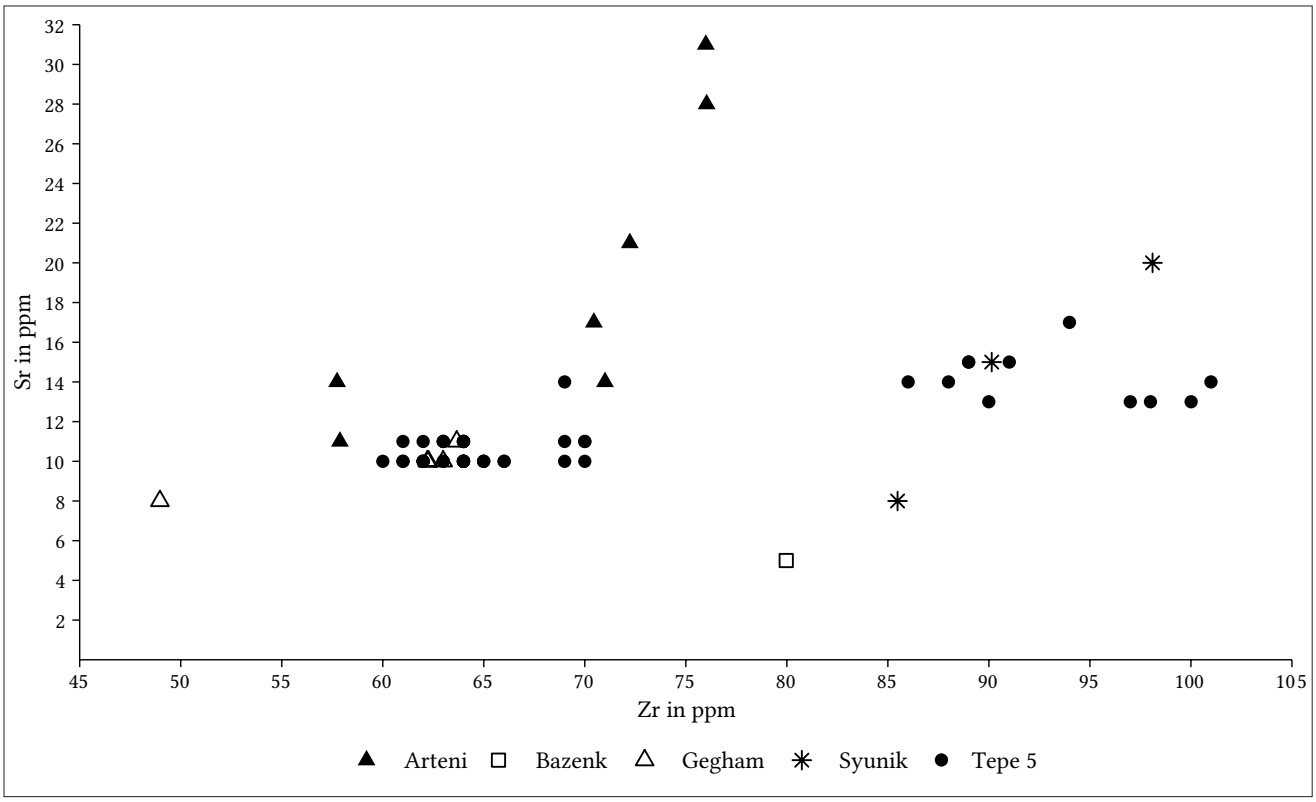

Fig. 340. Tepe 5. Scatterplot of obsidian artefacts (n=48) and sources (n=17) showing Zr/Sr-ratio. Only sample 0412 shows connections to the outcrops of Arteni

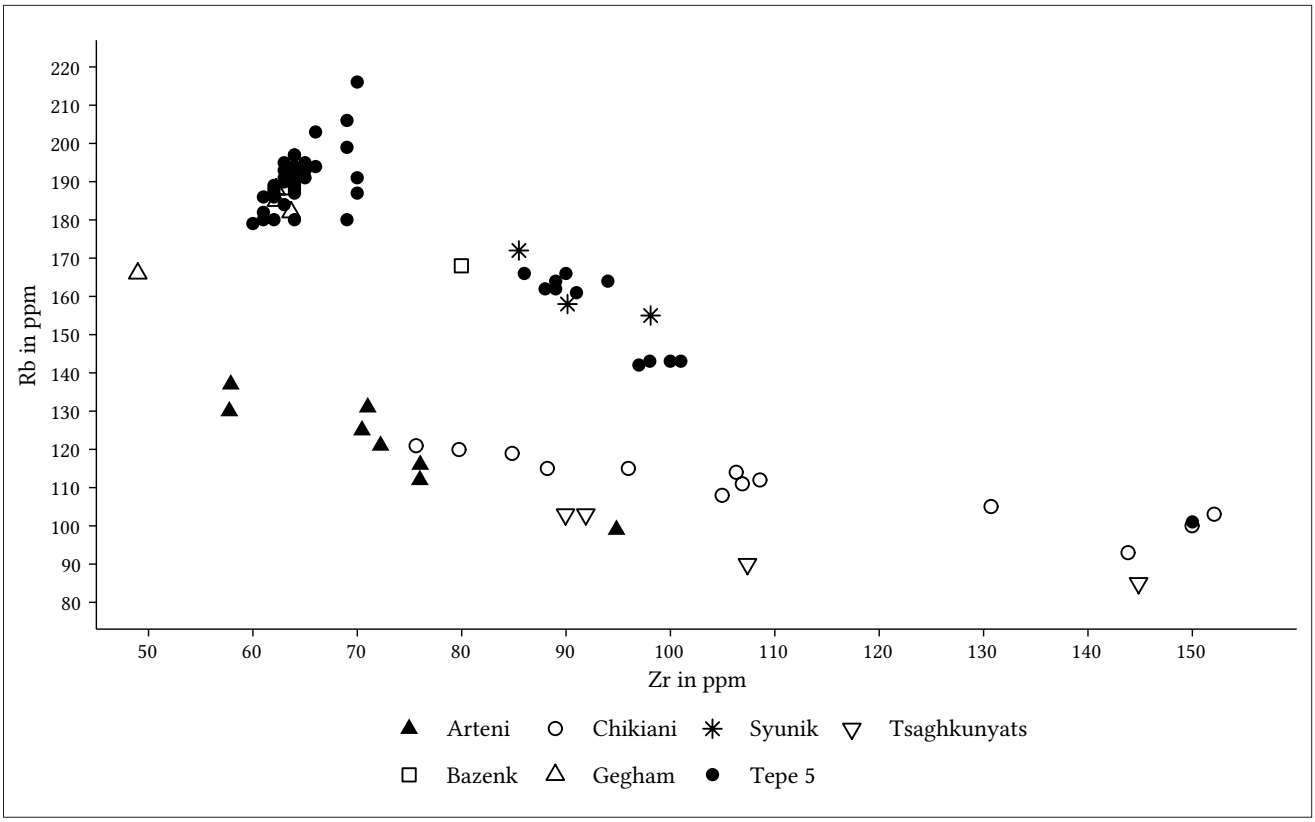

Fig. 341. Tepe 5. Scatterplot of obsidian artefacts (n=48) and sources (n=34) showing Zr/Rb-ratio. The obsidian of Tepe 5 shows strong connections with Gegham and Syunik

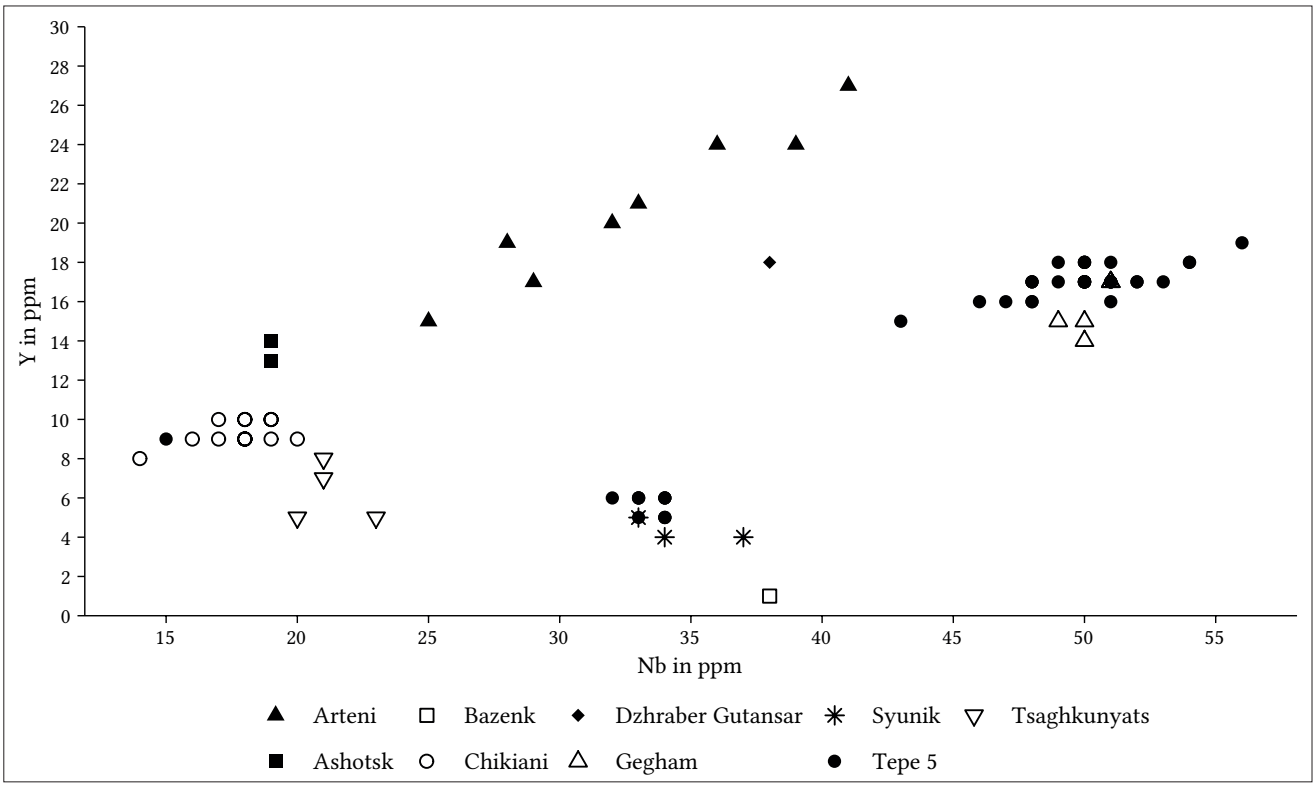

Fig. 342. Tepe 5. Scatterplot of obsidian artefacts (n=48) and reference material (n=37) showing Nb/Y-ratio. The most important sources for the obsidian of Tepe 5 were Gegham and Syunik

sources for locations in Georgia and as far as 500 km south-east of the source (Biagi/Gratuze 2016: 9–13. 31). Chronologically, exploitation ranges from the Palaeolithic to the historical periods (Biagi et al. 2017a: 1). Chikiani 2 and 3b were most intensively exploited by Chalcolithic and Bronze Age groups while Chikiani 1 was used to a lesser extent during these times (Biagi et al. 2017b: 16).

The outcrops of the Gegham massif, Geghasar and Spitaksar, are located in the south-west of Lake Sevan (Abedi et al. 2018: 408). Gegham obsidian is characterized by its low Ba- and Zr-values and by high Y/Zr-, Nb/Zr- (Chataigner/Gratuze 2014: 52–53) and Rb/Sr-ratios (Abedi et al. 2018: 411). Obsidian from these sites was intensively used in the Chalcolithic (Mentesh Tepe) as temper in pottery but also for tools (Palumbi et al. 2018: 129–131).

Syunik is another south Armenian source that supplied Chalcolithic Mentesh Tepe (Palumbi et al. 2018: 129–131) and settlements around Lake Urmia in Iran (Chataigner/Gratuze 2014: 64). The Syunik source comprises the outcrops of Bazenk, Sevkar, Mets Sevkar, Satanakar, Mets Satanakar and Pokr Satanakar (Abedi et al. 2018: 408). The chemistry of these outcrops is quite diverse. High values of Zr (Sevkar) are encountered, as are low Zr-values (Satanakar). The use of high altitude deposits as Gegham and Syunik apparently had its peak in the Bronze Age, when high temperatures and arid conditions lead to an increased transhumance and use of upland pastures (Chataigner/Gratuze 2014: 52–56. 67).

VII.3.2 The obsidian from Tepe 5

As the focus of our research was on ceramics, not all of the (eventually 192) obsidian objects from Tepe 5 could be sampled with p-XRF. To include as much variety as possible, obsidian was sorted for each context by colour and transparency. For each macroscopic group, one sample was selected for measuring. As a result, our sample includes 25 % of all obsidian pieces from Tepe 5 – 46 obsidian flakes and two artefacts (0489, 0502) out of 15 contexts (Table 37). All flakes derive from grave or pit fillings, topsoil or subsoil layers. Clearly dating to the Chalcolithic are finds from Pit-Complexes A and B. Assuming that Tepe 5 was once covered by a chalcolithic settlement most, if not all, finds deriving from Late Bronze Age or Early Iron Age grave fillings should be attributed to this period, too (ch. III).

Using the sourcing elements of Obsidian which can reliably be measured by p-XRF (Nb, Y, Zr, Sr, Rb) for a PCA (inertia of PC 1 87 %, PC 2 7 %; computed with variance-covariance matrix), it is clear that the majority of

Sample	Material	Gr.	Object	Context	Fe	Ni	Cu	As	Ag	Sn	Sb	Pb	Bi
0090	Copper		ring	KG-024	0.18	0.00	98.83	0.10	0.05	0.18	0.54	0.06	0.00
0219	Copper		fragment	KG-054	2.43	0.00	95.84	0.23	0.00	0.44	0.04	0.69	0.00
0232	Copper		fragment	KG-054	5.14	0.01	93.56	0.10	0.00	0.47	0.00	0.18	0.00
0342a	Copper		bead	KG-059	0.86	0.04	97.61	0.22	0.00	0.87	0.03	0.20	0.00
499,01	Copper		pendant	KG-095	1.51	0.03	97.29	0.23	0.00	0.14	0.00	0.54	0.00
499,02	Copper		pendant	KG-095	1.59	0.00	97.49	0.19	0.00	0.31	0.00	0.21	0.00
0344	Arsenic Copper	1	bead	KG-059	1.32	0.09	97.24	0.62	0.00	0.34	0.00	0.22	0.00
338a.01	Arsenic Copper	1	bead	KG-059	0.62	0.00	97.20	0.63	0.00	0.77	0.39	0.30	0.00
338a.02	Arsenic Copper	1	bead	KG-059	0.49	0.00	97.60	0.76	0.00	0.43	0.00	0.61	0.00
341a.02	Arsenic Copper	1	bead	KG-059	1.56	0.00	96.66	0.76	0.00	0.49	0.04	0.19	0.18
341a.03	Arsenic Copper	1	bead	KG-059	0.61	0.06	97.67	0.82	0.00	0.37	0.08	0.28	0.01
341a.01	Arsenic Copper	2	bead	KG-059	0.82	0.04	95.93	2.07	0.00	0.36	0.16	0.45	0.00
0343a	Arsenic Copper	2	bead	KG-059	1.74	0.05	94.66	2.69	0.00	0.19	0.15	0.22	0.00
0271a	Arsenic Copper	2	bead	KG-059	1.65	0.02	94.00	2.97	0.00	0.41	0.19	0.58	0.00
259.02	Arsenic Copper	2	eyelet	KG-059	2.26	0.00	92.92	3.00	0.00	1.10	0.21	0.25	0.00
0279	Arsenic Copper	3	eyelet	KG-059	2.03	0.01	88.79	7.32	0.01	0.46	0.34	0.83	0.02
0374a	Arsenic Copper	3	eyelet	KG-059	2.24	0.00	88.33	7.45	0.00	0.59	0.32	0.78	0.00
0263	Arsenic Copper	3	finger ring	KG-059	0.70	0.06	90.54	7.92	0.02	0.15	0.27	0.17	0.00
0345	Arsenic Copper	3	bracelet	KG-059	0.44	0.04	88.58	10.28	0.00	0.10	0.29	0.10	0.00
0302a	Tin Bronze	1	bead	KG-059	1.00	0.00	97.35	0.17	0.00	1.03	0.03	0.27	0.00
0512	Tin Bronze	1	bracelet	KG-074	0.69	0.02	97.96	0.04	0.00	1.06	0.00	0.07	0.00
0007	Tin Bronze	1	dagger	survey	2.78	0.10	94.90	0.07	0.00	1.28	0.00	0.40	0.00
0259.01	Tin Bronze	1	pendant	KG-059	0.56	0.03	96.41	0.07	0.00	2.53	0.00	0.29	0.00
0266	Tin Bronze	2	sheet	KG-059	0.66	0.02	92.86	1.84	0.03	3.89	0.18	0.40	0.00
0473	Tin Bronze	2	ring	KG-097	1.83	0.00	93.41	0.03	0.00	4.21	0.15	0.11	0.00
0180	Tin Bronze	2	disc	KG-043	0.08	0.01	94.21	0.05	0.00	5.48	0.00	0.12	0.00
0394	Tin Bronze	2	fragment	KG-057	0.97	0.00	91.76	0.16	0.06	6.37	0.05	0.45	0.00
0091	Tin Bronze	2	pommel	KG-024	0.14	0.06	91.37	0.39	0.07	7.28	0.07	0.59	0.01
0218	Tin Bronze	2	bead	KG-054	1.53	0.01	90.70	0.02	0.00	7.44	0.00	0.05	0.00
0212	Tin Bronze	2	bead	KG-053	1.41	0.00	90.62	0.01	0.00	7.51	0.00	0.23	0.00
0256	Tin Bronze	2	sheet	KG-063	1.23	0.03	90.02	0.06	0.04	8.10	0.24	0.11	0.00
0400	Tin Bronze	2	sheet	KG-00	0.56	0.03	90.88	0.00	0.03	8.40	0.00	0.02	0.00
0179	Tin Bronze	2	disc	KG-043	0.12	0.00	90.97	0.07	0.00	8.57	0.00	0.19	0.00
0089.02	Tin Bronze	3	dagger	KG-024	0.25	0.06	86.08	0.45	0.00	12.45	0.03	0.65	0.01
0089.01	Tin Bronze	3	dagger	KG-024	0.08	0.08	82.90	0.40	0.08	15.84	0.05	0.54	0.00
0262	Tin Bronze	4	sheet	KG-059	0.32	0.03	75.49	0.24	0.00	22.91	0.02	0.92	0.00
0276d	Tin Bronze	4	sheet	KG-059	0.05	0.00	68.28	0.37	0.00	30.11	0.00	1.10	0.02
0211.01	Leaded Tin Bronze		finger ring	KG-053	0.12	0.00	84.16	0.05	2.36	6.66	0.37	6.17	0.05
0211.02	Leaded Tin Bronze		finger ring	KG-053	1.99	0.00	76.74	0.00	0.22	11.14	0.00	9.47	0.04
0211.03	Leaded Tin Bronze		finger ring	KG-053	0.33	0.10	78.36	0.09	0.21	10.50	0.05	10.21	0.07
0390	Iron/Copper		bracelet	KG-057	34.22	0.00	62.66	0.01	0.00	1.26	0.00	0.16	0.09
0514	Iron/Copper		blade	KG-074	65.36	0.05	30.71	0.32	0.00	0.21	0.00	0.25	0.14
0249	Iron		fragment	KG-058	94.45	0.00	0.15	0.00	0.00	0.32	0.00	0.20	0.18
0258	Iron		fragment	KG-057	94.89	0.00	0.08	0.00	0.00	0.22	0.00	0.26	0.23
0260	Iron		fragment	KG-057	94.79	0.00	0.08	0.00	0.00	0.25	0.00	0.25	0.23
0277	Iron		fragment	KG-057	94.85	0.00	0.14	0.01	0.00	0.32	0.00	0.14	0.13
0386	Iron		fragment	KG-057	94.71	0.00	0.13	0.00	0.00	0.32	0.00	0.24	0.22
0435	Iron		fragment	KG-057	93.84	0.00	0.11	0.00	0.00	0.34	0.00	0.31	0.29
0471	Iron		knife	KG-097	94.52	0.00	0.19	0.00	0.00	0.46	0.00	0.18	0.16
0382	Iron		fragment	KG-057	95.03	0.00	0.07	0.00	0.00	0.16	0.02	0.32	0.30
0470	Silber		finger ring	KG-097	0.59	0.01	85.94	0.01	11.62	1.56	0.02	0.10	0.02
0519	Silber		earring	KG-077	0.21	0.00	56.59	0.13	37.79	1.20	0.00	3.82	0.16

Table 38. Measurement results of significant elements for the metal artefacts of Tepe 5 and a stray find from the survey (0007)

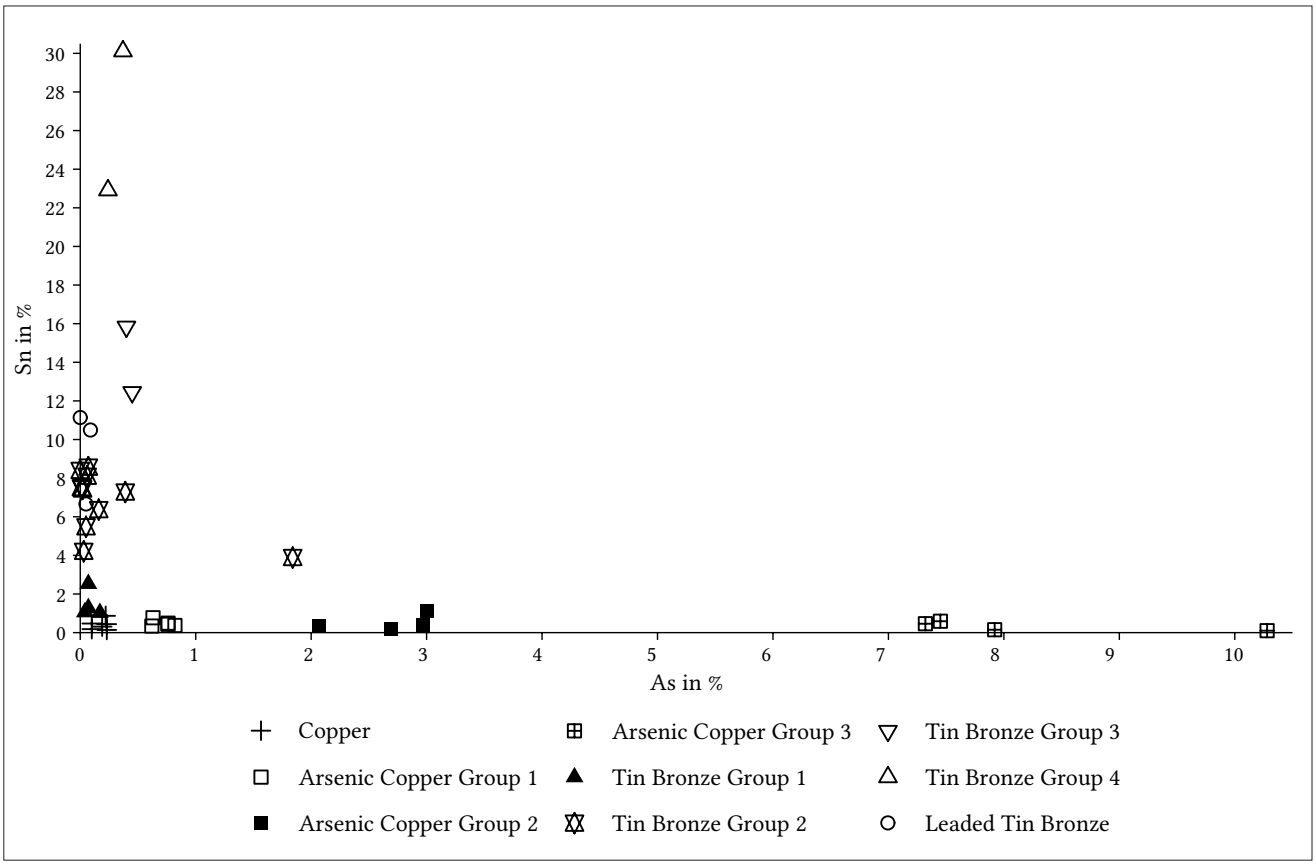

Fig. 343. Tepe 5. Scatterplot of copper (n=5), arsenic copper (n=13), tin bronze (n=17) and leaded tin bronze artefacts (n=1) showing Zr/Sr-ratio (n in this case referes to the numbers of objects not the number of measurements per object. Measurements of the same artefact can be identified in Table 38 by .0X)

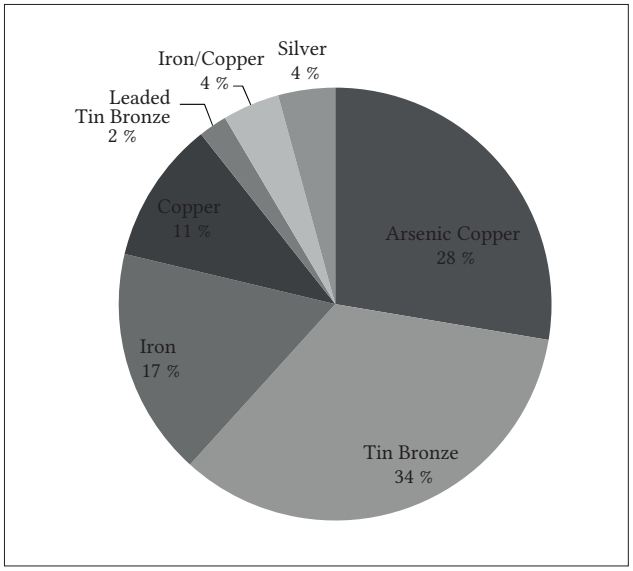

Fig. 344. Percentage of metals identified at Tepe 5 (the survey find 0007 is not included)

our objects match the sources of Gegham-Geghasar. Several show a strong relation with the sources of Syunik (0038, 0052, 0061, 0167, 0401, 0413, 0483) while only the arrowhead from Burial 6 (0489) can be attributed to a Chikiani outcrop. Interestingly, several objects whose sources are not included in this dataset (0079, 0405, 0485, 0493) seem also to be present at Tepe 5 (Fig. 338).

Going into more detail, the arrowhead 0489 (Burial 6) can be attributed to the Chikiani 3 outcrop, mining Area G with high Zr-values (Fig. 339). Objects from the Syunik outcrop can be divided into two groups – one related to Mets Sevkar (0079, 0167, 0405, 0485, 0493) and one to Pokr Sevkar (0038, 0052, 0061, 0401, 0413, 0483). The former includes those samples that could not be directly attributed by the PCA. 0412 shows a tendency to Pokr Arteni. As in the PCA, most objects included in this study derive from the Gegham Geghasar outcrops (Fig. 340). By looking at Rb-values, the same patterns as in the PCA are visible, while more detailed differentiation visible in the Sr-values cannot be picked up. In contrast, relations with Syunik, Mets Satanakar and Pokr Sevkar are closer when considering Rb-/Zr- values than those with Mets Sevkar. Also, no connections to Pokr Arteni can be observed (Fig. 341).

Adding the results of Nb-/Y-values (Fig. 342) the most conclusive interpretation of the measurements is, that

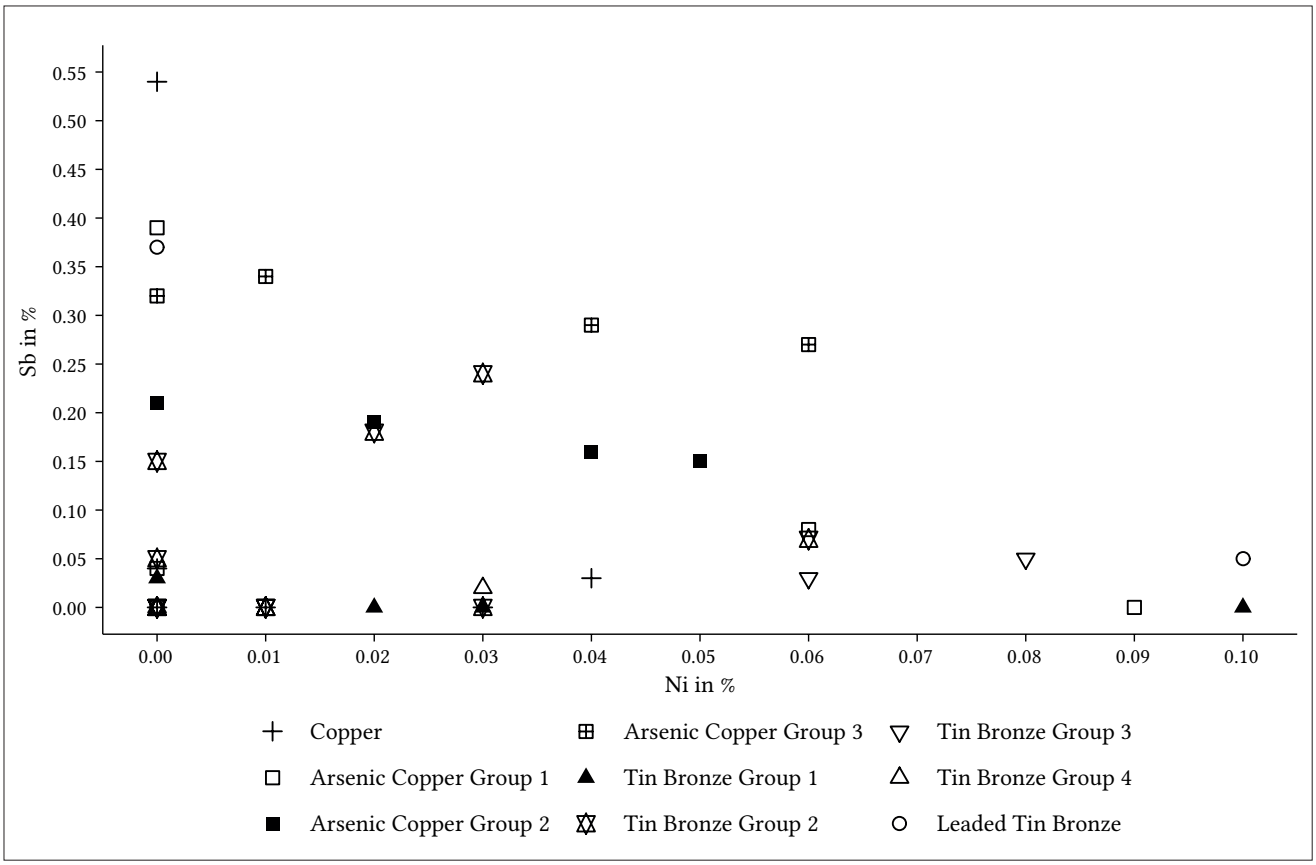

Fig. 345. Tepe 5. Scatterplot of copper (n=5), arsenical copper (n=13), tin bronze (n=17) and leaded tin bronze artefacts (n=1) showing Ni/Sb-ratio. For some arsenic copper artefacts, Ni- and Sb-values are increased

the bulk of the objects can be attributed to Gegham Geghasar including the re-used Late Bronze Age arrowhead from the Late Antique Burial 21 (0502, Fig. 133, 1). Other important obsidian sources for Tepe 5 were the Syunik outcrops Mets Sevkar and Pokr Sevkar (0038, 0052, 0061, 0079, 0167, 0401, 0405, 0413, 0483, 0485, 0493) while only one arrowhead (0489, Fig. 69, 1) from Burial 6 was produced from Chikiani 3 obsidian. As most finds are stray finds and/or can be attributed to the Early Chalcolithic settlement of Tepe 5, no further chronological breakdown of the Tepe 5 material is necessary. Both intensively used outcrops have been connected with Chalcolithic exploitation previously, for example at Mentesh Tepe.

VII.4 Metal analyses

According to our current understanding, the smelting of copper ores is first attested in the Balkans in the late 6th millennium BC, from where it spread to Anatolia. These objects include trace elements like As, Sb, Co, Ni and Pb as result of the smelting process (Garfinkel et al. 2014). In the Southern Caucasus, the earliest metallurgical evidence in the form of wastes, ore grinders and Cu residues appears with the Neolithic Shulaveri-Shomutepe culture of the mid-6th millennium BC (Courcier et al. 2016: 26). By the mid-5th millennium BC there is abundant evidence for a productive copper industry, best known from the site of Mentesh Tepe, 36 km to the west of Karacamirli. Inclusions of As occur rarely (Courcier et al. 2017: 526–528, with further references). The elements present in these pre-Bronze Age artefacts (As, S, Sb, and particularly Ni) and their relations point to the nearby Sevan-Akera ophiolites, which extends in a NW-SE direction along the northern flanks of the Lesser Caucasus (Courcier et al. 2008; Adamia et al. 2011: 493; Helwing et al. 2012; Courcier et al. 2016; 2017). Towards the Kura lowlands, this zone is bordered by the mining zones of Bolnisi-Madneuli (Georgia), Alaverdi-Kapan (Armenia) and Gadabay-Dashkesan (Azerbaijan). These mining areas probably supplied the Cu ore on which the southern and eastern Azerbaijani industries were based until the Iron Age.

Turning to precious metals, silver is known from the Halaf Culture settlement of Domuztepe in Turkey since

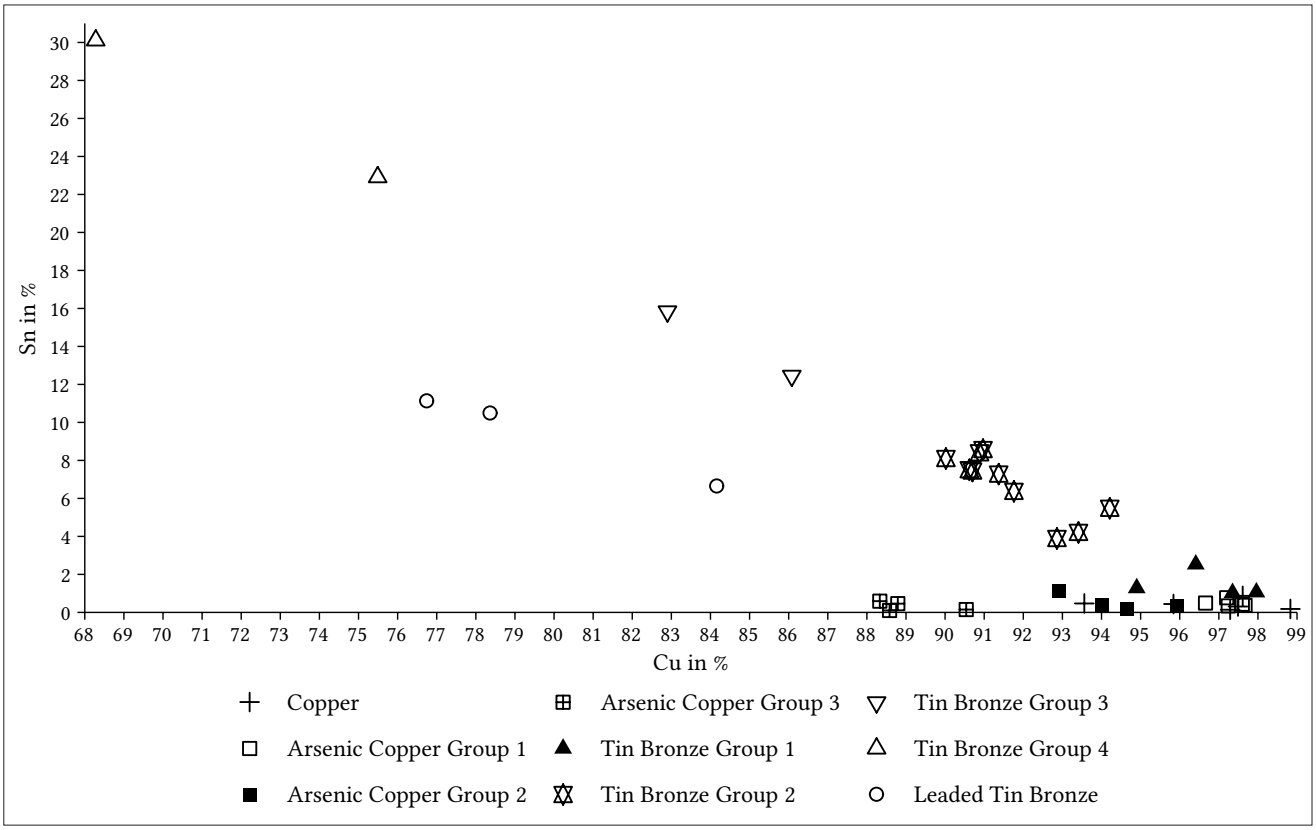

Fig. 346. Tepe 5. Scatterplot of copper (n=5), arsenical copper (n=13), tin bronze (n=17) and leaded tin bronze artefacts (n=1) showing Cu/Sn-ratio. Four Tin Bronze Groups can be differentiated by their Sn-content

the 6th millennium BC, but this is an isolated occurrence. The metal becomes more common in the second half of the 5th millennium BC when already large silver discs were produced in some places like Kotouc in Moravia (Hásek 1989). The use of natural local gold-silver-alloys was common until the 4th millennium BC when planned mining for silver and/or lead started. In the Northern Caucasus, Eastern Anatolia and in Iran the evidence for silver metallurgy is substantial (Hansen 2014: 398; Helwing 2014) but the only finds from the Kura valley are the objects discovered at Soyuq Bulaq (Courcier et al. 2008; Müseyibli 2014b). Normally, silver is made from argentiferous lead ores, as reflected in the chemical composition which includes at least 0.1 % Pb and 0.01 % Bi (Pernicka 2014: 154).

With ever larger numbers of finds, the current picture is that of a steady increase in metal production during the Aeneolithic/Chalcolithic, leading to a predominance of Cu-As alloys in the Early Bronze Age (Kura-Araxes) and a first, sporadic appearance of true bronze (Palumbi 2018; Meliksetyan/Pernicka 2010; Meliksetyan et al. 2011: Fig. 5; Bobokhyan 2015; Bobokhyan et al. 2017: 503).

A content of more than 2 % of As is indicative of alloying as no known natural ore contains that much. Some authors even assume that 0.5–1 % can be interpreted as added because in the early Chalcolithic phases, when arsenical copper was mainly used for needles and pins, increased hardness was not an important property (Borscher 2016: 29–30).

Tin bronze becomes the dominant alloy from the Middle Bronze Age onwards but new alloys continued to appear alongside the established ones, with zinc alloys in the Middle Bronze Age and antimony alloys in the Late Bronze Age (Meliksetyan et al. 2011: 204–205). Tin Bronze which comprises more than 1 % of Sn (in some cases more than 5 %) are perceived to be superior to arsenic alloys because of their increased hardness – especially at more than 10 % of Sn (Oudbashi et al. 2012: 159), but aesthetic considerations probably played a significant role in the production process (Pigott 1996: 159). Also, true bronze does not produce poisonous fumes during smelting and it is an alloy within which the amount of Sn can be controlled while the amount of arsenic often cannot (Lechtman 1996: 478). The last major innovation in metallurgy, the advent of iron objects is difficult to chart in the region, and throughout the earlier 1st millennium BC bronze artefacts make up a major proportion of the metallurgical production recovered.

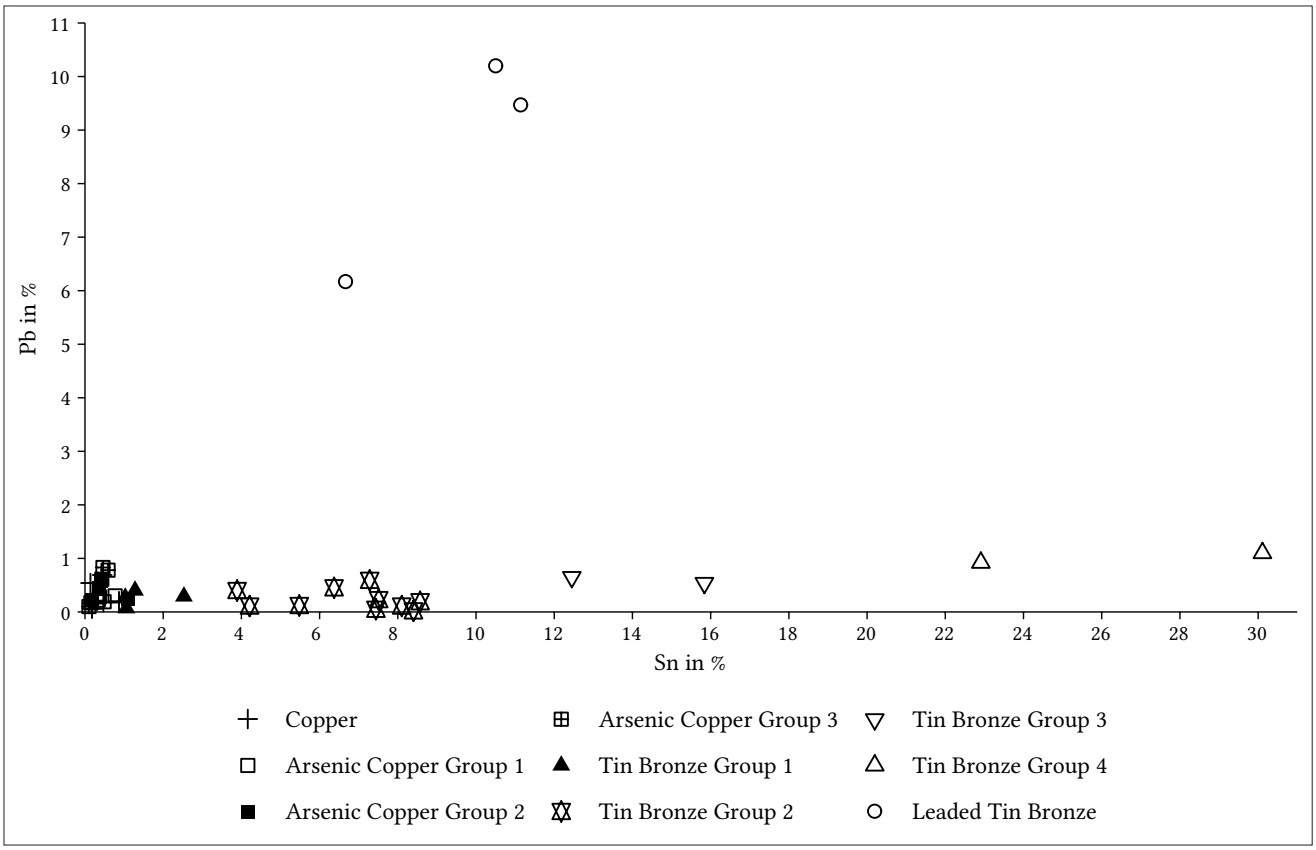

Fig. 347. Tepe 5. Scatterplot of copper (n=5), arsenical copper (n=13), tin bronze (n=17) and leaded tin bronze artefacts (n=1) showing Sn/Pb-ratio. Leaded tin bronze can be documented for Tepe 5

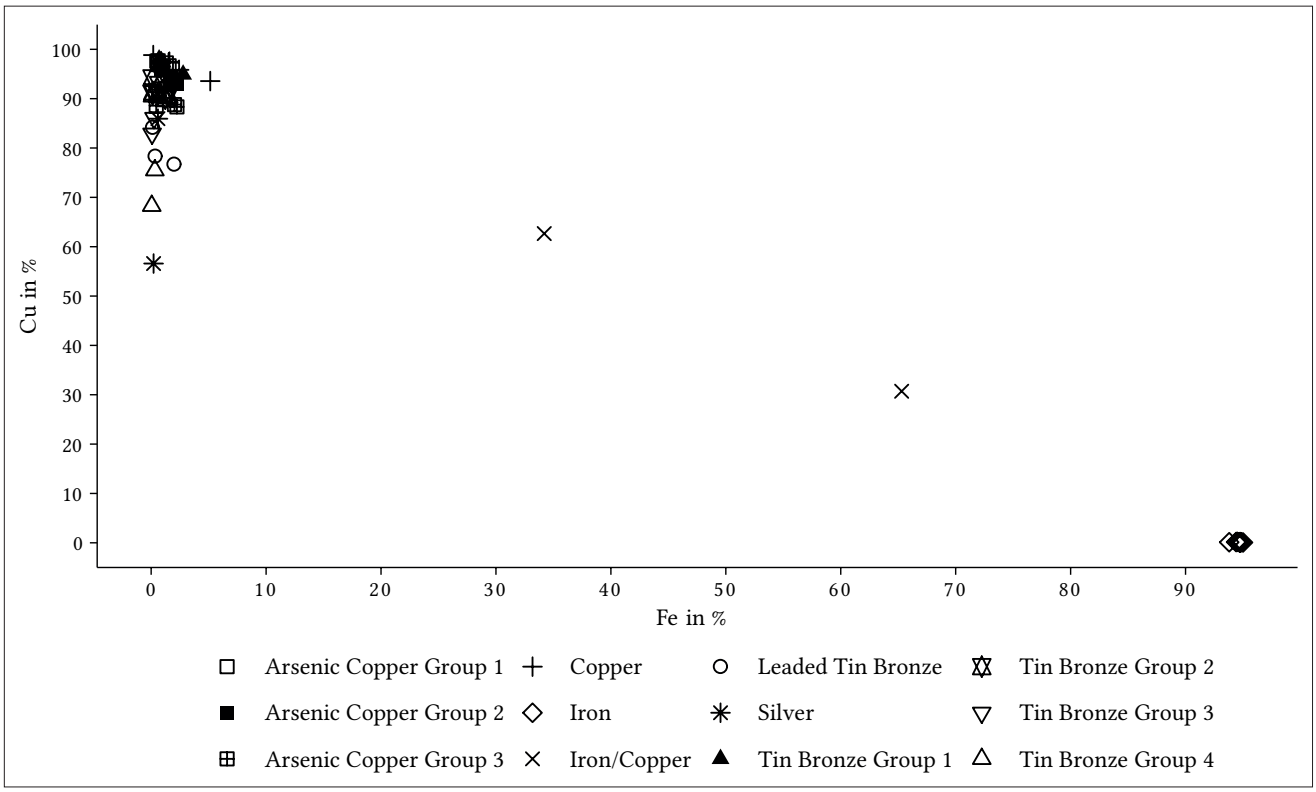

Fig. 348. Tepe 5. Scatterplot of copper (n=5), arsenical copper (n=13), tin bronze (n=17) and leaded tin bronze artefacts (n=1) showing Fe/Cu-ratio. The iron objects of Tepe 5 seem to consist of almost pure iron

The chemical characterization of copper alloys is crucial to understand the development of metal use in ancient societies. But for p-XRF the chemical matrix effects are poorly understood and the impact of calibration errors on the results is still troubling. As the fluorescence reflects from about 0.1 mm of depth, corrosion and the distance to the measuring window can cause less accurate or precise results. The impact of corrosion can be seen in a decrease of Zn and a relative increase of Sn. Tests with a portable Bruker HH p-XRF showed that the device was not able to produce very accurate quantitative data (Nicholas/Manti 2014: 1–2. 5. 8).

For these reasons, the results of 48 artefacts, sampled by a Bruker Tracer 5i and presented below, must be approached with caution. Starting in the year 2018, all bronze objects that were not completely corroded were analysed. Of the iron objects, only archaeologically identifiable artefacts were sampled. In 2019, bronze objects from Tepe 5, which had been brought to the museum from earlier seasons, were added.

VII.4.1 Copper

Five objects were found to be from nearly pure copper. (Table 38). The dagger 0089 (Fig. 47, 2), its pommel 0091 (Fig. 47, 1) and a ring (0090, Fig. 47, 3) were all found in subsoil layer KG-024 (ch. IV.8). As it is assumed that they belonged to one and the same object, this is a classic example of a composite tool: The ring consists of pure copper, dagger and pommel of different tin bronze alloys. Two copper fragments came from topsoil layer KG-054 (0219, 0232, ch. IV.8), while the pendant 0499 (Fig. 69, 2) was found in the Late Bronze Age Burial 6. One copper bead (0342a, Fig. 112, 12) came from Burial 14 (Early Iron Age – first quarter of the 1st millennium BC). Pendant and bead show comparable Cu-values, while the fragments yield lower, the ring even higher amounts. Due to the chronological differences between the burials, these relations should be interpreted as incidental.

VII.4.2 Arsenical Copper

Only the Early Iron Age Burial 13 yielded bronze objects with a high amount of As (> 0.5 %; Fig. 343), an alloy that is, as we have seen, present especially after the Late Chalcolithic, but continued to be used at least for another two-and-a-half millennia (Table 38).

Three groups can be differentiated, with objects containing less than 1 % As (0338a, 0344, 0341), between 1.9–3 % As (0271a, 0341, 0343, 0259.02) and more than 6.9 % of As (0263, 0279, 0345, 0374a). These high As-values can make the metal brittle. Sb- and Ni-values can be slightly increased compared to the tin bronze artefacts (Fig. 345). This might be a hint that ophiolithic ores were used. The ten artefacts made of arsenical copper (Table 38) are mostly beads (0271a, 0343a, 0344, 0338a, 0341a, Fig. 112, 6. 9–12) but also include a finger ring (0263, Fig. 112, 2), a bracelet (0345, Fig. 112, 1), two eyelets (0279, 0374a; Fig. 112, 3. 4) and another eyelet (sample 0259.02) still attached to pendant 0259 which was made of tin bronze (Fig. 112, 5).

Beads belong either in the low As-group or show medium As-values, which indicates that at least two different charges of beads were deposited in the burial. The eyelet on pendant 0259 was made of a medium As-rich alloy, while the other two eyelets are comparable in their As-value and belong to the As-rich group. Therefore, also these eyelets were not made from the same alloy. Finger ring and bracelet yield the highest amounts of As, also differing in their content.

VII.4.3 Tin Bronze

Tin bronze was used in 17 artefacts from Tepe 5 (Fig. 344). Again, it is possible to differentiate according to the tin content (Fig. 346) between those with less than 3 % Sn (0007, 0259.01, 0302a, 0512), between 3 % and 9 % Sn (0091, 0179, 0180, 0212, 0218, 0256, 0266, 0394, 0400, 0473), 10 % to 16.5 % Sn (0089) and with more than 22 % Sn (0262, 0276d).

Objects with low Sn-values show diverse amounts of Sn and belong to different artefact types. One tin bronze bead (0302a, Fig. 112, 9) and a pendant (0259.01, Fig. 112, 5) come from the Early Iron Age Burial 14, while the fragment of a bracelet (0512, Fig. 133, 2) belonging to Burial 1 (MBA/LBA transition) was found dislocated in Burial 21 (see ch. IV). Additionally, the dagger 0007, a surface find from the survey (grid Y62) not discussed here, belongs to this group.

Objects with medium low Sn-values include sheets from Burials 14 (0266) and 19 (0256, Fig. 130, 1), but also beads from topsoil layer KG-054 (0218) and possibly from the Late Bronze/Early Iron Age Burial 9 (0212, Fig. 144, 5). A fragment of a wire or needle was found in the fill of Pit-Complex B. Due to disturbances, this object may have originated from Early Iron Age Burial 8 (0394, Fig. 141, 9) while the knob of a dagger (0091, see above) comes from the subsoil layer KG-024. From the Late Antique Burial 27, a ring (0473, Fig. 152, 3), maybe belonging to the knife or dagger 0471 (see below), can be attributed to this group. The ornamented discs 0179 and 0180 (Burial 9, Fig. 90, 1–2) both belong to this group, too, but show different

contents of Sn. Therefore, it can be assumed that two separate alloys were used for those objects.[10]

Only dagger 0089 (subsoil layer KG-024) shows medium high Sn-values. As mentioned above, the pommel 0091 and the ring 0090 probably belong to this dagger as well.

Artefacts with the highest amount of Sn (> 22 %) are bronze sheets (0262, 0276d) from the Early Iron Age Burial 14 (Table 38). These high values should be treated with caution as the objects are strongly corroded and therefore possibly affected by surface enrichment. Nonetheless, high-tin bronzes are well known throughout the 2nd millennium BC. The differences in the alloys used for the production of these sheets suggest at least two different pieces of adornment.

A leaded tin bronze (or tin bronze with a high amount of lead that was probably added intentionally) – for the occurrence in Middle Bronze Age and Late Bronze Age contexts see A. Schachner (2005: 182) and K. Meliksetyan et al. (2011: 204–205) (Fig. 347) – is only attested once on Tepe 5: A finger ring (0211) with a round stone inlay was found in the Late Antique Burial 25 (Fig. 144, 2). To exclude that the high Pb-values were caused by the inlay, the finger ring was measured in different spots (on the rim of the inlay and twice on the ring itself). The Pb values stayed constant (Table 38).

VII.4.4 Iron

Ten mostly fragmented and heavily corroded iron objects were discovered (Fig. 348). All range in a very narrow Fe scale. Most samples derive from the fill KG-057 in Pit-Complex B (0258, 0260, 0277, 0382, 0386, 0435, Fig. 141, 1–5). It is unclear, weather these artefacts can be attributed to either the Early Iron Age Burials 8 or the Late Antique Burials 23 and 24. From Burial 15 comes the fragment 0249 (Fig. 122, 6), which can archaeologically be dated to Late Antiquity. The corroded iron handle 0471 from the Late Antique Burial 27 belonged to a knife or dagger (Fig. 152, 1). Two iron objects do not fit the cluster: the blade fragment 0514 from the Late Antique Burial 21 (Fig. 136, 1) and the bracelet 0390 in KG-057 (Fig. 141, 8). They both show a very high amount of copper (> 30 %) which might conceivably be indicative of a different production technology, but more likely reflects the highly corroded state of these two objects.

10 Unfortunately, none of the other typologically significant objects of Burial 9 were available for sampling.

VII.4.5 Silver

The Late Antique Burial 27 contained a silver finger ring with a frit bead inlay (0470, Fig. 152, 2). The visually inconspicuous ring is a silver object made from argentiferous lead ores (Table 38). The silver earring from the Medieval Burial 39 (0519, Fig. 172, 1) has a much lower silver content but too much for it to be considered a natural inclusion in a copper alloy.

VII.4.6 Summary

Five different groups of metals were identified among the 48 objects of Tepe 5 analysed by p-XRF. Copper alloys predominate, pure copper or iron and silver artefacts are less common. The greatest number stems from Burial 14, where several beads were investigated. This Early Iron Age Burial included artefacts of pure copper and tin bronze and is the only one that contained an object of arsenical copper. Tin bronze also occurred in the Middle/Late Bronze Age Burial 1, the Early Iron Age Burial 8, the Late Bronze/Early Iron Age Burials 9 and 19, as well in the Late Antique Burial 27. In tendency, lower Sn-values seem to occur in the earlier grave assemblages, but no strong correlation can be detected. Other than, for example, at Armenian sites (Meliksetyan et al. 2003: 313), the As content within the Tepe 5 objects stays well below 2 %. As no tin sources are known in Transcaucasia, this metal had to be imported (Meliksetyan et al. 2003: 313. 317), possibly from Eastern Anatolian sources. Datable pure copper artefacts were found in the Late Bronze Age Burial 6. Leaded tin bronze is only attested for the Late Antique Burial 25. Contexts for iron artefacts range from the Early Iron Age Burials 8 and 16 to Late Antiquity (Burials 15, 23 or 24), while most of them were found in the fills of Pit-Complex B. Silver was discovered in the Late Antique Burial 27 and the Medieval Burial 39 (Table 38). Possibly, for some of the arsenical copper artefacts ore from the Sevan-Akara-formation was used, and for the silver objects argentiferous lead ores.

VII.5 Conclusion

P-XRF analyses of pottery, soil, obsidian and metal from Tepe 5 have produced valuable insight into the procurement and use of raw materials and their further processing. For pottery it is possible to identify different pastes and raw material sources in the different periods of occupation of Tepe 5: The Early Chalcolithic, the Late Bronze Age, the Early Iron Age and Late Antiquity. No analyses

were possible for the Medieval graves, because they did not contain ceramic vessels. Delta clays were used in all prehistoric periods, as was mineral temper. Organic calcite temper was limited to the Early Chalcolithic while limestone temper was used exclusively in the Early Iron Age. Our Late Bronze/Early Iron Age pottery is archaeologically quite homogeneous, but there appear to be differences in the chemical fingerprints which would, if supported by a larger set of data, permit a chronological differentiation of Late Bronze/Early Iron Age pottery exclusively on analytical grounds. Most of the prehistoric pottery was produced from local clays, whose sources were at times a little bit further downstream or upstream on the Kura or her tributaries. Only with the Early Iron Age does appear pottery with no clear local chemistry, e. g. no clear relation to the clay samples included in this study (Early Iron Age Group 4). The Late Antique pottery shows a completely different chemical configuration and was not locally produced.

The obsidian artefacts of Tepe 5 can be traced back to at least three different sources in the Lesser Caucasus – Gegham-Geghasar, Syunik and Chikiani. The Early Chalcolithic community – to whose activities we owe the majority of our obsidian finds, was supplied with obsidian from Gegham-Gegasar (75 %), and to a lesser extent from Syunik (23 %), a pattern also seen at the contemporary settlement of Mentesh Tepe, c. 36 km to the west of Karacamirli. The Late Bronze Age arrowhead from Burial 6 had been worked from Chikiani obsidian.

A wide range of metals – copper, arsenical copper, tin bronze, leaded tin bronze, iron and silver – were used for the production of artefacts dating mainly from the Late Bronze and Early Iron Ages. Our analyses demonstrate the high variability of the alloying practice within the Late Bronze/Early Iron Age, with arsenic alloys and even pure copper remaining in use for particular classes of objects (beads, pendants).

VIII. Summary

Kai Kaniuth

The archaeological investigation of Karacamirli Tepe 5 took place within a framework of research centred on the Achaemenid (Late Iron Age) administrative complex surrounding the Gurban Tepe palace. This programme was primarily one of statistical archaeological survey and geophysical prospection, but soundings to ascertain particular features or to clarify stratigraphical successions were also part of the research design (Babaev et al. 2016; Babaev et al. in print). The small elevation of Tepe 5 is situated just outside the area demarcated by the previously known Achaemenid-period buildings of Gurban, Rizvan and Ilyas Tepes (Fig. 3). It came up as an area of potential interest in both survey and remote sensing. A geophysical prospection was carried out in 2015 employing the most sensitive geophysical equipment at our disposal. The interesting but ambiguous results suggested a further examination and exploratory trenches were laid out in the following field season.

Upon excavation, it immediately became apparent, that we were not dealing with another building complex, as was initially assumed, but with a place of burial. The importance of the discovery, the very complicated depositional sequence, the threat posed by ongoing agricultural modification of the immediately surrounding terrain and, last but not least, the chance to carry out an ambitious analytical programme, and thereby gather evidence unavailable from our other investigations, led us to continue these excavations in 2017.

Throughout the Holocene, Tepe 5 probably stood out as one of a series of small elevations of lighter-coloured, lime-rich soil on a Kura Terrace. These elevations were situated to the east of a small depression now partially dried with the help of a drainage canal to its west (Fig. 4), but which probably collected a fair amount of water running off from both east and west, forming a small lake or swamp.

The results reported by Jörg Faßbinder (ch. II) illustrate the relationship between the geophysical measurements and the refilled burial pits. This is an interesting methodological case study highlighting the mutually productive nature of archaeological and geophysical investigation. We were not able to tackle all research questions raised: The rectangular perimeter around Tepe 5 indicated in the magnetometer image could not be verified archaeologically, nor did we have the opportunity to check on the possibility that further archaeological features are located around the site. Its prominence through the millennia suggests, however, that much more was visible of (and possibly on) the hillock than there is today.

The occupational history of Tepe 5 lasted from the 5th millennium BC (Chalcolithic) to the Middle Ages (14th cent. AD). Except for the Chalcolithic contexts all periods of occupation were dated by radiocarbon analyses. Of 22 charcoal and bone samples submitted to two different laboratories, only one was discarded for inconsistency and sampling problems (the radiocarbon ages returned were too old by factor 10). The remaining dates showed very close inter-laboratory agreement and enabled a chronologically fine-grained discussion of all object categories from 46 burials (ch. IV), as well as of the associated human remains. The anthropological data (ch. V) was supplemented by isotope analyses (ch. VI), and a sizeable number of ceramic, metal and obsidian finds were studied by pXRF (ch. VII). In all, the precision of stratigraphic observation and the density of analytic data gathered provides one of the most detailed datasets in Transcaucasian archaeology. The restricted sample size cautions against broad generalizations from our findings, but the primary data presented will nonetheless constitute a point of reference for further studies.

The earliest archaeological traces on Tepe 5 date to the 5th millennium BC. We have no ^{14}C-dates for these contexts, and the chronology rests on ceramic parallels with Mentesh Tepe, 36 km to the west (ch. III). Tepe 5 is part of a string of Chalcolithic sites known, continuing with Rustepesi, just over 6 km to the west of Tepe 5, and Kechili III, another 5 km further west (Кесаманлы et al. 1976; 1978b; Narimanov 1987; Ceferov 2009). The ephemeral nature of the Tepe 5 contexts precludes their conclusive interpretation. The original surfaces have been

eroded, but the pits, which contained pottery and obsidian flakes, but no organic remains, suggest that they were not the refuse pits of a settlement, but rather of a specialised production area.

All Chalcolithic pottery is vegetable tempered, with different amounts of mineral temper. The sherds' archaeometric analysis (ch. VII) demonstrates the high variability within the material and also the technological options of its manufacturers. The choice of clays includes primarily local ones, probably collected in the immediate vicinity of the site itself, but deltaic clays were used, too, and are connected with specific vessel types. The obsidian fragments used in the Chalcolithic derive from two sources: Gegham-Geghasar (75 %) and Syunik-Mets Sevkar/Pokr Sevkar (25 %). The exploitation of Gegham obsidian sources may not seem an altogether logical choice given its remote locality and short seasonal accessibility (unless exploitation was limited to placer deposits), but Gegham has one of the widest distributions of any Caucasian source and supplied raw materials since the Late Neolithic. The distribution of Syunik obsidian is more restricted in its scope and seems to extend mostly towards the east, into the Mughan steppe, and south, to Nakhichevan and Iran (Abedi et al. 2018; Barge et al. 2018).

The occupants of Tepe 5 therefore participated in what has been called a multiple-source model typical for the Neolithic and Chalcolithic communities of Armenia and Azerbaijan, with their numerous local deposits, while sites in Georgia often relied on the one nearby source, Chikiani, exclusively (for the full argument, see Badalyan et al. 2004). In nearby Mentesh Tepe, an analytic programme of Chalcolithic obsidian artefacts also demonstrated that the majority of the raw material (63 %) came from Gegham, but that a whole range of other sources, among them Syunik, played a role, too (Palumbi et al. 2018: 126 Fig. 14. 17–18). Possibly, sample size is at the heart of these discrepancies. That, unlike at Mentesh Tepe (Lyonnet et al. 2012: 169–177), the lithic assemblage of Tepe 5 is exclusively made up of obsidian may partly be a function of the nature of our deposits.

After the Early Chalcolithic, Tepe 5 was not occupied for several millennia. This partially mirrors the regional settlement pattern, which is lacking in early 4th millennium (Leylatepe period) remains. Aggradation and avulsion of the Kura tributaries (Ollivier et al. 2015; 2016) are probably responsible for creating real or apparent local gaps in the settlement history. For the late 4th and early 3rd millennia BC, Kura-Araxes period sites are known at Osmanbozu, 8 km north-west of Tepe 5, as well as in two localities close to Gurban Tepe.

The next episode in the occupational history of Tepe 5 begins in the mid-2nd millennium BC[11]: The six oldest graves date to the 16th–15th cent. BC (Burials 1–5. 7). The precise nature and date of this transition from the Middle to the Late Bronze Age is still subject to debate, but the radiocarbon date obtained for Tepe 5 confirms the chronology brought forward by M. Gusejnova of a transition around 1500 BC (Гусейнова 2011). The Middle Bronze/Late Bronze Age transitional pottery was produced in a reducing atmosphere, resulting in a dark grey to black, usually polished sherd. Comparable wares and forms have a wide distribution into Eastern Georgia and the Armenian highlands, where they are associated with the Karmirberd (MB III) and Lchashen-Metsamor (LB) I horizons. Nearby, this same horizon was first met by six kurgan burials discovered one kilometre north of Tepe 5 (Асланов 1986; Гусеинова/Алиев 2008), which provided rare examples of horse trappings, cart fittings and rich ceramic inventories. Together, the two sites give a more balanced impression of the burial rites of the middle of the 2nd millennium BC. Even the Tepe 5 graves attest to far-ranging interconnections and a broad spectrum of artefacts available: Beads of frit, bronze, carnelian and cowrie shells form part of the latest of the elaborate Middle Bronze Age funerary assemblages.

From the Late Bronze Age onwards, human remains open another, albeit small window on the ancient cultures of the Kura basin. According to the little data available, the subsistence was based on a balanced diet low in fat, including plant, meat and dairy resources, as well as fresh-water fish. Certain physical traits and isotope analyses of human remains suggest that parts of the population were non-local. This would fit the assumption of a lifestyle in the Middle Bronze Age which included both seasonal and permanent mobility. From our sample, mobility was practiced within a region encompassing the Lesser Caucasus and its foothills. Only one burial from Tepe 5 (Burial 6) falls into the succeeding horizon, with dark-grey, pattern-burnished ceramics and typological links with the Lchashen-Metsamor 2-horizon. Interestingly, this burial contained an arrowhead manufactured from Chikiani obsidian.

The following five burials (nos. 8–12) contained fewer grave furnishings and a distinctive grey, medium hard to hard pottery which finds better local analogies in the contemporary graveyards of Zayamchay, Tovuzchay and Mingachevir. A single radiocarbon analysis sup-

11 This mirrors the situation at Kechili III, situated 11 km to the west, which was also unoccupied between the Chalcolithic and the Late Bronze Age, and then used as a burial ground.

ports a 12th/11th cent. BC date for this group of graves. Throughout the later 2nd millennium BC, usage of local and nearby riverine clays was confirmed to be the rule in the Tepe 5 sample. One grave assemblage containing conspicuous tin bronze headgear was associated with the skeletal remains of a probably non-local individual. The lack of colourful jewellery at this time may simply be an effect of the small sample size, which affects our ability to trace the wider interconnections of the Bronze Age population.

The Early Iron Age graves of the 9th–7th cent. BC (nos. 13–19) continue the predominantly local ceramic associations, although links with the Lesser Caucasus (Lchashen-Metsamor 4 and 5) persist. The settlement at Udabno in southern Kakheti now provides a comparable pottery corpus. Carnelian and frit beads reappear, but overall, the burial accoutrements are much reduced in number.

For the whole of the Late Bronze/Early Iron Age Khojaly-Gadabay-Culture, diverse alloying practices are attested, with pure and arsenical copper existing side by side with tin bronze. This matches information available from Armenia (Meliksetyan et al. 2011), Georgia (Kunze 2012) and eastern Anatolia (Isikli/Altunkaynak 2014). Everywhere in the Transcaucasus were local copper deposits available, some of them containing arsenic, as well. The tin, on the other hand, has not been successfully sourced, and its provenance is, therefore, a matter of debate (Cuénod et al. 2015). That metal alloying practices were highly variable is demonstrated by the Zayamchay finds, which are lacking arsenical copper, but show more tin bronzes than the burials from Tepe 5. In the Early Iron Age, the first iron fragments appear. Due to the small number of burials, our data goes only so far in helping with the establishment of a better periodization of Khojaly-Gadabay, particularly in its later stages.

Initially disappointing, but nonetheless interesting, is the fact that the burial tradition on Tepe 5 ceased when a large Achaemenid residence was built less than one kilometre to the west.

After a gap of almost one millennium, Tepe 5 was used as a graveyard again: Burials 21–27 were deposited in the later 3rd and 4th cent. AD. Chronologically the group is anchored by five ^{14}C-dates. The burial rites have changed by this time, allowing for even less variability in the depositional practice. The sole ceramic grave gift is a jug or pitcher, usually with traces of bitumen paint on the outside. Possibly, this is indicative of the contents: In one case, pine seeds were discovered within a pitcher, pointing to the consumption of resinated wine. The chemical signature of the pottery does not permit any links with known clay deposits, opening the possibility that pottery production had ceased to be a localized affair. Iron fragments now occur in most burials and tin bronze finger-rings are a regular find.

The circumstances that led to the Late Antique resurgence in burial activity are not known. They coincide, however, with a growth in settlement activity. The closest sites known from the Antique period are situated at Seyidlar (4 km to the south-east and provisionally dated between the 1st–3rd cent. AD; Jalilov 2007), Kechili I (12 km west of Tepe 5; Кесаманлы et al. 1978a), Qanli Tepe (6 km to the north-west, dated 1st–4th cent. AD; Кесаманлы/Джафаров 1977; 1979) and Uzumlu (5 km west of Tepe 5; Кесаманлы et al. 1978a).

The good state of preservation of the Late Antique skeletons offers new insights into the lifeways of the deceased: As in the Late Bronze/Early Iron Age, the local diet was variable and low in fat content. Fish continued to be a food resource in restricted supply, as were pheasants, which appear only in the sample from this period. Most deceased from this period were aged 40 and above, demonstrating on the one hand the non-representative nature of our data, but also suggesting that life expectancy was quite high. Given the age group interred on Tepe 5, the evidence collected of caries, tooth loss and healed fractures is not surprising. The only frequent epigenetic trait are lambdoid ossicles, found on c. 30 % of all Late Antique skeletons.

The latest and largest group of burials dates to the Middle Ages, between 1280 and 1400 AD (nos. 28–41, dated by a series of seven ^{14}C analyses). This episode in the history of the site postdates the destruction of the regional center, Shamkir (in AD 1239). The settlement history of the vicinity of Tepe 5 is not quite clear, but apart from an unnamed hill just northeast of Yeniabad/Bitdili dated to the 13th/14th cent. AD (Кесаманлы/Джафаров 1979), the sites of Ali-Godja II, situated just over 1 km north of Tepe 5 (Кәсәмәнлы/Чәфәров 1977) and Muncuqlu Tepe (9th–13th/14th cent. AD, Алиев/Велиев 1986; Алиев et al. 1988) are likely candidates for the settlements that might be related to the Tepe 5 burials.

Since no later archaeological features were observed, the state of preservation of these burials was better again than that of the preceding Late Antique horizon. The medieval skeletons were all interred in a stretched position, some turned on their sides. With the exception of several beads, a bronze disc and one silver earring, no grave goods can be attributed to this phase. While all this is not conclusive, the evidence does point to the deceased having belonged to the local Muslim population. For the first time we observe a fairly even age distribution, with children, adults and senile members all represented. The nutrition was highly variable, but only one individual

had consumed noticeably amounts of fish. Compared to the preceding periods, people consumed more fat and less protein. Three out of nine adult individuals showed evidence of nutritional deficiencies in the form of Harris lines, enamel hypoplasia or cribra orbitalia. The possibility that medieval populations of the 14th cent. AD were suffering from worsening living conditions is corroborated by the historical evidence at our disposal.

From the anthropological data available for altogether 38 individuals certain tendencies in the lifeways of the local populations can be deduced. Through time, the deceased seemed generally well-nourished and physically active. Wherever observable, lower activity or robustness could be explained by physical impairments. Together with the data from Mentesh Tepe, a first diachronic perspective on food resources used from the Neolithic to the Medieval period can now be developed. The rise in meat consumption from the Neolithic to the Bronze Age reported in a previous study (Herrscher et al. 2018a) finds both a continuation and a qualification in our data set, as the preponderance of dairy products over meat underscores the importance of pastoral herd management strategies. The lack of any C4 plants contrasts with several other studies on South Caucasian sites, some, as Mentesh Tepe, quite close, where millet is fairly abundant since the Early Bronze Age. The reasons for this pattern are not clear, but since the Karacamirli burials are by far the youngest studied to date, a first suggestion would be that millet cultivation was discontinued for other cereals during or after the Late Bronze Age.

The sample of burials represented in this study offers numerous points of departure for further research into the societies inhabiting the Middle Kura region between the Bronze Age and Medieval periods. To develop the research questions launched here it will be necessary to enlarge the corpus of remains subjected to thorough analysis, particularly in the field of physical anthropology. Most periods which are attested in the Qaracamirli/Yenikend region, with the exception of the Early Bronze Age (Kura Araxes) and Achaemenid/post-Achaemenid, left their mark on Tepe 5; but there remain many more questions which must be addressed, particularly with respect to the as yet unattested Neolithic and Middle Bronze periods.

Of more direct relevance to our survey project is the information provided by securely dated material, especially pottery, which was classified both typologically and technologically: As the close correspondence between the two kinds of analysis demonstrates, there is potential in using pXRF as a dating aid under controlled circumstances. The data and experience gained through our work at Tepe 5 will therefore greatly benefit our ongoing study of the region's settlement history.

IX. List of contexts

context	description	pottery	small finds	bones
KG-011	topsoil layer (north quadrants of square 6300/7990)	0033	0034	
KG-012	topsoil layer (2 m wide trench along northern side of square 6290/7990)			
KG-013	subsoil layer below KG-011 (SW corner of NW quadrant in square 6300/7990); identical with KG-015			
KG-014	subsoil layer below KG-011 (NW corner of NW quadrant in square 6300/7990); identical with KG-015	0035		
KG-015	subsoil layer below KG-011 (north quadrants of square 6300/7990) with vessel of Burial 18	0036	0037	
KG-016	rubbish pit	0045	0038–0044; 0046; 0047; 0050	
KG-017	subsoil layer below KG-012	0055	0048; 0052; 0061	
KG-018	fill material of Pit-Complex A (northern part)	0049	0051; 0053; 0056; 0057; 0060	0054
KG-019	lowest layer in rubbish pit KG-016	0062	0063	
KG-020	subsoil layer below KG-015	0064	0065; 0066	0067
KG-021	topsoil layer (2 m wide trench along north side of square 6310–6320/7990)	0072	0070; 0078	
KG-022	fill material of Pit-Complex A (southern part)	0073	0069; 0071; 0075; 0076; 0077; 0079; 0080	0074
KG-023	fill material of Pit-Complex A below KG-018 and KG-022	0082	0084; 0088; 0092; 0093; 0094; 0095; 0096; 0097; 0098; 0099; 0107	0083; 0554
KG-024	subsoil layer below KG-021	0086	0085; 0087; 0089; 0090; 0091; 0129; 0130; 0131; 0132; 0133; 0135	
KG-025	topsoil layer (SW quadrant of square 6300/7990)			
KG-026	Burial 7 (Pit-Complex A)	0100	0104; 0108; 0161	0105
KG-027	Burial 28 (Pit-Complex A)		0103; 0109	0106
KG-028	topsoil layer (2 m wide trench along southern side of square 6290/7990); identical with KG-012	0117		
KG-029	Burial 11 (Pit-Complex A)	0112	0110; 0114; 0116; 0118; 0119	0115
KG-030	southern part of Burial 20 (Pit-Complex A)			0113

(Continued on next page)

context	description	pottery	small finds	bones
KG-031	Burial 29	0121	0122–0124	0120
KG-032	Burial 13	0144	0068; 0139; 0145; 0167–0169; 0172; 0174; 0175; 0177	0137; 0166; 0553
KG-033	subsoil layer below KG-028; identical with KG-017	0127	0126; 0128	
KG-034	subsoil layer below KG-025	0125		
KG-035	Burial 42			0136
KG-036	Burial 30			0134
KG-037	topsoil layer (SE quadrant of square 6300/7990)	0138	0176; 0178	
KG-038	Burial 5 (Pit-Complex A)	0141	0101; 0140; 0142; 0147; 0151–0155; 0157–0160	0146
KG-039	SE part of Burial 4 (Pit-Complex A)			0163
KG-040	NW part of Burial 4 (Pit-Complex A)		0143; 0148; 0149a–b; 0150; 0156; 0162; 0171	0165
KG-041	Burial 10 (Pit-Complex A)	0164	0170	
KG-042	Burial 31			0173
KG-043	Burial 9		0179–0186; 0187a–e; 0198	0204
KG-044	Burial 2	0191; 0200	0188; 0189; 0195	
KG-045	Burial 32		0190	0193
KG-046	Burial 33		0225; 0226	0192
KG-047	eastern part of Burial 35		0202	0217
KG-048	Burial 34			0197
KG-049	rubbish pit	0196		
KG-050	Burial 36		0199	0203
KG-051	Burial 3	0201		
KG-052	Burial 37		0206; 0207	0205
KG-053	Burial 25		0210–0215	0208
KG-054	topsoil layer (southern quadrants of square 6290/7990 and northern quadrants of square 6290/7980)	0220	0218; 0219; 0223; 0224; 0232; 0246; 0248	
KG-055	Burial 16	0221	0222; 0228	
KG-056	pit at the eastern end of Pit-Complex B	0229	0230; 0231; 0233; 0234; 0236; 0238; 0242	
KG-057	central pit in Pit-Complex B that contained Burials 8, 23 and 24	0244; 0416–0419	0235; 0237; 0245; 0258; 0260; 0277; 0382; 0384–0386; 0389; 0390; 0394; 0395; 0397; 0399; 0401–0403; 0412; 0413; 0420; 0435	0247; 0404; 0414; 0415; 0421; 0552

(Continued on next page)

context	description	pottery	small finds	bones
KG-058	Burial 15 (Pit-Complex B)	0241	0239; 0240; 0249; 0253; 0254; 0278; 0280; 0282; 0305; 0317; 0379	0243
KG-059	Burial 14	0252	0251; 0255; 0257; 0259; 0261–0276a–d; 0279; 0281; 0283–0286; 0298–0304; 0306–0316; 0318–0345; 0349–0378; 0381	0346
KG-061	topsoil layer (northern quadrants of square 6300/7980)		0250	
KG-062	topsoil layer (removal of 2 m long section of the baulk between squares 6290/7980 and 6300/7980)			
KG-063	Burial 19		0256; 0396; 0407–0410	
KG-064	Burial 12	0347		
KG-065	Burial 17	0348		
KG-066	Burial 26 (Pit-Complex B)	0393	0380; 0383; 0388	0392
KG-073	Burial 38		0500; 0504; 0509a–b; 0510	0508
KG-074	Burial 21 (Pit-Complex C)	0506	0405; 0406 0426; 0438; 0444; 0447–0449; 0454; 0461; 0466; 0501–0503; 0505; 0512; 0514	0507; 0551
KG-076	Burial 43		0516	0515
KG-077	Burial 39		0519	0517
KG-089	Burial 40 (Pit-Complex B)			0387
KG-090	topsoil layer (southern quadrants of square 6300/8000)	0424		
KG-091	shallow pit in Burial 16 (Pit-Complex B)			
KG-092	Burial 44			0398
KG-093	Burial 41 (Pit-Complex C)			0480
KG-094	Burial 1 (Pit-Complex C)	0425	0423; 0427; 0428; 0436; 0437; 0439; 0440; 0450; 0452; 0453; 0456–0459; 0462–0465; 0476; 0513	0451; 0474
KG-095	western pit in Pit-Complex C that contained Burials 6 and 22	0498	0429; 0430–0434; 0469; 0481; 0483–0487; 0489; 0490; 0492–0494; 0499	0468; 0496; 0497
KG-096	Burial 45 (Pit-Complex C)			0445
KG-097	Burial 27	0472	0470; 0471; 0473	0455
KG-098	western part of Burial 35			0467
KG-099	Burial 46			0460
KG-100	large pit in square 6300/8000	0479	0446; 0478; 0482	
KG-101	narrow oblong pit in square 6300/8000			
KG-102	norther part of Burial 20		0488	0491

X. List of finds

(f) = found in the fill of the grave-pit

find-number	category	type of find	context	burial
0033	pottery		KG-011	
0034	small find	obsidian flake	KG-011	
0035	pottery		KG-014	
0036	pottery		KG-015	18
0037	small find	obsidian flake	KG-015	
0038	small find	obsidian flake	KG-016	
0039	small find	obsidian flake	KG-016	
0040	small find	obsidian flake	KG-016	
0041	small find	obsidian flake	KG-016	
0042	small find	obsidian flake	KG-016	
0043	small find	stone object	KG-016	
0044	small find	obsidian flakes	KG-016	
0045	pottery		KG-016	
0046	small find	stone object	KG-016	
0047	small find	flint flake	KG-016	
0048	small find	obsidian flake	KG-017	
0049	pottery		KG-018	
0050	small find	stone object	KG-016	
0051	small find	obsidian flake	KG-018	
0052	small find	obsidian flake	KG-017	
0053	small find	obsidian flake	KG-018	
0054	bones	animal bones	KG-018	
0055	pottery		KG-017	
0056	small find	obsidian flake	KG-018	
0057	small find	obsidian flake	KG-018	
0060	small find	obsidian flake	KG-018	
0061	small find	obsidian flake	KG-017	
0062	pottery		KG-019	
0063	small find	obsidian flakes	KG-019	
0064	pottery		KG-020	
0065	small find	obsidian flake	KG-020	
0066	small find	flint flake	KG-020	
0067	bones	animal bones	KG-020	
0068	small find	carnelian bead	KG-032	13
0069	small find	obsidian flake	KG-022	
0070	small find	obsidian flake	KG-021	
0071	small find	obsidian flake	KG-022	
0072	pottery		KG-021	
0073	pottery		KG-022	
0074	bones	animal bones	KG-022	
0075	small find	obsidian flake	KG-022	
0076	small find	obsidian flake	KG-022	
0077	small find	obsidian flake	KG-022	
0078	small find	obsidian flake	KG-021	
0079	small find	obsidian flake	KG-022	
0080	small find	obsidian flake	KG-022	
0082	pottery		KG-023	
0083	bones	animal bones	KG-023	
0084	small find	obsidian flake	KG-023	
0085	small find	obsidian flake	KG-024	
0086	pottery		KG-024	
0087	small find	obsidian flake	KG-024	
0088	small find	obsidian flake	KG-023	
0089	small find	bronze dagger	KG-024	
0090	small find	bronze ring	KG-024	
0091	small find	bronze knob	KG-024	

(Continued on next page)

find-number	category	type of find	context	burial
0092	small find	obsidian flake	KG-023	
0093	small find	obsidian flake	KG-023	
0094	small find	obsidian flake	KG-023	
0095	small find	obsidian flake	KG-023	
0096	small find	obsidian flake	KG-023	
0097	small find	obsidian flake	KG-023	
0098	small find	obsidian flake	KG-023	
0099	small find	obsidian flake	KG-023	
0100	pottery		KG-026	7
0101	small find	obsidian flake	KG-038	5 (f)
0103	small find	bronze ring	KG-027	28 (f)
0104	small find	obsidian flake	KG-026	7 (f)
0105	bones	human bones	KG-026	7
0106	bones	human bones	KG-027	28
0107	small find	obsidian flake	KG-023	
0108	small find	obsidian flake	KG-026	7
0109	small find	obsidian flake	KG-027	28 (f)
0110	small find	flint flake	KG-029	11 (f)
0112	pottery		KG-029	11
0113	bones	human bones	KG-030	20
0114	small find	obsidian flake	KG-029	11 (f)
0115	bones	human bones	KG-029	11 (f)
0116	small find	obsidian bones	KG-029	11 (f)
0117	pottery		KG-028	
0118	small find	obsidian flake	KG-029	11 (f)
0119	small find	obsidian flake	KG-029	11 (f)
0120	bones	human bones	KG-031	29
0121	pottery		KG-031	29
0122	small find	obsidian flake	KG-031	29 (f)
0123	small find	bronze disc	KG-031	29
0124	small find	obsidian flake	KG-031	29 (f)
0125	pottery		KG-034	
0126	small find	obsidian flake	KG-033	
0127	pottery		KG-033	
0128	small find	obsidian flake	KG-033	
0129	small find	obsidian flake	KG-024	
0130	small find	obsidian flake	KG-024	
0131	small find	obsidian flake	KG-024	
0132	small find	obsidian flake	KG-024	
0133	small find	obsidian flake	KG-024	
0134	bones	human bones	KG-036	30
0135	small find	obsidian flake	KG-024	
0136	bones	human bones	KG-035	42
0137	bones	human bones	KG-032	13
0138	pottery		KG-037	
0139	small find	obsidian flake	KG-032	13 (f)
0140	small find	obsidian flake	KG-038	5 (f)
0141	pottery		KG-038	5
0142	small find	obsidian flake	KG-038	5 (f)
0143	small find	frit bead	KG-040	4
0144	pottery		KG-032	13
0145	small find	clay bead	KG-032	13
0146	bones	human bones	KG-038	5
0147	small find	bronze bead	KG-038	5
0148	small find	frit bead	KG-040	4
0149a	small find	carnel. beads	KG-040	4
0149b	small find	bronze beads	KG-040	4
0150	small find	cowry shell	KG-040	4
0151	small find	bronze beads	KG-038	5
0152	small find	obsidian flake	KG-038	5
0153	small find	carnelian bead	KG-038	5
0154	small find	bronze beads	KG-038	5
0155	small find	bronze beads	KG-038	5
0156	small find	frit bead	KG-040	4
0157	small find	bronze beads	KG-038	5
0158	small find	brz. ornament	KG-038	5
0159	small find	bronze strip	KG-038	5
0160	small find	bronze strip	KG-038	5
0161	small find	obsidian flake	KG-026	7
0162	small find	bone beads	KG-040	4
0163	bones	human bones	KG-039	4
0164	pottery		KG-041	10
0165	bones	human bones	KG-040	4
0166	bones	human bones	KG-032	13

(Continued on next page)

find-number	category	type of find	context	burial
0167	small find	obsidian flake	KG-032	13 (f)
0168	small find	carnelian bead	KG-032	13
0169	small find	obsidian flake	KG-032	13 (f)
0170	small find	obsidian flake	KG-041	10 (f)
0171	small find	cowry shells	KG-040	4
0172	small find	obsidian flake	KG-032	13 (f)
0173	bones	human bones	KG-042	31
0174	small find	obsidian flake	KG-032	13 (f)
0175	small find	obsidian flake	KG-032	13 (f)
0176	small find	obsidian flake	KG-037	
0177	small find	obsidian flake	KG-032	13 (f)
0178	small find	obsidian flake	KG-037	
0179	small find	bronze disc	KG-043	9
0180	small find	bronze disc	KG-043	9
0181	small find	bronze torc	KG-043	9
0182	small find	bronze tubes	KG-043	9
0183	small find	brz. headband	KG-043	9
0184	small find	bronze chain	KG-043	9
0185	small find	bronze chain	KG-043	9
0186	small find	bronze chain	KG-043	9
0187a	small find	brz. chain	KG-043	9
0187b	small find	brz. fragments	KG-043	9
0187c	small find	bronze object	KG-043	9
0187d	small find	brz. button	KG-043	9
0187e	small find	bronze object	KG-043	9
0188	small find	obsidian flake	KG-044	2 (f)
0189	sample	charcoal	KG-044	2 (f)
0190	small find	obsidian flake	KG-045	32 (f)
0191	pottery		KG-044	2
0192	bones	human bones	KG-046	33
0193	bones	human bones	KG-045	32
0195	sample	charcoal	KG-044	2 (f)
0196	pottery		KG-049	
0197	bones	human bones	KG-048	34
0198	small find	bronze beads	KG-043	9
0199	small find	obsidian flake	KG-050	36 (f)
0200	pottery		KG-044	2
0201	pottery		KG-051	3
0202	small find	brick	KG-047	35 (f)
0203	bones	human bones	KG-050	36
0204	bones	human bones	KG-043	9
0205	bones	human bones	KG-052	37
0206	small find	bronze chain	KG-052	37 (f)
0207	small find	obsidian flake	KG-052	37 (f)
0208	bones	human bones	KG-053	25
0209	pottery		KG-053	25
0210	small find	bronze chain	KG-053	25 (f)
0211	small find	brz. finger ring	KG-053	25
0212	small find	bronze bead	KG-053	25 (f)
0213	small find	iron object	KG-053	25
0214	small find	iron fragments	KG-053	25
0215	small find	bronze chain	KG-053	25 (f)
0217	bones	human bones	KG-047	35
0218	small find	bronze sheet	KG-054	
0219	small find	brz. fragment	KG-054	
0220	pottery		KG-054	
0221	pottery		KG-055	16
0222	small find	frit bead	KG-055	16
0223	small find	frit bead	KG-054	1 (?)
0224	small find	frit bead	KG-054	1 (?)
0225	small find	obsidian flake	KG-046	33 (f)
0226	small find	obsidian flake	KG-046	33 (f)
0228	small find	frit bead	KG-055	16
0229	pottery		KG-056	
0230	small find	obsidian flake	KG-056	
0231	small find	obsidian flake	KG-056	
0232	small find	brz. fragments	KG-054	
0233	small find	obsidian flake	KG-056	
0234	small find	obsidian flake	KG-056	
0235	small find	obsidian flake	KG-057	23 (f)
0236	small find	obsidian flake	KG-056	
0237	small find	obsidian flake	KG-057	23 (f)
0238	small find	obsidian flake	KG-056	
0239	small find	obsidian flake	KG-058	15 (f)

(Continued on next page)

find-number	category	type of find	context	burial
0240	small find	obsidian flake	KG-058	15 (f)
0241	pottery		KG-058	15
0242	small find	obsidian flake	KG-056	
0243	bones	human bones	KG-058	15
0244	pottery		KG-057	23
0245	small find	obsidian flake	KG-057	23 (f)
0246	small find	obsidian flake	KG-054	
0247	bones	human bones	KG-057	8
0248	small find	obsidian flake	KG-054	
0249	small find	iron fragment	KG-058	15 (f)
0250	small find	brick	KG-061	
0251	small find	obsidian flake	KG-059	14 (f)
0252	pottery		KG-059	14
0253	small find	carnelian bead	KG-058	15
0254	small find	obsidian flake	KG-058	15 (f)
0255	small find	obsidian flake	KG-059	14 (f)
0256	small find	bronze object	KG-063	19
0257	small find	obsidian flake	KG-059	14 (f)
0258	small find	iron fragments	KG-057	23 (f)
0259	small find	brz. pendant	KG-059	14
0260	small find	iron fragment	KG-057	23 (f)
0261	small find	frit bead	KG-059	14
0262	small find	bronze sheet	KG-059	14
0263	small find	brz. finger ring	KG-059	14
0264	small find	frit bead	KG-059	14
0265	small find	frit bead	KG-059	14
0266	small find	bronze sheet	KG-059	14
0267	small find	frit bead	KG-059	14
0268	small find	frit bead	KG-059	14
0269	small find	carnelian bead	KG-059	14
0270	small find	frit bead	KG-059	14
0271a	small find	bronze beads	KG-059	14
0271b	small find	carnelian bead	KG-059	14
0272	small find	carnelian bead	KG-059	14
0273	small find	obsidian flake	KG-059	14 (f)
0274	small find	frit bead	KG-059	14
0275	small find	frit bead	KG-059	14
0276a	small find	frit beads	KG-059	14
0276b	small find	carnel. beads	KG-059	14
0276c	small find	clay bead	KG-059	14
0276d	small find	bronze sheet	KG-059	14
0277	small find	iron fragment	KG-057	23 (f)
0278	small find	obsidian flake	KG-058	15 (f)
0279	small find	bronze eyelet	KG-059	14
0280	small find	obsidian flake	KG-058	15 (f)
0281	small find	frit bead	KG-059	14
0282	small find	bead	KG-058	15
0283	small find	frit bead	KG-059	14
0284	small find	frit bead	KG-059	14
0285	small find	bronze sheet	KG-059	14
0286	small find	mollusc	KG-059	14
0298	small find	frit bead	KG-059	14
0299	small find	frit bead	KG-059	14
0300	small find	carnelian bead	KG-059	14
0301	small find	frit bead	KG-059	14
0302a	small find	bronze bead	KG-059	14
0302a	small find	frit bread	KG-059	14
0303	small find	frit bread	KG-059	14
0304	small find	frit bread	KG-059	14
0305	small find	carnelian bead	KG-058	15
0306	small find	carnelian bead	KG-059	14
0307	small find	frit bread	KG-059	14
0308	small find	frit bread	KG-059	14
0309	small find	frit bread	KG-059	14
0310	small find	frit bread	KG-059	14
0311	small find	carnelian bead	KG-059	14
0312	small find	frit bread	KG-059	14
0313	small find	frit bread	KG-059	14
0314	small find	frit bread	KG-059	14
0315	small find	frit bread	KG-059	14
0316	small find	carnelian bead	KG-059	14
0317	small find	carnelian bead	KG-058	15
0318	small find	frit bread	KG-059	14
0319	small find	frit bread	KG-059	14

(Continued on next page)

find-number	category	type of find	context	burial
0320	small find	frit bread	KG-059	14
0321	small find	frit bread	KG-059	14
0322	small find	frit breads	KG-059	14
0323	small find	frit bread	KG-059	14
0324	small find	frit bread	KG-059	14
0325	small find	frit bread	KG-059	14
0326	small find	frit bread	KG-059	14
0327	small find	frit bread	KG-059	14
0328	small find	frit bread	KG-059	14
0329	small find	frit bread	KG-059	14
0330	small find	frit bread	KG-059	14
0331	small find	frit bread	KG-059	14
0332	small find	frit bread	KG-059	14
0333	small find	carnelian bead	KG-059	14
0334	small find	frit bread	KG-059	14
0335	small find	frit bread	KG-059	14
0336	small find	carnelian bead	KG-059	14
0337a	small find	carnelian bead	KG-059	14
0337b	small find	frit beads	KG-059	14
0338a	small find	bronze beads	KG-059	14
0338b	small find	carnel. beads	KG-059	14
0339	small find	bronze sheet	KG-059	14
0340	small find	bronze sheet	KG-059	14
0341a	small find	bronze beads	KG-059	14
0341b	small find	carnelian bead	KG-059	14
0341c	small find	frit bead	KG-059	14
0342a	small find	bronze beads	KG-059	14
0342b	small find	carnel. beads	KG-059	14
0343a	small find	bronze beads	KG-059	14
0343b	small find	carnelian bead	KG-059	14
0344	small find	bronze beads	KG-059	14
0345	small find	brz. bracelet	KG-059	14
0346	bones	human bone	KG-059	14
0347	pottery		KG-064	12
0348	pottery		KG-065	17
0349	small find	frit bead	KG-059	14
0350	small find	frit bead	KG-059	14
0351	small find	frit bead	KG-059	14
0352	small find	frit bead	KG-059	14
0353	small find	frit bead	KG-059	14
0354	small find	frit bead	KG-059	14
0355	small find	frit beads	KG-059	14
0356	small find	frit bead	KG-059	14
0357	small find	frit beads	KG-059	14
0358	small find	frit bead	KG-059	14
0359	small find	frit beads	KG-059	14
0360	small find	frit bead	KG-059	14
0361	small find	carnelian bead	KG-059	14
0362	small find	frit bead	KG-059	14
0363	small find	frit bead	KG-059	14
0364	small find	frit bead	KG-059	14
0365	small find	frit bead	KG-059	14
0366	small find	carnelian bead	KG-059	14
0367	small find	frit bead	KG-059	14
0368	small find	frit bead	KG-059	14
0369	small find	frit bead	KG-059	14
0370	small find	frit bead	KG-059	14
0371	small find	frit bead	KG-059	14
0372	small find	frit bead	KG-059	14
0373	small find	frit bead	KG-059	14
0374a	small find	bronze eyelet	KG-059	14
0374b	small find	frit bead	KG-059	14
0375	small find	frit bead	KG-059	14
0376	small find	frit bead	KG-059	14
0377	small find	frit bead	KG-059	14
0378	small find	frit bead	KG-059	14
0379	small find	bead	KG-058	15
0380	small find	obsidian flake	KG-066	26 (f)
0381	small find	frit bead	KG-059	14 (f)
0382	small find	iron fragment	KG-057	23 (f)
0383	small find	obsidian flake	KG-066	26 (f)
0384	small find	obsidian flake	KG-057	23 (f)
0385	small find	mollusc	KG-057	23 (f)
0386	small find	iron fragments	KG-057	23 (f)

(Continued on next page)

find-number	category	type of find	context	burial
0387	bones		KG-089	40
0388	small find	obsidian flake	KG-066	26 (f)
0389	small find	frit bead	KG-057	23 (f)
0390	small find	bracelet	KG-057	23 (f)
0392	bones	human bones	KG-066	26
0393	pottery		KG-066	26
0394	small find	brz. fragment	KG-057	23 (f)
0395	small find	obsidian flake	KG-057	23 (f)
0396	small find	frit bead	KG-063	19
0397	small find	obsidian flake	KG-057	23 (f)
0398	bones	human bones	KG-092	44
0399	small find	obsidian flake	KG-057	23 (f)
0401	small find	obsidian flake	KG-057	23 (f)
0402	small find	obsidian flake	KG-057	23 (f)
0403	small find	flint flake	KG-057	23 (f)
0404	bones	human bones	KG-057	8
0405	small find	obsidian flake	KG-074	21 (f)
0406	small find	frit bead	KG-074	21 (f)
0407	small find	frit bead	KG-063	19
0408	small find	frit bead	KG-063	19
0409	small find	bone beads	KG-063	19
0410	small find	frit bead	KG-063	19
0411	sample	content of vessel 0419-01	KG-057	23
0412	small find	obsidian flake	KG-057	23 (f)
0413	small find	obsidian flake	KG-057	23 (f)
0414	bones	human bones	KG-057	24
0415	bones	human bones	KG-057	23
0416	pottery		KG-057	8, 23
0417	pottery		KG-057	8
0418	pottery		KG-057	8
0419	pottery		KG-057	23
0420	small find	spindle whorl	KG-057	23 (f)
0421	bones	astragalus	KG-057	23 (f)
0423	small find	frit bead	KG-094	1 (f)
0424	pottery		KG-090	
0425	pottery		KG-094	1
0426	small find	obsidian flake	KG-074	21 (f)
0427	small find	frit bead	KG-094	1 (f)
0428	small find	frit bead	KG-094	1 (f)
0429	small find	obsidian flake	KG-095	6 (f)
0430	small find	obsidian flake	KG-095	6 (f)
0431	small find	obsidian flake	KG-095	6 (f)
0432	small find	obsidian flake	KG-095	6 (f)
0433	small find	obsidian flake	KG-095	6 (f)
0434	small find	obsidian flake	KG-095	6 (f)
0435	small find	iron fragments	KG-057	23 (f)
0436	small find	frit bead	KG-094	1 (f)
0437	small find	frit bead	KG-094	1 (f)
0438	small find	carnelian bead	KG-074	21 (f)
0439	small find	frit bead	KG-094	1 (f)
0440	small find	frit bead	KG-094	1 (f)
0444	small find	frit bead	KG-074	21 (f)
0445	bones	human bones	KG-096	45
0446	small find	obsidian flake	KG-100	
0447	small find	frit beads	KG-074	21 (f)
0448	small find	frit bead	KG-074	21 (f)
0449	small find	frit bead	KG-074	21 (f)
0450	small find	frit bead	KG-094	1 (f)
0451	bones	animal bones	KG-094	1
0452	small find	frit bead	KG-094	1 (f)
0453	small find	frit bead	KG-094	1 (f)
0454	small find	frit bead	KG-074	21 (f)
0455	bones	human bones	KG-097	27
0456	small find	carnelian bead	KG-094	1 (f)
0457	small find	obsidian flake	KG-094	1 (f)
0458	small find	frit bead	KG-094	1 (f)
0459	small find	obsidian flake	KG-094	1 (f)
0460	bones	human bones	KG-099	46
0461	small find	obsidian flake	KG-074	21 (f)
0462	small find	obsidian flake	KG-094	1 (f)
0463	small find	obsidian flake	KG-094	1 (f)
0464	small find	frit bead	KG-094	1 (f)
0465	small find	obsidian flake	KG-094	1 (f)

(Continued on next page)

find-number	category	type of find	context	burial
0466	small find	frit bead	KG-074	21 (f)
0467	bones	human bones	KG-098	35
0468	bones	human bone	KG-095	6 (f)
0469	small find	obsidian flake	KG-095	6 (f)
0470	small find	silver ring	KG-097	27
0471	small find	iron handle	KG-097	27
0472	pottery		KG-097	27
0473	small find	bronze ring	KG-097	27
0474	bones	human bones	KG-094	1
0476	small find	obsidian flake	KG-094	1 (f)
0478	small find	obsidian flake	KG-100	
0479	pottery		KG-100	
0480	bones	human bones	KG-093	41
0481	small find	obsidian flake	KG-095	6 (f)
0482	small find	obsidian flake	KG-100	
0483	small find	obsidian flake	KG-095	6 (f)
0484	small find	obsidian flake	KG-095	6 (f)
0485	small find	obsidian flake	KG-095	6 (f)
0486	small find	obsidian flake	KG-095	6 (f)
0487	small find	obsidian flake	KG-095	6 (f)
0488	small find	obsidian flake	KG-102	20 (f)
0489	small find	ob. arrowhead	KG-095	6
0490	small find	frit bead	KG-095	6 (f)
0491	bones	human bones	KG-102	20
0492	small find	obsidian flake	KG-095	6 (f)
0493	small find	obsidian flake	KG-095	6 (f)
0494	small find	obsidian flake	KG-095	6 (f)
0496	bones	human bones	KG-095	22
0497	bones	human bones	KG-095	6
0498	pottery		KG-095	6
0499	small find	brz. pendant	KG-095	6 (f)
0500	small find	obsidian flake	KG-073	38 (f)
0501	small find	frit bead	KG-074	21 (f)
0502	small find	ob. arrowhead	KG-074	21
0503	small find	frit bead	KG-074	21 (f)
0504	small find	carnelian bead	KG-073	38
0505	small find	obsidian flake	KG-074	21 (f)

find-number	category	type of find	context	burial
0506	pottery		KG-074	21
0507	bones	human bones	KG-074	21
0508	bones	human bones	KG-073	38
0509a	small find	frit bead	KG-073	38
0509b	small find	frit beads	KG-073	38
0510	small find	stone pendant	KG-073	38
0512	small find	brz. bracelet	KG-074	21 (f)
0513	small find	obsidian flake	KG-094	1 (f)
0514	small find	iron blade	KG-074	21
0515	bones	human bones	KG-076	43 (f)
0516	small find	obsidian flake	KG-077	39 (f)
0517	bones	human bones	KG-077	39
0519	small find	silver earring	KG-077	39
0551	bones	animal bones	KG-074	21
0552	bones	animal bones	KG-057	23
0553	bones	animal bones	KG-032	13 (f)
0554	bones	animal bones	KG-023	

XI. Bibliography

Abbasova 2003
F. Abbasova, Bulaqbaşı abidələri (Bakı 2003)

Abdullayev/Leroy 2016
E. Abdullayev – S. A. G. Leroy, Provenance of clay minerals in the sediments from the Pliocene Productive Series, western South Caspian Basin, Marine and Petroleum Geology 73, 2016, 517–527

Abedi et al. 2018
A. Abedi – V. D. Mohammadi – D. Steiniger – M. Glascock, The provenance of Kul Tepe obsidian artifacts: Syunik and the highlands of Armenia as possible seasonal pastureland, Journal of Archaeological Science 21, 2018, 406–412

Acsádi/Nemeskéri 1970
G. Acsádi – J. Nemeskéri, History of human life span and mortality (Budapest 1970)

Adamia et al. 2011
S. Adamia – G. Zakariadze – T. Chkhotua – N. Sadradze – N. Tsereteli – A. Chabukiani – A. Gventsadze, Geology of the Caucasus: A Review, Turkish Journal of Earth Sciences 20, 2011, 489–544

Adamia et al. 2018
S. Adamia – T. Beridze – A. Chabukiani – K. Khmaladze – Z. Kutelia – G. Sadradze – N. Sadradze – S. Tvalchrelidze, Geodynamics, correlation of the main tectonic and metallogenic units of the Eastern Black Sea-Caspian Sea region, 2008, [https://events.donya-e-eqtesad.com] (02.11.2019)

Agayev 2006
G. Agayev, Short Report Excavations of Garajamirli I Settlement Site KP 321 – BTC ROW, Unpublished report for BTC Pipeline Co. (Baku 2006) [accessible through Maynard 2011]

Agayev 2007
G. Agayev, Excavations of Lak II Early Medieval Settlement KP 300 – BTC ROW (Baku 2007) [accessible through Maynard 2011]

Aggarwal 2014
C. C. Aggarwal, An Introduction to Cluster Analysis, in: C. C. Aggarwal – C. K. Reddy (eds.), Data Clustering: Algorithms and Applications (Boca Raton 2014) 1–27

Albarède 2003
F. Albarède, Geochemistry. An Introduction (Cambridge 2003)

Alizadeh et al. 2016
A. A. Alizadeh – I. S. Guliyev – F. A. Kadirov – L. V. Eppelbaum, Geosciences of Azerbaijan. Volume I: Geology, Regional Geology Reviews (Cham 2016)

Allen 1884
H. Allen, A system of human anatomy, including its medical and surgical relations (Philadelphia 1884)

AlQahtani et al. 2010
S. J. AlQahtani – M. P. Hector – H. M. Liversidge, Brief communication: The London atlas of human tooth development and eruption, American Journal of Physical Anthropology 142, 2010, 481–490

Ambrose/Norr 1993
S. H. Ambrose – L. Norr, Experimental Evidence for the Relationship of the Carbon Isotope Ratios of Whole Diet and Dietary Protein to Those of Bone Collagen and Carbonate, in: J. B. Lambert – G. Grupe (eds.), Prehistoric Human Bone – Archaeology at the Molecular Level (Heidelberg 1993) 1–37

Ambrose et al. 1997
S. H. Ambrose – B. M. Butler – D. B. Hanson – R. L. Hunter-Anderson – H. W. Krueger, Stable Isotopic Analysis of Human Diet in the Marianas Archipelago, Western Pacific, American Journal of Physical Anthropology 104, 1997, 343–361

Angel 1964
J. L. Angel, The reaction area of the femoral neck, Clinical Orthopaedics and Related Research 32, 1964, 130–142

Asanidze et al. 2019
L. Asanidze – Z. Lezhava – K. Tsikarishvili – G. Gaprindashvili – N. Chikhradze – J. Polk, Karst map of Georgia (Caucasus region) scale: 1:1.500.000. Carbonates and Evaporites (2019)

Aşurov 2008a
S. H. Aşurov, Çaparın son antik – ilk orta əsrlər abidəsi, in: M. Rəhimova et al. (eds), Şəmkir: arxeoloji irsi, tarixi və memarlığı: birinci respublika elmi-praktik konfransın materialları (28–29 noyabr 2007) (Bakı 2008) 196–206

Aşurov 2008b
S. H. Aşurov, Excavations of Late Antique and Early Medieval Period Chapel, Settlement and Burial Site KP 335/336 – BTC ROW (Baku 2008) [accessible through Maynard 2011]

Avetisyan 2003
P. Avetisyan, Ush bronzi arrajin p'uli hnagitakan hamalirneri arrandznats'man yev zhamanakagrut'yan harts'eri shurj (yst Harrichi yev hamazhamanakya hushardzanneri tvyalneri), in: А. Калантарян – P. C. Бадалян (eds.), Древнейшая Культура Армении 3. Материалы сессии, посвященной 70-летию Телемака Хачатряна (Ереван 2003) 52–60

Avetisyan/Bobokhyan 2008
P. Avetisyan – A. Bobokhyan, The Pottery Traditions of the Armenian Middle to Late Bronze Age 'Transition' in the Context of Bronze and Iron Age Periodization, in: K. S. Rubinson – A. Sagona (eds.), Ceramics in Transitions. Chalcolithic through Iron Age in the Highlands of the Southern Caucasus and Anatolia, ANES Suppl. 27 (Leuven 2008) 123–183

Babaev/Knauss 2010
I. Babaev – F. S. Knauss, Die achaimenidische Residenz bei Karačamirli: Ausgrabungen auf dem Gurban Tepe und auf Rizvan Tepe. 4. Vorbericht, Archäologische Mitteilungen aus Iran und Turan 42, 2010, 237–266

Babaev/Knauss 2016
I. Babaev – F. S. Knauss, Die achaimenidische Residenz bei Karačamirli. Ausgrabungen auf dem Gurban Tepe, auf dem Rizvan Tepe und bei Dara Yatax. Vorbericht über die 5., 6. und 7. Kampagne 2010, 2011, 2013, Archäologische Mitteilungen aus Iran und Turan 48, 2016, 143–188

Babaev et al. 2006
I. Babaev – I. Gagoshidze – F. S. Knauss, Ein Perserbau in Azerbajdzan. Ausgrabung auf dem Ideal Tepe bei Karačamirli 2006. Erster Vorbericht, Archäologische Mitteilungen aus Iran und Turan 38, 2006, 291–330

Babaev et al. 2009
I. Babaev – G. Mehnert – F. Knauss, Die achaimenidische Residenz auf dem Gurban Tepe. Ausgrabungen bei Karačamirli. 3. Vorbericht, Archäologische Mitteilungen aus Iran und Turan 41, 2009, 283–321

Babaev et al. 2016
I. Babaev – J. W. E. Fassbinder – Ch. Fink – K. Kaniuth – L. Lambers – St. Metz, Der Karacamirli-Survey – Vorbericht zu den Geländearbeiten 2013–2014, Archäologische Mitteilungen aus Iran und Turan 48, 2016, 189–218

Babaev et al. 2017a
I. Babayev – F. Knauss – K. Kaniuth – J. W. E. Fassbinder – M. Gruber – L. X. Mustafayev – Ü. R. Heydərova – F. Babayev, Beynəlxalq Azərbaycan-Almaniya Şəmkir-Qaracəmirli Arxeoloji Ekspedisiyasının Çöl-Tədqiqat İşləri Haqqında, Azərbaycanda arxeoloji tədqiqatlar 2015–2016, 2017, 478–488

Babaev et al. 2017b
I. Babayev – K. Kaniuth – L. X. Mustafayev – M. Gruber, 2016-ci ildə Şəmkir-Qaracəmirli Beynəlxalq arxeoloji ekspedisiyası tərəfindən MATM-ın Arxeologiya fonduna təhvil verilən arxeoloji tapıntılar, Milli Azərbaycan Tarixi Muzeyi 2017, 2017, 81–91

Babaev et al. (in print)
I. Babaev – J. W. E. Fassbinder – M. Gruber – K. Kaniuth – D. Lau – M. Schauer – M. Scheiblecker, Der Karacamirli-Survey – Vorbericht zu den Geländearbeiten 2015–2016, Archäologische Mitteilungen aus Iran und Turan

Badalyan/Avetisyan 2007
R. S. Badalyan – P. Avetisyan, Bronze and Early Iron Age archaeological sites in Armenia I. Mt. Aragats and its Surrounding Region, BAR International Series 1697 (Oxford 2007)

Badalyan et al. 2004
R. Badalyan – C. Chataigner – Ph. Kohl, Trans-Caucasian Obsidian: The Exploitation of the Sources and their Distribution, in: A. Sagona (ed.), A View from the Highlands. Archaeological Studies in honour of C. Burney, Ancient Near Eastern Studies 12 (Leuven) 437–465

Bahşaliyev 1997
V. B. Bahşaliyev, Nahçıvan Arkeolojisi – The Archaeology of Nakhichevan, Arkeoloji ve Sanat Yayınları: Deneme, Eleştiri ve Tarih Dizisi 18 (İstanbul 1997)

Bairamov et al. 2008
A. A. Bairamov – G. I. Aliyev – G. M. Hasanov – H. Y. Hasanov – T. A. Hasanov – A. J. Ismail-Zadeh – T. N.

Kangarli – V. V. Korobanov – A. I. Mamedov – A. V. Mamedov – H. V. Mustafayev – A. N. Nagiyev – A. A. Narimanov – M. I. Rustamov – Y. I. Zamanov, Geological Map of Azerbaijan Republic, in: A. A. Alizadeh (ed.), Geological Map of Azerbaijan Republic, 1:500.000, National Academy of Sciences of Azerbaijan Republic – Geology Institute (2008)

Bais 2001
M. Bais, Albania Caucasia. Ethnos, storia, territorio attraverso e fonti greche, latine e armene (Milano 2001)

Bataille/Bowen 2012
C. P. Bataille – G. J. Bowen, Mapping $^{87}Sr/^{86}Sr$ variations in bedrock and water for large scale provenance studies, Chemical Geology 304–305, 2012, 39–52

Beals et al. 1983
K. L. Beals – C. L. Smith – S. M. Dodd, Climate and the evolution of brachycephalization, American Journal of Physical Anthropology 62, 1983, 425–437

Beals et al. 1984
K. L. Beals – C. L. Smith – S. M. Dodd, Brain size, cranial morphology, climate, and time machines, Current Anthropology 25, 1984, 301–330

Bedrosian 1979
R. G. Bedrosian, The Turco-Mongol Invasion and the Lords of Armenia in the 13th–14th centuries (Ann Arbor 1979)

Behrendt et al. 2012
S. Behrendt – D. P. Mielke – O. Mecking, Die portable Röntgenfluoreszenzanalyse (P-RFA) in der Keramikforschung. Grundlagen und Potenzial, Restaurierung und Archäologie 5, 2012, 93–110

Belck 1893
W. Belck, Untersuchungen und Reisen in Transkaukasien, Hoch-Armenien und Kurdistan, I. Globus 63, 1893, 349–352

Bellary et al. 2013
S. S. Bellary – A. Steinberg – N. Mirzayan – M. Shirak – R. S. Tubbs – A. A. Cohen-Gadol – M. Loukas, Wormian bones: a review, Clinical Anatomy 26, 2013, 922–927

Bentley 2006
R. A. Bentley, Strontium Isotopes from the Earth to the Archaeological Skeleton: A Review, Journal of Archaeological Method and Theory 13, 2006, 135–187

Berry/Berry 1967
A. C. Berry – R. J. Berry, Epigenetic variation in the human cranium, Journal of Anatomy 101, 1967, 361–379

Bertram/Picchelauri 2005
J.-K. Bertram – K. Picchelauri, Vorbericht zu den Ausgrabungsarbeiten in Udabno (Ostgeorgien) im Jahre 2005, Archäologische Mitteilungen aus Iran und Turan 37, 2005, 323–364

Biagi et al. 2017a
P. Biagi – R. Nisbet – B. Gratuze, Discovery of obsidian mines on Mount Chikiani in the Lesser Caucasus of Georgia, Antiquity 91, 2017, e5, 1–8, [https://doi.org/10.15184/aqy.2017.39]

Biagi et al. 2017b
P. Biagi – R. Nisbet – B. Gratuze, Obsidian mines and their characterization. New aspects of the exploitation of the obsidian sources of Mt. Chikiani (Koyun Dag) in the Lesser Caucasus of Georgia, The Quarry 12, 2017, 2–24

Biagi/Gratuze 2016
P. Biagi – B. Gratuze, New Data on Source Characterization and Exploitation of Obsidian from the Chikiani Area (Georgia), Eurasiatica 6, 2016, 9–35

Bobokhyan et al. 2017
A. Bobokhyan – R. Kunze – K. Meliksetyan, Society and Metal in Bronze Age Armenia, in: E. Rova – M. Tonussi (eds.), At the Northern Frontier of Near Eastern Archaeology – Recent Research on Caucasia and Anatolia in the Bronze Age, Subartu 38 (Turnhout 2017) 501–523

Bocherens et al. 1996
H. Bocherens – P. L. Koch – A. Mariotti – D. Geraads – J.-J. Jaeger, Isotopic biogeochemistry (^{13}C, ^{18}O) of mammalian enamel from African Pleistocene hominid sites, Palaios 11, 1996, 306–318

Boggs 2009
S. Boggs, Petrology of sedimentary rocks (Cambridge 2009)

Bonamartini Corradi et al. 1996
A. Bonamartini Corradi – C. Leonelli – T. Manfredini – L. Pennisi – M. Romagnoli, Quantitative determination of pyrite in ceramic clay raw materials by DTA, Thermochimica Acta 287, 1996, 101–109

Bonsall et al. 2000
J. Bonsall – G. Cook – R. Lennon – D. Harkness – M. Scott – L. Bartosiewicz – K. McSweeney, Stable Isotopes, radiocarbon and the Mesolithic – Neolithic transition in the Iron Gates, Documenta Praehistorica 27, 2000, 119–132

Borscher 2016
L. C. Borscher, Reconstructing the Arsenical Copper Production Process in Early Bronze Age Southwest Asia (London 2016) [PhD-thesis: https://discovery.ucl.ac.uk/id/eprint/1529309]

Braund 1994
D. Braund, Georgia in Antiquity. A History of Colchis and Transcaucasian Iberia 550 BC–AD 562 (Oxford 1994)

Brodbeck-Jucker 2012
S. Brodbeck-Jucker, Die Keramik von Udabno in Ostgeorgien, in: A. Mehnert – G. Mehnert – S. Reinhold (eds.), Austausch und Kulturkontakt im Südkaukasus und seinen angrenzenden Regionen in der Spätbronze-/Früheisenzeit, Schriften des Zentrums für Archäologie und Kulturgeschichte des Schwarzmeerraumes 22 (Langenweißbach 2012) 123–137

Brodbeck-Jucker 2015
S. Brodbeck-Jucker, Some Aspects on the Pottery Finds from Udabno in Kakheti (Eastern Georgia), in: M. Işıklı – B. Can (eds.), International Symposium on East Anatolia-South Caucasus Cultures: Proceedings I (Cambridge 2015) 16–27

Brodbeck-Jucker 2019
S. Brodbeck-Jucker, Die Keramik von Udabno und ihre Stellung innerhalb des früheisenzeitlichen Südkaukasus, UPA 332 (Bonn 2019)

Brossmann et al. 2001
J. Brossmann – C. Czerny – J. Freyschmidt, Freyschmidt's »Köhler/Zimmer«: Grenzen des Normalen und Anfänge des Pathologischen in der Radiologie des kindlichen und erwachsenen Skeletts [14](Stuttgart/New York 2001)

Brothwell 1981
D. R. Brothwell, Digging Up Bones: The Excavation, Treatment and Study of Human Skeletal Remains (New York 1981)

Bryant/Froelich 1995
J. D. Bryant – P. N. Froelich, A model of oxygen isotope fractionation in body water of large mammals, Geochimica et Cosmochimica Acta 59, 1995, 4523–4537

Bryant et al. 1996
J. D. Bryant – P. L. Koch – P. N. Froelich – W. J. Showers – B. J. Genna, Oxygen isotope partitioning between phosphate and carbonate in mammalian apatite, Geochimica et Cosmochimica Acta 60, 1996, 5145–5148

Buckberry/Chamberlain 2002
J. L. Buckberry – A. T. Chamberlain, Age estimation from the auricular surface of the ilium: A revised method, American Journal of Physical Anthropology 119, 2002, 231–239

Burton/Hahn 2016
J. H. Burton – R. Hahn, Assessing the »Local« $^{87}Sr/^{86}Sr$ Ratio for Humans, in: G. Grupe – G. C. McGlynn (eds.), Isotopic Landscapes in Bioarchaeology (Berlin/Heidelberg 2016) 113–121

Burton/Price 1999
J. H. Burton – T. D. Price, Evaluation of bone strontium as a measure of seafood consumption, International Journal of Osteoarchaeology 9, 1999, 233–236

Burton/Price 2013
J. H. Burton – T. D. Price, Seeking the Local $^{87}Sr/^{86}Sr$ Ratio To Determine Geographic Origins of Humans, in: R. A. Armitage – J. H. Burton (eds.), Archaeological Chemistry VIII, American Chemical Society Symposium Series 1147 (Washington, D. C. 2013) 309–320

Burton et al. 1999
J. H. Burton – T. D. Price – W. D. Middleton, Correlation of Bone Ba/Ca and Sr/Ca due to Biological Purification of Calcium, Journal of Archaeological Science 26, 1999, 609–616

Byers 1991
S. Byers, Calculation of age at formation of radiopaque transverse lines, American Journal of Physical Anthropology 85, 1991, 339–343

Capo et al. 1998
R. C. Capo – B. W. Stewart – O. A. Chadwick, Strontium isotopes as tracers of ecosystem processes: theory and methods, Geoderma 82, 1998, 197–225

Ceferov 2009
H. Ceferov, Şamkircay hövzəsi tayfalarının Eneolit və Tunc Dövrü mədəniyyəti (1974–1979-cu ilin arxeoloji tədqiqatları əsasında), Azerbaycan Arxeologiyasi 12/2, 2009, 128–134

Chambrade/Metz 2017
M. L. Chambrade – S. Metz, Karacamirli 2017 – Fieldwork report (unpubl. field report)

Chataigner/Gratuze 2014
C. Chataigner – B. Gratuze, New Data on the Exploitation of Obsidian in the Southern Caucasus (Armenia, Georgia) and Eastern Turkey. Part 2: Obsidian Procurement from the Upper Palaeolithic to the Late Bronze Age, Archaeometry 56, 2014, 48–69

Chaumont 1985
M. L. Chaumont, s. v. Albania, Encyclopædia Iranica, I/8, 806–810 [an updated version is available online at http://www.iranicaonline.org/articles/albania-iranian-aran-arm (accessed on 26 February 2020)]

Chazin et al. 2019
H. Chazin – G. W. Gordon – K. J. Knudson, Isotopic perspectives on pastoralist mobility in the Late Bronze Age South Caucasus, Journal of Anthropological Archaeology 54, 2019, 48–67

Chenery et al. 2012
C. A. Chenery – V. Pashley – A. L. Lamb – H. J. Sloane – J. A. Evans, The oxygen isotope relationship between the phosphate and structural carbonate fractions of human bioapatite, Rapid Communications in Mass Spectrometry 26, 2012, 309–319

Clementz et al. 2009
M. T. Clementz – K. Fox-Dobbs – P. V. Wheatley – P. L. Koch – D. F. Doak, Revisiting old bones: coupled carbon isotope analysis of bioapatite and collagen as an ecological and palaeoecological tool, Geological Journal 44, 2009, 605–620

Coplen 1988
T. B. Coplen, Normalization of oxygen and hydrogen isotope data, Chemical Geology (Isotope Geoscience section) 72, 1988, 293–297

Coplen 2011
T. B. Coplen, Guidelines and recommended terms for expression of stable-isotope-ratio and gas-ratio measurement results, Rapid Communications in Mass Spectrometry 25, 2011, 2538–2560

Courcier 2014
A. Courcier, Ancient metallurgy in the Caucasus from the sixth to the third millennium BCE, in: B. W. Roberts – C. P. Thornton (eds.), Archaeometallurgy in global perspective (New York 2014) 579–664

Courcier et al. 2008
A. Courcier – A. Gasanova – A. Hauptmann, Ancient Metallurgy in the Caucasus during the Chalcolithic and Early Bronze Age: Recent Results from Excavations in Western Azerbaijan. Metalla 15, 2008, 21–34

Courcier et al. 2015
A. Courcier – B. Jalilov – I. Aliyev – F. E. O. Quliyev – M. Jansen – B. Lyonnet – N. Mukhtarov – N. Museibli, The Ancient Metallurgy in Azerbaijan from the End of the Neolithic to the Early Bronze Age (6th–3rd Millennium BCE): An Overview in the Light of New Discoveries and Recent Archaeometallurgical Research, in: G. Körlin – M. K. Prange – T. Stöllner – Ü. Yalcin (eds.), From Bright Ores to Shiny Metals – Festschrift for Andreas Hauptmann on the Occasion of 40 Years Research in Archaeometallurgy and Archaeometry, Der Anschnitt. Beiheft 29 (Bochum 2016) 25–36

Courcier et al. 2017
A. Courcier – M. Ragimova – N. Museibli – B. Jalilov, Metallurgical Developments in Azerbaijan from the Neolithic to the Early Bronze Age, in: E. Rova – M. Tonussi (eds.), At the Northern Frontier of near Eastern Archaeology – Recent Research on Caucasia and Anatolia in the Bronze Age, Subartu 38 (Turnhout 2017) 525–541

Cuénod et al. 2015
A. Cuénod – P. Bray – A. M. Pollard, The »Tin Problem« in the Prehistoric Near East: Further Insights from a Study of Chemical Datasets on Copper Alloys from Iran and Mesopotamia, Iran 53, 2015, 29–48

Cunningham et al. 2016
C. Cunningham – L. Scheuer – S. Black, Developmental Juvenile Osteology 2(London2016)

Dashdondog 2011
B. Dashdondog, The Mongols and the Armenians (1220–1335), Brill's Inner Asian Library 24 (Leiden 2011)

Deng/Han 2014
H. Deng – J. Han, Probabilistic Models for Clustering, in: C. C. Aggarwal – C. K. Reddy (eds.), Data Clustering: Algorithms and Applications (Boca Raton 2014) 61–86

DeNiro 1985
M. J. DeNiro, Postmortem preservation and alteration of in vivo bone collagen isotope ratios in relation to palaeodietary reconstruction, Nature 317, 1985, 806–809

DeNiro/Epstein 1976
M. J. DeNiro – S. Epstein, You are what you eat (plus a few ‰): the carbon isotope cycle in food chains, Geological Society of America Abstracts with Programs 6, 1976, 834–835

Dostiyev 2006
T. Dostiyev, Excavations of Hajialili I Settlement KP 301 – BTC ROW (Baku 2006) [accessible through Maynard 2011]

Dostiyev 2007a
T. Dostiyev, Short Report Excavations of Garajamirli II Settlement KP 323.57 – BTC ROW, Unpublished report for BTC Pipeline Co. (Baku 2007) [accessible through Maynard 2011]

Dostiyev 2007b
T. Dostiyev, Excavations of Lak I Settlement, KP 298 – BTC ROW (Baku 2007) [accessible through Maynard 2011]

Dostiyev 2008
T. Dostiyev, 2006–2007-ci illərdə Şəmkirin şəhər yerində aparılmış arxeoloji tədqiqatalar, in: M. Rəhimova et al. (eds), Şəmkir: arxeoloji irsi, tarixi və memarlığı: birinci respublika elmi-praktik kon-fransın materialları (28–29 noyabr 2007) (Bakı 2008) 31–60

Dostiyev 2009
T. Dostiyev, Orta əsr Şəmkir şəhər yeri. Şəmkir arxeoloji ekspedisiyasının tədqiqatlar 2009 (Bakı 2009)

Dostiyev 2012
T. Dostiyev, Medieval Shamkir in Light of Archaeological Excavations, IRS Heritage 11, 2012, 36–43

Dostiyev 2016
T. Dostiyev, Orta Əsr Şəmkir Şəhərində Tolerantliq, Azərbaycan Respublikasının Dini Qurumlarla İş üzrə Dövlət Komitəsi Jurnalı 5/46, 2016, 53–58

Dostiyev/Mammadov 2008
T. Dostiyev – A. Mammadov, Excavations of Hajialili III Settlement KP 302 – BTC ROW (Baku 2008) [accessible through Maynard 2011]

Drennan 2010
R. D. Drennan, Statistics for Archaeologists. A common sense approach (London/Heidelberg 2010)

Drief/Nieto 2000
A. Drief – F. Nieto, Chemical composition of smectites formed in clastic sediments. Implications for the smectite-illite transformation, Clay Minerals 35, 2000, 665–678

Dudwick 1990
N. Dudwick, The case of the Caucasian Albanians: Ethnohistory and ethnic politics, Paléorient 31, 1990, 377–383

Ebeye et al. 2016
O. A. Ebeye – D. E. Eboh – N. S. Onyia, Radiological assessment of age from epiphyseal fusion at the knee joint, Anatomy Journal 10, 2016, 1–7

Ehleringer/Osmond 1989
J. R. Ehleringer – C. B. Osmond, Stable isotopes, in: R. W. Pearcy – J. R. Ehleringer – H. A. Mooney – P. W. Rundel (eds.), Plant physiological ecology field methods and instrumentation (London 1989) 281–300

Elliott 2002
J. C. Elliott, Calcium Phosphate Biominerals, Reviews in Mineralogy and Geochemistry 48, 2002, 427–453

Erhardt 2014
E. B. Erhardt, SISUS: Stable Isotope Sourcing using Sampling [https://www.rdocumentation.org/packages/sisus]

Erhardt et al. 2014
E. B. Erhardt – B. O. Wolf – M. Ben-David – E. J. Bedrick, Stable Isotope Sourcing using Sampling, Open Journal of Ecology 4, 2014, 289–298

Ericksen 1991
M. F. Ericksen, Histologic estimation of age at death using the anterior cortex of the femur, American Journal of Physical Anthropology 84, 1991, 171–179

Fähnrich 2010
H. Fähnrich, Geschichte Georgiens, Handbuch der Orientalistik 8, 21 (Leiden 2010)

Fallucco et al. 2012
M. Fallucco – J. E. Janis – R. R. Hagan, The anatomical morphology of the supraorbital notch: clinical relevance to the surgical treatment of migraine headaches, Plastic and Reconstructive Surgery 130, 2012, 1227–1233

Fassbinder 2015
J. W. E. Fassbinder, Seeing beneath the farmland, steppe and desert soil: Magnetic prospecting and soil magnetism, Journal of Archaeological Science 56, 2015, 85–95

Fassbinder 2017
J. W. E. Fassbinder, Magnetometry for Archaeology, in: A. S. Gilbert (ed.), Encyclopedia of Geoarchaeology. Encyclopedia of Earth Sciences Series (Dordrecht 2017) 499–514

Fassbinder/Becker 2003
J. W. E. Fassbinder – H. Becker, Magnetometerprospektion des großen Kurgans 1 von Bajkara, Kasachstan, in: H. Parzinger – V. Zajbert – A. Nagler – A. Plešakov, Der große Kurgan von Bajkara. Studien zu einem skythischen Heiligtum, Archäologie in Eurasien 16 (Mainz am Rhein 2003) 131–136

Fassbinder et al. 1999
J. W. E. Fassbinder – W. E. Irlinger – N. Schleifer – H. Stanjek, Methodische Untersuchungen zur Magnetometerprospektion: Das frühmittelalterliche Gräberfeld von Alburg, Stadt Straubing, Niederbayern, Das archäologische Jahr in Bayern 1998, 1999, 112–114

Featherstone 2000
J. D. Featherstone, The science and practice of caries prevention, The Journal of the American Dental Association 131, 2000, 887–899

Featherstone 2004
J. D. Featherstone, The continuum of dental caries – evidence for a dynamic disease process, Journal of Dental Research 83 (suppl), 2004, 39–42

Finnegan 1978
M. Finnegan, Non-metric variation of the infracranial skeleton, Journal of Anatomy 125, 1978, 23–37

Finnegan/Faust 1974
M. Finnegan – M. A. Faust, Variants of the Femur, Research Report 14, 1974, 7–19

Flockhart et al. 2015
D. T. Flockhart – T. K. Kyser – D. Chipley – N. G. Miller – D. R. Norris, Experimental evidence shows no fractionation of strontium isotopes ($^{87}Sr/^{86}Sr$) among soil, plants, and herbivores: implications for tracking wildlife and forensic science, Isotopes in Environmental and Health Studies 51, 2015, 372–381

Fraley/Raftery 1998
C. Fraley – A. E. Raftery, How Many Clusters? Which Clustering Method? Answers Via Model-Based Cluster Analysis, The Computer Journal 41, 1998, 578–588

Fraley/Raftery 2002
C. Fraley – A. E. Raftery, Model-Based Clustering, Discriminant Analysis, and Density Estimation, Journal of the American Statistical Association 97, 2002, 611–631

Freyer 1986
H. D. Freyer, Interpretation of the Northern Hemispheric Record of $^{13}C/^{12}C$ Trends of Atmospheric CO_2 in Tree Rings, in: J. R. Trabalka – D. E. Reichle (eds.), The Changing Carbon Cycle: A Global Analysis (New York 1986) 125–150

Furtwängler/Knauss 1997
A. E. Furtwängler – F. S. Knauss, Archäologische Expedition in Kachetien 1996. Ausgrabungen in den Siedlungen Gumbati und Ciskaraant-Gora. 3. Vorbericht, Eurasia Antiqua 3, 1997, 353–387

Furtwängler et al. 1998
A. E. Furtwängler – F. S. Knauss – I. Motzenbäcker, Archäologische Expedition in Kachetien 1997. Ausgrabungen in Širaki. 4. Vorbericht, Eurasia Antiqua 4, 1998, 309–364

Gamkrelidze 2010
G. Gamkrelidze (ed.), Rescue Archaeology in Georgia: The Baku-Tbilisi-Ceyhan and South Caucasian Pipelines (Tbilisi 2010)

Gannes et al. 1998
L. Z. Gannes – C. M. del Rio – P. Koch, Natural abundance variations in stable isotopes and their potential uses in animal physiological ecology, Comparative biochemistry and physiology. Part A, Molecular & integrative physiology 119, 1998, 725–737

Garfinkel et al. 2014
Y. Garfinkel – F. Klimscha – S. Shalev – D. Rosenberg, The Beginning of Metallurgy in the Southern Levant: A Late 6th Millennium calBC copper awl from Tel Tsaf, Israel, PLoS ONE 9(3): e92591, [https://doi.org/10.1371/journal.pone.0092591]

Gass et al. 2019
A. Gass – S. V. Demidenko – J. W. E. Fassbinder – H. Parzinger – N. Prjamuchin, Früheisenzeitliche Kurgane und ihre Peripherien in Nekropolen der unteren Transwolga-Steppe im Fokus der archäologisch-geophysikalischen Untersuchungen, Acta Praehistorica et Archaeologica 51, 2019, 53–81.

Gelse et al. 2003
K. Gelse – E. Poschl – T. Aigner, Collagens – structure, function, and biosynthesis, Advanced Drug Delivery Reviews 55, 2003, 1531–1546

Geyer/Meeden 2017
C. J. Geyer – G. D. Meeden, rcdd: Computational Geometry [https://cran.r-project.org/web/packages/rcdd/index.html]

Glascock/Ferguson 2012
M. D. Glascock – J. R. Ferguson, Report on the Analysis of Obsidian Source Samples by Multiple Analytical Methods, [https://www.bruker.com/fileadmin/user_upload/8-PDF-Docs/X-rayDiffraction_ElementalAnalysis/HH-XRF/LabReports/Obsidian_Source_Samples.pdf] (28.06.2019)

Göhring et al. 2016
A. Göhring – M. Mauder – P. Kröger – G. Grupe, Using Gaussian Mixture Model clustering for multi-isotope analysis of archaeological fish bones for palaeobiodiversity studies, Rapid Communications in Mass Spectrometry 30, 2016, 1349–1360

Göhring et al. 2018
A. Göhring – M. Mauder – M. Vohberger – O. Nehlich – C. von Carnap-Bornheim – V. Hilberg – P. Kröger – G. Grupe, Palaeobiodiversity research based

on stable isotopes: Correction of the sea spray effect on bone carbonate $\delta^{13}C$ and $\delta^{18}O$ by Gaussian Mixture Model clustering, Palaeogeography, Palaeoclimatology, Palaeoecology 290, 2018, 673–686

Göhring et al 2019a
A. Göhring – C. von Carnap-Bornheim – V. Hilberg – C. Mayr – G. Grupe, Diet and species-specific oxygen isotope relationship and isotope spacing between structural carbonate and phosphate in archaeological mammalian bones, Archaeological and Anthropological Sciences 11, 2019, 2467–2487

Göhring et al. 2019b
A. Göhring – M. Mauder – P. Kröger – C. Mayr – C. von Carnap-Bornheim – V. Hilberg – G. Grupe, Evidence for sea spray effect on oxygen stable isotopes in bone phosphate – Approximation and correction using Gaussian Mixture Model clustering, Science of The Total Environment 673, 2019, 668–684

Golitko 2019
M. Golitko, The potential of Obsidian »Big Data«, Journal of the International Union for Prehistoric and Protohistoric Sciences 2, 2019, 83–98

Grauer/Roberts 1996
A. L. Grauer – C. A. Roberts, Paleoepidemiology, healing, and possible treatment of trauma in the medieval cemetery population of St. Helen-on-the-Walls, York, England, American Journal of Physical Anthropology 100, 1996, 531–544

Green et al. 2018
D. R. Green – G. Olack – A. S. Colman, Determinants of blood water δ18O variation in a population of experimental sheep: Implications for paleoclimate reconstruction, Chemical Geology 485, 2018, 32–43

Greiner et al. 2019
M. Greiner – A. Rodríguez-Navarro – M. F. Heinig – K. Mayer – B. Kocsis – A. Göhring – A. Toncala – G. Grupe – W. W. Schmahl, Bone incineration: An experimental study on mineral structure, colour and crystalline state, Journal of Archaeological Science: Reports 25, 2019, 507–518

Gruber 2019
M. Gruber, Besuch der Paradiesfestung bei Qalakənd, Rayon Gədəbəy (West-Aserbaidschan), Acta Praehistorica et Archaeologica 51, 2019, 33–52

Grupe 1998
G. Grupe, »Archives of Childhood« – The Research Potential of Trace Element Analyses of Ancient Human Dental Enamel, in: K. W. Alt – F. W. Rösing – M. Teschler-Nicola (eds.), Dental Anthropology: Fundamentals, Limits and Prospects (Vienna 1998) 337–347

Grupe 2014
G. Grupe, Application of isotopic mixing models for palaeodietary and paleoecological studies, Anthropologischer Anzeiger 71, 2014, 21–39

Grupe et al. 2015
G. Grupe – M. Harbeck – G. McGlynn, Prähistorische Anthropologie (Berlin/Heidelberg 2015)

Grupe et al. 2018
G. Grupe – D. Klaut – M. Mauder – P. Kröger – A. Lang – C. Mayr – F. Söllner, Multi-isotope provenancing of archaeological skeletons including cremations in a reference area of the European Alps, Rapid Communications in Mass Spectrometry 32, 2018, 1711–1727

Gülçur/Marro 2012
S. **Gülçur** – C. Marro, The view from the North – Comparative analysis of the Chalcolithic pottery assemblages from Norşuntepe and Ovçular Tepesi, Varia Anatolica 27, 2012, 305–352

Hacili 2010
Z. Hacili, Ceramics of Tovuzchay necropolis, in: Г. Г. Гамбашидзе (ed.), Международная научная конференция »Археология, этнология, фольклористика Кавказа«: Сборник кратких содержаний докладов : Тбилиси, 25–27 июня 2009 года (Тбилиси 2010) 276–279

Hacili 2012
Z. Hacili, Tovuzçay Hövzəsinin Son Tunc-İlk Dəmir dövrünə Aid Torpaq Qəbirləri (Tovuzçay və Qazqulu nekropollarının materialları əsasında), Arxeologiya və Etnoqrafiya 1, 2012, 215–218

Hagl et al. 2013
P. Hagl – C. Becker – G. Grupe, Establishment of dairying economy in the Bavarian Neolithic revealed by isotopic foodwebs, in: G. Grupe – G. McGlynn – J. Peters (eds.), Documenta Archaeobiologiae (Rahden 2013) 79–93

Hamer/Hamer 2004
F. Hamer – J. Hamer, The potter's dictionary of materials and techniques [5](Pennsylvania 2004)

Hančar 1932
F. Hančar, Die Nadelformen des prähistorischen Kaukasusgebietes, Eurasia Septentrionalis Antiqua 7, 1932, 113–182

Hančar 1934
F. Hančar, Kaukasus-Luristan, Eurasia Septentrionalis Antiqua 9, 1934, 47–112

Hanihara/Ishida 2001
T. Hanihara – H. Ishida, Frequency variations of discrete cranial traits in major human populations. IV. Vessel and nerve related variations, Journal of Anatomy 199, 2001, 273–287

Hansen et al. 1993
P. F. B. Hansen – K. Dam-Johansen – K. Østergaard, High-temperature reaction between sulphur dioxide and limestone. V. The effect of periodically changing oxidizing and reducing conditions, Chemical Engineering Science 7, 1993, 1325–1341

Hansen 2014
S. Hansen, Gold and silver in the Maikop Culture, in: H. Meller – R. Risch – E. Pernicka (eds.), Metalle der Macht – Frühes Gold und Silber. 6. Mitteldeutscher Archäologentag vom 17. bis 19. Oktober 2013 in Halle (Saale), Tagungen des Landesmuseums für Vorgeschichte Halle 11/II (Halle Saale 2014) 389–410

Harvati/Weaver 2006
K. Harvati – T. D. Weaver, Human cranial anatomy and the differential preservation of population history and climate signatures, The Anatomical Record Part A: Discoveries in Molecular, Cellular, and Evolutionary Biology 288, 2006, 1225–1233

Hässig et al. 2016
M. Hässig – T. Duretz – Y. Rolland – M. Sosson, Obduction of old oceanic lithosphere due to reheating and platereorganization: Insights from numerical modelling and the NE Anatolia – Lesser Caucasus case example, Journal of Geodynamics 96, 2016, 35–49

Haurowitz 1955
F. Haurowitz, Biochemistry – An Introductory Textbook (New York 1955)

Hefner et al. 2016
J. T. Hefner – M. A. Pilloud – J. E. Buikstra – C. C. M. Vogelsberg, A Brief History of Biological Distance Analysis, in: M. A. Pilloud – J. T. Hefner (eds.), Biological Distance Analysis: Forensic and Bioarchaeological Perspectives (San Diego 2016) 3–22

Helfert 2010
M. Helfert, Groß Gerau II. Die römischen Töpfereien von Groß-Gerau »Auf Esch« – Archäologische und archäometrische Untersuchungen zur Keramikproduktion im Kastellvicus, Frankfurter Archäologische Schriften 11 (Bonn 2010)

Helfert 2013
M. Helfert, Die portable energiedispersive Röntgenfluoreszenzanalyse (P-ED-RFA) – Studie zu methodischen und analytischen Grundlagen ihrer Anwendung in der archäologischen Keramikforschung, in: B. Ramminger – O. Stilborg – M. Helfert (eds.), Naturwissenschaftliche Analysen vor- und frühgeschichtlicher Keramik III. Methoden, Anwendungsbereiche, Auswertungsmöglichkeiten, Universitätsforschungen zur Prähistorischen Archäologie 238 (Bonn 2013) 13–47

Heling 1988
D. Heling, ›Ton- und Siltsteine‹, in: H. Füchtbauer (ed.), Sediment-Petrologie (Stuttgart 1988) 185–231

Helwing 2014
B. Helwing, Silver in the Early State Societies of Greater Mesopotamia, in: H. Meller – E. Pernicka – R. Risch (eds.), in: H. Meller – R. Risch – E. Pernicka (eds.), Metalle der Macht – Frühes Gold und Silber. 6. Mitteldeutscher Archäologentag vom 17. bis 19. Oktober 2013 in Halle (Saale), Tagungen des Landesmuseums für Vorgeschichte Halle 11/II (Halle Saale 2014) 411–421

Helwing et al. 2012
B. Helwing – B. Lyonnet – F. Guliyev – T. Aliyev – S. Hansen – G. Mirtskhulava, Ancient Kura 2010–2011. The first two seasons of joint field work in the Southern Caucasus, Archäologische Mitteilungen aus Iran und Turan 44, 2012, 1–190

Helwing et al. 2017
B. Helwing – T. Aliyev – B. Lyonnet – F. Guliyev – S. Hansen – G. Mirtskhulava, The Kura Projects. New Research on the Later Prehistory of the Southern Caucasus, Archäologie in Iran und Turan 16 (Berlin 2017)

Herrmann et al. 1990
B. Herrmann – G. Grupe – S. Hummel – H. Piepenbrink – H. Schutkowski, Prähistorische Anthropologie. Leitfaden der Feld- und Labormethoden (Berlin/Heidelberg/New York 1990)

Herrscher et al. 2014
E. Herrscher – G. Bedianashvili – M. Chkadua – N. Vanishvili – M. Abramishvili – E. Messager – L. Martin, Millet crop and consumption during the Late Bronze Age in Georgia: First human and animal isotopic evidence, American Journal of Physical Anthropology 153, 2014, 141

Herrscher et al. 2018a
E. Herrscher – M. Poulmarc'h – L. Pecqueur – E. Jovenet – N. Benecke – A. Decaix – B. Lyonnet – F. Guliyev – G. André, Dietary inferences through stable isotope analysis at the Neolithic and Bronze Age in the southern Caucasus (sixth to first millenium BC, Azerbaijan): From environmental adaptation to social impacts,

American Journal of Physical Anthropology 167, 2018, 856–875

Herrscher et al. 2018b
E. Herrscher – G. André – C. Bodet – C. Chataigner – A. Decaix – G. Goude – C. Hamon – F. Le Mort – B. Lyonnet – L. Martin – E. Messager – C. Oberlin – V. Ollivier – M. Poulmarc'h – C. Sermet – E. Vila, The origins of millet cultivation in the Caucasus: archaeological and archaeometric approaches, Préhistoires Méditerranéennes 6, 2018, 1–27

Higham et al. 2010
T. Higham – R. Warren – A. Belinskij – H. Härke – R. Wood, Radiocarbon Dating, Stable Isotope Analysis, and Diet-Derived Offsets in ^{14}C Ages from the Klin-Yar Site, Russian North Caucasus, Radiocarbon 52, 2010, 653–670

Hillson 2005
S. Hillson, Teeth ^{2}(Cambridge 2005)

Hillson/Antoine 2003
S. Hillson – D. Antoine, Ancient bones and teeth on the microstructural level, in: G. Grupe – J. Peters (eds.), Documenta Archaeobiologiae (Rahden 2003) 141–158

Hobson et al. 1999
K. A. Hobson – M. C. Drever – G. W. Kaiser, Norway Rats as Predators of Burrow-Nesting Seabirds: Insights from Stable Isotope Analyses, The Journal of Wildlife Management 63, 1999, 14–25

Howland et al. 2003
M. R. Howland – L. T. Corr – S. M. M. Young – V. Jones – S. Jim – N. J. Van Der Merwe – A. D. Mitchell – R. P. Evershed, Expression of the dietary isotope signal in the compound-specific $\delta^{13}C$ values of pig bone lipids and amino acids, International Journal of Osteoarchaeology 13, 2003, 54–65

Hubbe et al. 2009
M. Hubbe – T. Hanihara – K. Harvati, Climate Signatures in the Morphological Differentiation of Worldwide Modern Human Populations, The Anatomical Record 292, 2009, 1720–1733

Hummel 1929
J. Hummel, Das heimatkundliche Museum zu Helenendorf (Moskau 1929)

Hüseynov/Cəlilov 2008
M. M. Hüseynov – B. M. Cəlilov, Orta əsr Daşbulaq yaşayış yeri, in: M. Rəhimova et al. (eds), Şəmkir: arxeoloji irsi, tarixi və memarlığı: birinci respublika elmi-praktik konfransın materialları (28–29 noyabr 2007) (Bakı 2008) 226–238

Huseynov et al. 2007
M. Huseynov – G. Agayev – A. Gahraman – G. Safar, Long Report Excavations of Seyidlar Settlement KP 316 – BTC ROW, unpublished report for BTC Pipeline Co. (Baku 2007) [accessible through Maynard 2011]

Iacumin et al. 1996
P. Iacumin – H. Bocherens – A. Mariotti – A. Longinelli, Oxygen isotope analyses of co-existing carbonate and phosphate in biogenic apatite: a way to monitor diagenetic alteration of bone phosphate?, Earth and Planetary Science Letters 142, 1996, 1–6

IHPA NGO 2013
IHPA NGO, River Basin Management Plan for Central Kura Pilot Basin District: Agstafachay, Tovuzchay, Shamkirchay and Ganjachay River Basins [http://blacksea-riverbasins.net/sites/default/files/Ganja-Gazakh%20%20RBMP%20%20F%C4%B0NAL.pdf]

Isikli/Altunkaynak 2014
M. Isikli – G. Altunkaynak, Some Observations on Relationships between South Caucasus and North-Eastern Anatolia Based on Recent Archeo-Metallurgical Evidence, in: M. Kvachadze – M. Puturidze – N. Shanshashvili (eds.), Problems of Early Metal Age archaeology of Caucasus and Anatolia. Proceedings of the International Conference, November 19–23, 2014 (Tbilisi 2014) 73–93

Jalilov 2007
B. Jalilov, Short Report Excavations of Seyidlar II Antique Period Settlement KP 318 – BTC ROW, unpublished report for BTC Pipeline Co. (Baku 2007) [accessible through Maynard 2011]

Jalilov/Kvachidze 2007
B. Jalilov – V. Kvachidze, Excavations of Fakhrali Settlement KP 289 – BTC ROW (Baku 2007) [accessible through Maynard 2011]

Jim et al. 2004
S. Jim – S. H. Ambrose – R. P. Evershed, Stable carbon isotopic evidence for differences in the dietary origin of bone cholesterol, collagen and apatite: implications for their use in palaeodietary reconstruction, Geochimica et Cosmochimica Acta 68, 2004, 61–72

Johansen et al. 1986
O. S. Johansen – S. Gulliksen – R. Nydal, $\delta^{13}C$ and diet: analysis of Norwegian human skeletons, Radiocarbon 28, 1986, 754–761

Jordan/Zvelebil 2011
P. Jordan – M. Zvelebil, Ex Oriente Lux. The Prehistory of Hunter-Gatherer Ceramic Dispersals, in: P. Jordan – M. Zvelebil (eds.), Ceramics before farming – The

dispersal of pottery among prehistoric Eurasian hunter-gatherers (Walnut Creek 2011) 33–89

Kagerer/Grupe 2001
P. Kagerer – G. Grupe, Age-at-death diagnosis and determination of life-history parameters by incremental lines in human dental cementum as an identification aid, Forensic Science International 118, 2001, 75–82

Kakhiani et al. 2013
K. Kakhiani – A. Sagona – C. Sagona – E. Kvavadze – G. Bedianashvili – E. Massager – L. Martin – E. Herrscher – I. Martkoplishvili – J. Birkett-Rees – C. Longford, Archaeological Investigations at Chobareti in southern Georgia, the Caucasus, Ancient Near Eastern Studies 50, 2013, 1–138

Kettenhofen 1982
E. Kettenhofen, Die römisch-persischen Kriege des 3. Jahrhunderts n. Chr. nach der Inschrift Šāhpuhrs I. an der Kaʿbe-ye Zartošt (ŠKZ), Beihefte zum Tübinger Atlas des Vorderen Orients 55 (Wiesbaden 1982)

Kharazyan/Sargsyan 2005
E. Kharazyan – H. Sargsyan, Geological Map of Republic of Armenia [s. n.]

Kibaroğlu 2008
M. Kibaroğlu, Petrographische und geochemische Untersuchungen an archäologischer Keramik aus Nordost-Syrien, Südost-Anatolien, Ost-Anatolien und Ost-Georgien (Tübingen 2008) [PhD-Thesis: http://hdl.handle.net/10900/49155]

Kiguradze/Sagona 2003
T. Kiguradze – A. Sagona, On the Origins of the Kura-Araxes Cultural Complex, in: A. T. Smith – K. S. Rubinson (eds.), Archaeology in the Borderlands: Investigations in Caucasia and Beyond (Los Angeles 2003) 38–94

Kirakos Gandzaketsi 1986
Kirakos Gandzakets'i's history of the Armenians (translated by R. G. Bedrosian) (New York 1986)

Kirsanow/Tuross
K. Kirsanow – N. Tuross, Oxygen and hydrogen isotopes in rodent tissues: Impact of diet, water and ontogeny, Palaeogeography, Palaeoclimatology, Palaeoecology 310, 2005, 9–16

Knauss 2007
F. S. Knauss, Ein Perserbau auf dem Ideal Tepe bei Karačamirli (Aserbaidschan), ARTA 2007.002, 1–51

Knauss et al. 2010
F. Knauss – I. Gagoshidze – I. Babaev, A Persian Propylon in Azerbaijan. Excavations at Karacamirli, in: J. Nieling – E. Rehm (eds.), Achaemenid Impact in the Black Sea. Communication of Powers, BSS 11 (Aarhus 2010) 111–122

Knauss et al. 2013
F. Knauss – I. Gagoshidze – I. Babaev, Karačamirli: Ein persisches Paradies, ARTA 2013.004, 1–28

Knobbe et al. 2006
N. Knobbe – J. Vogl – W. Pritzkow – U. Panne – H. Fry – H. M. Lochotzke – A. Preiss-Weigert, C and N stable isotope variation in urine and milk of cattle depending on the diet, Analytical and Bioanalytical Chemistry 386, 2006, 104–108

Knott/Bailey 1998
L. Knott – A. J. Bailey, Collagen cross-links in mineralizing tissues: A review of their chemistry, function, and clinical relevance, Bone 22, 1998, 181–187

Kohlmeyer/Saherwala 1983
K. Kohlmeyer – G. Saherwala, Frühe Bergvölker in Armenien und im Kaukasus. Berliner Forschungen des 19. Jahrhunderts (Berlin 1983)

Kohn 1996
M. J. Kohn, Predicting animal $\delta^{18}O$: Accounting for diet and physiological adaptation, Geochimica et Cosmochimica Acta 60, 1996, 4811–4829

Kohn/Cerling 2002
M. J. Kohn – T. E. Cerling, Stable Isotope Compositions of Biological Apatite, in: M. J. Kohn – J. Rakovan – J. M. Hughes (eds.), Phosphates: Geochemical, Geobiological, and Materials Importance, reviews in Mineralogy and Geochemistry, The Mineralogical Society of America (Washington, D. C. 2002) 455–480

Kohn et al. 1996
M. J. Kohn – M. J. Schoeninger – J. W. Valley, Herbivore tooth oxygen isotope compositions: Effects of diet and physiology, Geochimica et Cosmochimica Acta 60, 1996, 3889–3896

Komsta/Novomestky 2015
L. Komsta – F. Novomestky, moments: Moments, cumulants, skewness, kurtosis and related tests [https://CRAN.R-project.org/package=moments]

Korfmann et al. 2003/2004
M. O. Korfmann – K. Picchelauri – J.-K. Bertram – G. Kastl, Erster Vorbericht zu den Vermessungs- und Ausgrabungsarbeiten in Udabno (Ostgeorgien) 2000–2004, Archäologische Mitteilungen aus Iran und Turan 35/36, 2003/2004, 175–224

Kornexl et al. 1997
B. E. Kornexl – T. Werner – A. Rossmann – H.-L. Schmidt, Measurement of stable isotope abundances in milk and milk ingredients – a possible tool for origin assignment and quality control, Zeitschrift für Lebensmitteluntersuchung und -Forschung A 205, 1997, 19–24

Krueger/Sullivan 1984
H. W. Krueger – C. H. Sullivan, Models for Carbon Isotope Fractionation Between Diet and Bone, in: J. R. Turnlund – P. E. Johnson (eds.), Stable Isotopes in Nutrition, ACS Symposium Series 258 (Washington, D. C. 1984) 205–222

Kulus/Dąbrowski 2019
M. J. Kulus – P. Dąbrowski, How to calculate the age at formation of Harris lines? A step-by-step review of current methods and a proposal for modifications to Byers' formulas, Archaeological and Anthropological Sciences 11, 2019, 1169–1185

Kunze 2012
R. Kunze, Interdisziplinäre Studien zu den Kleinfunden der Siedlungen Udabno I–III (Ostgeorgien) (Tübingen 2012) [PhD-thesis: http://nbn-resolving.de/urn:nbn:de:bsz:21-opus-69609]

Kushnareva 1997
K. Kh. Kushnareva, The Southern Caucasus in Prehistory. Stages of cultural and Socioeconomic Development from the Eighth to the Second Millennium B.C., University Museum Monograph 99 (Philadelphia 1997)

Lang 1955
D. M. Lang, Georgia in the Reign of Giorgi the Brilliant (1314–1346), Bulletin of the School of Oriental and African Studies, University of London 17, 1955, 74–91

Lechtman 1996
H. Lechtman, Arsenic Bronze: Dirty Copper or Chosen Alloy?, Journal of Field Archaeology 23/4, 1996, 477–514

Lee-Thorp et al. 1989
J. A. Lee-Thorp – J. C. Sealy – N. J. van der Merwe, Stable carbon isotope ratio differences between bone collagen and bone apatite, and their relationship to diet, Journal of Archaeological Science 16, 1989, 585–599

LeGeros/LeGeros 1984
R. Z. LeGeros – J. P. LeGeros, Phosphate Minerals in Human Tissues, in: J. O. Nriagu – P. B. Moore (eds.), Phosphate Minerals (Berlin 1984) 351–385

LeGeros et al. 1969
R. Z. LeGeros – O. R. Trautz – E. Klein – J. P. LeGeros, Two types of carbonate substitution in the apatite structure, Experientia 25, 1969, 5–7

Lengfelder et al. 2019
F. Lengfelder – G. Grupe – A. Stallauer – R. Huth – F. Söllner, Modelling strontium isotopes in past biospheres – Assessment of bioavailable $^{87}Sr/^{86}Sr$ ratios in local archaeological vertebrates based on environmental signatures, Science of The Total Environment 648, 2019, 236–252

Linford et al. 2007
N. Linford – P. Linford – L. Martin – A. Payne, Recent results from the English Heritage caesium magnetometer system in comparison with recent fluxgate gradiometers, Archaeological Prospection 14, 2007, 151–166

Longinelli/Peretti Padalino 1980
A. Longinelli – A. Peretti Padalino, Oxygen isotopic composition of water from mammal blood: first results, European Journal of Mass Spectrometry in Biochemical, Medicine and Environmental Research 1, 1980, 135–139

Longinelli 1984
A. Longinelli, Oxygen isotopes in mammal bone phosphate: A new tool for paleohydrological and paleoclimatological research?, Geochimica et Cosmochimica Acta 48, 1984, 385–390

Longinelli/Selmo 2011
A. Longinelli – E. Selmo, $\delta^{18}O$ values of Sus scrofa blood water and bone phosphate; a marked discrepancy between domestic and wild specimens, Rapid Communications in Mass Spectrometry 25, 2011, 3732–3734

Lordkipanidze 1991
O. Lordkipanidze, Archäologie in Georgien. Von der Altsteinzeit zum Mittelalter, Quellen und Forschungen zur prähistorischen und provinzialrömischen Archäologie 5 (Weinheim 1991)

Loukas et al. 2008
M. Loukas – D. G. Owens – R. S. Tubbs – G. Spentzouris – A. Elochukwu – R. Jordan, Zygomaticofacial, zygomaticoorbital and zygomaticotemporal foramina: anatomical study, Anatomical Science International 83, 2008, 77–82

Lovell/Grauer 2019
N. C. Lovell – A. L. Grauer, Analysis and interpretation of trauma in skeletal remains, in: M. A. Katzenberg – A. L. Grauer (eds.), Biological anthropology of the human skeleton [3](Hoboken 2019) 335–383

Ludwig 2010
N. Ludwig, Ostgeorgische Fundplätze des 1. Jahrtausends v. Chr. – Die Keramik, Schriften des Zentrums für

Archäologie und Kulturgeschichte des Schwarzmeerraumes 20 (Langenweißbach 2010)

Ludwig-Egermann 2012
N. Ludwig-Egermann 2012, Keramik ostgeorgischer Fundplätze am Übergang von der Spätbronze- zur Früheisenzeit, in: A. Mehnert – G. Mehnert – S. Reinhold (eds.), Austausch und Kulturkontakt im Südkaukasus und seinen angrenzenden Regionen in der Spätbronze-/Früheisenzeit, Schriften des Zentrums für Archäologie und Kulturgeschichte des Schwarzmeerraumes 22 (Langenweißbach 2012) 159–174

Luz et al. 1984
B. Luz – Y. Kolodny – M. Horowitz, Fractionation of oxygen isotopes between mammalian bone-phosphate and environmental drinking water, Geochimica et Cosmochimica Acta 48, 1984, 1689–1693

Luz/Kolodny 1985
B. Luz – Y. Kolodny, Oxygen isotope variations in phosphate of biogenic apatites, IV. Mammal teeth and bones, Earth and Planetary Science Letters 75, 1985, 29–36

Luz et al. 1990
B. Luz – A. B. Cormie – H. P. Schwarcz, Oxygen isotope variations in phosphate of deer bones, Geochimica et Cosmochimica Acta 54, 1990, 1723–1728

Lyonnet 2014
B. Lyonnet, The Early Bronze Age in Azerbaijan in the light of recent discoveries, Paléorient 40/2, 2014, 115–130

Lyonnet 2017
B. Lyonnet, Mentesh Tepe 2012–2014. The Pottery, in: B. Helwing – T. R. Aliyev – B. Lyonnet – F. Quliyev – S. Hansen – G. Mirtskhulava (eds.), The Kura Projects. New Research on the Later Prehistory of the Southern Caucasus, Archäologie in Iran und Turan 16 (Berlin 2017) 141–151

Lyonnet 2018
B. Lyonnet, Rethinking the ›Sioni cultural complex‹ in the South Caucasus (Chalcolithic period): New data from Mentesh Tepe (Azerbaijan), in: A. Batmaz – G. Bedianashvili – A. Michalewicz – A. Robinson (eds.), Context and Connection - Essays on the Archaeology of the Ancient Near East in Honour of Antonio Sagona, Orientalia Lovaniensia Analectica 268 (Leuven 2018) 547–567

Lyonnet/Quliyev 2017
B. Lyonnet – F. Quliyev, Mentesh Tepe (Azerbaijan), Preliminary Report on the 2012–2014 Excavations, in: B. Helwing – T. R. Aliyev – B. Lyonnet – F. Quliyev – S. Hansen – G. Mirtskhulava (eds.), The Kura Projects. New Research on the Later Prehistory of the Southern Caucasus, Archäologie in Iran und Turan 16 (Berlin 2017) 125–140

Lyonnet et al. 2012
B. Lyonnet – F. Quliyev – B. Helwing – T. R. Aliyev – S. Hansen – G. Mirtskhulava, Ancient Kura 2010–2011: The first two seasons of joint field work in the Southern Caucasus, Archäologische Mitteilungen aus Iran und Turan 44, 2012, 1–190

Lyonnet et al. 2016
B. Lyonnet – F. Quliyev – L. Bouquet – G. Bruley-Chabot – A. Samzun – L. Pecqueur – E. Jovenet – E. Baudouin – M. Fontugne – P. Raymond – E. Degorre – L. Astruc – D. Guilbeau – G. Le Dosseur – N. Benecke – C. Hamon – M. Poulmarc'h – A. Courcier, Mentesh Tepe, an early settlement of the Shomu-Shulaveri Culture in Azerbaijan, Quaternary International 395, 2016, 170–183

Mammadov/Agayev 2007
A. Mammadov – G. Agayev, Excavations of Hajialili II Settlement KP 300.98 – BTC ROW (Baku 2007) [accessible through Maynard 2011]

Manica et al. 2007
A. Manica – W. Amos – F. Balloux – T. Hanihara, The effect of ancient population bottlenecks on human phenotypic variation, Nature 448, 2007, 346–348

Manning et al. 2018
S. W. Manning – A. T. Smith – L. Khatchadourian – R. S. Badalyan – I. C. Lindsay – A. Greene – M. Marshall, A new chronological model for the Bronze and Iron Age South Caucasus: radiocarbon results from Project ArAGATS, Armenia, Antiquity 92, 2018, 1530-1551

Marro 2010
C. Marro, Where did Late Chalcolithic Chaff-Faced Ware originate? Cultural Dynamics in Anatolia and Transcaucasia at the Dawn of Urban Civilization (ca 4500–3500 BC), Paléorient 36/2, 2010, 35–55

Marro 2012
C. Marro, Is there a Post-Ubaid culture? Reflections on the transition from the Ubaid to the Uruk periods along the Fertile Crescent and beyond, Varia Anatolica 27, 2012, 13–38

Marro et al. 2009
C. Marro – V. Bakhshaliyev – S. H. Aşurov, Excavations at Ovçular Tepesi (Nakhchivan, Azerbaijan). First Preliminary Report : the 2006–2008 Seasons, Anatolia Antiqua 17, 2009, 31–87

Marro et al. 2011
C. Marro – V. Bakhshaliyev – S. H. Aşurov, Excavations at Ovçular Tepesi (Nakhchivan, Azerbaijan). Second Preliminary Report: the 2009–2010 Seasons, Anatolia Antiqua 19, 2011, 53–100

Marshall et al. 2007
J. D. Marshall – J. R. Brooks – K. Lajtha, Sources of variation in the stable isotopic composition of plants, in: R. Michener – K. Lajtha (eds.), Stable Isotopes in Ecology and Environmental Science [2](Oxford 2007) 22–60

Martin 1914
R. Martin, Lehrbuch der Anthropologie in systematischer Darstellung: mit besonderer Berücksichtigung der anthropologischen Methoden (Jena 1914)

Martin et al. 2008
C. Martin – I. Bentaleb – R. Kaandorp – P. Iacumin – K. Chatri, Intra-tooth study of modern rhinoceros enamel δ18O: Is the difference between phosphate and carbonate δ18O a sound diagenetic test?, Palaeogeography, Palaeoclimatology, Palaeoecology 266, 2008, 183–189

Martin et al. 2015
R. B. Martin – D. B. Burr – N. A. Sharkey – D. P. Fyhrie, Fatigue and Fracture Resistance of Bone, in: R. B. Martin – D. B. Burr – N. A. Sharkey – D. P. Fyhrie (eds.), Skeletal Tissue Mechanics [2](New York 2015) 423–482

Massler et al. 1941
M. M. Massler – I. Schour – H. G. Poncher, Developmental pattern of the child as reflected in the calcification pattern of the teeth, American Journal of Diseases of Children 62, 1941, 33–67

Mathé et al. 2009
V. Mathé – F. Lévêque – M. Druez, What interest to use caesium magnetometer instead of fluxgate gradiometer?, ArcheoSciences, revue d'archéométrie, suppl. 33, 2009, 325–327

Mauder et al. 2016
M. Mauder – E. Ntoutsi – P. Kröger – H.-P. Kriegel, Towards Predicting Places of Origin from Isotopic Fingerprints: A Case Study on the Mobility of People in the Central European Alps, in: G. Grupe – G. C. McGlynn (eds.), Isotopic Landscapes in Bioarchaeology (Berlin/Heidelberg 2016) 221–233

May 2010
T. May, The Conquest and Rule of Transcaucasia: The Era of Chormaq, in: J. Tubach – S. G. Vashalomidze – M. Zimmer (eds.), Caucasus during the Mongol Period – Der Kaukasus in der Mongolenzeit (Wiesbaden 2010) 129–151

May 2017
T. May (ed.), The Mongol Empire. A Historical Encyclopedia (Santa Barbara 2017)

May 2018
T. May, The Mongol Empire (Edinburgh 2018)

Maynard 2011
D. Maynard, The BTC Pipeline Archaeological Excavations in Azerbaijan, Archaeology Data Service [https://doi.org/10.5284/1000411]

Mayr et al. 2016
C. Mayr – G. Grupe – A. Toncala – C. M. Lihl, Linking Oxygen Isotopes of Animal-Bone Phosphate with Altimetry: Results from Archaeological Finds from a Transect in the Alps, in: G. Grupe – G. C. McGlynn (eds.), Isotopic Landscapes in Bioarchaeology (Berlin/Heidelberg 2016) 157–172

McCutchan et al. 2003
J. H. McCutchan – W. M. Lewis – C. Kendall – C. C. McGrath, Variation in trophic shift for stable isotope ratios of carbon, nitrogen, and sulfur, Oikos 102, 2003, 378–390

McLennan et al. 1990
S. M. McLennan – S. R. Taylor – M. T. McCulloch – J. B. Maynard, Geochemical and Nd-Sr isotopic composition of deep-sea turbidites: Crustal evolution and plate tectonic associations, Geochimica et Cosmochimica Acta 54/7, 1990, 2015–2050

McLennan 2001
S. M. McLennan, Relationships between the trace element composition of sedimentary rocks and upper continental crust, Geochemistry, Geophysics, Geosystems 2/4, 2001, 1–24

Mecking 2010
O. Mecking, Naturwissenschaftliche Untersuchung eines Töpferofens der Bernburger Kultur aus Erfurt-Gispersleben, in: B. Ramminger – O. Stilborg (eds.), Naturwissenschaftliche Analysen vor- und frühgeschichtlicher Keramik I. Methoden, Anwendungsbereiche, Auswertungsmöglichkeiten, Universitätsforschungen zur Prähistorischen Archäologie 176 (Bonn 2010) 117–126

Mecking et al. 2013
O. Mecking – D. P. Mielke – S. Behrendt, Methodenvergleich, Anwendungsbeispiele und Grundlagen der portablen Röntgenfloureszenzanalyse (P-RFA) in der Keramikforschung, in: B. Ramminger – O. Stilborg – M. Helfert (eds.), Naturwissenschaftliche Analysen vor- und frühgeschichtlicher Keramik III. Methoden, Anwendungsbereiche, Auswertungsmöglichkeiten, Uni-

versitätsforschungen zur Prähistorischen Archäologie 238 (Bonn 2013) 49–67

Meeden et al. 2017
G. Meeden – R. Lazar – C. J. Geyer, polyapost: Simulating from the Polya Posterior

Mehnert 2008
G. Mehnert, Skythika in Transkaukasien, Nomaden und Sesshafte 10 (Wiesbaden 2008)

Mekota et al. 2006
A.-M. Mekota – G. Grupe – S. Ufer – U. Cuntz, Serial analysis of stable nitrogen and carbon isotopes in hair: monitoring starvation and recovery phases of patients suffering from anorexia nervosa, Rapid Communications in Mass Spectrometry 20, 2006, 1604–1610

Meliksetyan et al. 2003
K. Meliksetyan – E. Pernicka – P. Avetisyan – H. Simonyan, Chemical and lead isotope characterisation of Middle Bronze Age bronzes and some Iron Age antimony objects (Armenia), in: Associazione Italiana di Metallurgia (ed.), International Conference Archaeometallurgy in Europe. Vol. 1 (Milan 2003) 311–318.

Meliksetyan et al. 2011
K. Meliksetyan – S. Kraus – E. Pernicka – P. Avetisyan – S. Devejian – L. Petrosyan, Metallurgy of Prehistoric Armenia, in: Ü. Yalcin (ed.), Anatolian Metal V (Bochum 2011) 201–210

Melzer/O'Leary 1987
E. Melzer – M. H. O'Leary, Anapleurotic CO_2 Fixation by Phosphoenolpyruvate Carboxylase in C_3 Plants, Plant Physiology 84, 1987, 58–60

Messager et al. 2015
E. Messager – E. Herrscher – L. Martin – E. Kvavadze – I. Martkoplishvili – C. Delhon – K. Kakhiani – G. Bedianashvili – A. Sagona – L. Bitadze – M. Poulmarc'h – A. Guy – D. Lordkipanidze, Archaeobotanical and isotopic evidence of Early Bronze Age farming activities and diet in the mountainous environment of the South Caucasus: a pilot study of Chobareti site (Samtskhe-Javakheti region), Journal of Archaeological Science 53, 2015, 214–226

Məmmədov 2006
T. M. Məmmədov, Qafqaz Albaniyası ilk orta əsrlərdə (Bakı 2006)

Minagawa/Wada 1984
M. Minagawa – E. Wada, Stepwise enrichment of ^{15}N along food chains: Further evidence and the relation between $\delta^{15}N$ and animal age, Geochimica et Cosmochimica Acta 48, 1984, 1135–1140

Mommsen 2007
H. Mommsen, Tonmasse und Keramik: Herkunftsbestimmung durch Spurenanalyse, in: G. A. Wagner (ed.), Einführung in die Archäometrie (Berlin/Heidelberg 2007) 179–195

Müseyibli 2004
N. Müseyibli, Zəyəmçay nekropolunda arxeoloji qazıntılar, Azərbaycan Arxeologiyası və Etnoqrafiyası 2, 2004, 58–74

Müseyibli 2007
N. Müseyibli, Böyük Kəsik eneolit dövrü yaşayış məskəni (Bakı 2007)

Müseyibli 2009
N. Müseyibli, Zəyəmçay nekropolunun qəbir tipləri, Azərbaycan Arxeologiyası 12/2, 2009, 37–57

Müseyibli 2014a
N. Müseyibli, Leylatəpə Mədəniyyətinin Xronologiyası və Dövrləşdirilməsi, Xəbərlər – Tarix, Fəlsəfə, Hüquq 2014/1, 2014, 91–109

Müseyibli 2014b
N. Müseyibli, The Grave Monuments and Burial Customs of the Leilatepe Culture (Baku 2014)

Müseyibli 2015
N. Müseyibli, The Leilatepe Archaeological culture: Its Near-Eastern Roots and its Place in the Caucasus Chalcolithic, in: M. Işıklı – B. Can (eds.), International Symposium on East Anatolia-South Caucasus Cultures: Proceedings I (Cambridge 2015) 58–75

Müseyibli 2016
N. Müseyibli, Some issues on general features of the Leilatepe Culture, Azərbaycan Arxeologiyası və Etnoqrafiyası 2016/1, 2016, 15–22

Müseyibli/Axundova 2013
N. Müseyibli – G. Axundova, Xocali – Gədəbəy Mədəniyyəti Karamikasının Ornamentlərinin Etnoarxeoloji Tədqiqi (Zəyəmçay və Tovuzçay nekropollarının materialları əsasında), Azərbaycan Arxeologiyası və Etnoqrafiyası 2, 2013, 11–26

Müseyibli/Kvachidze 2006
N. Müseyibli – V. Kvachidze, Excavations of a Muslim Cemetery KP 356 – BTC ROW (Baku 2006) [accessible through Maynard 2011]

Müseyibli/Nəcəfov 2019
N. Müseyibli – Ş. Nəcəfov, Zəyəmçay nekropolu (Bakı 2019)

Müseyibli et al. 2008
N. Müseyibli – G. Agayev – S. G. Ashurov – I. Aliyev – M. Huseynov – Ş. Nəcəfov – F. Quliyev, Excavations of Tovuzchai Necropolis KP 378 – BTC ROW (Baku 2008) [accessible through Maynard 2011]

Nagel/Strommenger 1985
W. Nagel – E. Strommenger, Kalakent – Früheisenzeitliche Grabfunde aus dem transkaukasischen Gebiet von Kirovabad/Jelisavetopol, BBV 4 (Berlin 1985)

Narimanishvili et al. 2018
G. Narimanishvili – N. Shanshashvili – D. Narimanishvili, Die Trialeti-Kultur – Das Leben, der Tod und die Prozessionsstraßen in die Ewigkeit, in: L. Giemsch – S. Hansen (eds.), Gold und Wein. Georgiens älteste Schätze. Begleitband zur Sonderausstellung 6. Oktober 2018 – 10. Februar 2019 Archäologisches Museum Frankfurt (Mainz 2018) 203–227

Nawroth 2011
M. Nawroth, Reisen in das Paradies: Berliner Forschungen des 19. Jahrhunderts im Kaukasusgebiet, in: M. Wemhoff – A. Kokowski (eds.), Das Silberne Pferd. Archäologische Schätze zwischen Schwarzem Meer und Kaukasus (Berlin 2011) 81–105

Nemətova 2008
M. S. Nemətova, Şəmkir kitabələri, in: M. Rəhimova et al. (eds), Şəmkir: arxeoloji irsi, tarixi və memarlığı: birinci respublika elmi-praktik konfransın materialları (28–29 noyabr 2007) (Bakı 2008) 320–324

Nesbitt et al. 1980
H. W. Nesbitt – G. Markovics – R. C. Price, Chemical processes affecting alkalis and alkaline earths during continental weathering, Geochimica et Cosmochimica Acta 44, 1980, 1659–1666

Nesbitt et al. 1990
H. W. Nesbitt – N. D. MacRae – B. I. Kronberg, Amazon deep-sea fan muds: light REE enriched products of extreme chemical weathering, Earth and Planetary Science Letters 100, 1980, 118–123

Nesbitt/Young 1982
H. W. Nesbitt – G. M. Young, Early Proterozoic climates and plate motions inferred from major element chemistry of lutites, Nature 299, 1982, 715–717

Neuwirth 2014
E. Neuwirth, RColorBrewer: ColorBrewer palettes [https://rdrr.io/cran/RColorBrewer/man/ColorBrewer.html]

Newsome et al. 2004
S. D. Newsome – D. L. Phillips – B. J. Culleton – T. P. Guilderson – P. L. Koch, Dietary reconstruction of an early to middle Holocene human population from the central California coast: insights from advanced stable isotope mixing models, Journal of Archaeological Science 31, 2004, 1101–1115

Nəcəfov 2008a
Ş. Nəcəfov, Zəyəmçay nekropolu qəbirlərinin xronologiyası, Azərbaycan Arxeologiyası 11, 2008, 55–64

Nəcəfov 2008b
Ş. Nəcəfov, Zəyəmçay nekropolunun daş örtüklü qəbirləri haqqında, in: M. Rəhimova et al. (eds), Şəmkir: arxeoloji irsi, tarixi və memarlığı: birinci respublika elmi-praktik konfransın materialları (28–29 noyabr 2007) (Bakı 2008) 155–167

Nəcəfov 2018
Ş. Nəcəfov, Late bronze and early iron age monuments in the BTC and SCP pipeline route: Zayamchay and Tovuzchay necropolis, in: P. M. Taylor (ed.), Pipelines to Cultural Heritage: Proceedings of an International Workshop (April 20–23, 2010, Baku, Azerbaijan) (Washington, D. C. 2018) 139–150

Nəcəfov et al. 2007
S. Nəcəfov – M. Huseynov – B. Jalilov, Excavations of Dashbulag Settlement KP 342 – BTC ROW (Baku 2007) [accessible through Maynard 2011]

Nicholas/Manti 2014
M. Nicholas – P. Manti, Testing the applicability of handheld portable XRF to the characterisation of archaeological copper alloys. art. 0904, in: J. Bridgland (ed.), ICOM-CC 17th Triennial Conference Preprints, Melbourne, 15–19 September 2014 (Paris 2014) 1–13

Noll 1991
W. Noll, Alte Keramik und ihre Pigmente. Studien zu Material und Technologie (Stuttgart 1991)

Odgers 1931
P. N. Odgers, Two Details about the Neck of the Femur. (1) The Eminentia. (2) The Empreinte, Journal of Anatomy 65, 1931, 352–362

Ogden et al. 2007
A. R. Ogden – R. Pinhasi – W. J. White, Gross enamel hypoplasia in molars from subadults in a 16th–18th century London graveyard, American Journal of Physical Anthropology 133, 2007, 957–966

Okrostsvaridze/Tormey 2013
A. V. Okrostsvaridze – D. R. Tormey, Phanerozoic continental crust evolution of the Inner Caucasian Microplate: The Dzirula massif, Episodes 36, 2013, 31–38

O'Leary 1988
M. H. O'Leary, Carbon isotopes in photosynthesis, BioScience 38, 1988, 328–336

Ollivier et al. 2015
V. Ollivier – M. Fontugne – B. Lyonnet, Geomorphic response and ^{14}C chronology of base-level changes induced by Late Quaternary Caspian Sea mobility (middle Kura Valley, Azerbaijan), Geomorphology 230, 2015, 109–124

Ollivier et al. 2016
V. Ollivier – B. Lyonnet – C. Chataigner, Base level changes, river avulsions and Holocene human settlement dynamics in the Caspian Sea area (middle Kura valley, South Caucasus), Quaternal International 395, 2016, 79–94

Ortner 2008
D. J. Ortner, Differential Diagnosis of Skeletal Lesions in Infectious Disease, in: R. Pinhasi – S. Mays (eds.), Advances in Human Palaeopathology (Chichester 2008) 191–214

Ortner/Putschar 1981
D. J. Ortner – W. G. Putschar, Identification of Pathological Conditions in Human Skeletal Remains (Washington, D. C. 1981)

Oudbashi et al. 2012
O. Oudbashi – M. Emami – P. Davami, Bronze in archaeology: A review of the archaeometallurgy of bronze in Ancient Iran, in: L. Collini (ed.), Copper Alloys – Early applications and current performance enhancing processes (Rijeka 2012) 153–178

Palumbi 2015
G. Palumbi, Technology and Cuisine. Experimenting with Chalcolithic obsidian-tempered pottery from the Southern Caucasus, ArchéOrient – Le Blog (Hypotheses.org), 3 July 2015 [http://archeorient.hypotheses.org/4347]

Palumbi et al. 2018
G. Palumbi – D. Guilbeau – L. Astruc – C. Chataigner – B. Gratuze – B. Lyonnet – G. Pulitani, Between cooking and knapping in the southern Caucasus. Obsidian-tempered ceramics from Aratashen (Armenia) and Mentesh Tepe (Azerbaijan), Quaternary International 468, 2018, 121–133

Paraskevas et al. 2009
G. Paraskevas – K. Natsis – S. Spanidou – A. Tzaveas – P. Kitsoulis – A. Raikos – B. Papaziogas – N. Anastasopoulos, Excavated-type of rhomboid fossa of the clavicle: a radiological study, Folia Morphologica 68, 2009, 163–166

Patond et al. 2015
S. Patond – B. Tirpude – V. Pande, Age estimation by radiological assessment of proximal tibial epiphysis, Al Ameen Journal of Medical Sciences 8, 2015, 144–149

Pellegrini et al. 2011
M. Pellegrini – J. A. Lee-Thorp – R. E. Donahue, Exploring the variation of the $\delta^{18}Op$ and $\delta^{18}Oc$ relationship in enamel increments, Palaeogeography, Palaeoclimatology, Palaeoecology 310, 2011, 71–83

Perizonius 1979
W. R. K. Perizonius, Non-metric cranial traits: Sex difference and age dependence, Journal of Human Evolution 8, 1979, 679–684

Pernicka 2014
E. Pernicka, Possibilities and limitations of provenance studies of ancient silver and gold, in: H. Meller – R. Risch – E. Pernicka (eds.), Metalle der Macht – Frühes Gold und Silber. 6. Mitteldeutscher Archäologentag vom 17. bis 19. Oktober 2013 in Halle (Saale), Tagungen des Landesmuseums für Vorgeschichte Halle 11/II (Halle Saale 2014) 153–164

Phillips 2011
D. L. Phillips, Mixing model in analyses of diet using multiple stable isotopes: a critique, Oecologia 127, 2011, 166–170

Phillips 2012
D. L. Phillips, Converting isotope values to diet composition: the use of mixing models, Journal of Mammalogy 93, 2012, 342–352

Phillips/Koch 2002
D. L. Phillips – P. L. Koch, Incorporating concentration dependence in stable isotope mixing models, Oecologia 130, 2002, 114–125

Phillips et al. 2014
D. L. Phillips – R. Inger – S. Bearhop – A. L. Jackson – J. W. Moore – A. C. Parnell – B. X. Semmens – E. J. Ward, Best practices for use of stable isotope mixing models in food-web studies, Canadian Journal of Zoology 92, 2014, 823–835

Picchelauri 1997
K. Picchelauri, Waffen der Bronzezeit aus Ost-Georgien, Archäologie in Eurasien 4 (Espelkamp 1997)

Pillay et al. 2000
A. E. Pillay – C. Punyadeera – L. Jacobson – J. Eriksen, Analysis of Ancient Pottery and Ceramic Objects Using X-Ray Fluorescence Spectrometry, X-Ray Spectrometry 29, 2000, 53–62

Piller 2012
Ch. K. Piller, The Caucasian Connection – Reflections on the Transition from the Late Bronze to the Early Iron Age in Northern Iran and Its Connections to the Southern Caucasus, in: A. Mehnert – G. Mehnert – S. Reinhold (eds.), Austausch und Kulturkontakt im Südkaukasus und seinen angrenzenden Regionen in der Spätbronze-/Früheisenzeit, Schriften des Zentrums für Archäologie und Kulturgeschichte des Schwarzmeerraumes 22 (Langenweißbach 2012) 305–317

Pin et al. 2003
C. Pin – S. Joannon – C. Bosq – B. Le Fèvre – P.-J. Gauthier, Precise determination of Rb, Sr, Ba, and Pb in geological materials by isotope dilution and ICP-quadrupole mass spectrometry following selective separation of the analytes, Journal of Analytical Atomic Spectrometry 18, 2003, 135–141

Plontke-Lüning 2015
A. Plontke-Lüning, Gustav Radde und die kaukasische Archäologie, Phasis 18, 2015, 213–237

Plummer et al. 2006
M. Plummer – N. Best – K. Cowles – K. Vines, CODA: Convergence Diagnosis and Output Analysis for MCMC, R News 6, 2006, 7–11

Podlesak et al. 2008
D. W. Podlesak – A.-M. Torregrossa – J. R. Ehleringer – M. D. Dearing – B. H. Passey – T. E. Cerling, Turnover of oxygen and hydrogen isotopes in the body water, CO_2, hair, and enamel of a small mammal, Geochimica et Cosmochimica Acta 72, 2008, 19–35

Pollard et al. 2007
M. Pollard – C. Batt – B. Stern – S. M. M. Young, Analytical Chemistry in Archaeology, Cambridge Manuals in Archaeology (Cambridge 2007)

Popkhadze et al. 2014
N. Popkhadze – R. Moritz – V. Gugushvili, Architecture of Upper Cretaceous rhyodacitic hyaloclastite at the polymetallic Madneuli deposit, Lesser Caucasus, Georgia, Open Geosciences 6/3, 2014, 308–329

Post 2002
D. M. Post, Using Stable Isotopes to Estimate Trophic Position: Models, Methods, and Assumptions, Ecology 83, 2002, 703–718

Poyart et al. 1975
C. F. Poyart – E. Bursaux – A. Freminet, The bone CO_2 compartment: evidence for a bicarbonate pool, Respiration Physiology 25, 1975, 89–99

Prescher 1997
A. Prescher, The craniocervical junction in man, the osseous variations, their significance and differential diagnosis, Annals of Anatomy – Anatomischer Anzeiger 179, 1997, 1–19

Price et al. 1992
T. D. Price – J. Blitz – J. Burton – J. A. Ezzo, Diagenesis in prehistoric bone: Problems and solutions, Journal of Archaeological Science 19, 1992, 513–529

Price et al. 2002
T. D. Price – J. H. Burton – R. A. Bentley, The Characterization of Biologically Available Strontium Isotope Ratios for the Study of Prehistoric Migration, Archaeometry 44, 2002, 117–135

Price et al. 2012
T. D. Price – M. Naum – P. Bennike – N. Lynnerup – K. M. Frei – H. Wagnkilde – T. Pind – F. O. Nielsen, Isotopic investigation of human provenience at the eleventh century cemetery of Ndr. Grødbygård, Bornholm, Denmark, Danish Journal of Archaeology 1, 2012, 93–112

Pritchard/Robbins 1990
G. T. Pritchard – C. T. Robbins, Digestive and metabolic efficiencies of grizzly and black bears, Canadian Journal of Zoology 68, 1990, 1645–1651

R Core Team 2018
R Core Team, R: A Language and Environment for Statistical Computing (Vienna 2018)

Ramminger et al. 2010
B. Ramminger – M. Helfert – O. Mecking, Zur Herkunftsbestimmung bandkeramischer Gefäße: Das Beispiel Herxheim, in: B. Ramminger – O. Stilborg (eds.), Naturwissenschaftliche Analysen vor- und frühgeschichtlicher Keramik I. Methoden, Anwendungsbereiche, Auswertungsmöglichkeiten, Universitätsforschungen zur Prähistorischen Archäologie 176 (Bonn 2010) 51–74

Rani et al. 2011
A. Rani – J. Chopra – A. Rani – R. Suniti – S. Mishra – A. Srivastava – P. Sharma – R. Diwan, A Study of

Morphological Features of Attachment Area of Costoclavicular Ligament on Clavicle and First Rib in Indians and its Clinical Relevance, Biomedical Research 22, 2011, 349–354

Rapp 2014a
St. Rapp, New Perspectives on »The Land of Heroes and Giants«: The Georgian Sources for Sasanian History, e-Sasanika 13, 2014, 1–32

Rapp 2014b
St. Rapp, The Sasanian World through Georgian Eyes: Caucasia and the Iranian Commonwealth in Late Antique Georgian Literature (Farnham 2014)

Rayfield 2012
D. Rayfield, Edge of Empires: A History of Georgia (London 2012)

Reimer et al. 2013
P. J. Reimer – E. Bard – A. Bayliss – J. W. Beck – P. G. Blackwell – Ch. Bronk Ramsey – C. E. Buck – H. Cheng – R. L. Edwards – M. Friedrich – P. M. Grootes – Th. P. Guilderson – H. Haflidason – I. Hajdas – Ch. Hatté – T. J. Heaton – D. L. Hoffmann – A. G. Hogg – K. A. Hughen – K. F. Kaiser – B. Kromer – S. W. Manning – M. Niu – R. W. Reimer – D. A. Richards – E. M. Scott – J. R. Southon – R. A. Staff – Ch. S. M. Turney – J. van der Plicht, IntCal13 and Marine13 Radiocarbon Age Calibration Curves 0–50,000 Years cal BP, Radiocarbon 55, 1869–1887

Reinhold 2007
S. Reinhold, Die Spätbronze- und frühe Eisenzeit im Kaukasus. Materielle Kultur, Chronologie und überregionale Beziehungen, Universitätsforschungen zur prähistorischen Archäologie 144 (Bonn 2007)

Reinhold 2009
S. Reinhold, Zyklopische Festungen und Siedlungen mit symmetrischem Grundriss – Überlegungen zu einem überregionalen Phänomen der kaukasischen Spätbronzezeit, in: J. Apakidze – B. Govedarica – B. Hänsel (eds.), Der Schwarzmeerraum vom Äneolithikum bis in die Früheisenzeit (5000–500 v. Chr.). Kommunikationsebenen zwischen Kaukasus und Karpaten. Internationale Fachtagung von Humboldtianern für Humboldtianer im Humboldt-Kolleg in Tiflis/Georgien (17.–20. Mai 2007) (Rahden 2009) 97–130

Reynolds 2009
D. Reynolds, Gaussian Mixture Models, in: S. Li – A. Jain (eds.), Encyclopedia of Biometrics (Boston 2009) 659–663

Rice 1987
P. M. Rice, Pottery Analysis. A Sourcebook (Chicago 1987)

Richards et al. 2006
M. P. Richards – B. T. Fuller – T. I. Molleson, Stable isotope palaeodietary study of humans and fauna from the multi-period (Iron Age, Viking and Late Medieval) site of Newark Bay, Orkney, Journal of Archaeological Science 33, 2006, 122–131

Robbins et al. 2002
C. Robbins – G. Hilderbrand – S. Farley, Incorporating concentration dependence in stable isotope mixing models: a response to Phillips and Koch (2002), Oecologia 133, 2002, 10–13

Robert/Bousquet 2018
C. Robert – R. Bousquet, Geowissenschaften: Die Dynamik des Systems Erde (Berlin 2018)

Robling/Stout 2007
A. G. Robling – S. D. Stout, Histomorphometry of Human Cortical Bone: Applications to Age Estimation: in: M. A. Katzenberger – S. R. Saunders (eds.), Biological Anthropology of the Human Skeleton (Hoboken 2007) 149–182

Rogers et al. 2000
N. L. Rogers – L. E. Flournoy – W. F. McCormick, The rhomboid fossa of the clavicle as a sex and age estimator, Journal of Forensic Sciences 45, 2000, 61–67

Roseman 2004
C. C. Roseman, Detecting interregionally diversifying natural selection on modern human cranial form by using matched molecular and morphometric data, Proceedings of the National Academy of Sciences of the United States of America 101, 2004, 12824–12829

Rösler 1892
E. Rösler, Zwei Gräber von Schuscha (Transkaukasien), Zeitschrift für Ethnologie 24 (Verhandlungen), 1892, 566–569

Rösler 1898a
E. Rösler, Archäologisch-ethnologischer Bericht über seine für die kaiserl. russ. Archäologische Commission unternommenen Untersuchungen im Gov. Elisabethpol im Februar und April 1897, Zeitschrift für Ethnologie 30 (Verhandlungen), 1898, 290–329

Rösler 1898b
E. Rösler, Neue Ausgrabungen und archäologische Forschungsreisen in Transkaukasien (Mai und Juli 1897),

Zeitschrift für Ethnologie 30 (Verhandlungen), 1898, 416–453

Rösler 1901
E. Rösler, Bericht über die für die kaiserl. russ. Archäologische Commission im Jahre 1899 unternommenen archäologischen Forschungen und Ausgrabungen in Transkaukasien, Zeitschrift für Ethnologie 33 (Verhandlungen), 1901, 78–150

Rösler 1902
E. Rösler, Archäologische Forschungen und Ausgrabungen in Transkaukasien, unternommen für die kaiserl. russ. Archäologische Commission im Jahre 1900, Zeitschrift für Ethnologie 34 (Verhandlungen), 1902, 137–191

Rozanov et al. 1998
A. Rozanov – L. Neretin – I. Volkov, Redox Nepheloid Layer (RNL) of the Black Sea – Its location, composition and origin, in: L. Ivanov – T. Oguz (eds.), Ecosystem modeling as a management tool for the Black Sea. Proceedings of the NATO TU Black Sea Project, Ecosystem Modelling as a Management Tool for the Black Sea, Zori Rossii, Ukraine 15–19 June, 1997, NATO Science Series 2.47 (Dordrecht 1998) 77–92

Rubinson 1976
K. S. Rubinson, The Trialeti Culture (Ann Arbor 1976)

Sagona 2014
A. Sagona, Rethinking the Kura-Araxes Genesis, Paléorient 40/2, 2014, 23–46

Sagona 2018
A. Sagona, The Archaeology of the Caucasus. From Earliest Settlements to the Iron Age, Cambridge World Archaeology (Cambridge 2018)

Sajko et al. 2011
S. Sajko – K. Stuber – M. Wessely, Growth Restart/Recovery Lines involving the vertebral body: a rare, incidental finding and diagnostic challenge in two patients, The Journal of the Canadian Chiropractic Association 55, 2011, 313–317

Saller 1957
R. Saller, Lehrbuch der Anthropologie in systematischer Darstellung: mit besonderer Berücksichtigung der anthropologischen Methoden (begründet von Rudolf Martin) Band 1 [3](Stuttgart 1957)

Saller 1959
R. Saller, Lehrbuch der Anthropologie in systematischer Darstellung: mit besonderer Berücksichtigung der anthropologischen Methoden (begründet von Rudolf Martin) Band 2 [3](Stuttgart 1959)

Saunders/Rainey 2008
S. R. Saunders – D. L. Rainey, Nonmetric Trait Variation in the Skeleton: Abnormalities, Anomalies, and Atavisms, in: M. A. Katzenberg – S. R. Saunders (eds.), Biological Anthropology of the Human Skeleton [2](Hoboken 2008) 533–559

Sawyer 1986
E. W. Sawyer, The influence of source rock type, chemical weathering and sorting on the geochemistry of clastic sediments from the Quetico Metasedimentary Belt, Superior Province, Canada, Chemical Geology 55, 1986, 77–95

Schachner 2005
A. Schachner, Von Bronze zu Eisen: Die Metallurgie des 2. und frühen 1. Jahrtausends v. Chr. im östlichen Transkaukasus, in: Ü. Yalcin (ed.), Anatolian Metal III. Der Anschnitt. Beiheft 18 (Bochum 2005) 175–190

Schaefer et al. 2009
M. Schaefer – S. Black – L. Scheuer, Juvenile Osteology: A Laboratory and Field Manual (San Diego 2009)

Schmahl et al. 2016
W. W. Schmahl – B. Kocsis – A. Toncala – G. Grupe, Mineralogic Characterisation of Archaeological Bone, in: G. Grupe – G. C. McGlynn (eds.), Isotopic Landscapes in Bioarchaeology (Berlin/Heidelberg 2016) 91–110

Schmahl et al. 2017
W. W. Schmahl – B. Kocsis – A. Toncala – D. Wycisk – G. Grupe, The Crystalline State of Archaeological Bone Material, in: G. Grupe – A. Grigat – G. C. McGlynn (eds.), Across the Alps in Prehistory: Isotopic Mapping of the Brenner Passage by Bioarchaeology (Cham 2017) 75–104

Schmidt 2003
H. L. Schmidt, Fundamentals and systematics of the non-statistical distributions of isotopes in natural compounds, Naturwissenschaften 90, 2003, 537–552

Schoeninger/DeNiro 1984
M. J. Schoeninger – M. J. DeNiro, Nitrogen and carbon isotopic composition of bone collagen from marine and terrestrial mammals, Geochimica et Cosmochimica Acta 48, 1984, 625–639

Schultz 1988
M. Schultz, Paläopathologische Diagnostik, in: R. Knussmann (ed.), Anthropologie. Handbuch der vergleichenden Biologie des Menschen. Band 1: Wesen und Methoden der Anthropologie. 1. Teil Wissenschaftstheorie, Geschichte, morphologische Methode (Stuttgart 1988) 480–496

Schwarz 1978
G. Schwarz, Estimating the Dimension of a Model, The Annals of Statistics 6, 1978, 461–464

Scott/Pilloud 2019
G. R. Scott – M. A. Pilloud, Dental Morphology, in: M. A. Katzenberg – A. L. Grauer (eds.), Biological Anthropology of the Human Skeleton [3](Hoboken 2019) 257–292

Scrucca et al. 2016
L. Scrucca – M. Fop – T. B. Murphy – A. E. Raftery, mclust 5: Clustering, Classification and Density Estimation Using Gaussian Finite Mixture Models, The R Journal 8, 2016, 289–317

Shackley 2012a
S. M. Shackley, An Introduction to X-Ray Fluorescence (XRF) Analysis in Archaeology, in: S. M. Shackley (ed.), X-Ray-Fluorescence Spectrometry (XRF) in Geoarchaeology (London/Heidelberg 2012) 7–44

Shackley 2012b
S. M. Shackley, Portable X-ray Fluorescence Spectrometry (pXRF): The Good, the Bad, and the Ugly, Archaeology Southwest Magazine 26, 2012, 1–8 [online exclusive essay: https://www.archaeologysouthwest.org/pdf/pXRF_essay_shackley.pdf]

Shishlina et al. 2016
N. I. Shishlina – Y. O. Larionova – I. A. Idrisov – E. S. Azarov, Variations in $^{87}Sr/^{86}Sr$ ratios in contemporary snail samples obtained from the eastern Caucasus, Arid Ecosystems 6, 2016, 100–106

Siegmund 2020
F. Siegmund, Statistik in der Archäologie – eine anwendungsorientierte Einführung auf Basis freier Software (Norderstedt 2020)

Slowikowski 2018
K. Slowikowski, ggrepel: Automatically Position Non-Overlapping Text Labels with ‚ggplot2' [https://rdrr.io/cran/ggrepel/]

Smith 1984
B. H. Smith, Patterns of molar wear in hunter-gatherers and agriculturalists, American Journal of Physical Anthropology 63, 1984, 39–56

Smith 2009
H. F. Smith, Which cranial regions reflect molecular distances reliably in humans? Evidence from three-dimensional morphology, American Journal of Human Biology 21, 2009, 36–47

Smith et al. 2009
A. T. Smith – R. S. Badalyan – P. Avetisyan, The Archaeology and Geography of Ancient Transcaucasian Societies. Volume 1. The Foundations of Research and Regional Survey in the Tsaghkahovit Plain, Armenia, OIP 134 (Chicago 2009)

Söllner et al. 2016
F. Söllner – A. Toncala – S. Hölzl – G. Grupe, Determination of Geo-dependent Bioavailable $^{87}Sr/^{86}Sr$ Isotopic Ratios for Archaeological Sites from the Inn Valley (Austria): A Model Calculation, in: G. Grupe – G. C. McGlynn (eds.), Isotopic Landscapes in Bioarchaeology (Berlin/Heidelberg 2016) 123–140

Speakman et al. 2011
R. J. Speakman – N. C. Little – D. Creel – M. R. Miller – J. G. Iñañez, Sourcing ceramics with portable XRF spectrometers? A comparison with INAA using Mimbres pottery from the American Southwest, Journal of Archaeological Science 38, 2011, 3483–3496

Sponheimer/Lee-Thorp 1999
M. Sponheimer – J. A. Lee-Thorp, Oxygen isotopes in enamel carbonate and their ecological significance, Journal of Archaeological Science 26, 1999, 723–728

Sponheimer/Lee-Thorp 2001
M. Sponheimer – J. A. Lee-Thorp, The oxygen isotope composition of mammalian enamel carbonate from Morea Estate, South Africa, Oecologia 126, 2001, 153–157

Steele/Bramblett 1988
D. G. Steele – C. A. Bramblett, The Anatomy and Biology of the Human Skeleton (College Station 1988)

Steele/Daniel 1978
K. W. Steele – R. M. Daniel, Fractionation of nitrogen isotopes by animals: a further complication to the use of variations in the natural abundance of ^{15}N for tracer studies, The Journal of Agricultural Science 90, 1978, 7–9

Stloukal/Hanakova 1978
M. Stloukal – H. Hanakova, Die Länge der Längsknochen altslawischer Bevölkerungen – Unter besonderer Berücksichtigung von Wachstumsfragen, Homo 24, 1978, 53–69

Stöllner 2018
Th. Stöllner, Das älteste Gold in Georgien im Kontext, in: L. Giemsch – S. Hansen (eds.), Gold und Wein. Georgiens älteste Schätze. Begleitband zur Sonderausstellung 6. Oktober 2018 – 10. Februar 2019 Archäologisches Museum Frankfurt (Mainz 2018) 120–139

Stuart-Macadam 1985
P. Stuart-Macadam, Porotic hyperostosis: representative of a childhood condition, American Journal of Physical Anthropology 66, 1985, 391–398

Sullivan/Krueger 1981
C. H. Sullivan – H. W. Krueger, Carbon isotope analysis of separate chemical phases in modern and fossil bone, Nature 292, 1981, 333–335

Surkhayev 2012
M. M. Surkhayev, Monuments of the early stage of Late Bronze Age in Northwestern Azerbaijan (15th–8th centuries BC), in: A. Mehnert – G. Mehnert – S. Reinhold (eds.), Austausch und Kulturkontakt im Südkaukasus und seinen angrenzenden Regionen in der Spätbronze-/Früheisenzeit, Schriften des Zentrums für Archäologie und Kulturgeschichte des Schwarzmeerraumes 22 (Langenweißbach 2012) 251–260

Taylor 2018
P. M. Taylor (ed.), Pipelines to Cultural Heritage: Proceedings of an International Workshop (April 20–23, 2010, Baku, Azerbaijan) (Washington, D.C. 2018)

Taylor/Maynard 2011
P. M. Taylor – D. Maynard, Archaeological Excavations on the BTC Pipeline, Azerbaijan, Internet Archaeology 29, 2011 [http://intarch.ac.uk/journal/issue29/btc_toc.html]

Taylor et al. 2011
P. M. Taylor – Ch. R. Polglase – N. Müseyibli – J. M. Koller – T. A. Johnson, Past and Future Heritage in the Pipelines Corridor. Azerbaijan – Georgia – Turkey (Washington, D.C. 2011)

Telkkä et al. 1962
A. Telkkä – A. Palkama – P. Virtama, Prediction of stature from radiographs of long bones in children, Journal of Forensic Sciences 7, 1962, 474–479

Thompson/Galvin 1983
D. D. Thompson – C. A. Galvin, Estimation of age at death by tibial osteon remodeling in an autopsy series, Forensic Science International 22, 1983, 203–211

Tieszen/Fagre 1993
L. L. Tieszen – T. Fagre, Effect of Diet Quality and Composition on the Isotopic Composition of Respiratory CO_2, Bone Collagen, Bioapatite, and Soft Tissues, in: J. B. Lambert – G. Grupe (eds.), Prehistoric Human Bone – Archaeology at the Molecular Level (Berlin/Heidelberg 1993) 121–155

Trąbska/Trybalska 2010
J. Trąbska – B. Trybalska, Barium phosphates and sulphates in archaeological pottery, in: B. Ramminger – O. Stilborg (eds.), Naturwissenschaftliche Analysen vor- und frühgeschichtlicher Keramik I. Methoden, Anwendungsbereiche, Auswertungsmöglichkeiten, Universitätsforschungen zur Prähistorischen Archäologie 176 (Bonn 2010) 41–49

Trotter/Gleser 1958
M. Trotter – G. C. Gleser, A re-evaluation of estimation of stature based on measurements of stature taken during life and of long bones after death, American Journal of Physical Anthropology 16, 1958, 79–123

van der Boon et al. 2017
A. van der Boon – K. F. Kuiper – G. Villa – W. Renema – M. J. M. Meijers – C. G. Langereis – E. Aliyeva – W. Krijgsman, Onset of Maikop sedimentation and cessation of Eocene arc volcanism in the Talysh Mountains, Azerbaijan, Geological Society, London, Special Publications 428, 2017, 145–169**Vogel 1978**
J. C. Vogel, Isotopic Assessment of the Dietary Habits of Ungulates, South African Journal of Science 74, 1978, 298–301

Veliyev et al. 2018
A. Veliyev – A. Bayramov – J. Ibrahimov – S. Mammadov – G. Alizhadeh, Geological Setting and Ore Perspective of the New Discovered Gadir Low Sulfidation Epithermal Deposit, Gedabek NW Flank, Lesser Caucasus, Azerbaijan, Universal Journal of Geoscience 6/3, 2018, 78–101

Vincent et al. 2016
S. J. Vincent – W. Braham – V. A. Lavrishchev – J. R. Maynard – M. Harland, The formation and inversion of the western Greater Caucasus Basin and the uplift of the western Greater Caucasus: Implications for the wider Black Sea region, Tectonics 35, 2016, 2948–2962

von Cramon-Taubadel 2014
N. von Cramon-Taubadel, Evolutionary insights into global patterns of human cranial diversity: population history, climatic and dietary effects, Journal of anthropological sciences 92, 2014 43–77

Walker 1986
P. L. Walker, Porotic hyperostosis in a marine-dependent California Indian population, American Journal of Physical Anthropology 69, 1986, 345–354

Walker et al. 2009
P. L. Walker – R. R. Bathurst – R. Richman – T. Gjerdrum – V. A. Andrushko, The causes of porotic hyperostosis and cribra orbitalia: a reappraisal of the iron-defi-

ciency-anemia hypothesis, American Journal of Physical Anthropology 139, 2009, 109–125

Wapler et al. 2004
U. Wapler – E. Crubezy – M. Schultz, Is cribra orbitalia synonymous with anemia? Analysis and interpretation of cranial pathology in Sudan, American Journal of Physical Anthropology 123, 2004, 333–339

Warnes et al. 2017
G. R. Warnes – B. Bolker – G. Gorjanc – G. Grothendieck – A. Korosec – T. Lumley – D. MacQueen – A. Magnusson – J. Rogers, gdata: Various R Programming Tools for Data Manipulation [https://rdrr.io/cran/gdata/]

Warnes et al. 2018
G. R. Warnes – B. Bolker – T. Lumley, gtools: Various R Programming Tools [https://rdrr.io/cran/gtools/]

Wasserman et al. 1958
R. H. Wasserman – F. W. Lengemann – C. L. Comar, Comparative Metabolism of Calcium and Strontium in Lactation, Journal of Dairy Science 41, 1958, 812–821

White/Folkens 2005
T. D. White – P. A. Folkens, The Human Bone Manual (San Diego 2005)

White et al. 2004
C. White – F. J. Longstaffe – K. R. Law, Exploring the effects of environment, physiology and diet on oxygen isotope ratios in ancient Nubian bones and teeth, Journal of Archaeological Science 31, 2004, 233–250

Wickham 2016
H. Wickham, ggplot2: elegant graphics for data analysis (New York 2016)

Wronkiewicz/Condie 1987
D. J. Wronkiewicz – K. C. Condie, Geochemistry of Archean shales from the Witwatersrand Supergroup, South Africa: Source-area weathering and provenance, Geochimica et Cosmochimica Acta 51, 1987, 2401–2416

Xəlilov 2008
M. C. Xəlilov, Şəmkirin alban dövrü arxeoloji abidələri, in: M. Rəhimova et al. (eds), Şəmkir: arxeoloji irsi, tarixi və memarlığı: birinci respublika elmi-praktik konfransın materialları (28–29 noyabr 2007) (Bakı 2008) 207–215

Xiong/Li 2014
H. Xiong – Z. Li, Clustering Validation Measures, in: C. C. Aggarwal – C. K. Reddy (eds.), Data Clustering: Algorithms and Applications (Boca Raton 2014) 571–605

Zar 2010
J. H. Zar, Biostatistical analysis [5](Upper Saddle River 2010)

Zischow 2004
A. S. Zischow, Die bronzezeitlichen Fundplätze des Tsalka-Plateaus in Trialeti/Georgien im Kontext der Bronzezeit Transkaukasiens (Tübingen 2004) [MA-Thesis: http://hdl.handle.net/10900/46258]

Russian

Аббасова 1988
Ф. Ə. Аббасова, Азербајҹанын JTCAT експедисијасы II Јеникенд дəстəсинин 1988-ҹи илде апардығы чəл-тəдгигат ишләринин һесабаты, Arxeologiya və Etnoqrafiya İnstitutu elmi arxivi, h-500 (Bakı 1988)

Абилова 1960
Г. А. Абилова, Краткий отчет об археологической экспедиции 1957 года в Кедабекский район, материалы по истории Аэербайджана 3, 1960, 9–104

Авалов 2008
Э. В. Авалов, Крепость Шамкир – выдающийся памятник зодчества Азербайджана, M. Rəhimova et al. (eds), Şəmkir: arxeoloji irsi, tarixi və memarlığı: birinci respublika elmi-praktik konfransın materialları (28–29 noyabr 2007) (Bakı 2008) in: 245–254

Алиев 1987
А. А. Алиев, Исследования городища Мунджуглутепе, Археологические открытия (1985 г.), 1987, 546

Алиев/Велиев 1986
А. А. Алиев – Ф. И. Велиев, Археологические Раскопки в поселении Мунджуглутепе в 1985 году, Археологические и этнографические изыскания в Азербайджане (1985 г.), 1986, 62–63

Алиев et al. 1988
А. А. Алиев – В. А. Асадов – Ф. Аббасов, Работы Еникендской экспедиции, Археологические открытия (1986 г.), 1988, 453–454

Алиев n. d.
А. А. Алиев, Археологическое обследование в районе

Еникендского гидроузла, Arxeologiya və Etnoqrafiya İnstitutu elmi arxivi, h-309 (Bakı not dated)

Асланов 1986
Г. М. Асланов, Исследование курганов в Еникендского гидроузла в 1985 году, Археологические и этнографические изыскания в Азербайджане (1985 г.), 1986, 19–20

Асланов et al. 1959
Г. М. Асланов – Р. М. Ваидов – Г. И. Ионе, Древний Мингечаур (эпоха энеолита и бронзы) (Баку 1959)

Алиев 1991
В. Г. Алиев, Культура эпохи средней бронзы Азербайджана (Баку 1991)

Ахундов 1986
Д. А. Ахундов, Архитектура древнего и раннесредневекового Азербайджана (Баку 1986)

Ваидов 1954
Р. М. Ваидов, Раннесредневековое городище Судагылан, Краткие сообщения ИА РАН 54, 1954, 127–139

Ваидов 1961
Р. М. Ваидов, Минкәчевир. III–VIII Әсрләрдә (Археоложи газынты материаллары әсасында) (Баку 1961)

Варазашвили 1992
В. Л. Варазашвили, Раннеземледельческая культура иоро-алазанского бассейна (Тбилиси 1992)

Гогадзе 1972
Э. М. Гогадзе, Периодизация и генезис курганной культуры Триалети (Тбилиси 1972)

Гуммель 1940
Я. И. Гуммель, Археологические очерки (Баку 1940)

Гусейнова 1989
М. А. Гусейнова, Керамика Восточного Закавказья эпохи поздней бронзы и раннего железа (XIV–IX вв. до н.э.) (Баку 1989)

Гусейнова 2011
М. А. Гусейнова, Из истории Южного Кавказа. Ходжалы-Гедабекская культура Азербайджана (XVI–IX вв до н.э.) (Баку 2011)

Гусейнова/Алиев 1992
М. А. Гусейнова – И. Н. Алиев, Раскопки на поселении Алыгоджа Шамхорского района, in: A. A. Abbasov (ed.), Azərbaycanda arxeologiya və etnoqrafiya elmlərinin son nəticələrinə həsr olun-muş elmi konfransın materialları (Bakı 1992) 121–122

Гусейнова/Алиев 2008
М. А. Гусейнова – И. Н. Алиев, Среднебронзовые курганы с. Гараджамирли Шамкирского района Азербайджана, in: M. Rəhimova et al. (eds.), Şəmkir: arxeoloji irsi, tarixi və memarlığı: birinci respublika elmi-praktik konfransın materialları (28–29 noyabr 2007) (Bakı 2008) 129–154

Деведжян 1981
С. Г. Деведжян, Лори-Берд. Результаты раскопок 1969–1973 гг. (Ереван 1981)

Джафарзаде 1938
И. М. Джафарзаде, Циклопические сооружения Азербайджана, Труды Азербайджанского филиала Академии наук СССР 55, 1938, 5–54

Джафаров et al. 1982
Г. Ф. Джафаров – Г. П. Кесаманлы – И. Г. Нариманов, Археологические раскопки в зоне строительства Шамхорской ГЕС, Археологические и этнографические изыскания в Азербайджане (1978 г.), 1982, 9–11

Есаян/Погребова 1985
М. Н. Погребова – С. А. Есаян, Скифские памятники Закавказья (Москва 1985)

Ивановский 1911
А. А. Ивановский, По Закавказью. Археологические наблюдения и исследования 1893, 1894 и 1896 гг. (Москва 1911)

Казиев 1960
С. М. Казиев, Археологические раскопки в Мингечауре: Альбом кувшинных погребений (Баку 1960)

Квачидзе 2008
В. А. Квачидзе, Погребальный обряд Заямчайского некрополя Шамкирского района (Раскопки 2003-го года), in: M. Rəhimova et al. (eds.), Şəmkir: arxeoloji irsi, tarixi və memarlığı: birinci respublika elmi-praktik konfransın materialları (28–29 noyabr 2007) (Bakı 2008) 168–179

Кежушов/Аббасова 1987
Р. Б. Кежушов – Ф. Ә. Аббасова, Азәрбајҹан ССР ЕА Тарих институту ЈТС АТ експедисијасының Јеникәнд дәстәсинин 1987–чи ил чәл-тәдгигат ишләринин (һесабаты), Arxeologiya və Etnoqrafiya İnstitutu elmi arxivi, h-461 (Bakı 1987)

Кесаманлы 1981
Г. П. Кесаманлы, Исследование Шамхорской экспедиции, Археологические открытия (1980 г.), 1981, 420–421

Кесаманлы 1999
Г. П. Кесаманлы, Археологические памятники эпохи бронзы и раннего железа Дашкесанского района (Баку 1999)

Кесаманлы 2003
Г. П. Кесаманлы, Раскопки на поселении Битдили, Azərbaycan Arxeologiyası və Etnoqrafiyası 2, 2003, 55–58

Кесаманлы/Гусейнова 1986
Г. П. Кесаманлы – М. А. Гусейнова, Археологические памятники Кедабекского района (Баку 1986)

Кесаманлы/Джафаров 1977
Г. П. Кесаманлы – Г. Ф. Джафаров, Работы в зоне строительства Шамхорской ГЭС, Археологические открытия (1976 г.), 1977, 492–493

Кесаманлы/Джафаров 1979
Г. П. Кесаманлы – Г. Ф. Джафаров, Раскопки на поселении Битдили, Археологические и этнографические изыскания в Азербайджане (1976 г.), 1979, 8–11

Кесаманлы et al. 1976
Г. П. Кесаманлы – М. А. Гусейнова – Г. Ф. Джафаров – С. М. Кашкай – Г. Г. Асланов, Новые памятники в районе строительства Шамхорской ГЭС, Археологические открытия (1975 г.), 1976, 502

Кесаманлы et al. 1978a
Г. П. Кесаманлы – Г. Ф. Джафаров – И. А. Бабаев, Работы Шамхорского отряда, Археологические открытия (1977 г.), 1978, 498–499

Кесаманлы et al. 1978b
Г. П. Кесаманлы – Г. Ф. Джафаров – М. А. Гусейнова – Г. Г. Асланов, Археологические работы в зоне строительства Шамхорской ГЕС, Археологические и этнографические изыскания в Азербайджане (1975 г.), 1978, 23–26

Кесаманлы et al. 1980
Г. П. Кесаманлы – Г. Ф. Джафаров – И. А. Бабаев, Археологические Исследования в зоне строительства Шамхорской ГЭС, Археологические и этнографические изыскания в Азербайджане (1977 г.), 1980, 6–9

Кәсәмәнлы/Ҷәфәров 1977
Һ. П. Кәсәмәнлы – Һ. Ф. Ҷәфәров, Шамхор археложи експедисижасы Шамхор дәстәсинин 1977-чи ил тәдгигатларынын һесабаты, Arxeologiya və Etnoqrafiya İnstitutu elmi arxivi, h-216 (Bakı 1977)

Куфтин 1941
Б. А. Куфтин, Археологические раскопки в Триалети (Тбилиси 1941)

Мамиашвили 1988
Н. Ф. Мамиашвили, Могильник первой половины I тысячелетия до н. э. из Сагареджо, Труды Кахетской Археологической Експедитсии 8, 1988, 72–112

Мартиросян 1964
А. А. Мартиросян, Армения в эпоху бронзы и раннего железа (Ерева́н 1964)

Менабде/Кигурадзе 1981
М. В. Менабде – Т. В. Кигурадзе, Археологические памятники с. Сиони (Тбилиси 1981)

Мещанинов 1932
И. И. Мещанинов, Циклопические сооружения Закавказья, Известия Государственной Акад Истории Материальной Культуры XIII 4–7, 1932, 1–105

Минкевич-Мустафаева 1962
Н. В. Минкевич-Мустафаева, О датировке и хронологических этапах некоторых памятников Азербайджана эпохи пздней бронзы и раннего железа, Материальная культура Азербайджана 4, 1962, 109–139

Нариманов 1987
И. Г. Нариманов, Культура древнейшего земледельческо-скотоводческого населения Азербайджана (Эпоха энеолита VI–IV тысячелетия до н. э.) (Баку 1987)

Парцингер et al. 2018
Г. Парцингер – А. Гасс – Й. Фассбиндер, Исследования межкурганного пространства могильников скифского времени северного кавказа с применением магнитометрии, in: А. А. Тишкин (ed.), Современные решения актуальных проблем евразийской археологии, Вып. 2 (Барнаул 2018) 91–98

Погребова 2011
М. Н. Погребова, История Восточного Закавказья. вторая половина II – начало I тыс. до н.э. (по археологическим данным) (Москва 2011)

Расулоглы 1993
Т. Расулоглы, Циклопические сооружения на территории Азербайджана (Баку 1993)

Реслер 1902
Э. Реслер, Елисаветпольекая губерния, Отчетъ Императорской Археологической Комиссии (1899 г.), 1902, 57–90

Реслер 1905
Э. Реслер, Археологическия изследования Э. А. Реслера в Елисаветпольсной губ. в 1901 году., Известия Императорской Археологической Комиссии 16, 1905, 1–26

Сурхаев 2005
М. М. Сурхаев, Предметы вооружения и конской упряжи из курганов №1 и №2 Гараджамирли (Азербайджан), in: Эдубба вечна и постоянна. Материалы конференции, посвящённой 90-летию со дня рождения И. М. Дьяконова (Санкт-Петербург 2005) 234–241

Хачатрян 1975
Т. С. Хачатрян, Древняя культура Ширака III–I тыс. до н. э (Ереван 1975)

Хачатрян 1979
Т. С. Хачатрян, Артикский некрополь. Каталог (Ереван 1979)

Шарифов 1929
Д. М. Шарифов, Раскопки близ с. Човдар, Ганджинского уезда, Известия АЗКОМСТАРИСА выпуск 4, тетрадь 2, 1929, 239–260